

ESSENTIALS OF IGNEOUS AND METAMORPHIC PETROLOGY

B. RONALD FROST | CAROL D. FROST

Essentials of Igneous and Metamorphic Petrology

All geoscience students need to understand the origins, environments, and basic processes that produce igneous and metamorphic rocks. This concise textbook, written specifically for one-semester undergraduate courses, provides students with the key information they need to understand these processes. Topics are organized around the types of rocks to expect in a given tectonic environment, rather than around rock classifications: this is much more interesting and engaging for students, as it applies petrology to real geologic environments. This textbook includes over 250 illustrations and photos, and is supplemented by additional color photomicrographs made freely available online. Application boxes throughout the text encourage students to consider how petrology connects to wider aspects of geology, including economic geology, geologic hazards, and geophysics. End-of-chapter exercises allow students to apply the concepts they have learned and to practice interpreting petrologic data.

B. Ronald Frost is a professor of geology at the University of Wyoming, where he performs wide-ranging research on igneous and metamorphic petrology as well as ore deposits. He has authored more than 110 scientific papers on topics ranging from serpentinization and the metamorphism of serpentinites, ocean floor metamorphism, granulites, thermobarometry, the geochemistry of granites, and melting of sulfide ore deposits. He has conducted extensive field research in the Precambrian basement of Wyoming, as well as in Siberia, Greenland, northern Canada, and the Broken Hill area of Australia. He received the Alexander von Humboldt Research Award from the German government. He has been an associate editor for the *Journal of Metamorphic Geology* and *Geochimica et Cosmochimica Acta*, and currently serves on the editorial board of the *Journal of Petrology*. He is a member of the American Geophysical Union, the Society of Economic Geologists, and the Geochemical Society, and a fellow of the Mineralogical Society of America. He has taught mineralogy, petrology, optical mineralogy, and ore deposits for more than thirty-five years.

Carol D. Frost is a professor in the Department of Geology and Geophysics at the University of Wyoming. She investigates the origin and evolution of the continental crust, the provenance of clastic sedimentary rocks, and granite petrogenesis, and she applies isotope geology and geochemistry to environmental issues including water coproduced with hydrocarbons and geological sequestration of carbon dioxide. She is the author of more than 120 scientific papers. She is a fellow of the Mineralogical Society of America and serves as the science editor for the Geological Society of America's journal, *Geosphere*. She was awarded the CASE Wyoming Professor of the Year award in 2001. In 2008, she received her university's highest faculty award, the George Duke Humphrey medal, recognizing teaching effectiveness, distinction in scholarly work, and distinguished service to the university and to the state. She has served in the administration of the University of Wyoming as director of the School of Energy Resources, associate vice president for research and economic development, and vice president for special projects, and she currently serves as associate provost.

The two authors are unrelated.

Essentials of Igneous and Metamorphic Petrology

B. Ronald Frost

UNIVERSITY OF WYOMING

Carol D. Frost

UNIVERSITY OF WYOMING



CAMBRIDGE
UNIVERSITY PRESS

CAMBRIDGE
UNIVERSITY PRESS

32 Avenue of the Americas, New York, NY 10013-2473, USA

Cambridge University Press is part of the University of Cambridge.

It furthers the University's mission by disseminating knowledge in the pursuit of education, learning, and research at the highest international levels of excellence.

www.cambridge.org

Information on this title: www.cambridge.org/9781107696297

© B. Ronald Frost and Carol D. Frost 2014

This publication is in copyright. Subject to statutory exception and to the provisions of relevant collective licensing agreements, no reproduction of any part may take place without the written permission of Cambridge University Press.

First published 2014

Printed in the United States of America

A catalogue record for this publication is available from the British Library.

Library of Congress Cataloging in Publication data

Frost, Bryce Ronald, 1947- Essentials of igneous and metamorphic petrology / B.

Ronald Frost, Carol D. Frost. p. cm.

Includes bibliographical references and index.

ISBN 978-1-107-02754-1 (hardback : alk. paper)

1. Igneous rocks. 2. Metamorphic rocks. I. Frost, Carol D.
(Carol Denison) II. Title.

QE461.F767 2014

552'.1-dc23 2013012168

ISBN 978-1-107-02754-1 Hardback

ISBN 978-1-107-69629-7 Paperback

Cambridge University Press has no responsibility for the persistence or accuracy of URLs for external or third-party Internet Web sites referred to in this publication and does not guarantee that any content on such Web sites is, or will remain, accurate or appropriate.

Contents

List of Figures	page xi	2.5.1 <i>The Ternary System $Mg_2SiO_4 - CaAl_2Si_2O_8 - CaMgSi_2O_6$</i>	30
List of Tables	xix	2.6 Implications for Petrology	31
List of Maps	xx	Summary	32
List of Boxes	xxii	Questions and Problems	32
Preface	xxiii	Further Reading	35
Acknowledgments	xxv		
1		3	
.....		
Introduction to Igneous Petrology	1	Introduction to Silicate Melts and Magmas	36
1.1 Introduction	1	3.1 Introduction	36
1.2 The Scope of Igneous Petrology	2	3.2 The Role of Volatiles	37
1.3 Classification of Igneous Rocks	2	3.2.1 <i>Role of H_2O</i>	37
1.3.1 <i>Preliminary Classification</i>	3	3.2.2 <i>Role of CO_2</i>	38
1.3.2 <i>IUGS Classification of Plutonic Rocks</i>	3	3.3 Physical Properties of Magma	39
1.3.3 <i>IUGS Classification of Volcanic and Hypabyssal Rocks</i>	5	3.3.1 <i>Temperature</i>	39
1.4 Igneous Textures	5	3.3.2 <i>Heat Capacity and Heat of Fusion</i>	39
1.4.1 <i>Crystal Size</i>	6	3.3.3 <i>Viscosity</i>	39
1.4.2 <i>Crystal Shape</i>	7	3.3.4 <i>Density</i>	40
1.5 Igneous Structures	8	3.4 The Ascent of Magmas	40
1.5.1 <i>Structures in Volcanic Flows</i>	8	3.5 Magmatic Differentiation	42
1.5.2 <i>Structures in Pyroclastic Deposits</i>	10	3.5.1 <i>Partial Melting</i>	42
1.5.3 <i>Structures in Hypabyssal Rocks</i>	12	3.5.2 <i>Crystallization Processes</i>	42
1.5.4 <i>Structures in Plutonic Rocks</i>	14	3.5.3 <i>Liquid-liquid Fractionation</i>	43
Summary	16	3.5.4 <i>Assimilation</i>	43
Questions and Problems	16	3.5.5 <i>Magma Mixing</i>	44
Further Reading	17	Summary	44
		Questions and Problems	45
		Further Reading	46
2		4	
.....		
An Introduction to Igneous Phase Diagrams	18	The Chemistry of Igneous Rocks	47
2.1 Introduction	18	4.1 Introduction	47
2.2 The Phase Rule	19	4.2 Modal Mineralogy versus Normative Mineralogy	48
2.3 The Lever Rule	20	4.3 Variation Diagrams Based on Major Elements	48
2.4 Two Component Systems Involving Melt	21	4.4 Major Element Indices of Differentiation	51
2.4.1 <i>Binary Systems with a Eutectic</i>	21	4.4.1 <i>Modified Alkali-lime Index</i>	53
2.4.2 <i>Binary Systems with a Peritectic</i>	24	4.4.2 <i>Iron Enrichment Index</i>	54
2.4.3 <i>Binary Systems with a Thermal Barrier</i>	26	4.4.3 <i>Aluminum Saturation Index</i>	55
2.4.4 <i>Binary Systems with Solid Solution</i>	27	4.4.4 <i>Alkalinity Index</i>	56
2.4.5 <i>Binary Systems with Partial Solid Solution</i>	29	4.5 Identification of Differentiation Processes Using Trace Elements	56
2.5 Phase Diagrams of Ternary Systems	29		

4.5.1	<i>Use of Trace Elements to Model Melting and Crystallization Processes</i>	57
4.5.2	<i>Graphical Representations of Trace Element Compositions</i>	58
4.6	Application of Stable and Radioactive Isotopes in Igneous Petrology	59
4.6.1	<i>Geochronology</i>	60
4.6.2	<i>Isotopic Tracing of Magma Sources</i>	60
	Summary	61
	Questions and Problems	62
	Further Reading	64

5

	Basalts and Mantle Structure	65
5.1	Introduction	65
5.2	Basalt Petrology	66
5.2.1	<i>Classification</i>	66
5.2.2	<i>Chemistry and Petrography</i>	66
5.3	Melt Generation from the Mantle	67
5.3.1	<i>Mantle Composition</i>	67
5.3.2	<i>Crust and Mantle Structure</i>	67
5.3.3	<i>Mechanisms for Partial Melting of the Mantle</i>	68
5.3.4	<i>The Process of Mantle Melting</i>	68
5.3.5	<i>Origin of Tholeiitic versus Alkali Basalts</i>	69
5.4	Environments where Magmas are Generated	70
	Summary	70
	Questions and Problems	71
	Further Reading	71

6

	Oceanic Magmatism	72
6.1	Introduction	72
6.2	The Petrology and Structure of the Ocean Crust	73
6.2.1	<i>Ophiolites as a Model of the Ocean Crust</i>	73
6.2.2	<i>Refinements of the Ophiolite Model</i>	74
6.3	Petrography and Geochemistry of Oceanic Magmatism	78
6.3.1	<i>Mid-ocean Ridge Basalt</i>	78
6.3.2	<i>Off-ridge Magmatism</i>	80
	Summary	86
	Questions and Problems	86
	Further Reading	87

7

	Convergent Margin Magmatism	88
7.1	Introduction	88
7.2	Oceanic and Continental Arcs	89
7.2.1	<i>Island Arc Magmatism</i>	89
7.2.2	<i>Continental Arc Magmatism</i>	89
7.2.3	<i>Structure of Island and Continental Arcs</i>	91
7.2.4	<i>Examples of Island and Continental Arcs</i>	92
7.3	Petrographic Characteristics of Island and Continental Arc Rocks	97
7.3.1	<i>Petrography of Island Arc Rocks</i>	97
7.3.2	<i>Petrography of Continental Arc Rocks</i>	99
7.4	Geochemical Characteristics of Convergent Margin Magma Series	99
7.4.1	<i>Comparison of Oceanic and Arc Differentiation Trends</i>	99
7.4.2	<i>Comparison of Island and Continental Arc Magma Series</i>	100
7.4.3	<i>Comparison of Oceanic and Continental Arc (Cordilleran) Plutonic Complexes</i>	102
7.4.4	<i>Geochemical Identification of Contrasting Processes Forming Segum and Mount Saint Helens</i>	103
7.5	Magma Generation at Convergent Margins	104
	Summary	105
	Questions and Problems	106
	Further Reading	106

8

	Intracontinental Volcanism	107
8.1	Introduction	107
8.2	Continental Flood Basalt Provinces	108
8.2.1	<i>The Columbia Plateau – Snake River Plain Province</i>	109
8.2.2	<i>Petrography and Chemistry of Continental Flood Basalts</i>	111
8.2.3	<i>Models for the Generation of Continental Flood Basalts</i>	111
8.3	Bimodal Volcanism	112
8.3.1	<i>Bimodal Volcanism in the Yellowstone – Snake River Plain Province</i>	112

8.3.2	<i>Geochemistry of the Yellowstone – Snake River Plain Bimodal Suite</i>	114	10.4.1	<i>The Etive Granite</i>	150
8.3.3	<i>Models for the Generation of Bimodal Volcanism</i>	115	10.4.2	<i>Geochemistry and Origin of Caledonian Granites</i>	151
8.4	<i>Alkaline Volcanism</i>	115	10.5	<i>Review of the Four Main Granite Types</i>	152
8.4.1	<i>Sodic Alkaline Magmatism of the East African Rift</i>	116		<i>Summary</i>	156
8.4.2	<i>Potassic Alkaline Volcanism</i>	118		<i>Questions and Problems</i>	156
8.5	<i>Origin of the Chemical Diversity of Intracontinental Basaltic Magmas</i>	121		<i>Further Reading</i>	156
	<i>Summary</i>	122			
	<i>Questions and Problems</i>	122			
	<i>Further Reading</i>	122			
9			11		
.....				
	Intracontinental Plutonism	124		Introduction to Metamorphic Petrology	157
9.1	<i>Introduction</i>	124	11.1	<i>Introduction</i>	157
9.2	<i>Layered Mafic Intrusions</i>	126	11.2	<i>The Scope of Metamorphism</i>	158
9.2.1	<i>The Bushveld Intrusion</i>	128	11.3	<i>Types of Metamorphism</i>	158
9.2.2	<i>Mineralogical Variation in LMIs</i>	128	11.3.1	<i>Regional Metamorphism</i>	158
9.2.3	<i>Granitic Rocks Associated with LMIs</i>	129	11.3.2	<i>Contact Metamorphism</i>	158
9.2.4	<i>Tectonic Environments of LMIs</i>	130	11.3.3	<i>Burial Metamorphism</i>	158
9.3	<i>Anorthosites and Related Rocks</i>	130	11.3.4	<i>Dynamic Metamorphism</i>	159
9.3.1	<i>Archean Anorthosites</i>	131	11.3.5	<i>Hydrothermal Metamorphism</i>	159
9.3.2	<i>Massif Anorthosites</i>	132	11.4	<i>Basic Goals of Metamorphic Petrology</i>	159
9.4	<i>Ferroan Granites</i>	134	11.5	<i>Identification of Protolith</i>	159
9.4.1	<i>The Pikes Peak Batholith</i>	135	11.5.1	<i>Rocks of Clearly Sedimentary Parentage</i>	159
9.4.2	<i>The Composition of Ferroan Granites</i>	136	11.5.2	<i>Rocks of Clearly Igneous Parentage</i>	161
9.5	<i>Alkaline Complexes</i>	138	11.5.2	<i>Rocks of Uncertain Parentage</i>	161
9.5.1	<i>Geology of the Ilimaussaq Intrusion</i>	138	11.6	<i>Determination of Metamorphic Textures</i>	161
	<i>Summary</i>	141	11.6.1	<i>Stability Range of Single Minerals</i>	161
	<i>Questions and Problems</i>	142	11.6.2	<i>Stability of Mineral Assemblages</i>	162
	<i>Further Reading</i>	143	11.6.3	<i>Metamorphic Facies</i>	162
			11.6.4	<i>Thermobarometry</i>	162
			11.7	<i>Metamorphic Textures</i>	162
			11.7.1	<i>Primary Textures</i>	162
			11.7.2	<i>Metamorphic Textures</i>	164
			11.8	<i>Naming a Metamorphic Rock</i>	166
				<i>Summary</i>	167
				<i>Questions and Problems</i>	168
				<i>Further Reading</i>	169
10			12		
.....				
	Interpretation of Granitic Rocks	144		Interpretation of Metamorphic Phase Diagrams	170
10.1	<i>Introduction</i>	144	12.1	<i>Introduction</i>	170
10.2	<i>Classification of Granitic Rocks</i>	145	12.2	<i>A Little History</i>	171
10.2.1	<i>Mineralogical Classification</i>	145	12.3	<i>Use of Chemographic Projections</i>	171
10.2.2	<i>Classification Based on Opaque Oxides</i>	145	12.3.1	<i>Chemographic Projections in a Two-Component System</i>	172
10.2.3	<i>Alphabetic Classification</i>	145	12.3.2	<i>Chemographic Projections in a Three-Component System</i>	173
10.2.4	<i>Geochemical Classification</i>	145			
10.3	<i>Peraluminous Leucogranites</i>	146			
10.3.1	<i>Himalayan Leucogranites</i>	148			
10.3.2	<i>Geochemistry of Peraluminous Leucogranites</i>	148			
10.4	<i>Caledonian Granites</i>	149			

12.3.3 <i>Chemographic Projections in Systems with Four and More Components</i>	175
Summary	176
Questions and Problems	176
Further Reading	179

13

Metamorphic Facies and the Metamorphism of Mafic Rocks 180

13.1 Introduction	180
13.2 Definition of Metamorphic Facies	181
13.3 Facies of Regional Metamorphism	181
13.3.1 <i>Greenschist Facies</i>	181
13.3.2 <i>Blueschist Facies</i>	182
13.3.3 <i>Amphibolite Facies</i>	183
13.3.4 <i>Very Low-Temperature Metamorphism</i>	184
13.3.5 <i>Granulite Facies</i>	185
13.3.6 <i>Eclogite Facies</i>	185
13.4 Facies of Contact Metamorphism	185
13.5 Textural Changes during Metamorphism	186
13.6 Mafic Mineral Assemblages at Increasing Temperature and Pressure	187
13.6.1 <i>Relations at Very Low Temperatures</i>	187
13.6.2 <i>Relations at Low Pressure with Increasing Temperature</i>	188
13.6.3 <i>Relations at Low Temperature with Increasing Pressure</i>	189
Summary	189
Questions and Problems	189
Further Reading	190

14

Thermobarometry and the Conditions of Metamorphism 191

14.1 Introduction	191
14.2 Review of Thermodynamics	192
14.2.1 <i>Free Energy</i>	192
14.2.2 <i>Effect of Changes in Pressure and Temperature on ΔG</i>	192
14.2.3 <i>The Equilibrium Constant</i>	192
14.2.4 <i>Activity-composition Relations</i>	193
14.3 Thermobarometers	194
14.3.1 <i>Geothermometry</i>	194
14.3.2 <i>Geobarometry</i>	195
14.3.3 <i>Thermobarometry</i>	196
14.4 Conditions of Metamorphism	197
14.4.1 <i>The Pressure and Temperature Conditions for the Metamorphic Facies</i>	198

14.4.2 <i>The Upper Temperature Limits to Metamorphism and Migmatites</i>	199
14.4.3 <i>Upper Pressure Limit of Metamorphism</i>	200
Summary	201
Questions and Problems	202
Further Reading	202

15

Metamorphism of Peridotitic Rocks 203

15.1 Introduction	203
15.2 The Process of Serpentinization	204
15.3 Prograde Metamorphism of Serpentine: Reactions in the System $\text{CaO-MgO-SiO}_2\text{-H}_2\text{O}$	204
15.4 Role of Minor Components	208
15.4.1 <i>Iron</i>	208
15.4.2 <i>Aluminum</i>	210
15.5 Metaperidotites and Metamorphic Facies	211
15.6 Role of CO_2 in Metamorphism of Peridotites	212
15.7 Metasomatism of Peridotites	214
15.8 Examples of Metaperidotites in the Field	215
15.8.1 <i>Malenco Serpentinite</i>	215
15.8.2 <i>Ingalls Peridotite</i>	217
Summary	218
Questions and Problems	218
Further Reading	219

16

Metamorphism of Pelitic Rocks 220

16.1 Introduction	220
16.2 Chemographic Projections for Pelitic Systems	221
16.2.1 <i>Chemographic Projections for Continuous Reactions</i>	221
16.2.2 <i>AMF Projections for Pelitic Rocks</i>	223
16.3 Progressive Metamorphism of Pelitic Rocks: Barrovian Metamorphism	224
16.3.1 <i>The Protolith: The Mineralogy of Shale</i>	224
16.3.2 <i>Low-Grade Metamorphism of Pelitic Rocks</i>	224
16.3.3 <i>Barrovian Metamorphism of Pelitic Schists</i>	225
16.4 Comparison between Barrovian and other P-T Conditions for Metamorphism of Pelitic Rocks	229
16.4.1 <i>Correlation of Barrovian Zones to Metamorphic Facies</i>	229

16.4.2 <i>Pressure Information from Metapelitic Rocks</i>	230	Summary	259
Summary	233	Questions and Problems	260
Questions and Problems	234	Further Reading	261
Further Reading	236		
17		Appendix: Review of Mineralogy	263
Metamorphism of Calcareous Rocks and the Role of Fluids in Metamorphism	237	A.1 Introduction	263
17.1 Introduction	237	A.2 Leucocratic Rock-forming Minerals	263
17.2 Metamorphism of Impure Dolomitic Marble	238	A.2.1 <i>Quartz</i>	263
17.2.1 <i>Stability of Metamorphic Assemblages in T-X Space</i>	239	A.2.2 <i>Feldspars and Feldspathoids</i>	263
17.2.2 <i>Examples of How Mineral Assemblages Can Monitor Fluid Flow in Aureoles</i>	240	A.2.3 <i>Carbonates</i>	268
17.3 Buffering of other Fluid Components	242	A.3 Ferromagnesian Minerals	268
17.4 Buffering of pH	244	A.3.1 <i>Olivine</i>	268
Summary	246	A.3.2 <i>Pyroxenes</i>	269
Questions and Problems	247	A.3.3 <i>Amphiboles</i>	272
Further Reading	248	A.3.4 <i>Phyllosilicates</i>	274
		A.4 Aluminum-excess Minerals	277
		A.4.1 <i>Aluminosilicates (Andalusite, Kyanite, and Sillimanite)</i>	277
		A.4.2 <i>Garnets</i>	278
		A.4.3 <i>Staurolite</i>	278
		A.4.4 <i>Cordierite</i>	278
		A.4.5 <i>Chloritoid</i>	279
		A.5 Ca-Al Silicates	279
		A.5.1 <i>Clinozoisite-Epidote</i>	279
		A.5.2 <i>Prehnite</i>	279
		A.5.3 <i>Pumpellyite</i>	279
		A.5.4 <i>Lawsonite</i>	280
		A.5.5 <i>Laumontite</i>	280
		A.6 Oxide, Sulfide, and other Nominally Opaque Phases	280
		A.6.1 <i>Fe-Ti Oxides (Magnetite and Ilmenite)</i>	280
		A.6.2 <i>Other Spinel Minerals</i>	280
		A.6.3 <i>Fe Sulfides</i>	280
		A.6.4 <i>Graphite</i>	281
		A.6.5 <i>Rutile</i>	281
		A.7 Accessory Minerals	281
		A.7.1 <i>Zircon</i>	281
		A.7.2 <i>Sphene (or Titanite)</i>	281
		A.7.3 <i>Apatite</i>	281
		A.7.4 <i>Monazite</i>	281
		Summary	282
		References	283
		Index	297
18			
Regional Occurrence and Tectonic Significance of Metamorphic Rocks	249		
18.1 Introduction	249		
18.2 Metamorphism along Convergent Plate Margins	250		
18.2.1 <i>Characteristics of Low-Temperature, High-Pressure Belts</i>	250		
18.2.2 <i>Characteristics of Low-Pressure, High-Temperature Belts</i>	250		
18.2.3 <i>Tectonic Interpretation</i>	250		
18.3 Metamorphism in Continental Collisions	251		
18.3.1 <i>Examples of Continental Collisions</i>	252		
18.4 Metamorphism in Rifting Terrains	253		
18.5 Sea Floor Metamorphism	254		
18.6 Granulite Terranes	255		
18.7 Metamorphism in Archean Terrains	257		
18.7.1 <i>Greenstone Belts</i>	258		
18.7.2 <i>Gneiss Terrains</i>	258		
18.7.3 <i>Tectonic Interpretation of Archean Metamorphic Belts</i>	259		

Figures

1.1	IUGS classification of plutonic rocks based upon modal mineralogy	page 4	2.3	A ternary diagram for the system $x - y - z$ showing where phase E with the composition of x_2yz plots	21
1.2	IUGS classification of gabbroic rocks	5	2.4	Phase diagram showing a portion of the system $\text{NaCl-H}_2\text{O}$	22
1.3	IUGS classification of ultramafic rocks	5	2.5	Phase diagram for the system $\text{CaAl}_2\text{Si}_2\text{O}_8 - \text{CaMgSi}_2\text{O}_6$ at one bar	22
1.4	IUGS classification of volcanic rock based on modal mineralogy	6	2.6	Phase diagram for the system $\text{CaAl}_2\text{Si}_2\text{O}_8 - \text{CaMgSi}_2\text{O}_6$ showing the crystallization path for a melt with composition X	23
1.5	IUGS classification of volcanic rocks based on chemical composition, in weight percent oxide	7	2.7	Phase diagram for the system $\text{Mg}_2\text{SiO}_4 - \text{SiO}_2$	24
1.6	Photomicrographs showing textures in volcanic rocks	8	2.8	Phase diagram for the system $\text{Mg}_2\text{SiO}_4 - \text{SiO}_2$ showing the equilibrium crystallization path for a melt with composition X	24
1.7	Photomicrographs showing textures in plutonic igneous rocks	9	2.9	(A) Phase diagram for the system $\text{Mg}_2\text{SiO}_4 - \text{SiO}_2$ showing the path followed by fractional crystallization. (B) The sequences of mineral assemblages encountered in a hypothetical magma chamber of composition X that underwent fractional crystallization	25
1.8	Structures of volcanic rocks	10	2.10	Phase diagram for the system $\text{NaSiO}_4 - \text{SiO}_2$	26
1.9	Classification of pyroclastic rocks	11	2.11	Phase diagram for the system $\text{NaSiO}_4 - \text{SiO}_2$ showing how crystallization of two melts with similar compositions can produce very different residual melts	26
1.10	Photomicrographs of pyroclastic rocks	12	2.12	(A) Phase diagram for the system $\text{CaAl}_2\text{Si}_2\text{O}_8 - \text{NaAlSi}_3\text{O}_8$ (Bowen, 1913) (B) Phase diagram for the system $\text{Mg}_2\text{SiO}_4 - \text{Fe}_2\text{SiO}_4$ (Bowen and Schairer, 1935)	27
1.11	Sketch showing the relative scale of aerial distribution of pyroclastic air fall deposits from strombolian and plinian eruptions	13	2.13	Phase diagram for the system $\text{Mg}_2\text{SiO}_4 - \text{Fe}_2\text{SiO}_4$ showing the path followed by a melt with composition x during (A) equilibrium crystallization and (B) fractional crystallization	28
1.12	Diagram of the formation of a pyroclastic flow deposit by the collapse of a lava dome	13	2.14	Phase diagram for the system $\text{NaAlSi}_3\text{O}_8 - \text{KAlSi}_3\text{O}_8$ at high water pressures	28
1.13	Photo of a lava dome and pyroclastic flow within the caldera of Mount Saint Helens	14	2.15	Ternary phase diagram for the system $x - y - z$	29
1.14	(A) Geologic sketch map of Shiprock in New Mexico, USA, showing dikes (linear features) radiating out of a volcanic neck (irregular gray shape). The volcanic neck, called Shiprock, is about 600 meters high. (B) View of Shiprock and dikes from the southeast	14	2.16	Ternary phase diagram for the system $\text{Fo} - \text{An} - \text{Di}$ showing the crystallization path followed by melts of the composition X and Y. D = ternary peritectic and E = ternary eutectic	30
1.15	Photo of chilled Tertiary dike intruding and baking adjacent Cretaceous sedimentary rocks, southern Colorado, USA	15			
1.16	(A) Biotite-rich xenolith in granodiorite dike cutting the Laramie anorthosite complex, Wyoming, USA. (B) Fine-grained granodiorite autolith in granite, floor of main terminal building	15			
2.1	Phase diagram for the one-component system Al_2SiO_5	19			
2.2	Diagram showing olivine solid solutions. Points a, b, and c refer to olivine with different amounts of Fe and Mg	20			

2.17 Ternary phase diagram showing the sequence of rocks produced from a melt with a composition Y that has undergone fractional crystallization and crystal settling	31	4.3 Harker diagrams for the Red Mountain pluton, Wyoming, USA	50
3.1 Schematic diagram showing the structure of a silicate melt	37	4.4 Diagram showing the effect of fractional crystallization on the trend followed by magmas on a Harker diagram	51
3.2 Diagram showing how the solution of H ₂ O into a silicate melt breaks silica polymers, replacing the bridging oxygen with OH	37	4.5 Diagram showing that the geochemical composition of dacite is consistent with its origin by mixing of rhyolite and andesite magmas	51
3.3 (a) Effect of water on the melting temperature of albite. (b) How the phase relations control the melting and movement of melts in the crust	38	4.6 Harker diagrams comparing trends in the Sherman batholith and the Red Mountain pluton, Wyoming, USA	51
3.4 Comparison of molar volume of water in melt and in fluid at 800°C	38	4.7 Photographs showing the relationships between the rock units composing the Sherman batholith, Wyoming, USA	52
3.5 Diagram showing how the solution of CO ₂ into a silicate melt enhances polymerization	38	4.8 . Harker diagram showing the variation of CaO and Na ₂ O + K ₂ O in three batholiths	53
3.6 Solubility of CO ₂ into tholeiitic basalt	39	4.9 Plot of MALI (Na ₂ O + K ₂ O – CaO) vs. SiO ₂ showing where calcic, calc-alkalic, alkali-calcic, and calcic rocks plot	54
3.7 Relationship between viscosity, temperature, and composition of melts at 1 bar	40	4.10 Fe* [FeO ^{tot} /(FeO ^{tot} +MgO)] vs SiO ₂ diagram comparing the ferroan Red Mountain pluton, Wyoming, USA with the magnesian Tuolumne batholith, California, USA	54
3.8 Stopped block of gabbro that sank through the magma chamber, where it deformed layers of anorthosite accumulating on the magma chamber floor. Laramie anorthosite complex, USA	41	4.11 Aluminum Saturation Index (ASI) vs. SiO ₂ diagrams	55
3.9 (A) Photo of alkali feldspar mantled with plagioclase (reverse zoning), a texture known as rapakivi texture. Mantled feldspars indicate a change in crystallization conditions. Ksp = alkali-feldspar, Pl = plagioclase, Qz = quartz. Sherman batholith, Wyoming, USA. (B) Resorbed crystal of quartz (Qz) in an olivine-bearing (Ol) groundmass. The anhedral crystal shape and reaction rim around the quartz suggest that this crystal was entrained into a magma in which quartz was not stable	43	4.12 Classification of alkaline rocks, shown on a plot of Alkalinity Index (AI) versus Feldspathoid Silica Saturation Index FSSI	56
3.10 The Hortavær complex was constructed by multiple injections of diorite (dark lenses) intruded into a syenitic magma chamber (light-colored rock), north central Norway	44	4.13 Variation of trace element concentrations during fractional crystallization of a magma according to the Rayleigh law	58
4.1 Diagram showing the behavior of compatible (path A) and incompatible (path B) elements during differentiation of a melt	48	4.14 Variation in Zr content of rocks from the Red Mountain pluton, Laramie anorthosite complex, Wyoming, USA	58
4.2 Harker diagrams showing the compositional variation in the Sherman batholith, Wyoming, USA	49	4.15 Rare earth element patterns of lunar rocks	59
		4.16 Nb and Y contents of rocks from the Sherman batholith, Laramie Mountains, Wyoming, USA	59
		4.17 Contour diagram showing the regional variation in initial ⁸⁷ Sr/ ⁸⁶ Sr of Mesozoic granitic rocks in central California	60
		5.1 The basalt tetrahedron showing the differences in normative composition between alkali basalt, olivine tholeiite, and quartz tholeiite	66

5.2	The major layers of the crust and mantle, along with characteristic S-wave velocities for each layer	67	7.5	Granodiorite of the Tuolumne pluton in Yosemite National Park, California	95
5.3	Diagram showing how adiabatic decompression of the mantle (arrow) can lead to melting even if the mantle is dry	68	7.6	Plot of $\text{FeO}^{\text{tot}}/(\text{FeO}^{\text{tot}}+\text{MgO})$ showing the different differentiation trends for arc magmas and oceanic tholeiites	100
5.4	Simplified phase diagram for the system Fo-Di-En at about 20 kbar	69	7.7	Alkalis- FeO^{tot} -MgO (AFM) diagram comparing the differentiation trends of tholeiitic rocks (as indicated by the lavas of the Galapagos) and calc-alkalic rocks (as indicated by the lavas of the Cascades)	100
5.5	Pseudoternary projection from plagioclase on to the olivine-diopside-quartz plane showing how location of the basalt eutectic changes with increasing pressure	69	7.8	The chemical trends of island arc rocks, represented by Seguam, compared to continental arc rocks from Mount Saint Helens and Tuolumne	101
6.1	Petrologic and seismic profile for an ideal ophiolite	73	7.9	Plot of weight percent SiO_2 versus weight percent K_2O showing the composition variation of volcanic rocks from various island arcs	101
6.2	Morphology of (A) fast (East Pacific Rise), (B) slow (Mid-Atlantic Ridge), and (C) ultra-slow (Gakkel Ridge, Arctic Ocean) spreading centers	75	7.10	QAP diagram showing the compositional ranges of rocks found in calcic (C) and calc-alkalic (CA) batholiths	102
6.3	Cross-sections of oceanic crust beneath the Mid-Atlantic ridge	76	7.11	The chemical trends of plutonic island and continental arc rocks as represented by Seguam and Tuolumne	102
6.4	Cross-sections of the ocean crust as obtained in several IODP drill holes	76	7.12	Variation diagrams showing the differences in trends exhibited by Seguam and Mount Saint Helens volcanic rocks, which reflect different processes of magmatic differentiation	103
6.5	Pseudoternary projection from plagioclase onto the olivine-clinopyroxene-quartz plane showing the composition range of MORB glasses	78	8.1	The aerial extent (in dark shading) of the four units of the Columbia River basalts	110
6.6	Compositions of basalt glasses from the Narrowgate region of the FAMOUS valley, Mid-Atlantic Ridge	80	8.2	Major element compositions of the Columbia River Basalt Groups	111
6.7	Geochemical trends of volcanoes on the Galapagos Islands and Iceland, both of which straddle oceanic ridges	81	8.3	A portion of the northwestern United States showing the location of the Snake River Plain, Craters of the Moon volcanic rocks, Cedar Butte rhyolite volcano, the Yellowstone Caldera, and the calderas formed by the Yellowstone hot spot as it moved across Idaho, dashed where approximate	112
6.8	The island of Hawaii is a compound volcanic edifice formed by five overlapping shield volcanoes	82	8.4	Geochemical trends in the volcanic rocks of the Yellowstone – Snake River Plain province	114
6.9	Comparison of the compositions of early Hawaiian basalts (as exemplified by Loihi), the main stage tholeiites, and the late-stage alkali basalts projected onto the normative Qz-Nph-Ol triangle	83	8.5	Geochemical trends for the Boina, Nyambeni, and Suswa volcanoes	117
7.1	Schematic cross-section of a typical island arc	92	8.6	Geochemical trends for the rocks from Mount Vesuvius	119
7.2	Photo of Pyre Peak, Seguam Island, Alaska	92	8.7	Major diamond-producing regions of the world	120
7.3	Mount Saint Helens prior to the eruption of May 1980	94			
7.4	Diagram showing the geologic history of Mount Saint Helens volcano	95			

9.1	Photos of layering in igneous rocks. (A) Layering in feldspathic peridotite. Relatively resistant layers are richer in plagioclase than the less resistant layers. Rum intrusion, Scotland. Photo courtesy of Michael Cheadle. (B) Layering in gabbros from the Rum intrusion. Layering is based on modal variation of olivine, augite, and plagioclase. Photo by Michael Cheadle. (C) Layering of chromite in anorthosite, Bushveld intrusion, South Africa. Photo by Michael Cheadle. (D) Layering in nepheline syenites, Ilimaussaq intrusion, southern Greenland.	127	9.9	Photo of the Ilimaussaq intrusion taken on the southeast shore of Kangerdluarssuk fjord looking northeast. Kakortokite composed of cumulus minerals on the floor of the complex in the foreground, naujaite is the sodalite-rich floating cumulates in the background, and lujavrite is the horizon sandwiched between the two.	141
9.2	Photograph of the Dufek intrusion exposed on 1840 m Neuberg Peak in Antarctica. The Frost pyroxenite is a major marker in the intrusion and extends for about thirty-five kilometers alongstrike. Photo by Michael Cheadle.	127	9.10	Flow sheet showing how the range of rock types found in intracontinental magmatism are related. Modified after Frost and Frost (2011).	142
9.3	Stratigraphic cross-section across the Bushveld complex showing the variation in olivine and plagioclase compositions. After Atkins (1969).	130	10.1	P-T diagram showing the relation between the water-saturated granite solidus and two common dehydration melting curves for pelitic rocks	149
9.4	Photo showing agglomeration of coarse plagioclase grains in leucogabbro, a texture common in Archean anorthosites. The pencil in the upper right is fifteen centimeters long. Fiskensæset intrusion, west Greenland. Photo by John Myers.	131	10.2	South face of Bhagirtahi III, showing fifteen-hundred-meter-thick tourmaline-garnet and two-mica bearing leucogranite sill, Garhwal Himalaya, North India	149
9.5	Schematic cross section of the Fiskensæset intrusion. Modified after Myers (1976).	132	10.3	Chemical characteristics of peraluminous leucogranites	151
9.6	Google Earth image showing layering in the Poe Mountain anorthosite. Light-colored anorthosite layers tend to weather in relief, whereas darker leucogabbroic layers tend to erode from low topography.	135	10.4	Comparison of the chemical characteristics of Caledonian-type Etive granite (stippled area) with Cordilleran granites (shaded area)	152
9.7	Geochemical characteristics of ferroan granites associated with mafic intrusions and anorthosites. Data from Anderson, Frost, and Frost (2003), Barker and colleagues (1975), Kleeman and Twist (1989), Smith and colleagues (1999), and Scoates and colleagues (1996).	137	10.5	Comparison of the geochemical characteristics of peraluminous leucogranites, Caledonian granites, ferroan granites, and Cordilleran granites	153
9.8	Schematic cross-section of the Ilimaussaq intrusion. Modified after Andersen, Bohse, and Steenfelt (1981).	140	10.6	QAP diagram showing the differentiation path followed by various granite types.	155
			11.1	Relict sedimentary textures in metamorphic rocks	163
			11.2	Relict igneous textures in metamorphic rocks	163
			11.3	Textures in metamorphic rocks	164
			11.4	Illustrations comparing the relationship between schistosity, foliation, and lineation in metamorphic rocks	165
			12.1	Chemography for the two-component system a-b with phases V, W, Y, Z	172
			12.2	Topology for the hypothetical two-component system a-b shown in Figure 12.1	172
			12.3	Topology for the hypothetical two-component system a-b shown in Figure 12.1.,	

with divariant assemblages identified using chemographic projections.	173	14.3 Calcite – dolomite solvus after Goldsmith and Heard (1961)	195
12.4 Chemographic diagram for a hypothetical three-component system x-y-z	173	14.4 Location of the equilibrium anorthite = grossular + kyanite + quartz and isopleth lines showing the displacement of this equilibrium in systems with plagioclase and garnet solid solutions	195
12.5 Topology for the hypothetical three-component system x-y-z	173	14.5 Thermobarometry from an assemblage sillimanite-garnet-biotite-plagioclase-quartz	196
12.6 Topology for the hypothetical three-component system x-y-z, with divariant assemblages identified using chemographic projections	173	14.6 P-T diagrams showing multi-equilibria thermometry of a granulite with the assemblage orthopyroxene-clinopyroxene-garnet-plagioclase-quartz	197
12.7 Same topology as Figure 12.6 showing the assemblages found in two hypothetical bulk compositions, p and q	174	14.7 P-T conditions of metamorphism showing the conditions for UHP and UHT metamorphism and the approximate conditions for the metamorphic facies	198
12.8 A. Chemography for the system MgO-SiO ₂ -H ₂ O showing projection from H ₂ O to the MgO-SiO ₂ plane	175	14.8 Comparison of the P-T conditions for granite minimum melt (Luth, Jahns, and Tuttle, 1964) and the beginning of hornblende breakdown (Spear, 1981)	199
12.9 ACF diagram plotting common metamorphic minerals	176	14.9 Photograph of charnockite dike in amphibolite in the Wind River Range, Wyoming	199
13.1 ACF diagram for mineral stabilities at amphibolite facies showing the approximate fields where pelitic, mafic, and calc-silicate rocks occur	181	14.10 Photograph of migmatitic paragneiss, Teton Range, Wyoming	200
13.2 Approximate P-T stabilities for the metamorphic facies	182	15.1 Photographs and photomicrographs of textures in metaperidotites	206
13.3 ACF diagram showing the stable assemblages in mafic rocks in greenschist facies	182	15.2 P-T diagram showing mineral stabilities in the system CaO-MgO-SiO ₂ -H ₂ O	207
13.4 ACF projection showing mineral relationships in mafic rocks in amphibolite facies	183	15.3 Chemographic projections showing assemblages in the divariant fields in Figure 15.2	207
13.5 Schematic diagram comparing the P-T stabilities of anorthite-forming and hornblende-forming reactions	183	15.4 Diagram showing the relation between X _{Mg} of olivine and X _{Mg} of other silicates	208
13.6 Photograph of a garnet amphibolite with plagioclase rims (Pl) around the garnet (Grt)	184	15.5 P-T diagram comparing the breakdown of Mg-talc with Fe-talc	209
13.7 ACF diagrams showing mineral relations in weakly metamorphosed mafic rocks	184	15.6 Isobaric T-X _{Mg} diagram for the reaction talc = orthopyroxene + quartz + H ₂ O at 3 kbar	209
13.8 ACF diagram showing mineral relations in mafic rocks in granulite facies	185	15.7 P-T diagram showing the divariancy of reactions in natural metaperidotites due to the presence of iron	210
13.9 Photomicrographs showing textures typical of metabasic rocks	186	15.8 P-T diagram showing important reactions in high-temperature peridotites	210
14.1 P-T diagram showing how the decrease in the molar volume of H ₂ O affects the slope of the dehydration reaction olivine + tremolite = enstatite + diopside + H ₂ O	192		
14.2 Diagram showing how the Fe and Mg contents of biotite and garnet vary as a function of T	194		

15.9	Phase diagram showing the stability fields of garnet, spinel, and plagioclase in high-T peridotites	211	melting (reproduction of Figure 10.1). (B) photomicrograph of pelitic gneiss that underwent melting via the reaction biotite + plagioclase + sillimanite + quartz = garnet + melt. From central Massachusetts.	229
15.10	Photomicrograph in PPL of garnet in a garnet peridotite	211		
15.11	P-T diagram for the system H_2O showing the relation between liquid, vapor, and supercritical fluid	212	16.13 Photographs and photomicrographs of pelitic rocks in blueschist, granulite, and whiteschist facies	230
15.12	T-X diagram showing the mutual solubilities of H_2O and CO_2	213	16.14 AFM projections for pelitic rocks in granulite facies	230
15.13	T-X diagram showing mineral relations in the system $\text{MgO-SiO}_2\text{-H}_2\text{O-CO}_2$ at three kilobars	213	16.15 AFM projection for common pelitic assemblages in blueschist facies	230
15.14	T-X diagram showing mineral relations in the system $\text{MgO-SiO}_2\text{-H}_2\text{O-CO}_2$ at three kilobars and low temperatures	214	16.16 AFM projections for mineral assemblages in whiteschist (i.e., eclogite-facies pelitic rocks)	231
15.15	Diagrams showing meta-somatic zones found at the margin of metaperidotite bodies	214	16.17 P-T diagram showing the location of bathograds and bathozones	231
15.16	Metasomatic blackwall zone between metagabbro (now rodingite) and metaperidotite	215	16.18 Photomicrographs of pelitic rocks from a range of bathozones	232
16.1	Isobaric T-X diagram showing the breakdown of talc to orthopyroxene + quartz	221	16.19 Bathozones (numbered) in New England	233
16.2	Isobaric, isothermal $\text{FeSiO}_3\text{-MgSiO}_3\text{-SiO}_2$ chemographic projections displaying the continuous nature of the reaction talc = enstatite + quartz + H_2O	221	17.1 Ternary diagrams showing the minerals that form in impure dolomitic limestones during metamorphism	238
16.3	Diagram showing the behavior of chemographic projections in continuous reactions	222	17.2 T-X diagram showing mineral stabilities during metamorphism of impure dolomitic marbles	239
16.4	Diagram showing the relation between continuous reactions and discontinuous reaction	223	17.3 T-X diagram showing the paths followed during (1) internal control of fluid composition (buffering) and (2) external control of fluid composition (infiltration)	240
16.5	Construction of the AFM projection for metapelitic compositions	223	17.4 Isobaric T-X diagram showing the fluid path followed in the contact aureole of the Alta stock	241
16.6	A typical AFM projection from muscovite for middle amphibolite facies (kyanite zone)	224	17.5 Isobaric T-X diagram showing the path followed by the fluid during metamorphism in the Marysville stock	242
16.7	AFM projections showing transition from the chlorite zone (A) to the biotite zone (B)	226	17.6 Sketch map of the opaque mineral assemblages surrounding the ore body at Ducktown, Tennessee	243
16.8	AFM projection for the garnet zone	227	17.7 Plot of the $\log f_{\text{S}_2}$ vs $\log f_{\text{O}_2}$ showing the variation of fluid composition adjacent to the ore body at Ducktown, Tennessee	244
16.9	AFM projections showing the transition from the garnet to the staurolite zones	227	17.8 Sketch of alteration around a quartz-pyrite vein in granodiorite from porphyry copper deposit in Ajo, Arizona	244
16.10	AFM projection for the kyanite zone	228		
16.11	AFM projections for the sillimanite zone	228	18.1 P-T diagram showing the clockwise path followed in a metamorphic terrain during continental over-thrusting. Three stages	
16.12	(A) P-T diagram showing two dehydration melting curves in pelitic rocks and a possible path followed during decompression			

- in the path are labeled, 1 = rapid burial by thrusting, 2 = heating, 3 = uplift due to interaction between erosion and isostasy (after England and Thompson, 1984). 251
- 18.2 A comparison between the assemblages recorded in metamorphic terrane (the metamorphic field gradient) and the P-T path followed by the rocks during metamorphism. A, B, C, D = localities in a metamorphic belt in order of increasing grade. 252
- 18.3 Structure of the Alpine orogeny as exemplified by exposures on the Matterhorn. 252
- 18.4 Metamorphic alteration in IODP holes 1256D, 745B, 1309D. Locations for these holes are given in Figure 7.2. Sources of data as in Figure 7.3. 256
- 18.5 Environments of granulite metamorphism: (1) crystallization of mafic magma to become gabbro, (2) dehydration during melting of granite, (3) metamorphism associated with CO₂ fluxing from mafic magma, and (4) crystallization of felsic magma to form pyroxene-bearing felsic rocks. Modified after Frost and Frost (1987). 255
- 18.6 Google Earth image of gneiss terranes (light) and greenstone terranes (dark) in the Pilbara craton of northwestern Australia. Arrows indicate the dip direction of the foliations in the gneiss and in the greenstone. Structural trends after Van Kranendonk and colleagues (2002). 258
- A.1 The system Ab-An-Or showing the names of the various feldspars. (After Deer, Howie, and Zussman, 1963.) Mineral abbreviations as on Table 2.1. 264
- A.2 Crystallographic sketch of plagioclase showing the orientation of albite twins (010), the basal cleavage (001), and pericline twins (which form on a rhombic section). 265
- A.3 Figure showing what a plagioclase grain would look like when oriented normal to X. Both (010) cleavage and the albite twin plane are razor sharp and both sets of twins show the same birefringence (A). The twins will go to extinction with the same amount of rotation clockwise (B) and counter-clockwise (C). Using the chart shown on Figure 2.4, the composition of this plagioclase can be identified as An₃₂. 266
- A.4 Graph showing the relation between plagioclase composition and rotation angle to extinction when looking down the X-axis. From Heinrich (1965). 266
- A.5 Schematic phase diagrams for the alkali feldspars. A. Phase relations for anhydrous magmas that solidify at relatively high temperatures. a = stability region for sanidine, b = stability for orthoclase, c = stability for microcline. B. Phase relations for magmas with H₂O that crystallize at lower temperatures. 267
- A.6 Diagram showing the approximate composition ranges for the three pyroxene quadrilateral solution series. A-B shows the line of section displayed as a T-X diagram in Figure A.7. Mineral fields from Lindsley and Frost (1992). 269
- A.7 Schematic T-X diagram showing the phase relations between augite, pigeonite, and orthopyroxene along section A-B in Figure A.6. 270
- A.8 Isothermal sections of the pyroxene quad at 800°, 900°, 1000°, and 1100°C showing how the pigeonite stability field expands with increasing temperature. Modified from Lindsley and Frost (1992). 271
- A.9 Sketches of exsolution textures in pyroxenes. A. Orthopyroxene with narrow lamellae of augite. B. Orthopyroxene with wide lamellae of augite (inverted pigeonite). C. Augite host with exsolution of orthopyroxene. 271
- A.10 Compositional range of sodic pyroxenes in igneous rocks and in metabasites. Compiled from data in Deer, Howie, and Zussman (1978). 272
- A.11 Diagram showing the composition range of the quadrilateral amphiboles. 273
- A.12 Diagram showing the composition range of sodic amphiboles in igneous and metamorphosed mafic rocks. Fields defined by data from Brown (1974) and Deer, Howie, and Zussman (1997). 274
- A.13 Diagram showing the compositional range of hornblende from igneous and metamorphic rocks. Fields defined by data from Deer, Howie, and Zussman (1997). 275

- | | | | |
|--|-----|---|-----|
| A.14 Phase diagram showing the P-T stabilities of the aluminosilicate minerals. Data from Pattison (1992). | 277 | tie lines show the approximate compositions of coexisting phases. Modified after Lindsley (1991). | 282 |
| A.15 Diagram showing the composition relations between the ilmenite and magnetite solid solutions at magmatic temperatures. Dashed | | A.16 Bowen's reaction series showing the minerals that will crystallize during differentiation of a basaltic magma. | 282 |

Tables

3.1	Viscosities of Magmas and Common Substances	page 41	13.1	Metamorphic Facies as Defined by Mineral Assemblages in Mafic Rocks	181
4.1	Alkali-Lime Classification for Igneous Rocks	53	13.2	Diagram Showing the Changes in Mineralogy in Mafic Rocks at Very Low T	187
4.2	Classification of Rocks by Aluminum Saturation	55	13.3	Diagram Showing the Changes in Mineralogy in Mafic Rocks with Increasing T	188
5.1	Global Rates (km ³ /yr) of Cenozoic Magmatism	70	13.4	Diagram Showing the Changes in Mineralogy in Mafic Rocks with Increasing P at Low P	188
8.1	Ages and Dimensions of Major Continental Flood Basalt Provinces	109	14.1	Analysis of Olivine from New Caledonia	193
9.1	Major Layered Mafic Intrusions	126	14.2	Equilibria in the Assemblage Opx-Cpx-Gar-Plag-Q	197
9.2	Differences between Archean and Massif Anorthosites	132	15.1	Reactions Occurring during Metamorphism of Peridotitic Rocks	205
9.3	Major Anorthosite Complexes	134	15.2	Relationship between Metamorphic Facies and Mineral Assemblages in Metaperidotites	211
10.1	The Four Major Granitic Rock Types in Order of Decreasing Relative Abundance	153	17.1	Mineral Reactions in Impure Dolomitic Marbles	239
11.1	Clearly Sedimentary Protoliths	160	17.2	Reactions around the Ducktown Ore Body	242
11.2	Igneous Protoliths or Protoliths of Uncertain Parentage	161	A.1	Abbreviation for Minerals	264
11.3	Common Rock Names for Metamorphic Rocks	166	A.2	Carbonate Minerals Commonly Found in Metamorphic Rocks	268
12.1	Coordinates for Phases in the System MgO-SiO ₂ -H ₂ O	176			

Maps

1.1	Geologic map of the Matachewan and Mistassini dike swarms in the southern portion of the Canadian Shield	page 15	8.6	Major diamond-producing regions of the world. Filled circles = diamonds sourced from kimberlite, open square = diamonds sourced from lamproite.	120
6.1	Map showing select ophiolite belts around the world	73	9.1	Distribution of major layered mafic intrusions around the world	126
6.2	Tectonic map of the ocean basins showing mid-ocean ridges, convergent margins, transform faults, and areas discussed in the text	75	9.2	Geologic map of the Bushveld Complex after Vermaak and Von Gruenewaldt (1981). Inset shows location within the Republic of South Africa. Age data after Cawthorn and colleagues (2012) and Scoates and Friedman (2008).	129
6.3	Map showing the location of oceanic islands (points) and oceanic plateau (shaded)	82	9.3	Worldwide distribution of massif anorthosites (filled circles) and Archean anorthosites (open circles). The box outlines an area encompassing the Grenville anorthosites; the names of the individual Grenville anorthosites are given in Map 9.4.	131
7.1	World map showing active island arcs and continental margin magmatism	89	9.4	Geologic map showing the Archean and Proterozoic provinces of North America and the distribution of Proterozoic massif anorthosites and ferroan granites. Age ranges of ferroan rocks given in millions of years.	135
7.2	Geologic map of Seguam island, central Aleutian arc, Alaska, USA	92	9.5	Geologic map of the Laramie anorthosite complex. Inset shows its location within Wyoming, USA. Box indicates the area shown in Figure 9.6. Modified after Frost et al. (2010).	136
7.3	Geologic map of Tobago, West Indies, showing a cross-section through the Cretaceous oceanic arc complex that exposes both plutonic and volcanic rocks	93	9.6	Geologic map of the Pikes Peak batholith. Modified after Scott and colleagues (1978), Bryant, McGrew, and Wobus (1981), and Hutchinson (1976).	137
7.4	Geologic map of Mount Saint Helens, Cascade Range, Washington, prior to the 1980 eruption	94	9.7	Geologic map of the Ilimaussaq intrusion. Inset shows its location in Greenland. Modified after Ferguson (1964).	140
7.5	Geologic map of the Tuolumne pluton (after Bateman and Chappell, 1979)	98	10.1	Geologic map of the Manaslu granite after Colchen, Le Forte, and Pecher (1980)	150
8.1	Locations of major continental flood basalt provinces (shaded areas) and of major continental rifts (heavy lines)	108	10.2	Geologic map of Scotland showing the locations of the Caledonian granites	151
8.2	Map showing the relation between the Colombia River basalts, the Oregon Plateau volcanic belt, the Snake River Plain, Yellowstone, and the direction of movement of the Juan de Fuca plate relative to North America	109	10.3	Geologic map of the Etive granite after Frost and O'Nions (1985)	152
8.3	World map showing the major alkaline magmatism provinces	119	15.1	Metamorphic geology of the Val Malenco area of Italy and Switzerland.	
8.4	Map of the East African rift showing the locations of the Boina, Nyambeni, and Suswa volcanoes, all of which are sodic alkaline rocks (filled stars), and Nyiragongo, which is a potassic alkaline volcano (unfilled star)	116			
8.5	Geologic sketch of the Roman province in Italy showing the location of major eruptive centers	117			

(A) The regional and contact metamorphic isograds, (B) Detailed map of the contact aureole. Modified after Trommsdorff and Evans (1974) and Peretti (1988).	215	18.1 Paired metamorphic belts from the island of Honshu, Japan. Inset shows the increase in metamorphic grade in the blueschist belt toward the continent. Modified after Miyashiro (1973).	250
15.2 Geologic map of the contact aureole at Paddy-Go-Easy pass, Central Cascades, Washington (after Frost, 1975).	216	18.2 Map of rocks recording the Alpine metamorphism in the Western Alps. Modified after Frey and colleagues (1974).	253
16.1 Map showing the distribution of metamorphic zones in southeastern Scotland as defined by assemblages in pelitic rocks	225	18.3 Distribution of terrains within the Superior province, with the granulite terrains labeled. After Thurston (2002).	257
17.1 Map of the contact aureole of the Alta stock in Utah	241	18.4 Distribution of metamorphic facies in the Eastern Goldfields subprovince of the Yilgarn Archean province. After Binns, Gunthorpe, and Groves (1976).	259
17.2 Geologic map of the contact aureole around the Marysville stock, Montana, USA	242		

Boxes

6.1	Ocean Drilling (with photo)	<i>page 77</i>	8.1	Volcanic Hazards in Intracontinental Environments	113
6.2	Ore Deposits in Ocean Crust (with photo)	84	9.1	Ore Deposits Associated with LMIs	125
6.3	Volcanic Hazards from Oceanic Volcanism (with photo)	85	9.2	Ore Deposits Associated with Anorthosite Complexes	138
7.1	Volcanic Hazards (with table)	90	9.3	Enrichment of REEs in Alkaline Plutons	133
7.2	Porphyry Copper Deposits	91	10.1	Ore Deposits and Granites (photo)	147
7.3	Volcanic Hazards Associated with Convergent Margin Magmatism: Explosive Volcanism and Pyroclastic Deposits (with figure)	96	10.2	Granite Pegmatites (photo)	154
			14.1	The Dynamic Earth	201
			15.1	Petrology and Geophysics	217
			17.1	Hydrothermal Ore Deposits and Hydrothermal Alteration	245

Preface



Petrology, from the Greek words *petra*, meaning rock, and *logos*, meaning knowledge, is the study of rocks and the conditions in which they form. It includes igneous, metamorphic, and sedimentary petrology. Igneous and metamorphic petrology are commonly taught together because both disciplines depend on the use of chemistry and phase diagrams. In contrast, sedimentary petrology is often combined with stratigraphy because both of these sciences depend on understanding the physical processes that accompany the deposition of sediments. Igneous and metamorphic petrology share common foundations; for example, both use phase diagrams to understand the conditions that control the crystallization of various minerals. However, there are important differences between the disciplines. In igneous petrology, the bulk composition of the rock is important because it gives clues to the tectonic environment in which it formed. Metamorphic petrology is not so much concerned with the bulk chemistry of the rocks as with the use of mineral assemblages to determine the conditions under which the rock crystallized. Because igneous rocks may later be transformed into metamorphic rocks, this book begins with igneous petrology and takes up metamorphic petrology second.

In contrast to many petrology textbooks, which are written for the upper-level undergraduate and graduate student audience, this book is accessible to introductory-level geology students who may have taken few earth science courses beyond physical geology and mineralogy. It aims to convey the essential petrologic information that is needed by all geoscientists no matter what their eventual specialization, be it geophysics, geochemistry, economic geology, geohydrology, or indeed any aspect of the Earth system.

This book focuses on the fundamental principles that govern the mineralogy of igneous and metamorphic rocks. For igneous petrology, this involves an understanding of how the mineralogy of igneous rocks reflects the equilibria that govern the crystallization of minerals from magma and how the geochemistry of a rock reflects its magmatic differentiation. The book uses several major element discrimination diagrams, including Fe-index, modified alkali-lime index, and aluminum saturation index, to compare and contrast magmatic suites that form in different tectonic environments. These simple geochemical parameters effectively highlight the different magmatic processes that create magmatic suites formed at oceanic and continental divergent plate boundaries, in arcs formed at oceanic and continental convergent margins, and in oceanic and continental intraplate tectonic settings.

In metamorphic petrology, the mineral assemblages in metamorphic rocks depend fundamentally upon the protolith of the rock as well as on the mineral reactions that take place at successively higher temperatures and pressures. Starting with ultramafic protoliths, which are the simplest, the text describes how pressure, temperature, and fluid composition affect the mineral assemblages in progressively more complex systems, including pelitic and calcareous protoliths. This book emphasizes chemographic projections as a way to determine the metamorphic mineral assemblages that occur together at specific metamorphic conditions. In addition, the text discusses the environments where various types of metamorphism are found and the tectonic significance of different types of metamorphic belts.

Throughout the textbook the authors have provided examples of how petrology relates to other areas of geology, including economic geology, geologic hazards, and geophysics. These short vignettes help students make connections between the study of igneous and metamorphic rocks and other fields of geology and illustrate the value of a fundamental understanding of petrology.

Acknowledgments



This textbook is the result of several decades of experience teaching igneous and metamorphic petrology at the University of Wyoming. The authors began writing this material when what had been two separate, semester-long courses in igneous and metamorphic petrology were combined into one and the existing textbooks were more exhaustive than the new course format could accommodate. They would like to acknowledge the hundreds of students who used successive versions of the igneous and metamorphic petrology course packet and provided edits and suggestions. They are especially grateful to those former students who went on to become geoscience faculty members and who have encouraged the authors to convert the course packet into a commercially published textbook.

The authors also wish to thank the external reviewers for their helpful suggestions and the editors and staff at Cambridge University Press for their expertise and patience in seeing the book through to publication. Too, they warmly acknowledge their colleagues at the University of Wyoming and elsewhere for providing a stimulating and rewarding environment in which to pursue petrologic teaching and research. Last, Carol Frost acknowledges with gratitude her family's forbearance while this textbook underwent repeated revision over many evenings, weekends, and holidays.

Chapter 1

Introduction to Igneous Petrology

1.1 Introduction

Igneous petrology is the study of magma and the rocks that solidify from magma. Thus igneous petrologists are concerned with the entire spectrum of processes that describe how magmas are produced and how they ascend through the mantle and crust, their mineralogical and geochemical evolution, and their eruption or emplacement to form igneous rocks. Igneous petrology requires a working knowledge of mineralogy. Readers who wish to review the characteristics of the major rock-forming igneous minerals will find a concise summary in Appendix 1. The appendix emphasizes the identification of rock-forming minerals in hand sample and in thin section. In addition, the appendix includes descriptions of minerals found in minor abundance but commonly occurring in igneous rocks, including accessory minerals that contain trace amounts of uranium and are important geochronometers.

Before geologists can understand the origin of igneous rocks, they must classify and describe them. This chapter introduces the classification of igneous rocks using the mineralogical classification system recommended by the International Union of Geological Sciences (IUGS) Subcommission on the Systematics of Igneous Rocks, which has the advantage that it is relatively simple and can be applied in the field. For rocks that are too fine-grained to name using this classification, a geochemical classification can be employed instead. The simplest of these, the total alkali versus silica classification, is introduced in this text.

Finally, this chapter introduces basic terminology that describes the textural and structural features of igneous rocks. Descriptions of igneous textures document crystal shape, size, and the arrangement of the various minerals, glass, and cavities in the rock. Igneous structures are larger-scale features that are the result of rock-forming processes. The textures and structures preserved in igneous rocks provide information about their evolution, emplacement, and crystallization, all of which are fundamental goals of igneous petrology.

1.2 The Scope of Igneous Petrology

All rocks ultimately derive from magmas, which solidify to form igneous rocks. Consider, for example, the history of a shale. Such a rock is now composed of clay minerals. These clay minerals may have formed by weathering of a sedimentary rock that contained rock fragments and mineral grains. These components in turn may have been produced by erosion of a granitic gneiss. Before it was metamorphosed, this gneiss may have been a granodiorite, which is an igneous rock formed by crystallizing magma. As this example illustrates, the study of igneous petrology forms a foundation from which to study metamorphic and sedimentary rocks.

Igneous petrology is the study of the classification, occurrence, composition, origin, and evolution of rocks formed from magmas. The discipline can be divided into two components: **igneous petrography**, which is the description and classification of igneous rocks; and **igneous petrogenesis**, which is the study of the origin and evolution of igneous rocks. There are many different ways to approach the study of igneous petrology. **Field geology** is very important to the study of igneous petrology because important information is contained in the field relationships between rock units, the structure of an igneous rock, and its texture and physical appearance. For example, volcanologists depend heavily on their field observations during an eruption, and on the distribution of ash, lava, and other volcanic ejecta formed as the result of the eruption, to model the processes that occurred within a volcano before and during an eruption. **Laboratory identification** of the minerals in a thin section of an igneous rock, along with the chemical composition and age of a rock, are important means of classifying and relating it to other rocks with which it is spatially associated.

Another important way to study igneous rocks is through geochemistry. **Major-element geochemistry** can determine whether a suite of rocks is related through a process such as magmatic differentiation or mixing. **Trace-element geochemistry** is used to identify the role various minerals may have played as either crystallizing phases or residual phases in a suite of rocks. **Isotope geochemistry**, which can involve both radiogenic and stable isotopes, can determine whether a suite of rocks formed from a single magma, or whether a more complex, multi-source process was involved.

Because magmas that crystallize beneath Earth's surface are not observable and lavas erupted on the surface are hot and often dangerously explosive, geologists find it difficult to study the formation of igneous rocks directly. Therefore **experimental petrology** is an important aspect of igneous petrology in which the pressures and temperatures required for igneous rocks to form and evolve are reproduced in the laboratory. For many rocks, field and petrographic description does not provide conclusive proof of the process by which they formed. For these rocks, data gathered from experimental petrology are essential.

1.3 Classification of Igneous Rocks

One of the most tedious aspects of igneous petrography is the mastery of terminology. Innumerable, and often inscrutable, names have been applied to igneous rocks over the past few centuries as petrology grew in importance and sophistication. Much igneous terminology is arcane because in the early days of the science, petrologists did not have access to experimental data, phase diagrams, isotopic systems, or thermodynamic data and thus their work was mainly descriptive as opposed to quantitative. One way they described rocks was to name them. Among the more picturesque names is **charnockite**, which was named after the rock that formed the tombstone of Job Charnock, the founder of Calcutta (now Kolkata), India. Charnockite is a name given to an orthopyroxene-bearing granite, but there is no way to determine that from the origin of the name unless one was to desecrate Job Charnock's tombstone by sampling it for thin section and chemical analysis.

Unfortunately, like charnockite, most of the rock names that arose early in the development of igneous petrology do not provide much insight into the origin or evolution of the rock they describe. Many of the rock names based on type locality were given in the nineteenth or early twentieth century. Over time, geologists recognized the necessity of a more systematic rock classification scheme. In 1972, the IUGS Subcommission on the Systematics of Igneous Rocks published a rock classification system that has been widely adopted, and use of many of the old rock names has been abandoned (Streckeisen, 1976; LeMaitre et al., 1989; LeBas and Streckeisen, 1991).

There are two basic approaches to the naming of rocks. A rock can be classified either according to the minerals

that make it up or by its chemical composition. The first approach has the benefit that geologists can name rocks in the field by identifying their mineralogy; however, it is not very helpful for classifying fine-grained rocks. Alternately, a chemical classification requires analytical data, and therefore is not useful in the field, but it does provide a means of naming fine-grained or glassy rocks. The compositions of most igneous rocks can be expressed in nine oxides: SiO_2 , TiO_2 , Al_2O_3 , Fe_2O_3 , FeO , MgO , CaO , Na_2O , and K_2O . These combine to form the major rock-forming igneous minerals, which include pyroxene, olivine, garnet, amphibole, mica, quartz, plagioclase, alkali feldspar, feldspathoid, magnetite, and ilmenite. Most rocks contain only a few of these minerals. The IUGS classification uses both mineralogical and chemical data, but emphasizes classification on the basis of mineralogy.

1.3.1 Preliminary Classification

Igneous rocks are divided into the general categories of **plutonic**, **hypabyssal**, and **volcanic** depending on their grain size. Plutonic rocks characteristically have coarse or medium grain sizes (>1 mm) and are inferred to have crystallized deep in the crust. Hypabyssal and volcanic rocks are fine-grained to glassy. Volcanic rocks crystallize at the surface and hypabyssal rocks crystallize at shallow depths, typically less than a kilometer. Because the grain size of an igneous rock is determined by the cooling rate of the magma and this is a function both of magma temperature and the ambient temperature of the rocks into which the magma was emplaced, grain size generally increases with depth but there is no specific depth associated with the transition from plutonic to hypabyssal rocks.

In addition to classification according to grain size, we can describe the general composition of a rock using the terms **felsic**, **mafic**, and **ultramafic**. Rocks rich in quartz, feldspars, or feldspathoids are light colored and are called *felsic*. The term *felsic* combines parts of the words **feldspars** (and **feldspathoids**) and **silica**. Darker-colored rocks rich in ferromagnesian minerals are called *mafic*. The term *mafic* reflects the enrichment of these rocks in **magnesium** and **iron (Fe)**. Ultramafic rocks are essentially free of any felsic minerals.

1.3.2 IUGS Classification of Plutonic Rocks

Because plutonic rocks are relatively coarse-grained so that their constituent minerals can be easily identified,

either in hand specimen or in thin section, they are the most straightforward group of igneous rocks to classify. The IUGS classification is based on the modal amounts of the common minerals, which are divided into five groups:

- Q quartz
- A alkali feldspar, including albite with up to five mole percent anorthite ($<\text{An}_{50}$)
- P plagioclase with composition An_{50} to An_{100}
- F feldspathoids: nepheline, sodalite, analcite, leucite, cancrinite
- M mafic minerals: olivine, pyroxenes, amphiboles, micas, and opaque minerals, and accessory minerals such as zircon, apatite, sphene, allanite, garnet, and carbonate.

Rocks containing less than 90 percent mafic minerals ($M < 90$) are classified according to the amounts of Q, A, P, and F minerals they contain, whereas rocks containing more than 90 percent mafic minerals are classified according to the proportions of major mafic minerals. Felsic and mafic rocks typically have far less than 90 percent mafic minerals and ultramafic rocks far more.

Because rocks never contain both quartz and feldspathoids, felsic and mafic rocks can be classified in terms of three components, either QAP or FAP. Triangular plots of the three components are shown in Figure 1.1 along with the names assigned to rocks containing particular proportions of Q, A, P, and F minerals. However, some rocks are not uniquely defined by QAP or FAP alone. For example, both diorite and gabbro fall in the same portion of the QAP triangle. They are distinguished primarily on the basis of plagioclase composition: plagioclase in diorite is more sodic than An_{50} , whereas that in gabbro is more calcic. Because the IUGS classification does not consider the composition of the plagioclase, it cannot distinguish these two rock types. A third rock name is assigned to the gabbro/diorite portion of the QAP triangle: anorthosite. Anorthosite is a special name applied to rocks that contain more than 90 percent plagioclase. Because the IUGS classification is based only on the proportion of Q, A, P, and F minerals, it does not distinguish between rocks with only 10 percent ferromagnesian minerals and rocks with up to 90 percent ferromagnesian minerals. Therefore,

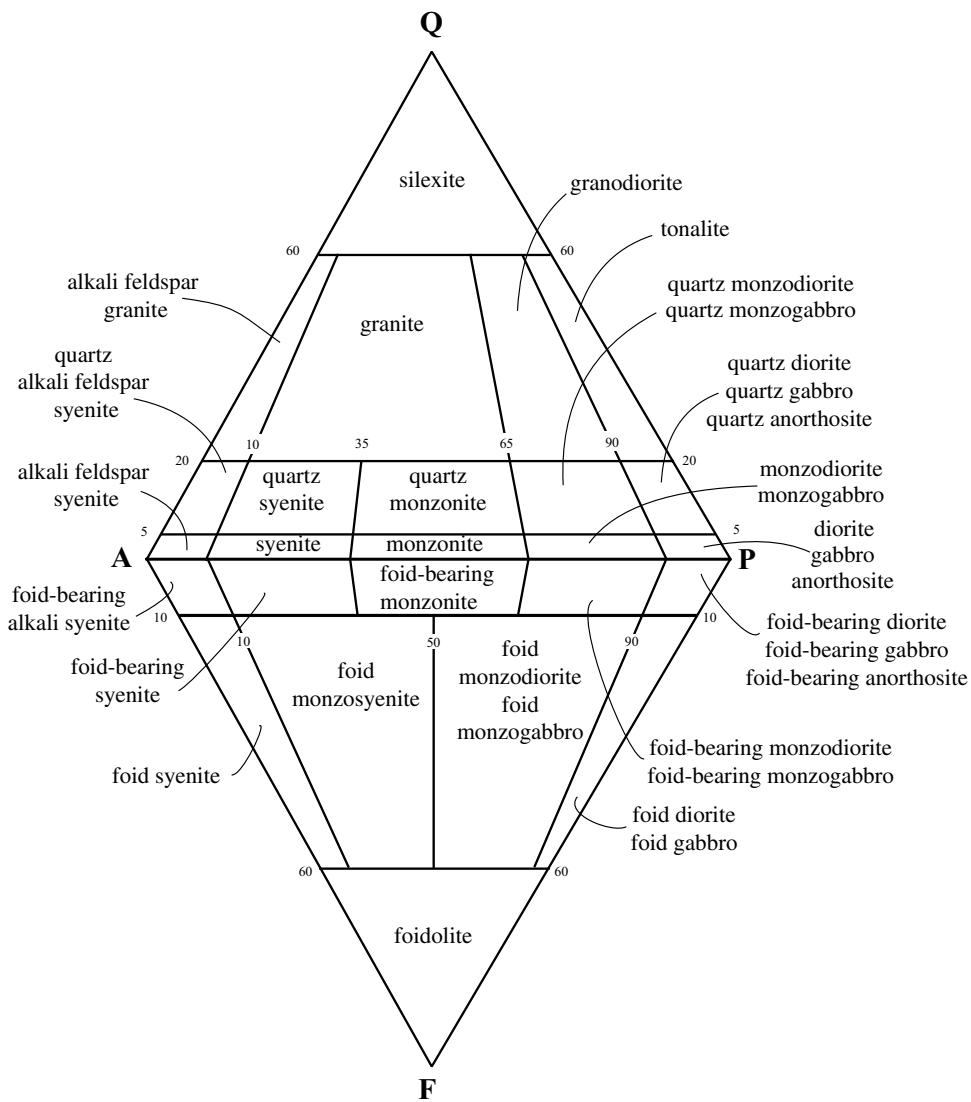


Figure 1.1 IUGS classification of plutonic rocks based upon modal mineralogy. A = alkali feldspar, F = feldspathoid, P = plagioclase, Q = quartz. After Streckeisen (1976).

anorthosite occupies the same part of the triangle as do the diorites and gabbros that have considerably higher mafic mineral contents. This classification scheme can be further specified by adding the names of the major mafic minerals present, with the most abundant placed closest to the rock name. For example, a biotite-hornblende tonalite contains more hornblende than biotite.

Mafic rocks can be further subdivided according to the proportion of plagioclase, orthopyroxene, clinopyroxene, olivine, and hornblende they contain (Figure 1.2). Strictly speaking, the term *gabbro* applies to a rock consisting of augite and calcic plagioclase, although the term is also

broadly applied to any rock consisting of calcic plagioclase and other ferromagnesian minerals. For example, troctolite, a rock with olivine + calcic plagioclase, and norite, a rock with orthopyroxene + calcic plagioclase, are included in the gabbro family. Though not shown in Figure 1.2, rocks consisting of calcic plagioclase and hornblende are, quite logically, called hornblende-gabbros. Most gabbroic rocks contain between 35 and 65 percent mafic minerals. If they contain less than this, the rock name may be prefixed by **leuco-**, meaning light. If they contain more than 65 percent mafic minerals, they may be prefixed by **mela-**, meaning dark.

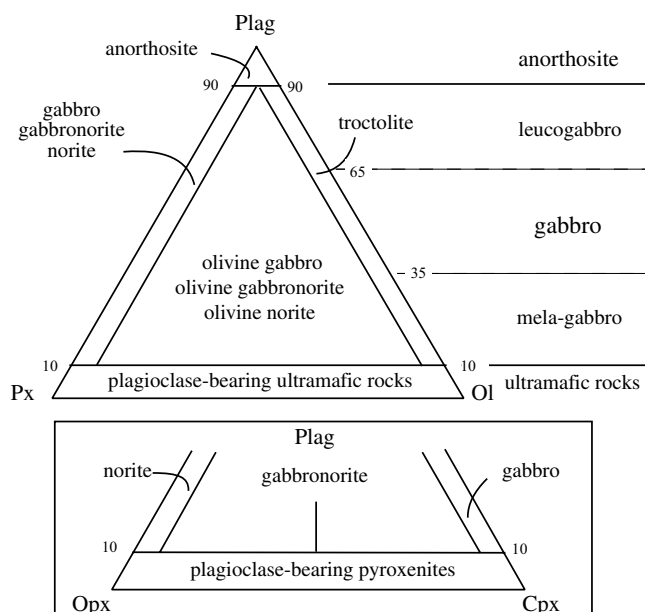


Figure 1.2 IUGS classification of gabbroic rocks. Ol = olivine, Plag = plagioclase, Px = pyroxene. Inset shows classification with regards to the type of pyroxene. Opx = orthopyroxene, Cpx = augite. After Streckeisen (1976).

Ultramafic rocks contain little or no plagioclase and thus require their own classification scheme based on ferromagnesian mineral content. Ultramafic rocks containing more than 40 percent olivine are called peridotites, whereas ultramafic rocks containing more than 65 percent pyroxene are called pyroxenites (Figure 1.3). Peridotites and pyroxenites are further divided depending on the relative proportions of orthopyroxene, clinopyroxene, and olivine. The presence of other mineral phases can be used to further specify the name of the ultramafic rock; for instance, lherzolite that contains garnet is called garnet lherzolite.

Charnockites (orthopyroxene-bearing granitic rocks), lamprophyres (mafic and ultramafic rocks with mafic phenocrysts), carbonatites (igneous carbonate-rich rocks), and pyroclastic rocks have their own classification schemes (LeMaitre et al., 1989).

1.3.3 IUGS Classification of Volcanic and Hypabyssal Rocks

Whenever possible, the IUGS recommends that volcanic rocks be classified on the basis of modal mineralogy. The

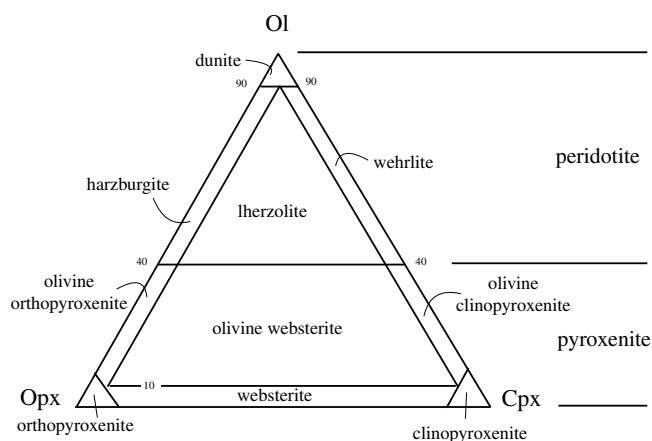


Figure 1.3 IUGS classification of ultramafic rocks. Ol = olivine, Opx = orthopyroxene, Cpx = clinopyroxene. After Streckeisen (1976).

names for volcanic and hypabyssal rocks determined in this way are given in Figure 1.4. There are a few plutonic rock types for which there are no volcanic equivalents, such as anorthosite and ultramafic rocks. These plutonic rocks usually represent accumulations of crystals, and no liquid of that composition ever existed. The only ultramafic lava solidifies to form a rare rock called **komatiite**, which occurs almost exclusively in ancient Archean terrains. It is the volcanic equivalent of peridotite.

If the volcanic rocks are so fine-grained that minerals cannot be identified, then they must be classified on the basis of chemical composition. The IUGS has recommended that volcanic rocks be classified based upon their total alkali and silica contents (TAS) (LeBas et al., 1986) (Figure 1.5). The TAS diagram has as its x-axis the weight percent of SiO_2 of the rock, and as its y-axis the weight percent $\text{Na}_2\text{O} + \text{K}_2\text{O}$ of the rock. The diagram is then divided into fifteen fields. Classification using this chemical approach gives rock names that are typically consistent with the names based on the QAPF diagram.

1.4 Igneous Textures

Petrologists use textures and structures to interpret how igneous rocks crystallized. The terms *texture* and *structure* are nearly interchangeable, although **texture** of a rock refers to the small-scale appearance of the rock: the size, shape, and arrangement of its constituent phases,

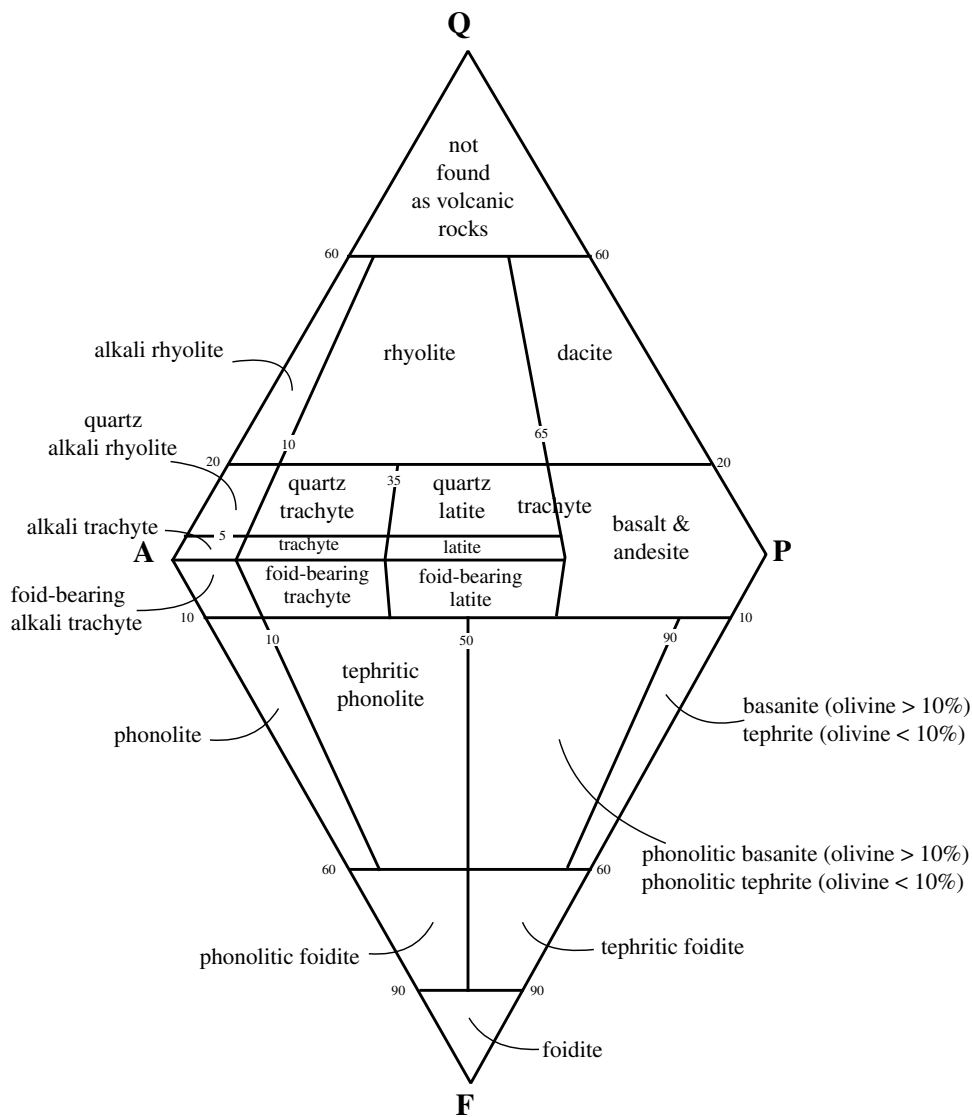


Figure 1.4 IUGS classification of volcanic rock based on modal mineralogy. Abbreviations as in Figure 1.1. After Streckeisen (1980).

including minerals, glass, and cavities. The **structure** of a rock refers to larger-scale features recognizable in the field, such as banding, mineral zonation, or jointing. Textures may provide information about cooling and crystallization rates and the phase relations between minerals and magma at the time of crystallization. Structures indicate the processes active during the formation of rocks and the mechanisms of differentiation.

1.4.1 Crystal Size

Igneous textures, including the size and shape of minerals, provide information about the crystallization history of igneous rocks. The size of the crystals that form when a

melt crystallizes involves a complex interaction between the rate at which crystals nucleate and the rate at which essential elements diffuse to the surface of the growing crystal. The rate at which elements move through a melt may not change much during cooling, but the rate of nucleation is strongly dependent on how close the melt is to the equilibrium crystallization temperature. No nucleation will occur at the equilibrium crystallization temperature because it requires some energy to nucleate a crystal. The melt has to be somewhat undercooled (i.e., cooled below the equilibrium crystallization temperature) before crystals can nucleate. The further the melt temperature is below the equilibrium crystallization temperature the faster the nucleation will be.

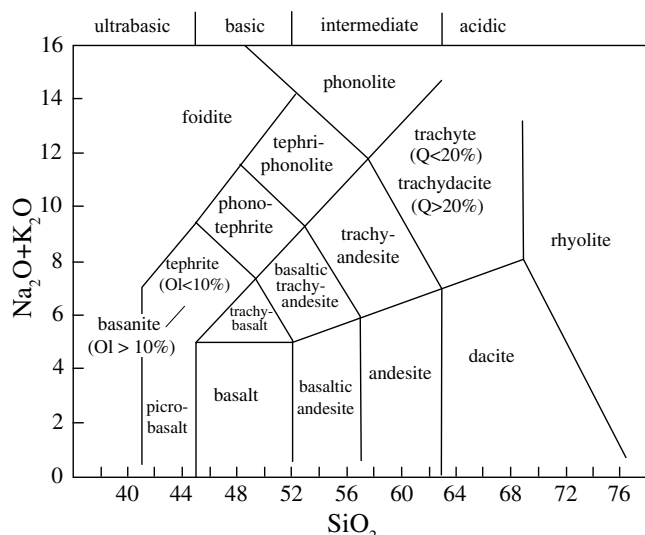


Figure 1.5 IUGS classification of volcanic rocks based on chemical composition, in weight percent oxide. Q = quartz, Ol = olivine. After LeBas et al. (1986).

Consequently, one important variable that controls the size of minerals in an igneous rock is the cooling rate of the igneous magma. In a slowly cooled magma, which will form a plutonic rock, nucleation will be slow and nutrients will have ample time to migrate through the melt to grow large (up to centimeter-sized) crystals. Such a coarse-grained rock is said to be **phaneritic**. If a magma cools quickly, as in a hyperbyssal or a volcanic rock, then nucleation will be rapid and many nuclei will compete for resources, producing an **aphanitic**, or fine-grained rock. In some volcanic rocks, the magma cooled so rapidly that no nuclei at all could form and the resulting texture is **glassy**.

Another variable that varies grain size is the presence of volatile components or elements, such as H_2O or F, that decrease the viscosity of the melt and, hence, enhance the ability of essential elements to reach the face of a growing crystal. Melts with an abundance of these elements may crystallize extremely coarse-grained crystals in the form of a pegmatite. These **pegmatites** may have grain sizes up to a meter or more.

1.4.2 Crystal Shape

Petrologists use the shape of crystals and how the various minerals are arranged in an igneous rock to decipher the crystallization history of a rock. A mineral growing in a

melt will tend to have grain boundaries that are **euhedral**, that is, they are bounded by well-formed crystal faces. The thin section of nepheline basalt shown in Figure 1.6A is composed of euhedral crystals of augite and olivine contained in a fine-grained matrix. The textures shown in the thin section suggest that the augite and olivine began to crystallize from the melt and had grown to sizes of one to five millimeters before the lava erupted. The fine-grained matrix indicates that the melt in which the crystals were entrained chilled quickly and solidified as volcanic glass. A close examination of Figure 1.6A shows that the matrix is not all glass; a few extremely small grains of augite are also present. These probably nucleated shortly before the basalt erupted and solidified.

Crystals that are relatively large compared to the minerals composing the matrix of igneous rocks are called **phenocrysts**. In Figure 1.6A, the contrast in size between the phenocrysts and the matrix is obvious. However, few igneous rocks have a matrix so dominated by glass. More typically, the matrix will undergo some degree of crystallization. For example, the basalt shown in Figure 1.6B contains phenocrysts of equant olivine and elongate plagioclase in a matrix of finer-grained olivine, augite, plagioclase, and glass. Relations are similar in the andesite shown in Figure 1.6C, except the plagioclase in the andesite is stubbier than the plagioclase in the basalt. Phenocrysts of quartz may occur in highly siliceous melts, such as dacite and rhyolite (Figure 1.6D), and the presence of quartz phenocrysts is one way to identify these rocks in the field.

Many of the textures characteristic of volcanic rocks also help petrologists interpret plutonic rocks. The early crystallizing minerals form a matrix of interlocking euhedral grains, in a texture called **cumulate** texture. The minerals that formed later are constrained to grow in the interstices of these cumulus grains. These **postcumulus** grains are **anhedral**, which means they are not bounded by crystal faces. Examples of cumulate texture are shown in Figure 1.7A, a gabbro consisting of cumulus plagioclase and postcumulus augite, and in Figure 1.7B, a pyroxenite with cumulus orthopyroxene and postcumulus plagioclase. Some granitic rocks contain tabular plagioclase or potassium-feldspar; for example the granodiorite shown in Figure 1.7C contains distinctly tabular plagioclase. The plagioclase has the same stubby aspect ratio as plagioclase of similar composition in the volcanic rock shown

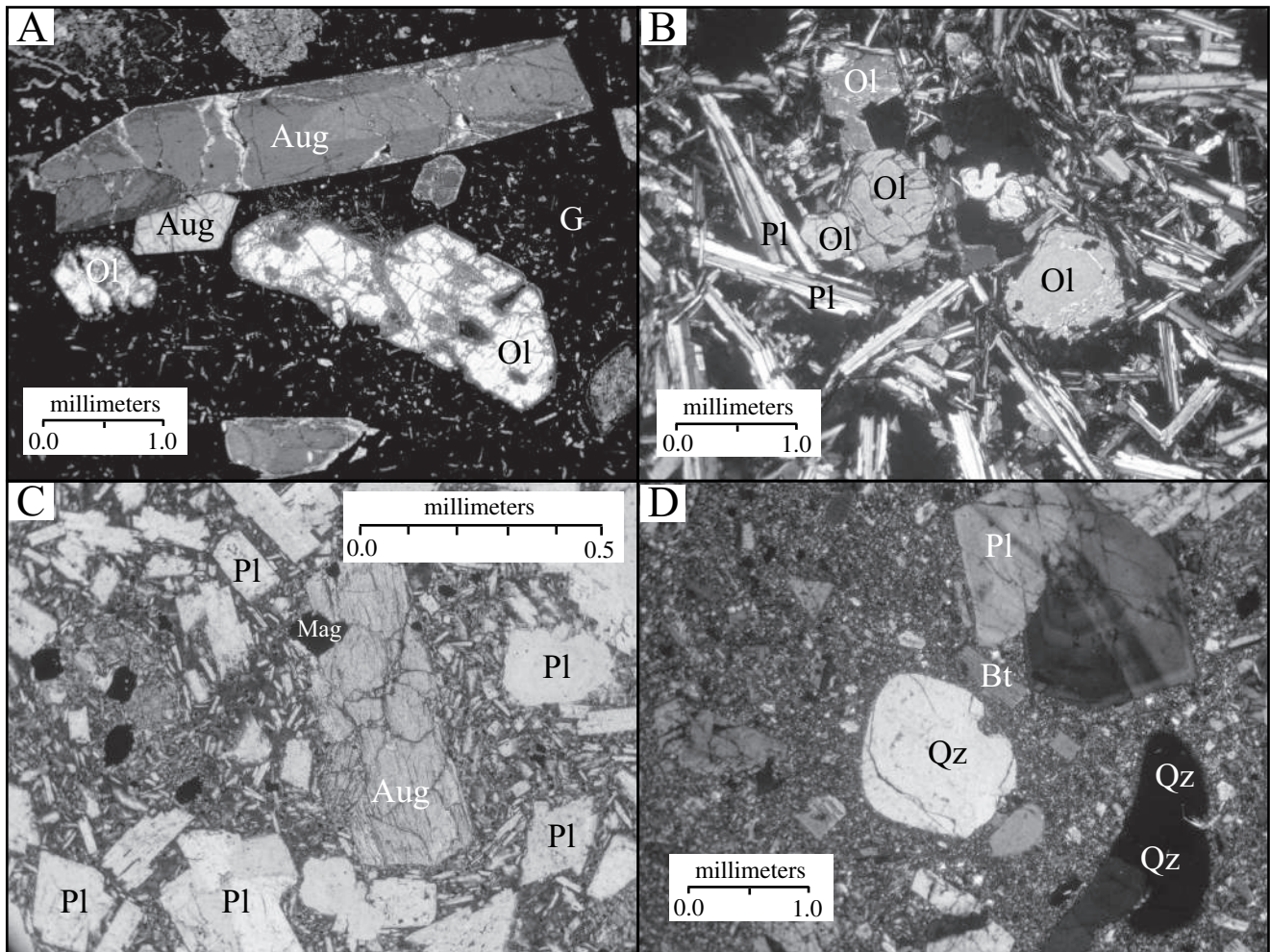


Figure 1.6 Photomicrographs showing textures in volcanic rocks. (A) Glassy nepheline basalt containing phenocrysts of olivine (Ol), augite (Aug), and glass (G) erupted near the Kaiserstuhl, Southern Germany. Crossed polarized light (XPL). (B) Olivine tholeiite containing phenocrysts of olivine (Ol) and plagioclase (Pl) in a matrix of fine-grained olivine, augite, plagioclase, and glass from the Snake River Plain, Idaho, USA. XPL. (C) Andesite with phenocrysts of augite (Aug), plagioclase (Pl) and magnetite (Mag) in matrix of fine-grained plagioclase, augite, and glass from Soufriere volcano, St. Vincent. Plane polarized light (PPL). (D) Dacite consisting of quartz (Qz), plagioclase (Pl), and biotite (Bt) in a matrix of quartz, plagioclase, and glass. XPL.

in Figure 1.6C. The concentric zoning in this plagioclase records changes in composition as plagioclase grain grows in the granodioritic melt.

In some plutonic rocks, the magma solidifies after relatively coarse-grained minerals have formed, making a rock called a **porphyry**. This rock has a texture that is characterized by euhedral grains dispersed in a finer-grained matrix (Figure 1.7D). A porphyritic texture tells a geologist that the rock underwent a complex cooling history. First, it cooled slowly, during which time the phenocrysts grew, followed by sudden cooling that caused the rapid solidification of the rest of the melt.

1.5 Igneous Structures

Igneous rocks exhibit a wide variety of forms. Mafic volcanic rocks occur mostly as **flows**; felsic volcanic rocks may also form flows, but also commonly form **pyroclastic** rocks, or rocks fragmented while still hot. Hypabyssal rocks may form as **lava domes**, **dikes**, or **sills**, and plutonic rocks occur as plutons and batholiths, as well as dikes and sills.

1.5.1 Structures in Volcanic Flows

Lava flows may range in thickness from less than a meter to more than ten meters. Mafic lava flows are often divided

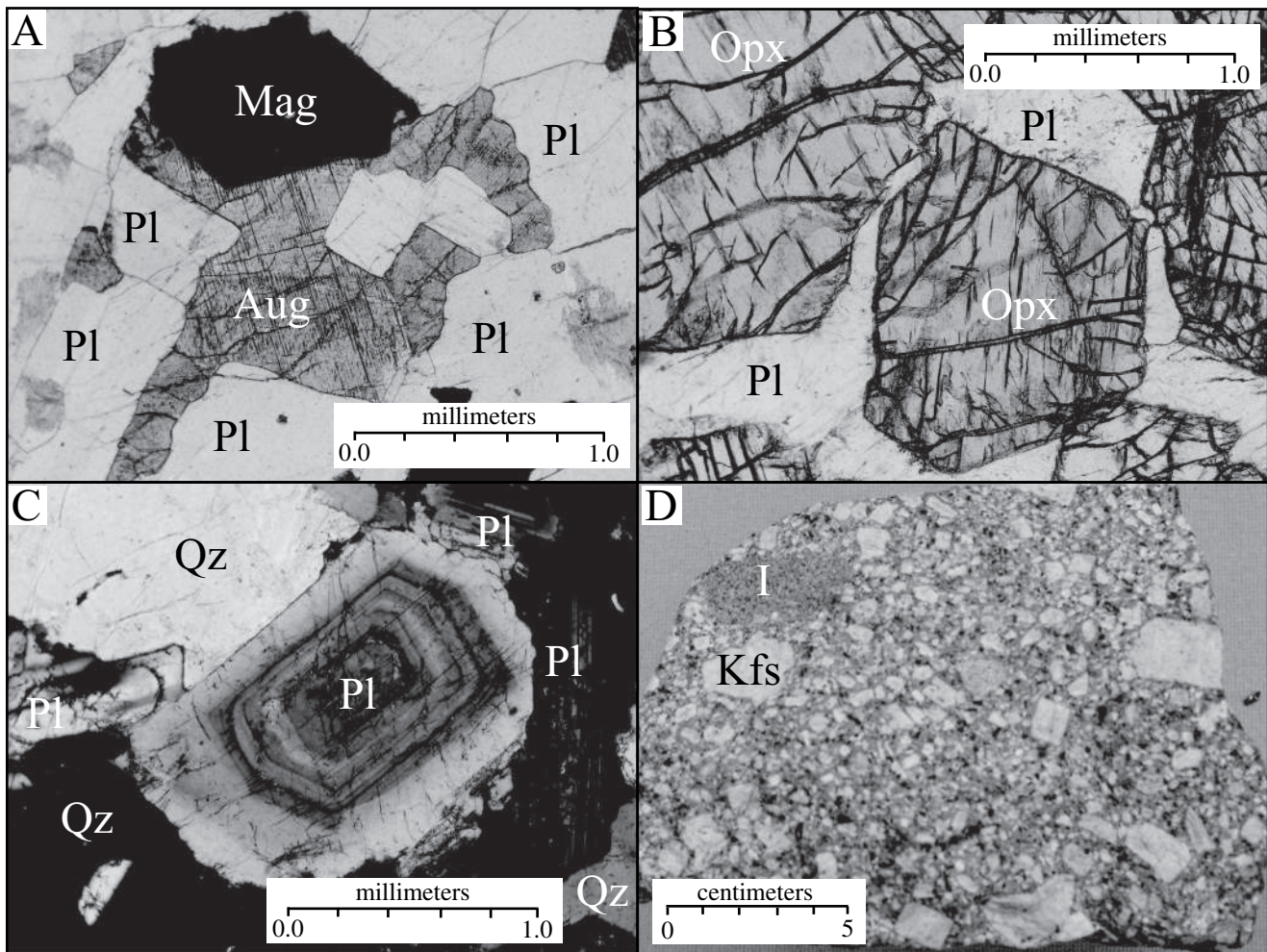


Figure 1.7 Photomicrographs showing textures in plutonic igneous rocks. (A) Plane-polarized light (PPL) photomicrograph showing euhedral (i.e., cumulus) plagioclase (Pl) and magnetite (Mag) surrounded by anhedral (i.e., postcumulus) augite (Aug). Gabbro from the Skaergaard intrusion, Greenland. (B) Photomicrograph in PPL showing euhedral orthopyroxene (Opx) and anhedral plagioclase (P) in a feldspathic pyroxenite from the Stillwater intrusion, Montana, USA. (C) Photomicrograph in crossed polarized light (XPL) showing compositionally zoned, euhedral plagioclase (Pl) surrounded by anhedral quartz (Qz). Biotite-hornblende granodiorite from Blue Mountains, Oregon, USA. Field of view for all photomicrographs is 2.5 mm. (D) Photograph of a granite porphyry dike containing phenocrysts of K-feldspar (Kfs) in a fine grained matrix of K-feldspar, plagioclase, quartz, biotite, and hornblende. The rock also contains an inclusion (I), which is interpreted as an autolith composed of chilled material from the margin of the dike. Willow Creek pass, Colorado, USA.

into two types: blocky lava is known as *aa* (Figure 1.8A), and a massive lava with a ropey surface is called *pahoehoe* (Figure 1.8B). Pahoehoe texture forms on relatively hot lavas but as the lava cools, the surface breaks apart, making *aa*. These names are etymologically Hawaiian; abundant lava flows in Hawaii allowed native Hawaiians ample time to develop a terminology comparing the textures of the flows. In cross-section, many flows, particularly those that ponded before completely crystallizing,

show **columnar jointing** (Figure 1.8C). Columnar jointing forms by contraction that cracks the rock as heat from the flow dissipates to the ground surface. The vertically oriented columns, which are typically hexagonal in cross-section, are commonly relatively wide at the base of the flow and more narrow at the top.

Where basalts erupt or flow into water, they form **pil-lows** (Figure 1.8D). The magma that contacts water is chilled and quenches, forming a distinctive lobate, or

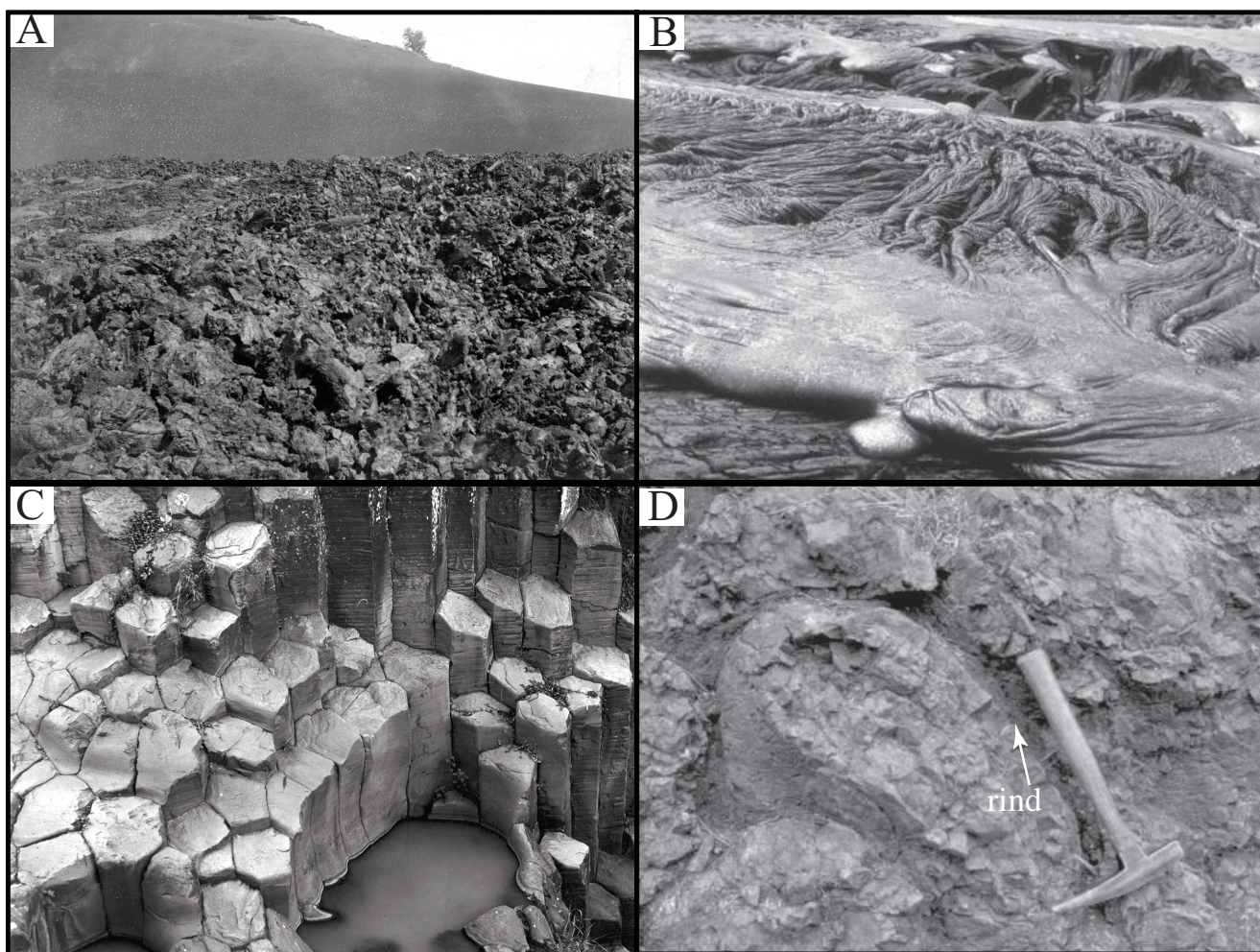


Figure 1.8 Structures of volcanic rocks. (A) Blocky or aa lava flow in Snake River Plain, Idaho, USA. United States Geologic Survey photo library I.C. 738. (B) Ropey or pahoehoe lava from 1972–74 eruption of Kilauea volcano, Hawaii, USA. United States Geological Survey photo library HVO 221ct. (C) Columnar jointing in basalt, San Miguel Regla, Hidalgo, Mexico. United States Geologic Survey photo library Fries, C.4. (D) Pillow in basalt from Curaçao, Netherlands Antilles. Note the rind on the pillow.

“pillow,” shape. As lava continues to flow, it breaks the solidified crust of the initial pillow to form another lobe. A pillow basalt is constructed of hundreds of these nested lobes. In cross-section, the pillows have a rounded top and a tail that points downward. Pillow basalts are diagnostic of subaqueous volcanism and because they are well preserved in the geologic record, they allow geologists to identify underwater eruptions up to billions of years old.

Commonly, gas bubbles exsolved from the magma gather at the top of a flow. Solidification of the melt will produce a rock pocked by holes from these exsolved gas bubbles. The holes are called **vesicles**, and they are key evidence of lava flows because gas bubbles are unlikely in hyperbyssal rocks. Vesicles are also important markers of

the top of a flow, something that may be difficult to recognize in complexly deformed volcanic rocks.

1.5.2 Structures in Pyroclastic Deposits

Pyroclastic deposits are classified according to two factors: the size of the fragments within the deposit and the relative abundance of glass, crystals, and rock fragments (Figure 1.9). Fragments larger than thirty-two millimeters in diameter are called either *bombs* or *blocks*. **Bombs** are clots of magma that were partly or entirely plastic when erupted. Shapes of bombs are controlled by the initial fluidity of the magma, length and velocity of flight through the air, and deformation on impact. **Blocks** are erupted fragments of solid rock. Solid or liquid materials

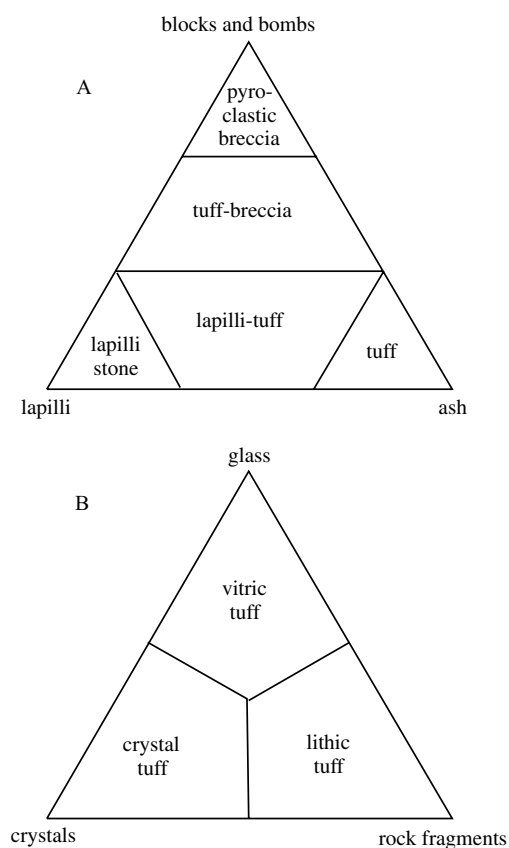


Figure 1.9 Classification of pyroclastic rocks. After (A) Fisher (1966) and (B) Pettijohn (1975).

between four and thirty-two millimeters in size at the time of eruption are called **lapilli**. Finely spun glass threads are called *Pele's hair*; *accretionary lapilli* are spheroidal, concentrically layered pellets formed by accretion of ash and dust by condensed moisture in eruption clouds. **Ash** (Figure 1.10A) is incoherent ejecta less than four millimeters in diameter and may be vitric, crystal, or lithic ash depending on the proportion of glass, crystals, or rock fragments. **Pumice** and **scoria** are ejecta of melt that have a porosity of 30 to 80 percent. Scoria is andesitic or basaltic in composition, whereas pumice has intermediate to siliceous composition. Because the vesicles in pumice are isolated, pumice may have a density less than that of water and can float. **Tuff** is consolidated volcanic ash. The crystal-vitric tuff shown in Figure 1.10B contains both glassy material – ash and pumice – and crystals of quartz. The vitric tuff in Figure 1.10C contains pumice fragments flattened by the weight of the overlying pyroclastic material.

Pyroclastic deposits are also classified by their areal extent and their structure, and give geologists information on the eruption process. One type of pyroclastic deposit is a **pyroclastic fall** deposit that forms from pyroclastic material that falls directly out of the sky. Because of their mode of formation, pyroclastic fall deposits mantle topography with a uniform thickness of ash over a local area. Over large areas, pyroclastic fall deposits show systematic decreases in thickness and grain size away from the source. An isopach map can show the location of the vent, the wind direction, and the height of the eruption column. We can define two end members of a spectrum of pyroclastic fall deposits. In a **strombolian** eruption, the eruption column is low (1–3 km) and the fragments accumulate around the vent, forming the cone. This type of eruption is named after Stromboli, a volcano north of Sicily that has had frequent, rather quiet eruptions since historical times. In a **plinian** eruption, the eruption column is high (20–50 km) and pumice and ash are spread as a thin sheet covering areas up to 10^6 km² (Figure 1.11). This type of eruption is named after Pliny the Younger, who in 79 CE wrote elaborate letters describing the eruption of Vesuvius that destroyed Pompeii (and killed his uncle, Pliny the Elder). Plinian and strombolian deposits are generally coarse-grained and are produced by explosive exsolution of volatiles that blows apart the magma. If a vent is situated where water has ready access, the mechanism of explosion changes fundamentally. Magma is torn apart by exsolving gases and mixes with water. Rapid vaporization triggers a thermal explosion and further fragmentation. These **phreatomagmatic** explosions are more violent and produce fine-grained deposits composed of glassy ash or **hyaloclastite**.

Another type of pyroclastic deposit is a **pyroclastic flow deposit**. These deposits form from avalanches of pyroclastic fragments that move down topographic lows and fill depressions. Their movement is broadly analogous to other natural debris flows (e.g., rock flows and mud flows). The deposits are characterized by poorly sorted material with a continuum of sizes from large blocks to fine ash because there is little room and time for sorting in a fast-moving avalanche of closely packed particles. In contrast, air fall deposits are usually well sorted because during transport through the high atmosphere the particles are sorted according to size and density. Because pyroclastic flows are gravity controlled, they infill topographic lows instead of mantling topography. As with air fall deposits,

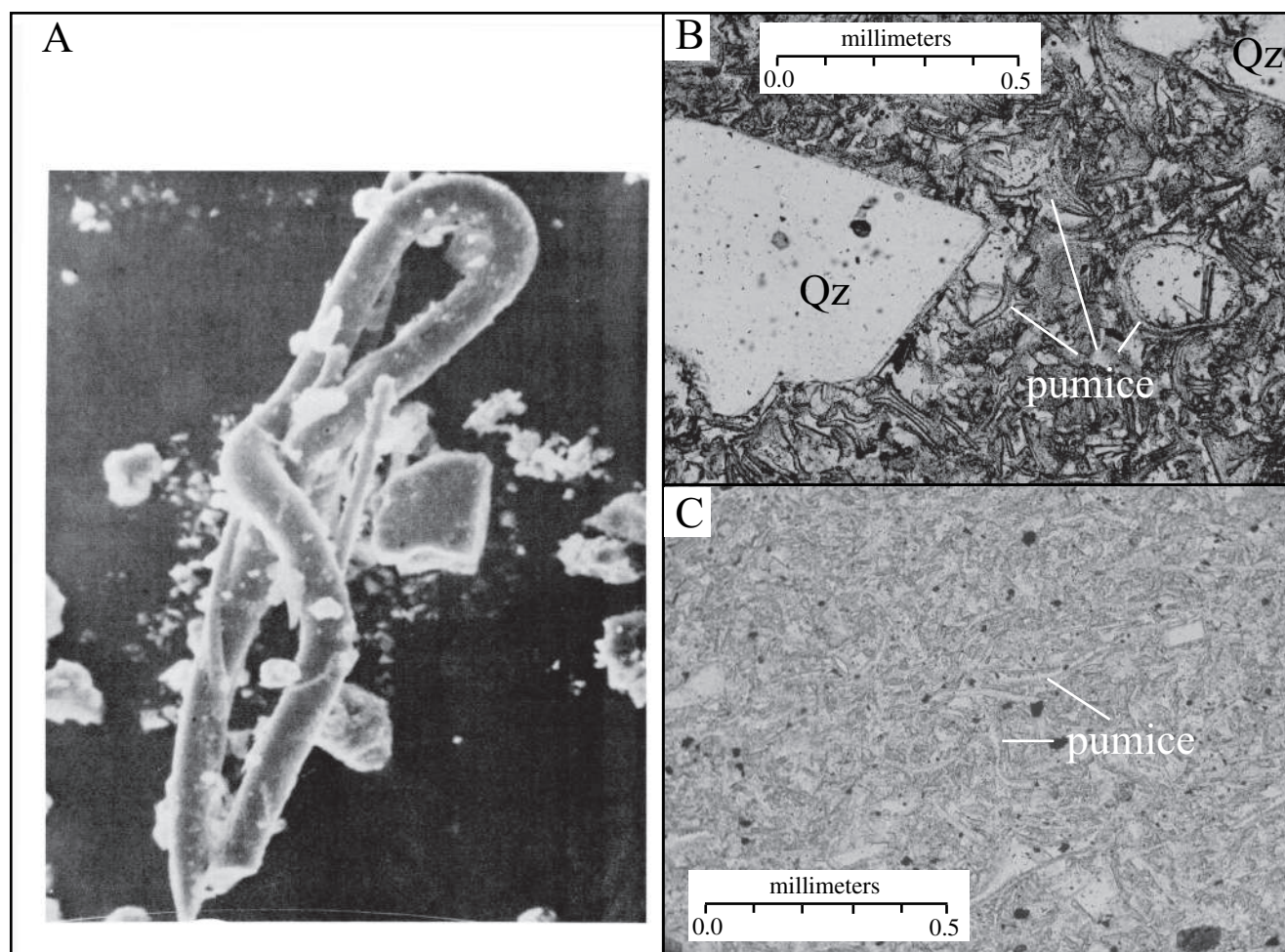


Figure 1.10 Photomicrographs of pyroclastic rocks. (A) Ash from Mount Saint Helens collected in Laramie, Wyoming after the May 18, 1980 eruption. Length of the glass strand is 200 μm . (B) Crystal vitric tuff showing crystals and crystal fragments of quartz (Qz) in a matrix of pumice. PPL, FOV = 1.25 mm. Bandolier, New Mexico, USA. (C) Vitric tuff showing pumice fragments more compressed than those in Figure 1.9a. Lava Creek Tuff, Yellowstone, Idaho, USA. PPL, FOV = 1.25 mm.

pyroclastic flows vary by several orders of magnitude in their volume and dispersal.

Pyroclastic flow deposits may also form when a growing lava dome collapses (Figure 1.12). Growing lava domes are unstable and commonly break up to form landslides. If the melt is close to water saturation at the time the landslide forms, sudden decompression of the underlying magma could lead to explosion, which triggers an avalanche of hot blocks, ash, and gas. These deposits are typically monolithologic. Transported individual blocks can reach tens of meters in diameter. The pyroclastic flow deposits of Mont Pelée that formed on the island of Martinique in 1902 originated by collapse of a lava dome.

If the temperature of emplacement is sufficiently hot, pyroclastic deposits sometimes undergo processes of

welding after deposition (Figure 1.11C). Welding occurs when particles are fused together by solid-state diffusion at particle contacts. For rhyolitic glass the minimum temperature for welding is 625°C at 1 atm. and 590°C at 10 atm. If the glass is sufficiently ductile (i.e., hot), the pumice and ash particles deform as they weld under the weight of the overlying deposit. The end result is a rock in which all porosity is removed and pumices are deformed in streaks or **fiamme**.

1.5.3 Structures in Hypabyssal Rocks

Hypabyssal rocks are rocks that crystallized at shallow depths. Magmas emplaced near the surface cool relatively quickly, and hypabyssal rocks are, therefore, typically fine-grained but lack evidence that they ever erupted on

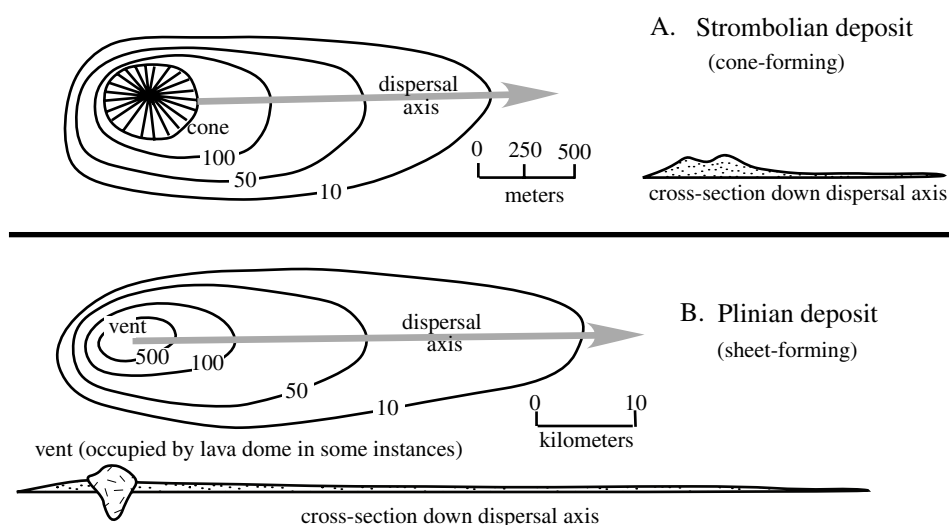


Figure 1.11 Sketch showing the relative scale of aerial distribution of pyroclastic air fall deposits from strombolian and plinian eruptions.

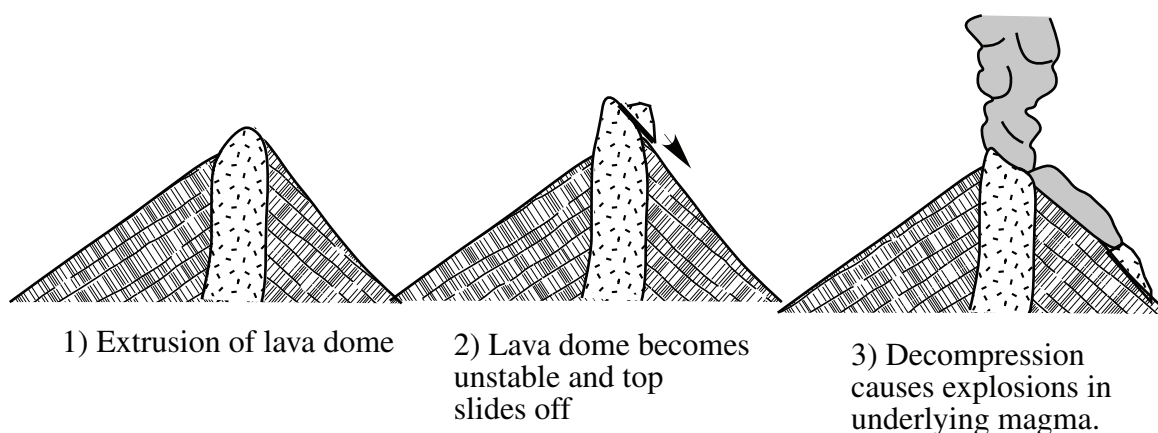


Figure 1.12 Diagram of the formation of a pyroclastic flow deposit by the collapse of a lava dome.

the surface. Examples of hypabyssal rocks include **lava domes, volcanic necks, dikes, and sills**.

Lava domes include both hypabyssal and eruptive classes of igneous structures. They form from highly viscous lava that forms bulging, dome-shaped bodies that may be several hundred meters high (Figure 1.13). The surface of the dome may be made of fragmented lava (much like aa) that erupted on the surface of the dome but didn't manage to flow far. Beneath the surface, the dome consists of magma that shallowly solidified and was pushed into the domal shape by magma intruding from below.

Some volcanoes erupt easily eroded, fragmented rocks. As such, the volcano itself may not survive as a topographic

feature. As the volcanic edifice erodes away, the vent of the volcano, which is made of rock that is more resistant to erosion, may remain. This irregularly shaped spire of hypabyssal rock is called a *volcanic neck* (Figure 1.14). Volcanic necks are common features in some volcanic terrains.

Dikes are tabular bodies of igneous rock that form when magma solidifies within a subterranean fracture. Dikes can range from centimeters to kilometers in thickness, although the thickness of hypabyssal dikes tends to be on the order of meters. Dikes can form on a local scale during the eruption of single volcanoes. Some volcanic necks have dikes radiating out from them that may extend for more than ten kilometers (Figure 1.14). These



Figure 1.13 Photo of a lava dome and pyroclastic flow within the caldera of Mount Saint Helens. The dome and flow occurred as part of the eruptive activity of March–April 1982. Photo by Richard Waitt. From the United States Geological Survey Earthquake Information Bulletin, 14, September–October 1982.

dikes indicate that, in addition to the eroded fragmental rocks, the fossil volcano erupted magma supplied by fissures now occupied by dikes.

When magma intrudes sedimentary rocks, they commonly parallel sedimentary bedding, rather than forcing fractures across bedding planes. Such intrusions are called **sills**. The term *sill* also applies to dikes that have intruded parallel to metamorphic layering in metamorphic rocks.

Chilled margins are a common, distinctive feature of hypabyssal sills and dikes. (Figure 1.15). When magmas are emplaced at fairly shallow depths, the ambient temperature is not very high and the magma on the margin of the dike or sill may chill very rapidly and be fine-grained. The fine-grained margins of the dike or sill insulate the magma in the interior of the dike or sill, allowing it to cool more slowly, becoming coarser grained.

When the crust fractures in an extensional tectonic environment, intrusion of magma into the resulting faults produces a **dike swarm**. A dike swarm consists of many dikes with similar orientation and chemistry that extend over tens to hundreds of kilometers. Dike swarms are best exposed in Precambrian terrains (Map 1.1) where erosion has stripped away the sedimentary cover. The compositions, dates, and orientations of Precambrian dike swarms

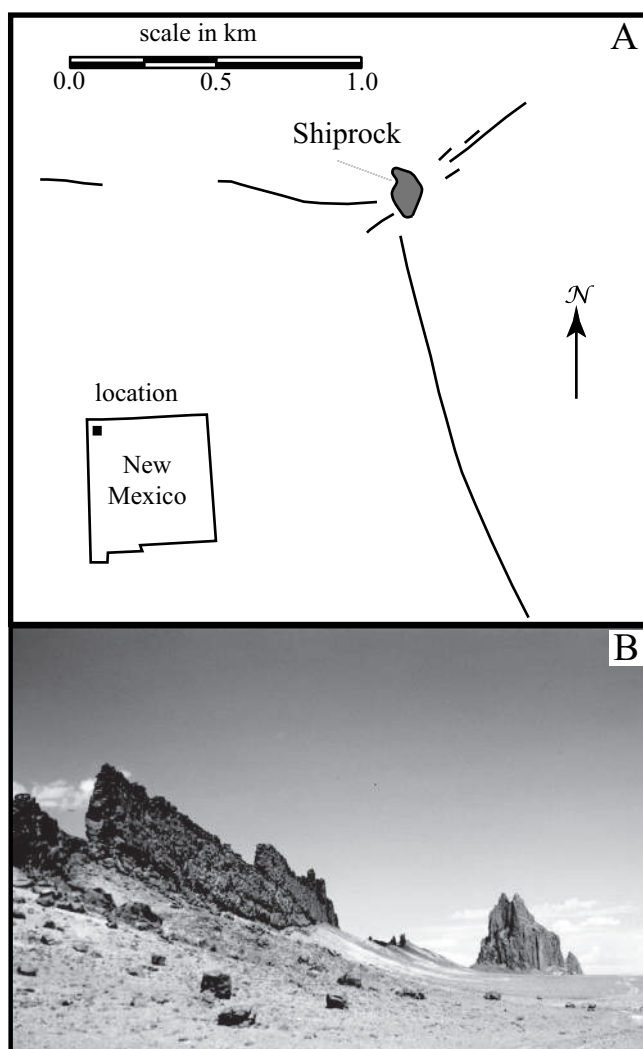


Figure 1.14 (A) Geologic sketch map of Shiprock in New Mexico, USA, showing dikes (linear features) radiating out of a volcanic neck (irregular gray shape). The volcanic neck, called Shiprock, is about 600 meters high. (B) View of Shiprock and dikes from the southeast. Photo from the United States Geological Survey photo library, McKee, 1007ct.

may be used to reconstruct Precambrian continental configurations.

1.5.4 Structures in Plutonic Rocks

Plutonic rocks occur as irregularly shaped bodies known as **plutons**. A pluton larger than forty mi^2 in outcrop is called a **batholith**, although large batholiths are composed of many individual plutons. For example, the Sierra Nevada batholith, which is exposed over an area of about 600 x

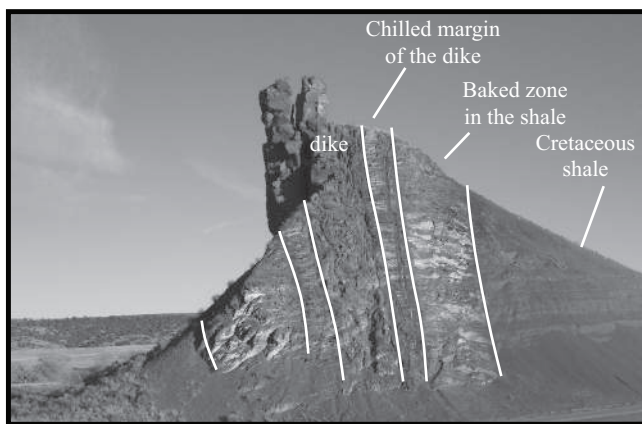
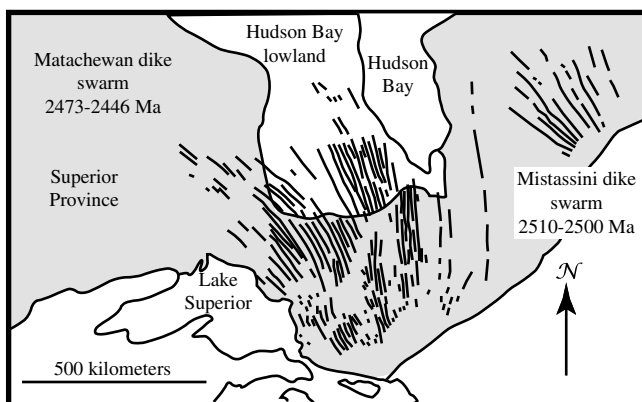


Figure 1.15 Photo of chilled Tertiary dike intruding and baking adjacent Cretaceous sedimentary rocks, southern Colorado, USA. Photo by Eric Erslev.



Map 1.1 Geologic map of the Matachewan and Mistassini dike swarms in the southern portion of the Canadian Shield. Dikes in the Hudson Bay lowland are mapped aeromagnetically. Modified after Buchan et al. (2007).

200 km in eastern California, consists of hundreds of separate plutons that were emplaced over a time period that ranges over most of the Mesozoic, though the bulk of the batholith was emplaced throughout the Cretaceous. The term *batholith* is usually applied to granitic rocks. Large plutons composed of mafic rocks are more commonly referred to as *intrusions*.

Plutons emplaced in shallow environments may preserve chilled margins, although those intruded deeper in the crust may not. Igneous intrusions commonly contain blocks of exotic rock that range from centimeters to kilometers in size. In some occurrences, the inclusions are fragments plucked off the country rock during the intrusion of

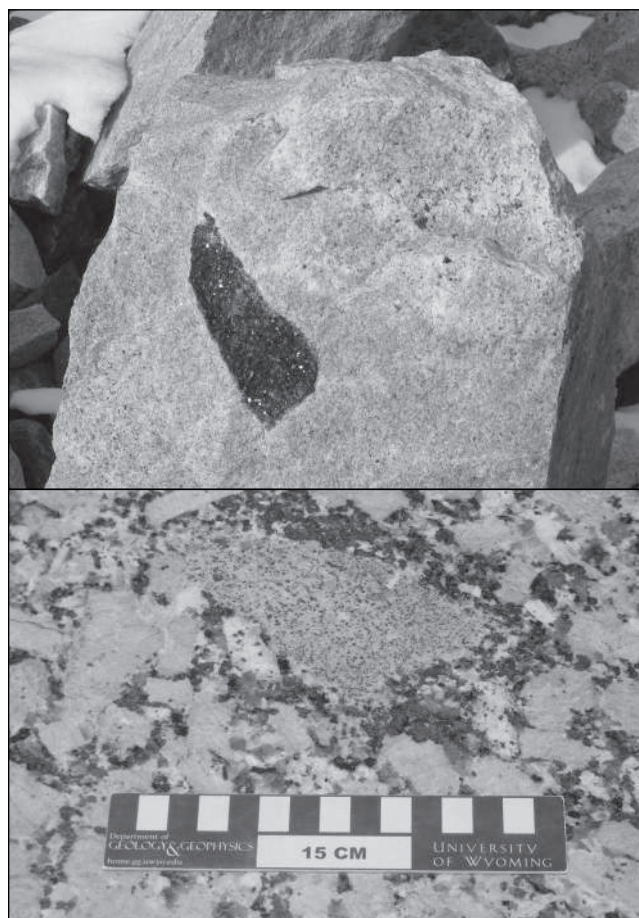


Figure 1.16 (A) Biotite-rich xenolith in granodiorite dike cutting the Laramie anorthosite complex, Wyoming, USA. (B) Fine-grained granodiorite autolith in granite, floor of main terminal building, Denver International Airport.

the magma or that foundered into the magma from the roof of the intrusion. Such fragments of country rock are called **xenoliths** (Figure 1.16A); the term *xeno-* means foreign. In some plutons, inclusions consist of pieces of a slightly older intrusion that was clearly part of the same magma sequence as the host rock. These types of enclaves are called **autoliths** (Figure 1.16B). If it is unclear whether the inclusion is related to the host rock, the term **enclave** can be used.

Dikes are also present in plutonic rocks, although because they were emplaced at relatively great depth (and hence relatively high temperatures), they seldom show chilled margins. Because dikes in plutonic environments tend to be emplaced into a relatively warm environment, they may also be as coarse-grained as the rocks they intrude, unlike hypabyssal dikes.

Summary

- Igneous rocks form by solidification of magma, either on Earth's surface (extrusive or volcanic rocks), near the surface (hypabyssal rocks), or at depth (plutonic rocks).
- Igneous rocks are classified either on the basis of the proportions of quartz, feldspars, and mafic minerals or by their geochemical composition.
- The texture and structures preserved in igneous rocks allow geologists to interpret the environment in which the rocks formed.

Questions and Problems

Problem 1.1. Determine the rock names for coarse-grained rock samples with the following proportions of alkali feldspar, plagioclase, and quartz.

	A	B	C
Alkali feldspar	0.55	0.37	0.1
Plagioclase	0.22	0.36	0.49
Quartz	0.23	0.27	0.41

Problem 1.2. Determine the rock names for coarse-grained rock samples with the following mineral proportions.

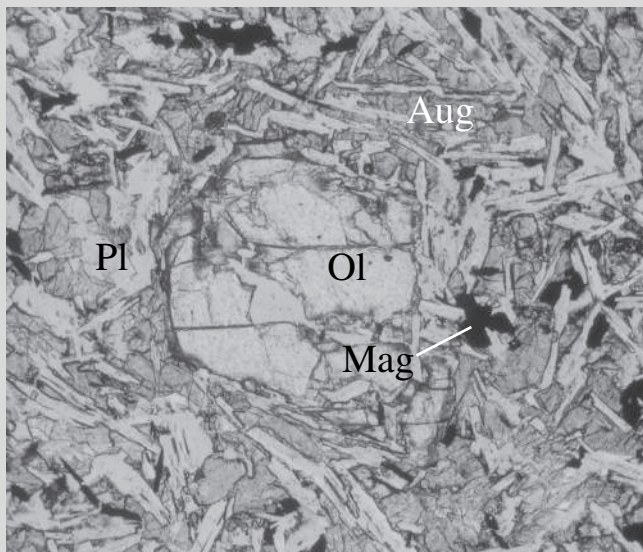
	A	B	C
Alkalifeldspar	15	3	0
Plagioclase	46	64	92
Quartz	21	2	3
Biotite	3	5	0
Hornblende	13	15	5

Problem 1.3. A coarse-grained rock sample consists of 15 percent plagioclase, 35 percent augite, and 50 percent enstatite. What is the name of this rock according to the IUGS classification?

Problem 1.4. Determine the rock names for volcanic rock samples with the following compositions:

	A	B	C
SiO ₂	54.7	70.97	60.06
TiO ₂	1.71	0.33	0.83
Al ₂ O ₃	16.34	13.72	16.51
FeO*	11.58	3.11	7.68
MnO	0.24	0.06	0.17
MgO	2.36	0.32	0.38
CaO	6.75	1.5	3.14
Na ₂ O	4.14	3.67	4.57
K ₂ O	1.47	5.22	5.58
P ₂ O ₅	0.71	0.06	0.25

Problem 1.5. Figure P1.1 is a photomicrograph of a trachyandesite with augite (Aug), magnetite (Mag), olivine (Ol), and plagioclase (Pl). Determine the order in which these minerals crystallized and explain your reasoning.



Further Reading

.....

LeBas, M. J., et al., 1986, Chemical classification of volcanic rocks based on the total alkali-silica diagram. *Journal of Petrology*, 27, 745–50.

LeMaitre, R. W., et al., 1989, *A classification of igneous rocks and glossary of terms*. Blackwell Scientific Publishers, Oxford, UK.

MacKenzie, W. S., Donaldson, C. H., and Guilford, C., 1982, *Atlas of igneous rocks and their textures*. John Wiley & Sons, New York.

Thorpe, R. S., and Brown, G. C., 1993, *The field description of igneous rocks*. John Wiley & Sons, New York.

Chapter 2

An Introduction to Igneous Phase Diagrams

2.1 Introduction

Silicate melts are chemically complex. Not only does it take more than nine elements to characterize most igneous rocks, melts also contain a number of volatile components, including H_2O , CO_2 , HF , and HCl . Despite the complexity of natural igneous melts, phase diagrams of mineral relations in chemically simple systems provide a way to understand the processes by which igneous rocks crystallize. These phase diagrams may not duplicate the crystallization process exactly, but they can help identify the factors that control the crystallization of minerals from melts. Surprisingly, many of the relations illustrated in simple phase diagrams can be extended to igneous rocks, despite their chemical complexity. This chapter begins with a review of the phase rule and lever rule, both of which are prerequisite to an understanding of phase diagrams. It then covers how to interpret the crystallization and melting relations in the various types of binary phase diagrams. Finally, this chapter provides a brief introduction to ternary and pseudoternary phase diagrams. Throughout these discussions the emphasis is on how relations in phase diagrams can be used to interpret crystallization and phase relations in igneous rocks.

2.2 The Phase Rule

The phase rule is a simple equation that predicts the number of minerals and melts that will be present as a function of physical conditions such as pressure and temperature. It is based in chemical thermodynamics, the branch of chemistry that studies how changes in temperature, pressure, and chemical composition affect equilibria. In this section the applications of thermodynamics will be mostly graphical, through the use of phase diagrams. Some thermodynamic definitions provide a necessary background for understanding the phase rule and phase diagrams. Among them are:

System – that part of the universe that is under consideration. Systems typically are described by their chemical constituents. For example, crystallization of olivine from a melt can be modeled by the system $\text{Mg}_2\text{SiO}_4 - \text{Fe}_2\text{SiO}_4$. Because minerals may have complex chemical formulae and referring to geological systems by their chemical constituents can be cumbersome, geologists commonly refer to systems informally with the names of the mineral end members. For example, the system $\text{Mg}_2\text{SiO}_4 - \text{Fe}_2\text{SiO}_4$ may be referred to as the system forsterite – fayalite, and the system $\text{CaAl}_2\text{Si}_2\text{O}_8 - \text{CaMgSi}_2\text{O}_6$ may be called the system anorthite – diopside.

Phase – a homogenous, mechanically separable part of a system. Phases are separated from one another by interfaces. Geologists usually think of the phases in a rock as the minerals that are present; however, during the evolution of an igneous rock a silicate melt phase may be present as well as, perhaps, an H_2O -rich or a CO_2 -rich fluid phase.

Component – a chemical constituent of a system. The phase rule quantifies the minimum number of components, or chemical constituents, needed to define all the phases in the system. The components of a system are often listed in terms of oxides, as in the model system for olivine. However, in applying the phase rule it is important to identify the *minimum* number of components that define a system. For example, a system containing the phases andalusite, sillimanite, and kyanite can be described as having a single component: Al_2SiO_5 . It would be a mistake to call this a two-component system (i.e., Al_2O_3 and SiO_2). In this book, components are given either as chemical compositions (e.g., Mg_2SiO_4) or as abbreviations for mineralogic end members (for example, Fo for Mg_2SiO_4).

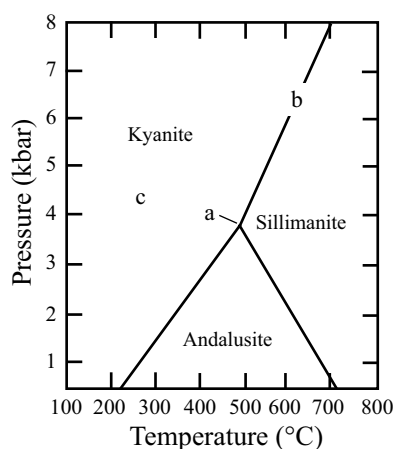


Figure 2.1 Phase diagram for the one-component system Al_2SiO_5 (from Holdaway, 1971). Points a, b, and c are examples of invariant, univariant, and divariant assemblages, respectively.

(Common abbreviations for minerals are listed in Table A.1 in the appendix.)

Variance. Variance (or degrees of freedom) refers to the number of variables that have to be constrained before the equilibrium conditions of a system can be known. This is best understood by considering the phase diagram for the system Al_2SiO_5 (Figure 2.1). If all three aluminosilicates are in equilibrium in a rock, then the crystallization conditions of the rock are known; it must have formed at the aluminosilicate triple point (i.e., point a in Figure 2.1 at 550°C and 4.5 kilobars). Such an assemblage has no degrees of freedom and is known as invariant. If only two aluminosilicates are present in equilibrium, for example, kyanite and sillimanite (point b, Figure 2.1), then the rock must have crystallized along the reaction curve kyanite = sillimanite. This assemblage has one degree of freedom (i.e., it is univariant), meaning that if one variable, either pressure or temperature, is known, then the other is defined by the univariant curve kyanite \rightleftharpoons sillimanite. Finally, an assemblage with only one aluminosilicate (such as point c in Figure 2.1) reveals only that the rock crystallized in one of the fields in the phase diagram. This assemblage has two degrees of freedom (it is divariant), and it is necessary to define both temperature and pressure to better constrain its crystallization conditions.

Although these relations are relatively simple for a one-component system such as that treated earlier in this chapter, they become progressively more complex as the number of components in a system increases. In complex

natural systems, it is often helpful to use the phase rule. This simple equation relates variance, the number of components, and the number of phases in an assemblage. The phase rule is written as:

$$\phi + f = C + r$$

where ϕ = the number of phases, f = the degrees of freedom (variance), C = the number of components, and r describes the number of environmental variables in the system. In a system at 1 bar, such as in many igneous phase diagrams, temperature is the only environmental variable and $r = 1$. In systems where the variables are both temperature and pressure (the most common situation in metamorphic petrology), $r = 2$. Because the most common variables are pressure and temperature, the phase rule is often written as:

$$\phi + f = C + 2$$

The phase rule is a basic equation that tells how much information is needed to define a system. The equation has two parts. One part is the variable r . This describes the number of physical unknowns in the system. The other part of the equation determines, given a system with a certain number of components, how many phases are needed to write a reaction. One way to understand this is to recall how to solve equations with multiple variables: if there are x unknowns then x equations are required to solve it uniquely. This can be expressed as: $R + f = U$, where R = number of reactions, f = degrees of freedom (variance), and U = number of unknowns. The phase rule says that the number of phases equals R , and the number of components + the number of environmental unknowns equals U .

2.3 The Lever Rule

In addition to indicating pressure and temperature, phase diagrams communicate information about composition of the phases. The **lever rule** is used to locate compositions on a phase diagram. For example, olivine compositions vary from Fe_2SiO_4 to Mg_2SiO_4 (Figure 2.2). All olivine compositions will plot somewhere on the line b-c, depending on the ratio of Fe to Mg in the olivine. Pure fayalite plots at b, whereas pure forsterite plots at c. Intermediate olivine plots somewhere between b and c.

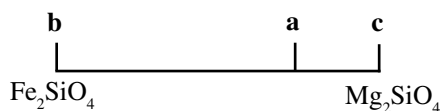


Figure 2.2 Diagram showing olivine solid solutions. Points a, b, and c refer to olivine with different amounts of Fe and Mg.

The variable that describes the composition of olivine is called *mole fraction* and is abbreviated as $X_{\text{Fe}_2\text{SiO}_4}$, X_{Fa} , $X_{\text{Fe}}^{\text{Ol}}$, or sometimes $X_{\text{Fe}_2\text{SiO}_4}^{\text{Ol}}$.

Mole fraction is the molar ratio of components in a solution. For olivine, the ratio is:

$$X_{\text{Fe}}^{\text{Ol}} = \frac{\text{Fe}_2\text{SiO}_4}{\text{Fe}_2\text{SiO}_4 + \text{Mg}_2\text{SiO}_4} \quad (2.1)$$

Since all olivine compositions share the SiO_4 framework, reaction 2.1 simplifies to:

$$X_{\text{Fe}}^{\text{Ol}} = \frac{\text{Fe}}{(\text{Fe} + \text{Mg})} \quad (2.2)$$

Olivine is usually a binary solution of Fe and Mg that can be expressed as:

$$X_{\text{Fe}}^{\text{Ol}} = (1 - X_{\text{Mg}}^{\text{Ol}}) \quad (2.3)$$

Since point b in Figure 2.2 has no magnesium, it has $X_{\text{Fe}}^{\text{Ol}} = 1.0$ and $X_{\text{Mg}}^{\text{Ol}} = 0.0$. Likewise, since point c has no Fe, it has $X_{\text{Fe}}^{\text{Ol}} = 0.0$ and $X_{\text{Mg}}^{\text{Ol}} = 1.0$. As X_{Fe} increases, the olivine plots closer to b and further from c. The lever rule indicates the exact location an olivine with a given X_{Fe} will plot on Figure 2.2, expressed as a distance of X_{Fe} , the total distance from c toward b. For example, point a is located 25 percent of the way from c toward b and 75 percent of the way from b toward c. It has the composition $X_{\text{Fe}}^{\text{Ol}} = 0.25$ or $X_{\text{Mg}}^{\text{Ol}} = 0.75$.

A phase composed of three components can be plotted on a ternary diagram, where each apex of the triangle is the composition of a component. Consider phase E in Figure 2.3, which has the formula x_2y_2z . By normalizing the ions so they total to one (i.e., there are four ions so dividing the stoichiometric coefficient of each by four), phase E can be represented by the following molar ratios $x:y:z = 0.5:0.25:0.25$. Point E in the x-y-z triangle (Figure 2.3) must lie on a line connecting all points that contain

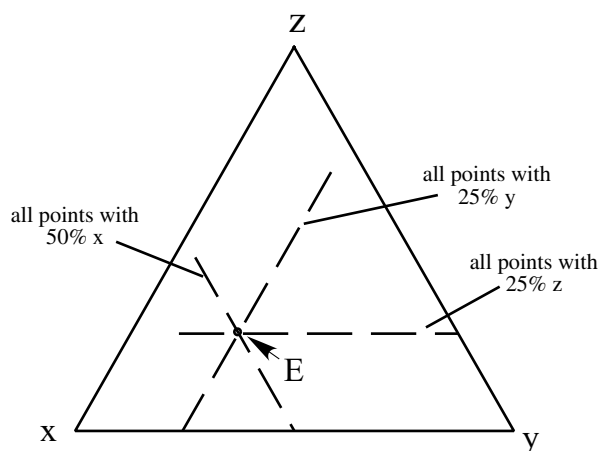


Figure 2.3 A ternary diagram for the system $x - y - z$ showing where phase E with the composition of x_2yz plots.

50 percent of x . The same operation can be performed to find lines marking the locus of points containing 25 percent y and 25 percent z , and the intersection of the three lines represents the composition of phase E.

2.4 Two Component Systems Involving Melt

The phase rule and the lever rule provide the basis for interpreting phase diagrams. The simplest phase diagrams are one-component systems. Melting relations in these systems are simple; because the melt has a fixed composition, it can be treated the same as any other phase in the system. For example, adding a field for Al_2SiO_5 melt in Figure 2.1 requires only a curve at high temperature for the melting of sillimanite or kyanite. On the other hand, it is not so simple to show melt relations in a two-component system because the melt is a solution involving both components. In these systems, it is necessary to understand how melt interacts with various types of solids. Five types of binary phase diagrams with melts can be recognized. These are:

- 1) binary systems with a eutectic;
- 2) binary systems with a peritectic;
- 3) binary systems with a thermal barrier;
- 4) binary systems with solids that have a complete solid solution; and

- 5) binary systems with solids that have a partial solid solution.

On each of these phase diagrams it is possible to identify the paths the melt would follow during:

- 1) **Equilibrium crystallization** is the process whereby the crystallizing minerals remain in contact with the melt throughout the crystallizing process.
- 2) **Fractional crystallization** is a process in which crystallizing minerals are immediately extracted from the melt and do not react with it further. In nature, fractional crystallization can occur in one of two processes: 1) crystals may be removed from communication with the melt when they sink to the bottom of a magma chamber, or 2) crystals may be left behind as the melt moves away in a process called **filter pressing**.
- 3) **Equilibrium melting** is a process whereby the melt and the residuum remain in communication throughout the melting process.
- 4) **Fractional melting** models a system where melt is extracted from a system as soon as it forms and does not react further with the residuum.

2.4.1 Binary Systems with a Eutectic

Effect of additional components on the melting temperature of a phase. An example of a two-component system with a melt is the system $H_2O - NaCl$, which is composed of the phases ice, salt, and melt (i.e., water). Ice is a solid that contains very little salt, and salt is a solid that contains very little H_2O . Liquid water, on the other hand, can contain a large amount of salt. At surface conditions, salt is not completely miscible with water, but this system is so familiar that it is a good one with which to introduce binary phase diagrams. A simple rule for the melting of most substances is that the temperature at which the solid will melt is highest when the melt has the same composition as the solid. In other words, addition of any component to a melt will reduce the melting temperature of solids in equilibrium with that melt.

The $H_2O - NaCl$ system offers a well-known example of this rule. What happens when salt is spread on an icy sidewalk? Of course, the ice melts. Figure 2.4 shows the effect of salt on the melting temperature of ice. This effect

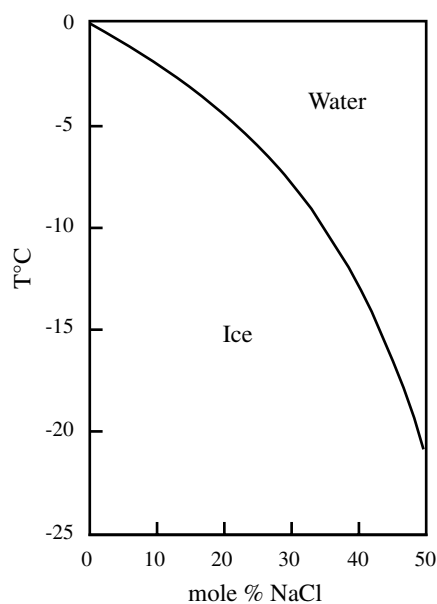


Figure 2.4 Phase diagram showing a portion of the system NaCl-H₂O.

is not a magical property of NaCl – anything that can dissolve in water will depress the freezing temperature. Why is this?

When ice (or any phase) is in equilibrium with its melt, the molecules of H₂O are leaving the surface of the ice crystal and entering the water (i.e., the ice is melting) at the same rate as the molecules of H₂O are leaving the water and adhering to the ice (i.e., the water is freezing). What happens with the addition of a component, such as NaCl, that can dissolve in the water but not in ice? The rate at which H₂O molecules in the water adhere to the ice depends on the rate at which these molecules collide with the surface of the ice. The addition of NaCl to the water affects the rate at which H₂O molecules collide with the surface because some of the water molecules will be bonded to Na⁺ or Cl⁻ rather than impacting the surface of the ice. These molecules will not bond with the ice, and thus the rate at which water freezes to form ice is lower than the rate at which ice melts to form water. If the temperature stays the same, the ice will melt. To equalize the rate of melting with the rate of freezing would require lowering the temperature (Figure 2.4).

The CaAl₂Si₂O₈ – CaMgSi₂O₆ phase diagram. The system CaAl₂Si₂O₈ – CaMgSi₂O₆ (anorthite – diopside) (Figure 2.5) is another good example of how an additional component depresses the melting point of any phase. Pure

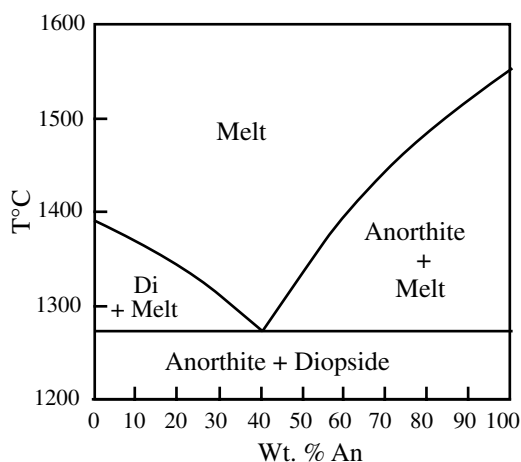


Figure 2.5 Phase diagram for the system CaAl₂Si₂O₈ – CaMgSi₂O₆ at one bar (Bowen, 1915).

anorthite melts at 1553°C. Addition of even a small amount of CaMgSi₂O₆ to the melt will cause anorthite to melt at lower temperatures. Similarly, diopside melts at 1392°C, and the addition of CaAl₂Si₂O₈ to a diopside-rich system will cause diopside to melt at lower temperatures. The curve showing the freezing point depression of anorthite (or of diopside) is the **liquidus**. The two liquidus curves meet at 1274°C. This point is a **eutectic** and represents the lowest temperature at which melt may be present in this system. It is important to note that the melting temperature for this system (and other silicate phase diagrams shown in this chapter) is much higher than the temperature of most silicate melts because additional components depress the melting temperature.

Relationships in Figure 2.5 are best understood by applying the phase rule. Since the system is isobaric, the phase rule should be: $\phi + f = C + 1$. The system has two components, so when three phases are present there are no degrees of freedom (i.e., an invariant point), when two phases are present there is one degree of freedom (i.e., a univariant line), and when only one phase is present there are two degrees of freedom (i.e., a divariant field). There is only one place on the diagram where three phases are present, and that is the eutectic where diopside, anorthite, and melt coexist. At the eutectic, there are no degrees of freedom, the temperature is 1274°C, and the melt has a fixed composition (40 percent anorthite). There are three places on the diagram where two phases occur. These are the fields labeled *diopside + anorthite*, *diopside + melt*, and

anorthite + melt in Figure 2.5. The *diopside + anorthite* field lies at temperatures below the eutectic. Diopside and anorthite have fixed composition (located at either end of the diagram). The univariant nature of the field is represented by the fact that at any temperature below 1274° diopside and anorthite of fixed composition will coexist. In the field labeled *anorthite + melt*, the two phases are anorthite (of fixed composition) and a melt of variable composition. The univariant nature of this field is represented by the fact that at a given temperature the composition of the melt is fixed at the point where the isotherm for that temperature intersects the liquidus. Alternatively, if a melt composition is specified to be in equilibrium with anorthite, then the temperature at which *anorthite + melt* occurs is fixed. The one-phase field in Figure 2.5 is labeled *melt*. The composition of the melt is not constrained in this field so even if the temperature is fixed, there is no constraint on the composition of the melt. Likewise, if the melt composition is fixed, the temperature is not constrained.

Equilibrium crystallization. During equilibrium crystallization of a melt in the system $\text{CaAl}_2\text{Si}_2\text{O}_8 - \text{CaMgSi}_2\text{O}_6$, the first phase to crystallize depends on the starting composition. For example, consider a melt with the composition 40 percent diopside and 60 percent anorthite (composition X in Figure 2.6). During cooling the composition of this melt is unchanged until it hits the anorthite-melt liquidus at 1400°C and anorthite begins to crystallize. Extraction of a small amount of anorthite makes the melt richer in $\text{CaMgSi}_2\text{O}_6$, and crystallization ceases unless the temperature cools further. As the temperature continues to fall, more anorthite crystallizes out of the melt, making the melt progressively richer in $\text{CaMgSi}_2\text{O}_6$. Eventually, at the eutectic (1274°C), the melt becomes saturated in diopside and diopside crystallizes out along with anorthite. At this point, a small drop in temperature will cause the remaining melt to crystallize in a mixture of 60 percent diopside and 40 percent anorthite. If the initial melt has more diopside than the eutectic composition, then diopside is the initial mineral to crystallize. The composition of this melt becomes richer in $\text{CaAl}_2\text{Si}_2\text{O}_8$ and migrates toward the eutectic composition, where the final melt will crystallize.

Equilibrium melting. Equilibrium melting follows the same path as equilibrium crystallization but in reverse. A rock with diopside + anorthite begins melting at 1274°C, regardless of the proportion of diopside and anorthite in

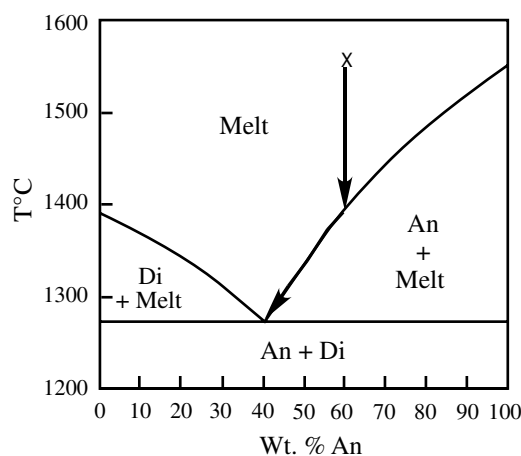


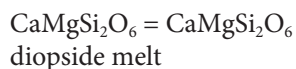
Figure 2.6 Phase diagram for the system $\text{CaAl}_2\text{Si}_2\text{O}_8 - \text{CaMgSi}_2\text{O}_6$ showing the crystallization path for a melt with composition X.

the rock. Rocks with different amounts of diopside and anorthite generate different amounts of melt at the eutectic, but all rocks in this system begin melting at the same temperature. Around the eutectic, a small increase in temperature produces extensive melting. If the rock contains more than 40 percent $\text{CaAl}_2\text{Si}_2\text{O}_8$, all the diopside melts during this eutectic event and with increasing temperature, the melt composition moves up the *anorthite + melt* liquidus as more anorthite melts. If the rock contains less than 40 percent $\text{CaAl}_2\text{Si}_2\text{O}_8$, anorthite is depleted and the melt moves along the *diopside + melt* liquidus as diopside melts.

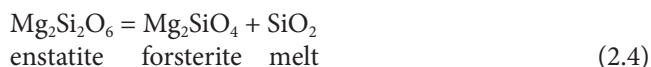
Fractional crystallization and fractional melting. In fractional crystallization, a crystal is removed from communication with the melt as soon as it forms. In systems such as $\text{CaAl}_2\text{Si}_2\text{O}_8 - \text{CaMgSi}_2\text{O}_6$, the fractional crystallization path is the same as the equilibrium crystallization path because there is no reaction between the crystals and the melt. In fractional melting, the melt is extracted from the solids as soon as it forms. In the diopside – anorthite system the melt forms at the eutectic temperature (1274°C) with a composition 60 percent diopside and 40 percent anorthite. This melt composition is constant as long as diopside and anorthite are present. Once either diopside or anorthite is depleted, melting ceases until the temperature reaches the melting temperature of the residual phase, be it anorthite (at 1553°C) or diopside (at 1492°C).

2.4.2 Binary Systems with a Peritectic

Most minerals melt to form a liquid of the same composition as the solid, a process called **congruent melting**. For congruent melting, the reaction can be written:



However, not all minerals melt congruently. When enstatite, for example, is heated to its melting point, the melt is more silica rich than enstatite, and the remaining solid converts from enstatite to olivine. This process is called **incongruent melting**. The reaction for the melting of enstatite is called a **peritectic** reaction and can be written:



The phase diagram for the system Mg_2SiO_4 – SiO_2 is shown in Figure 2.7. As with the $\text{CaAlSi}_3\text{O}_8$ – $\text{CaMgSi}_2\text{O}_6$ diagram, a eutectic where melt reacts to enstatite and silica exists. In this system, however, an additional invariant point occurs where forsterite, enstatite, and melt coexist. This point is the peritectic and it represents the equality expressed by reaction (2.4). The difference between a eutectic and a peritectic is that at a eutectic, a melt reacts to form two solid phases, whereas at the peritectic, a solid phase reacts with the melt to form another solid phase. As the temperature falls through a peritectic, the solid phases in equilibrium with the melt change, but the melt is not necessarily consumed.

Equilibrium crystallization. Figure 2.8 shows an enlargement of the portion of the phase diagram for the system Mg_2SiO_4 – SiO_2 that contains the peritectic and eutectic. Equilibrium crystallization of melts that are more silica rich than point P will follow very similar paths to those of melts in the system diopside – anorthite. On cooling, the melt hits a liquidus, either the silica + melt liquidus or the enstatite + melt liquidus, at which point either silica or enstatite crystallize out, eventually driving the melt to the enstatite + silica eutectic (point E). However, if the bulk composition lay on the forsterite side of point P, then the crystallization process will be very different. For example, a melt with the composition X in Figure 2.8 begins crystallizing forsterite and, as crystallization proceeds, the composition of the melt is driven to progressively more silica-rich compositions

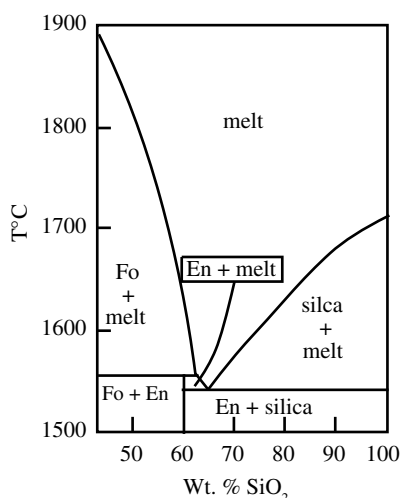


Figure 2.7 Phase diagram for the system Mg_2SiO_4 – SiO_2 (Bowen and Andersen, 1914).

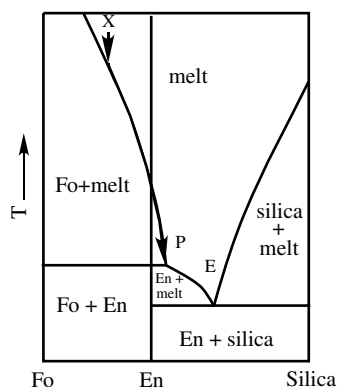


Figure 2.8 Phase diagram for the system Mg_2SiO_4 – SiO_2 showing the equilibrium crystallization path for a melt with composition X.

until the melt becomes more siliceous than enstatite. Even so, olivine continues to crystallize until the melt reaches the composition of the peritectic. At this temperature (1556°C), olivine reacts with the melt to form enstatite by reaction (2.4). This reaction proceeds until one phase is completely consumed. If the bulk composition of the melt lies between olivine and enstatite, the melt is used up resulting in the final assemblage of olivine + enstatite. Alternately, if the bulk composition of the melt lies between that of enstatite and P, the reaction at the peritectic consumes olivine and a small amount of melt remains. Continued cooling causes more enstatite to crystallize driving the melt to the eutectic (1543°C), at

which point silica and enstatite crystallize together until the melt is consumed.

Equilibrium melting. Equilibrium melting follows the inverse path of equilibrium crystallization. Melting of the assemblage quartz + enstatite begins at the eutectic (1543°C). If the solid assemblage has more quartz than the eutectic composition, enstatite is depleted by melting at the eutectic and the melt moves up the silica + melt curve until all the quartz is depleted from the rock. If the solid assemblage has more enstatite than the eutectic composition, quartz is depleted by melting at the eutectic and the melt moves up the enstatite + silica curve. If the rock contained less enstatite than the composition of the peritectic, then this mineral is depleted from the solid assemblage before reaching the peritectic. If the rock contained more enstatite than the peritectic composition (point P in Figure 2.8), then at 1556°C enstatite is entirely removed from the assemblage by reaction with the melt to form olivine. Melt then traverses the olivine-melt curve until attaining the same bulk composition of the original assemblage. If the original assemblage contained olivine + enstatite, then melting begins at 1556°C. After enstatite is depleted from the rock by peritectic melting, the melt composition moves along the olivine + melt curve. Melting ceases when the melt composition is the same as the original bulk composition of the system.

Fractional crystallization. In the system diopside – anorthite, it is unimportant whether the system undergoes equilibrium crystallization or fractional crystallization; the end product of crystallization is the same. In a system with a peritectic, however, the path followed during fractional crystallization is different from the trajectory followed during equilibrium crystallization. Equilibrium crystallization of a melt with a composition X will cease at the peritectic (point P in Figure 2.8), where all the melt is consumed by reaction (2.4). During fractional crystallization, the olivine is entirely extracted from the system as soon as it forms. As a result, when the melt reaches P, olivine is not available to react with the melt. Since olivine is absent, the melt moves down the liquidus past P, and enstatite begins to crystallize in place of olivine. Enstatite crystallization drives the melt to E, the enstatite-silica eutectic (Figure 2.9A). Thus, in fractional crystallization, all melts reach the eutectic regardless of initial composition.

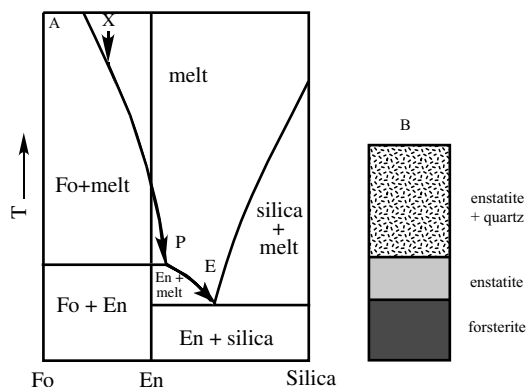


Figure 2.9 (A) Phase diagram for the system Mg_2SiO_4 – SiO_2 showing the path followed by fractional crystallization. (B) The sequences of mineral assemblages encountered in a hypothetical magma chamber of composition X that underwent fractional crystallization.

Whereas magmas that crystallize by the process of equilibrium crystallization form a rock with the same bulk composition as the original magma, magmas undergoing fractional crystallization form a series of rocks of different compositions. Consider what rock sequence would result if a melt of composition X was emplaced into a magma chamber and crystallized entirely by fractional crystallization (Figure 2.9B). If the first grains to crystallize, olivine, sink to the bottom of the magma chamber, they form a layer of pure dunite. As the subsequent melt crosses the peritectic, enstatite crystallizes and may accumulate above the olivine-rich layer. At the eutectic, the remainder of the melt crystallizes to an assemblage of 60 percent enstatite and 40 percent quartz. The sum of the abundances of olivine, enstatite, and quartz in this theoretical magma chamber will equal the initial bulk composition of the magma. Applying the lever rule defines the exact proportions of the minerals formed in Figure 2.9B. (In this calculation, keep in mind that the proportions calculated will be in weight percent because those are the units in which the phase diagram is plotted.)

Fractional melting. In fractional melting, a rock with the original assemblage enstatite + silica, melting begins at 1543°C (the eutectic temperature; Figure 2.7). If enstatite is depleted during melting, quartz melts next when the temperature reaches 1712°C. If quartz depletes during melting, the next melting occurs at the peritectic (1556°C) where enstatite converts to olivine. Further melting occurs

only when the temperature increases to the melting point of olivine (1890°C).

Petrologic importance. The peritectic reaction for the system $\text{Mg}_2\text{SiO}_4 - \text{SiO}_2$ is critical in igneous petrology because it provides a mechanism by which olivine-saturated melt can evolve to form silica-saturated rocks. Magnesian olivine and quartz are incompatible, yet it is not uncommon for olivine-bearing igneous rocks to evolve toward silica-saturated, residual melts. Because during fractional crystallization, a melt (even one with a complex composition) can pass through the orthopyroxene peritectic, it may produce a silica-enriched melt while leaving an olivine-rich residue behind.

2.4.3 Binary Systems with a Thermal Barrier

If a binary system has an interior phase that melts congruently, the resulting phase diagram has a **thermal barrier**. A phase diagram with a thermal barrier can be conceptualized as two binary phase diagrams, each of which has a eutectic, that are joined at the interior phase. A good example is the system $\text{NaAlSi}_3\text{O}_8 - \text{SiO}_2$, which has the interior phase albite (Figure 2.10). Albite melts congruently, meaning this system has two eutectics, one where the melt crystallizes to nepheline + albite and another where the melt crystallizes to silica + albite. As noted previously, the highest temperature at which any phase melts is when it melts to its own composition. Thus if a melt in the $\text{NaAlSi}_3\text{O}_8 - \text{SiO}_2$ system has the composition of pure albite, it will crystallize directly to albite. If however, a small amount of silica or nepheline is added to the system, the melt will crystallize at a lower temperature than the pure albite system.

Equilibrium Crystallization. Figure 2.11 details the system $\text{NaAlSi}_3\text{O}_8 - \text{SiO}_2$ to show the effect of a thermal barrier on equilibrium crystallization. Consider two melts, X and Y, that have very similar composition; X is slightly less siliceous than albite whereas Y is slightly more siliceous. Upon crystallizing albite, melt X moves toward Ne-rich compositions and eventually reaches the nepheline + albite eutectic. In contrast, crystallization of albite from melt Y drives the melt composition to more silica-rich compositions and eventually to the albite + silica eutectic. Because crystallization of the melt always involves extraction of albite, there is no way a melt can move from the silica-saturated field to the nepheline-saturated field, making the albite composition a thermal barrier. Since a

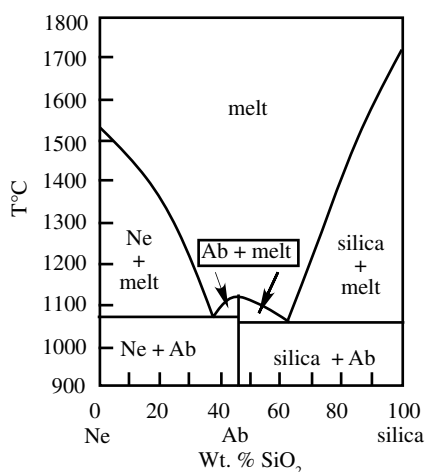


Figure 2.10 Phase diagram for the system $\text{NaSiO}_4 - \text{SiO}_2$ (Schairer and Bowen, 1956).

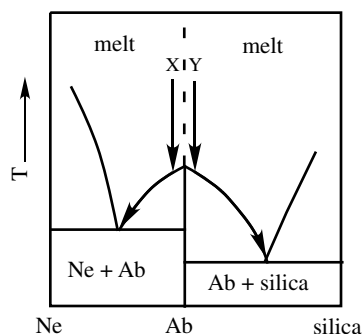


Figure 2.11 Phase diagram for the system $\text{NaSiO}_4 - \text{SiO}_2$ showing how crystallization of two melts with similar compositions can produce very different residual melts.

system with a thermal barrier is simply a system with two eutectics, the paths followed by fractional crystallization, equilibrium melting, and fractional melting will be similar to those observed in a system with a single eutectic.

Petrologic importance. The thermal barrier represented by the albite composition plays an important role in the evolution of igneous rocks. As noted previously, in the system $\text{Mg}_2\text{SiO}_4 - \text{SiO}_2$, fractional crystallization may drive melts across the olivine-orthopyroxene peritectic, allowing melts to evolve from an olivine-saturated composition to a quartz-saturated one. However, because albite imposes a thermal barrier, there is no similar way a nepheline-saturated melt can evolve to quartz-saturated compositions by fractional crystallization. The thermal barrier means that two basaltic melts with only slightly different compositions (one slightly silica saturated and one slightly nepheline saturated) will evolve two distinctly different residual

melts, one rhyolitic (equivalent to the albite-silica eutectic in Figure 2.11) and the other phonolitic (equivalent to the nepheline-albite eutectic in Figure 2.11).

2.4.4 Binary Systems with Solid Solution

A binary system involving two end members that have complete solid solution can have only two phases, a melt and a solid, both of which are solutions between compositional extremes. The system never has three phases, so it cannot have a eutectic because a binary eutectic requires two solid phases and the melt phase. A phase diagram for this system displays two univariant lines: one is the **liquidus**, which gives the composition of the liquid at any given temperature, the other is the **solidus**, which gives the composition of the solid. Good examples of binary systems with solid solutions are the melting relations of the plagioclase ($\text{CaAl}_2\text{Si}_2\text{O}_8 - \text{NaAlSi}_3\text{O}_8$) and olivine ($\text{Mg}_2\text{SiO}_4 - \text{Fe}_2\text{SiO}_4$) series (Figure 2.12). When the plagioclase solid solution melts, the melt is always more sodium rich than the coexisting plagioclase mineral (Figure 2.12A). Similarly, an olivine in equilibrium with a melt is always more iron rich than the associated melt (Figure 2.12B). The crystallization and melting relations can be illustrated in the olivine system, although the relations are the same for the plagioclase system.

Equilibrium crystallization. In the system $\text{Mg}_2\text{SiO}_4 - \text{Fe}_2\text{SiO}_4$, a cooling melt of the composition x (Fo_{75}) will begin to crystallize at around 1790°C (see Figure 2.13A). The olivine that crystallizes from this melt has the composition o_1 (approximately Fo_{90}). As cooling proceeds, the extraction of magnesian olivine enriches the melt in iron. In equilibrium crystallization, olivine remains to react with the melt, so the olivine present becomes more iron rich as well. Both the olivine and the melt become more iron rich (see heavy arrows in Figure 2.13A). Although both olivine and melt progressively more iron rich, the bulk composition of the system does not change because the abundances of olivine and melt change in tandem. Olivine becomes more abundant and melt becomes less abundant until, at 1628°C , olivine (o_2) matches the composition of the bulk system (Fo_{75}). The last melt to crystallize at this temperature (m_2) has the composition Fo_{44} .

Fractional crystallization. If the $\text{Mg}_2\text{SiO}_4 - \text{Fe}_2\text{SiO}_4$ system undergoes fractional crystallization, each batch of crystallizing olivine is removed from reaction with the

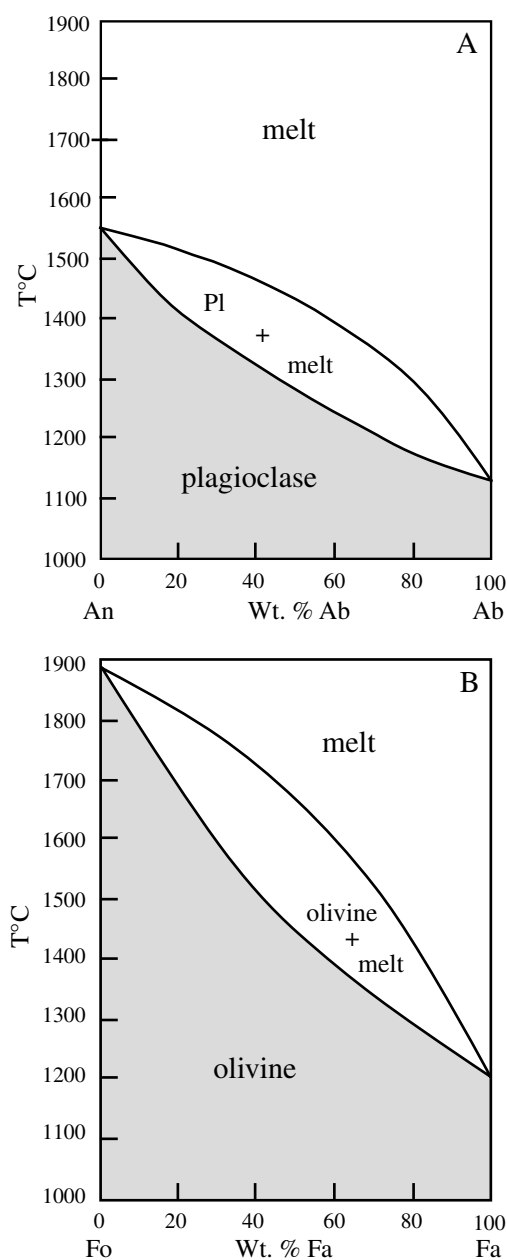


Figure 2.12 (A) Phase diagram for the system $\text{CaAl}_2\text{Si}_2\text{O}_8 - \text{NaAlSi}_3\text{O}_8$ (Bowen, 1913) (B) Phase diagram for the system $\text{Mg}_2\text{SiO}_4 - \text{Fe}_2\text{SiO}_4$ (Bowen and Schairer, 1935).

melt. As with equilibrium crystallization, the first olivine to crystallize from a melt of Fo_{75} will be Fo_{90} . Subsequent removal of this Fo_{90} olivine will make the melt more Fe rich. However, because the olivine does not react with the melt, fractional crystallization causes the melt to move all the way to Fo_0 . After crystallization ceases, rather than having a rock with olivine of a single composition,

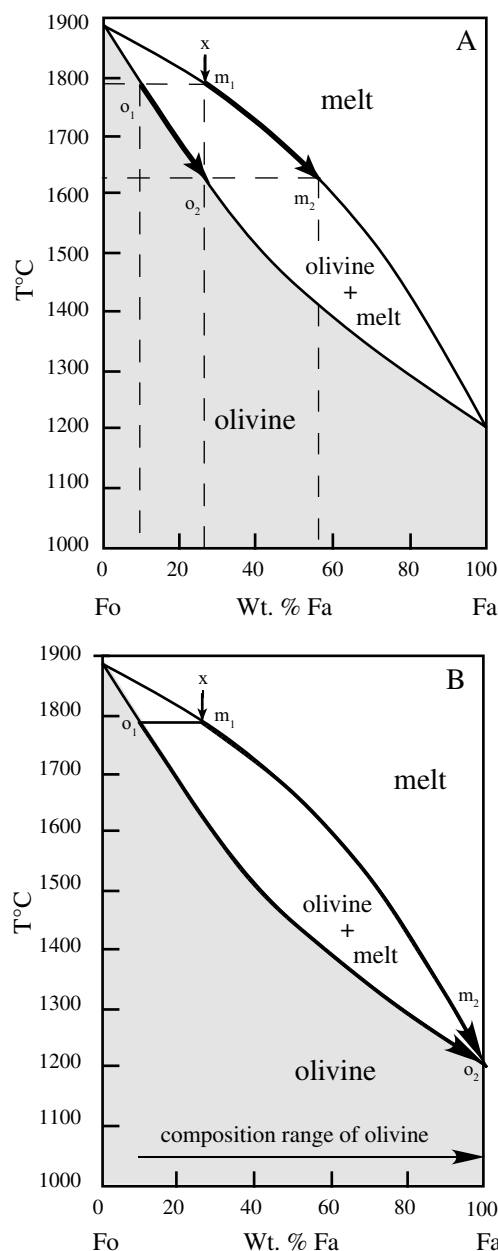


Figure 2.13 Phase diagram for the system $\text{Mg}_2\text{SiO}_4 - \text{Fe}_2\text{SiO}_4$ showing the path followed by a melt with composition x during (A) equilibrium crystallization and (B) fractional crystallization.

the rock contains olivine with a composition that ranges across the spectrum, from Fo_{90} to Fo_0 (Figure 2.13B).

Equilibrium and fractional melting. Melting is the inverse of the crystallization processes. During equilibrium melting, olivine of Fo_{75} generates a melt with Fo_{44} and proceeds with olivine becoming simultaneously less abundant and more magnesian. Melting ceases when the

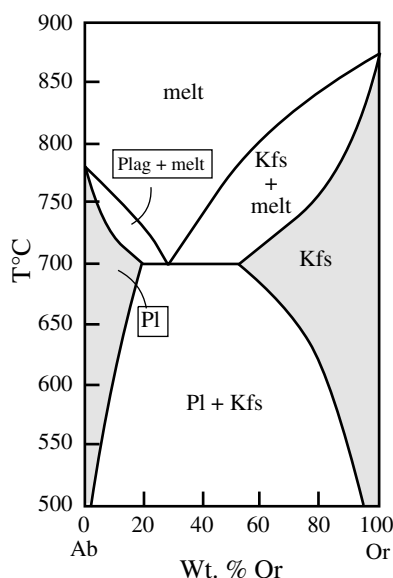


Figure 2.14 Phase diagram for the system $\text{NaAlSi}_3\text{O}_8 - \text{KAlSi}_3\text{O}_8$ at high water pressures (Morse, 1970).

last bit of olivine has melted, at which point the olivine will be around Fo_{10} . Fractional melting is complementary to fractional crystallization. As with equilibrium melting, the first melt to form from an olivine of Fo_{75} will be Fo_{44} . This melt, however, will be extracted from the system so any olivine that melts as T will be more Mg-rich than Fo_{75} . The residual olivine becomes more magnesian as melting progresses until the last olivine to melt has a composition of Fo_{100} .

Petrologic importance. Fractional crystallization of olivine (or any ferromagnesian mineral) extracts magnesium preferentially from a melt, leaving the melt relatively enriched in iron. Olivine easily equilibrates with the melt by simple exchange of Fe and Mg, and zoned olivines are rare in igneous rocks. Because of this phenomenon, most differentiated rocks evolved in this system are enriched in iron relative to magnesium. Fractional and equilibrium crystallization of plagioclase follows processes similar to fractional and equilibrium crystallization of olivine. The first plagioclase to crystallize is more calcic than the coexisting melt (Figure 2.12A), and both the plagioclase and the melt will become more sodic as crystallization proceeds. Plagioclase commonly does not equilibrate easily with the melt, because doing so requires the exchange between calcium and aluminum in the plagioclase and sodium and silicon in the melt. Since both the aluminum and silicon are tightly bound in the tetrahedral site,

equilibration is very slow. This slow diffusion explains why zoned plagioclase is so commonly encountered in igneous rocks, as well as why evolved rocks are enriched in sodium relative to calcium.

2.4.5 Binary Systems with Partial Solid Solution

Systems with partial solid solution phases have phase diagrams similar to those that show complete solid solution; both have a liquidus and a solidus. A good example is shown in Figure 2.14, which diagrams the system $\text{KAlSi}_3\text{O}_8 - \text{NaAlSi}_3\text{O}_8$ at high water pressure. This system contains a eutectic corresponding to the point where the last melt crystallizes to a mixture of K-feldspar and albite, as well as two liquidus lines (one for the melt in equilibrium with albite and one for melt in equilibrium with K-feldspar), two solidus lines, and two **solvus** lines that reflect the extent of the solid solution of sodium in orthoclase and potassium into albite. The K-feldspar that crystallizes at the eutectic contains about 45 percent albite and albite that crystallizes at the eutectic contains 20 percent orthoclase. If the original melt contained less than 45 percent albite, the melt crystallizes to K-feldspar solid solution in much the same way that a melt in the system albite – anorthite crystallizes to a plagioclase solid solution. Likewise, if the melt contained less than 20 percent K-feldspar, an albite solid solution will crystallize without the melt ever reaching the eutectic.

The last melt present during crystallization of a melt that originally had a composition with between 20 percent and 55 percent orthoclase will reach the eutectic. Unlike the system shown in Figure 2.6, where the solid phases have fixed compositions, both albite and K-feldspar will change composition during crystallization. If the melt composition lies to the orthoclase-rich side of the eutectic, the first phase to crystallize will be K-feldspar. As crystallization proceeds, both K-feldspar and the melt become enriched in Na until arriving at the eutectic. At the eutectic, albite with the composition $\text{Ab}_{80}\text{Or}_{20}$ begins to crystallize in equilibrium with orthoclase composed of $\text{Ab}_{45}\text{Or}_{55}$. If this system is rapidly cooled, as in volcanic rocks, the feldspars will retain their high-T compositions. However, if the system is slowly cooled, the feldspars will re-equilibrate along the solvus, with albite becoming more sodic and K-feldspar becoming more potassic.

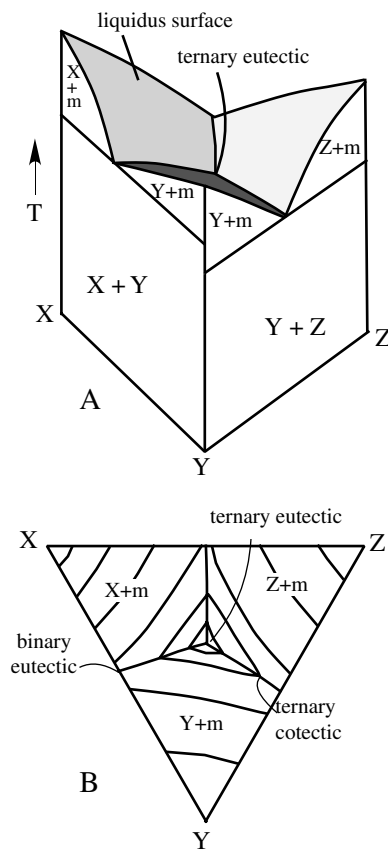


Figure 2.15 Ternary phase diagram for the system $x - y - z$. (A) Perspective view of ternary T-composition diagram. (B) Liquidus projection with thermal contours. After Cox, Bell, and Pankhurst (1979).

2.5 Phase Diagrams of Ternary Systems

Ternary systems involving a melt include four variables: temperature and three chemical components. Phase relations in this system are displayed on a three-dimensional diagram (Figure 2.15A) in which the base is an equilateral triangle that shows the compositional variation in the system. The temperature axis is perpendicular to this base. Each of the three sides of the diagram consists of a binary diagram. In Figure 2.15A these are the binary systems X-Y, Y-Z, and X-Z (note that the system X-Z lies at the back of Figure 2.15A). Each of the binary diagrams in Figure 2.15A is a simple binary with a eutectic. The alternative way to show phase relations in a ternary diagram is to use a **polythermal projection**, wherein temperature variation is drawn as contours (Figure 2.15B).

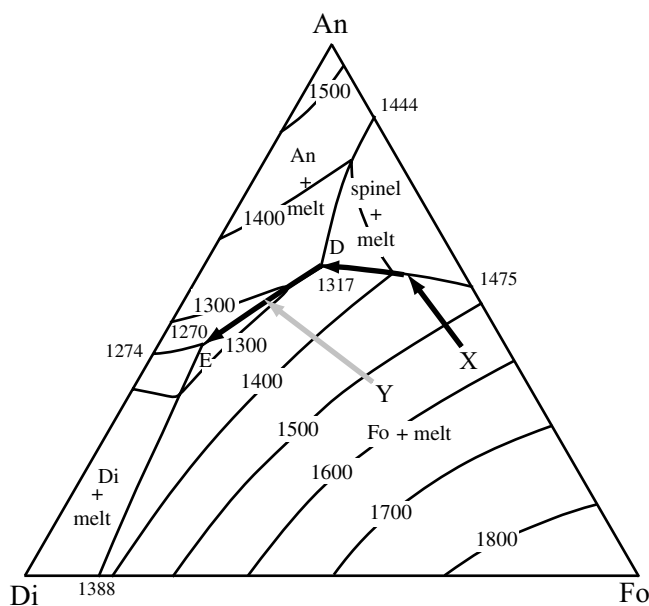


Figure 2.16 Ternary phase diagram for the system Fo – An – Di showing the crystallization path followed by melts of the composition X and Y. D = ternary peritectic and E = ternary eutectic. After Osborn and Tait (1952).

Just as an additional component causes depression of a freezing point in a one-component system, addition of a third component to a binary system causes depression of the temperature of a binary eutectic (Figure 2.15B). When a new component is added, the binary eutectic is no longer invariant; instead, it becomes univariant. This univariant curve is called a **cotectic**. Figure 2.15 shows three ternary cotectics that intersect at a ternary eutectic. As is the eutectic in a binary diagram, the ternary eutectic is an invariant point that reflects the lowest temperature at which a melt phase can exist.

2.5.1 The Ternary System

$\text{Mg}_2\text{SiO}_4 - \text{CaAl}_2\text{Si}_2\text{O}_8 - \text{CaMgSi}_2\text{O}_6$

The ternary system $\text{Mg}_2\text{SiO}_4 - \text{CaAl}_2\text{Si}_2\text{O}_8 - \text{CaMgSi}_2\text{O}_6$ is an analog for a basaltic melt. Figure 2.16 shows that the system has four, rather than three, fields of primary crystallization. In addition to fields of olivine + melt, diopside + melt, anorthite + melt, the system requires an additional field for spinel + melt. The composition of spinel lies outside of the Fo-An-Di compositional triangle. A system that has one or more phases that lie outside of the plane

of a ternary diagram is known as a **pseudoternary** system. Even though, strictly speaking, the system Fo – An – Di is pseudoternary, for most compositions it behaves like a true ternary system.

Equilibrium crystallization. Consider how crystallization proceeds for a melt with the composition X on Figure 2.16. The first crystals, olivine, form at temperatures slightly below 1600°C. As temperature falls, the crystallization of olivine drives the melt composition directly away from the olivine apex. At temperatures slightly above 1400°C, spinel joins olivine as a crystallizing phase. As temperature falls to 1317°C (at point D), spinel reacts with the melt to make forsterite + plagioclase. Point D is a ternary peritectic that is analogous to the binary peritectic in the system Fo – SiO_2 . A melt that was originally rich in spinel component is exhausted at the peritectic, whereas melts with a composition like X consume spinel by the peritectic reaction. At temperatures below 1317°C, olivine and plagioclase are the crystallizing phases and their crystallization drives the melt along the cotectic toward the eutectic (point E). At the eutectic (1270°C), diopside joins the crystallizing phases and olivine + diopside + plagioclase crystallize together until the melt is entirely consumed.

If the melt started with the composition Y on Figure 2.16, olivine crystallization forces the melt composition directly away from the Fo apex and toward the plagioclase-olivine cotectic (gray line in Figure 2.16). Melts of this composition miss the peritectic at point D and intersect the plagioclase-olivine cotectic at temperatures slightly below 1300°C. Plagioclase then joins the crystallizing assemblage, driving the melt composition to the eutectic.

Fractional Crystallization. As in simple binary systems, such as that illustrated in Figure 2.9, fractional crystallization produces a range of rocks from a magma of a fixed composition. Now, consider what happens to a melt of composition Y in Figure 2.17 during fractional crystallization. The olivine formed during initial crystallization stages sinks to the bottom of the magma chamber, accumulating a layer of dunite. Once the melt reaches the cotectic, fractional crystallization deposits a layer of plagioclase + olivine, producing a rock called a troctolite. Once the eutectic is reached, the residual melt crystallizes to an assemblage

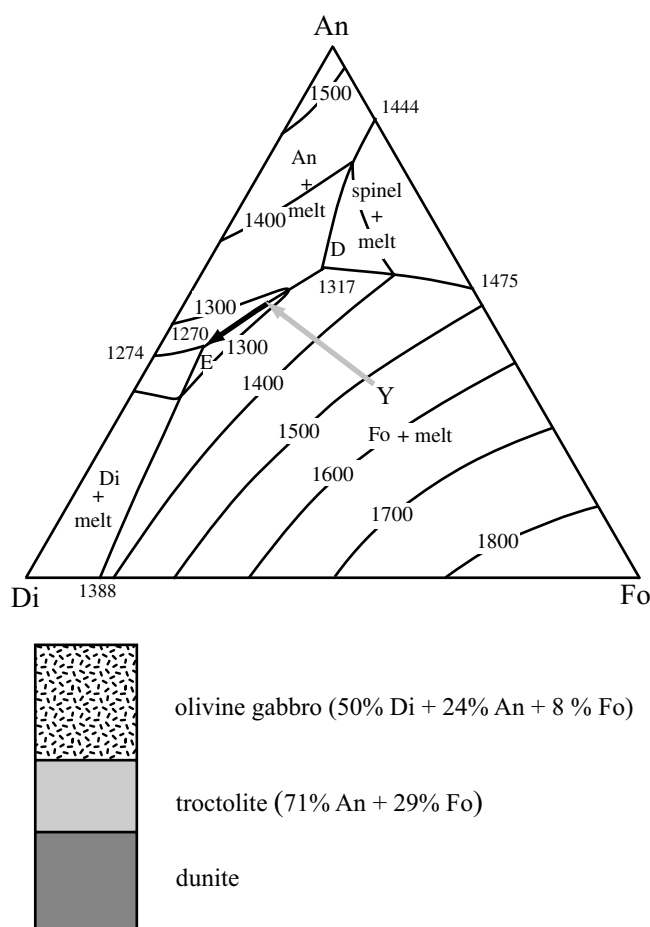


Figure 2.17 Ternary phase diagram showing the sequence of rocks produced from a melt with a composition Y that has undergone fractional crystallization and crystal settling. Mineral proportions are determined from the lever rule.

of diopside, anorthite, and olivine, which together compose olivine gabbro. Although the layered sequence of rocks formed by this process (shown schematically in Figure 2.17) is an extreme simplification, it provides a good illustration of the kinds of crystallization processes that may form layered mafic intrusions discussed in Chapter 9.

2.6 Implications for Petrology

Phase diagrams from simplified systems provide considerable insight into how igneous melts crystallize and evolve. Most important, these display how igneous melts crystallize over a wide range of temperature. Primitive basaltic lavas erupt at temperatures around

1200°C, whereas granite melts may remain liquid at temperatures below 700°C, and melts of alkaline rocks may survive to even lower temperatures. Even in simple systems, crystallization occurs over a range of temperatures before the eutectic is reached; for example, melts with a composition X or Y in Figure 2.16 will crystallize over a range of 200° to 300°C. Phase diagrams show how eutectic melting can form a substantial amount of melt over a very small temperature range. Because natural silicate melts contain a large number of elements, true eutectic melting is probably a rare occurrence in nature but nevertheless, partial melting of silicate rocks may still generate a large amount of melt over a narrow temperature range.

The range of temperatures over which crystals and melts coexist provides ample opportunity for fractional crystallization. As noted earlier, two types of reactions allow melts to change composition during fractional crystallization. One is by means of peritectic reactions, the most important of which is the reaction between olivine and melt to make orthopyroxene (Figure 2.7). If olivine is preferentially extracted from a melt, it will cause silica to be enriched in the residual melt (Figure 2.9). The other is through continuous reactions such as those shown in Figure 2.12. Fractional crystallization of plagioclase will preferentially deplete Ca from the melt and leave Na behind. Similarly, fractional crystallization of ferromagnesian silicates will enrich the melt in Fe. For this reason, fractional crystallization of most melts will tend to produce residual melts enriched in SiO_2 and that have higher FeO/MgO and $\text{Na}_2\text{O/CaO}$ than the original melt.

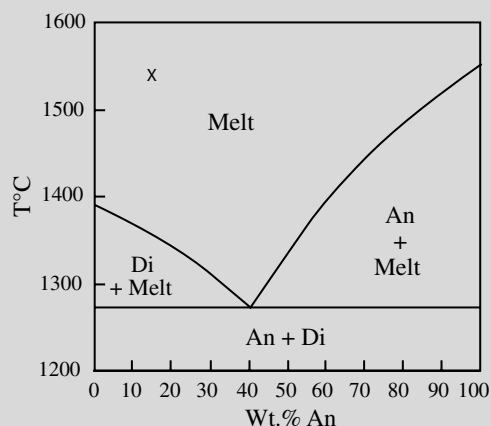
Finally, phase diagrams show that albite forms a thermal divide that cannot be crossed by fractional crystallization (Figure 2.10). This provides important insights into how nepheline-bearing rocks may form. Melts relatively poor in Na_2O will crystallize toward silica-saturated compositions (Figure 2.11). However, fractional crystallization of alkalic melts, which are rich in Na_2O , will follow a different trend. Rather than becoming more silica rich, alkalic melts may evolve progressively lower silica contents, with the result that nepheline will eventually crystallize (Figure 2.11). As with melts relatively poor in Na_2O , fractional crystallization will enrich alkalic melts in FeO/MgO and $\text{Na}_2\text{O/CaO}$.

Summary

- The melting temperature of most phases is decreased when additional components are added to the melt.
- In eutectic melting, large volumes of melt may be generated with small changes in temperature. Although true eutectic melts probably do not occur in nature, many common melts, such as basalts and granites, may be “eutectic-like.”
- Olivine-bearing melts may differentiate to silica-bearing melts, but nepheline-bearing melts cannot differentiate to quartz-bearing melts. Thus there are two distinct series of evolved igneous rocks, those that are silica-saturated and those that are nepheline-saturated.
- Differentiation via fractional crystallization enriches residual melts in Fe over Mg and Na (+ K) over Ca.

Questions and Problems

Problem 2.1. Figure P2.1 shows the phase diagram for the system diopside-anorthite.



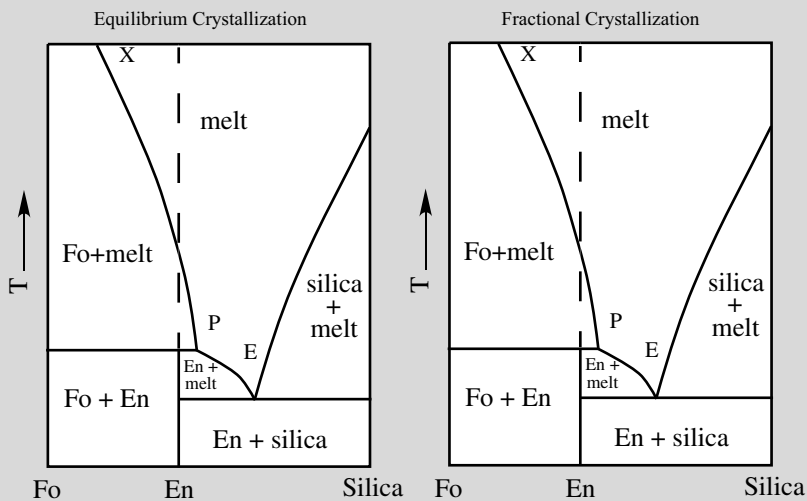
- 1) Draw the path of crystallization for a melt with composition X.
- 2) At what temperature does crystallization begin?
- 3) At what temperature does crystallization cease?
- 4) What is the composition of the melt at the eutectic?

Problem 2.2. Answer the following questions assuming fractional crystallization in the system illustrated on Figure P2.1.

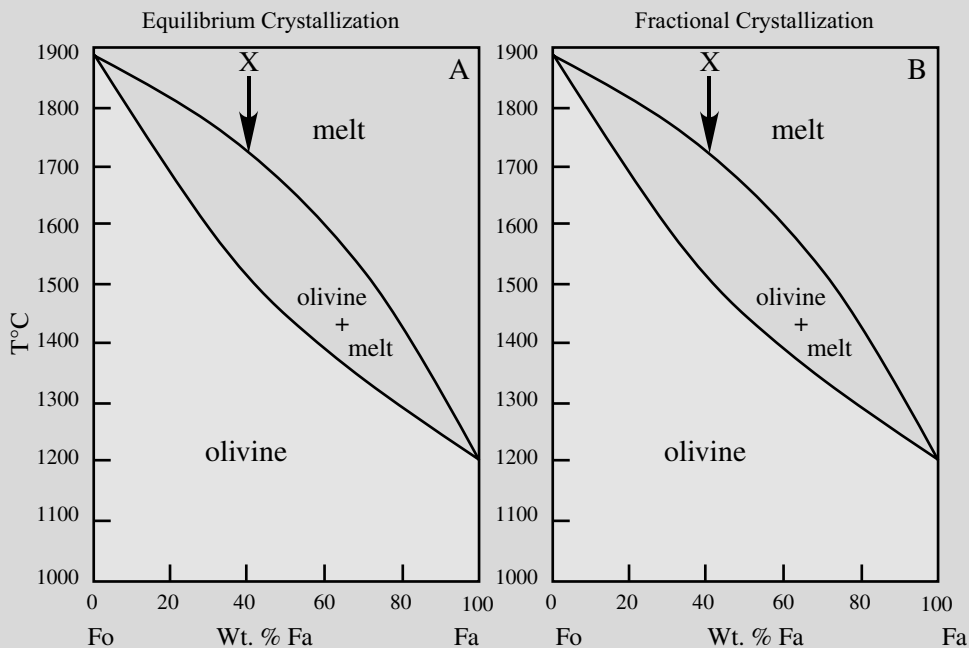
- 1) What proportion of the original melt will crystallize out as diopside before anorthite appears?
- 2) Sketch the layers and label the minerals found in each, assuming that as the melt underwent fractional crystallization the minerals that crystallized sank to the magma chamber floor.

Problem 2.3. Figure P2.2 shows the phase diagram for a portion of the system $\text{Fe}_2\text{SiO}_4 - \text{SiO}_2$. For both **equilibrium** and **fractional** crystallization:

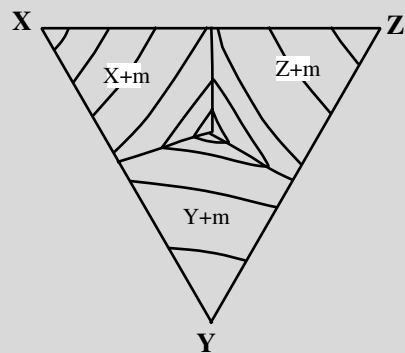
- 1) Show the path followed by the liquid composition and
- 2) What are the final minerals to crystallize? In what proportion are they?



Problem 2.4. Figure P2.3 shows phase diagrams for the system forsterite – fayalite. Show the path of the fluid composition for both equilibrium crystallization and fractional crystallization.



Problem 2.5. Figure P2.4 shows a ternary diagram for the hypothetical system XYZ.



1) Label:

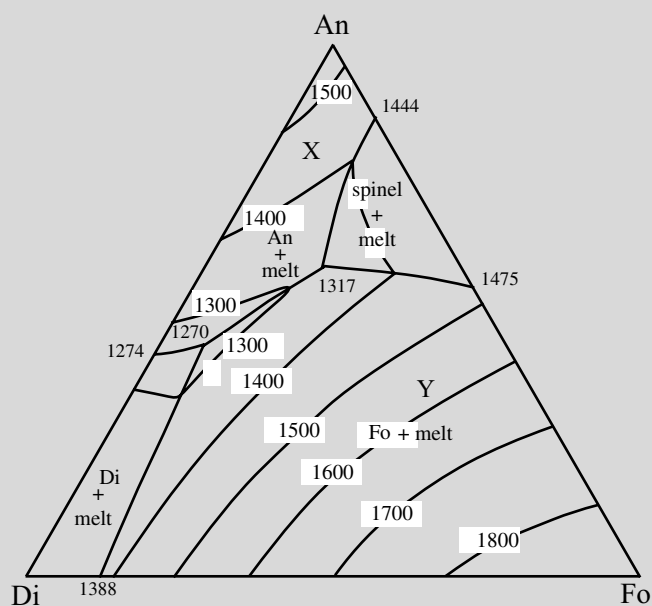
- a) the ternary eutectic
- b) the binary cotectic
- c) a binary eutectic

2) On the phase diagram in Figure P2.4, show the composition of the initial melts a, b, and c that will crystallize on each the following paths:

- a) Melt a – Z + melt – X + Y + melt – X + Y + Z
- b) Melt b – Y + melt – Y + Z + melt – X + Y + Z
- c) Melt c – X + melt – X + Y + melt – X + Y + Z

3) One of the crystallization paths listed on question 2 is impossible. Which is it?

Problem 2.6. Figure P2.5 shows the system An-Di-Fo and two melt compositions, X and Y.



- 1) Show the crystallization path followed by each melt during fractional crystallization.
- 2) Assume that fractional crystallization occurred and the crystals that formed sank to the bottom of the magma chamber. Show the sequence of rocks and relative proportion of minerals in each layer of rock formed by this process from each melt composition.

Further Reading

.....

Bowen, N. L., 1928, *The evolution of igneous rocks*. Mineola, NY: Dover.

Cox, K. G., Bell, J. D., and Pankhurst, R. J., 1979, *The interpretation of igneous rocks*. London: George Allen and Unwin, chapters 2 and 3, pp. 42–144.

Morse, S. A., 1980, *Basalts and phase diagrams*. Berlin: Springer-Verlag.

Chapter 3

Introduction to Silicate Melts and Magmas

3.1 Introduction

Igneous rocks form by crystallization of silicate melts.¹ As melt moves through the mantle and crust, it almost invariably carries crystals. These crystals may be minerals that crystallized from the melt as it cooled or they may be **xenocrysts**, foreign crystals incorporated into the melt from the rocks through which the melts ascended. This mixture of melt and crystals is called a **magma**.

Silicate minerals are highly ordered at the atomic scale, consisting of an oxygen framework in which the cations sit in two major types of sites: tetrahedral sites and octahedral sites. Tetrahedral sites contain Si (and to a lesser extent Al) and, depending on the mineral, they may occur as isolated tetrahedra or as linked tetrahedral (polymers) that form chains, sheets, or frameworks. The octahedral sites lie elsewhere in silicate structure and bond various tetrahedrally bonded polymers together. Cations typically found in octahedral coordination include Fe, Mg, Ca, and Na.

Silicate melts also have these structures at the molecular scale. When a silicate mineral melts, the long-range order disappears, but, unless the melt is taken to temperatures far above the liquidus, the short-range order is maintained. The octahedral and tetrahedral sites remain in the melt, but the polymers formed from the interlocked silica tetrahedra are discontinuous (Figure 3.1). The smaller ions, primarily Si, Al, and P, are called **network-forming ions** because they occupy the tetrahedral sites that help polymerize the melt. The larger ions (Fe, Ca, Mg, Na, etc.) are referred to as **network-modifying ions** because their presence will tend to depolymerize the melt. Because granites are rich in network-forming ions such as SiO_2 and Al_2O_3 , granitic melts consist of many linked tetrahedra and hence have a high degree of polymerization making them viscous. In contrast, rocks rich in network-modifying ions, such as basalt, are not strongly polymerized. Such melts will be more fluid than the granitic melts.

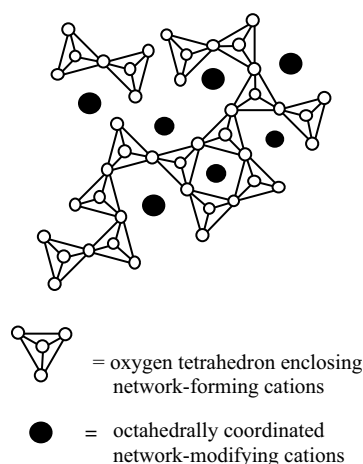


Figure 3.1 Schematic diagram showing the structure of a silicate melt. Small ions (Si and Al) occupy the silica tetrahedra and are called the network-forming ions; larger ions occur in sites outside the tetrahedral polymers and are called network-modifying ions.

3.2 The Role of Volatiles

The presence of volatile components (most commonly H_2O and CO_2) plays an important role in silicate melts. These volatiles not only affect the melting temperature of rock and the viscosity of the melt, they affect the processes that accompany melt ascent and solidification and provide an important mechanism for eruption of lavas.

3.2.1 Role of H_2O

Water plays a critical role in igneous petrology. Not only does water pressure determine the presence or absence of hydrous ferromagnesian silicates, the presence of water has a major effect on the properties of silicate melts. Water reacts with the bridging oxygens to break the silicate network (Figure 3.2) by a reaction such as:



Because of this behavior, H_2O is more soluble in the highly polymerized granitic melts than in the less polymerized basaltic melts. Furthermore, because solution of water into a melt depolymerizes the melt, addition of water to a silicate melt will decrease its viscosity.

The addition of water to a silicate melt also decreases the temperature of crystallization. The effect of water on the melting of albite is shown in Figure 3.3. Albite is a fairly good model for the melting of granite because both

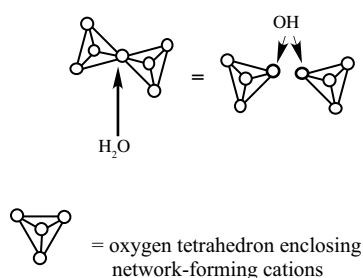


Figure 3.2 Diagram showing how the solution of H_2O into a silicate melt breaks silica polymers, replacing the bridging oxygen with OH.

albite and granite melts are dominated by network-forming elements. In a dry system, granite and albite will melt at very high temperatures (900°C or above). Increasing water pressure will cause melting to occur at progressively lower temperatures. This has an important effect on the behavior of melt in the crust. For example, a dry melt generated deep in the crust, such as at point A in Figure 3.3B, will become superheated as it rises in the crust because decompression leads it away from the dry solidus. Thus, it may be erupted at temperatures as high as 75°C above the solidus. In contrast, although a water-saturated melt (point B in Figure 3.3B) may form at low temperatures, it cannot move to much shallower levels without crystallizing. This means that any granitic melt emplaced into the crust or erupted on the surface must have been undersaturated in water at the depth where it was originally formed (point C, Figure 3.3B).

When a silicate melt crystallizes in the crust, the water originally bound into the melt structure is released as fluid. To understand the importance of this process, one must understand how the volume of water vapor changes as a function of pressure (Figure 3.4). At pressures above about 3,000 bars, the molar volume of H_2O in the melt is nearly the same as that in the fluid. Water exsolved from the melt at these pressures should disperse through the grain boundaries of the country rocks without much dilational effect. Melts emplaced at shallower levels (i.e., at lower pressures) will exsolve water that has a much higher molar volume. For example, melt crystallized at 1,000 bars will exsolve fluid with a molar volume more than three times larger than that of the H_2O dissolved in the melt. When such a melt crystallizes, the water released will hydrofracture the rock and produce a halo of veins around the intrusion. A melt crystallizing at 100 bars will

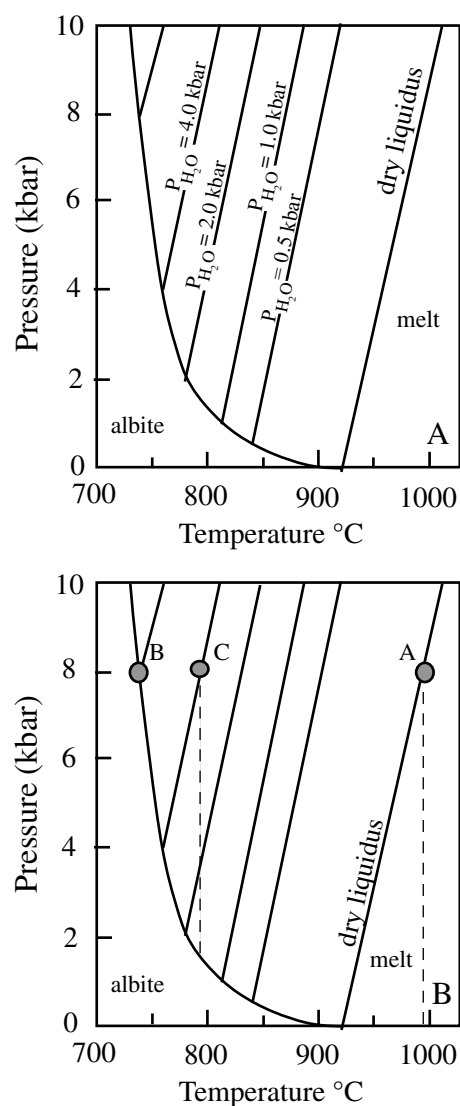


Figure 3.3 (a) Effect of water on the melting temperature of albite. (b) How the phase relations control the melting and movement of melts in the crust. The behavior of melts at points A, B, and C are discussed in the text. After Burnham (1979).

exsolve an aqueous fluid that occupies a volume nearly fifty times that of the H_2O dissolved in the melt. This volume change is so huge that melts crystallizing at shallow levels may exsolve water explosively, producing caldera-type eruptions.

3.2.2 Role of CO_2

Silicate melts contain dissolved water and carbon dioxide, as well as other volatile components such as halogens. Carbon dioxide may be the dominant volatile constituent

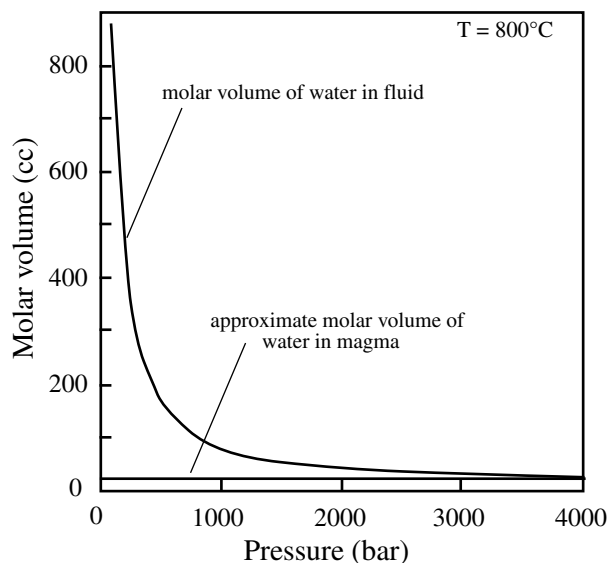


Figure 3.4 Comparison of molar volume of water in melt and in fluid at $800^\circ C$. Data from Burnham, Holloway, and Davis (1969).

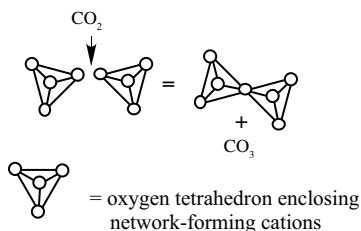
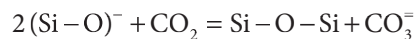


Figure 3.5 Diagram showing how the solution of CO_2 into a silicate melt enhances polymerization.

in melts at depth, whereas water may be incorporated into melts mainly as they pass through the crust. CO_2 -rich fluid inclusions are found in many volcanic and plutonic rocks. Therefore it is important to consider the effect of adding CO_2 on the viscosity of a melt. CO_2 dissolves into the melt by the following reaction:



As shown schematically in Figure 3.5, solution of CO_2 into a melt increases the polymerization of the melt.

Carbon dioxide has a greater solubility in melts with low polymerization, such as basalts, than in ones with few network modifiers, such as albite-quartz melts, because the

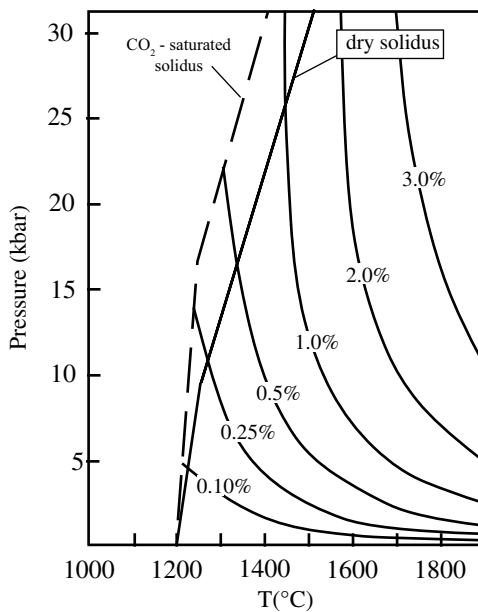


Figure 3.6 Solubility of CO_2 into tholeiitic basalt. After Spera and Bergman (1980).

latter have few nonbridging oxygens with which the CO_2 may bond. Like water, solubility of CO_2 into a melt lowers its melting temperature (Figure 3.6). However, the effect of CO_2 on the melting temperature of a silicate rock is far less extreme than that of water because CO_2 has a much lower solubility. CO_2 is most soluble in basaltic melts at high pressure. This means that as a basaltic melt rises in the crust it will exsolve CO_2 . By the time the melt erupts it will consist of a mixture of silicate melt and CO_2 -rich vapor. This vapor can become one of the major driving forces for eruption of basaltic melts, and indeed the most abundant volatiles emitted during volcanic eruptions are H_2O and CO_2 .

3.3 Physical Properties of Magma

3.3.1 Temperature

Magma temperatures are difficult to measure directly. The temperature of flowing lavas or lava lakes can be measured with a pyrometer or with a thermocouple, and these direct measurements are supplemented with experimental determinations of silicate melting temperatures in the laboratory. The temperature of intrusive magmas is even harder to determine, and for these petrologists rely on experimental results and temperatures calculated from the compositions of coexisting minerals.

Extrusion temperatures for lavas are mostly in the range of 800° to $1,200^\circ\text{C}$. The temperature of basaltic magma is higher than that of rhyolitic magma. Basalts are rarely much hotter than the temperature at which their first minerals crystallize; that is, they are rarely superheated. In contrast, some rhyolites may erupt at temperatures up to 200°C above their liquidus temperature. The temperature of intrusive magmas is probably lower than that of extrusive lavas. Water plays a role in this relationship because the solubility of water in silicate melts increases with increasing pressure. The increased water content of plutonic rocks has the additional effect of depressing liquidus temperatures to the extent that some granitic magmas may have been intruded at temperatures around 700°C .

3.3.2 Heat Capacity and Heat of Fusion

Heat capacity, C_p , is defined as the amount of heat that must be added to raise the temperature of one gram of melt by one degree Celsius. Mathematically this is expressed as:

$$C_p = dH/dT$$

where dH is the amount of heat (enthalpy) that must be added and dT is the change of temperature. Another heat term involved in producing igneous melts is the heat of fusion, dH_f . This variable defines the amount of heat that must be added to a rock already at the melting temperature to produce one gram of melt. One unusual feature of silicate melts is the great difference in these two quantities. C_p is typically 0.3 cal/g deg for most rocks, whereas dH_f is typically $65\text{--}100 \text{ cal/g}$. This means it takes about the same amount of heat to melt a given mass of rock as it takes to raise its temperature by 200° or 300°C (McBirney, 1993). This huge heat of fusion makes ascending magmas an efficient means for moving heat through the crust. Crystallization of magmas in the deep crust releases heat necessary for high-grade metamorphism, whereas at shallow crustal levels, crystallization may provide the heat that drives hydrothermal circulation associated with many ore deposits.

3.3.3 Viscosity

The viscosity of a melt is a measure of its resistance to flow. It is a function of a number of properties, most importantly the composition of the melt, including the types and amounts of dissolved gases such as H_2O and CO_2 , and its temperature. The viscosity of *magmas* is more complicated

than that of silicate *melts* because most magmas contain crystals suspended in the melt. These crystals vary in size and shape, which also affect viscosity. The density of suspended crystals is particularly important: viscosity may be very different when crystals are abundant (greater than >40 percent by volume) than in more dilute suspensions of crystals in melt (Petford, 2009). Although quantification is difficult, viscosity is an important control on fundamental igneous processes including the rate of magma transport in dikes and sills.

Disregarding the complexities introduced by crystal-bearing magmas, it is possible to gain a sense of the variations in viscosities by considering melts of different compositions and temperatures. The compositional control on viscosity of a given melt may be predicted to an extent by determining the ratio of network-forming ions to network-modifying ions. The extent of polymerization is given by the ratio R , which is the total number of oxygen atoms divided by the sum of the network-forming ions in the melt:

$$R = O / (Si + Al + P)$$

Smaller values of R indicate more polymerized melts, which will be more viscous than melts with larger R values, which indicate melts that are less polymerized and therefore more fluid. The range of R extends from around two for pure silica melts to four for a pure forsterite melt.

Viscosity is also temperature dependent: the higher the temperature, the less viscous (more fluid) the melt. Temperature is related to viscosity (η) by the Arrhenius equation:

$$\eta = Ae^{E/RT}$$

where A is a constant, E is the activation energy for viscous flow, R is the gas constant, and T is temperature. Activation energy correlates to R value and is higher for more polymerized melts (Scarfe, 1973). Experimental measurements of the viscosity of melts with different values of R show that rhyolitic melts will have a viscosity nearly 1,000 times higher than that of a tholeiite at the same temperature (Figure 3.7). Figure 3.7 also shows that the viscosity of a melt increases as temperature falls; between 1,200°C and 1,150°C the viscosity of tholeiitic melt nearly doubles.

The differences in viscosity of silicate magmas affect the shapes and processes associated with volcanic rocks. For example, basaltic magmas, which have low R values and

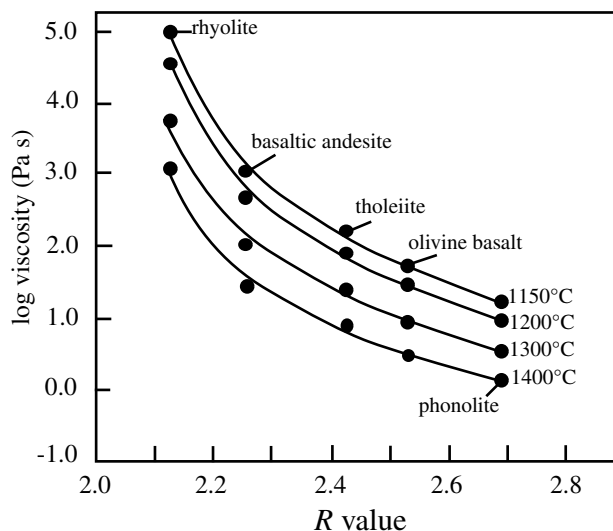


Figure 3.7 Relationship between viscosity, temperature, and composition of melts at 1 bar. After Scarfe (1973).

which are extruded at high temperatures, tend to be fluid (similar to ketchup; see Table 3.1) and may flow for long distances, forming shield volcanoes or flood basalts. In contrast, rhyolite magmas, which have high R values and are erupted at low temperature, tend to have high viscosity, and their behavior is more akin to Silly Putty (Table 3.1). Rhyolitic magmas may form steep-sided domes or, if the magma is too viscous for gas to escape, they may erupt explosively.

3.3.4 Density

Density is an important property that affects the behavior of magmas in various ways: it is one of the factors controlling whether magmas rise through the crust, whether crystals settle out, and whether ions diffuse readily. The density of magmas varies from around 2.2 to 3.1 g/cm³. Density rises with increasing pressure; it falls with increasing temperature. In general, mafic magmas are denser than felsic ones, mainly because mafic magmas are typically richer in heavy oxides such as CaO and FeO, whereas felsic magmas are richer in lighter oxides such as SiO₂, Al₂O₃, and Na₂O.

3.4 The Ascent of Magmas

Most magmas are less dense than the surrounding country rocks, and therefore tend to ascend. The ascent velocity of a body of magma depends on its density and viscosity. At

Table 3.1 Viscosities of Magmas and Common Substances

Material	Viscosity (Pa s)	Wt. % SiO ₂	Temperature (°C)
ASE motor oil	2×10^1		20
Ketchup	$\sim 5 \times 10$		20
Basalt	$10\text{--}10^2$	45–52	1,200
Peanut butter	$\sim 2.5 \times 10^2$		20
Crisco®	2×10^3		20
Andesite	$\sim 3.5 \times 10^3$	58–62	1,200
Rhyolite	$\sim 10^5$	73–77	1,200
Rhyolite	$\sim 10^8$	73–77	800

Source: From Philpotts and Ague, 2009 and sources therein.

depth, magmas may ascend as diapirs, plastically deforming as they push aside the country rocks. The velocity of ascent is approximated by Stokes Law:

$$V = \frac{2g\Delta\rho r^2}{9\eta_w}$$

where V is the velocity, g = the force of gravity, r is diapir radius, $\Delta\rho$ is the density contrast between wallrock and magma, and the viscosity subscript refers to the wallrock (w). From this equation it is clear that velocity is greatest for magma bodies of large size and when magmas ascend through wallrocks with low viscosity.

Magmas may also rise through fractures, forming sheet-like intrusions known as dikes. In this situation, the buoyancy force causing the magma to rise is sufficient to fracture the rock. The fractures may be the site of multiple intrusions of magma, which may be of similar or contrasting composition. A set of subparallel dikes, usually composed of basalt, is referred to as a dike swarm (Map 1.1). Radial dikes may emanate from a central magma body, such as the conduit feeding a volcano (Figure 1.14). Magmas cool as they fill fractures to form dikes because dikes commonly have a very large ratio of surface area to volume. If enough magma travels along a fracture, the wall rock may be thermally eroded, and a more cylindrical conduit may form. Cylindrical geometry is much more favorable for transporting magma with a minimum of heat loss, and it is the common shape of kimberlite diatremes.

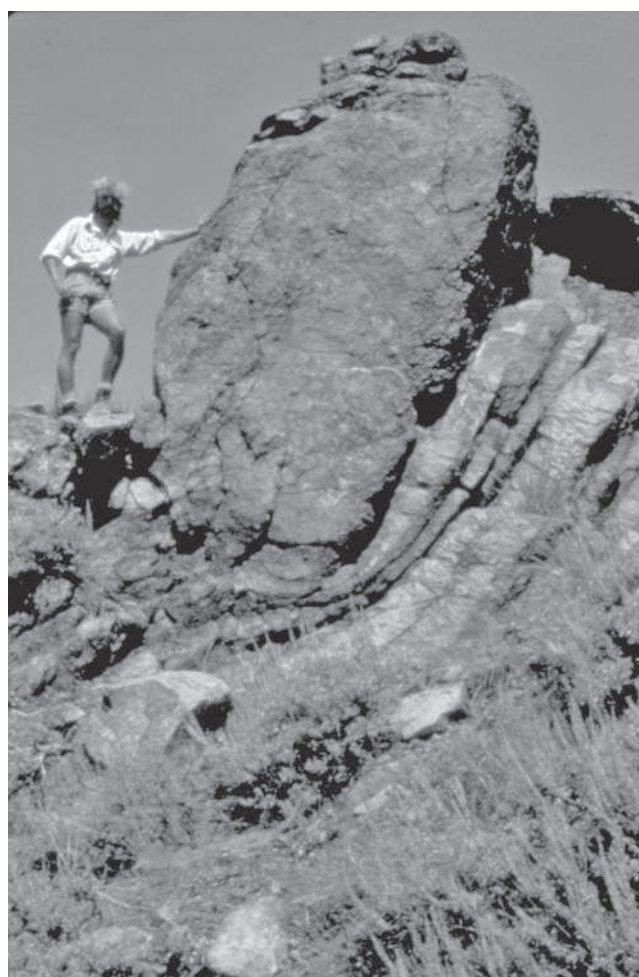


Figure 3.8 Stopped block of gabbro that sank through the magma chamber, where it deformed layers of anorthosite accumulating on the magma chamber floor. Laramie anorthosite complex, USA.

At shallow levels, magma ascent may be primarily by **stopping**. In this process, wallrocks are fractured and founder into the magma (Figure 3.8). The magma loses heat both to the wall rock and by assimilation of the stopped blocks. For this reason, it is unlikely that magmas ascend great distances by this process, and ascent by stopping may be limited to the uppermost few kilometers of the magma's rise.

Because not all magma bodies will be of the appropriate temperature, size, density, or viscosity to rise all the way to the surface of the earth, it is worth remembering that those magmas extruded on the surface may not be representative of magmas formed at depth.

3.5 Magmatic Differentiation

Magmatic differentiation refers to all the mechanisms by which a parent magma may give rise to igneous rocks of various compositions. These processes include the crystallization of mineral phases and separation of the residual liquid (fractional crystallization), separation of two melts (liquid immiscibility), mixing of separate magmas, and assimilation of country rock either as a solid or as a partial melt into the parent magma. It is also possible to produce a diversity of rock types by partially melting solid rock and removing the melt, leaving behind a refractory residue. Because magmas originate by processes of melting, these mechanisms will be examined first.

3.5.1 Partial Melting

Partial melting, also referred to as *partial fusion* or *anatexis*, is the process by which melt is produced in a proportion less than the whole. Partial melting can be considered by examining the two end member models introduced in the discussion of phase diagrams in Chapter 2:

Equilibrium melting. The partial melt that forms continually reacts and equilibrates with the remaining solid until the moment the melt is removed. Up to the point of segregation, the bulk composition of the system remains constant.

Fractional melting. The partial melt is removed in infinitely small increments so that it cannot interact with the residual solid. The bulk composition of the solid continually changes because melt, which is of a different composition than the initial solid, is lost from the system.

Which of these end member processes most closely approximates partial melting in nature will depend on the ability of the melt to separate from the residual crystals. This in turn depends on many factors that control the microscopic geometry of the partial melt within the solid rock. Models of melt production and segregation in the mantle suggest melts can escape from the solid matrix after relatively small degrees of melting. Assuming that compaction drives expulsion of partial melt, MacKenzie (1984) suggested melt will be expelled once the melt represents 3 percent or more of the total volume. MacKenzie and O’Nions (1991) present

evidence based on the inversion of rare earth element concentrations that melt segregation in the mantle can occur when melt fractions are less than 1 percent. More recently, Rabinowicz and Toplis (2009) considered the combined effect of shear segregation related to the ductile flow of the mantle and compaction, and determined that, depending on the viscosity of the solid mantle, basaltic melts will be expelled at melt fractions between 3.5 and 10 percent.

3.5.2 Crystallization Processes

Crystallization of solid phases from a melt also presents opportunities to form rocks of a different composition than the original melt. Like partial melting processes, crystallization can be considered by examining the two end member models discussed in Chapter 2:

Equilibrium crystallization. Crystals remain in contact with the residual liquid after they form and continually react and equilibrate with the liquid. In this case, the bulk composition of the final solids are the same as the original melt composition, and no magmatic differentiation takes place.

Fractional crystallization. Crystals are removed from the residual liquid as soon as they are formed, either by gravitational settling or floating. In this process, the bulk composition of the remaining liquid changes as crystals form and are removed.

It is possible to segregate liquid from crystals by mechanisms other than gravitational separation. The liquid remaining before crystallization may be complete and can be squeezed out in a process called **filter pressing**. A buoyant liquid in a mush of loosely packed crystals may migrate to a zone of lower pressure, just as water is driven out of a pile of accumulating and compacting sediments. Another mechanism, **flow segregation**, may separate crystals from the remaining melt during flow through a dike or along the walls of a pluton. Nearest the contact with country rock, the velocity gradient is steepest and a zone of maximum shear is present. This shearing results in a force that tends to drive crystals out of the zone of maximum shear and toward the interior of the flow. Crystals are thus found in the areas of lowest velocity gradient; in a dike they may be concentrated in the center, and the margins of the dike are much finer grained.

3.5.3 Liquid-Liquid Fractionation

Magmas may become compositionally zoned by two different processes: boundary layer fractionation and immiscibility. **Boundary layer fractionation** results when the magma along the margins of the chamber acquires a density different from the rest of the magma, either by absorption of water from the country rocks or by partial melting or crystallization. This liquid then rises and collects under the roof of the magma chamber, or less commonly may sink and collect at the bottom. This process was important in the formation of the Bishop Tuff, an extensive, compositionally stratified deposit distributed over much of the western United States. The 0.77-million-year-old tuff is postulated to have been erupted from a compositionally zoned magma chamber beneath what is now Long Valley caldera in southern California (Hildreth, 1979). Because of the high viscosity of silicic magmas, crystal settling is unlikely to be an effective process of magmatic differentiation. Instead, Hildreth proposed that absorption of water from the wall rocks produced a water-enriched boundary layer that was less dense than the magma in the interior of the chamber. This magma rose to the top of the chamber, producing a compositionally stratified magma chamber. Another boundary layer process that may produce stratification results from cooling of magma along the walls and roof. Crystallization of the cooler magma along the margin of the chamber may leave a less dense interstitial liquid that rises along the walls toward the top, where it forms a stratified cap to the magma chamber (Sawka, Chappell, and Kistler, 1990).

Certain melt compositions may separate into two or more **immiscible** (i.e., unmixable) liquids. Immiscibility is thought most common in mafic melts, which may separate into a sulfide liquid and a mafic silicate liquid. Immiscibility is also likely to occur in alkaline melts rich in CO_2 and that may separate into a high-alkali silicate liquid and a carbonate-rich liquid. Iron-rich basaltic melts may separate into a felsic silica-rich liquid and a mafic iron-rich liquid. If the two liquids formed have very different densities, then they may separate very effectively, as oil does from water. If the magma is very viscous and crystal-rich, the two liquids may not separate as well, and small droplets be evident in the interstices between early crystallizing minerals. Evidence of this process is preserved as solid inclusions of (Na, K) Cl

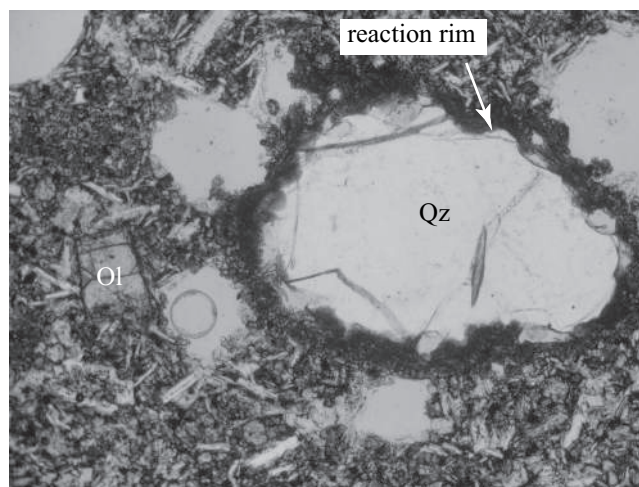
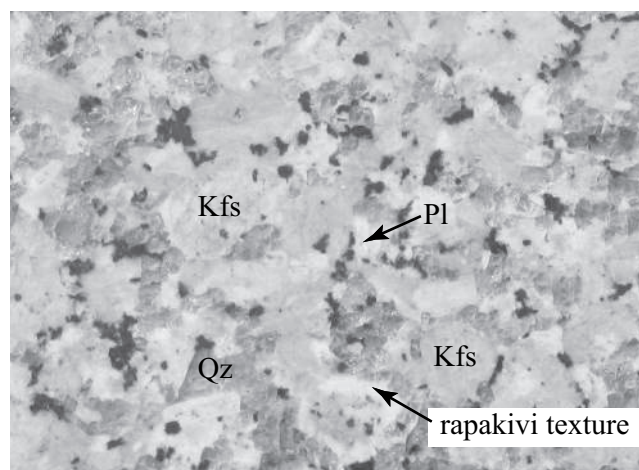


Figure 3.9 (A) Photo of alkali feldspar mantled with plagioclase (reverse zoning), a texture known as rapakivi texture. Mantled feldspars indicate a change in crystallization conditions. Ksp = alkali-feldspar, Pl = plagioclase, Qz = quartz. Sherman batholith, Wyoming, USA.. (B) Resorbed crystal of quartz (Qz) in an olivine-bearing (Ol) groundmass. The anhedral crystal shape and reaction rim around the quartz suggest that this crystal was entrained into a magma in which quartz was not stable.

in K-feldspar in the monzosyenites of the Laramie anorthosite complex, Wyoming, USA, which suggests these rocks formed from a magma that contained immiscible droplets of a chloride-rich melt (Frost and Touret, 1989).

3.5.4 Assimilation

Magmas may also change composition by assimilating material from their country rocks. *Assimilation*,

sometimes referred to as *contamination*, may occur in two ways:

Bulk assimilation occurs when blocks of wall rock are stoped into the magma and completely melt.

Assimilation of partial melts occurs when the wall rocks are heated to their solidus and begin to melt. It is important to remember that the composition of the first melts are usually different than the bulk composition of the rock, and hence the compositional effect on the magma is not identical to that from bulk assimilation.

Both assimilation of bulk rock and partial melt require thermal energy for melting. The melt necessarily becomes cooler, so much so that it may begin to crystallize. Crystallization releases heat of fusion, a positive feedback that helps assimilation proceed. Therefore assimilation is usually accompanied by crystallization (assimilation + fractional crystallization, often abbreviated as AFC).

Various textural features may evidence assimilation. Xenocrysts, crystals inherited from the country rock that would not normally be expected to crystallize from the melt, may be present. **Reversely zoned crystals**, such as plagioclase with calcic rather than sodic rims, suggest the melt has changed its composition and that the composition of the phases crystallizing from the melt has changed in a manner not normally associated with differentiation by simple fractional crystallization (Figure 3.9A). **Resorbed crystals**, those that show textural evidence of remelting may (but do not always) result from changes in melt composition, which may cause a previously crystallizing phase to be out of equilibrium with the contaminated melt (Figure 3.9B).

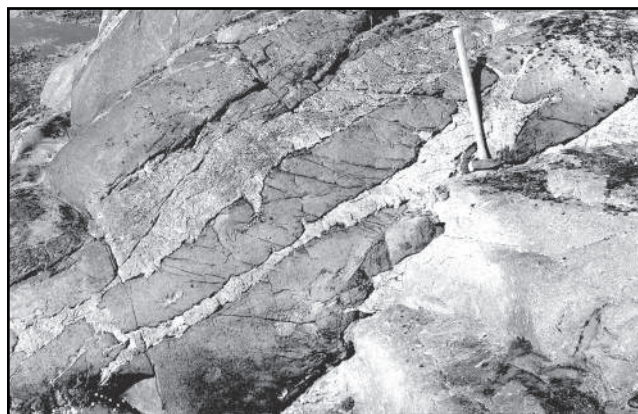


Figure 3.10 The Hortavær complex was constructed by multiple injections of diorite (dark lenses) intruded into a syenitic magma chamber (light-colored rock), north central Norway.

3.5.5 Magma Mixing

If two magmas are introduced into the same magma chamber, they may mix and form a magma of intermediate composition. The magmas may be independently derived, or may have formed by boundary layer fractionation and consequently rehomogenize. If the two magmas do not completely homogenize, then evidence of commingled melts may remain. Intrusion of denser mafic magma into a felsic magma chamber sometimes forms a sheet of mafic magma near the floor of the magma body. Thermal contrasts between the magmas cause the mafic magma to chill, forming lobate margins and other structures recording the presence of both mafic and felsic magmas within a chamber (Figure 3.10).

Summary

- Silicate melts are composed of network-forming ions, such as Si, Al, and P, that occupy tetrahedral sites. These form linked tetrahedra that polymerize the melt. Larger ions including Fe, Ca, Mg, and Na, form network-modifying ions that tend to depolymerize the melt. Granitic melts are richer in network-forming ions and are more strongly polymerized (and more viscous) than basaltic melts.
- The presence of H₂O in silicate melts tends to break the silicate networks and depolymerize the melt. Carbon dioxide has the opposite effect, and increases the polymerization of the melt.
- In general, mafic magmas are denser than felsic ones.
- Magma viscosity is a function of composition, temperature, and the kinds, quantities, and geometries of crystals present.

- Magmas are typically less dense than the surrounding rock, and hence have a tendency to rise. Magmatic ascent is an important mechanism to transport deep heat to the shallow crust.
- A diversity of igneous rocks can be produced by partial melting solid rock, extracting the melt, and leaving behind a more refractory residue. Partial melting may be fractional, in which infinitely small increments are removed from the remaining solid. Equilibrium melting describes the process by which partial melt continually reacts and equilibrates with the solid until melting is complete.
- A suite of igneous rocks with a variety of compositions may also form by equilibrium or fractional crystallization.
- Other processes that differentiate magmas include immiscible liquid-liquid fractionation, assimilation, and magma mixing.

Questions and Problems

Problem 3.1. Referring to the albite-H₂O system as an analog for granite (Figure 3.3), answer the following:

- How does increasing pressure affect the amount of H₂O that can be dissolved in a granitic melt?
- How does addition of H₂O affect the melting point of the granitic rock?
- What is the effect of dissolution of H₂O on the viscosity of the granitic melt?
- How does the ascent of a rising H₂O-saturated magma compare to that of a rising H₂O-undersaturated magma?

Problem 3.2. Aqueous fluids can be released during the late stages of crystallization of a magma in a magma chamber.

- Refer to Figure 3.3 to explain how crystallization at a constant pressure can lead a magma to become H₂O saturated.
- At what pressures might the aqueous fluid released hydrofracture the rock? Discuss your answer in terms of the molar volume of H₂O.
- Why might porphyritic texture result (like that shown in Figure 1.7D) when H₂O is lost from a magma body?

Problem 3.3. Use Stoke's Law to estimate the ascent velocity (in cm/s) of a magma diapir:

$$V = \frac{2g\Delta\rho r^2}{9\eta_w}$$

- Calculate ascent velocity for a 10 km diameter diapir with a density of 2.6 g/cm³ through mid-crustal wall rocks with a density of 3.0 g/cm³ and a viscosity of 10²¹ Pa s. (Recall that g = 980 cm/sec² for Earth and 1 Pa s = 10 g/cm s.)
- What will affect the ascent rate more: decreasing the diapir diameter to 1 km, or increasing viscosity of the wall rocks to 10²⁴ Pa s, a value representative of upper crustal rocks? Present calculations to support your answer. On the basis of these simple calculations, does diapiric ascent appear to be an effective mechanism for moving magmas through the upper crust?

Further Reading

.....

Hess, P. C., 1980, Polymerization model for silicate melts. In *Physics of magmatic processes*, ed. R. B Hargreaves. Princeton, NJ: Princeton University Press, 3–48.

McBirney, A. R., 2007, *Igneous petrology*, 3rd ed. Jones and Bartlett, Boston, Chapter 2.

Petford, N., 2009, Which effective viscosity? *Mineralogical Magazine*, 73, 167–91.

Winter, J. D., 2010, *Principles of igneous and metamorphic petrology*, 2nd ed., New York: Prentice Hall, Chapter 11.

Notes

.....

- 1 Almost all igneous rocks form from silicate melts, but there are rare exceptions. Carbonatites, for example, form from carbonate melts and some high-temperature sulfide deposits form from sulfide melts. Iron-oxide or Fe-Ti oxide melts have been postulated to form in some environments.

Chapter 4

The Chemistry of Igneous Rocks

4.1 Introduction

An important way of classifying suites of igneous rocks is by the variation in their chemical compositions. Indeed, igneous geochemistry is a complex field wherein major, minor, and trace element characteristics, as well as isotopic compositions, help determine the origin and evolution of igneous rocks. Most of this subject is beyond the range of an introductory course. However, because geochemistry is integral to the classification of igneous rocks, it is essential to provide an introduction to this topic.

The chemical formulas of the common rock-forming minerals are composed of relatively few elements referred to as **major elements**. Most rocks contain more than 1.0 weight percent of each of the major element oxides SiO_2 , Al_2O_3 , FeO and Fe_2O_3 , MgO , CaO , Na_2O , and K_2O . Because the major element composition of a rock reflects its mineralogy, major element oxide concentrations can be used to calculate what is referred to as the **normative mineralogy** of a rock. This topic is explained in the following section. **Minor elements** typically make up 0.1 to 1.0 weight percent of a rock. These include TiO_2 , MnO , and P_2O_5 . **Trace elements** compose less than 0.1 percent of a rock; they are expressed as elements as opposed to oxides and their concentrations are reported in parts per million by weight.

4.2 Modal Mineralogy versus Normative Mineralogy

The relative abundance of minerals in a rock is known as its **mode**. Modal abundances are expressed in volume percent. In rocks with individual minerals that can be distinguished by color, or that can be stained to mark minerals with distinct colors, the mode can be determined using image analysis programs. Modes can also be determined by *point-counting* under the petrographic microscope. In this method, the mineral under the cross-hairs is identified. The rock is advanced systematically a specific distance across the microscope stage, and successive minerals under the cross-hairs are identified in a grid of points. The total number of points occupied by each mineral is converted to a volume percent. Although it is relatively easy to obtain modal mineralogy for plutonic rocks using these methods, it is very difficult to do so with extrusive rocks, which are finer-grained and may partially consist of glass.

To help overcome the difficulties in obtaining modes for fine-grained rocks, four petrologists, C. Whitman Cross, Joseph P. Iddings, Louis V. Pirsson, and Henry S. Washington, introduced the **norm** (Cross et al., 1902). Their calculated mineralogical composition, based on the major element oxide abundances of the rock, is called the CIPW norm after the initial letters of their surnames. The CIPW norm calculations assume the melt crystallizes to anhydrous phases (olivine, pyroxenes, and Fe-Ti oxides); no hydrous phases are allowed. Biotite would be expressed as normative orthopyroxene + K-feldspar, hornblende by normative orthopyroxene + clinopyroxene + plagioclase. Therefore, unless the rocks are anhydrous, the norm will not include the same assemblage as the mode. Moreover, unlike the mode and the IUGS classification system, both of which are reported in volume percent, the CIPW norm is reported in weight percent. Nevertheless, normative calculations can be very helpful. Not only does the norm provide a means to compare plutonic rocks with volcanic rocks, it can also help demonstrate how the geochemistry of a rock reflects its mineralogy. For example, a corundum-normative granite contains more alumina than can be accommodated in feldspar alone, and a nepheline-normative rock does not contain enough silica to form quartz.

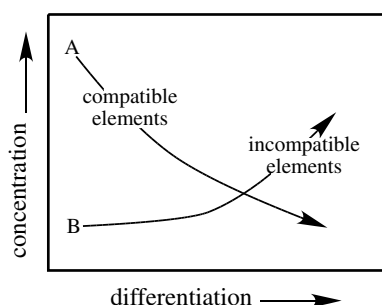


Figure 4.1 Diagram showing the behavior of compatible (path A) and incompatible (path B) elements during differentiation of a melt.

4.3 Variation Diagrams Based on Major Elements

Suites of igneous rocks, such as a series of lavas erupted from a single volcano, can be inferred to originate from a common parent magma. Thus, the variation in their compositions arises from magmatic differentiation. One of the main mechanisms by which a suite of rocks of different compositions may crystallize from a common parental magma is by crystal-liquid fractionation. As is clear from the phase diagrams examined in Chapter 2, crystallizing minerals incorporate certain elements into their structure and in doing so, leave behind melt of different composition.

Two common terms describe the behavior of elements during the differentiation of a melt. A **compatible** element is one that is preferentially fractionated from a melt into the crystallizing phases. In other words, the element is **compatible** with the crystallizing minerals. Because these elements are preferentially extracted during crystallization, the abundances of compatible elements in the melt should decrease with increasing fractionation (Figure 4.1, path A). In contrast, *incompatible* elements are not compatible with the crystallizing phases. Because they are preferentially retained in the melt rather than incorporated into crystallizing phases, the abundances of these elements in the residual melt should increase with increasing differentiation (Figure 4.1, path B).

Because each element behaves differently during magmatic differentiation, one way to assess differentiation in a suite of igneous rocks is to plot the weight percent of the various oxides in the rocks against some monitor of differentiation. Because the first minerals that crystallize

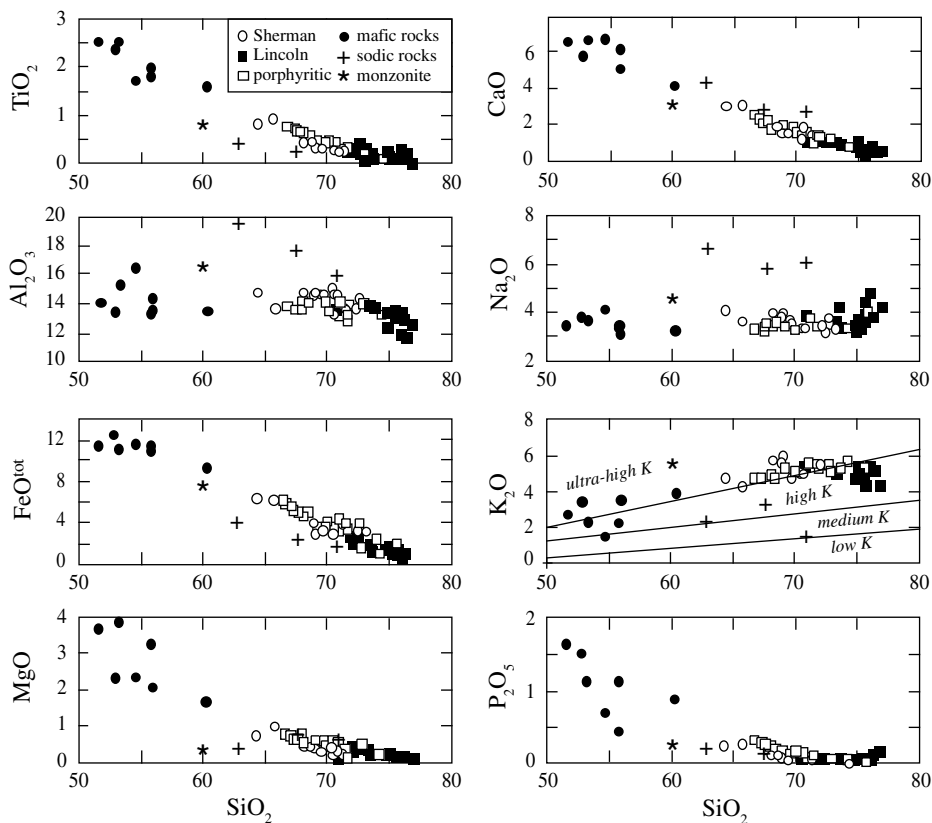


Figure 4.2 Harker diagrams showing the compositional variation in the Sherman batholith, Wyoming, USA. After Frost et al. (1999).

out of a mafic melt are silica poor (olivine has < 40 percent SiO_2 , calcic plagioclase has < 50 percent SiO_2), differentiation typically causes the residual melts to become enriched in silica (i.e., silica behaves as an incompatible element). Therefore, examining the variation of each element against the weight percent SiO_2 is a common strategy for monitoring differentiation in a series of related igneous rocks (Figures 4.2 and 4.3). Such diagrams are called Harker diagrams, after their inventor, Alfred Harker (Harker, 1909). In Harker diagrams, the weight percent of elements incorporated into early crystallizing phases, such as ferromagnesian minerals and calcic plagioclase (CaO , FeO , MgO , and TiO_2), tends to decrease with increasing silica content. Weight percent Al_2O_3 may also decrease with increasing SiO_2 , but the change commonly is not as extreme as for CaO or MgO . In contrast, the weight percent of the alkalis (Na_2O and K_2O) typically increases with increasing silica as these accumulate in the magma until alkali feldspars crystallize.

Harker diagrams cannot always illustrate the processes occurring during differentiation of basaltic magmas

because substantial differentiation may take place in basalt without discernibly affecting SiO_2 content. In studying basalts, petrologists may choose to plot weight percent oxides as a function of weight percent MgO instead of SiO_2 (see Map 8.2). Fractional crystallization of olivine will enrich a melt in FeO while depleting it in MgO (see Figure 2.11B), thus weight percent MgO is a good monitor of differentiation in mafic magmas that undergo minimal changes in silica. It is important to note that, whereas increasing differentiation is marked by *increases* in silica, increasing differentiation is marked by *decreases* in MgO . Both chemical variations as a function of SiO_2 and chemical variations as a function of MgO give petrologists important information on suites of igneous rocks. If a suite of rocks forms a simple array on the diagram, there is good reason to suspect the rocks are all related, by differentiation of a common magma, from melting of a similar source, or through mixing of magmas. Conversely, if the samples scatter across the diagram instead of forming an array, the rocks are probably unrelated. Variation diagrams can be used to distinguish suites of rocks formed

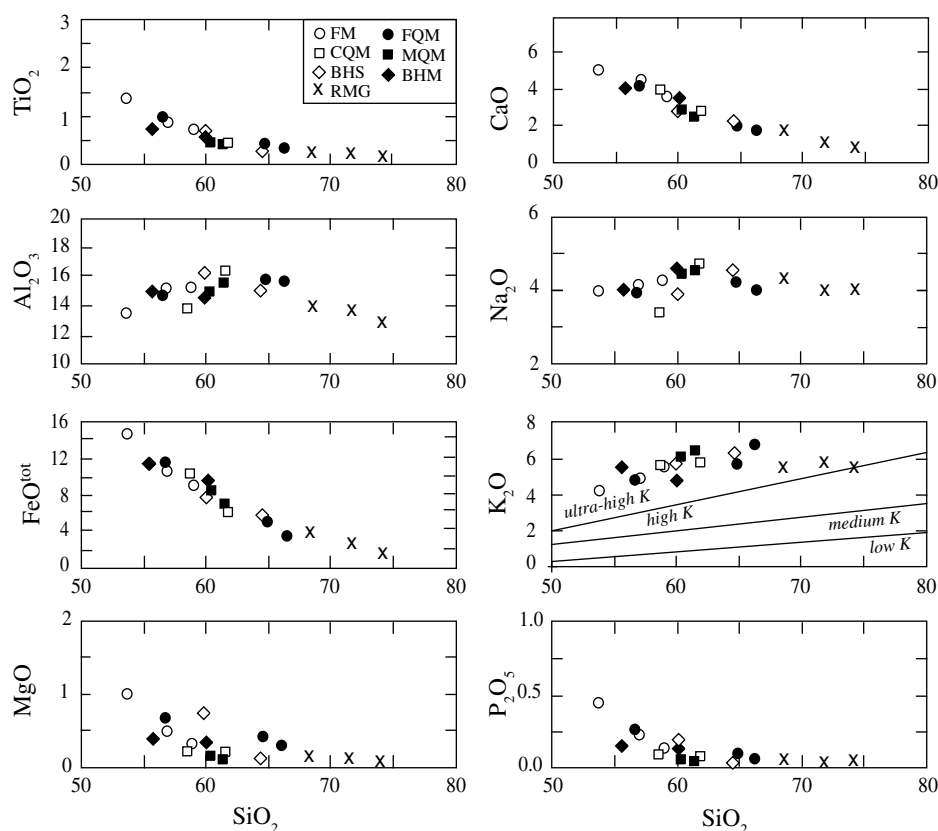


Figure 4.3 Harker diagrams for the Red Mountain pluton, Wyoming, USA. FM = fayalite monzonite, CQM = clinopyroxene quartz monzonite, BHS = biotite-hornblende syenite, RMG = Red Mountain pluton, FQM = fine-grained quartz monzonite, MQM = medium-grained quartz monzonite, BHM = biotite-hornblende monzonite. After Anderson, Frost, and Frost (2003).

by fractional crystallization from those formed by magma mixing. Figure 4.4 shows how fractional crystallization of olivine and anorthite would affect the Al_2O_3 and SiO_2 contents of a suite of rocks. Consider a melt of composition M_1 . As olivine begins to crystallize, it enriches the residual magma in both SiO_2 and Al_2O_3 and drives the melt composition along the vector (V_1) that extends directly away from the olivine composition. Lava erupted after some olivine crystallization may have composition M_2 . If plagioclase then begins to crystallize and olivine ceases to crystallize, the residual liquid will follow a trajectory along vector V_2 . In all likelihood olivine and plagioclase will crystallize together. If they do, then the residual magma will evolve along a path determined by the relative abundances of olivine and plagioclase. Figure 4.4 shows the situation in which olivine and plagioclase crystallize in equal abundances, driving the melt along vector V_3 . This demonstration shows how a suite of rocks related by fractional crystallization will form curved arrays on a Harker diagram. The trajectories of these arrays will change in tandem with the composition and abundances of the crystallizing phases.

Harker diagrams can also determine whether a suite of rocks is related by mixing. For example, consider an andesite volcano that has a few dacite and rhyolite domes on its flanks. In a Harker diagram, the Al_2O_3 , CaO , and K_2O contents of these three rocks form a linear array (Figure 4.5). This configuration suggests the dacite may have formed by mixing the andesite magma, perhaps ascending from depth, and a rhyolite magma, which may have been derived in the crustal.

Harker diagrams cannot *prove* any particular process has taken place. Rather they simply indicate whether a certain process is *consistent* with the major element data. To be certain of the process, the trends inferred from major elements must agree with trace element, isotopic, and field evidence. Two good examples of suites formed by magma mixing and fractional crystallization are the Sherman batholith and the Red Mountain plutons (Figures 4.2 and 4.3). Both are 1.43 Ga plutons that occur in the Laramie Mountains of southeastern Wyoming, USA. Although the trends look similar, there are important differences between the two. Observe how the samples from the Sherman batholith form linear trends,

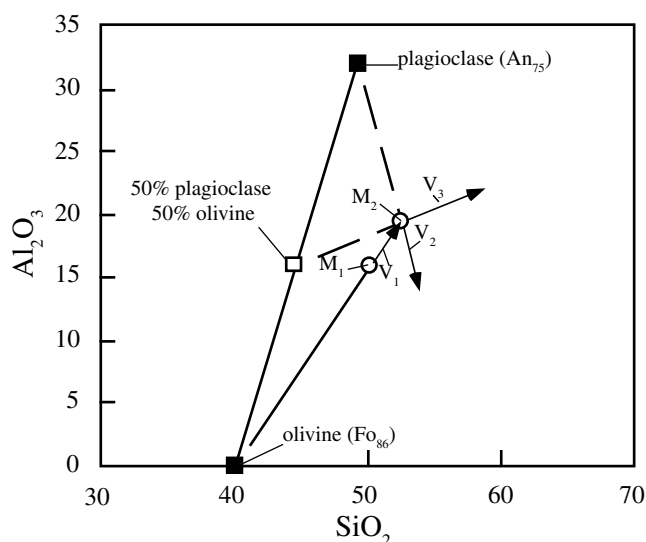


Figure 4.4 Diagram showing the effect of fractional crystallization on the trend followed by magmas on a Harker diagram. See text for discussion.

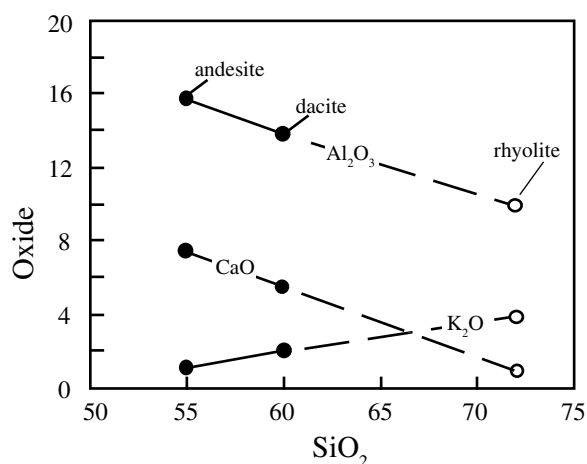


Figure 4.5 Diagram showing that the geochemical composition of dacite is consistent with its origin by mixing of rhyolite and andesite magmas.

whereas those from the Red Mountain pluton form curves (Figure 4.6). This suggests the rocks of intermediate composition in the Sherman batholith may have formed as the result of magma mixing, whereas the suite of rocks in Red Mountain pluton may have formed by fractional crystallization.

These conclusions are supported by field evidence. The Sherman batholith consists of the eponymous Sherman granite, a porphyritic granite, a fine-grained granite called the Lincoln granite, and mafic dikes and enclaves (Figure 4.7). Mafic and Lincoln granite magmas

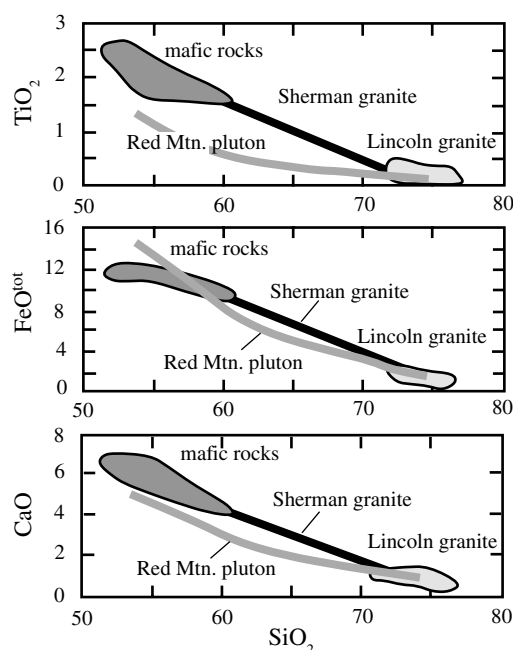


Figure 4.6 Harker diagrams comparing trends in the Sherman batholith and the Red Mountain pluton, Wyoming, USA. Data from Figures 5.2 and 5.3. See text for discussion.

commingled (Figure 4.7A) and mixed to form less mafic hybrid magma (Figure 4.7B). Mafic enclaves (Figure 4.7C) assimilated into the Sherman granite produced variable mafic mineral contents (Figure 4.7D). Rims of plagioclase on crystals of potassium feldspar indicate that the composition of the Sherman magma and the composition of the stable, crystallizing feldspar were changed during magma mixing (Figure 4.7E). The porphyritic granite was produced by mixing of the Sherman granite with the Lincoln granite, and also contains potassium feldspar rimmed with plagioclase (Figure 4.7F). The Red Mountain pluton, in contrast, is a small, compositionally zoned pluton cut by fine-grained dikes that appear to represent magma expelled during crystallization (Anderson, Frost, and Frost, 2003).

4.4 Major Element Indices of Differentiation

In addition to Harker diagrams, other chemical variation diagrams can help identify the differentiation history of a magma. Many of the commonly used indices of differentiation are based on major elements. The alkali-lime index, iron enrichment index, aluminum saturation index, and alkalinity index have been used for many decades to

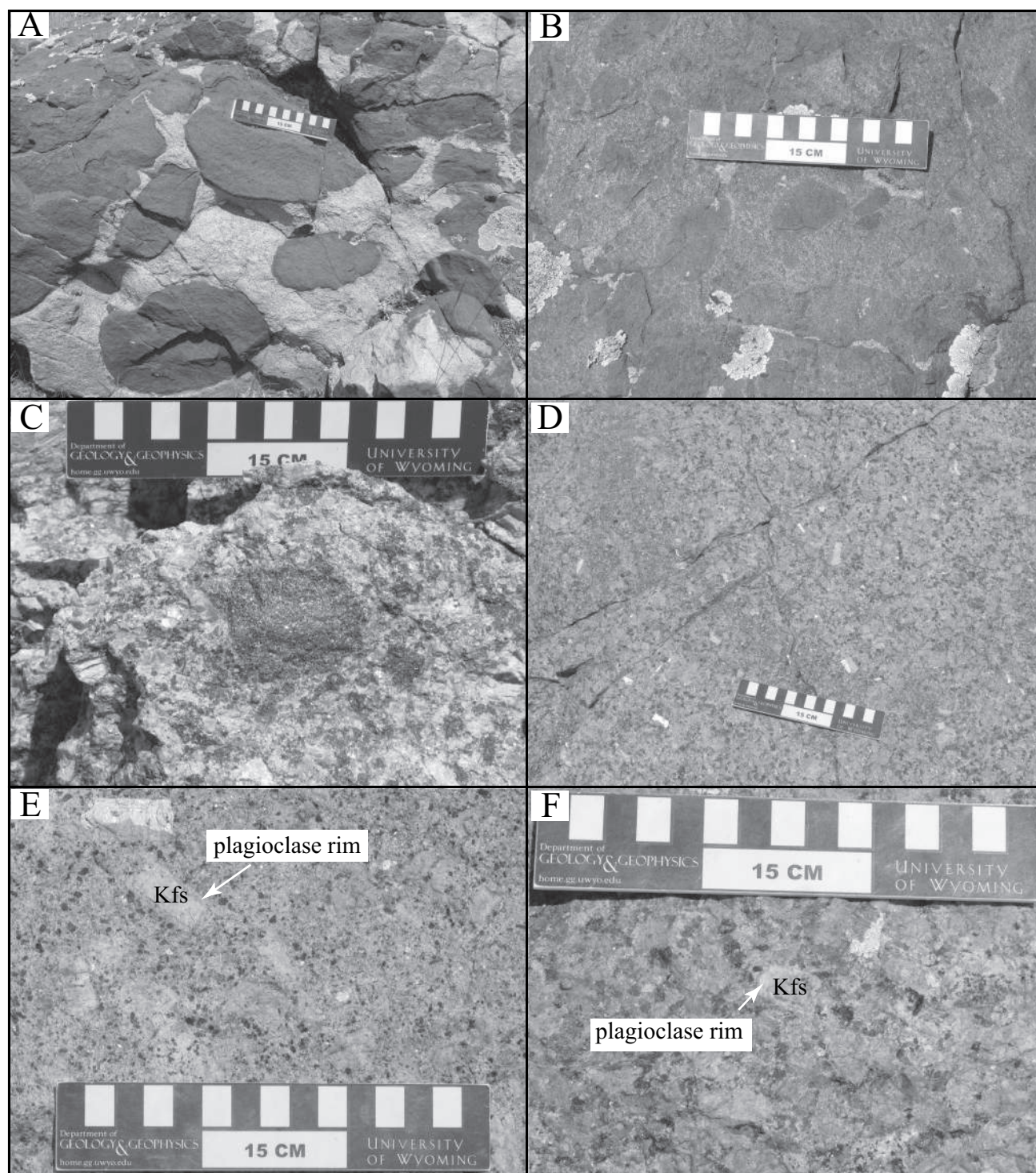


Figure 4.7 Photographs showing the relationships between the rock units composing the Sherman batholith, Wyoming, USA. (A) The fine-grained Lincoln granite and mafic magmas commingle, forming pillows of mafic magma and lobate and cusped contacts between the two magmas. (B) Intermediate magma is formed by mixing of mafic and granite magmas; mafic enclaves are visible within the hybrid host rock. (C) Mafic enclaves in the Sherman granite. (D) Heterogeneous assimilation of mafic material produces Sherman granite with variable mafic mineral contents. (E) Rims of plagioclase on crystals of potassium feldspar (arrow) indicate that magma mixing changed the composition of the Sherman magma, and also changed the composition of the stable, crystallizing feldspar. (F) The porphyritic granite, which is interpreted to form by mixing of the Sherman granite with the Lincoln granite, also contains potassium feldspar rimmed with plagioclase (arrow).

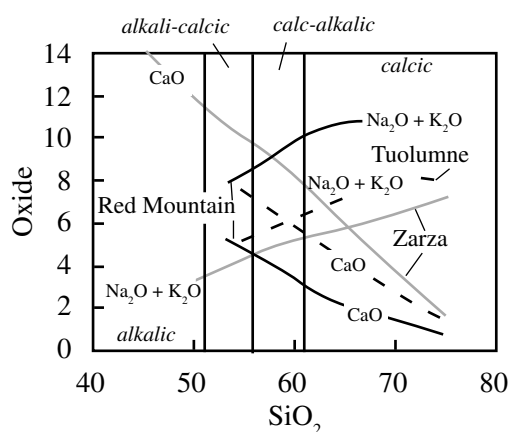


Figure 4.8 Harker diagram showing the variation of CaO and $\text{Na}_2\text{O} + \text{K}_2\text{O}$ in three batholiths. Dark solid lines = Red Mountain pluton, Wyoming, USA (Anderson, Frost, and Frost, 2003). Dark dashed line = Tuolumne pluton, Sierra Nevada batholith, California, USA (Bateman and Chappell, 1979). Dashed line = Zarza pluton, Baja California, Mexico (Tate et al., 1999).

categorize series of rocks and to identify the processes that produced their spectrum of compositions.

4.4.1 Modified Alkali-lime Index

An important chemical control on the differentiation history of a magma is the relative abundances of CaO, Na_2O , and K_2O because these elements are important constituents of feldspars. If CaO is high relative to Na_2O and K_2O , then the first feldspar to crystallize will be rich in anorthite ($\text{CaAl}_2\text{Si}_2\text{O}_8$), which is relatively rich in Al_2O_3 and poor in silica. Crystallization of this feldspar, therefore, will enrich the residual melt in SiO_2 and deplete it in alumina. In contrast, if the alkalis are abundant relative to CaO then the first feldspar to crystallize will be rich in $\text{NaAlSi}_3\text{O}_8$ and KAlSi_3O_8 . The alkali feldspar components are richer in silica and poorer in alumina than is anorthite. Thus if the first feldspars to crystallize from a melt are rich in alkali components, they will deplete the melt in silica and enrich it in alumina. As a result, alkaline rocks commonly differentiate to silica-depleted compositions, whereas calcic rocks tend to differentiate to silica-enriched compositions. Decades ago, Peacock (1931) recognized the importance of the relative abundances of CaO to the alkalis by introducing the Alkali-lime Index.

For most igneous rock series, CaO decreases with increasing silica on a Harker diagram, whereas Na_2O and

Table 4.1 Alkali-Lime Classification for Igneous Rocks

Alkali-Lime Index (wt % SiO_2 where $\text{CaO} = \text{Na}_2\text{O} + \text{K}_2\text{O}$)	Name
< 51%	Alkalic
51–56%	Alkali-calcic
56–61%	Calc-alkalic
>61%	Calcic

K_2O increase. Consequently, with increasing silica on a Harker diagram the curves for CaO and $\text{Na}_2\text{O} + \text{K}_2\text{O}$ will intersect (Figure 4.8). If the rocks are from a relatively alkalic suite, the intersection will occur at relatively low silica; whereas if the rocks are from a relatively calcic suite, the curves will intersect at relatively high silica. As a monitor of the relative abundances of lime and alkalis in a suite of rocks, Peacock (1931) defined the Alkali-lime Index as the silica content at which the two curves intersect. He coined four terms to describe the relative alkalinity of a magma suite: alkalic, alkali-calcic, calc-alkalic, and calcic (Table 4.1). The terms derived by Peacock (1931) have attained wide acceptance in the petrologic community but have been used so loosely that the original meaning has been all but lost. It is common to apply the term *calc-alkalic* to describe magmas associated with island arc magmatism, irrespective of their Alkali-lime Index. In this book we use the term in its strict geochemical sense.

There are several problems with the Alkali-lime Index as proposed by Peacock. One problem is the difficulty comparing many suites in a single diagram because each suite is defined by two lines, so only a few suites will overwhelm the diagram with lines. Another problem is that this index is easily applicable only in rock suites with a range in silica content that covers the value where CaO and $\text{Na}_2\text{O} + \text{K}_2\text{O}$ intersect (for example, note that the CaO and $\text{Na}_2\text{O} + \text{K}_2\text{O}$ curves for the Red Mountain pluton do not intersect in Figure 4.7). Finally, it is difficult to apply this analysis to single samples or to rock suites with little variation in silica contents. To address this problem, Frost and colleagues (2001) introduced the variable $\text{Na}_2\text{O} + \text{K}_2\text{O} - \text{CaO}$, which they called the **modified alkali-lime index** (MALI). At the silica content where the CaO and $\text{Na}_2\text{O} + \text{K}_2\text{O}$ curves cross, the modified alkali-lime index is 0.0. At higher silica contents it is positive, and at lower

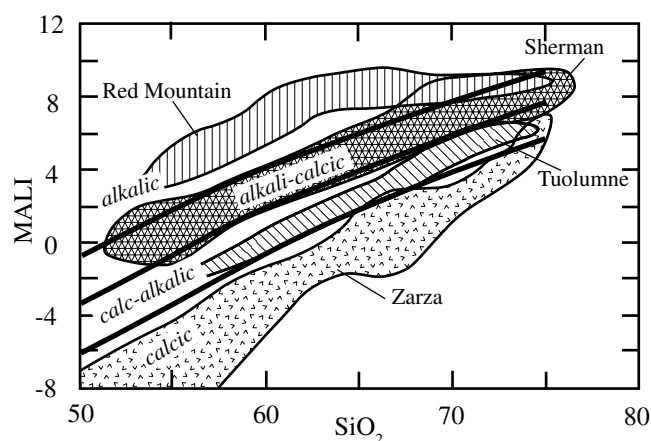


Figure 4.9 Plot of MALI ($\text{Na}_2\text{O} + \text{K}_2\text{O} - \text{CaO}$) vs. SiO_2 showing where calcic, calc-alkalic, alkali-calcic, and alkalic rocks plot. The composition ranges for the Red Mountain, Sherman, Tuolumne, and Zarza plutons are shown for comparison.

values it is negative. *Alkalic*, *alkali-calcic*, *calc-alkalic*, and *calcic* rocks occupy distinct fields on a plot of the modified alkali-lime index against silica. Four examples are plotted in Figure 4.9: the Red Mountain pluton, which is alkalic; the Sherman batholith, which is alkali-calcic; the Tuolumne pluton, which is calc-alkalic; and the Zarza pluton, which is calcic.

The differences in Alkali-lime Index are reflected mineralogically in the compositions of the feldspars. In a calcic rock suite, the first plagioclase to crystallize is relatively calcic (for example, An_{80}), and K-spar joins the crystallization trend rather late in the differentiation sequence. A plutonic suite following a calcic differentiation trend tends to span compositions from gabbro – dacite – quartz diorite – granodiorite (see Figure 1.1). A volcanic suite may follow the trend basalt – andesite – dacite – rhyolite (see Figure 1.4). In contrast, an alkalic suite first forms plagioclase that is relatively sodic (for example, An_{50}), and K-spar crystallizes relatively early in the differentiation trend. A plutonic, alkalic suite may follow the trend gabbro – monzonite – syenite – quartz syenite – granite (Figure 1.1), whereas an alkalic volcanic suite may include basalt – trachyte – quartz trachyte – rhyolite (Figure 1.4).

4.4.2 Iron Enrichment Index

Decades ago petrologists recognized that differentiation in some suites leads to distinctive iron enrichment, whereas

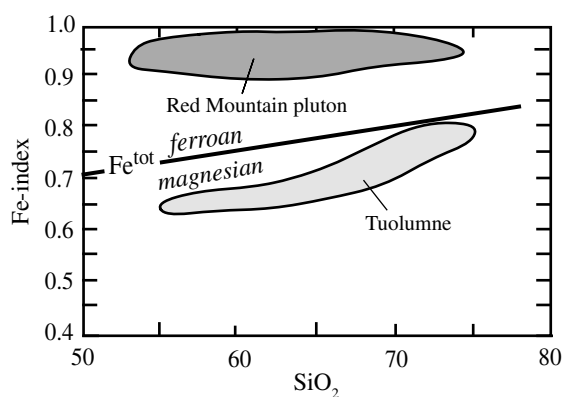


Figure 4.10 $\text{Fe}^* [\text{FeO}^{\text{tot}}/(\text{FeO}^{\text{tot}} + \text{MgO})]$ vs SiO_2 diagram comparing the ferroan Red Mountain pluton, Wyoming, USA with the magnesian Tuolumne batholith, California, USA.

in other suites this iron enrichment is modest or lacking (Nockolds and Allen, 1956). The **iron enrichment index** (Fe-index) $[(\text{FeO} + 0.9\text{Fe}_2\text{O}_3) / (\text{FeO} + 0.9\text{Fe}_2\text{O}_3 + \text{MgO})]$ measures the extent to which total iron became enriched during the differentiation of a magma. It is important to note that the “iron enrichment,” measured by the Fe-index, is relative to magnesia. Although the absolute abundance of FeO, Fe_2O_3 , and TiO_2 increase with differentiation during the early fractionation of most basalts, once Ti-magnetite and ilmenite begin to crystallize these oxides become compatible and decrease with differentiation. Thus iron enrichment could take place in some suites even as the absolute abundance of iron decreases provided that iron abundance decreases at a slower rate than the depletion of MgO from the melt.

Differentiation associated with iron enrichment was originally referred to as the *Skaergaard trend*, whereas that lacking iron enrichment was called the *Cascade trends* (Miyashiro, 1974). Because nothing in the definition of either a tholeiite or a calc-alkalic rock that deals with iron, Frost and colleagues (2001) proposed renaming these trends *ferroan* and *magnesian*, respectively, so that the names reflect the chemical variables on which the distinction is based. Figure 4.10 compares the compositional trend followed by the Red Mountain pluton, which is strongly iron enriched, to the magnesian Tuolumne suite. Rocks following a ferroan trend undergo iron enrichment before becoming enriched in alkalis, whereas those following a magnesian trend show only minimal iron enrichment.

A number of differentiation processes may cause iron enrichment, including the fractional crystallization of

olivine from a magma. In contrast, fractional crystallization of magnetite will deplete the melt in iron and enrich it in silica. For this reason, relatively reduced melts, which inhibit magnetite crystallization, will follow a ferroan crystallization trend, whereas oxidized rocks will follow a more magnesian trend. Additionally, crystallization of biotite and hornblende may play an important role in determining the degree of iron enrichment. Unlike olivine and the quadrilateral pyroxenes, which cannot accommodate much ferric iron, both biotite and hornblende can contain considerable Fe^{3+} (as well as ferrous Fe^{2+}). Therefore crystallization of hornblende and biotite represents an additional means for extracting Fe from a melt thus inhibiting iron enrichment.

4.4.3 Aluminum Saturation Index

Yet another parameter for characterizing igneous rocks is the **aluminum saturation index (ASI)** ($\text{Al}/(\text{Ca} + 1.67\text{P} + \text{Na} + \text{K})$) (Table 4.2). The index was originally defined by Shand (1943); the phosphorous component was added by Zen (1988) to take into account Ca residing in apatite. This change was needed so that rocks with an aluminum saturation index of >1.0 would also be corundum normative. The major hosts for aluminum in igneous rocks are the feldspars. This parameter indicates whether the alkalis needed to make feldspars balance the abundance of aluminum, or whether there is excess of either alkalis or aluminum. Most mafic rocks are **metaluminous** and have neither excess aluminum nor alkalis. In such rocks the alkalis are mostly accommodated in feldspars, and the remaining calcium (and minor sodium) are found in hornblende or augite.

Granitic rocks may be metaluminous, peraluminous, or peralkaline. If there is an excess of aluminum over alkalis (i.e., the molecular ratio of $\text{Al}/(\text{Ca} + \text{Na} + \text{K}) > 1.0$), then the rock is said to be **peraluminous**. Figure 4.11A compares the composition of two granites from the western United States. The Harney Peak granite in the Black Hills of South Dakota is strongly peraluminous, whereas the Tuolumne pluton in the Sierra Nevada of California is metaluminous and ASI increases with increasing silica content. Figure 4.11B shows where common minerals in granites plot on an ASI diagram. By construction, feldspars have $\text{ASI} = 1.0$ (i.e., the alkalis and the aluminum are balanced). Augite and hornblende have low ASI indices because they contain substantial amounts of calcium that

Table 4.2 Classification of Rocks by Aluminum Saturation

Aluminum Saturation Index (in moles)	Rock Name
$\text{Al}/(\text{Ca} + \text{Na} + \text{K}) > 1.0$	Peraluminous
$\text{Al}/(\text{Ca} + \text{Na} + \text{K}) < 1.0$ and $(\text{Na} + \text{K}) < \text{Al}$	Metaluminous
$(\text{Na} + \text{K}) > \text{Al}$	Peralkaline

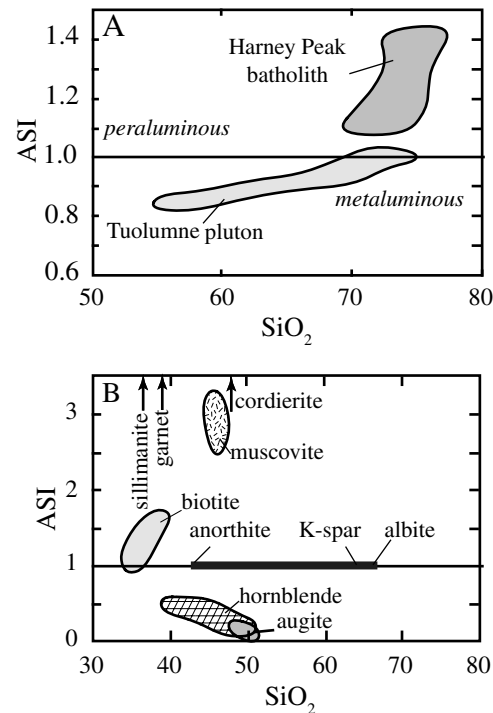


Figure 4.11 Aluminum Saturation Index (ASI) vs. SiO_2 diagrams. (A) Comparison of the peraluminous Harney Peak granite, South Dakota, USA (Nabelek, Russ-Nabelek, and Denison, 1992) and the metaluminous Tuolumne pluton, California, USA (Bateman and Chappell, 1979). (B) Diagram comparing where common minerals from granites plot. Heavy gray line illustrates the composition range for the feldspars.

is not balanced by aluminum. Orthopyroxene has widely varying ASI, but it is not shown on Figure 4.11B because it usually has only small amounts of either alkalis or aluminum, and hence doesn't affect the abundance of those elements in rocks. In its ideal formula, $(\text{KFe}_3\text{AlSi}_3\text{O}_{10}(\text{OH})_2)$, biotite would have $\text{ASI} = 1.0$, but natural biotites usually contain excess aluminum substituting for iron and are hence weakly peraluminous. Muscovite is strongly

peraluminous, as are sillimanite, garnet, and cordierite, which typically contain little or no alkalis.

Thus the ferromagnesian minerals found in a granite (or a rhyolite) reflect the aluminum saturation of that rock. Metaluminous rocks contain minerals with low ASI, such as augite and hornblende. Augite and hornblende should be absent in peraluminous rocks. In weakly peraluminous rocks, the extra aluminum may be accommodated in biotite, but strongly peraluminous rocks should be marked by the presence of an aluminum-rich mineral in the rock. Common aluminous minerals found in granitic rocks are muscovite and garnet; cordierite and sillimanite are rarer.

4.4.4 Alkalinity Index

The **alkalinity index** (AI) $(AI = (Al - (Na + K)))$ measures the relative abundances of aluminum and alkalis. Alkaline rocks are defined as those that have higher sodium and potassium contents than can be accommodated in feldspar alone (Shand, 1943). If there is an excess of alkalis over aluminum, the rocks are **peralkaline** and AI will be less than zero. Sorensen (1974) recognized three subgroups of alkaline rocks. In the first, silica is adequate but alumina is deficient, so the minerals that accommodate the excess alkalis include sodic pyroxenes and sodic amphiboles, making peralkaline granites and their volcanic equivalents, pantellerite and comendite. In the second subgroup, alumina is adequate but silica is deficient. These rocks contain feldspathoids along with micas, hornblende, and/or augite and form rocks such as metaluminous nepheline syenite. In the third subgroup, both alumina and silica are deficient and both feldspathoids and sodic pyroxenes and/or amphiboles crystallize. These rocks include peralkaline nepheline syenites.

To distinguish these three types of alkaline rocks, Frost and Frost (2008) defined one additional index, the *Feldspathoid Silica Saturation Index* (FSSI):

$$FSSI = (Q - (Lct + 2Nph))/100$$

Where Q, Lct, and Nph are the normative quartz, leucite, and nepheline contents, respectively. This index is positive for quartz-saturated rocks, for which it expresses the excess amount of silica. For silica-undersaturated rocks, it represents the amount of silica that must be added to make it silica saturated. The equation for FSSI involves multiplying the normative nepheline content by two because

AI	+	Metaluminous Si-undersaturated contain nepheline with Ca-pyroxenes, Ca-amphiboles, or biotite	Metaluminous Si-saturated contain quartz with Fe-Mg-Ca-pyroxenes, Ca-amphiboles, or biotite
	-	Peralkaline Si-undersaturated (Al-deficient) contain nepheline with Na-pyroxenes and Na-amphiboles	Peralkaline Si-saturated (Al-deficient) contain quartz with Na-pyroxenes and Na-amphiboles
		-	+
		FSSI	

Figure 4.12 Classification of alkaline rocks, shown on a plot of Alkalinity Index (AI) versus Feldspathoid Silica Saturation Index FSSI. Alkaline rocks occupy the shaded portions of the diagram. They may be silica-undersaturated (top left corner), alumina-deficient (bottom right corner), or both silica and alumina deficient (bottom left corner). From Frost and Frost (2008).

two formula units of quartz must be added to nepheline to make albite:



Only one formula unit of quartz must be added to leucite to make K-feldspar:



Using the FSSI and AI indices, Frost and Frost (2008) developed a matrix showing how the subgroups of alkaline rocks are related to “normal” granitic rocks (Figure 4.12). The shaded quadrants of this diagram are occupied by the three subgroups of alkaline rocks, namely the metaluminous, Si-undersaturated rocks; the peralkaline, Si-undersaturated rocks; and the peralkaline, Si-saturated rocks. The fourth quadrant is occupied by metaluminous and peraluminous, Si-saturated rocks.

4.5 Identification of Differentiation Processes Using Trace Elements

Trace elements, which are present in rocks in concentrations of less than 0.1 percent by weight, include the *transition metals* Sc, Ti, V, Cr, Mn, Co, Ni, Cu, and Zn, the *rare earth elements* La, Ce, Nd, Sm, Eu, Gd, Tb, Dy, Ho, Er, Tm, Yb, and Lu, and other trace elements, including Cs, Rb, Ba,

Sr, Y, Zr, Hf, Nb, Ta, Pb, Th, and U. Trace elements are useful fingerprints of the origin of igneous rocks and igneous processes because they exhibit a range in concentration far greater than for major elements. For example, in most igneous rocks, CaO varies between 0 and 10 weight percent. However, Sr, which behaves chemically much like Ca, may vary from 10s of ppm to 1,000s of ppm in those same igneous rocks. Therefore, a process that affects the concentration of Ca may affect the concentration of Sr by a much greater magnitude, making it more likely that the process can be detected and identified by considering the Sr content.

Because of their wide variations in abundance, trace elements can be used to identify and quantify processes of crystallization and partial melting. For elements with low concentration (that is, for trace elements), the element is partitioned between minerals and melt according to the relationship:

$$D = \frac{C_i^{\text{mineral}}}{C_i^{\text{melt}}} \quad (4.1)$$

D is called a **partition coefficient** and C_i is the concentration of any trace element in either the melt or the crystal. D can be measured from experiments or by comparing the concentration of a trace element in phenocrysts in volcanic rocks with that of its glassy matrix. D values are strongly composition dependent, so different values apply to mafic magmas than to felsic magmas.

Magmas will be in equilibrium with more than one mineral phase as they crystallize. To describe this situation, we define a **bulk distribution coefficient**, D_B , which is calculated from the weight proportions (w) of each mineral in the assemblage:

$$D_B = \sum_{i=1}^n w_i D_i \quad (4.2)$$

Those elements that behave compatibly (i.e., those that preferentially concentrate in the minerals) have D_B greater than 1. In contrast, those elements that are incompatible and concentrate in the melt have D_B less than 1. In general, compatible elements have ionic radii and charge similar to those of major elements like Mg, Fe, Ca, and Na and therefore can substitute crystallizing minerals for them. Incompatible elements may have either much larger or smaller radii or too high a charge to occupy major sites in the lattices of common rock-forming minerals.

4.5.1 Use of Trace Elements to Model Melting and Crystallization Processes

A number of simple models can resolve melting and crystallization processes from trace element concentrations of rocks, and the reader is referred to more complete treatments of this topic in Shaw (2006). This section will consider a single example to illustrate the power of this approach: a model of trace element partitioning during fractional crystallization. The theoretical variation of trace element concentrations during fractional crystallization can be calculated from the Rayleigh equation:

$$C_i/C_i^0 = F^{(D-1)} \quad (4.3)$$

where C_i is concentration of element i in the melt after a certain amount of fractionation has taken place, C_i^0 is the concentration of element i in the initial melt, and F is melt fraction remaining. The Rayleigh equation allows petrologists to calculate how the concentration of trace elements change during fractional crystallization (Figure 4.13). From Figure 4.13 it is clear that highly compatible elements (such as those with $D_B > 10$) are quickly removed from the melt, whereas highly incompatible elements (such as those with $D_B < 0.5$) can accumulate very high abundances in the last fraction of the melt to crystallize. This is the reason pegmatites, which form from the last remaining granitic melt, commonly contain high concentrations of incompatible elements such as Li, B, and Be.

The abundances of trace elements in minerals and rocks can be used to test various hypotheses for the origin of igneous rocks. For example, consider the idea that crystallization and removal of plagioclase from the lunar tholeiite produces residua that form the basaltic lunar rock type known as KREEP. This lunar material, first found during the *Apollo 12* mission, is named for its unusually high contents of potassium (K), rare earth elements (REE), and phosphorus (P). Given that the rare earth element Ce has $D = 0.1$ between plagioclase and basaltic liquid, and that KREEP have 200 ppm Ce and the initial tholeiitic parental magma had 18 ppm, how much plagioclase must be removed from a magma with the composition of the lunar tholeiite to produce a KREEP basalt? Substituting the concentration into equation (4.3):

$$200/18 = F^{(0.1-1)}$$

$$11 = F^{(-0.9)}$$

$$0.07 = F, \text{ the fraction of liquid remaining}$$

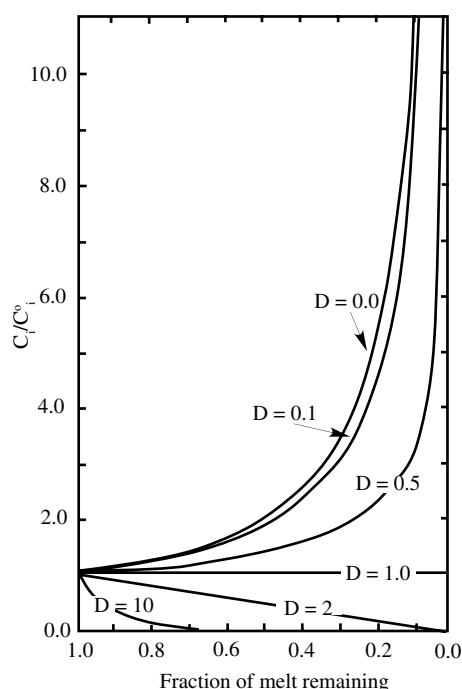


Figure 4.13 Variation of trace element concentrations during fractional crystallization of a magma according to the Rayleigh law. The diagram illustrates the rapid removal of highly compatible elements from the magma during crystallization, and the resulting enrichment of highly incompatible elements in the magma. From Cox, Bell, and Pankhurst (1979).

This indicates that if 93 percent of the magma crystallized as plagioclase, then the 7 percent residual liquid would have the correct concentration of Ce. This calculation suggests that if KREEP is formed by removal of plagioclase from a tholeiitic magma, then KREEP is a highly differentiated basaltic rock type.

4.5.2 Graphical Representations of Trace Element Compositions

Trace element compositions may be portrayed graphically in a number of ways. First, they can be plotted on Harker diagrams, similar to how major elements are portrayed. With trace elements percent SiO_2 is on the x-axis and the trace element concentration, usually in ppm, on the y-axis. An example of this graphical treatment is shown in Figure 4.14. Zirconium contents in rocks of the Red Mountain pluton, a monzonitic to granitic pluton associated with the Laramie anorthosite complex, decrease from 2,000–3,000 ppm in the most mafic parts of the pluton to less than 300 ppm in the most siliceous granites.

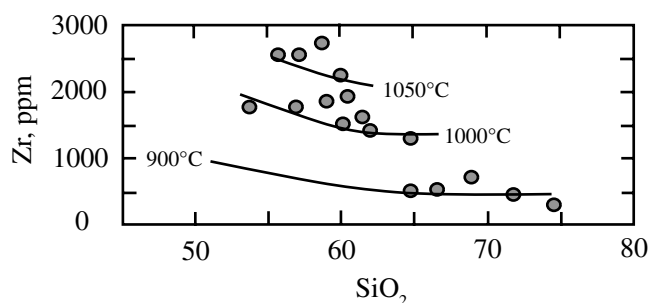


Figure 4.14 Variation in Zr content of rocks from the Red Mountain pluton, Laramie anorthosite complex, Wyoming, USA. The contours show the temperature at which zircon saturates in the Red Mountain pluton melts (Watson and Harrison, 1983). The Red Mountain rocks contain fayalite and clinopyroxene and probably crystallized from hot magmas, but they probably did not begin to crystallize at temperatures much above 1,000°C. Zircon probably crystallized early, accumulating in the solid phase in those samples that have greater than 1,000 ppm Zr and lie above the 1,000°C isotherm. From Anderson, Frost, and Frost (2003).

This decrease is related to crystallization of zircon, which incorporates zirconium, thereby depleting the remaining magma in this element.

The rare earth elements are among the most commonly used trace elements in petrology. They are typically plotted as a group, arranged by increasing atomic number along the x-axis in a **rare earth element (REE) diagram**. The y-axis is the element concentration in the sample divided by its concentration in primitive chondritic meteorites. Because even-numbered atomic elements are more abundant in the solar system than odd-numbered atomic elements, normalizing to chondritic composition smooths the saw-tooth pattern that would be obtained if the sample concentrations alone were plotted. An example of the rare earth diagram is shown in Figure 4.15, in which REE compositions of lunar anorthosite, quartz tholeiite, and KREEP are plotted. The normalized abundances make smooth curves except for excursions for the element Eu. Of the REEs, Eu is the only element that can be present in magmas in the 2+ oxidation state, which allows Eu^{2+} to substitute for Ca^{2+} in plagioclase. The large positive Eu anomaly in the REE pattern of anorthosite reflects incorporation of Eu^{2+} in feldspar. The negative Eu anomaly in the REE pattern of high-K and KREEP basalts are consistent with their interpretation as the residual magmas following plagioclase crystallization and formation of lunar

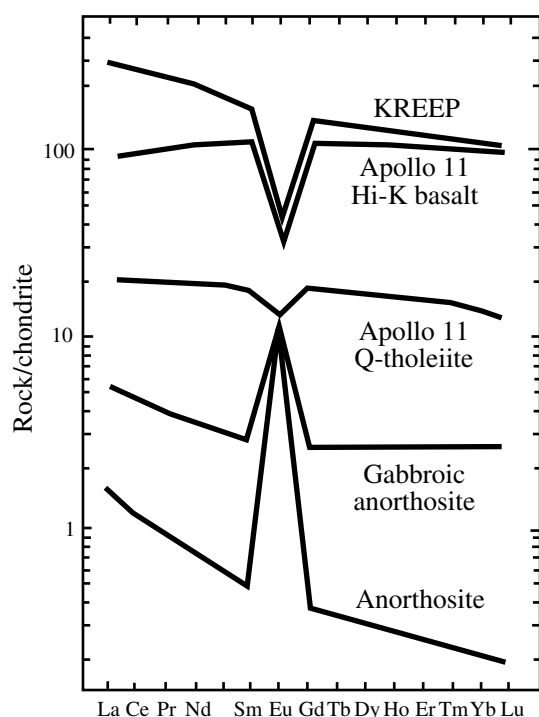


Figure 4.15 Rare earth element patterns of lunar rocks. The gap between neodymium and samarium is occupied by promethium, which has no stable isotopes. From Taylor (1975).

anorthosite. The quartz tholeiite, with its intermediate REE abundances and nearly flat pattern, could approximate the composition of the parent magma from which anorthosite and residual KREEP basalt formed.

Different tectonic environments involve different conditions of melting or different source rocks, and they tend to generate magmas with different trace element compositions. For example, mid-ocean ridge basalt tends to be depleted in the light rare earth elements relative to the heavy rare earth elements, and are typically depleted in Nb. This has led to the use of trace element abundances to indicate the origin for rocks that have subsequently been deformed or removed from their original setting (e.g., Pearce, Harris and Tindle, 1984; Pearce and Peate, 1995). It is important to remember that this is an empirical approach, and that variables including the exact composition of the source rocks, the extent of differentiation, magma mixing and assimilation, and subsequent metamorphism may lead to incorrect interpretations. Consider one of the widely used **discrimination diagrams** for granitic rocks shown in Figure 4.16, which plots the Nb and Y contents of the granitic rocks from the Sherman batholith. The plot shows

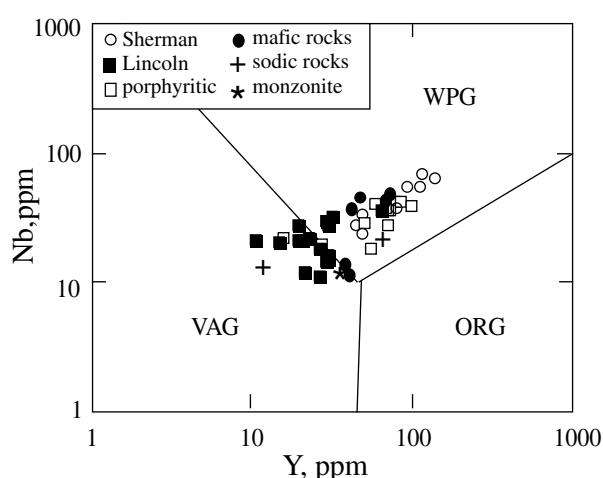


Figure 4.16 Nb and Y contents of rocks from the Sherman batholith, Laramie Mountains, Wyoming, USA. Most samples plot in the within-plate granite (WPG) field, but the highly differentiated Lincoln granite samples (which probably have assimilated some continental crust) extend into the volcanic-arc granite (VAG) field. From Frost et al. (1999).

that the Sherman granite samples plot within the field for within-plate granites (WPG), whereas the Lincoln and a few of the porphyritic granites trend into the field for volcanic arc granites (VAG). Because both these granites are part of a single batholith, they must have formed in a single tectonic setting. The fact that they plot in two different parts of the discrimination diagram could reflect the fact that the Lincoln granite probably originated from a different source than the Sherman. If Lincoln magmas were produced by partial melting of the country rock and these country rocks originally formed in a volcanic arc, then the Lincoln granite may plot in the VAG field even though the batholith formed far from an active volcanic arc.

4.6 Application of Stable and Radioactive Isotopes in Igneous Petrology

Elements are characterized by the number of protons in the nucleus; for example, carbon always contains six protons. The number of neutrons in the nucleus of a particular element can vary; for example, carbon may have six, seven, or eight neutrons. As a result of the variation in neutrons, a carbon element may have the atomic weight of twelve, thirteen, or fourteen. Neutron variants of a single element are called **isotopes**, and they can be either stable or radioactive. A radioactive isotope undergoes decay and

produces another isotope. For example, ^{14}C is a radioactive isotope referred to as the **parent** isotope, and it decays to form ^{14}N , the **daughter** isotope.

The sources of magmas and the processes that have affected them, as well as the crystallization and metamorphic ages of rocks, can be identified from their isotopic compositions (see Faure, 1986 for a more complete treatment of isotope geology). The stable isotopes of relatively light elements such as H, C, and O behave differently than one another as a function of the large relative differences in mass between their isotopes. This difference in behavior is called **mass fractionation**. The H and O isotopic compositions are different for meteoric water than magmatic water, thus the H and O isotopic composition of igneous rocks facilitate identifying rocks affected by hydrothermal circulation of meteoric water, or recognizing magmas that assimilated sedimentary rock, which would have interacted with meteoric water on Earth's surface. The isotopic composition of C in carbonate minerals, graphite, or diamond in igneous rocks can distinguish near-surface and deep-seated sources of carbon incorporated by those minerals.

4.6.1 Geochronology

Ratios comparing radioactive parent to radiogenic daughter isotopes can preserve time information inferred from the constant rate of decay that characterizes each parent isotope. In geology, this field of investigation, called **geochronology**, is extensive and involves the use of many parent-daughter pairs with varying parent isotope decay rates. Deciding which radiometric system best suits any particular problem involving the determination of age of a geologic event depends on decay rate, elemental abundances, and chemical behavior of the parent and daughter elements. For example, Precambrian rocks may be dated using the ^{238}U - ^{206}Pb and ^{235}U - ^{207}Pb parent-daughter pairs, which have two different, but relatively slow decay rates (10^8 to 10^9 year half lives), whereas the date a tree was burned in a fire pit by some prehistoric Native American is better determined from the abundance of ^{14}C , half of which will decay in 5,730 years.

4.6.2 Isotopic Tracing of Magma Sources

Another important application of isotope geology is in igneous petrogenesis, the study of magmatic sources. Isotopic compositions of heavy elements that have one

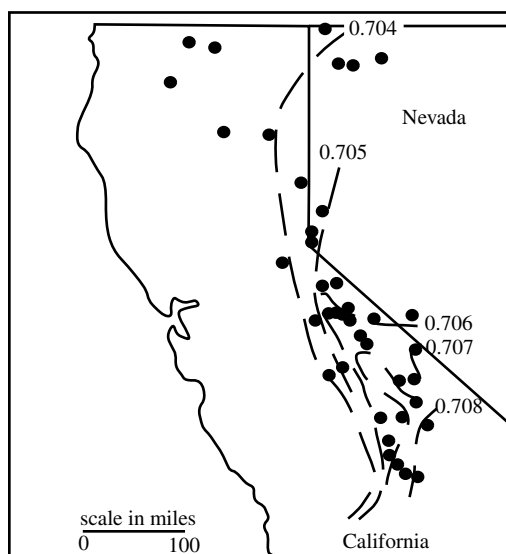


Figure 4.17 Contour diagram showing the regional variation in initial $^{87}\text{Sr}/^{86}\text{Sr}$ of Mesozoic granitic rocks in central California. Solid dots indicate locations of analyzed samples. From Kistler and Peterman (1973).

or more radiogenic isotope, including Sr, Nd, Hf, and Pb, vary from depending on their location in Earth. The variations in $^{87}\text{Sr}/^{86}\text{Sr}$, $^{143}\text{Nd}/^{144}\text{Nd}$, $^{176}\text{Hf}/^{177}\text{Hf}$, $^{208}\text{Pb}/^{204}\text{Pb}$, $^{207}\text{Pb}/^{204}\text{Pb}$, and $^{206}\text{Pb}/^{204}\text{Pb}$ are partly a function of age of the rock: the amounts of radiogenic daughter isotopes, ^{87}Sr , ^{143}Nd , ^{176}Hf , and ^{208}Pb , ^{207}Pb , and ^{206}Pb , increase with time as their parent isotopes decay, whereas the abundance of the non-radiogenic isotopes ^{86}Sr , ^{144}Nd , ^{177}Hf , and ^{204}Pb stay the same. However, the rate at which these radiogenic daughters are produced depends not just on time, but also on the abundance of the radioactive parent isotope. Consider ^{87}Sr , which forms by decay of ^{87}Rb . The granitic parts of the continental crust contain relatively high amounts of Rb, but the mantle has comparatively little Rb. Over geologic timescales, this difference in abundances has produced a mantle with low $^{87}\text{Sr}/^{86}\text{Sr}$ of around 0.703, whereas the present-day continental crust contains rocks that have average $^{87}\text{Sr}/^{86}\text{Sr}$ of around 0.715. The isotopes of Sr (and Nd, Hf, and Pb) have relatively similar mass differences so they do not fractionate measurably during geologic processes. When a partial melt forms from a source region, the melt has exactly the same $^{87}\text{Sr}/^{86}\text{Sr}$ as its source region. Therefore a magma with $^{87}\text{Sr}/^{86}\text{Sr}$ of 0.720 cannot have formed by partially melting the mantle, but instead was generated somewhere in the crust. Measurements of potential source rocks narrow down the possible crustal

sources. Note, however, that the isotopic composition of a magma is also unaffected by crystallization: the growing crystals acquire the same $^{87}\text{Sr}/^{86}\text{Sr}$ ratio present in the magma. Isotopic tracers can “see through” the process of fractional crystallization and consequently they retain information about the magma source(s).

An early demonstration of the usefulness of radiogenic isotope ratios for magma source identification was provided by Kistler and Peterman (1973). They determined the $^{87}\text{Sr}/^{86}\text{Sr}$ isotopic compositions of granites from Mesozoic batholiths of California (Figure 4.17). Plotted in Figure 4.17 are contours drawn from the $^{87}\text{Sr}/^{86}\text{Sr}$ of the granitic rocks at the time they crystallized. This is referred to as the **initial** $^{87}\text{Sr}/^{86}\text{Sr}$ because the subsequent decays of ^{87}Rb to produce additional ^{87}Sr

after the rock solidified has been determined and subtracted out. Kistler and Peterman’s data (1973) show the initial $^{87}\text{Sr}/^{86}\text{Sr}$ of the granitic rocks is a function of geographic location, and that the ratios increase to the south and east. To the west of the contour defining $^{87}\text{Sr}/^{86}\text{Sr} = 0.704$ is an area composed of relatively young, mainly mantle-derived volcanic rocks and volcanogenic sediment. To the east of the $^{87}\text{Sr}/^{86}\text{Sr} = 0.706$ contour are Precambrian to Triassic carbonates, shale, and sandstones. The $^{87}\text{Sr}/^{86}\text{Sr}$ of the Mesozoic granites shows how they inherited their Sr isotopic compositions from the compositional differences in the crust they intruded. Kistler and Peterman (1978) later used the $^{87}\text{Sr}/^{86}\text{Sr} = 0.706$ contour to approximate the edge of Precambrian crust in the western United States.

Summary

- The **norm** is the calculated mineral abundances that would be present in a rock if it were anhydrous. It is used to compare fine-grained rocks with coarse-grained rocks and to classify fine-grained rocks.
- Suites of rocks derived from a common parent magma obtain their various compositions by **magmatic differentiation**, most commonly through crystallization and removal of minerals from a magma.
- **Compatible elements** are preferentially incorporated into phases crystallizing from a melt and decrease in abundance in the magma as differentiation proceeds.
- **Incompatible elements** are incompatible with phases crystallizing from a melt and increase in abundance in the magma during differentiation.
- **Harker diagrams** are a common way of graphically illustrating igneous rock composition. They can identify crystal fractionation or magma mixing.
- Indices of differentiation include:
 - **Modified Alkali-lime index (MALI)**: categorizes rock suites as alkalic, alkali-calcic, calc-alkalic, and calcic.
 - **Iron-enrichment index (Fe-index)**: identifies ferroan versus magnesian suites.
 - **Aluminum-saturation index (ASI)**: distinguishes between peraluminous, metaluminous, or peralkaline rocks.
 - **Alkalinity Index (AI)**: distinguishes whether rocks are peralkaline.
 - **Feldspathoid Silica Saturation Index (FSSI)**: along with the AI, helps distinguish the various types of alkaline rocks.
- It is important to distinguish between alkalic, peralkaline, and alkaline rocks because these terms, though similar, describe different conditions. Alkalic rocks have $(\text{Na}_2\text{O} + \text{K}_2\text{O})$ that is high relative to CaO as defined by the alkali-lime index. These rocks tend to have K-feldspar and albitic plagioclase. Alkaline rocks are rocks that contain more K and Na than can be accommodated in feldspar. Peralkaline rocks have an excess of K and Na compared to AI and therefore contain sodic pyroxenes or amphiboles.

- Because variations of trace element concentrations in igneous rocks are of much greater magnitude than the variation in major element concentrations, trace elements provide more sensitive indicators of igneous processes, and can be used to quantitatively model those processes.
- Isotopic compositions of igneous rocks can provide information about the timing of events, and can be used to identify source rocks and various processes including assimilation and water-rock interaction.

Questions and Problems

Problem 4.1. What is the difference between normative and modal mineralogy?

Problem 4.2. Using the normative calculation software available for download from the Volcano Hazards Program of the U.S. Geological Survey (http://www.volcanoes.usgs.gov/observatories/yvo/.../other/NormCalc_JBL.xls), calculate the norm for the four samples from Table Pr.4.2. Which rocks are silica-saturated? If the rocks were anhydrous, what mafic minerals would be present?

	Shasta	Tuolumne	Brome	Mt. Megantic
	82-91a	4	BR15	MG21
SiO ₂	63.14	62.78	61.13	62.15
TiO ₂	0.57	0.70	0.87	0.38
Al ₂ O ₃	16.88	15.74	18.16	17.71
Fe ₂ O ₃	1.54	2.07	1.25	0.37
FeO	2.43	3.22	2.35	3.68
MnO	0.07	0.09	0.17	0.09
MgO	3.59	2.50	0.69	0.30
CaO	5.89	4.80	1.58	1.35
Na ₂ O	4.11	3.25	7.01	5.26
K ₂ O	1.18	3.22	5.37	6.75
P ₂ O ₅	0.17	0.17	0.00	0.00
LOI	0.3	0.35	0.00	0.00
Sum	99.57	98.89	98.58	98.04

Data from Bateman and Chappell (1979), Eby (1985), and Grove et al. (2005). LOI = Loss on Ignition, an indication of the volatile content of the rock.

Problem 4.3. Show that weight percent FeO = 0.9 weight percent Fe₂O₃

Problem 4.4. Construct templates for Fe-index, MALL, and ASI variation diagrams.

- The boundary between ferroan and magnesian fields is described by (Frost and Frost (2008): $\text{FeO}^* = 0.46 = 0.005 \text{ SiO}_2$; it is applicable for 48 percent to 75 percent SiO₂.

b. The boundaries on the MALI diagram are as follows (Frost et al., 2001):

alkali – alkali-calcic:

$$\text{Na}_2\text{O} + \text{K}_2\text{O} - \text{CaO} = -41.86 + 1.112 * \text{wt.\% SiO}_2 - 0.00572 \text{ wt.\% SiO}_2^2$$

alkali-calcic – calc-alkalic:

$$\text{Na}_2\text{O} + \text{K}_2\text{O} - \text{CaO} = -44.72 + 1.094 * \text{wt \% SiO}_2 - 0.00527 \text{ wt.\% SiO}_2^2$$

calc-alkalic – calcic:

$$\text{Na}_2\text{O} + \text{K}_2\text{O} - \text{CaO} = -45.36 + 1.0043 * \text{wt \% SiO}_2 - 0.00427 \text{ wt.\% SiO}_2^2$$

c. ASI is the molecular ratio $\text{Al}/(\text{Ca} + \text{Na} + \text{K})$ (Shand, 1943). Derive the equation that converts weight per cent oxide to molecular ratio of these ions.

Problem 4.5. Plot the analyses from Shasta volcano (below) on Fe-index, MALI, and ASI diagrams. Describe these andesites and dacites based on where they plot on these diagrams.

	SiO ₂	TiO ₂	Al ₂ O ₃	FeO ^{tot}	MnO	MgO	CaO	Na ₂ O	K ₂ O	P ₂ O ₅	LOI	Sum
82–91b	63.32	0.57	16.73	3.749	0.07	3.71	6.02	4.09	1.11	0.17	0.26	99.69
82–96	62.96	0.58	17.01	4.033	0.08	3.44	5.93	4.19	1.2	0.16	0.25	99.73
82–97	63.38	0.59	16.62	4.268	0.07	3.03	5.19	4	1.56	0.14	0.47	99.23
83–45	62.98	0.52	17.51	3.877	0.08	2.64	5.52	4.93	1.27	0.16	0.98	99.78
83–54	63.8	0.59	16.14	4.102	0.08	3.11	5.31	4.59	1.57	0.13	0.77	99.69
83–55	62.44	0.63	16.36	4.479	0.08	3.52	5.89	4.32	1.41	0.14	0.61	99.48
97–4	62.21	0.61	17.03	4.374	0.08	3.45	5.95	4.16	1.26	0.18	0.01	99.78
97–6	61.51	0.65	16.81	4.185	0.08	3.57	6.06	4.1	1.23	0.23	0.6	98.87
99–12A	56.9	0.36	17.1	5.382	0.11	5.9	8.82	3.03	0.74	0.13	0.4	99.07
99–12B	55.7	0.54	16.8	6.561	0.14	6.08	9.23	2.88	0.48	0.13	0.19	99.27
99–13	61.5	0.6	17	4.392	0.08	3.47	5.97	3.95	1.24	0.23	0.2	98.92
99–14	61.7	0.6	17	4.293	0.08	3.45	5.92	4	1.23	0.23	0.24	98.98
99–16	61.5	0.65	16.7	4.158	0.08	3.53	6.02	3.98	1.24	0.27	0.56	98.59
99–17	62.4	0.57	17	3.879	0.07	3.21	5.86	4.06	1.2	0.22	0.43	98.9
99–18	61.4	0.65	16.8	4.158	0.08	3.53	6.07	3.98	1.23	0.27	0.45	98.63
FeO _{tot} is total iron expressed as FeO												
Data from Grove et al., 2005.												

Problem 4.6. The partition coefficient, D, for Sr between plagioclase and melt is 2. If the initial Sr concentration of a melt is 200 ppm, what will the concentration of the melt be after plagioclase crystallizes, leaving 50 percent of the melt remaining? Do the calculation using equation 4.3 and check by solving the problem graphically using Figure 4.13.

Problem 4.7. Are the rare earth elements compatible or incompatible in plagioclase? Answer by inspection of Figure 4.15. (Recall that anorthosite is a rock composed of 90–100 percent plagioclase.)

Problem 4.8. The continental crust has been derived by partial melting of the mantle over geologic time and the formation of the continental crust from those partial melts.

- a) Assuming that for mantle melting the bulk distribution coefficient of Sr is greater than one and the bulk distribution coefficient of Rb is less than one, suggest how the Rb/Sr of the mantle from which partial melts were extracted (the depleted mantle) has changed during that time.
- b) As a result, how will the $^{87}\text{Sr}/^{86}\text{Sr}$ of the depleted mantle differ from the continental crust?
- c) Is your reasoning compatible with the observed variations in $^{87}\text{Sr}/^{86}\text{Sr}$ of granites in California shown in Figure 4.17? Explain.

Further Reading

.....

Cox, K. G., Bell, J. D., and Pankhurst, R. J., 1979, *The interpretation of igneous rocks*. Boston: G. Allen and Unwin.

Frost, B. R., Arculus, R. J., Barnes, C. G., Collins, W. J., Ellis, D. J., and Frost, C. D., 2001, A geochemical classification of granitic rock suites. *Journal of Petrology*, 42, 2033–48.

Frost, B. R. and Frost, C. D., 2008, A geochemical classification for feldspathic rocks. *Journal of Petrology*, 49 (11), 1955–69.

Rollinson, H. R., 1993, *Using geochemical data: evaluation, presentation, interpretation*. Harlow, New York: Longman/Wiley.

Chapter 5

Basalts and Mantle Structure

5.1 Introduction

Basalts are the most common rock type on the surface of Earth. The oceanic crust, which covers more than 70 percent of the surface of Earth, is composed of basalt and its intrusive equivalent, gabbro. Basalts dominate the rocks on oceanic islands and are also widespread on the continents. One of the major petrologic discoveries in the twentieth century was that basalts are partial melts of the mantle (Green and Ringwood, 1969). With this insight, basalts became more than simply interesting volcanic rocks: they took on significance as probes of the mantle. The chemistry of basalts, including their major and trace element compositions as well as their isotope geochemistry, provides direct evidence about the nature and composition the mantle that is difficult to obtain by other means. This chapter describes the petrology of basalts, the structure and composition of the mantle from which they are derived, and the various processes by which the mantle may partially melt to form basaltic magmas.

5.2 Basalt Petrology

5.2.1 Classification

Because basalts are typically fine-grained to glassy rocks, the most common classification is based upon normative (as opposed to modal) mineralogy. One of the best ways to visualize basalt chemistry is by use of the basalt tetrahedron (Yoder and Tilley, 1962) (Figure 5.1). The basalt tetrahedron has the apices of normative augite (Aug), quartz (Qz), nepheline (Nph), and olivine (Ol). Normative albite (Ab) plots one third of the way toward Nph from Qz and normative hypersthene (Hyp) plots midway between Ol and Qz. Because Hy never coexists with Nph, the Ol-Ab-Aug plane is always present. This plane is called the **plane of critical silica undersaturation** and separates Hyp-normative bulk compositions from Nph-normative bulk compositions. The Nph-normative basalts are called **alkali basalts**; the Hyp-normative basalts are called **tholeiites**. Because the Mg-rich olivine found in basalts never coexists with quartz, the Hyp-Ab-Aug plane is also important to basalt petrology. This plane is called the **plane of silica saturation** and it separates quartz-saturated tholeiites (i.e., **quartz tholeiites**) from olivine-saturated tholeiites (i.e., **olivine tholeiites**).

5.2.2 Chemistry and Petrography

The normative differences between the two basalt types reflect their subtle differences in chemistry. As their name implies, alkali basalts are richer in alkalis (Na_2O and K_2O) and poorer in CaO than are tholeiites. As such, they plot in the alkalic or alkali-calcic fields of Peacock (1931), whereas tholeiites are typically calcic or calc-alkalic. Important, alkali basalts have slightly lower silica contents than tholeiites (46–48 percent compared to 48–52 percent). Because alkali feldspars (for example, albite, $\text{NaAlSi}_3\text{O}_8$) contain more silica than calcic feldspars ($\text{CaAl}_2\text{Si}_2\text{O}_8$), crystallization of alkali feldspar will deplete silica from a rock more effectively than will crystallization of calcic feldspar. Thus the combination of relatively high alkalis and low silica explains why alkali basalts are nepheline normative. In addition to the differences in major element abundances, alkali basalts also tend to be richer in incompatible elements than tholeiites. As we noted in Chapter 4, incompatible elements are elements incompatible with crystallizing silicates but compatible with melt. These elements, such as TiO_2 , Fe_2O_3 , and rare earth

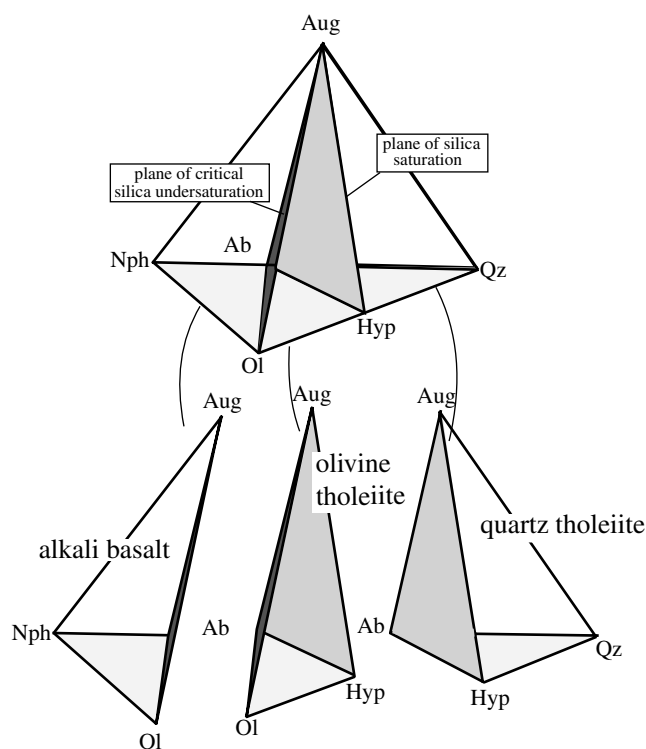


Figure 5.1 The basalt tetrahedron showing the differences in normative composition between alkali basalt, olivine tholeiite, and quartz tholeiite. After Yoder and Tilley (1962).

elements, are likely to be concentrated in the magma as it crystallizes or are likely to be the first elements to enter a melt when melting begins.

The chemical differences between tholeiites and alkali basalts are reflected in the following petrographic differences. Tholeiites typically contain olivine only as a phenocryst. The olivine commonly shows signs of resorption or reaction to pigeonite or hypersthene. Groundmass phases include pyroxenes and plagioclase. The augite in tholeiites is typically colorless, indicating that it is poor in ferric iron and titanium. Some quartz tholeiites may contain groundmass quartz or vesicles lined with a silica mineral, although in many quartz tholeiites the excess silica will be hidden in its glassy matrix. Alkali basalts contain olivine as both phenocrysts and groundmass. The augite tends to be pleochroic because it contains small amounts of ferric iron and titanium. There may be a late-stage alkali feldspar, often anorthoclase, in the groundmass. In most alkali basalts the normative nepheline is hidden in the residual glass, however, if the basalt is very alkalic, nepheline may appear in the groundmass. Such a basalt is called a **basanite**.

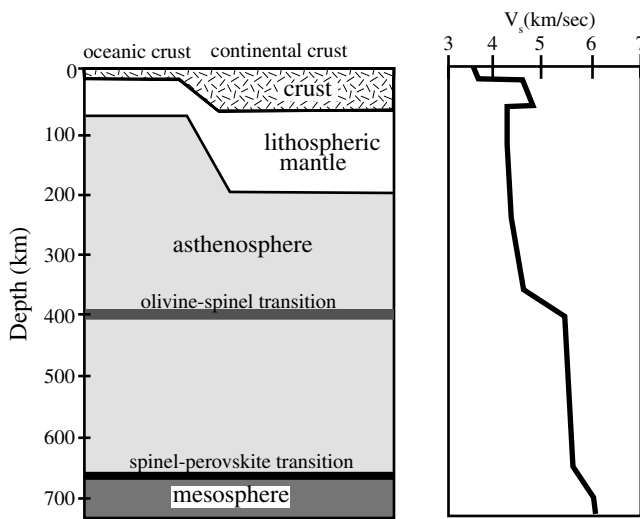


Figure 5.2 The major layers of the crust and mantle, along with characteristic S-wave velocities for each layer.

As depicted in Figure 2.9, in the system nepheline – silica, albite is a thermal barrier. Melts on the silica side of the albite composition evolve to a quartz-bearing eutectic, whereas melts on the nepheline side evolve to a nepheline-bearing eutectic. This behavior extends to more complex silicate systems as well. Those melts that lie to the nepheline side of the olivine-albite-diopside plane in Figure 5.1 (i.e., alkali basalts) differentiate toward Nph-saturation, whereas those melts on the hypersthene side (i.e., tholeiites) differentiate toward Hyp- or Qz- saturation. As a result, alkali basalts and tholeiites follow very different differentiation paths. During differentiation, alkali basalts evolve to form nepheline-bearing rocks, such as phonolites or their plutonic equivalents, nepheline syenites (i.e., the rocks on the lower half of the IUGS diagrams shown in Figures 1.1 and 1.4). Tholeiites, in contrast, evolve toward silica saturation, forming residual magma with trachytic or rhyolitic composition.

5.3 Melt Generation from the Mantle

5.3.1 Mantle Composition

Because the mantle cannot be directly sampled, petrologists deduce its composition indirectly. The proxy evidence includes:

Evidence from mantle-derived melts. The compositions of partial melts derived from the mantle, particularly mid-ocean ridge basalts and ocean island basalts,

place important constraints on the composition of the mantle.

The composition of rocks of mantle origin. Samples of rock that formed in the mantle can be found at Earth's surface and give important indications of the rocks that compose the upper mantle. Mantle rocks occur as xenoliths in basalts or kimberlites, as well as **ophiolites** (discussed further in Chapter 6), which represent pieces of the upper mantle and oceanic crust that have been thrust onto the continents.

The composition of chondritic meteorites. Chondritic meteorites have a similar composition to the bulk composition of Earth. The composition of the mantle can be estimated by taking the chondrite composition and subtracting those elements thought to make up Earth's core and crust.

Geophysical evidence. The geophysical properties of the mantle, in particular its density and seismic velocity, allow geologists to construct a fairly robust picture of mantle structure and place some constraints on composition.

These various kinds of evidence suggest the mantle has the composition of lherzolite: a peridotite dominated by olivine that contains both orthopyroxene and clinopyroxene (see Figure 1.3). An aluminous mineral is also present: either plagioclase, spinel, or garnet. Depth is the primary control determining which aluminum-bearing mineral is present; plagioclase forms at the shallowest levels, whereas garnet forms at greatest depth.

5.3.2 Crust and Mantle Structure

Geophysical evidence indicates the outer 700 kilometers of Earth consist of the following major layers (Figure 5.2):

Oceanic or continental crust. Oceanic crust is between three and ten kilometers thick, and continental crust is up to eighty kilometers thick. The base of the crust is defined by the Moho, the seismic discontinuity across which S-wave velocity increases from around 3.5 km/s in the crust to 4.5 km/s in the mantle.

Lithospheric mantle. Lithospheric mantle is the upper portion of the mantle that deforms brittly. It is defined by relatively high S-wave velocities of around 4.5 to 5 km/s. It extends to about 80 kilometers depth beneath the oceans, and to around 200 kilometers beneath continents.

Asthenosphere. The asthenosphere extends from the base of the lithosphere to around 660 km depth. It is a relatively weak zone that deforms by creep. S-wave velocities

are lower than in the lithospheric mantle, and may be attenuated in part because of the presence of a partial melt. Together, the asthenosphere and lithospheric mantle compose the **upper mantle**.

Mesosphere. The mesosphere is the part of the mantle below the asthenosphere, extending to the outer core. Its upper boundary is marked by a change in seismic velocity and density thought to correspond to a change in mineral structure in response to increasing pressure. The mesosphere is coincident with the **lower mantle**.

5.3.3 Mechanisms for Partial Melting of the Mantle

The normal temperatures encountered at increasing depth in the mantle (the dashed line indicating the geothermal gradient in Figure 5.3) are always below the solidus for fluid-absent lherzolite. Under ordinary circumstances, therefore, the mantle is solid. However, a number of phenomena can generate mantle melting. First, the normal geothermal gradient could be perturbed, so that it is locally hot enough to melt. This may occur beneath ocean islands at “hot spots” such as Hawaii.

Second, the temperature at which melting begins could be lowered by addition of a component to dry lherzolite. The addition of CO_2 and/or H_2O to peridotite lowers the solidus significantly (Figure 5.3). This means that the addition of CO_2 and even small amounts of H_2O can lower the solidus enough melt can be produced from lherzolite at the temperatures and pressures thought typical of the normal mantle thermal regime (Figure 5.3). Because subduction carries water-rich fluids along with oceanic crust into the mantle, this process is likely an important mechanism for adding fluids that depress the mantle solidus and trigger partial melting.

A third mechanism that may produce melting is decompression of ascending mantle. Mantle material may ascend either as part of convection cells or as diapirs. The temperature gradient across the center of a convection cell is approximately adiabatic; that is, no heat is transferred in or out of the mass under consideration. For mantle materials, the adiabatic gradient is around $0.3^\circ\text{C}/\text{km}$, which means that mantle rising adiabatically does not cool appreciably as it ascends. By comparison, the melting point gradient of anhydrous mantle is much steeper (Figure 5.3). This relationship is shown by the arrow in Figure 5.3, which indicates the P-T path of a rising mantle diapir that originally lay on the mantle geotherm. As

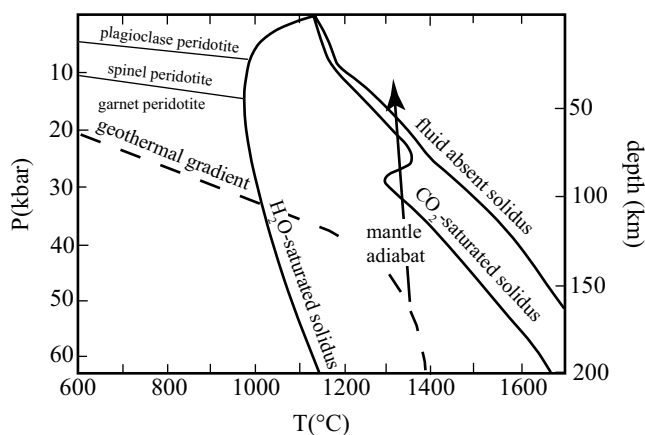


Figure 5.3 Diagram showing how adiabatic decompression of the mantle (arrow) can lead to melting even if the mantle is dry. Modified from Philpotts and Ague (2009).

the diapir is decompressed adiabatically, it will melt when it crosses the fluid-absent solidus at around fifty kilometers depth, even if the mantle lacked any fluid component such as CO_2 or H_2O . (If the mantle contains CO_2 or H_2O , then melting begins at greater depth.) Because mid-ocean ridges are located above up-going limbs of convection cells, decompression melting is particularly important at mid-ocean spreading centers.

5.3.4 The Process of Mantle Melting

The composition of partial melts of the mantle and their residual solids can be illustrated in the simplified system Di-Fo-En (Figure 5.4). Lherzolite plots near the center of this ternary system. On heating, the first melt to form is of eutectic composition (point X). As melting proceeds, the residual solids will become progressively more olivine-rich (gray arrow in Figure 5.4). After about 25 percent melting, the diopside (as well as most of the aluminous phase, spinel or garnet) will have been completely incorporated into the melt, and the residue will consist only of olivine and orthopyroxene (i.e., the rock will be a harzburgite). If melting proceeds further, the melt composition will become increasingly enriched in the orthopyroxene component (black arrow in Figure 5.4), while the residua becomes enriched in olivine.

Production of basaltic melts therefore leaves the mantle enriched in olivine. This leads to the common terminology applied to peridotites. A **fertile** lherzolite (a lherzolite from which a basaltic melt can be extracted) contains abundant green (i.e., Al_2O_3 -rich) spinel as well as clinopyroxene that may be rich in minor components such as TiO_2 and Na_2O . In a **depleted** lherzolite (a lherzolite from which a partial

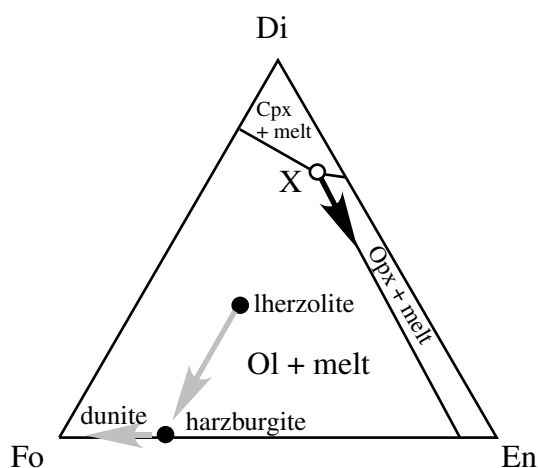


Figure 5.4 Simplified phase diagram for the system Fo-Di-En at about 20 kbar. Black arrow shows the path followed by the melt during melting of lherzolite; gray arrows show the path followed by the residua.

melt has been extracted), the spinel is Cr rich and less abundant than in fertile lherzolite, and the clinopyroxene has lower Na_2O and TiO_2 contents. Extremely depleted mantle rocks include harzburgite (a peridotite with little or no clinopyroxene) or dunite, which contains olivine with only minor amounts of orthopyroxene and clinopyroxene.

5.3.5 Origin of Tholeiitic versus Alkali Basalts

As noted at the beginning of this chapter, there are two main basalt types, tholeiitic and alkalic. It is natural to ask how melting of the mantle can produce basalts of varying compositions. Possible explanations include:

1. *The alkalic and tholeiitic basalts come from two different sources with different compositions.* As discussed in Chapter 9, mantle-derived, alkaline magmas display a wide range of compositions, from hyper-potassic magmas, such as those of the Roman province of Italy, to highly sodic magmas, such as those from the East African Rift. It is appealing to invoke a heterogeneous mantle to explain this broad compositional spectrum. If the extreme compositional range observed in alkaline rocks does reflect heterogeneous mantle, then the same heterogeneity may also explain lesser compositional differences, such as those that distinguish tholeiites and alkali basalts.
2. *Both alkali basalts and tholeiites come from the same kind of source but they represent melting at different pressures or different degrees of partial melting.* Most

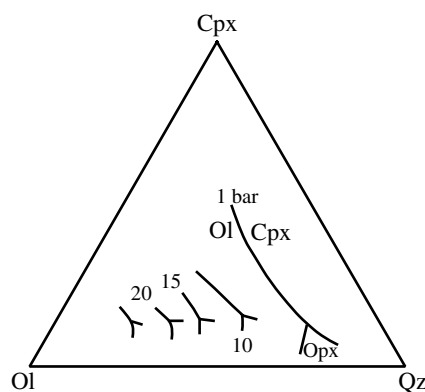


Figure 5.5 Pseudoternary projection from plagioclase on to the olivine-diopside-quartz plane showing how location of the basalt eutectic changes with increasing pressure. Modified from Elthon (1989).

alkali basalts differ only slightly in composition from tholeiites, so a substantial difference in source composition is not required. Furthermore, in some places, like Hawaii, the basalt types grade from alkalic to tholeiitic during the eruptive history of a volcanic center. To explain this, many petrologists argue that alkali basalts and tholeiitic basalts come from a single mantle source. Evidence supporting this argument derives from the fact that augite in the mantle is the major source of Na_2O , K_2O , TiO_2 , and other incompatible elements enriched in alkali basalts. As noted earlier, augite is the first silicate depleted from melting of lherzolite. If Na_2O is extracted preferentially from this pyroxene during early stages of partial melting of the mantle, then the first melts are alkaline. As melting proceeds, the magmas become progressively more calcic, approaching tholeiite in composition.

Another possible explanation for the origin of the different basalt compositions relates to the pressure of melting. Figure 5.5 shows the effect of pressure on the olivine-orthopyroxene-clinopyroxene-plagioclase eutectic as projected from an aluminous phase (plagioclase, spinel, or garnet). This diagram, which is called a **pseudoternary** diagram, is read in a similar way to Figure 2.15 as long as the projected phase – plagioclase (or spinel or garnet at higher pressure) – is always present. Figure 5.5 shows that increasing pressure moves the eutectic away from silica toward olivine, meaning melts generated at high pressure will likely have less silica than those produced at lower pressure. Thus alkali basalts may be generated from the

same mantle as tholeiites either by lower degrees of partial melting, or at higher pressure, or both.

5.4 Environments where Magmas are Generated

Igneous activity observed today is confined to relatively few tectonic environments:

Constructive plate margins. These are divergent plate boundaries, such as mid-ocean ridges and back-arc spreading centers, where mantle upwells, decompression melting occurs, and magma is emplaced into the rift. Magmatism in this environment is described in Chapter 6.

Destructive plate margins. These are convergent plate boundaries that are either ocean-ocean or ocean-continent collision zones. In these collisions, water subducted

into the mantle via the downgoing, hydrated plate induces melting in the overlying mantle. The resulting magmatism forms ocean islands and continental margin arcs discussed in Chapter 7.

Oceanic intraplate regions. These manifest as islands and sea floor plateau that decorate the ocean floor and that were probably caused by hot spot magmatism. Oceanic intraplate magmatism is described in Chapter 6.

Continental intraplate regions. Within-plate continental magmatism produces igneous rocks that manifest a substantial range in composition because the magmas form by a number of processes and because the rocks that partially melt are compositionally varied reflecting a range of mantle and continental sources. Continental intraplate volcanism and plutonism are the subjects of Chapters 8 and 9, respectively.

Summary

- Basalts are classified as alkali basalts, quartz tholeiites, and olivine tholeiites based on their normative mineralogy.
- Alkali basalts evolve toward nepheline saturation and form phonolites and nepheline syenites. Tholeiites evolve toward silica saturation and form trachytes and rhyolites.
- The mantle is composed of an upper lithospheric mantle, which overlies the asthenosphere and mesosphere.
- The temperatures and pressures in the mantle encountered along a typical geothermal gradient are always below the solidus for dry melting of the mantle, so the mantle is normally solid.
- Partial melting of the mantle produces basaltic magmas. Melts are generated by perturbing the normal geothermal gradient to raise the temperature of the mantle, lowering the melting point by adding water or CO₂ or other components, or by bringing the mantle to shallower depths and producing melt by decompression.
- Alkali basalts and tholeiites could come from different mantle sources, or form from the same mantle source by different degrees of melting, or melting at different pressures.
- The tectonic environments that generate the greatest volume of magma are at constructive plate margins, both at mid-ocean ridges and in back-arc spreading centers (Table 5.1). Subduction zones are the second most voluminous sites of magmatism, followed by oceanic intraplate regions where ocean islands and plateau are formed. Lesser volumes of magma form within continental plates, but this tectonic setting creates the most variety of igneous rock compositions.

Table 5.1 Global Rates (km³/yr) of Cenozoic Magmatism

Location	Volcanic rocks	Plutonic rocks
Constructive plate boundaries	3.0	18.0
Destructive plate boundaries	0.4–0.6	2.5–8.0
Continental intraplate regions	0.03–0.1	0.1–1.5
Oceanic intraplate regions	0.3–0.4	1.5–2.0
Global total	3.7–4.1	22.1–29.5

Sources: Crisp (1983) and McBirney (1993)

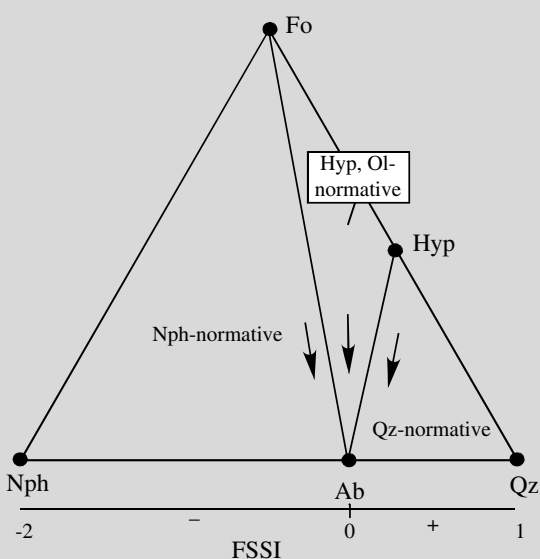
Questions and Problems

Problem 5.1. Describe three mechanisms by which the mantle may partially melt. Give the tectonic environments in which each of these mechanisms may operate.

Problem 5.2. What are the mineralogical and chemical differences between alkali and tholeiitic basalt? What rock types represent the extreme differentiates of each?

Problem 5.3. What rocks that can be collected at Earth's surface provide the best information about the composition of the mantle? Explain your answer.

Problem 5.4. Use the figure below (from Frost and Frost, 2008) to relate the FSSI index (Chapter 4) to the basalt tetrahedron (Figure 5.1). Give the range of FSSI for alkali basalt, olivine tholeiite, and quartz tholeiite.



Further Reading

McBirney, A. R., 2007, *Igneous petrology*, 3rd ed. Jones and Bartlett, Boston, Chapter 1.

McKenzie, D. and Bickle, M. J., 1988, The volume and composition of melt generated by the extension of the lithosphere. *Journal of Petrology*, 29, 625–79.

Philpotts, A. R. and Ague, J. J., 2009, *Principles of igneous and metamorphic petrology*, 2nd ed., Cambridge University Press, Cambridge, Chapter 23.

Wilson, M., 1989, *Igneous petrogenesis: A global tectonic approach*. Unwin Hyman, London, Chapter 3.

Chapter 6

Oceanic Magmatism

6.1 Introduction

Because it is covered by kilometers of water, ocean crust was long inaccessible to direct observation by geologists. Today, however, our knowledge of the ocean floor comes from two sources, the study of fragments of the ocean floor that have been thrust onto the land, called **ophiolites**, and from ship-based geophysical and geological studies that burgeoned during the Second World War and were followed by the Deep Sea Drilling Program (DSDP), which began in 1968. These investigations provided the foundation that underpins our understanding of oceanic magmatism. This chapter first discusses the structure and stratigraphy of ophiolites and to what extent they provide models that help understand the ocean crust. A description of advances achieved by recent research of the ocean floor based on geophysical studies and ocean drilling follows. Finally, this chapter describes the magmatic suites that compose ocean islands and oceanic plateau.



Map 6.1 Map showing select ophiolite belts around the world. Ophiolites occur along the trends indicated by bold lines. Stars show particularly well-known occurrences. Data from Irwin and Coleman (1974).

6.2 The Petrology and Structure of the Ocean Crust

6.2.1 Ophiolites as a Model of the Ocean Crust

Geologists have long recognized that an association of peridotite (in many places hydrated to serpentinite), gabbro, basalt, and deep-water chert are exposed in many places around the world (Map 6.1). In some localities, these rocks form a complete stratigraphic section, but in many places one or more of these rock types exist within fault-bounded tectonic slices. As early as the 1820s this association was called an **ophiolite**, but before the advent of plate tectonics, the significance of these rocks was cryptic. Geologists attending the September 1972 Penrose Conference defined the stratigraphy of a typical ophiolite, shown in Figure 6.1 (Anonymous, 1972). Implicit in the definition is the assumption that ophiolites are fragments of oceanic crust thrust onto the continents, and thus the stratigraphy described at the Penrose Conference represents an idealized cross-section of the oceanic crust.

The uppermost layer in an ophiolite is composed of deep-water sediments, mostly pelagic mud, although chert may be common in some places. The thickness of

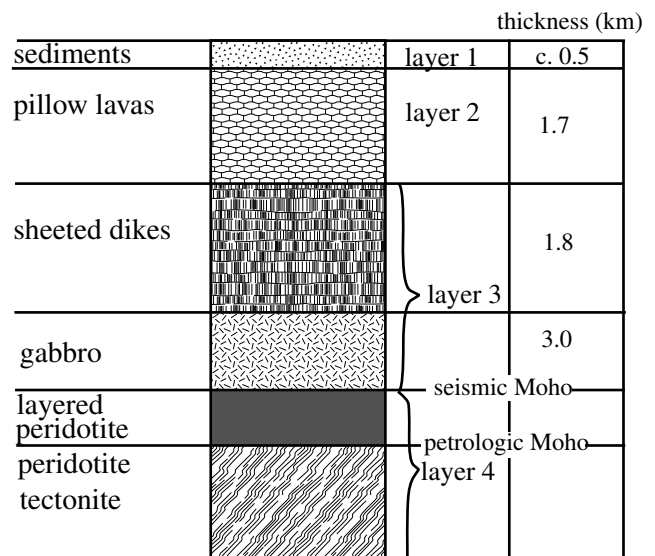


Figure 6.1 Petrologic and seismic profile for an ideal ophiolite (Anonymous, 1972).

this layer depends on the age of the crust. On juvenile oceanic crust there are no sediments; the thickness of the sediment layer generally increases with age. A kilometer or so of pillow basalts, which represent lavas that were erupted directly onto the ocean floor, underlie the

sediments. The pillow basalts grade into sheeted dikes, a horizon that may be over a kilometer thick. Sheeted dikes are dikes that consistently chilled on one side only. They are interpreted to have been emplaced into a spreading center, with each new dike intruded into the core of a preceding dike. Below the sheeted dikes lie several kilometers of gabbro. The top of the gabbro is directionless, but toward the bottom it may be layered or foliated. This layer is interpreted to have crystallized from an intrusive body of basaltic magma. Below this lies layered peridotite, which is much denser than the overlying gabbro. The contact between peridotite and gabbro is the location of a distinct change in seismic velocity marking the Moho. However, because these peridotites are interpreted to have formed as cumulates from the basaltic magma, they are unrelated to underlying mantle and actually represent an ultramafic portion of the crust. Below the cumulate peridotites is a highly deformed peridotite, which is interpreted as mantle depleted by partial melting during basalt genesis. Petrologically this is true mantle, even though it is impossible to distinguish it seismically from the overlying cumulate peridotite.

6.2.2 Refinements of the Ophiolite Model

Nearly as soon as the Penrose ophiolite model was proposed, geologists began to debate whether the model describes a true picture of the ocean crust (Miyashiro, 1975; Moores, 1982). It quickly became evident that ophiolites form in diverse tectonic environments, and not all reflect ocean-floor stratigraphy produced at mid-ocean spreading centers. Some ophiolites, such as the Troodos ophiolite in Cyprus, contain basalts more closely related compositionally to arc basalts than to mid-ocean ridge basalts (Miyashiro, 1973) and evidently formed above newly initiated subduction zones. These are called **suprasubduction-zone** ophiolites (Pearce, Lippard, and Roberts, 1984). Observations suggest ophiolites form in a wide range of tectonic environments and thus resist a simplified, “one-size-fits-all” model. In addition to forming above subduction zones, ophiolites form by back-arc spreading as did the Rocas Verdes ophiolite in Chile (Stern and de Wit, 2003), at the contact between a back-arc and an arc as did the Bay of Islands ophiolite in Canada (Kurth-Velz, Sassen, and Galer, 2004), or in an oceanic spreading center as did the Macquarie Island ophiolite in the south Pacific (Varne, Brown, and Faloon, 2000) and the Oman

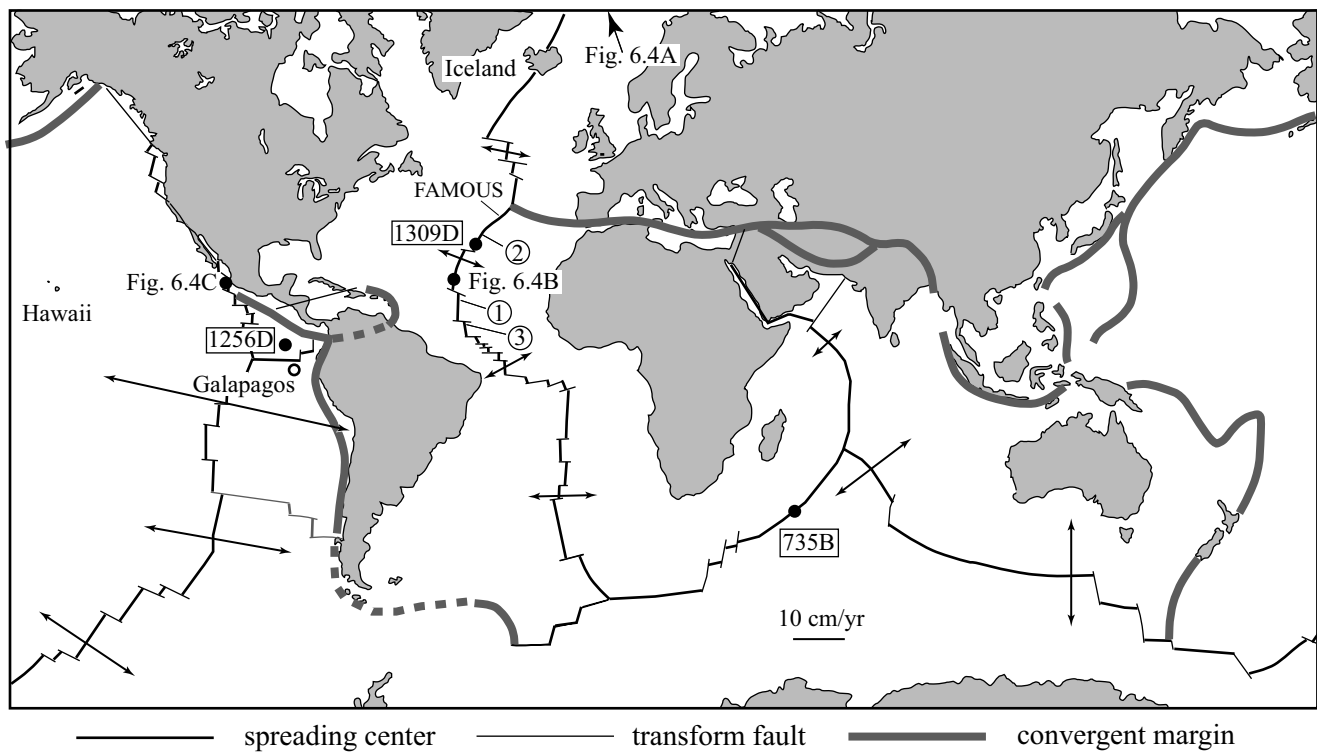
ophiolite on the Arabian Peninsula (Boudier and Nicolas, 2011). Map 6.1 shows the global distribution of these and other major ophiolites.

A second problem with the ophiolite model arose in the 1990s and 2000s when seismic surveys and deep-ocean drilling showed the stratigraphy of the oceanic crust is far more complex than the ophiolite model suggested. Geophysical studies revealed significant differences in spreading rates among oceanic ridges (Map 6.2) and that ridges with different spreading rates have different morphology (Figure 6.2), which translates into differences in crustal cross-section.

Fast-spreading centers. The East Pacific Rise (EPR) is an example of a fast-spreading center (half-rate 6–7 cm/yr). Fast-spreading centers are characterized by a 2.5 to 3.0 kilometer-wide zone of magma extrusion, which forms a smooth topographic high of around 200 meters (Figure 6.2A). Flat lava plains made of ponded lava lakes and small volcanic hills composed of sediment-free pillow lavas occur along the ridge axis. There is either no axial valley or only one that is poorly developed.

Seismic studies of the EPR appear to image large sub-axial magma chambers beneath fast-spreading centers. These magma chambers appear to be periodically replenished from below with fresh batches of mantle magma. Between additions of magma, fractional crystallization takes place. Lavas erupt when the magma pressure exceeds the lithostatic pressure and the strength of the chamber roof, probably coincident with addition of magma into the chamber. The crustal cross-section beneath a fast-spreading ridge is similar to that described by the ophiolite model.

Slow- and ultra-slow-spreading centers. The Mid-Atlantic Ridge (MAR) is a typical slow-spreading center (half-rate 1–2 cm/yr), and the Gakkel Ridge under the Arctic Ocean is an ultra-slow-spreading ridge (half-rate 0.1 cm/year) (Figure 6.2B, C). Unlike fast-spreading centers, slow- and ultra-slow-spreading centers tend to have a well-defined axial valley. The slow-spreading center is characterized by a twenty-five to thirty-kilometer-wide axial valley bounded by mountains. Within this broad valley is a second, well-defined inner valley, three to nine kilometers wide, where volcanic activity is concentrated (Figure 6.2B, C). Small volcanic hills occur within this inner valley, showing that volcanic activity is neither spatially nor temporally continuous.



Map 6.2 Tectonic map of the ocean basins showing mid-ocean ridges, convergent margins, transform faults, and areas discussed in the text. The length of the spreading rate vector arrows is proportional to the spreading rate. Numbers refer to cross-sections shown in Figure 6.3. Numbers in boxes refer to IODP drill holes shown in Figure 6.4. Modified from Brown and Mussett (1981) with additional data from Dick and colleagues (2000), Teagle and colleagues (2006), and Blackman and colleagues (2011).

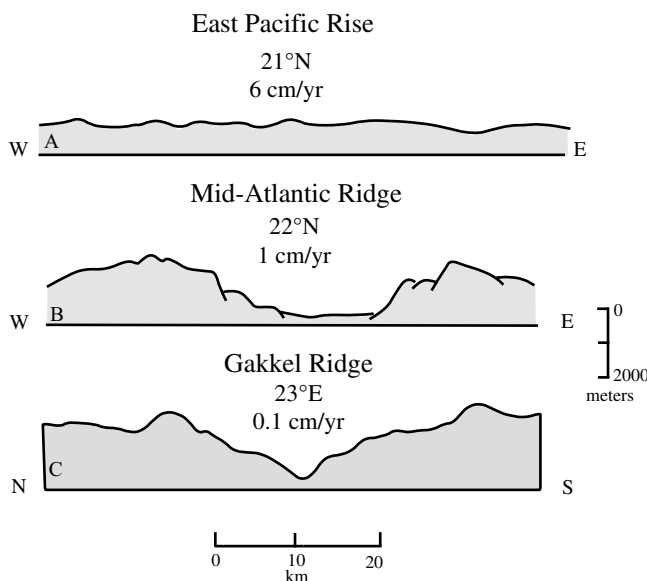


Figure 6.2 Morphology of (A) fast (East Pacific Rise), (B) slow (Mid-Atlantic Ridge), and (C) ultra-slow (Gakkel Ridge, Arctic Ocean) spreading centers. Data from Basaltic Volcanism Study Project (1981) and Cochran (2008).

A sub-crustal magma chamber beneath slow-spreading centers must either be about the width of the inner valley floor (three kilometers), or each volcanic hill may have a small (<1.5 kilometer-wide) magma chamber beneath it. The second hypothesis is more consistent with geophysical data, which does not observe attenuated S-waves as would be expected if a large magma chamber existed.

The crust beneath the slow-spreading centers is more poorly layered and more heterogeneous than the ophiolite model predicts. This is shown in surveys of fractures zones off of the Mid-Atlantic Ridge, where cross-sections of the oceanic crust are exposed (Figure 6.3). Because magma is not constantly supplied, extension at slow- and ultra-slow-spreading is partially or completely accommodated by faulting. These extensional faults produce crustal sections that eliminate some of the units in the ophiolite stratigraphy. In some places the basalt flows from the spreading centers are in fault contact with gabbro; in others the basalt is in contact with serpentinized peridotite. In many places in slow- and ultra-slow-spreading ridges this

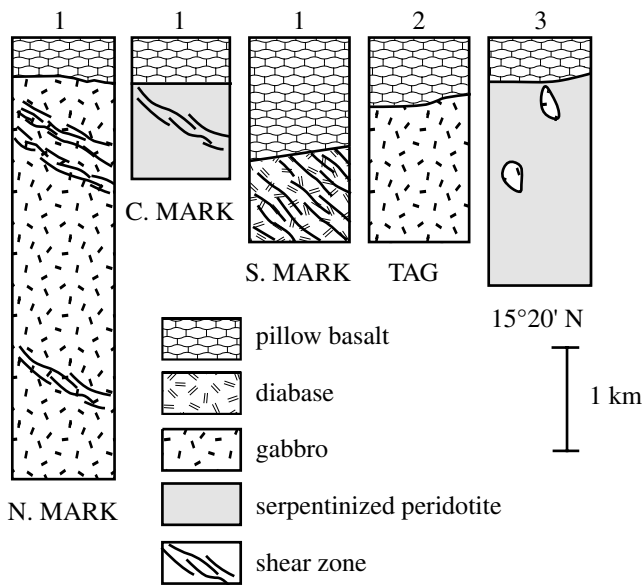


Figure 6.3 Cross-sections of oceanic crust beneath the Mid-Atlantic ridge. Numbers refer to locations in Map 6.2. After Karson (1998).

extension has stripped the crust from the mantle, exposing serpentinized peridotite directly on the sea floor.

Four decades of ocean drilling have revealed a great petrologic variability to the ocean crust (see Box 6.1). Deep drill cores in fast-spreading crust, such as Integrated Ocean Drilling Program (IODP) hole 1256D, show relations similar to what the ophiolite model predicts (Teagle et al., 2011) (Figure 6.4). However, drill holes into gabbroic crust exposed in slow-spreading ridges (IODP holes 375B and 1309D) show relations that are much more complex (Dick et al., 2000; Blackman et al., 2011) (Figure 6.4). Core from hole 375B from the Southwest Indian ridge contains mainly gabbro with minor amounts of oxide gabbro. The section is cut by several large, ductile shear zones. In contrast, core from hole 1309D from the Mid-Atlantic ridge contains a complex series of gabbro and oxide gabbro interlayered with screens of peridotite. Magmatic differentiation produced the oxide gabbro retrieved from holes 375B and 1309D. As explained in Chapter 2, crystallization of olivine (and any other Fe-Mg silicate) removes Mg from a melt preferentially to iron (Figure 2.11). Eventually this saturates the melt in Fe-Ti

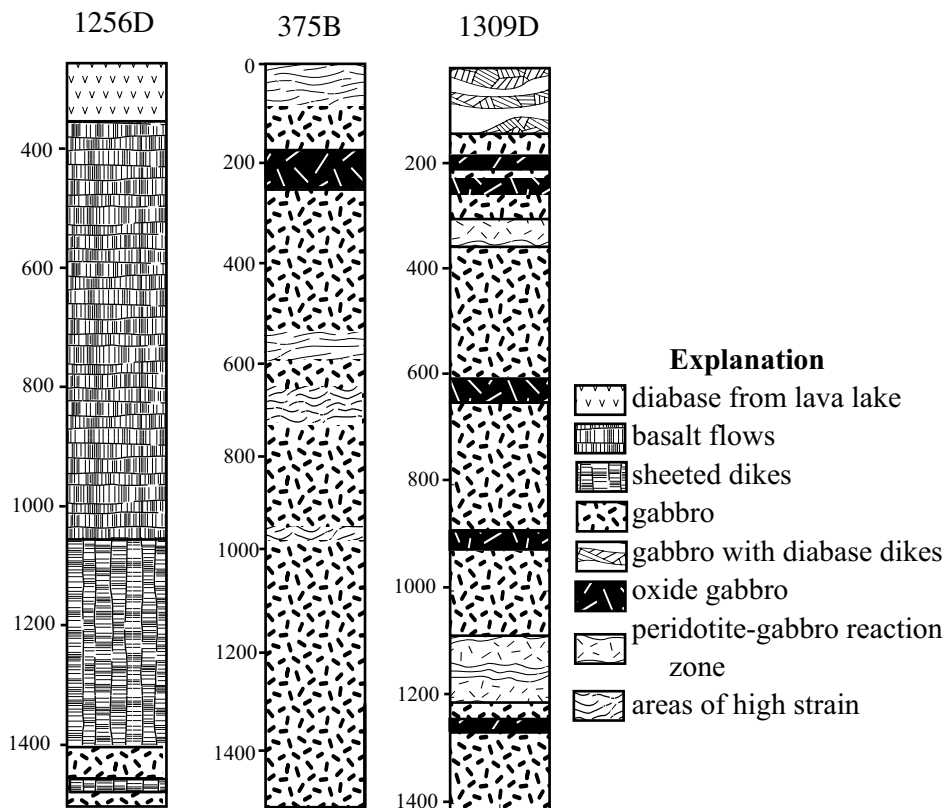


Figure 6.4 Cross-sections of the ocean crust as obtained in several IODP drill holes. Data from Dick and colleagues (2000), Teagle and colleagues (2006), and Blackman and colleagues l. (2011).

BOX 6.1 | OCEAN DRILLING

Before ocean drilling programs commenced, the only information scientists had about the composition of the ocean floor was obtained by dredging. Beginning in 1968, the United States' National Science Foundation (NSF) began a program to obtain samples of the ocean floor by drilling. The initial drilling project, entirely funded by the NSF, was called the Deep Sea Drilling Project (DSDP). In 1975, France, Germany, Japan, the Soviet Union, and the United Kingdom jointly funded the drilling program. DSDP ran from 1968 until 1983 using the research vessel *Glomar Challenger*. The *Glomar Challenger* was retired in 1983 and the drilling program resumed in 1985 as the Ocean Drilling Program (ODP) then, in 2003, as the Integrated Ocean Drilling Program (IODP), which uses the research vessel *Joides Resolution* and is ongoing today. Currently the drilling program is supported by twenty-six countries, including the United States, the European Union, the United Kingdom, Japan, China, India, Australia, and New Zealand.

One of the major scientific themes of the IODP is to study the petrology of the ocean crust to understand the geochemical and geodynamic processes involved in the solid Earth system. The scientific value of ocean drilling became apparent within the first years of drilling. The first cores substantiated the young age of the ocean crust and the dynamics of sea floor spreading, geologic observations and processes that now underpin discussions of plate tectonics. Ocean drilling verified that the primary transfer of energy and material from the deep Earth to the surface occurs via sea floor spreading and the creation of oceanic crust at mid-ocean ridges, as well as by upwelling magmas that form ocean islands, ocean plateau, and island arcs. Further drilling documented that sea floor spreading involves not only magmatic addition to the crust but locally, may include tectonic denudation as well. As a result of sea floor tectonics, a considerable area of the ocean floor is underlain by serpentinized mantle peridotite. Ocean drilling has enabled descriptions of the kinds of reactions involved in the alteration of the sea floor, including serpentinization; these reactions have proven critical to modeling the geochemistry of ocean water. Recent findings suggest that MORBs interact extensively with the mantle through which they move, producing hybrid troctolites whose existence was previously unexpected. In total, these observations help petrologists understand the evolution of mantle-derived basaltic magmas and the formation of oceanic crust.



Box 6.1 Rainbow over the drilling rig of the *Joides Resolution* 30°N on the Mid-Atlantic Ridge.

oxides (magnetite and ilmenite), producing the oxide gabbro. The presence of multiple oxide gabbro horizons in holes 375B and 1309D means the holes penetrated several discrete igneous bodies, each of which had differentiated to oxide gabbro. A significant amount of troctolite and olivine-rich troctolite is also present and these are inferred to have formed by reaction between the peridotitic mantle and the basalt emplaced into the spreading center (Blackman et al., 2011).

In summary, the data obtained from recent drilling of the sea floor shows that, although some or all of the components of an ophiolite may be present at any given locale, oceanic crust is immensely more complex than the ophiolite model implies. Fast-spreading centers produce crustal stratigraphy closest to the ophiolite model, but in slow-spreading areas faults truncate the stratigraphy and the gabbroic sequence consists of multiple injections of magma that interacted with the peridotite host rocks and differentiated in place.

6.3 Petrography and Geochemistry of Oceanic Magmatism

Oceanic magmatism occurs in two distinct environments: at mid-ocean ridges and at off-ridge locations where ocean islands and oceanic plateau are formed. The basalts erupted in each of these two environments are chemically and petrographically distinct. Volumetrically the most important environment is along mid-ocean ridges where new oceanic crust continually forms as tectonic plates diverge (Map 6.2). The basalt erupted here is olivine and quartz-normative tholeiite; these basalts are referred to as **mid-ocean ridge basalts (MORB)**. A significant volume of basaltic magma is also erupted from vents not located on ridges; this **off-ridge magmatism** occurs on ocean islands and oceanic plateau. The rocks erupted off-ridge are referred to as **ocean island basalts (OIB)**, and they include both tholeiitic and alkali basalts.

6.3.1 Mid-ocean Ridge Basalt

The fine-grained groundmass of MORB reflects rapid cooling of magma extruded into a cold submarine environment. Phenocryst assemblages in glassy basalts suggest the first minerals to crystallize are olivine + spinel. As the magma differentiates, plagioclase joins the crystallizing assemblage. Finally a groundmass consisting of

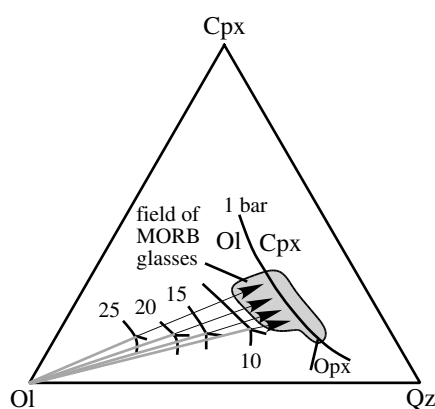


Figure 6.5 Pseudoternary projection from plagioclase onto the olivine-clinopyroxene-quartz plane showing the composition range of MORB glasses. Also shown are the eutectics for aluminous peridotite at 1 bar and 10, 15, 20, and 25 kilobars. See text for discussion. Modified after Elthon (1989).

plagioclase + Ca-rich clinopyroxene (augite) + olivine forms. Olivine compositions are typically Fo_{65-91} . The spinel is Mg and Cr rich, and is frequently found as inclusions in olivine. Plagioclase is typically An_{88-40} (Grove and Bryan, 1983) and is commonly more Ca-rich in basalts erupted on the Mid-Atlantic ridge than those erupted on the East Pacific rise. The presence of more sodic plagioclase on the East Pacific rise suggests magmas differentiate to a greater extent at fast-spreading centers where large magma chambers may be present (Hekinian, 1982).

Trace element characteristics of MORB suggest the type of mantle source rock from which partial melts are extracted is spinel or plagioclase lherzolite, rather than the high-pressure phase, garnet lherzolite. This mineralogy is consistent with geophysical studies of P- and S-wave attenuation, which suggest that the melting begins at depths of sixty to eighty kilometers, and the melt segregates at about twenty kilometers to rise and feed the magma chambers. At minimum, 20 percent partial melting is required to produce the most MgO-rich MORB compositions (Wilson, 1989).

The origin of MORB is summarized in Figure 6.5, which shows the system olivine-clinopyroxene-quartz-plagioclase as projected from anorthite to the olivine-clinopyroxene-quartz plane (see also Figure 5.5). Heavy lines on this pseudoternary projection are the locations of the olivine-clinopyroxene, olivine-orthopyroxene, and orthopyroxene-clinopyroxene cotectics in the presence of an aluminous phase at one bar, and ten, fifteen, twenty,

and twenty-five kilobars. At one bar the aluminous phase is plagioclase, at ten, fifteen, and twenty kilobars it is spinel, and at twenty-five kilobars it is garnet. This diagram clearly illustrates that increasing pressure stabilizes clinopyroxene with respect to olivine and orthopyroxene. This occurs because at increasing pressure clinopyroxene is progressively enriched in Na and Al.

To understand how to read Figure 6.5, consider a dry mantle diapir that begins melting at twenty-five kilobars. The first melt has a composition that lies on the olivine-orthopyroxene-diopside “eutectic.” (The quotation marks recognize that in a pseudoternary projection, the eutectic does not lie in the plane of the diagram.) If this high-pressure melt moves to shallower crustal levels (i.e., to lower pressure), for example to a pressure of ten kilobars, then the original melt will no longer lie on the “eutectic.” Rather it will lie in the field of primary olivine crystallization. As olivine crystallizes, it drives the residual melt composition directly away from the olivine apex as the light grey arrow originating at olivine and passing through the “eutectic” composition shows. All melts derived by fractional crystallization of olivine from the twenty-five-kilobar “eutectic” lie along the dark portion of the arrow. Partial melting at a range of mantle depths and fractional crystallization of olivine during magma ascent will produce the observed compositional range of MORB glasses (gray field in Figure 6.5).

Figure 6.5 implies that the range in compositions of MORB results from a number of processes. First, magmas form by partial melting at various depths, producing parent magmas with a limited but varying composition. These magmas start to crystallize during ascent into the ridge center. When the magmas pond at low pressures (i.e., less than ten kilobars), magmas originating from different depths mix. These composite melts move to shallow magma chambers where their compositions are further changed by low-pressure differentiation. Finally, observations from IODP hole 1309D suggest the magmas interact with their mantle host rocks at relatively shallow crustal levels and that this process further affects the compositions of MORB (Blackman et al., 2011).

These multiple processes result in a small but significant range in the major element composition of erupted MORB. The composition of basalt liquids erupted on the sea floor can be determined from the composition of basalt glass. Compositions of basalt glasses from the Narrowgate region

of the FAMOUS valley, Mid-Atlantic Ridge (Figure 6.6) show that although SiO_2 contents are relatively constant, MgO varies between 7 to 9 percent. As the observed phenocrysts – olivine, plagioclase, and augite – crystallize, MgO in the remaining melt decreases. Thus, plotting the basalt glass compositions as a function of MgO indicates the behavior of the other major elements as a function of magmatic differentiation. The decrease in Al_2O_3 and CaO with decreasing MgO is consistent with the crystallization of plagioclase and olivine. Crystallization of these phases alone would not result in the observed decrease in CaO; another calcium-rich phase, augite, is required to account for the observed compositional range of basalt glasses. Both FeO^{tot} and TiO_2 behave incompatibly in MORB and increase with decreasing MgO, indicating that neither ilmenite nor Ti-magnetite were crystallizing during the limited fractionation of these rocks. This geochemical dataset indicates that minor differentiation occurs during emplacement of MORB onto the sea floor. More extensive differentiation by crystal fractionation would not be expected, given the rapid cooling of the magma in contact with seawater.

There are two places where hot spot activity has produced enough tholeiitic lava to produce islands that rise above sea level – Iceland and the Galapagos Islands. Iceland is located on the Mid-Atlantic Ridge, and the Galapagos Islands sit slightly off axis of the Galapagos spreading center. Both localities represent places where basalts formed by upwelling and decompression of mantle at a spreading center and are also affected by complex interaction with a mantle plume or hot spot (Harpp et al., 2002; O'Connor et al., 2007). Whereas basalt generated at mid-ocean ridges is commonly considered “normal,” or N-MORB, basalts at locations on or near hot spots exhibit higher concentrations of incompatible elements and may be referred to as “enriched,” or E-MORB. In addition to enrichments in incompatible elements, both Iceland and the Galapagos contain volcanoes that have erupted lavas with a wide range of compositions, from basalt to rhyolite (Carmichael, 1964; McBirney and Williams, 1969). Lavas from both centers show similar differentiation trends (Figure 6.7). The magma undergoes extensive differentiation when a large change in $\text{FeO}^*/(\text{FeO}^* + \text{MgO})$ ratio coincides with a minimal change in silica content. This trend results from the crystallization of olivine and pyroxenes without participation of Fe-Ti oxides. Such differentiation

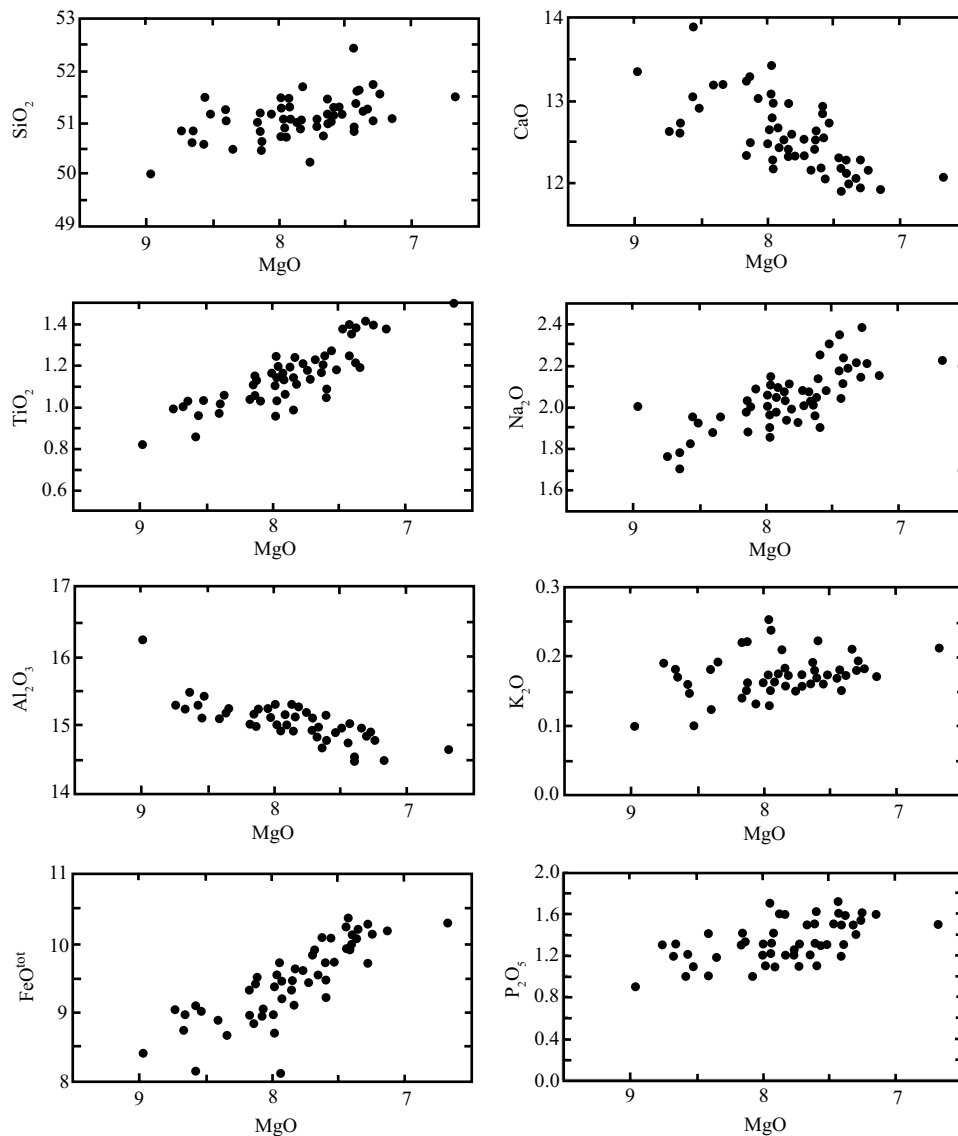


Figure 6.6 Compositions of basalt glasses from the Narrowgate region of the FAMOUS valley, Mid-Atlantic Ridge. Data from Stakes, Shervais, and Hopson (1984).

enriches the magma in iron and leads to the formation of ferrobasalt, a basalt with more than 13 percent FeO^* and less than 6 percent MgO (McBirney and Williams, 1969). As such, the rhyolites formed by differentiation of these basalts are ferroan, metaluminous, and calc-alkalic (in Iceland) to alkali-calcic and alkalic (in the Galapagos) (Figure 6.7).

6.3.2 Off-ridge Magmatism

Off-ridge magmatism falls into three broad categories:

1. **Seamounts:** these submarine volcanic structures either never grow enough to breach sea level or if they do, they are eroded and subside. In the tropics, they may
2. **Oceanic island volcanoes:** these immense volcanoes rise up to ten thousand meters above the ocean floor and have dimensions greater than the largest

be capped with coral reef deposits, but as the volcano subsides only a guyot (a flat-topped seamount that lies just below sea level) remains. Seamounts are most abundant in the Pacific, where they number between twenty-two thousand and fifty-five thousand (Batiza, 1982). Many seamounts appear along fracture zones, which may provide conduits for the magma. Others form linear chains that show a progressive age relationship, and that suggest a genetic relationship with ocean island volcanoes.

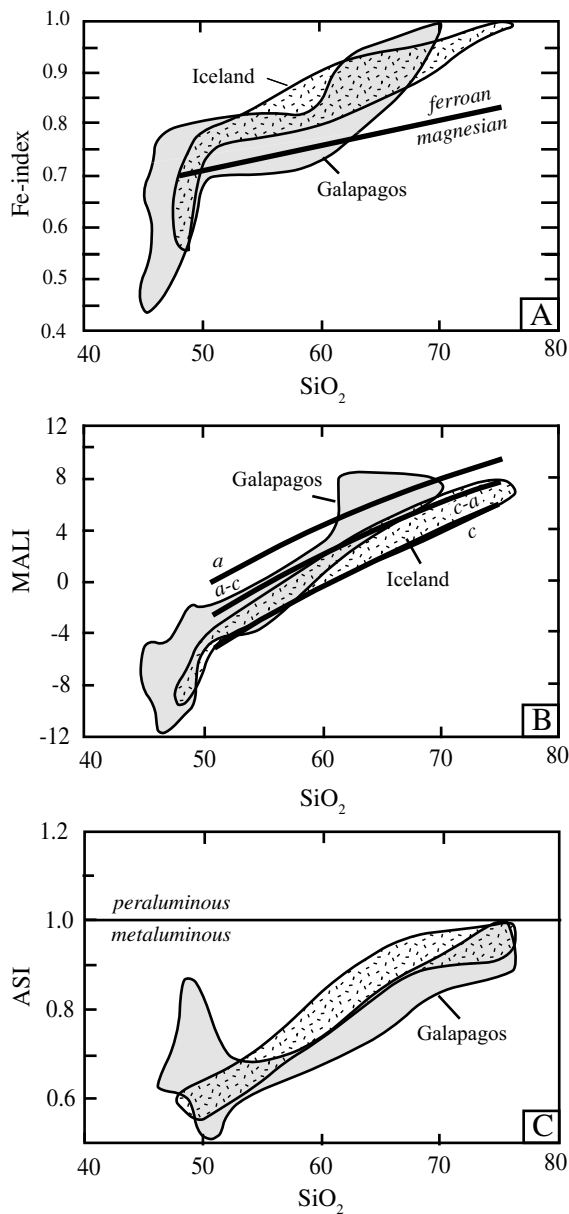


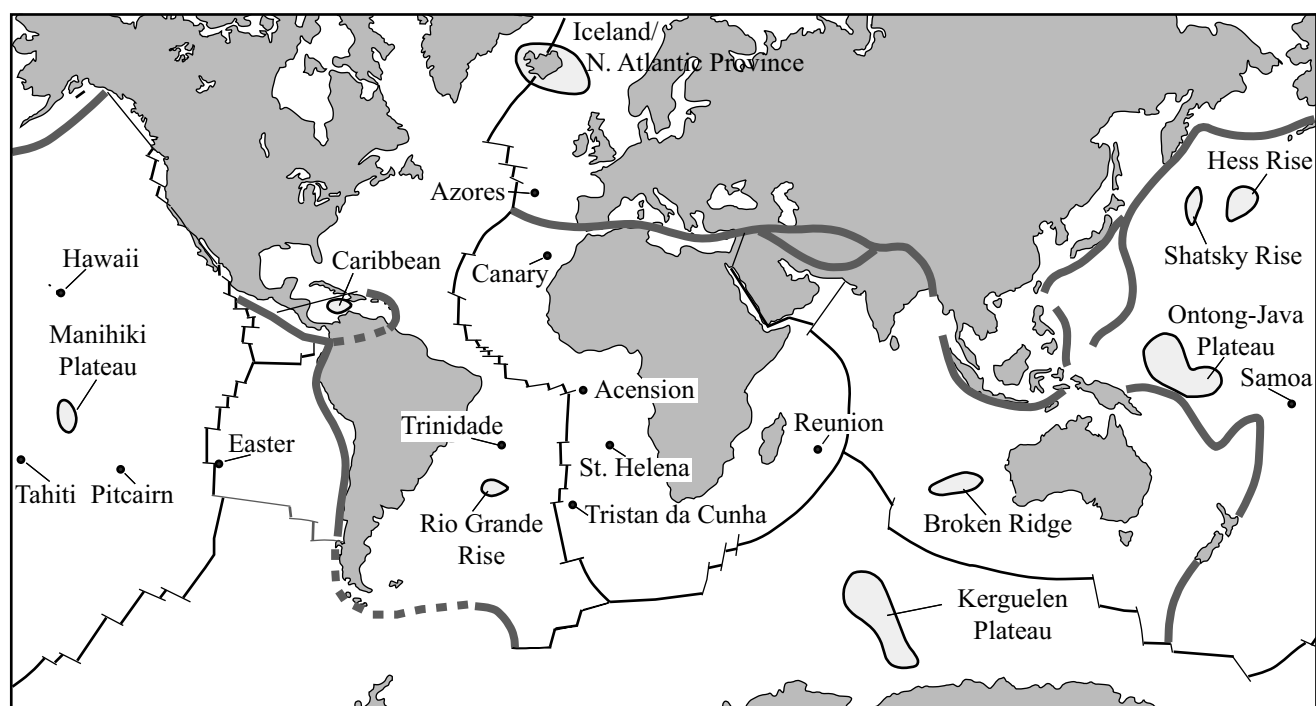
Figure 6.7 Geochemical trends of volcanoes on the Galapagos Islands and Iceland, both of which straddle oceanic ridges. Data from McBirney and Williams (1969) and Carmichael (1964).

mountains on the continents. Usually an ocean island volcano has several centers, suggesting the focus of magmatic activity migrates with time. Ocean island volcanoes may be single islands, or in fast-spreading oceans like the Pacific, they may form linear chains. A good example is the Hawaii-Emperor chain, a chain of seamounts and subaerial oceanic islands that stretches

from Hawaii nearly to Kamchatka. In this chain, the oldest volcanoes lie at the northwest end, and the active, but still submarine, volcano of Loihi is situated at the east end. Locations of some ocean islands are shown in Map 6.3.

3. **Oceanic plateau:** Oceanic plateau are topographic highs within ocean basins that have an area of several 100 km² and rise an average of a thousand meters above the ocean floor. Large, well-studied oceanic plateau include the Ontong-Java plateau in the western Pacific Ocean and the Kerguelen plateau in the southern Indian Ocean (Map 6.3). Oceanic plateau lie on thickened oceanic crust that may be between ten and thirty-five kilometers thick. Many form at or near mid-ocean spreading centers, and appear to have formed by immense, short-lived eruptions of tholeiitic basalt (Kerr, 2004). Because of their thickness, they are not easily subducted and instead fragments of oceanic plateau may accrete to continental margins. For example, the Ontong-Java plateau collided with the Solomon Islands (Neal et al., 1977; Petterson et al., 1997), and the Caribbean plateau collided with northwestern South America (Kerr et al., 1997). Oceanic plateau are similar to continental flood basalts (see Chapter 8) in that both involve large, rapid outpourings of basalt. Both are sometimes referred to as "large igneous provinces" (Coffin and Eldholm, 1992).

A plume or hot spot model appears to explain many of the intraplate volcanic features of the ocean floor, especially many oceanic island volcanoes and plateau. Plumes may originate from a thermal boundary layer at the core-mantle boundary, or at the base of the upper mantle at 670 kilometers. The rising plume of solid material undergoes decompression melting as it shallows. The composition of the basalt magma depends on the depth and extent of melting and the composition of the mantle diapir. A short-lived voluminous eruption of this basalt may form an oceanic plateau, whereas a plume that produces magma over a longer period of time will build an oceanic island volcano. As plate motion carries the overlying oceanic crust across the plume, the site of volcanic activity shifts to that part of the ocean floor that is directly above the plume. In this way, a chain of hot spot volcanoes develops across the ocean crust at the pace of plate motion.



Map 6.3 Map showing the location of oceanic islands (points) and oceanic plateau (shaded). Plateau locations are after Coffin and Eldholm (1992).

6.3.2.1 Hawaii: An Example of an Oceanic Island Volcano

The Hawaii-Emperor island chain is over two thousand kilometers long. The easternmost island, Hawaii, is the only volcanically active island, although to its east the submarine volcanic center of Loihi is developing (Figure 6.8). Five overlapping shield volcanoes build the island of Hawaii, of which only Kilauea and Mauna Loa are active. Mauna Loa, at 4,170 meters above sea level, and Mauna Kea, at 4,205 meters, have the highest relief above base level of any mountain on earth (>10,000 meters), which indicates the huge amounts of magma involved in their formation. The focus of volcanism on Hawaii moves six centimeters a year, which is essentially identical to the movement rate of the Pacific plate. A stationary hot spot appears to explain the spatial relationships of Hawaiian volcanism very well.

Structure. The Hawaiian islands are associated with a large-amplitude, free-air gravity anomaly, which can be explained in terms of a huge volcanic load that downwarps the oceanic lithosphere. The crust beneath Hawaii is fifteen to twenty kilometers thick, as opposed to five to six kilometers in the adjacent Pacific. The lithosphere is

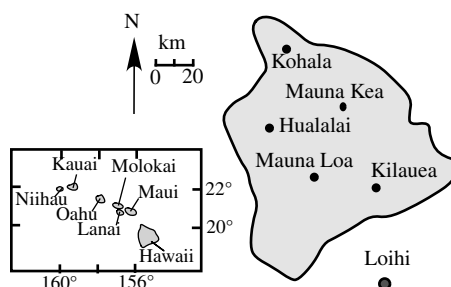


Figure 6.8 The island of Hawaii is a compound volcanic edifice formed by five overlapping shield volcanoes.

estimated to be relatively thin at less than ninety kilometers (Forsyth, 1977). The distribution of magma-related earthquake hypocenters has been used to construct the three-dimensional layout of the magma chamber and feeder conduit for the active volcanic center of Kilauea. It appears that melting occurs below sixty kilometers depth, and this magma is transported up through narrow conduits to shallow magma chambers (Wright, 1984). The main magma storage area is a zone, three kilometers in diameter, which extends from three to six kilometers depth. As magma fills the magma reservoirs

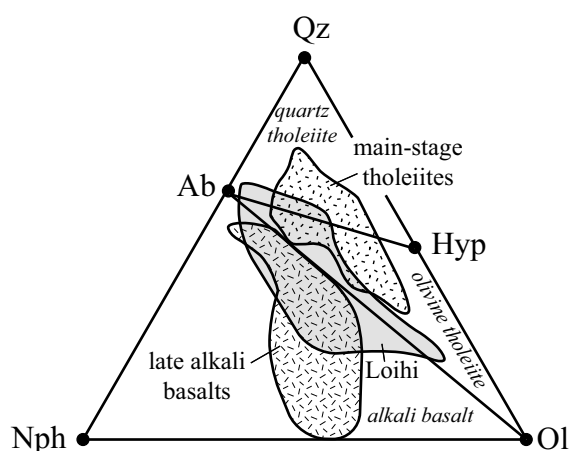


Figure 6.9 Comparison of the compositions of early Hawaiian basalts (as exemplified by Loihi), the main stage tholeiites, and the late-stage alkali basalts projected onto the normative Qz-Nph-Ol triangle. Data from MacDonald (1968), Fodor and colleagues (1992), Frey and Clague (1983), Hawkins and Melchior (1983), Muir and Tilley (1957), Ren and colleagues (2009), Wilkinson and Hensel (1988), and West and colleagues (1992).

the summit of the volcano inflates, as is measured by tilt meters. After a major eruption, it takes a period of months for the Kilauea magma chamber to refill (Ryan, Koyanagi, and Fiske, 1981; Dzurisin, Koyanagi, and English, 1984).

Evolution of an oceanic island volcano. Nearly all oceanic island volcanoes exhibit a complex pattern of igneous evolution, although the pattern is not the same for all ocean islands. At Hawaii, four characteristic stages can be identified. The first, the pre-shield stage, is seen at Loihi, the seamount south of Hawaii constructed of alkali basalt and tholeiite (Figure 6.9). The second, the shield-building stage, consists of large volumes of tholeiitic basalt. As volcanism wanes, the eruptions become more explosive and more alkaline in composition. The volume of magma produced during this post-shield stage is only about one percent of the total production of the volcano. A long period of dormancy and erosion initiates the post-erosional stage of volcanism. Again the eruptions are explosive, and the magmas produced are highly alkaline and silica poor. The rock types produced are alkali basalts and nepheline-bearing basalts. The amount of time between stages varies from volcano to volcano, and can be between one hundred thousand years to two million years. On the island of Hawaii, Mauna Loa and Kilauea are in the shield-

building stage, while the three older volcanoes (Mauna Kea, Hualalai, and Kohala) are between the post-shield stage and the post-erosional stage.

Petrography and geochemistry. Hawaii is a little unusual compared to other oceanic island volcanoes in the large volume of tholeiite and small volume of alkaline rock it has produced. Most other hot spots, such as the Azores, St. Helena, and Tristan da Cunha, have a larger proportion of alkaline rocks. Oceanic island tholeiites are similar to MORB, but may have orthopyroxene as well as olivine, spinel, clinopyroxene, and Fe-Ti oxides. In terms of major element chemistry, these tholeiites have higher K_2O and TiO_2 relative to MORB, but lower Al_2O_3 contents. Alkali basalts commonly contain ultramafic xenoliths, whereas ultramafic xenoliths are rare in tholeiites.

Magma sources for Hawaii volcanism. Neodymium, strontium, and lead isotopic data from Hawaiian volcanic centers strongly suggest that no single mantle source of magma can produce all the rock types found there. The interaction of an upper mantle source that also supplies the mid-ocean ridges with a lower-mantle plume source can account for much of the isotopic variability at oceanic island volcanic centers. In addition some ocean island lavas require the incorporation of a material that has isotopic characteristics like the crust. One possible contributor is the subduction of oceanic crust. The subcontinental lithosphere also may be recycled into the mantle and could become incorporated into oceanic island magmas. A combination of sources, along with different degrees of partial melting, seems to be involved, although the processes are complex and the details remain incompletely resolved.

6.3.2.2 Ontong-Java: An Example of an Oceanic Plateau

The Ontong-Java plateau is the largest known oceanic plateau, with a volume of 44.4 million km^3 occupying an area of 1.9 million km^2 of Pacific sea floor (Kerr, 2004). It is composed of tholeiitic basalt erupted in two short episodes at 122 ± 3 and 90 ± 4 million years (Neal et al., 1997). The crust on the Ontong-Java plateau averages thirty-six kilometers thick, and the plateau sits two to three kilometers above the surrounding sea floor today.

Although all lavas are tholeiitic basalts with between six and eight percent MgO, Neal and colleagues (1997) identified two groups of lavas on the basis of incompatible

BOX 6.2 | ORE DEPOSITS IN OCEANIC CRUST

Most ophiolites lack economic mineral deposits, but two types of important ore deposits are locally found in ophiolites: chromite and copper-bearing, massive sulfide deposits.

Chrome: Concentrations of chromite are common in the peridotite tectonite portion of an ophiolite (see Figure 6.1). In some localities the chrome concentration is rich enough to be ore grade. Because the peridotite and chromite bodies within an ophiolite have been subjected to ductile deformation within the mantle, the ore bodies have a discontinuous, pod-like shape. Hence they are called **podiform chromite** deposits to distinguish them from chromite deposits associated with layered mafic intrusions, which are called **stratiform chromite** deposits (see Box 9.1). Although the stratiform deposits are much larger than podiform deposits, podiform deposits contain chromite much richer in chrome, and are therefore valuable despite their smaller size. The chromite deposits of Kazakhstan and Turkey, the third and fourth largest chrome producers in the world after South Africa and India, come from ophiolites.



Box 6.2 Copper ingot in the shape of an oxhide, from Cyprus, circa 1225–1150 BCE. Artifact held by the British Museum, London. Photo used with permission. © The Trustees of the British Museum / Art Resource, NY.

Copper: Associated with pillow basalts in some ophiolites are massive sulfide deposits consisting of pyrite, pyrrhotite, chalcopyrite, and sphalerite. How these deposits formed was a great mystery until the discovery of “black smokers” on the sea floor (Corliss et al., 1979). Geologists now recognize that the intrusion of gabbroic rocks at a ridge crest drives circulation of hydrothermal fluid through the overlying basalts. As these fluids react with the basaltic crust, they extract metals, mostly Fe, Cu, and Zn, as well as sulfur from the sulfides in the basalt. When these fluids are expelled into the sea, the sulfides precipitate as “black smoke,” which cools and deposits as **volcanogenic massive sulfide (VMS)** deposits. The most famous ophiolite-hosted VMS deposits are associated with the Troodos ophiolite in Cyprus. Copper has been mined on Cyprus since the fourth millennium CE. Copper mining ceased in 1979, but there has recently been interest in restarting production.

BOX 6.3 | VOLCANIC HAZARDS FROM OCEANIC VOLCANISM

Despite the fact that oceanic volcanism is by far the most voluminous magmatism on Earth, it is associated with comparatively low volcanic hazard. This is partly because most eruptions take place under the ocean where eruptions are isolated from the atmosphere by a kilometer or more of seawater. Equally important, oceanic magmas are dominated by highly fluid basalt that generally lacks the explosive nature of arc magmatism. However, oceanic magmatism is not without its volcanic hazards, as any air traveler to Europe in the summer of 2011 could tell you. The eruption of the Eyjafjallajökull volcano in Iceland ejected a plume of ash that disrupted air travel to western Europe for weeks. This ash plume was small compared to the fissure eruption of Laki, also on Iceland, in 1783. Laki is the largest fissure eruption in history, and the volcanic gases emitted by the eruption killed many of the livestock on the island as well as approximately a quarter of the population because of famine and fluorine poisoning.

The islanders living on Hawaii are accustomed to the volcanic hazards of the island, which they attribute to activity of the goddess Pele. Volcanic eruptions and associated destruction of human structures are part of Hawaii's history. In the most recent of Pele's tricks, slow-moving lava flows from Kilauea overran the Kalapana Gardens Subdivision near Hilo. Much of the area was destroyed in 1986; the last house was overrun in 1990. One of the owners of the last houses to be engulfed in lava said they stayed until the last minute because "it is very easy to outrun a lava flow."



Box 6.3 Lava from Kilauea engulfing the Kalapana Gardens Subdivision in 1990, causing residents to abandon their community as it was consumed by the slow-moving flows.

Photo from U.S.G.S. Hawaii Volcano Observatory, <http://hvo.wr.usgs.gov/kilauea/history/1990Kalapana/>.

element concentrations and isotopic compositions. They suggested the two types of basalt were likely the product of variable degrees of partial melting from multiple mantle sources. Based on the range of major element compositions recorded in the basalts, Neal and colleagues (1997) concluded that the parent magmas subsequently underwent crystal fractionation of olivine followed by clinopyroxene and plagioclase. Gabbroic enclaves in some of the flows evince removal of clinopyroxene and plagioclase during the later stages of differentiation. The apparent complexity of the processes that acted over geologically short periods of time is a reminder that much remains to

understand about the genesis of oceanic plateau and how they differ from oceanic islands.

One potentially important aspect of the formation of oceanic plateau is their possible impact on Earth's environment. There is tantalizing evidence of temporal correlations between the formation of oceanic plateau and other large igneous provinces and oceanic anoxia, rapid global warming, and mass extinctions. Beyond the temporal coincidence, the causal links between these global impacts and the outpouring of large quantities of basaltic magma are not well established, representing a fruitful area for future research.

Summary

- Ophiolites are commonly used as a simplified model for ocean crust. The stratigraphy of an ophiolite from top to bottom is: pillow basalt, sheeted dikes, gabbro, cumulate peridotite, and deformed peridotite.
- Ophiolites may form in back-arc spreading centers, in suprasubduction zone settings, or in mid-ocean spreading centers.
- Oceanic crust is more complex than the ophiolite model suggests. Parts of the crust may be excised by faults, and the gabbroic horizon may involve multiple injections of melt that may interact with mantle host peridotite and evolve toward oxide gabbro.
- Ocean islands and oceanic plateau form above mantle plumes ("hot spots"). Basaltic magma forms by decompression melting within rising mantle diapirs. The composition of the basalt magma varies depending on the depth and extent of partial melting and the composition of the mantle involved.
- Tholeiites are found in MORB, ocean islands, and oceanic plateau.
- Alkali basalts are found on many ocean islands, and on some of these islands they have evolved to extremely alkaline magmas.

Questions and Problems

Problem 6.1. Compare and contrast fast mid-ocean spreading centers with slow- and ultra-slow- mid-ocean spreading centers. Include in your comparison:

- topography and dimensions of the ridge,
- stratigraphy and structure of the rocks produced,
- differences in plagioclase compositions, and
- magma volumes and differentiation histories.

Problem 6.2. How can hotspot tracks be used to determine plate motion? What assumptions are involved?

Problem 6.3. What types of basalt are found at mid-ocean ridges? At oceanic islands? What might account for any differences?

Problem 6.4. Plot data for MORB glasses from the FAMOUS area and basalts from Galapagos on Fe-index, MALI, and ASI diagrams. How do the two groups of basalts differ? How might these differences relate to the presence or absence of mantle plume activity?

Further Reading

.....

Basaltic Volcanism Study Project, 1981, *Basaltic volcanism on the terrestrial planets*. Pergamon Press, Inc., New York, sections 1.2.5, 1.2.6, 6.2.1, and 6.2.2.

Hekinian, R., 1982, *Petrology of the ocean floor*. Amsterdam, Elsevier.

Kerr, A., 2004, Oceanic plateaus. In Holland, H. D. and Turekian, K. K., *Treatise on geochemistry*, Vol. 3, *The Crust*. Amsterdam, Elsevier, 537–65.

McBirney, A. R., 2007, *Igneous petrology*, 3rd ed. Jones and Bartlett, Boston, Chapter 8.

Winter, J. D., 2010, *Principles of igneous and metamorphic petrology*, 2nd ed., Prentice Hall, New York, Chapters 13 and 14.

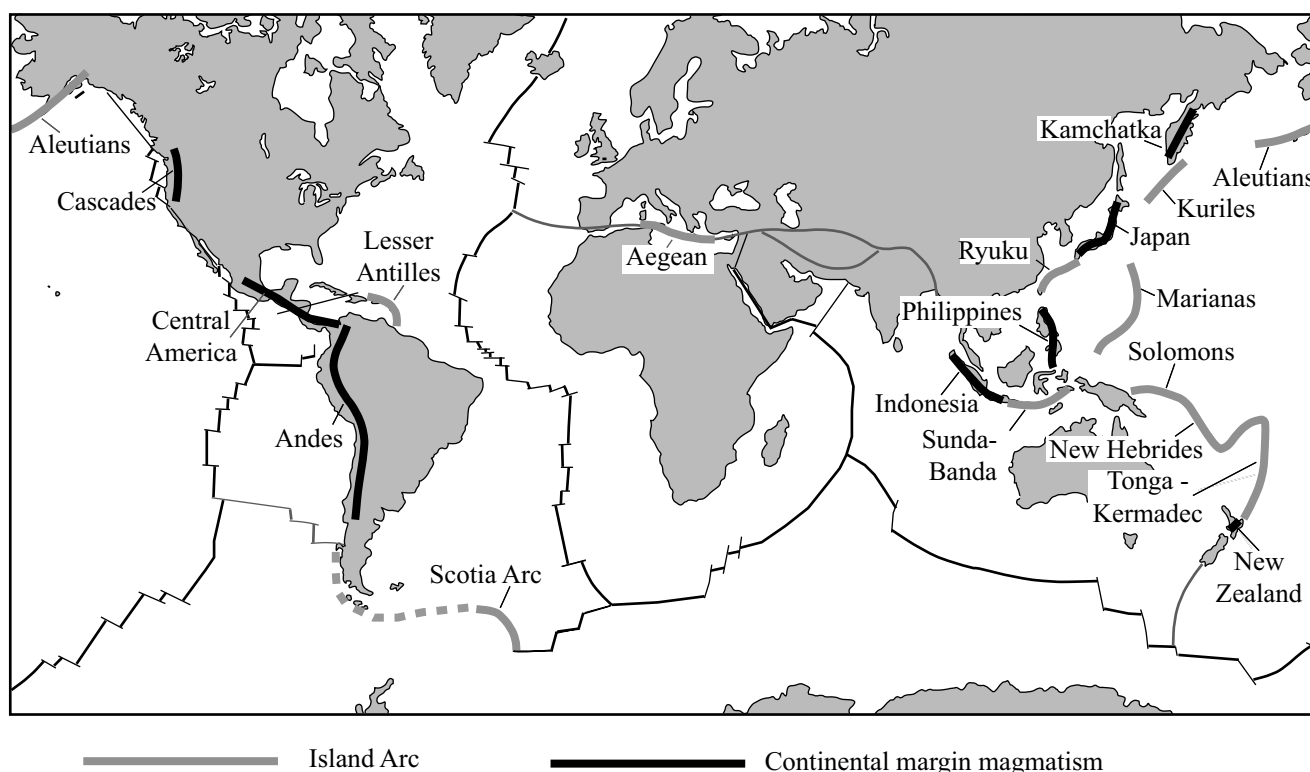
Chapter 7

Convergent Margin Magmatism

7.1 Introduction

Subduction produces some of the major topographic features on Earth and consumes large amounts of oceanic crust each year. At modern rates it would take only 160 million years to subduct an area equal to that of the entire surface of Earth. Regardless of whether the overriding plate is oceanic or continental, convergent plate margins share many of the same characteristics. This includes a deep (six thousand to eleven thousand meters deep) oceanic trench marking the plate boundary, chains of volcanoes on the overriding plate located about 100–200 kilometers inboard from the trench, and a dipping zone of seismicity called the Benioff zone, which includes shallow, intermediate, and deep-focus earthquakes. This marks the plane of descent of the oceanic lithosphere into the mantle. The volcanoes and plutonic rocks above the Benioff zones are constructed of magmas that range from basalt to rhyolite, with andesite the dominant composition. Volcanism in this tectonic setting is frequently highly explosive. This, coupled with the fact that large population centers are located in the shadow of many of these volcanoes, makes study of arc magmatism important for hazard prediction. The volcanic and plutonic rocks formed at convergent margins are also relevant to the study of the growth and evolution of the continental crust. Insofar as convergent margin magmas transfer material from the mantle to the crust, they represent a mechanism by which continents form and grow. The volume and composition of crust formed at subduction zones is therefore of considerable interest to geologists interested in the formation and development of continental crust over Earth's history.

This chapter introduces the main features of oceanic and continental arc magmatism using well-studied examples of arc volcanic and plutonic complexes. The petrography and geochemistry of island and continental arcs provide important clues to the petrogenesis of arc magmas, although the details of the process remain poorly understood.



Map 7.1 World map showing active island arcs and continental margin magmatism.

7.2 Oceanic and Continental Arcs

We can divide convergent margin volcanism into two groups, even though the overall tectonic setting is similar in each. First, **island arc magmatism** generates melts in response to subduction which are injected into oceanic crust with little contamination by crustal melting. The second is **continental arc magmatism**, wherein subduction zone magmas ascend through and interact with continental crust. Although many of the magmatic processes are the same in both environments, the resulting magma suites have somewhat different compositions that relate to whether the magmas traversed continental crust during their ascent into and through the overriding plate.

7.2.1 Island Arc Magmatism

Subduction of one oceanic plate beneath another has produced currently active oceanic island arcs, including the Aleutian, Kurile, Marianas, Ryuku, Sunda-Banda, Solomon, New Hebrides, and Tonga-Kermadec arcs of the

western Pacific; the Lesser Antilles of the Caribbean; and Scotia in the southern Atlantic Ocean (Map 7.1). In these young island arcs the plutonic rocks are rarely exposed, so that most of the petrologic information available comes from extrusive materials. In some island arc terranes, erosion has exposed their plutonic roots. A good example is Tobago in the West Indies, where the crust has tilted to expose a cross-section that includes arc basement, and plutonic rocks underlying a volcanic sequence (Frost and Snoke, 1989; Snoke et al., 2001).

7.2.2 Continental Arc Magmatism

Whereas oceanic island arcs are formed by the subduction of one oceanic plate beneath another, continental margin magmatism results from the more complex tectonic environment in which the overriding plate is continental. Magmas generated in this environment today occur along the west coast of North and South America, Japan, New Zealand, and along the Aegean Sea (Map 7.1). The eruptions of both continental and

BOX 7.1 VOLCANIC HAZARDS

There are approximately 600 active arc volcanoes in the world. When these volcanoes erupt they may cause loss of life and damage to property by a number of different processes. Some destruction is a direct result of the eruption: ash falls, pyroclastic flows, debris avalanches, explosions, and emission of volcanic gases and acid rain all may cause damage and death. Other hazards are indirect: the volcanic eruptions may trigger earthquakes, tsunamis, and post-eruption famine. Fortunately, volcanic eruptions are relatively infrequent events and they involve less economic loss and human casualties than other natural hazards such as floods, hurricanes, and earthquakes. Nevertheless, there have been thirty-two eruptions since 1000 CE that killed more than 300 people. Moreover, approximately 10 percent of the world's people live near potentially dangerous volcanoes (Tilling, 1989).

The Volcanic Explosivity Index (VEI) was developed to provide an estimate of the magnitude of volcanic eruptions. It is a logarithmic index based upon the volume of material ejected by an eruption (Newhall and Self, 1982). The scale ranges from zero for small, nonexplosive eruptions of lava to eight for huge, paroxysmal eruptions of pyroclastic material and injection of significant amounts of ash into the stratosphere (Table 7.1). As one might expect, the larger the eruption the less frequent it is likely to be. Mason and colleagues (2004) identified five eruptions with a VEI of seven or greater in the last ten thousand years, the most recent being Tambora in 1815. There has been no eruption with a VEI of eight in that time. The entrainment of ash from Tambora into the stratosphere caused the following summer to be much cooler than usual. In the past two million years, only six eruptions with VEIs of eight or greater have occurred, and they were cataclysmic. Eruptions on this order of magnitude may have caused "volcanic winters" with significant effects on life on the planet.

Table 7.1 Volcanic Explosivity Index

VEI	Volume	Plume	Frequency	Example	Death toll
0	$< 10^4 \text{ m}^3$	$< 100 \text{ m}$	constant	Kilauea	4 since 1900
1	$> 10^4 \text{ m}^3$	100–1000 m	daily	Nyiragongo (2010)	245
2	$> 10^6 \text{ m}^3$	1–5 km	weekly	Galeras (1993)	9
3	$> 10^7 \text{ m}^3$	3–15 km	few months	Nevado del Ruiz (1985)	23,000
4	$> 0.1 \text{ km}^3$	10–25 km	$\leq \text{yr}$	Eyjafjallajökull (2010)	0
5	$> 1 \text{ km}^3$	20–35 km	$\leq 10 \text{ yrs}$	Mount Saint Helens (1980)	57
6	$> 10 \text{ km}^3$	$> 30 \text{ km}$	$\leq 100 \text{ yrs}$	Mt. Pinatubo (1990)	700
7	$> 100 \text{ km}^3$	$> 40 \text{ km}$	$\leq 1,000 \text{ yrs}$	Tambora (1815)	92,000
8	$> 1,000 \text{ km}^3$	$> 50 \text{ km}$	$\leq 10,000 \text{ yrs}$	Toba (70,000 yrs BP)	Unknown

BOX 7.2 | PORPHYRY COPPER DEPOSITS

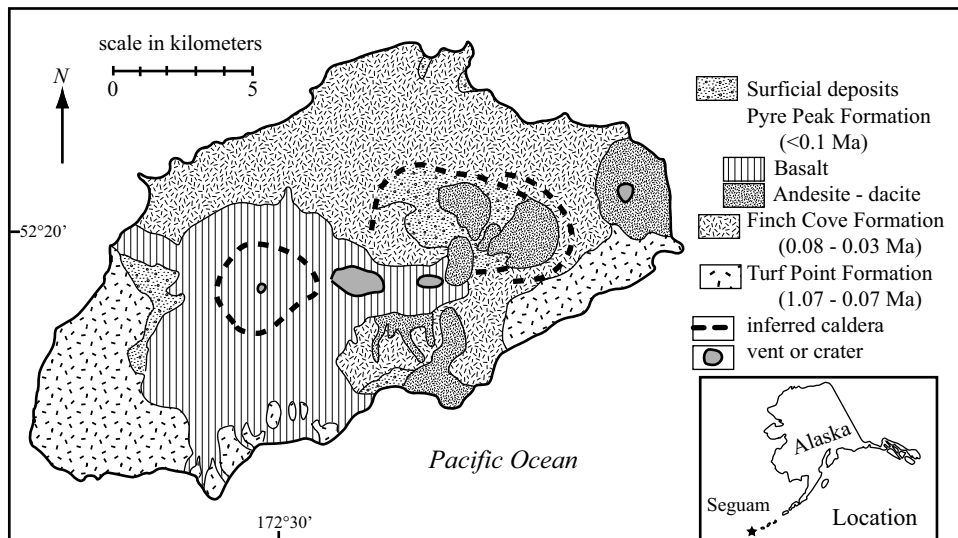
A major economic characteristic of arc magmatism is the occurrence of porphyry copper deposits. These deposits supply nearly three-fourths of the world's copper, half of the molybdenum, and around one-fifth of the gold (Sillitoe, 2010). Porphyry copper deposits are associated with shallow intrusions in arc settings. Typical examples include the Bingham mine in Utah, El Teniente in Chile, and the Ok Tedi Mine in Papua New Guinea. There is no consistent relationship between porphyry deposits and the composition of the host rocks, which may range from diorite to granodiorite in calc-alkalic suites and from diorite to syenite in more alkalic suites (McMillan and Panteleyev, 1988). Instead, the common feature of the host plutons for porphyry Cu deposits is their shallow level of emplacement. The shallow emplacement level means that, during crystallization of the igneous pluton, the aqueous fluids exsolved from the magma undergo a large volume increase (Figure 3.2). This causes hydrofracturing of the rocks within, above, and around the intrusion, allowing circulation of fluids through the rock. Because transition metals such as Cu, Mo, and Au and elements such as Cl and S behave incompatibly in silicate melts, these become enriched during the fractionation of the melt and will, in turn, fractionate into the exsolving fluids. The metals, which are dissolved in the fluid as chloride complexes, are transported through the fractured rocks and precipitated as the fluids become neutralized by reaction with the country rock (see Chapter 17).

island arc volcanoes represent a significant geologic hazard (Box 7.1).

Not only are volcanic edifices common in continental arcs, some arcs have been eroded deeply enough to expose granitic batholiths that formed beneath the volcanoes. These batholiths represent some of the most voluminous granitic intrusions in the world. Late Mesozoic subduction along the western margin of North and South America produced several large granitic batholiths, including the Coast Range batholith of western Canada, the Sierra Nevada batholith of California, and the Peninsular Ranges batholith of California and Baja California. The magmatic arc along the western margin of North America has been more deeply eroded than the corresponding arc in South America: huge andesite volcanoes still cap much of the Andes. These large batholiths, known as Cordilleran batholiths after the extensive mountain chains along western North and South America, are not single intrusions of granite but rather composite bodies made up of numerous plutons that range in composition. Arc batholiths are important as a source of metals, including copper, molybdenum, and gold (Box 7.2).

7.2.3 Structure of Island and Continental Arcs

Cross-sections through island and continental arcs can be divided into four regions: the trench, fore-arc, arc, and back-arc. Arcs are marked by a distinctive negative gravity anomaly over the trench that is paired with a positive anomaly over the fore-arc (Figure 7.1). The negative gravity anomaly near the trench is caused by the presence of relatively light, water-saturated sediments in the fore-arc, whereas the positive gravity anomaly over the fore-arc reflects the presence of cold dense subducted lithosphere beneath the arc. The trench and fore-arc are marked by low heat flow, while the arc and back arc are characterized by high heat flow. The low heat flow over the fore-arc is produced by the cold slab that lies beneath it. The high heat flow over the arc and back-arc is caused by the heat carried to high crustal levels by hot magma. The down-going slab in subduction zones is marked by the Benioff zone earthquakes along its plunging surface.



Map 7.2 Geologic map of Segum island, central Aleutian arc, Alaska, USA. From Singer, Myers, and Frost (1992).

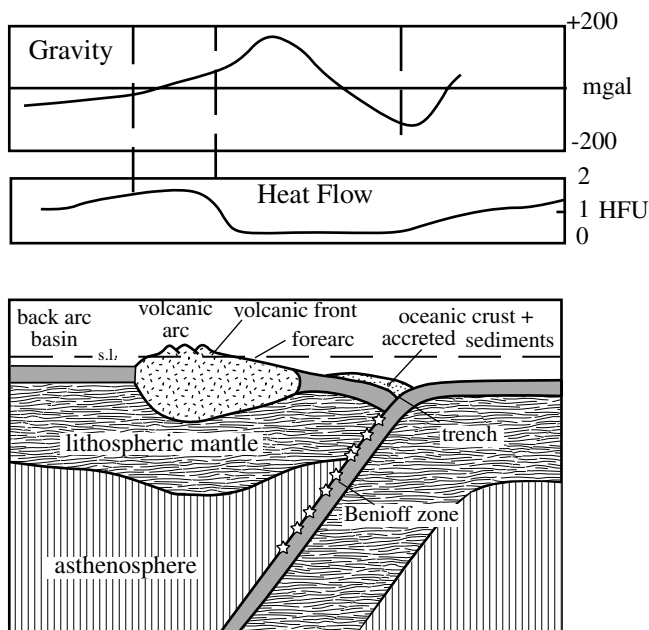


Figure 7.1 Schematic cross-section of a typical island arc. The graphs above show the gravity and heat flow profiles across the arc. Stars indicate locations of earthquake epicenters. s.l. = sea level, HFU = heat flow units. Modified from Gill (2010).



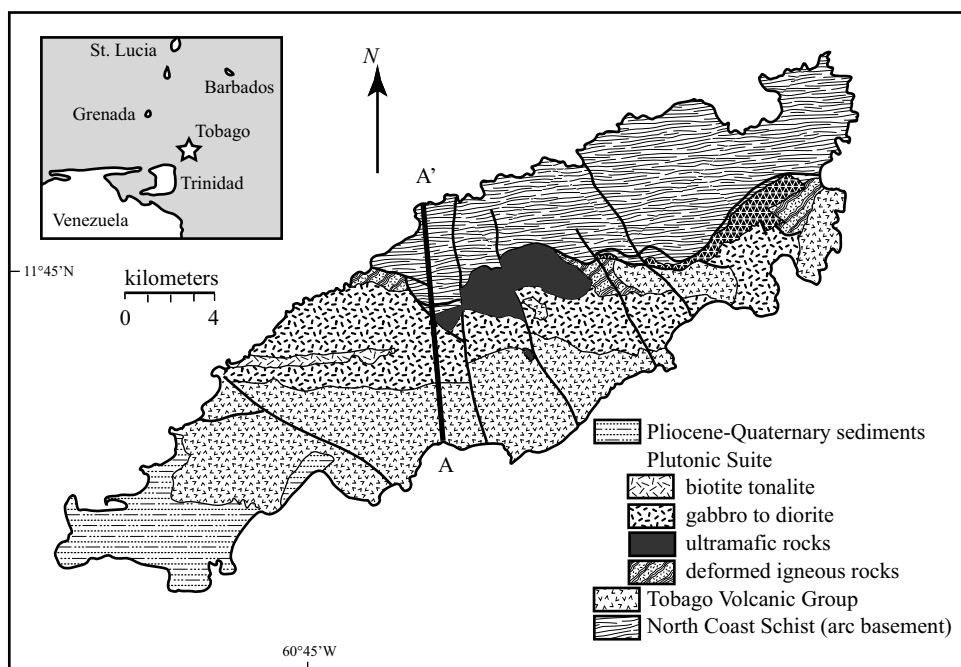
Figure 7.2 Photo of Pyre Peak, Segum Island, Alaska. Note characteristic steep-sided cone of the composite volcano breached by a summit caldera. Photo by Brad Singer, used with permission.

7.2.4 Examples of Island and Continental Arcs

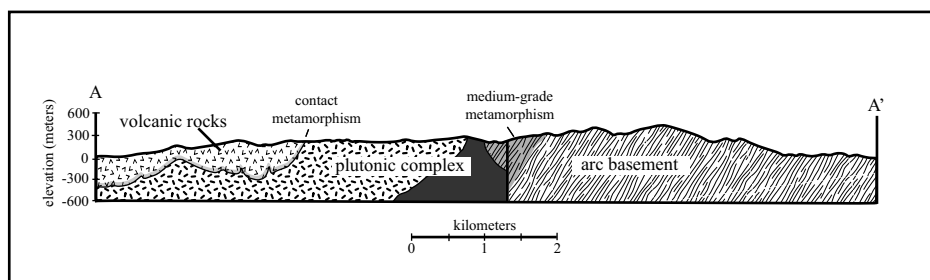
7.2.4.1 Island Arc Volcano – Segum, Aleutian Islands, Alaska

Segum, an island in the middle of the Aleutian chain, is dominated by Pyre Peak, the highest of the young volcanic edifices on the island (Figure 7.2). In this portion

of the chain, modern volcanoes are built atop Eocene to Miocene arc crust (Singer, Myers, and Frost, 1992). The subaerial lavas of Segum consist of three major eruptive phases (Map 7.2). The oldest of these three units is the Turf Point Formation, which consists of flows that range from 1.1 to 0.07 million years old. Overlying this, the Finch Cove Formation ranges in age from 0.08 to 0.03 million years old. The deposits from the youngest eruptive phase compose the Holocene Pyre Peak Formation, which occupies the western half of the island. The most recent volcanic activity on Segum occurred in May 1993.



Map 7.3 Geologic map of Tobago, West Indies, showing a cross-section through the Cretaceous oceanic arc complex that exposes both plutonic and volcanic rocks. From Frost and Snoke (1989).



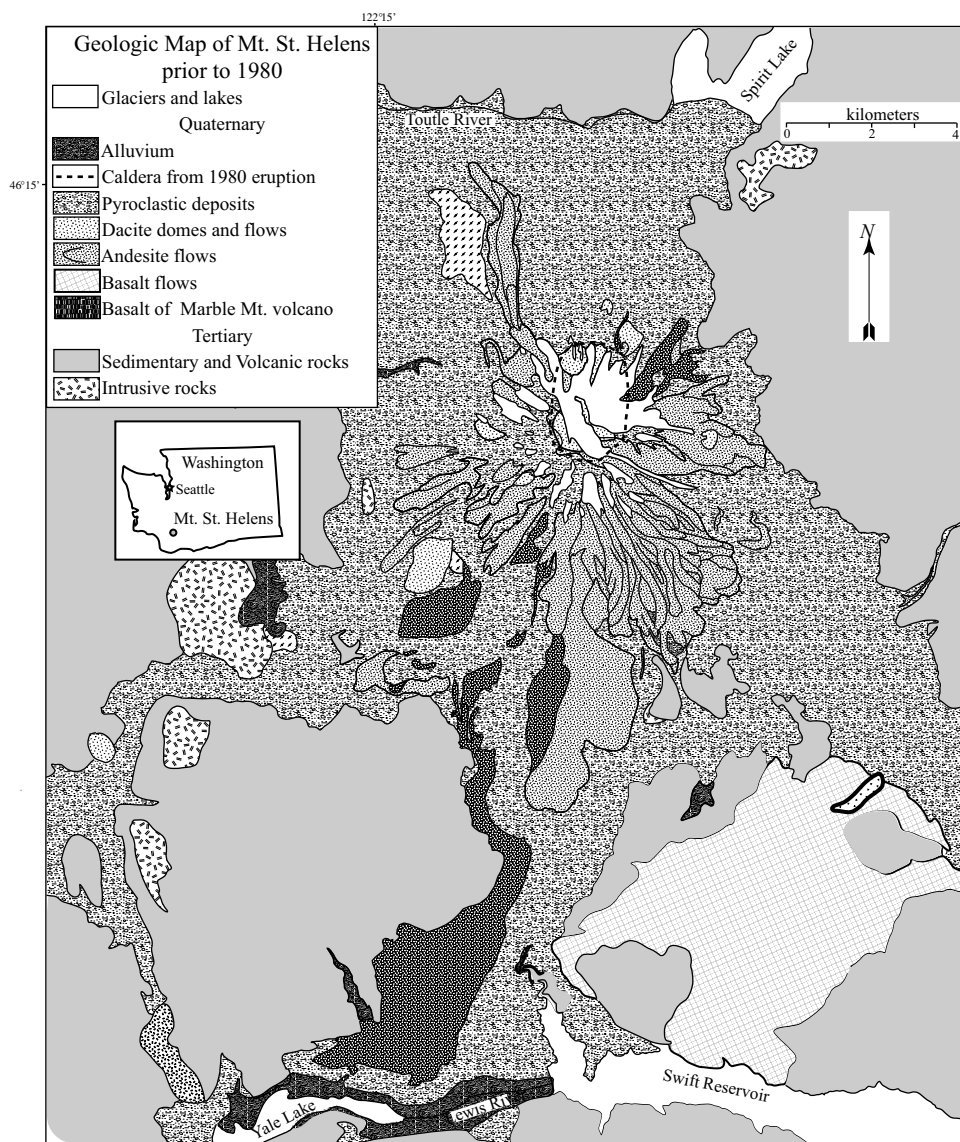
The geochemical studies of Seguan were conducted on the Turf Point formation where the wave-cut cliffs on the island shore expose a cross-section through the eruptive sequence. The Turf Point Formation consists of about 70 percent basalt, 15 percent andesite, and 15 percent dacite. Similar abundances of these rocks are found in both the Finch Cove and Pryor Peak Formations.

7.2.4.2 Island Arc Plutonic Complex – Tobago, West Indies

The island of Tobago lies at the northeast corner of the South American shelf in the southern Caribbean. The island preserves a crustal cross-section through a 105–103-million-year-old (Albian) oceanic island arc (Snoke et al., 2001). The arc is built on older, metamorphosed, and deformed Cretaceous arc rocks referred to as

the North Coast Schist (Map 7.3). Both plutonic rocks and volcanic rocks of the Albian arc are exposed. The plutonic rocks of the oceanic arc include ultramafic rocks, gabbro and diorite, and a small volume of tonalite. The ultramafic rocks include dunite, wehrlite, olivine clinopyroxenite, and hornblendite. The gabbroic rocks include olivine melagabbro, hornblende gabbro, and gabbro-norite. Mineralogical layering in the gabbro unit has been interpreted to result from crystal accumulation, and texturally the ultramafic and gabbroic rocks appear to be cumulate rocks.

Parts of the plutonic complex intruded and contact metamorphosed the volcanic rocks of the Tobago plutonic-volcanic complex, which include volcanoclastic breccias and lava flows. Volcanogenic mudstone, sandstone, and grit are also found within the volcanic sequence. Both plutonic and volcanic rocks are cross-cut by a suite of mafic



Map 7.4 Geologic map of Mount Saint Helens, Cascade Range, Washington, prior to the 1980 eruption. Heavy dashed line shows the extent of the caldera produced by that eruption. Inset shows location in the state of Washington. Modified after Hopson (2008).



Figure 7.3 Mount Saint Helens prior to the eruption of May 1980. Photo from the USGS.

dikes interpreted by Frost and Snoke (1989) as similar in composition to the basaltic parent magmas from which the Tobago plutonic and volcanic rocks formed.

7.2.4.3 Continental Arc Volcano – Mount Saint Helens, Washington

Before its explosive eruption on May 18, 1980, Mount Saint Helens, located in southern Washington state, was a stratovolcano rivaling Mount Fuji for its symmetry (Figure 7.3). The geologic map of Mount Saint Helens before the eruption displays many of the features distinctive of continental arc volcanoes (Map 7.4). One characteristic is that the Mount Saint Helens volcano erupted basalt, andesite, and dacite lavas. The basalt flows extended

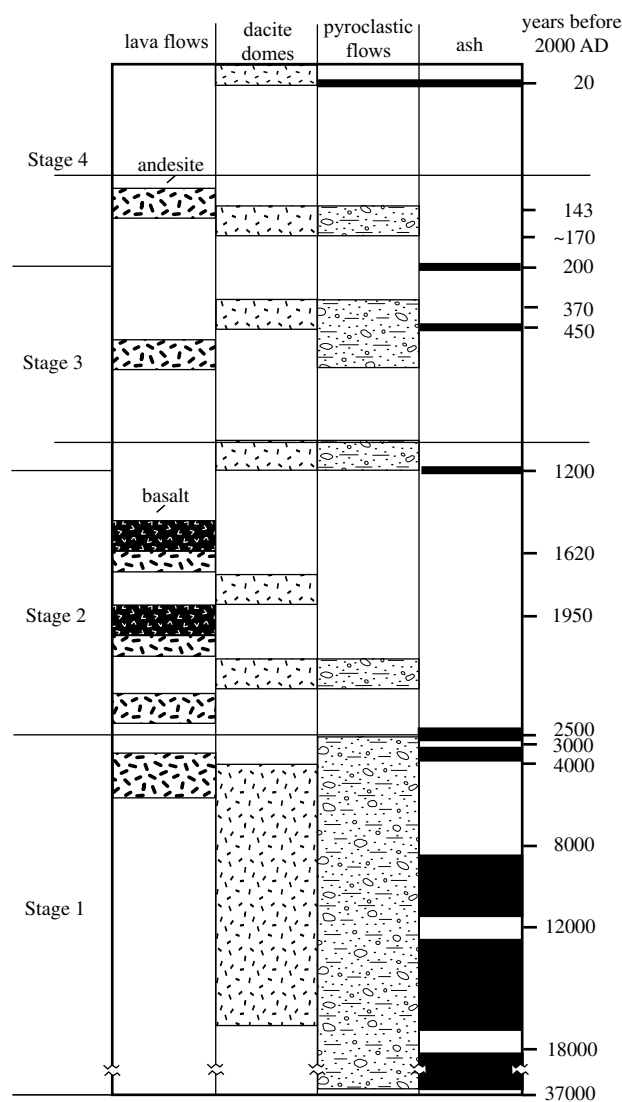


Figure 7.4 Diagram showing the geologic history of Mount Saint Helens volcano. Modified after Hopson (2008).

up to twenty kilometers from the vent (Map 7.4). The fluid basalt formed lava tubes that flowed through a thick forest of large trees typical of the Pacific Northwest rain forest, solidifying around the tree trunks. After the trees rotted away, the flow was littered with huge holes, several feet in diameter, where the trees used to stand. The andesite flows were much more viscous than the basalt flows. Most andesite froze on the slopes of the mountain, although a few flowed about eight kilometers from the vent. Dacite volcanism formed domes, which seldom exceed a kilometer in diameter. In addition to forming domes, the dacite volcanism and, to a lesser extent, the andesite volcanism produced pyroclastic flows that flowed down the



Figure 7.5 Granodiorite of the Tuolumne pluton in Yosemite National Park, California. Photo by Arthur W. Snoke.

mountain and into the valleys of the Toutle and Lewis rivers, which drain the north and south sides of the volcano, respectively.

Even before a magnitude 4.1 earthquake on March 15, 1980 marked the awakening of Mount Saint Helens, the volcano was recognized as the most active volcano in the Cascades arc, which extends from northern California to southern British Columbia. Geologists had determined that over the past forty thousand years Mount Saint Helens had erupted lavas, emplaced dacitic domes, produced pyroclastic flows, and emitted ash (Figure 7.4). Several events had occurred within the last 200 years. Because of extensive petrologic study and an extensive monitoring program, the 1980 eruption of Mount Saint Helens was predicted successfully, minimizing loss of life (Box 7.3).

7.2.4.4 Continental Arc (Cordilleran) Batholith – The Tuolumne Pluton

A classic example of a Cordilleran batholith is the Tuolumne pluton in the Sierra Nevada batholith, which is spectacularly exposed in Yosemite National Park in California (Figure 7.5). The Tuolumne pluton makes up only a small portion of the immense Sierra Nevada batholith, which is over 500 kilometers long by 50 to 80 kilometers wide, and is composed of up to 200 separate plutons. The majority of exposed rock in the Tuolumne pluton is granodiorite, rather than true granite (Map 7.5). Many other Cordilleran batholiths are similarly dominated by granodiorite. Another important feature of the Tuolumne pluton is that it is composite, meaning that it formed from multiple intrusive episodes (Map 7.5). Earlier, relatively mafic phases including

BOX 7.3 | VOLCANIC HAZARDS ASSOCIATED WITH CONVERGENT MARGIN MAGMATISM: EXPLOSIVE VOLCANISM AND PYROCLASTIC DEPOSITS

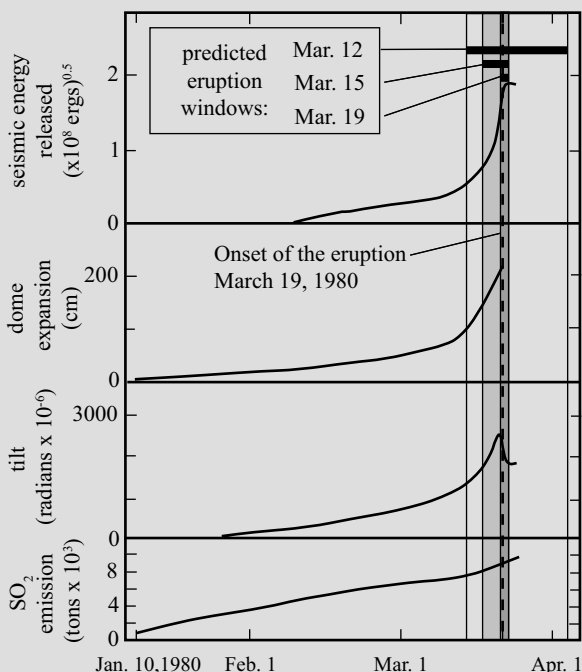
The intermediate to felsic magmas of magmatic arcs are characterized by high water contents and high viscosity (see Chapter 4). These magmas lead to explosive volcanism, in contrast to the relatively quiescent basaltic volcanism of oceanic magmas. Explosive magmatism produces pyroclastic deposits, which may form by multiple mechanisms. One mode of origin is collapse of a growing lava dome. Growing lava domes are unstable, and commonly break up to form landslides. If the melt is close to water saturation at the time the landslide forms, sudden decompression of the underlying magma can lead to explosion, which triggers an avalanche of hot blocks, ash, and gas. Transported individual blocks can reach tens of meters in diameter. The pyroclastic flow deposits of Mount Saint Helens associated with the climactic eruption on May 18, 1980 formed by this mechanism (Christiansen and Peterson, 1981).

Pyroclastic flow deposits also may form by collapse of a vertical eruption column. Magma is disrupted by expanding gases within the conduit and discharges pumice, ash, and gases as a mixture into the air. A turbulent jet structure is formed, mixing cold air into the sides of the column. This air is heated by the ash, expanding the column, and lowering its density. The mixture of ash and gas is almost always denser than the surrounding atmosphere when first discharged. In addition, the amount of kinetic energy available from gas expansion is only enough to discharge the mixture to a few kilometers height at most. To produce a column thirty to fifty kilometers high, as is typical for continental arc volcanoes, the discharged mixture must absorb and heat enough air to lower the density of the mixture to less than that of the atmosphere. The mixture is then buoyant and rises as a convective plume, like smoke from a forest fire or an exhaust pipe. In columns where the whole or part of the mixture is still denser than the atmosphere by the time all kinetic energy is lost, collapse occurs and forms a density current of ash and hot gases. Because gases have very low viscosity and density, the particles settle rapidly to form a dense avalanche or pyroclastic flow. These flows can travel several tens of kilometers at velocities up to 10 to 300 m/sec. The July 22, 1980 eruptions of Mount Saint Helens included pyroclastic flows of this origin (Christiansen and Peterson, 1981).

Arc volcanoes, including Mount Saint Helens, have produced massive eruptions (VEI scale five and six; see Box 7.1), many of which have resulted in extreme loss of life. Relatively recent eruptions on this scale include Krakatoa in 1883, Katmai in 1911, and Mount Pinatubo in 1990. Because volcanic eruptions can have disastrous consequences for people living near the volcano, petrologists and volcanologists seek to understand the plumbing of volcanoes to characterize and mitigate volcano hazards. Because Mount Saint Helens was so close to population, geologists studied the development of the volcanic edifice attentively. Researchers established seismographs around the volcano to sense the movement of magma and tiltmeters around the edifice to recognize how the mountain inflated as the magma moved into the shallower plumbing. These measurements provided the basis for a series of successively narrowing predictive windows that proved remarkably accurate (Swanson et al., 1985; Tilling, 1989; Box 7.3).

The information obtained from the eruption of Mount Saint Helens became indispensable in predicting the eruption of Mount Pinatubo ten years later. Scientists from the Philippine Institute of Volcanology and Seismology, working closely with those from the United States Geological Survey, were able to monitor emissions of volcanic gases and to use earthquakes to follow the movement of magma into the volcano from a depth of thirty-two kilometers. They used these data to predict the eruption far enough in advance that people living on the volcano's slopes were able to evacuate before the eruption. These

(continued)

BOX 7.3 (CONT.)

Box 7.3 Evidence of potential volcanic activity at Mount Saint Helens became increasingly compelling through the early months of 1980, when seismic activity, dome expansion, inflation of the edifice, and SO₂ emissions increased. Geologists issued series of warnings of a volcanic eruption with successively narrowing predictive windows, all of which accurately predicted the March 19 event. Modified from Swanson et al. (1985).

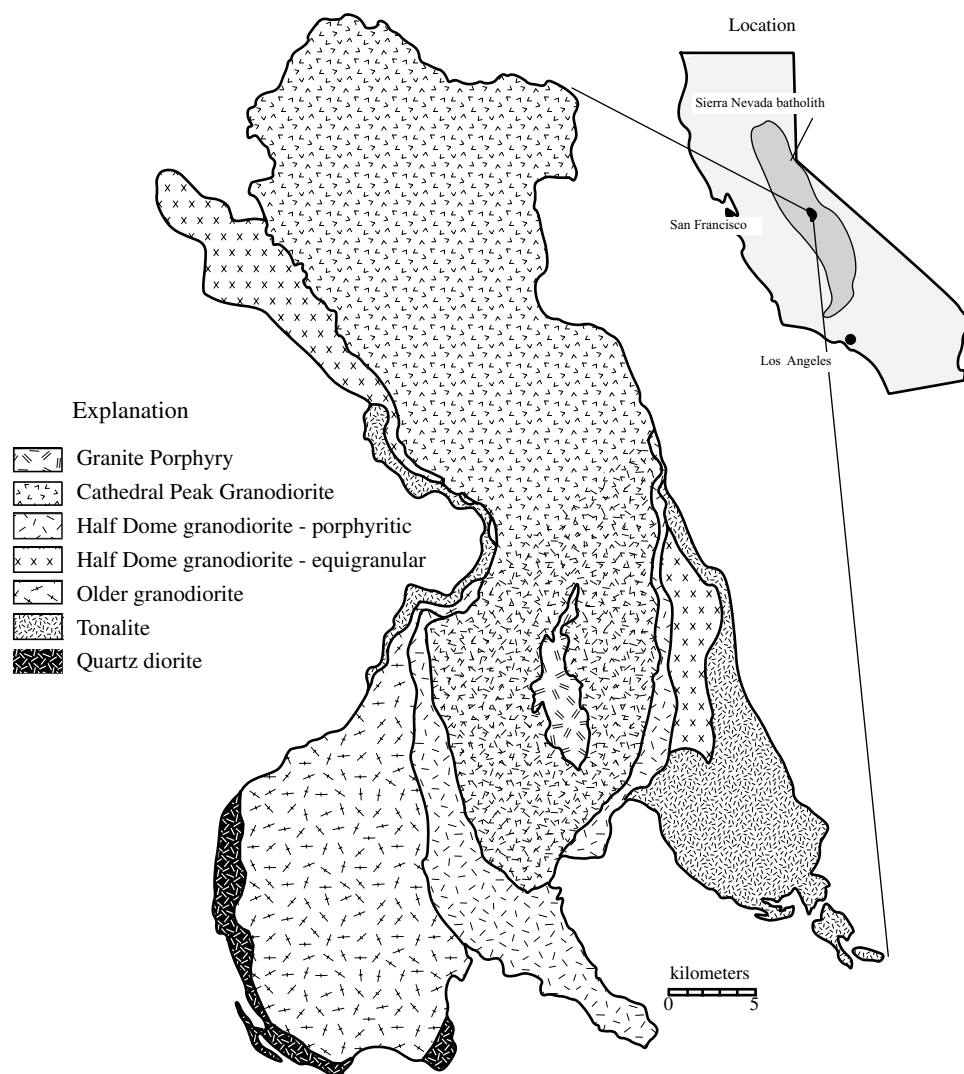
efforts saved an estimated five thousand lives and at least \$250 million in property (Newhall, Hendley, and Stauffer, 1997). These results indicate that in the future, geologists will be able to predict volcanic eruptions with sufficient accuracy that eruptions of arc volcanoes threatening cities from Seattle to Tokyo. Hazard forecasts could give the millions of people who live in the shadows of these beautiful mountains enough time to avoid the immediate effects of volcanic eruptions.

quartz diorite and tonalite form a discontinuous annulus around the batholith. Progressively younger and more evolved intrusions are nested within the interior of the pluton. Field relations indicate that the sheets and blocks of the earlier quartz diorite and tonalite were incorporated into the younger, more evolved magmas as they were emplaced in the interior portions of the batholith (Bateman and Chappell, 1979; Miller, Miller, and Paterson, 2005).

7.3 Petrographic Characteristics of Island and Continental Arc Rocks

7.3.1 Petrography of Island Arc Rocks

The Turf Point Formation lavas on Seguan are a calcic island arc suite that span a compositional range from basalt to rhyodacite. This suite consists of an anhydrous phenocryst assemblage of plagioclase, olivine, clinopyroxene,



Map 7.5 Geologic map of the Tuolumne pluton (after Bateman and Chappell, 1979). Inset shows the location of the batholith within the Sierra Nevada batholith, and the location of the Sierra Nevada batholith in California.

orthopyroxene, magnetite, and rare ilmenite. The proportions of the phenocryst phases vary between basalts, basaltic-andesites, andesites, and dacites, but even the dacites and rhyodacites lack hydrous minerals such as hornblende and biotite (Singer, Myers, and Frost, 1992).

The calcic lavas of Seguam differ from those of other Aleutian volcanoes and from most of the volcanoes of the Pacific and Lesser Antilles arcs, which tend to be calc-alkalic. Many calc-alkalic island arc suites are dominated by voluminous, two-pyroxene andesites. Such rocks are typically phenocryst rich, containing an assemblage of hypersthene, augite, and plagioclase. Plagioclase usually is andesine and commonly shows complex zoning. Olivine phenocrysts may occur, but they are rarely in equilibrium with the pyroxenes and may be xenocrysts from the mantle. Some andesites may contain phenocrysts of

hornblende in addition to, or even to the exclusion of, the pyroxenes. In addition to andesite, calc-alkalic island arcs commonly erupt small volumes of evolved dacite. Like the andesites, dacitic lavas from these suites are phenocryst rich. The key phenocryst for dacite is quartz, which occurs with complexly zoned andesine. Ferromagnesian minerals may include pyroxenes, hornblende, cummingtonite, or biotite.

Alkali-calcic to alkalic, high-K series island arc rocks are around 50 percent basalt, 40 percent andesite, and 10 percent dacite. They are distinguished from calc-alkalic suites by a higher abundance of biotite. Alkalic island arc suites occur in Fiji and Sunda in the Pacific, and in Grenada in the southern Lesser Antilles.

The plutonic rocks associated with modern island arc volcanoes are rarely exposed, but older complexes, such as

Tobago, indicate that the plutonic roots of island arc volcanoes are composed of ultramafic to gabbroic cumulate rocks with lesser amounts of more siliceous tonalite (Frost and Snoke, 1989). Some mafic layered intrusions appear to represent the roots of arc volcanoes. The Duke Island mafic-layered intrusion in southeastern Alaska, described in Chapter 9, is interpreted as a sub-arc intrusion. Other examples include the Proterozoic Mullen Creek and Lake Owen complexes of southeastern Wyoming, which are composed of mafic and ultramafic cyclic units that suggest repeated intrusion of mafic magma into a sub-arc magma chamber (Premo and Loucks, 2000). Other plutonic arc rocks, such as the Jurassic Smartville complex of northern California, are dominated by unzoned gabbros or zoned plutons composed of olivine gabbro in the core with quartz diorite rims (Beard and Day, 1988). A common feature in all these examples of island arc plutons is the preservation of both cumulate and differentiated rocks in the complexes.

7.3.2 Petrography of Continental Arc Rocks

Magma series erupted along continental margins are compositionally similar to those erupted in island arcs, except that arcs erupting through continents have a greater abundance of silica-rich rock types, such as dacite and rhyolite. Much of this felsic material occurs as pyroclastic flow deposits. Continental margin magmatism contains significant amounts of andesite and dacite, which are petrologically similar to rocks of those compositions erupted in island arcs. Continental margin magmatic arcs may also contain rhyolite, which may be distinguished from dacite by the presence of phenocrystic sanidine.

Plutonic rocks are more commonly exposed in continental margin magmatic arcs than in island arcs. Rock types are generally gabbro, diorite, tonalite, granodiorite, and granite. The minerals characteristic of these rocks are plagioclase, alkali feldspar, quartz, amphibole, biotite, and magnetite and ilmenite. Pyroxenes, both clinopyroxene and orthopyroxene, may be found locally. Sphene and apatite are common accessory minerals, even in the mafic rocks, whereas allanite is common in highly differentiated granites. As with most slowly cooled rocks, there is evidence of subsolidus growth of minerals such as biotite, amphibole, and chlorite due to the interaction of solid rocks with high-temperature hydrothermal fluids. Grain boundaries also may be

altered by post-crystallization reactions resulting in a sutured texture.

Pyroxene is dominantly augite, sometimes joined by hypersthene in intermediate composition plutonic rocks. In many diorites, clinopyroxene is rimmed by hornblende. Amphibole is mainly hornblende and, unlike in the volcanic rocks, it is abundant and often well-formed in plutonic rocks, reflecting that the plutonic rocks crystallized with higher water activity than the volcanic rocks. The color of the hornblende ranges from green to brown and tends to correlate with increasing amounts of TiO_2 . Biotite is a common mafic mineral in granitic rocks. Plagioclase is the major rock-forming mineral in nearly all plutonic rocks. It is often complexly zoned, and myrmekite is common. Alkali feldspar is found only interstitially in mafic granitic rocks, but becomes more abundant in more felsic rocks. Orthoclase is the most common alkali feldspar, whereas microcline is found in the most differentiated rocks and forms under volatile-rich conditions. Exsolution textures are common, and magmatic fluid may be the cause of perthite coarsening (Parsons, 1978). Granophyric intergrowths are characteristic of the most differentiated granitic rocks, which form from the most volatile-rich magmas. Granophyres may form under conditions of supercooling, either by reduction in temperature as the magma rises in the crust, or by sudden loss of volatiles from the system (Vernon, 2004). Magnetite and ilmenite are the major opaque oxides.

7.4 Geochemical Characteristics of Convergent Margin Magma Series

7.4.1 Comparison of Oceanic and Arc Differentiation Trends

The tholeiitic basalts from oceanic and island arc environments are similar in terms of major element composition, but they follow different differentiation trends. This is best illustrated on a plot of Fe^* versus SiO_2 (Figure 7.6). During differentiation, tholeiitic melts from oceanic environments become enriched in Fe relative to Mg. The ferromagnesian silicates in the lavas become increasingly enriched in their iron end members as differentiation progresses. Only late in the differentiation history of oceanic tholeiites do the melts undergo silica enrichment (see data for the Galapagos and Iceland in Figure 6.9). In contrast, most arc magma suites show strong enrichment

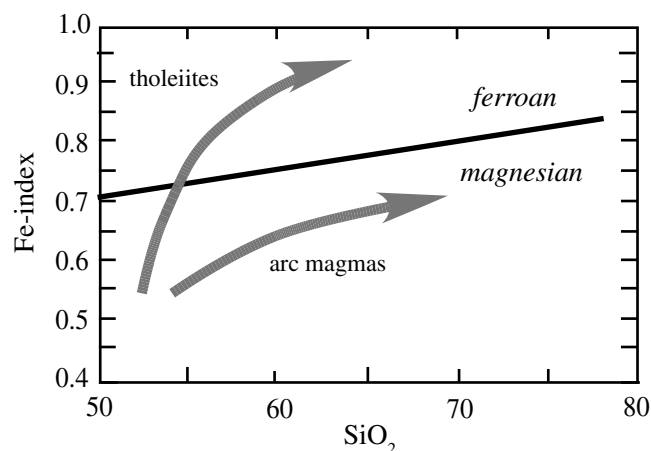


Figure 7.6 Plot of $\text{FeO}^{\text{tot}}/(\text{FeO}^{\text{tot}} + \text{MgO})$ showing the different differentiation trends for arc magmas and oceanic tholeiites.

in silica with increasing differentiation, but the ferromagnesian silicates show only moderate increases in the Fe/(Fe+Mg) ratio.

In terms of the classification discussed in Chapter 5, oceanic magmas are typically ferroan, whereas those from magmatic arcs are magnesian. These different trends are caused by the fact that the oceanic tholeiitic magmas tend to be more reducing than the arc magmas, and as a result Fe-Ti oxides crystallize relatively late in the former. The crystallization of olivine extracts Mg preferential to Fe and this causes the melts to become iron enriched, a feature noted earlier in the formation of oxide gabbros in oceanic crust. In contrast in arc magmas, Fe-Ti oxides crystallize relatively early, inhibiting the iron enrichment of the residual magma and causing the evolving magmas to become enriched in silica (Frost and Lindsley, 1992).

The two differentiation trends are often shown in a ternary diagram plotting $(\text{Na}_2\text{O} + \text{K}_2\text{O}) - \text{FeO}^{\text{(total)}} - \text{MgO}$ (Figure 7.7). On such a diagram differentiation drives the oceanic magmas (magmas from the Galapagos as an example) toward the iron apex before alkalis become enriched. In contrast the magmatic arc magmas (often called “calc-alkalic,” *senso lato*), as exemplified by magmas of Mount Saint Helens and other Cascade volcanoes, evolve toward the alkali apex without increases in FeO.

7.4.2 Comparison of Island and Continental Arc Magma Series

Although island and continental arc magma series both tend to be magnesian, there are some important differences

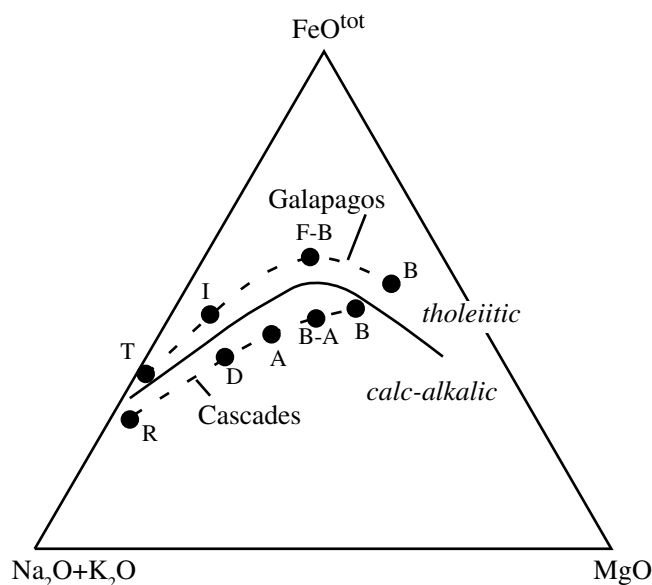


Figure 7.7 Alkalis- FeO^{tot} -MgO (AFM) diagram comparing the differentiation trends of tholeiitic rocks (as indicated by the lavas of the Galapagos) and calc-alkalic rocks (as indicated by the lavas of the Cascades). CA = calc-alkalic, TH = tholeiite, A = andesite, B = basalt, B-A = basaltic andesite, D = dacite, F-B = ferrobasalt, I = icelandite, R = rhyolite, T = trachyte. From Irvine and Barager (1971) and Wilson (1989).

in alkali content. This is shown in Figure 7.8, where fields for Seguam, Tobago, Mount Saint Helens, and Tuolumne all follow magnesian differentiation trends, but Seguam and Tobago are calcic whereas Mount Saint Helens and Tuolumne are calc-alkalic (Figure 7.8B). Arc volcanoes also may be characterized according to their trends on a plot of K_2O versus silica (Figure 7.9). A few arc volcanoes, such as St. Kitts, are poor in K_2O . These magmas are referred to in Figure 7.9 as the low-K series and are calcic by the MALI classification. Some arcs, such as those of the Solomon Islands, are potassic and define a high-K series. These are alkali-calcic by the MALI classification. Most arc volcanoes, including Mount Saint Helens and the more differentiated lavas of Seguam, fall into what we refer to as the medium-K series. As noted in Figure 7.9, some researchers have called this medium-K group the “calc-alkalic” series even though Seguam is calcic (Figure 7.8). Volcanic rocks of this composition are so common in arcs that the term “calc-alkalic” commonly is used to describe island arc magmas in general. However, because the term has a strictly defined geochemical connotation and because some arc suites are calcic and some

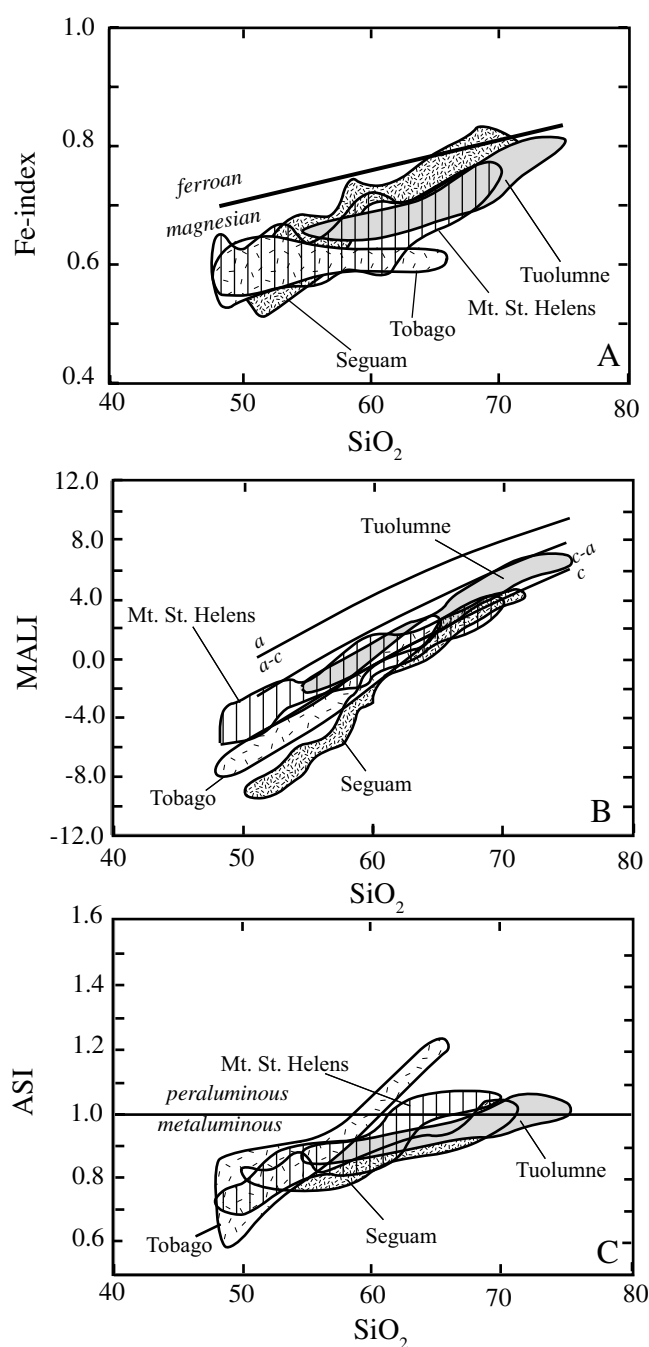


Figure 7.8 The chemical trends of island arc rocks, represented by Seguam, compared to continental arc rocks from Mount Saint Helens and Tuolumne. Data from Bateman and Chappell (1979), Halliday and colleagues (1983), Singer, Myers, and Frost (1992), and Smith and Leeman (1993).

are alkali-calcic, it is not advisable to use the word "calc-alkalic" loosely to refer to island arc magmatism.

There are several explanations for the variations in K_2O in arc lavas. One is based on the observation that in some

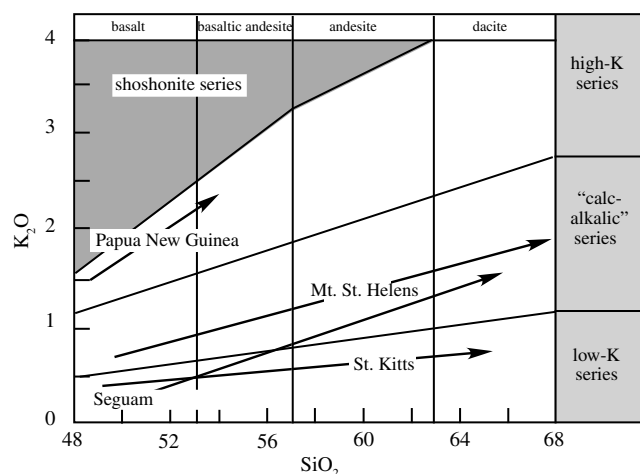


Figure 7.9 Plot of weight percent SiO_2 versus weight percent K_2O showing the composition variation of volcanic rocks from various island arcs. b.a. = basaltic andesite. Data from Brown et al. (1977), Johnson, Mackenzie, and Smith (1978), Halliday and colleagues (1983), Singer, Myers, and Frost (1992), and Smith and Leeman (1993).

arcs there is a spatial pattern along the axis of the arc. In the Lesser Antilles, for example, the lavas vary from low-K magmas at St. Kitts at the northern end of the arc, to "calc-alkalic" magmas in the center of the island chain, to high-K lavas at the southern end at Grenada (Brown et al., 1977). This variation correlates with the amount of sediment, which is a rich source of K_2O , being carried into the trench, which increases southward toward South America.

Another pattern observed in some arcs is a correlation between K_2O content and a volcano's distance from the subduction zone. The alkali content of volcanoes in an island arc tends to increase with increasing depth to the Benioff zone. Volcanoes erupting close to the trench (i.e., from relatively shallow melting depths) tend to be calcic in terms of the Peacock classification (see Chapter 5). Volcanoes erupting further away from a trench (i.e., relatively deep melting) are calc-alkalic, whereas those that are erupted farthest from a trench are alkali-calcic. Most of this change is related to an increase in K_2O in the magma with increasing depths of melting (Marsh and Carmichael, 1974).

In comparison to island arcs, calcic suites are uncommon along active continental margins. Instead, calc-alkalic suites are most typical. As with island arcs, the K_2O content of continental margin volcanism increases

inland from the coast, with alkalic suites occurring on the landward side of the volcanic front. A good example of a high-K magmatic suite occurs in the Absaroka Mountains, which lie on the eastern margin of Yellowstone National Park in Wyoming. The Absaroka Mountains lie more than a thousand kilometers inboard from the west coast of North America and host an unusually potassic suite that has provided the names *absarokaite* and *shoshonite* and given the name to the shoshonite series (see Figure 7.9).

7.4.3 Comparison of Oceanic and Continental Arc (Cordilleran) Plutonic Complexes

As the Tobago plutonic complex documents (Map 7.2), island arc plutonic rocks are dominated by ultramafic and gabbroic cumulates with only small volumes of tonalite. By contrast, continental arc plutons are composed mainly of granodiorite with subsidiary granite and quartz diorite. On the QAP diagram the oceanic arc plutons like Tobago define a slightly different differentiation trend from the continental arc batholiths such as Tuolumne (Figure 7.10). Tuolumne follows a differentiation trend of quartz diorite to granodiorite, with minor granite, with minor early gabbro or diorite (the trend marked C-A). Oceanic arc plutons like Tobago have lower abundance of alkalis; they are less likely to contain granodiorite or granite and typically follow a trend from gabbro and diorite to quartz-diorite to tonalite (marked C in Figure 7.10).

The divergent differentiation trends of oceanic and continental arc plutonic complexes illustrated on the QAP diagram are also evident on plots of Fe-index and MALI (Figure 7.11). Although both Tobago and Tuolumne are magnesian, Tobago is dominated by calcic rocks and Tuolumne by calc-alkalic ones. The ultramafic and gabbroic cumulates exposed on Tobago account for the lower silica contents of that island arc's plutonic complex compared to the continental arc rocks that extend to more siliceous compositions.

Also shown in Figure 7.11 is the compositional range of the Sierra Nevada batholith, of which Tuolumne is a small part. The granitic rocks of the batholith are dominantly magnesian, although a few of the most siliceous granites are ferroan. The granitic rocks define a large field on a MALI diagram that covers the range from calcic to alkali (Figure 7.11B). This broad range in

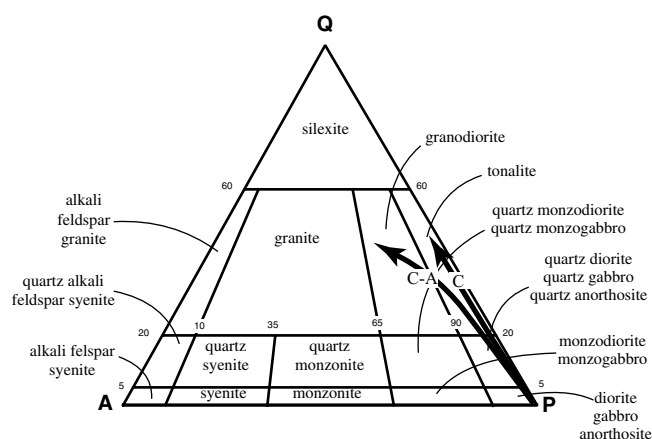


Figure 7.10 QAP diagram showing the compositional ranges of rocks found in calcic (C) and calc-alkalic (CA) batholiths (after Frost and Frost, 2008).

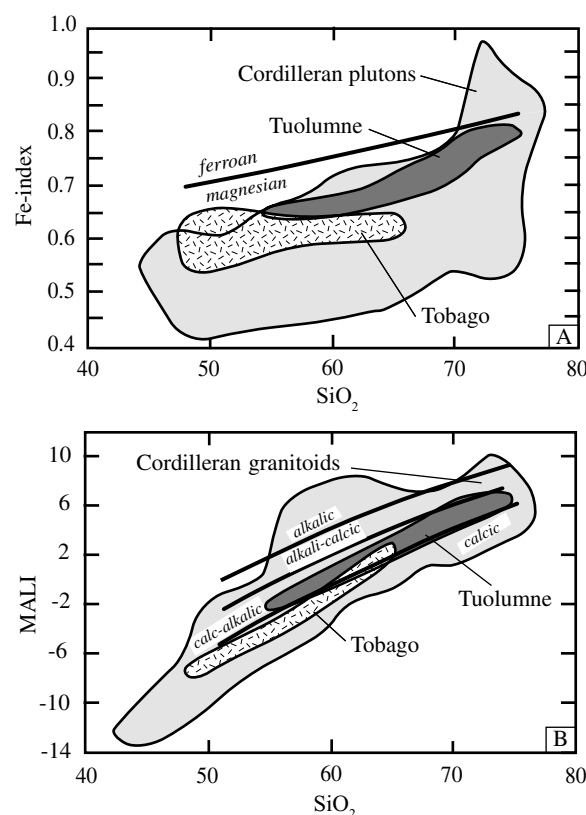


Figure 7.11 The chemical trends of plutonic island and continental arc rocks as represented by Segum and Tuolumne. Also shown is the field for Cordilleran batholiths. Data from Bateman and Chappell (1979), Halliday and colleagues (1983), Singer, Myers, and Frost (1992), Smith and Leeman (1993), and Frost and colleagues (2001).

composition correlates to geographic location. Plutons on the western part of the Sierra Nevada tend to be calcic, those in the core Sierra Nevada are calc-alkalic, and those lying in the eastern Sierra Nevada are alkali-calcic or alkalic. As was observed for arc volcanic rocks, this change in composition may reflect a shift to more alkalic compositions farther inboard from the subduction zone. In addition, the inboard plutons may have incorporated more continental crust, which also is indicated by their increase in initial Sr isotopic composition from west to east (Figure 4.12).

7.4.4 Geochemical Identification of Contrasting Processes Forming Seguam and Mount Saint Helens

Although both Seguam and Mount Saint Helens have erupted basalt, andesite, and dacite, the two rock suites developed by very different processes. Geochemical studies (Halliday et al., 1983; Smith and Leeman, 1992) strongly suggest the range of rock compositions from Mount Saint Helens formed from mixing two melts: a mantle-derived basaltic melt and a crustally derived dacite melt. In contrast, Singer, Myers, and Frost (1992) concluded Seguam formed by closed-system fractional crystallization.

Evidence for these different processes is seen in geochemical variation diagrams (Figure 7.12A, B). The plots of TiO_2 and FeO^{tot} abundances from Seguam define a distinct inflection at 60 percent SiO_2 , and TiO_2 increases with increasing silica up to this inflection point. The inflection indicates the appearance of Fe-Ti oxides (ilmenite or titanomagnetite) on the liquidus, after which point iron and titanium are removed from the melt by incorporation into crystallizing oxides. In contrast, the TiO_2 and FeO concentrations in rocks from Mount Saint Helens form straight trends on variation diagrams, a feature explained by mixing basaltic and dacitic magma. This hypothesis is supported by Sr isotopic data (Figure 7.12C). As described in Chapter 4.6, in a closed system $^{87}\text{Sr}/^{86}\text{Sr}$ will increase over time as ^{87}Rb decays to ^{87}Sr . The decay rate for ^{87}Rb is slow enough that the $^{87}\text{Sr}/^{86}\text{Sr}$ ratio for a magma varies little over the lifetime of a volcano. Figure 7.12C shows that the $^{87}\text{Sr}/^{86}\text{Sr}$ of lavas from Seguam remains constant regardless of the silica content of the rock, a pattern consistent with closed-system fractionation of a magma with a particular $^{87}\text{Sr}/^{86}\text{Sr}$. By contrast, the $^{87}\text{Sr}/^{86}\text{Sr}$ for rocks from Mount Saint Helens increases with increasing silica.

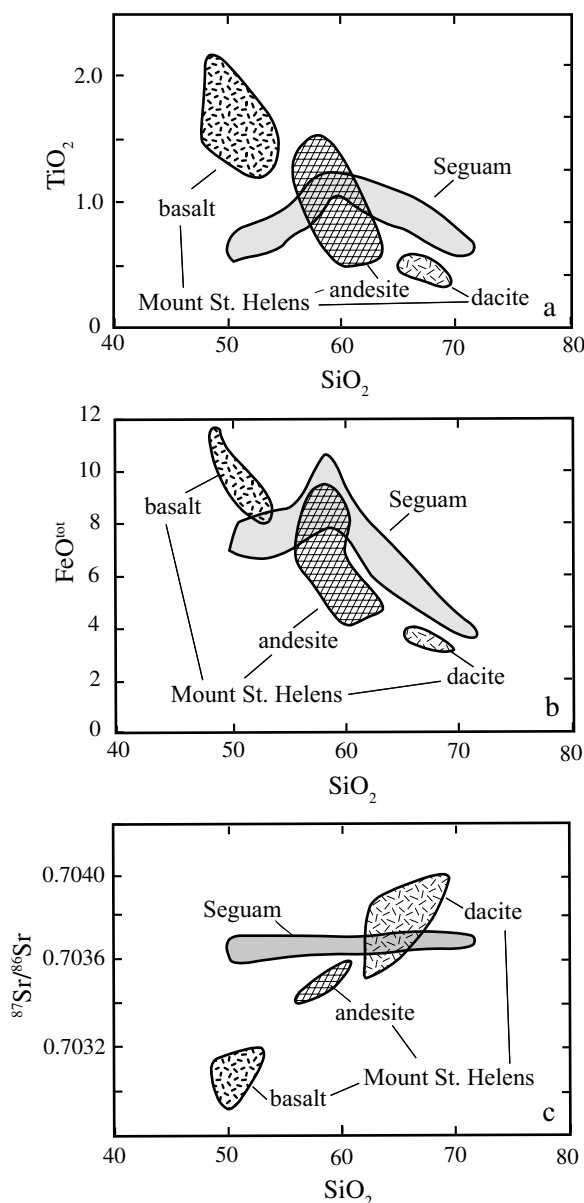


Figure 7.12 Variation diagrams showing the differences in trends exhibited by Seguam and Mount Saint Helens volcanic rocks, which reflect different processes of magmatic differentiation. Data from Singer, Myers, and Frost (1992), Halliday and colleagues (1983), and Smith and Leeman (1993).

This pattern would be expected if a dacitic melt with a relatively high $^{87}\text{Sr}/^{86}\text{Sr}$ ratio mixed with a basaltic melt with a low $^{87}\text{Sr}/^{86}\text{Sr}$ signature.

This evidence led Halliday and colleagues (1983) and Smith and Leeman (1993) to conclude that the various rock types on Mount Saint Helens formed from mixed magma. Intrusion of hot basaltic magma melted mafic country

rock to produce a dacitic melt. The two initial melts, the crustal dacite melt and the basalt mantle-derived melt, then mixed in various proportions to produce the andesites. On the other hand, Singer, Myers, and Frost (1992) concluded that Segua formed from mafic melt that differentiated in a closed system to form the more evolved rocks, including the andesites, dacites, and rhyodacites.

7.5 Magma Generation at Convergent Margins

The sources of arc magmas are the subject of long and continuing debate. Compared to oceanic magmas at ridges or within oceanic plates, a more diverse combination of materials may be involved or in some way, influence the magmas in arc settings (Figure 7.2):

1. *Seawater* is the ultimate source for most of the H_2O that appears in island arc magmas. It is trapped in pore spaces in sea floor sediment and gets incorporated into oceanic crust during metamorphism, and is subducted along with the oceanic crust.
2. *Oceanic crust* consists of basalt, gabbro, and sea floor sediments including clays, carbonates, and chert. Oceanic crust may be incorporated into arc magmas in two environments. Subducted oceanic crust could melt at depth, or the oceanic crust on which the arc volcano is built could melt as magmas pass through it. During subduction, the cold crust is heated by the surrounding mantle and possibly also by frictional heating at the surface of the slab.
3. *The mantle wedge above the subducted slab* consists of two components. One is the mantle lithosphere, forty to seventy kilometers thick, which is depleted in some constituents because MORB melts have already been extracted. These depleted rocks are unlikely to melt readily. The other component is the asthenospheric mantle, which consists of lherzolites likely to be more fertile than those in the lithosphere and that could melt if they were to interact with fluids discharged by the subduction zone.
4. *Continental crust.* Unlike island arc magmas, magmas by subduction along continental margins must pass into and through continental crust. Many of the

differences between continental margin magmas and island arc magmas can be attributed to the fact that continental margin magmas must pass through a ~50 km thick section of continental crust. Almost without exception these magmas appear to interact with the crust through which they pass, both assimilating that crust and undergoing fractional crystallization as they cool. In some places, the effects of assimilation are easily recognized. If the overriding continental plate contains Precambrian crust, the distinctive isotopic characteristics of those ancient rocks will be imprinted in the contaminated magmas. In areas where the overlying crust contains young metasedimentary rocks, which are not isotopically distinguishable from mantle-derived magmas, crustal assimilation is harder to identify.

The thermal regime of the subduction zone is very important in controlling magma production. Generally speaking, the system will be hotter if the convergence rate is slower, since this will minimize the depression of isotherms where cool lithosphere is subducted into the mantle. Likewise, if the subducted slab is young, it will be warmer and the system will be hotter. Numerical models by Peacock (1991) suggest that young, warm, oceanic crust and its veneer of sediment may partially melt rather than dehydrate as it descends into the mantle. On the other hand, older, cooler crust may dehydrate and release fluids that flux the overlying mantle wedge, lowering its melting point such that the mantle partially melts.

Recently, investigators have recognized that at subduction-zone pressures and temperatures, hydrous fluids polymerize, not unlike silicate melts, which enhances their ability to dissolve solutes, particularly silica and alkalis. Because of this behavior of aqueous fluids, at high enough temperatures there is a continuum between aqueous solutions and hydrous melts (Manning, 2004). Thus, depending upon conditions, the down-going slab releases fluids that range from silicate melts to aqueous fluids. Polymerized aqueous fluids can dissolve and transport a wide variety of chemical compounds into the overlying mantle. These fluids can produce partial melting of the mantle wedge and these magmas may carry a geochemical signature of the slab, even if the slab itself didn't melt.

Arc magmas may rise diapirically and pond in magma chambers at depths of thirty kilometers or less, accumulating

at the base of the crust or within it. Some magma chambers appear to form within a few hundred meters of the surface. Here magmas may differentiate and may assimilate the surrounding crustal wall rocks. Evidence for high-level magma chambers comes from several observations. The existence of craters at the summits of volcanoes is evidence of shallow magma chambers. They are formed by eruption of large volumes of magma and the subsequent foundering of the overlying rock into the space previously occupied by the magma. In addition, many andesite flows contain inclusions of cumulate plutonic autoliths. These autoliths typically are gabbro or diorite in composition, and provide evidence that crystals were accumulating within a magma chamber before eruption. The presence of plagioclase restricts their formation to depths shallower than thirty kilometers, since plagioclase does not usually crystallize at greater depths. The attenuation of S-waves, shallow volcanic tremors, and the deformation of the ground surface associated with the filling of shallow magma chambers all

reinforce petrographic indications from mineral assemblages of low-pressure crystallization.

Finally, the composition of continental arc magmas may be affected by assimilation of crust during magma ascent and emplacement. As described earlier in this chapter, because the isotopic composition of mantle-derived magmas commonly is distinct from that of crustal melts, the interaction of mantle and crust sources may be identified isotopically. Section 7.4.4 described the interaction of crustal melts with more mafic arc magmas at Mount Saint Helens, as evidenced by the contrasting Sr isotopic compositions between basalts and dacites (Figure 7.12C). In another example, the incorporation of Precambrian crust in magmas of the Sierra Nevada batholith is indicated by higher $^{87}\text{Sr}/^{86}\text{Sr}$ isotope ratios of the granitic rocks in the eastern portions of the batholith (Section 7.4.3 and Figure 4.12). Partial melts of continental crust tend to be felsic and are a major reason continental arcs contain more siliceous rocks on average than island arcs.

Summary

- Oceanic and continental arcs form on an overriding oceanic or continental plate, respectively, above a subducting oceanic plate.
- Magmas from arcs typically follow a magnesian differentiation trend in contrast to the ferroan trend exemplified by oceanic tholeiites.
- Island arc magmas may be calcic, calc-alkalic, or alkalic. The K_2O content correlates spatially either with position along the arc (as in the Lesser Antilles), or with increasing distance from the subduction zone (as in the Sierra Nevada batholith).
- The common volcanic rock types associated with arcs are basalts, andesites, dacites, and minor rhyolites. Magmatic arcs on continental margins tend to produce magmas that are more siliceous than arcs in oceanic environments.
- Arc volcanism is commonly associated with explosive eruptions, which form pyroclastic deposits. These pose considerable hazards to human and other life.
- Oceanic arc plutonic complexes typically contain ultramafic and gabbroic cumulates as well as differentiated rocks such as tonalites.
- The plutonic roots of continental arcs are exposed as Cordilleran granitic batholiths, dominantly granodiorite. Cordilleran batholiths tend to be magnesian, calcic to calc-alkalic, and metaluminous. The most siliceous rocks may be peraluminous, mainly due to interaction with continental crust.
- A combination of sources may contribute to arc magmas, including the oceanic crust of the down-going slab and its carapace of subducted sediment, the overlying mantle wedge, and the oceanic or continental crust of the overriding plate. Variations in the thermal regime of the subduction zone system and the characteristics of the fluid or melt released from the subducted slab, as well as the composition and amount of interaction with the overriding plate, may account for the petrologic, geochemical, and isotopic differences observed in arc magmas.

Questions and Problems

Problem 7.1. Construct a table comparing the petrography and geochemical composition of island arc magmas to mid-ocean ridge magmas and to ocean island magmas.

Problem 7.2. What are the essential differences between island and continental arc magmatic suites? What are possible causes of those differences?

Problem 7.3. Describe the sequence of rock types erupted during stage 2 of Mount Saint Helens shown in Figure 7.4. What magma chamber processes could have produced this sequence of eruptive products?

Problem 7.4. Are volcanic and plutonic suites from continental arcs identical, except that one was erupted on Earth's surface and the other crystallized at depth? Why or why not?

Further Reading

Gill, R., 2010, *Igneous rocks and processes: A practical guide*. Wiley-Blackwell, Oxford, Chapter 6.

McBirney, A. R., 2007, *Igneous petrology*, 3rd ed., Jones and Bartlett, Boston, Chapter 9.

Wilson, M., 1989, *Igneous petrogenesis: A global tectonic approach*. Unwin Hyman, London, Chapters 6 and 7.

Winter, J. D., 2010, *Principles of igneous and metamorphic petrology*, 2nd ed., Prentice Hall, New York, Chapters 16 and 17.

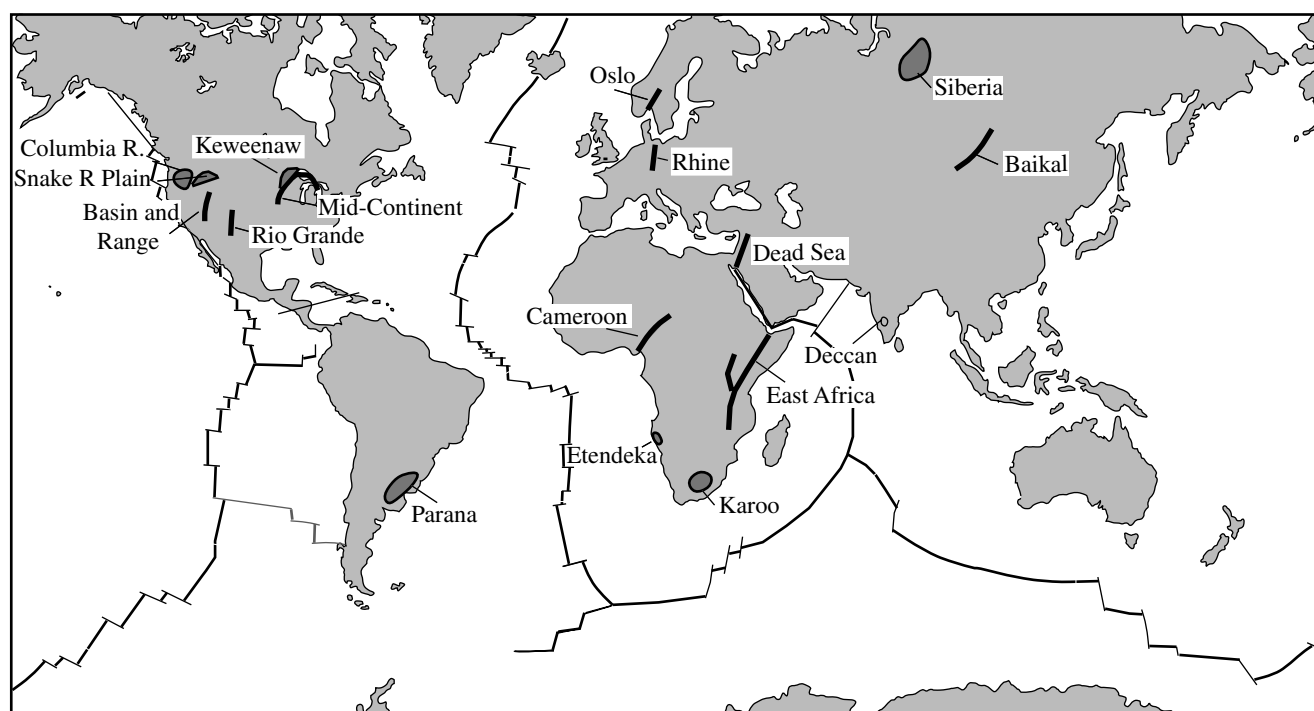
Chapter 8

Intracontinental Volcanism

8.1 Introduction

Although continental intraplate magmatism produces only a small proportion of the igneous rocks erupted on Earth, it produces the largest variety of rock types. This diversity of intracontinental igneous rocks results from various combinations of mantle, continental lithosphere, and crustal sources. Different combinations and proportions of these sources, together with processes of magmatic differentiation, create a broad spectrum of igneous suites. Intracontinental magmatism is addressed in this and the following chapter. This chapter is concerned with intracontinental volcanism, whereas the next chapter describes plutonic rocks that formed in an intraplate environment. The discussion of volcanism precedes that of plutonism because the tectonic environment of young volcanic rocks is typically the most straightforward. The information assembled in this chapter is then used to address the origin of intracontinental plutonic rocks, the tectonic environments of which are not always definitive. It is important to keep in mind that in many instances intrusions are spatially related to coeval volcanic rocks, and hence the division of this topic into two chapters is somewhat arbitrary.

Intracontinental volcanism is typically associated with mantle plumes or rifts. Plume-related magmatism in intracontinental settings is analogous to that in oceanic environments: volcanic centers define tracks of progressively younger magmatism approaching the present site of the plume. The plume track along the Snake River Plain in Idaho is comparable to the one that produced the Hawaii-Emperor island chain in the Pacific Ocean. Intracontinental volcanism associated with active continental rift zones includes the Basin and Range province and the Rio Grande rift of the southwestern United States, the Rhine graben of Europe, the East African rift zone (including the Red Sea), and the Cameroon volcanic line of Africa, the Baikal rift in Siberia, and the southeast Australia rift zone (Map 8.1). Of these, the East African rift system involves the greatest volumes of magma (500,000 km³ compared to 12,000 km³ in the Rio Grande rift). Continental rift zones form above areas of local lithospheric extension and are characterized by a central depression, uplifted flanks, and a thinning of the underlying crust. These structures are associated with high heat flow, broad zones of regional uplift, and magmatism. The rift zones are usually tens of kilometers wide and tens to a few hundred kilometers long. The Basin and Range province is unusual among continental rifts in that it extends hundreds of kilometers in both length and breadth. Some rift zones, such as the East African rift, represent continental crust undergoing the first stages of continental breakup. These may eventually evolve into Atlantic-type, rifted continental margins. Other rift zones are the products of “escape tectonics.” In these zones, the continent outboard of a continental collision extends in response to that collision. Examples include the Rhine graben, which formed in response to the Alpine collision, and the Baikal rift, which formed in response to the Himalayan collision.



Map 8.1 Locations of major continental flood basalt provinces (shaded areas) and of major continental rifts (heavy lines).

It is difficult to generalize about the composition of lavas erupted in continental rifts. In some environments, rifting involves eruption of huge volumes of tholeiitic basalt as flood basalt, such as in the Rio Grande rift. In other areas, such as the East African rift, magmatism involves the formation of individual, point-source volcanoes that may range in composition from tholeiitic to alkaline. Most alkaline rocks are rich in sodium, rather than potassium, although potassic alkaline rocks are present as well. This chapter examines this wide range of primary magmas, their origin, and their differentiation to form a wide range of derivative magmas.

8.2 Continental Flood Basalt Provinces

Perhaps the most dramatic examples of continental volcanism are flood basalts. Large areas of the continents have been covered by great thicknesses of basaltic magma that appear to have been fed from fissures rather than from central vents. Some of these flood basalts, such as the Keweenawan basalts in the north central United States, are clearly related to rifts; for others the relationship is cryptic. Continental flood basalt provinces, together with oceanic plateau (see Chapter 6), are sometimes referred to as **large**

igneous provinces (LIPs). The volume of lava produced in these provinces is far greater than any continental volcanism occurring today. Most continental flood basalts are tholeiitic, and they appear to form in extensional environments. Although they form lava sequences one to ten kilometers thick, the surface upon which the lavas flowed never seems to have developed much relief. Apparently, the underlying rocks subsided to form a basin of about the same extent as the lavas that flowed out, so that mass was simply transferred from depth to the surface.

Map 8.1 shows the distribution of major continental flood basalt provinces in the world; the ages and dimensions of the provinces are given in Table 8.1. Many of the flood basalts erupted during continental breakup or during failed continental rifting. The Karoo, Paraná, and Deccan provinces evolved in tensional environments associated with the breakup of Gondwana during the Jurassic and Cretaceous. These provinces form a band that parallels the Atlantic margin of Gondwana. A plume source is implicated in the origin of other occurrences of continental flood basalts. The Columbia River basalts and the lavas of the Snake River Plain and Yellowstone may be the product of a single plume (Camp, 1995). Mantle plumes are commonly associated with divergent plate margins;

Table 8.1 Ages and Dimensions of Major Continental Flood Basalt Provinces

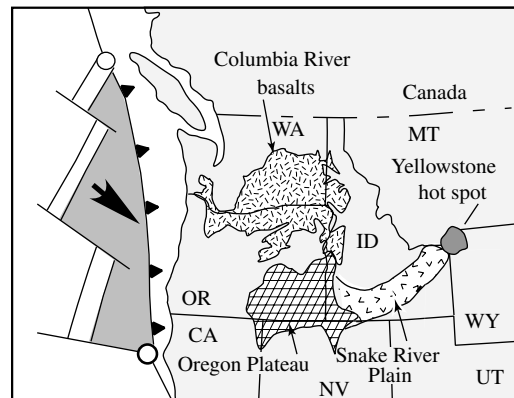
Flood basalt	Location	Age (Ma)	Area (km ²)	Thickness (m)
Snake River Plain	Idaho, USA	16–present	$.5 \times 10^5$	up to 1,200
Columbia River	WA, ID, OR, USA	16–6	2.0×10^5	>1,500
Deccan Traps	India	65–50	$>5.0 \times 10^5$	>2,000
Paraná Plateau	Brazil	149–119	12×10^5	1,800
Karoo	S. Africa	206–216	$>1.4 \times 10^5$	9,000
Siberian Traps	Russia	245–216	$>15 \times 10^5$	3,500
Keweenaw	Lake Superior, USA	1200–1050	$>1.0 \times 10^5$	12,000

many ocean islands, including Iceland, the Galapagos, Bouvet, and Tristan da Cunha are located on mid-ocean ridges. Continental flood basalt provinces may be related to rifting and to plume activity. For example, the Etendeka and Paraná flood basalt provinces were formed over the Tristan hot spot during the opening of the South Atlantic Ocean (Mohriak et al., 2002).

8.2.1 The Columbia Plateau – Snake River Plain Province

One of the youngest and best preserved continental flood basalt provinces in the world is the Columbia Plateau – Snake River Plain province of Washington, Oregon, and Idaho. The basaltic volcanism composes part of a swath of Miocene and younger basaltic (and minor rhyolite) volcanism that extends across the northwestern United States, including the Columbia Plateau, the Oregon Plateau, and to the east, the Snake River Plain and Yellowstone (Map 8.2). Between six and seventeen million years ago, approximately 200,000 km³ of relatively aphyric basaltic lavas covered an area of about 200,000 km² in the Columbia Plateau. Since the Miocene, a much smaller volume of basaltic lava has been erupted in the Snake River Plain, where the last eruption took place only two thousand years ago.

The Columbia River basalts have been divided into four major units, which are, from oldest to youngest, the Imnaha, Grande Ronde, Wanapum, and Saddle Mountains basalts (Figure 8.1). The Picture Gorge basalt is a smaller unit coeval with the Grande Ronde basalt. The Grande Ronde flow is by far the largest by volume, and was erupted over a narrow time interval of 0.42 million years beginning at 15.79 million years ago (Barry et al., 2010). This age is somewhat younger than the 16.5 million year age



Map 8.2 Map showing the relation between the Columbia River basalts, the Oregon Plateau volcanic belt, the Snake River Plain, Yellowstone, and the direction of movement of the Juan de Fuca plate relative to North America.

for the Steens basalt, one of the major basalt flows of the southeastern Oregon Plateau that is considered part of the Columbia River Basalt Group (Brueseke et al., 2007; Baksi (2010). Like the Grande Ronde basalt, the Steens basalt was erupted over a very short time of 0.2 million years (Baksi, 2010). The origin of the Columbia River basalts is the subject of ongoing debate. Some authors emphasize the location of the basalt province east of the Cascades arc in a back-arc setting and propose a magma source in the shallow mantle akin to that supplying arcs. Alternatively, the fact that huge volumes of basalt were erupted over a very short period of time has led others to conclude that the eruption of the Steens basalt marked the onset of hotspot volcanism in western North America (see discussion and reply in Hooper et al., 2007). Hooper and colleagues (2007) proposed that one edge of the plume died out over

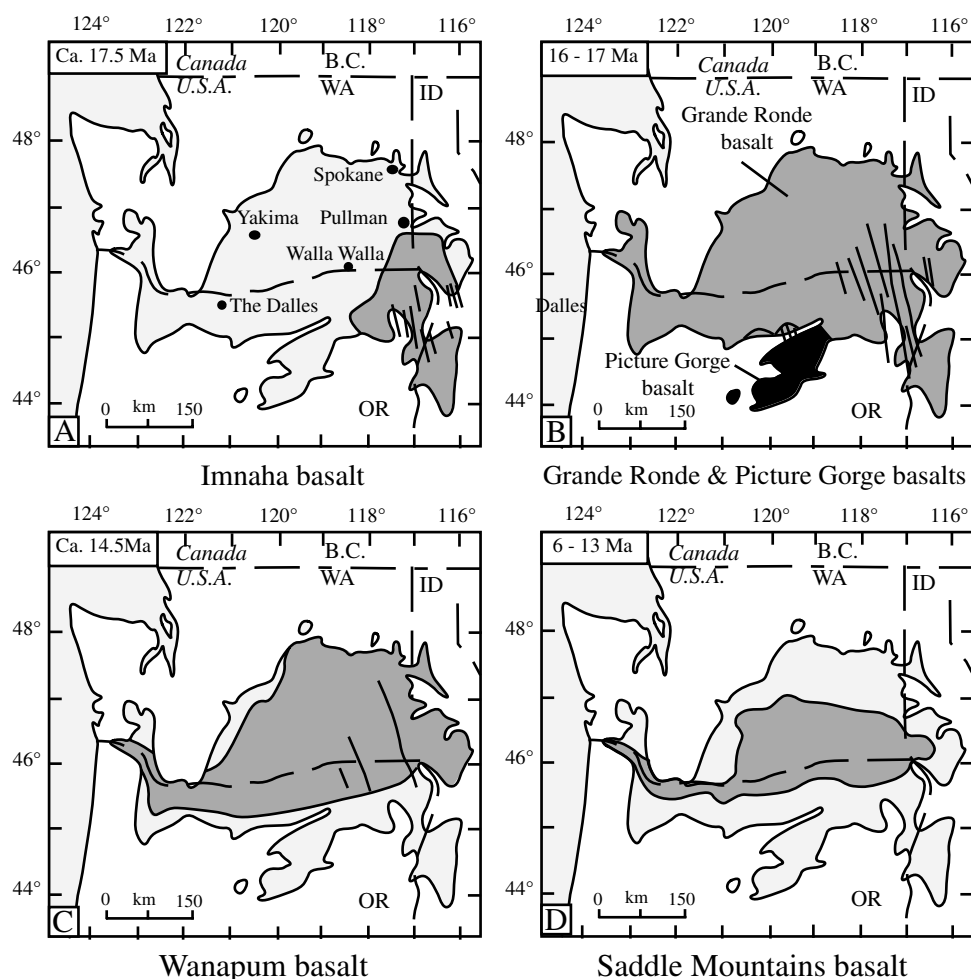


Figure 8.1 The aerial extent (in dark shading) of the four units of the Columbia River basalts. Light shading gives the modern extent of the Columbia River basalts. The location of the fissures are marked with heavy lines. From Swanson and colleagues (1979).

six million years ago after the eruption of the Columbia River basalts, while the main portion of the plume produced the basaltic and rhyolitic volcanism of the Snake River Plain. The rhyolite volcanism of the Snake River Plain becomes younger to the east as the North American plate drifted westward over the head of the plume. The locus of the plume-related volcanism is now centered over Yellowstone and the eastern Snake River Plain.

Chemistry of the Columbia River basalts. The Columbia River basalts show a differentiation trend typical of tholeiitic suites, with moderate increases in SiO_2 accompanied with considerable decreases in CaO and decreases in MgO (Figure 8.2). Figure 8.2 shows that as the suites differentiate to lower MgO , they display an increase in silica. However, at any value of MgO there is a considerable range in SiO_2 among the eruptive suites. This suggests each suite experienced a different degree of crustal

assimilation. The well-defined trend on the CaO versus MgO diagram is consistent with fractionation of clinopyroxene and plagioclase, which produces residual lavas poorer in both of those two oxides. The increase in K_2O with decreasing MgO indicates that potassium was behaving incompatibly; no K-bearing phase, such as K-feldspar, was crystallizing in these basalts. TiO_2 behaved incompatibly in the Imnaha, Grande Ronde, and Picture Gorge basalts, indicating that the Ti-bearing phase, such as Ti-magnetite or ilmenite, was not crystallizing. In both the Saddle Mountains and Wanapum basalts, the TiO_2 reaches a maximum at $\text{MgO} \sim 5.0$ percent, which indicates the composition where ilmenite or Ti-magnetite began to crystallize.

A key point indicated by the data shown in Figure 8.2 is that each formation in the Columbia River Basalt Group has a distinct geochemical signature. The oldest unit, the

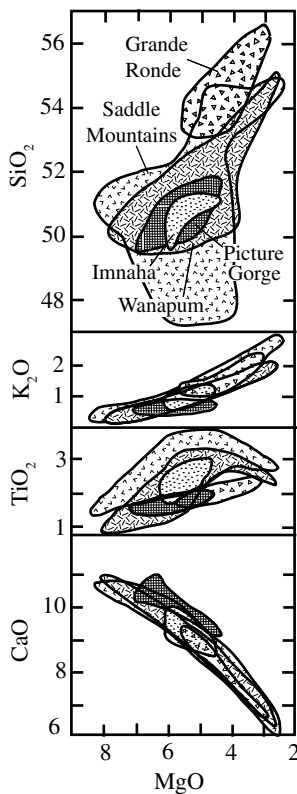


Figure 8.2 Major element compositions of the Columbia River Basalt Groups. From Hess (1989) and Hooper and Swanson (1990).

Imnaha basalt, has a relatively restricted compositional range, and SiO_2 and MgO compositions are near those of primitive mantle-derived basalts. Despite the huge volume of basalt erupted in the Grand Ronde basalts, these basalts have a rather restricted range in composition, which is richer in SiO_2 and poorer in MgO than the Imnaha basalt. Compared to the Grande Ronde, the time-correlative Picture Gorge is less evolved chemically and has lower SiO_2 and higher MgO (Figure 8.2). The smaller lava volumes of the Wanapum and Saddle Mountains formations were erupted with highly variable chemical compositions.

Two end member models describe the formation of the Columbia River basalts: either each eruption represents a new batch of mantle-derived magma, or the basalts formed from a single large batch of magma that ponded and differentiated in a chamber at depth from which eruptions tapped magma periodically. Since the lavas do not systematically become more evolved with decreasing eruptive age, the geochemical data best support the first alternative.

8.2.2 Petrography and Chemistry of Continental Flood Basalts

Flood basalt lavas typically are aphyric and phenocrysts are scarce. When phenocrysts are present, plagioclase is the most abundant mineral; it is accompanied by augite + pigeonite and Ti-magnetite and lesser amounts of olivine. This mineral assemblage is indicative of shallow-level crystallization. There are some distinct differences between continental flood basalts and MORB. In both rock types, plagioclase is the dominant phenocryst phase, but in MORB, olivine and Mg-Cr spinel are very common, whereas in continental flood basalts, augite and sometimes pigeonite are the main ferromagnesian minerals.

In terms of major element chemistry, continental flood basalts are similar to MORB. One important difference is the Fe-index, which is typically higher in continental flood basalts ($\text{FeO}^{\text{tot}}/(\text{FeO}^{\text{tot}} + \text{MgO}) = 0.7\text{--}0.8$; Hooper, 2000) than in MORB ($\text{FeO}^{\text{tot}}/(\text{FeO}^{\text{tot}} + \text{MgO}) = 0.5\text{--}0.6$; Stakes, Shervais, and Hopson, 1984). Either continental flood basalts are generated from sources that have more Fe than N-MORB-source mantle, such as E-MORB mantle (see Figure 6.7), or magmatic differentiation lowered the Mg content.

8.2.3 Models for the Generation of Continental Flood Basalts

The petrography, major and trace element chemistry, and isotope geochemistry suggest fundamental differences between continental flood basalts and oceanic basalts, some of which may be due to subcontinental lithospheric mantle and continental crust contamination of flood basalts (Hooper et al., 2007).

Continental flood basalts contain a low-pressure phenocryst assemblage. Consequently, it is reasonable to assume that at least part of the differentiation that produces continental flood basalts takes place at shallow depths, and that gabbroic and ultramafic cumulates lie beneath the flood basalt provinces. Cox (1980) envisions a two-stage process: basaltic sills near the base of the crust that undergo partial crystallization. The residual magmas, which are now less MgO rich, rise through a network of dikes toward the surface. The magmas may pond again near the surface and undergo further fractional crystallization to produce the low-temperature phenocryst assemblage.

Ascent through a system of dikes provides ample opportunity for crustal contamination. The extent of contamination will vary with the temperature of the magma, the flux of magma through the dikes, the width of the dikes, and the composition (and solidus temperature) of the crust through which they pass. Where flow in the dikes is turbulent, magma will erode its walls and become more contaminated than if flow were laminar. The Columbia River basalts appear to have been contaminated at two levels: first, at the base of the crust by the subcontinental lithosphere or lower crust, and second at shallower crustal levels where assimilation of continental material occurred during magma ascent (Hooper et al., 2007).

8.3 Bimodal Volcanism

The Columbia River flood basalt province contains essentially no coeval rhyolites, but most flood basalt provinces and many tholeiitic volcanoes in rifts erupt rhyolite as well as basalt (Bryan et al., 2002). In fact the association of basaltic rocks and rhyolite with a comparative lack of intermediate rocks is common enough in rifted areas to carry its own term – **bimodal volcanism**.

8.3.1 Bimodal Volcanism in the Yellowstone – Snake River Plain Province

A good example of bimodal volcanism is seen in the Snake River Plain – Yellowstone system, which, as noted earlier, appears to be located along a continuation of the plume track that may have formed the Columbia River basalt and Oregon Plateau (Figure 8.3). The Yellowstone – Snake River Plain province erupted in a two-stage process. The first event involved rhyolitic caldera eruptions that migrated from west to east across Idaho during the past fifteen million years (Perkins and Nash, 2002). This age progression is caused by the westward migration of North America over a stationary hot spot. Indeed, the fact that the apparent eastward migration of the calderas matches the rate of the westward movement of the North America plate is one of the strongest arguments that the Yellowstone – Snake River Plain volcanism is caused by a mantle hot spot. The famous thermal features of Yellowstone National Park are the result of the magmatic heat that remains after the most recent eruption in this series, a massive eruption that formed the Yellowstone Caldera six hundred forty thousand years ago. The second

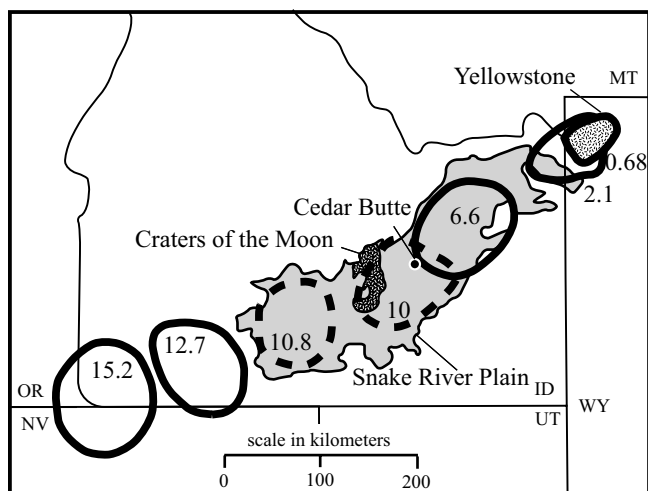


Figure 8.3 A portion of the northwestern United States showing the location of the Snake River Plain, Craters of the Moon volcanic rocks, Cedar Butte rhyolite volcano, the Yellowstone Caldera, and the calderas formed by the Yellowstone hot spot as it moved across Idaho, dashed where approximate. Numbers give the ages for the caldera eruptions in millions of years. Modified after Perkins and Nash (2002) and McCurry et al. (2008).

series of events involved the eruption of extensive flood basalts that filled most of the calderas formed by the rhyolitic eruptions.

The eruptions of the Yellowstone Caldera produced voluminous deposits of fayalite-bearing, high-silica rhyolitic tuffs, which record some of the world's most catastrophic volcanic events (Box 8.1). The presence of fayalite in these tuffs indicates that the magma was iron enriched. The remnants of similar iron-enriched, high-silica rhyolites, found on the margins of the Snake River Plain across southern Idaho and northern Nevada, were used to determine the locations and ages of the calderas that have long been buried by the basaltic Snake River Plain lavas.

The Snake River Plain volcanism is dominated by olivine tholeiite, but locally, including at Cedar Butte, the plain is dotted with small rhyolite volcanoes. Like the rhyolite from Yellowstone, the rhyolite from the small rhyolite volcanoes in the Snake River Plain is iron enriched. Additionally, the rhyolite is isotopically indistinguishable from the basalts of the Snake River Plain, causing McCurry and colleagues (2008) to conclude that the rhyolite was produced by extreme differentiation of the Snake River Plain tholeiitic basalt. This association of rhyolite with basalt is typical of bimodal volcanism. In many

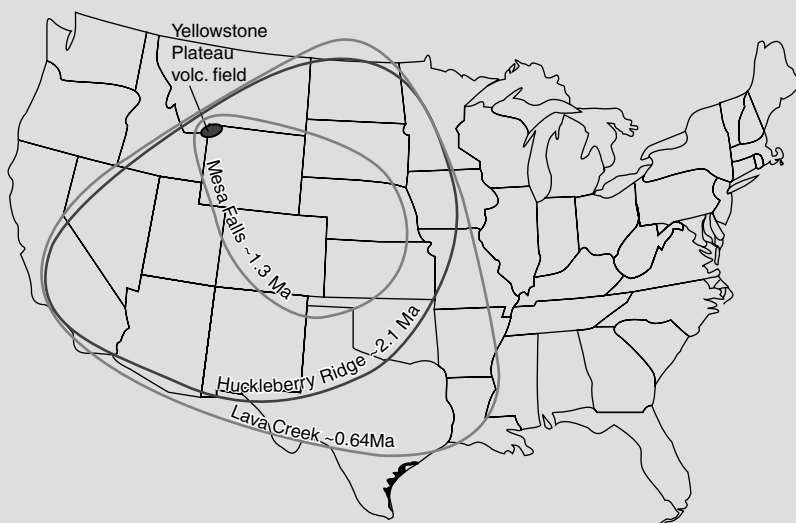
BOX 8.1 VOLCANIC HAZARDS IN INTRACONTINENTAL ENVIRONMENTS

Arc volcanoes account for more eruption-related fatalities in the past thousand years than eruptions in any other tectonic setting (Box 7.1). However, some of the largest volcanic eruptions derive from intracontinental volcanoes. The Yellowstone volcanic field has erupted catastrophically three times over the past 2.1 million years:

Eruption	Date	Volume of ejecta
Huckleberry Ridge	~2.1 Ma	2,500 km ³
Mesa Falls	~1.4 Ma	280 km ³
Lava Creek	~0.64 Ma	1,000 km ³

Each eruption produced extensive blankets of hot rhyolitic ash that covered much of western and central North America (Box 8.1). Each eruption also resulted in the formation of a caldera when the ground collapsed above the partially emptied magma chamber.

Eruptions on this scale are rarest, but the hazards they pose are the most significant. Each eruption at Yellowstone probably lasted for a day to weeks. The area closest to the volcanic centers was overrun by ash flows, and a larger area was affected by ash falls. Fine ash encircled the globe, cooling climate for several years. The U.S. Geological Survey estimates that the probability of another major, caldera-forming eruption in Yellowstone is so small as to be below the threshold of calculation (Christiansen et al., 2007). However, the area remains geologically active, and the hydrothermal features – including geysers, hot springs, and fumaroles – draw millions of visitors to Yellowstone National Park each year.



Box 8.1 The extent of ash fall deposits from the three major caldera-forming eruptions of the Yellowstone Plateau volcanic field: the Huckleberry Ridge ash bed (~2.1 Ma), the Mesa Falls ash bed (~1.3 Ma), and the Lava Creek ash bed (~0.64 Ma). From Christiansen and colleagues (2007).

rift environments, only basalt and rhyolite are found and lavas with intermediate silica contents are conspicuously missing. In the Snake River Plain, lavas with intermediate silica contents are found in the four-hundred-thousand-year-old lava flows from Cedar Butte, which record a complete geochemical transition from basalt to rhyolite in the Snake River Plain magmatic system (Figure 8.4).

8.3.2 Geochemistry of the Yellowstone – Snake River Plain Bimodal Suite

The differentiation trends of intracontinental, plume-related magmas (Figure 8.4) are distinctly different from those of arc magmas (Figure 7.8). The notable increase in the Fe-index with only a minor change in silica is probably an indication that magnetite and ilmenite didn't begin crystallizing until late in the fractionation history of the lavas. The lack of Fe-Ti oxides in the initial crystallizing assemblage leads to the formation of rhyolites that are strongly enriched in iron over magnesium (Figure 8.4A). Similar to the iron index, MALI of Snake River Plain basalts shows a strong increase with only a minor change in silica before following a trend parallel to the alkalic – alkali-calcic boundary (Figure 8.4B). This trend is probably caused by fractionation of clinopyroxene at relatively high pressures, conditions that suppress plagioclase crystallization (Frost and Frost, 2011). Crystallization of clinopyroxene extracts CaO from the melt without changing the K_2O or Na_2O contents, unlike crystallization of plagioclase.

The rhyolitic tuffs of Yellowstone lie at the silica-rich margins of the Snake River trends in Figure 8.4. The Yellowstone rhyolites, however, are a little less iron enriched than the rhyolites of Cedar Butte: they border on being calc-alkalic instead of alkali-calcic. In addition, the Yellowstone rhyolites are slightly peraluminous instead of metaluminous (Figure 8.4C). Isotopic studies of the intracaldera Yellowstone rhyolitic rocks indicate that they formed dominantly by differentiation of tholeiitic basalt but may contain up to 15 percent crustal components (Hildreth, Halliday, and Christiansen, 1991). The compositional differences between the Yellowstone rhyolites and those of Cedar Butte can be explained by this crustal contamination. The continental crust in the area, as indicated by the gneisses exposed in the adjacent Wind River Mountains, is dominated by magnesian calc-alkalic granitic rocks (Frost et al., 1998). Melting of these granitic rocks likely produces mildly peraluminous

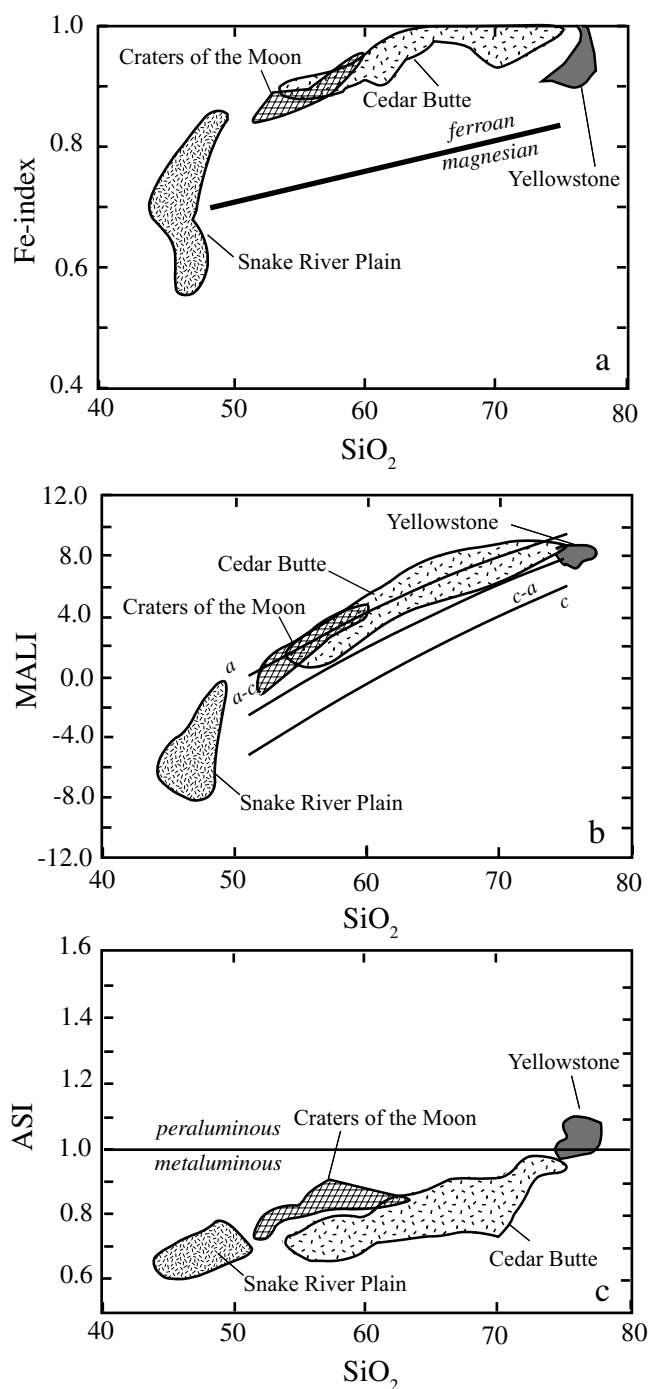


Figure 8.4 Geochemical trends in the volcanic rocks of the Yellowstone – Snake River Plain province. In Figure 8.4 A: c = calcic, c-a = calc-alkalic, a-c = alkali-calcic, a = alkalic. Data from McCurry et al. (2008), McCurry (unpublished data), and Hildreth, Halliday, and Christiansen (1991).

magnesian calc-alkalic melts that, when added to the melts of Cedar Butte composition, could produce the magmas of Yellowstone.

8.3.3 Models for the Generation of Bimodal Volcanism

Models for the origin of bimodal volcanism must both identify the sources of the basaltic and rhyolitic magmas and also explain the near absence of intermediate composition lavas. The source of the basaltic components in bimodal suites is the least controversial aspect of the problem; a mantle source is almost certainly required. Mantle-derived tholeiitic basalt may be produced either when the asthenosphere upwells during rifting or when a mantle plume ascends. This tholeiitic basalt may pond at the base of the crust, where it would differentiate along a tholeiitic trend, producing magmas enriched in FeO/(FeO + MgO). Contamination of the primary magma by subcontinental lithosphere and the continental crust may occur in bimodal associations, just as it does in flood basalts. Eruption of these magmas accounts for the basalt flows in bimodal associations.

The origin of the rhyolitic rocks in bimodal associations is more contentious. One possibility is that the basaltic magma stalled at depth continues to differentiate until producing andesitic to rhyolitic magmas. These magmas may assimilate continental crust as they evolve, and crustal contamination may be reflected in their isotopic compositions. As the magmas become more siliceous and accordingly more buoyant, triggering ascent to shallower depths or eruption at the surface. This hypothesis is favored for the eastern Snake River Plain, where an unusual continuum of magma compositions is preserved in a few Quaternary volcanic centers (McCurry et al., 2008; Figure 8.4).

To explain the lack of intermediate compositions typical of bimodal associations, Frost and Frost (1997) proposed that partial remelting of earlier formed differentiates could produce granitic melts. These, too, could assimilate felsic crust prior to eruption on the surface. Hildreth, Halliday, and Christiansen (1991) identified partial melts of Cenozoic basalt as a possible source of Yellowstone rhyolites and were able to quantify varying amounts of crustal assimilation using Sr, Nd, and Pb isotopic data.

A third mechanism to produce the rhyolitic magmas in bimodal associations is partial melting of felsic crust in

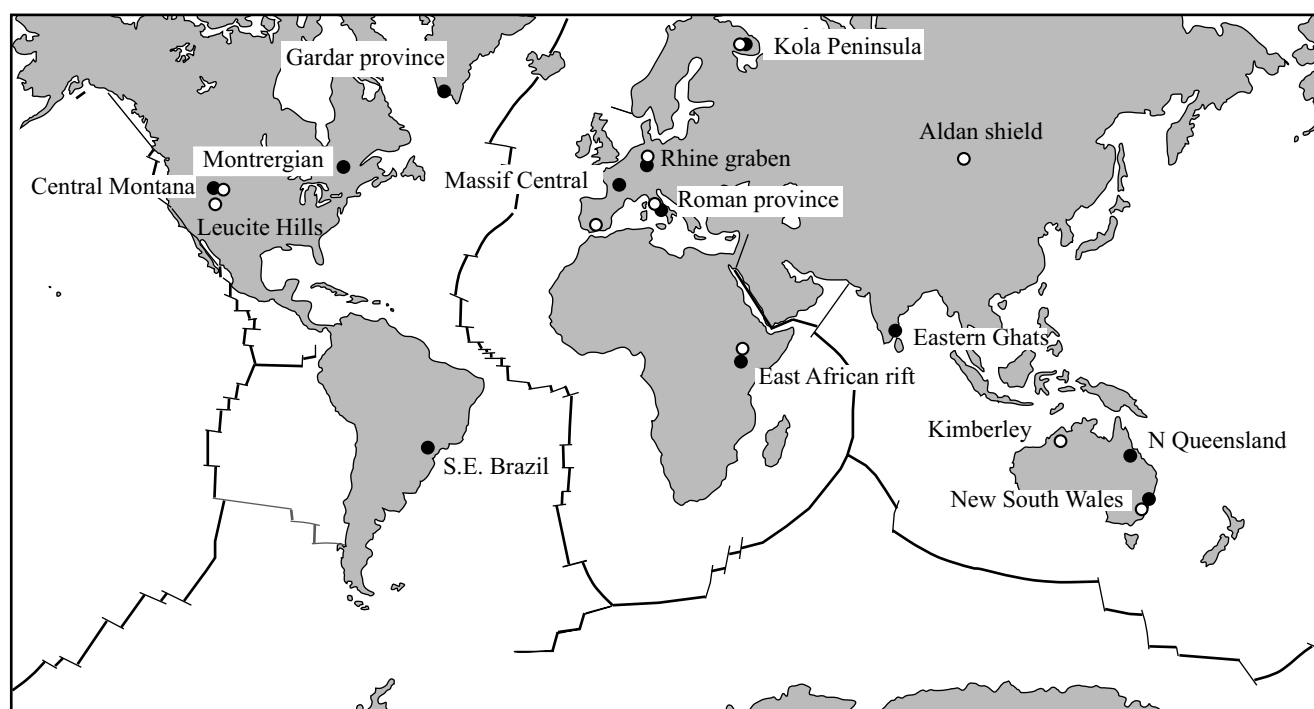
response to heating by tholeiitic magma. This mode of origin accounts for the lack of intermediate rocks. However, as Christiansen and McCurry (2007) pointed out, rocks formed by crustal melting tend to be magnesian and calc-alkalic, whereas the silicic volcanic rocks in bimodal associations are typically ferroan and alkali-calcic to alkalic. Nevertheless, it seems likely that rhyolites formed in extensional environments associated with tholeiitic basalt may include a spectrum from those that are formed exclusively by fractionation or partial melting of basalt and its subsequent differentiates, to those that were produced largely or entirely by partial melting of felsic crust.

8.4 Alkaline Volcanism

Small volumes of alkaline volcanic and intrusive rocks occur in intracontinental settings (Map 8.3). Alkaline rocks are so named because they have relatively high abundances of (Na + K). Most commonly, alkaline rocks are unusually rich in sodium; however, potassic alkaline rocks do occur. As noted in Chapter 4, three broad classes of alkaline rocks exist: nepheline-bearing rocks that are metaluminous (i.e., there are enough alkalis to stabilize nepheline, but not enough to make sodic amphiboles and pyroxenes); nepheline-bearing rocks that are peralkaline (i.e., there are enough alkalis to form sodic pyroxenes and amphiboles); and quartz-bearing rocks that are peralkaline (Figure 4.11). The rocks associated with alkaline magmatism range from mafic to felsic silicate rocks and carbonatites.

Alkali and nepheline basalts. These basalts typically contain plagioclase, olivine, and augite rich in titanium and sodium. The absence of orthopyroxene in the groundmass allows one to distinguish alkali basalt from tholeiite. Many alkali basalts do not contain nepheline as a modal phase; it is a normative component hiding in the glass phase. Nepheline is a groundmass phase in the nepheline basalts. These rocks include basanite, where olivine is present with nepheline, and tephrite, where olivine is absent.

Trachyte. The primary mineral in trachyte is alkali feldspar. Metaluminous trachyte may contain minor phenocryst phases including calcic pyroxene, iron-rich olivine, hornblende, and Fe-Ti oxides. In peralkaline trachyte, the groundmass phase is sodic pyroxene and sodic amphibole. Trachyte is close to SiO₂ saturation, and so trachyte can be either quartz bearing or nepheline bearing. With



Map 8.3 World map showing the major alkaline magmatism provinces. Sodic alkaline rocks are shown in filled circles; potassic alkaline magmatism is shown in open circles.

increasing silica, quartz trachyte grades into rhyolite; with decreasing silica trachyte grades into trachytic phonolite.

Phonolite. Phonolite is a felsic volcanic rock that contains nepheline and alkali feldspar. The groundmass minerals include alkali feldspar, pyroxene, and amphibole. In peralkaline phonolites, the pyroxenes and amphiboles are Na rich (aegirine or riebeckite/arfvedsonite).

Peralkaline rhyolites. Peralkaline rhyolites contain alkali feldspar and quartz as the main phenocryst phase. The presence of sodic pyroxenes and amphiboles distinguishes peralkaline from metaluminous rhyolites.

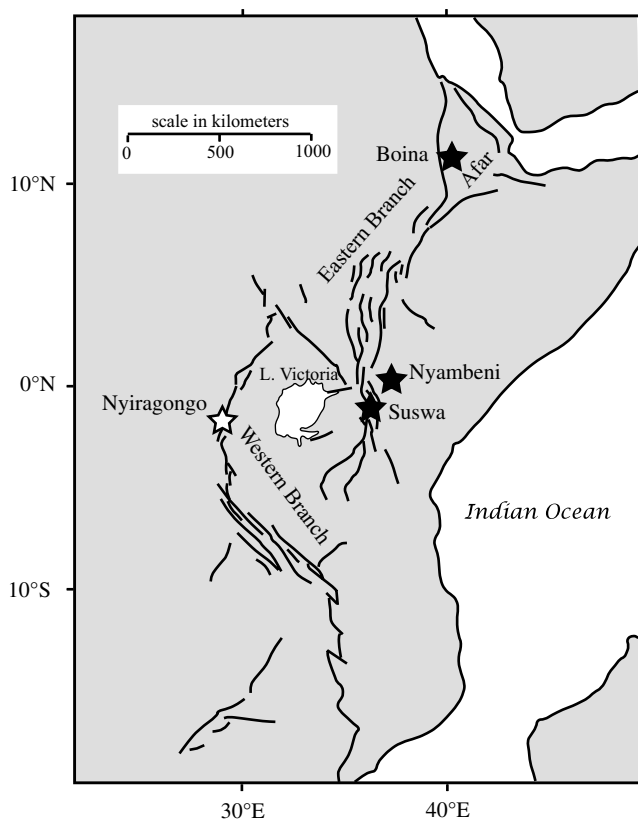
Carbonatites. Carbonatites contain at least 50 percent carbonate minerals, mostly calcite, although Ol Doinyo Lengai, a volcano of the East African rift in Tanzania, has erupted sodium carbonate. Other minerals include sodic pyroxenes and amphiboles, and Mg-rich biotite, which may form by unmixing of a carbonate-rich melt from phonolite or alkali basalt.

8.4.1 Sodic Alkaline Magmatism of the East African Rift

The East African rift, one of the great alkaline provinces in the world, extends sixty-five hundred kilometers from

the Red Sea to Mozambique (Map 8.4). Volcanoes in the rift, which have been erupted from the Miocene to Holocene, include compositions that range from tholeiitic to highly alkaline basalts. Most of the volcanoes in the East African rift have erupted sodic lavas, although a few, such as Nyiragongo, are potassic. Three volcanoes from the East African rift are described to provide examples of the range in compositions present and some of the different differentiation processes capable of producing those compositions. One is the Quaternary Boina volcano from the Afar region, which consists of mildly alkaline olivine tholeiite, ferrobasalt, trachyte, and peralkaline rhyolite (Barberi et al., 1975). The Nyambeni range consists of multiple volcanic centers in Kenya that have been active from Pliocene to Holocene. These have erupted a series of lavas ranging from highly alkaline basalts (basanite and tephrite) to phonolite with minor peralkaline phonolite (Brotzu, Morbidelli, and Piccirillo, 1983). Mount Suswa is a Quaternary volcano in Kenya that has erupted peralkaline trachytes and phonolites; basaltic rocks are absent (Nash, Carmichael, and Johnson, 1969).

Trends on the Fe-index and MALI diagrams. During differentiation, the basaltic rocks of the Boina volcano



Map 8.4 Map of the East African rift showing the locations of the Boina, Nyambeni, and Suswa volcanoes, all of which are sodic alkaline rocks (filled stars), and Nyiragongo, which is a potassic alkaline volcano (unfilled star).

show a strong increase in the iron ratio with only a minor change in silica content (Figure 8.5A), defining a trend very similar to rocks from the Snake River Plain (compare Figure 8.5A to Figure 8.4). This early iron enrichment probably indicates that substantial differentiation took place before magnetite began to crystallize. Nyambeni shows an iron enrichment trend similar to Boina, but because the primary magma was undersaturated with respect to silica, differentiation never led to significant silica enrichment and Nyambeni. The rocks from Suswa are restricted to an iron-rich composition. Because iron-rich melts are never derived directly from the mantle, the melts from Suswa must have formed from differentiation of a parent melt that was not erupted.

On a MALI diagram (Figure 8.5B), the lavas of Boina form a narrow trend that initially increases until the rocks lie in the alkalic field and then plateau at high silica. The increase at low silica can be explained by substantial

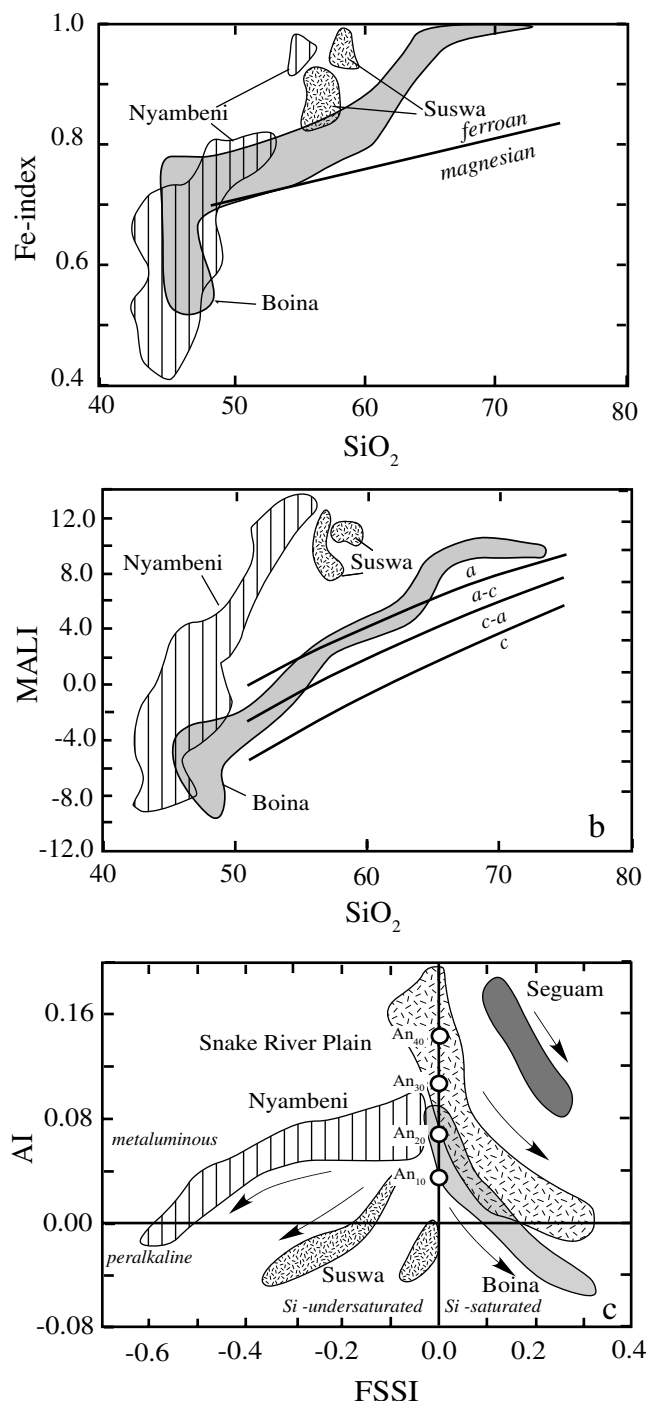


Figure 8.5 Geochemical trends for the Boina, Nyambeni, and Suswa volcanoes. a. Fe-index versus silica, b. MALI versus silica (a = alkalic, a-c = alkali-calcic, c-a = calc-alkalic, c = calcic). c. AI versus FSSI. Trends for Craters of the Moon and Seguam are shown for comparison in data from Barberi et al. (1975), Brotzu, Morbidelli, and Piccirillo (1983), Nash, Carmichael, and Johnson (1969), Singer, Myers, and Frost (1992) and from references cited in Figure 8.4.

fractionation of augite, which extracts CaO from the melt, while the plateau at high silica may be produced by the fractionation of aegirine and sodic amphibole, which extract Na₂O from the melt. Rocks from Nyambeni form a broad field with a very steep increase in relative MALI with minor change in silica.

Trends on the AI – FSSI diagram. On a plot of alkalinity index versus FSSI (feldspathoid silica-saturation index) (see Figure 4.11), compositional data from each of the three volcanoes define separate fields that radiate from FSSI = 0.0, which represents the albite thermal barrier (Figure 8.5C; c.f. Figure 2.10). As noted in Chapter 2, fractional crystallization of magmas slightly to the right of this barrier can move the composition of a melt farther to the right (toward higher silica contents). In the same way, a magma slightly to the left of this barrier may differentiate to compositions farther to the left (toward lower silica contents), but in neither case can the melt composition cross this barrier. The rocks from Boina become increasingly silica rich during differentiation (as indicated by the arrow in Figure 8.5C), but also become more alkaline. In contrast, the rocks from Nyambeni reflect a decrease in silica with differentiation. The rocks from Suswa define two groups, each of which show increasing alkalinity and decreasing silica abundance with increasing differentiation. These trends of increasing alkalinity with increasing differentiation are not unique to alkaline rocks, as indicated by the fact that the lavas from the Snake River Plain and Seguam show similar trends. These trends are a manifestation of the crystallization of plagioclase, because, as indicated in Figure 2.11A, crystallization of plagioclase will extract Ca from a melt, enriching it in alkalis. In a Ca-bearing melt that is sodium-rich, CaO will preferentially enter plagioclase, leaving the pyroxene enriched in Na₂O. This effect, called the “plagioclase effect” by Bowen (1945), means crystallization of plagioclase can drive a melt that was originally metaluminous into the peralkaline field. The positions of An₁₀, An₂₀, An₃₀, and An₄₀ are shown in Figure 8.5 to show how extraction of plagioclase of these compositions could have caused the trends observed (although the differentiation was certainly more complex than that).

Figure 8.5C shows a suite of rocks derived from a basaltic parent will evolve to become peralkaline through fractional crystallization depending on the relative abundances of CaO and Na₂O in the parent rock. Rock suites

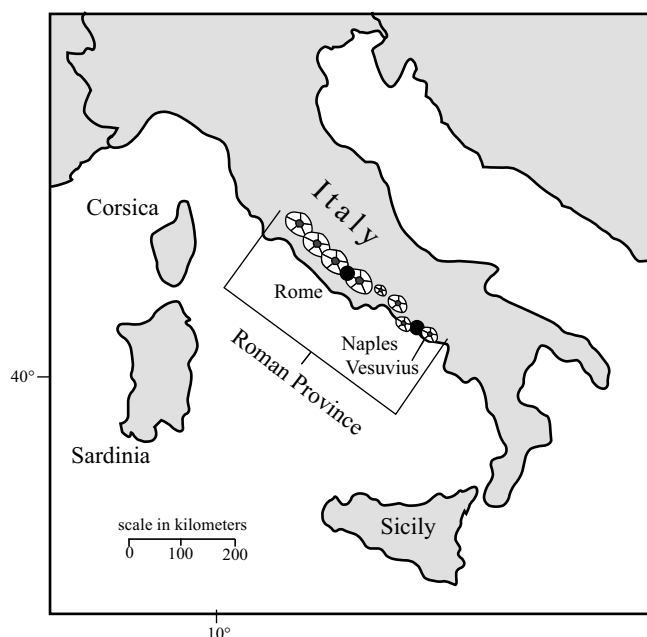
such as Seguam, which are relatively calcic, do not become peralkaline during differentiation. In contrast those that are sodium rich may become peralkaline if significant amounts of plagioclase fractionate.

Implications for the evolution of Boina, Nyambeni, and Suswa volcanoes. As noted in Chapter 4, geochemical variation diagrams such as those in Figure 8.5 cannot prove a suite of rocks evolved through fractional crystallization, but the fact that the rocks from Boina and Nyambeni form tight trends strongly supports this contention. The fact that Sr isotopes are similar for the basaltic and rhyolitic rocks of Boina and that the trace elements behave in a manner consistent with fractional crystallization (Barberi et al., 1975) is strong corroboration that the suite of rocks erupted by Boina evolved through fractional crystallization. Similarly the well-defined trends on major and trace variation diagrams in the Nyambeni lavas suggest derivation through fractional crystallization (Brotzu, Morbidelli, and Piccirillo, 1983). The same cannot be said for the rocks from Suswa because they occupy two separate fields in the discrimination diagrams, particularly in Figure 8.5. Based on whole rock and trace element chemistry, Nash, Carmichael, and Johnson (1969) argued that Suswa volcano erupted melts from different sources at different times, although each of the individual batches of melt may have evolved toward increasing peralkalinity and decreasing silica activity.

8.4.2 Potassic Alkaline Volcanism

Although most alkaline rocks are sodic (i.e., have Na₂O > K₂O), a number are potassic. In some localities, such as in the East African rift, potassic alkaline magmas are clearly rift related. In other localities, such as the Roman province, the tectonic environment is cryptic at best. In this section, Mount Vesuvius from the Roman province exemplifies potassic alkaline volcanism. Another group of mafic potassic alkaline rocks, kimberlites and lamproites, forms small bodies (often a kilometer or less across) that are important as hosts of diamonds. This section also discusses the origins of kimberlites and lamproites and the diamonds they contain.

Mount Vesuvius and the Roman Province. Mount Vesuvius is the southern-most volcano in the Roman province, a group of potassic alkaline volcanoes that extends for more than 500 kilometers along the west coast of Italy (Map 8.5). Mount Vesuvius is a recent cone (less



Map 8.5 Geologic sketch of the Roman province in Italy showing the location of major eruptive centers. Modified after Corticelli and colleagues (2002).

than nineteen thousand years old) built in the caldera of Mount Somma, an older volcano active from thirty-nine thousand to nineteen thousand years ago. Long periods of quiescence punctuated by explosive eruptions characterize the activity of Vesuvius (Di Renzo et al., 2007). One of these eruptions buried Pompeii in 79 CE, an event witnessed by Pliny the Younger. His letters on the eruption of Vesuvius (*Epistulae* VI.16 and VI.20) are certainly some of the earliest geologic descriptions of a volcanic eruption. Because of Pliny's letters, eruptions such as those of Vesuvius are called "plinian."

Over the last nineteen thousand years, Vesuvius has erupted about 50 km³ of magma with wide ranging composition. Trachyte from Vesuvius may be either nepheline- or quartz-normative, whereas phonotephrite and phonolite are both nepheline- and leucite-normative (Di Renzo et al., 2007). The rocks from Mount Vesuvius do not form any clear trends on chemical discrimination diagrams (Figure 8.6), which is not surprising considering that both quartz-saturated and nepheline-saturated rocks are involved. Lack of a simple trend indicates the evolution of the rocks from Vesuvius did not involve simple fractional crystallization. In fact, Di Renzo and colleagues (2007) postulate that the melting of a heterogeneous

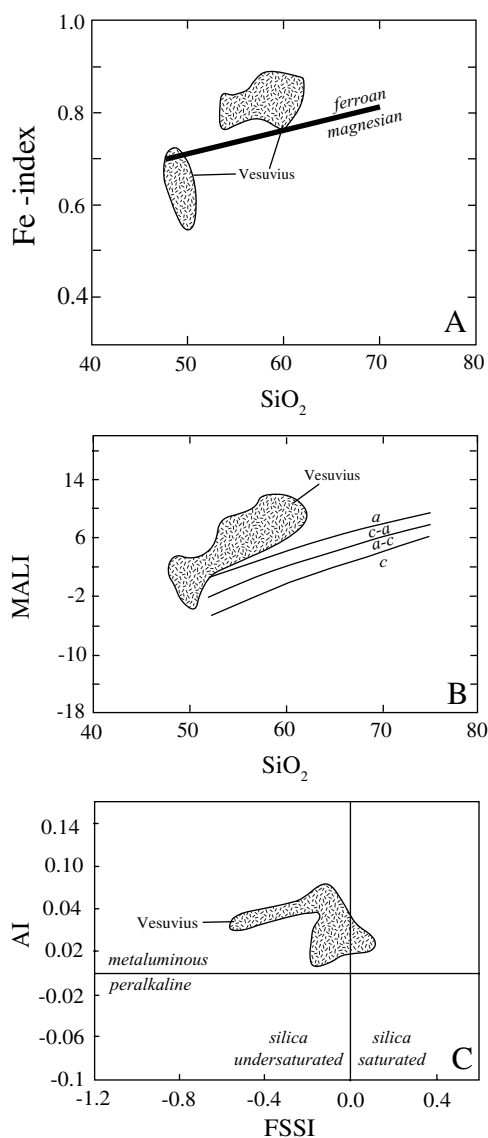
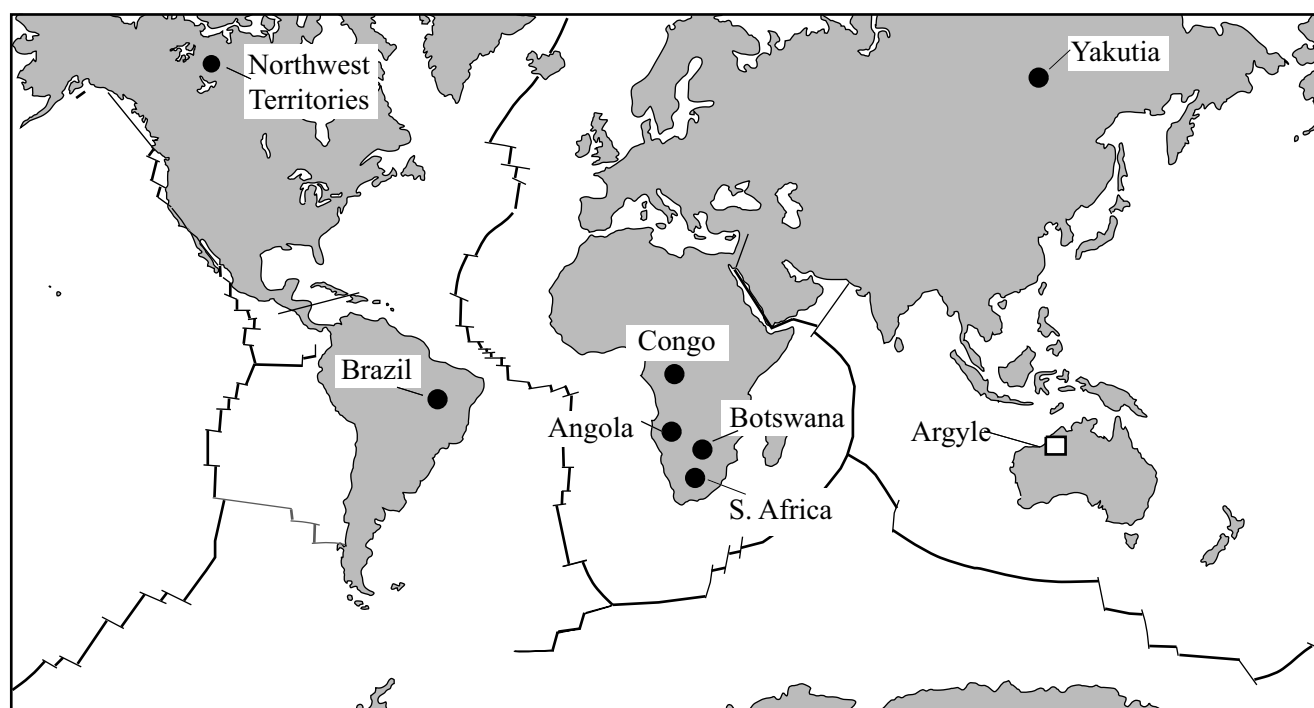


Figure 8.6 Geochemical trends for the rocks from Mount Vesuvius. Data from Di Renzo and colleagues (2007).

source area, crustal contamination, and magma mixing could all have been involved in the evolution of the lavas from Vesuvius.

Kimberlites and lamproites. Kimberlites and lamproites occur almost exclusively within continental plates, typically erupting through Precambrian crust (Dawson, 1967; Mitchell and Bergman, 1991) (Map 8.6). Kimberlites and lamproites have similar major element compositions and the two rock types are often grouped together (Mitchell and Bergman, 1991). Both are potassic ultramafic rocks that contain olivine and phlogopite. The tectonic environment that produces such rocks is often enigmatic, and



Map 8.6 Major diamond-producing regions of the world. Filled circles = diamonds sourced from kimberlite, open square = diamonds sourced from lamproite.

may be different for different occurrences. These potassic mafic rocks are interesting because 1) they may bear xenocrystic diamond, and 2) they have exotic mineralogies (and names) that give petrologists important information about the mantle.

Kimberlites are products of continental intraplate magmatism, confined to regions of the crust underlain by ancient cratons; no occurrences have been described from oceanic environments or young fold belts. Kimberlites don't appear to be associated with continental rifts, although in some cases their location can be correlated with zones of weakness in the crustal lithosphere. Kimberlites cluster in small volcanic diatremes, sills, and dikes. Some kimberlite provinces have experienced multiple episodes of kimberlite magmatism – southern Africa, Wyoming, and Russia in particular.

Kimberlites appear to originate at depths of 100–200 kilometers and ascend into the crust as a kimberlite magma. At relatively shallow depths (maybe around two kilometers), they exsolve a CO_2 -rich fluid and the fluid-rich magma erupts explosively to the surface (Dawson, 1967; Mitchell, 1986). This rapid emplacement results in brecciation of the host rock as well as fragmentation of the conduit up which the melt moves. As a result,

kimberlites consist of a fragmented and altered ground-mass containing olivine, phlogopite, diopside, apatite, spinel, and ilmenite. Many of these minerals have been partially or completely altered to serpentine and carbonate. Kimberlites also often include lithic fragments and xenocrysts from crustal and mantle rocks through which they ascend. The diamonds commonly present in kimberlites are usually found within garnet peridotites or eclogite xenoliths; rarely they are found as xenocrysts within the kimberlite itself.

Lamproites occur mainly as dikes, minor intrusions, and flows (Mitchell and Bergman, 1991). Like kimberlites, lamproites are associated with lineaments that may reflect zones of lithospheric weakness. Some of the classic lamproite occurrences include the Leucite Hills, Wyoming; Smoky Buttes, Montana; and occurrences in Antarctica, southern Spain, and western Australia (Map 8.6). Most lamproites are Cenozoic, in contrast to kimberlites, which are exclusively pre-Cenozoic. Like kimberlites, lamproites may host diamonds.

Lamproites are characterized by major phases of phlogopite, olivine, diopside, sanidine, and leucite. In most rocks, olivine is partially or totally pseudomorphed by serpentine, iddingsite, carbonate, or quartz. Fresh leucite

is also rare, commonly replaced by sanidine, analcite, quartz, zeolite, or carbonate. Lamproites may contain diamonds, but the diamonds tend to be much smaller than those found in kimberlites. One explanation for this size disparity is that lamproites are emplaced at a slower velocity than the explosive emplacement of kimberlite. Whereas kimberlites can carry the larger xenoliths and the larger diamond xenocrysts to crustal levels, in lamproites, those diamonds and larger xenoliths will sink into the mantle before arriving at shallow crustal levels.

8.5 Origin of the Chemical Diversity of Intracontinental Basaltic Magmas

The preceding sections illustrated how a wide variety of mantle-derived rocks of basaltic composition erupted in continental settings. These intracontinental mafic rocks range from voluminous tholeiitic flood basalts through alkali basalts to highly alkaline sodium-rich or potassium-rich mafic magmas. A reasonable question to ask is: What causes this extreme variability of magma compositions? As noted in Chapter 5, alkali basalts could form by small degrees of partial melting of a normal mantle. However, it is difficult to adopt this explanation for the origin of the highly alkaline basaltic rocks, such as those that formed the Nyam Beni eruptive centers, or for potassic magmas such as those that feed the Roman province. These highly alkaline melts must have been derived from a mantle whose composition was different from the “normal” mantle that produces tholeiites.

This process by which the composition of the mantle has changed is called **metasomatism**, which technically describes any metamorphic process that changes the composition of a rock. Metasomatized mantle is increasingly recognized as a precursor for alkaline magmatism, both in the East African rift (Rosenthal et al., 2009) and in the Roman province (Bianchini, Beccaluva, and Siena, 2008; Nikogosian and Van Bergen, 2010). Movement of Na-bearing fluid through the mantle will produce hornblende-rich veins, whereas K-bearing fluids will produce phlogopite. Preferential melting of these veins will produce sodium-enriched and potassium-enriched alkaline magmas. Mantle xenoliths brought up in alkali basalts provide compelling evidence for metasomatism (Dawson and Smith, 1988; Meshesha et al., 2011). The mineralogical composition in these veins and their abundance in the mantle are likely to be irregularly distributed. Thus

melting of a metasomatized mantle is likely to produce a wide variety of magmas. This explains why areas such as the East African rift and the Roman province erupt such a wide variety of lavas (Bianchini, Beccaluva, and Siena, 2008; Nikogosian and Van Bergen, 2010).

Having established how highly alkaline magmatism can derive from a heterogeneous, metasomatized mantle, the next question concerns the source of the fluids that metasomatized the mantle. Because both Na_2O and K_2O are enriched in the crust over the mantle, one reasonable source is through subduction (Bianchini, Beccaluva, and Siena, 2008; Markl, Marks, and Frost, 2010). If a subduction zone entrained substantial sea floor sediment, dewatering of these rocks may produce a K-rich fluid that could metasomatize the overlying mantle. Alteration of basaltic rocks on the sea floor causes albite to form from calcic plagioclase. Subduction of these rocks provides a source for sodium-rich fluids that can affect the composition of the overlying lithosphere (Markl, Marks, and Frost, 2010). It is important to emphasize that this type of metasomatism must have occurred before (in some areas millions of years before) alkaline melts generated. The thermal event that produced the alkaline melts is in no way directly related to subduction.

The fact that metasomatized mantle enriched in K_2O or Na_2O melts to produce alkaline rocks may explain observations from the Roman province. The Roman province lies above a steep east-directed subduction zone (Bianchini, Beccaluva, and Siena, 2008), in an area where one would expect broadly calc-alkalic volcanism. Indeed calc-alkalic magmas are found locally in the Roman province (Boria and Conticelli, 2007). One proposal to explain why the magmatism in the Roman province is highly potassic suggests that, unlike most arcs, the mantle under the Roman Province had been previously invaded by K-rich fluids derived from an earlier subduction event (Bianchini, Beccaluva, and Siena, 2008). Thus, although this book describes igneous rocks in the context of the tectonic environment where they are most frequently occur, it is important to note that the factors controlling the composition of mantle melts are many and include mantle composition, degree of melting, and temperature and pressure conditions of melting. The tectonic environment usually controls the conditions of melting, but not the composition of the mantle that partially melts in these environments. For this reason, a variety of magma compositions may be produced by mantle melting in any given tectonic environment.

Summary

- Intracontinental volcanism includes continental flood basalts, bimodal associations of basalt and rhyolite associations, and alkaline rocks.
- Intracontinental volcanism is usually associated with mantle plumes or rifts.
 - Hotspot-related magmatism in intracontinental settings defines tracks of progressively younger volcanic centers recording the movement of the plate over a plume.
 - Rift-related volcanism may be associated with broad areas of extension, such as in the Basin and Range in southwestern United States, or in narrower rifts such as the East African rift.
- A wide range of lavas is erupted in continental rifts.
 - Flood basalt provinces are dominated by large volumes of tholeiitic basalt.
 - Bimodal associations are composed of tholeiitic basalt and ferroan rhyolite.
 - Rift-related volcanism may range in composition from tholeiitic to alkaline.
 - Kimberlites and lamproites are unusual mafic, high-potassium magmas that may transport diamonds to the surface.
- The wide range of mantle-derived rocks of basaltic composition, from tholeiitic basalt, through alkali basalt, to alkaline sodium or potassium-rich mafic magmas, may reflect:
 - different degrees of partial melting of the mantle, and/or
 - variations in the composition of the mantle sources.
- Alkaline rocks are commonly attributed to partial melting of mantle that is compositionally heterogeneous as a result of metasomatism.

Questions and Problems

Problem 8.1. Compare and contrast oceanic plateau and continental flood basalt provinces.

Problem 8.2. Calculate the approximate plate velocity for the North American plate from the age of volcanic centers along the Snake River Plain and Yellowstone shown in Figure 8.3. What is the direction of plate motion?

Problem 8.3. Provide at least two explanations for the absence of intermediate compositions of volcanic rocks found in bimodal volcanic suites.

Problem 8.4. What is metasomatism?

Problem 8.5. What are the similarities and differences between kimberlites and lamproites?

Further Reading

Eldholm, O. and Coffin, M. F., 2000, Large igneous provinces and plate tectonics. In *The history and dynamics of global plate motions*, eds. M. A. Richards, R. G. Gordon, and R. D. van der Hilst. Geophysical Monograph 121, American Geophysical Union, Washington DC, pp. 309–26.

- McBirney, A. R., 2007, *Igneous petrology*, 3rd ed., Jones and Bartlett, Boston, Chapter 11.
- Mitchell, R. H., 1995, *Kimberlites, orangeites, and related rocks*. Plenum, New York.
- Pierce, K. L., and Morgan, L. A., 1992, The track of the Yellowstone hot spot: volcanism, faulting, and uplift. In *Regional geology of eastern Idaho and western Wyoming*, eds. P. K. Link, M. A. Kuntz, and L. B. Platt. Geological Society of America Memoir 179, pp. 1–52.
- Sørensen, H. (ed.), 1974, *The Alkaline rocks*, John Wiley & Sons, New York.
- Winter, J. D., 2010, *Principles of igneous and metamorphic petrology*, 2nd ed., Prentice Hall, New York, Chapters 15, 19.

Chapter 9

Intracontinental Plutonism

9.1 Introduction

The previous chapter described the wide variety of volcanic rocks produced in intracontinental settings through the participation of different source magmas that have differentiated through fractional crystallization, crustal assimilation, or magma mixing. Intracontinental magmatism also produces a variety of plutonic rocks, including layered mafic intrusions, Archean and massif anorthosites, alkaline intrusions, and ferroan granites that are compositionally distinct from igneous rocks found in arc environments. Some of these plutonic rocks are associated with the coeval volcanic rocks described in the previous chapter, which allows geologists to ascribe a tectonic environment to those plutons. Many intracontinental plutons, however, are not spatially and temporally related to volcanic rocks, so their tectonic environment must be determined by inference.

This chapter discusses the textures, occurrence, and compositions of four categories of plutonic rocks found in an intracontinental environment. Layered mafic intrusions are described first. These bodies, many of which exhibit spectacular layering, are also important sources for chrome, nickel, cobalt, and other platinum group elements. The second group of rocks are anorthosites, rocks composed of at least 90 percent plagioclase that occur in two associations. Archean anorthosites occur as dikes and sills, and as their name suggests, they are most common in the Archean rock record. Massif anorthosites are batholith size bodies of anorthosite that are relatively abundant in the Proterozoic, but Phanerozoic examples are also known. Associated with massif anorthosite is the third group of intrusions, ferroan granites, also introduced in this chapter. However, ferroan granites are as likely to occur where anorthosite is absent. As the name implies, ferroan granites are iron rich and contain more potassium feldspar than plagioclase, giving them a pink color. The final group of intracontinental plutonic rocks is alkaline intrusions. These intrusions are uncommon but contain unusual minerals and host scarce metals in high demand for personal electronics and clean energy technologies (Box 9.1).

BOX 9.1 | ORE DEPOSITS ASSOCIATED WITH LMIS

Chrome: Layered mafic intrusions host important deposits of Cr, Ni, Co, and platinum group elements (PGEs: Pt, Pd, Ru, Rh, Os, Ir). The partition coefficient, D , for Cr between chromite and melt is on the order of fifteen hundred, which means the Cr content of chromite is about fifteen hundred times that of the melt. Chrome deposits are found in the ultramafic portions of a layered mafic intrusion where chromite-rich layers may be more than five meters thick. These deposits are thought to result from the injection of a new magma into a magma body. The mixing of the melt in the intrusion with the new melt may drive the melt into the primary field of chromite crystallization (Duke, 1988), producing chromite-rich layers at the base of the intrusion. In some LMIs, these chromite deposits extend for kilometers and are called **stratiform chromite** deposits to distinguish them from **podiform chromite** deposits found in ophiolites (see Box 6.1). The biggest chrome deposit in the world is the Bushveld intrusion in South Africa; it supplies more than 70 percent of the world's chrome (see photo of chromite layers in Figure 9.1C). Chrome deposits from the base of the Stillwater intrusion in Montana were mined during World War II, but are not mined today in part because the chromite in the Stillwater is not as pure as that in the Bushveld.

Platinum Group Elements: In the process of differentiation, the basaltic magma in the magma chamber of a layered intrusion becomes saturated in sulfur, causing a separate sulfide melt to form along with the silicate melt. The sulfide melt is mostly composed of FeS, but economically important elements such as Cu, Ni, Co, and the platinum group elements are strongly fractionated into sulfide melts. If, during the formation of a layered mafic intrusion, the sulfide melt was in communication with a large volume of silicate melt, it might sequester enough of these elements to form an ore deposit, particularly if the sulfide melt was concentrated into a limited horizon. Layered mafic intrusions that contain important platinum ore bodies include the Bushveld, Great Dyke, and Stillwater intrusions.

Nickel: The partition coefficient for Ni between olivine and melt is around four, which means crystallization of olivine will deplete the melt of nickel. Therefore, nickel sulfide ore bodies are only found in intrusions where sulfur saturation occurred before significant olivine crystallized. Intrusions in which this occurred include Sudbury, which being quartz saturated, never crystallized olivine, and Duluth, which attained early sulfur saturation because of assimilation of S-rich pelitic country rocks.

Iron, Titanium, and Vanadium: Ferric iron, titanium, and vanadium behave as incompatible elements during early crystallization of mafic igneous intrusions until magnetite and ilmenite begin crystallizing. In the Bushveld intrusion, cumulate magnetite began crystallizing at the base of the upper zone, and the upper zone contains more than twenty layers up to ten meters thick that are rich in vanadium-bearing titaniferous magnetite. Magnetite concentrations are also found in irregular plugs and pegmatitic bodies within portions of the main zone (Willemse, 1969). These magnetite-rich areas are economic mainly because of their high concentrations of vanadium, and they make South Africa the world leader in the production of this metal.

9.2 Layered Mafic Intrusions

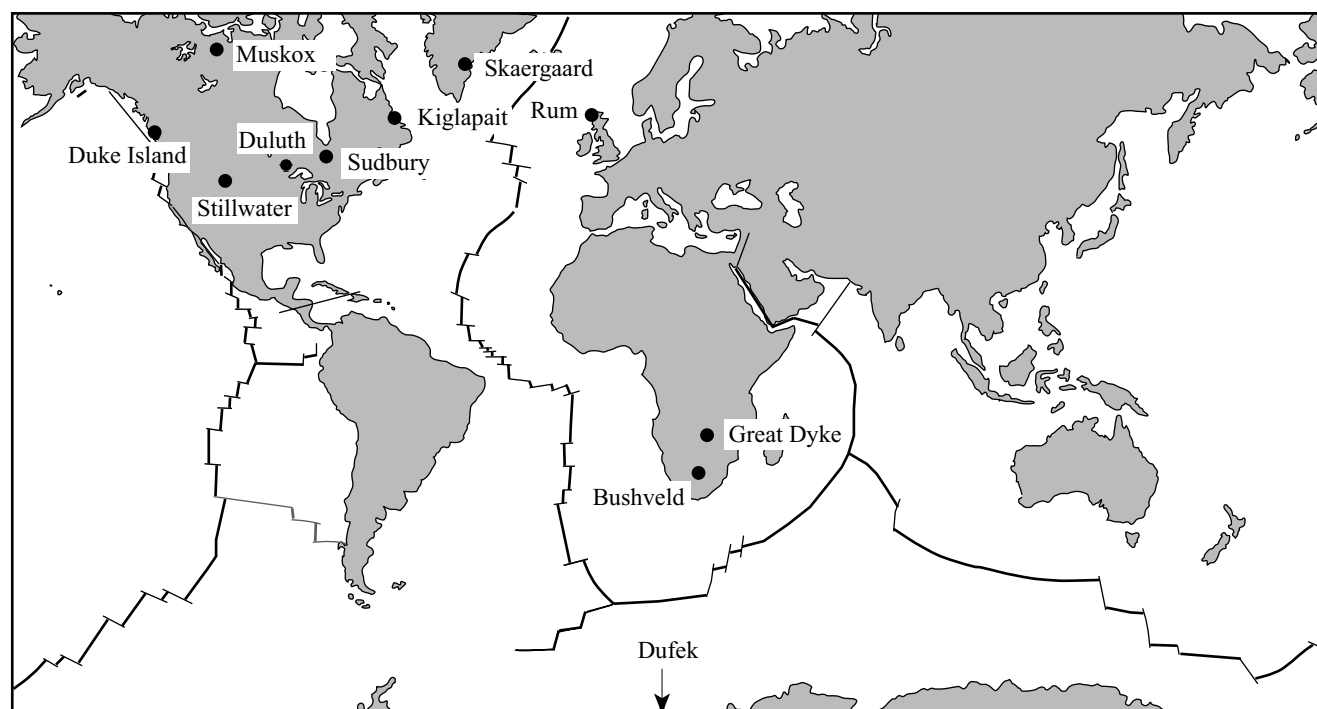
Layered mafic intrusions (LMIs) are some of the most important types of igneous bodies; the locations of some of the best-studied LMIs are shown in Map 9.1 and their size and age are given in Table 9.1. Not only do these

Table 9.1 Major Layered Mafic Intrusions

Name	Location	Age	Area (km ²)
Bushveld	S. Africa	2054 Ma	66,000
Dufek	Antarctica	Jurassic	50,000
Duluth	Minnesota, USA	1.1 Ga	4,700
Stillwater	Montana, USA	2.7 Ga	4,400
Muskox	Northwest Territories, Canada	1.2 Ga	3,500
Great Dyke	Zimbabwe	2575 Ma	3,300
Sudbury	Ontario, Canada	1849 Ma	1,300
Kiglapait	Labrador, Canada	1.3 Ga	250
Skaergaard	Greenland	Tertiary	100
Duke Island	Alaska, USA	Cretaceous	~100
Rum	Scotland	Tertiary	~100

intrusions preserve spectacular igneous textures and structures, they provide petrologists with critical insights into the differentiation processes of mafic melts. In addition, some LMIs host chrome, nickel, and platinum deposits. Although most layered mafic intrusions are Precambrian in age (Table 9.1), layered mafic intrusions have formed throughout Earth's history. A distinctive feature of LMIs is their igneous layering (Figure 9.1). Layering is also found in oceanic gabbros and in gabbroic and ultramafic intrusions associated with arc volcanoes, but large-scale, persistent layering is the hallmark of layered mafic intrusions.

Igneous layering is postulated to form by accumulation of minerals on the floor of an igneous intrusion. Usually the magma from which it forms is mafic, because mafic magmas are fluid enough to allow minerals to sink during the crystallization of the melt. Layering, however, is not unknown in felsic intrusions, and in both compositions, layering forms on all scales. Kilometer-scale layering is governed by the appearance or disappearance of key minerals, such as olivine or plagioclase, during the crystallization of an igneous body. The base of many layered intrusions is marked by ultramafic horizons rich in olivine, pyroxene, and locally chromite (Figure 9.1A). The first appearance of cumulus plagioclase typically marks the transition from ultramafic to gabbroic composition



Map 9.1 Distribution of major layered mafic intrusions around the world.

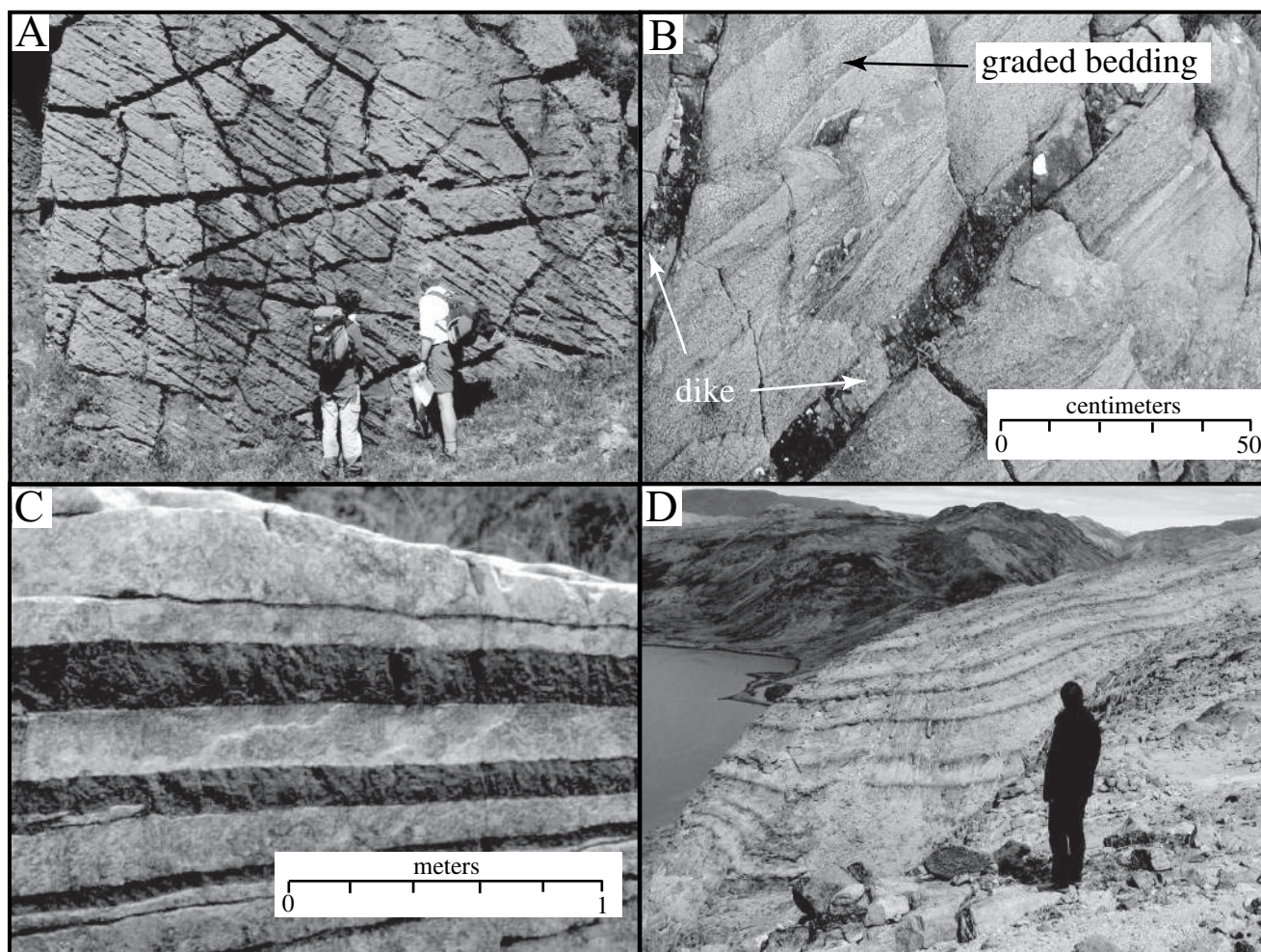


Figure 9.1 Photos of layering in igneous rocks. (A) Layering in feldspathic peridotite. Relatively resistant layers are richer in plagioclase than the less resistant layers. Rum intrusion, Scotland. Photo courtesy of Michael Cheadle. (B) Layering in gabbros from the Rum intrusion. Layering is based on modal variation of olivine, augite, and plagioclase. Photo by Michael Cheadle. (C) Layering of chromite in anorthosite, Bushveld intrusion, South Africa. Photo by Michael Cheadle. (D) Layering in nepheline syenites, Ilimaussaq intrusion, southern Greenland.

and forms a horizon that often can be traced from pluton to pluton across the entire intrusion.

In addition to the kilometer-scale layers, most layered intrusions contain layering on the meter scale. Many processes have been postulated for the formation of these small-scale layers. They could be caused by the injection of new magma into a magma chamber, which causes a new mineral, such as olivine or chromite, to crystallize and sink to the floor of the chamber. Such a process could have formed the Frost Pyroxenite, a narrow layer that is a major marker extending for more than thirty-five kilometers in the Dufek intrusion in Antarctica (Figure 9.2). Small-scale layering may also be caused by density currents containing

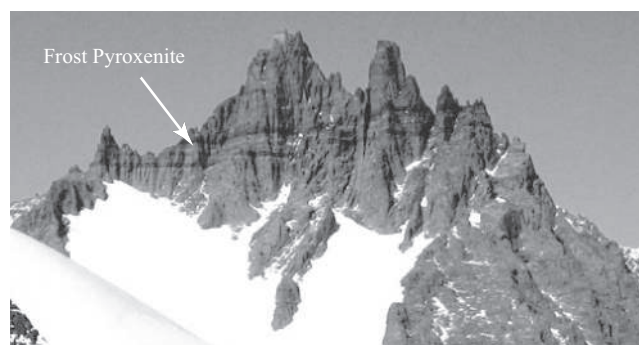


Figure 9.2 Photograph of the Dufek intrusion exposed on 1840 m Neuberg Peak in Antarctica. The Frost pyroxenite is a major marker in the intrusion and extends for about thirty-five kilometers alongstrike. Photo by Michael Cheadle.

crystals that crystallized on the relatively cool walls of the magma chamber and then slid onto the floor of the chamber. These crystals could accumulate as graded layers (Figure 9.1B) similar to graded beds formed by turbidity currents in sedimentary environments. Such a process may also have produced the unusual chromite layers in anorthosite (Figure 9.1C) found in the Bushveld intrusion in South Africa (Voordouw, Gutzmer, and Beukes, 2009). Another process forming layered rocks is postulated from the Ilimaussaq intrusion (Figure 9.1D), where periodic eruptions and magma chamber degassing could have produced layering by (Pfaff et al., 2008). Because high water pressure depresses the crystallization temperature of a silicate melt (Figure 3.3), each time fluid was released the crystallization temperature increased and a small amount of melt crystallized. The denser minerals (the dark bands) in Figure 9.1D sank to the bottom of the chamber before the less dense feldspars and feldspathoids. As crystallization of minerals proceeded, the fluids in the remaining melt increased, inhibiting further crystallization until another degassing event occurred. Understanding the processes by which igneous layering forms is the subject of ongoing research because these processes provide insights into the chemical evolution of intrusions over time.

9.2.1 The Bushveld Intrusion

The largest and arguably the most important layered mafic intrusion in the world is the 2.05 Ga Bushveld intrusion in South Africa (Map 9.1). The Bushveld intrusion, which contains a stratigraphy nearly eight thousand meters thick, is layered on scales ranging from less than a meter to hundreds of meters. The intrusion forms a complex bowl shape in which the shallower portions of the intrusion are exposed as one moves inward from the margins. The intrusion is capped by a series of granitic rocks and felsic volcanic rocks, which are the youngest units in the intrusive complex. The Bushveld is considered to have formed from a mafic magma that differentiated in place, although in detail the crystallization history is complex. Locally the base of the intrusion contains a narrow zone of fine-grained gabbroic rock, known as the **marginal zone** (Map 9.2), which is interpreted to represent the chilled magma that produced the intrusion. Above this is the **lower zone**, a sequence of peridotite and pyroxenite more than a kilometer thick. These rocks formed by the accumulation of early crystallizing phases including olivine,

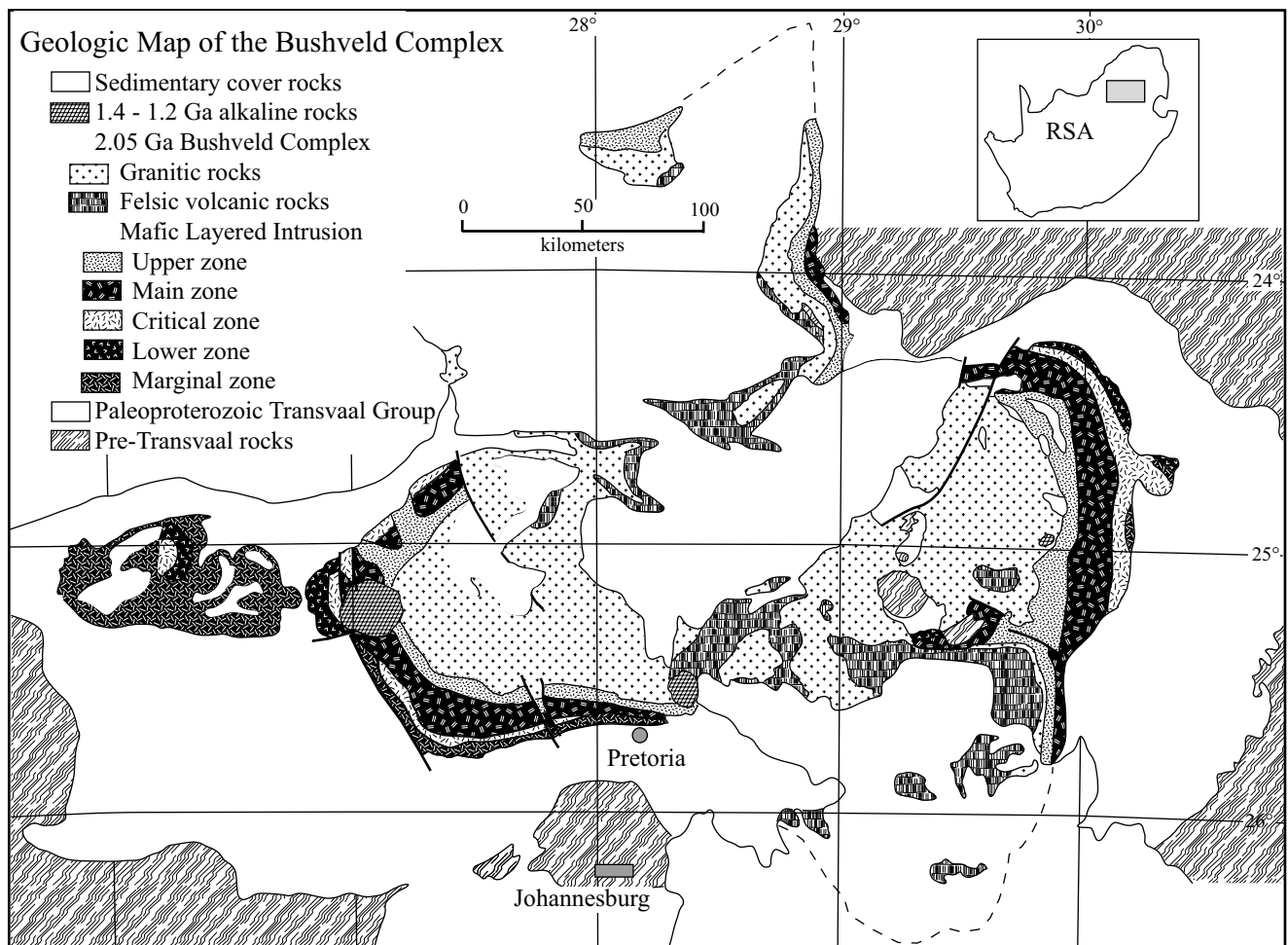
chromite, orthopyroxene, and clinopyroxene. Plagioclase, where present in the lower zone, occurs in the interstices of the ferromagnesian minerals. Above the lower zone are three thick gabbroic horizons: the **critical zone**, marked by the appearance of plagioclase; the **main zone**, marked by the disappearance of chromite; and the **upper zone**, marked by the appearance of cumulus magnetite.

9.2.2 Mineralogical Variation in LMIs

Because the rocks from layered mafic intrusions usually consist of varying proportions of cumulus and postcumulus grains, whole rocks analyses of these rocks do not retain direct information about melt compositions. For example, a rock from the base of an intrusion with 40 percent chromite and 60 percent olivine could contain around 16 percent Cr_2O_3 . There is no melt that has anywhere near that Cr content; analyses with this composition would merely show that Cr has been concentrated by accumulation of chromite. To understand the chemical variation present within layered mafic intrusion, therefore, it is better to use mineral chemistry, because the composition of olivine, for example, that formed at any point in the crystallization of a melt will be the same regardless of whether the rock contains nearly 100 percent cumulus olivine or only a few percent postcumulus olivine.

Figure 9.3 shows that, at increasing stratigraphic positions in the Bushveld intrusion, the plagioclase becomes increasingly more sodic and the ferromagnesian silicates become more iron rich (Atkins, 1969). These are exactly the kind of chemical changes one would expect of olivine and plagioclase formed by fractional crystallization. As Figure 2.11 demonstrated, olivine always is higher in $\text{Mg}/(\text{Mg}+\text{Fe})$ and plagioclase always is higher in $\text{Ca}/(\text{Ca}+\text{Na})$ than the melt from which they crystallize. Fractional crystallization of olivine and plagioclase will therefore preferentially extract MgO and CaO from a melt, leaving the residual melt relatively enriched in FeO and Na_2O .

The mineralogy of most layered mafic intrusions is broadly similar to the Bushveld in that the intrusions record a differentiation trend with ferromagnesian minerals becoming enriched in iron relative to magnesium and plagioclase becoming more sodic at progressively higher stratigraphic levels. In detail, however, each pluton is distinct. Some of these differences reflect differences in silica abundance. Like the Bushveld, the middle zones of the Skaergaard intrusion in Greenland contain no olivine;



Map 9.2 Geologic map of the Bushveld Complex after Vermaak and Von Gruenewaldt (1981). Inset shows location within the Republic of South Africa. Age data after Cawthorn and colleagues (2012) and Scoates and Friedman (2008).

low-Ca pyroxene is present instead (Wager and Brown, 1967). By contrast, the Kiglapait intrusion in Canada contains no orthopyroxene and olivine occurs throughout (Morse, 1980); the Dufek intrusion in Antarctica contains no olivine or quartz, only pyroxenes (Himmelberg and Ford, 1976), and Sudbury in Canada is quartz saturated throughout (Naldrett et al., 1970). In most of the large layered intrusions, magnetite appears only in the upper portions of the stratigraphy, but in a few intrusions, as exemplified by the Duke Island intrusion, magnetite appears in the ultramafic horizons (Irvine, 1974). As a result of magnetite extraction, the Duke Island intrusion, located in Alaska, does not show the extreme iron enrichment characteristic of the Bushveld. Intrusions like the Duke Island are therefore considered of arc affinity, rather than rift associated. The early appearance of magnetite in

these intrusions inhibits iron enrichment during differentiation and produces magnesian rocks (c.f. Figure 7.6).

9.2.3 Granitic Rocks Associated with LMIs

The uppermost portions of some layered mafic intrusions contain granites and granophyres (granites containing fine-grained intergrowths of quartz and feldspar) that appear to derived from extreme fractional crystallization of the basaltic parent melt. These granitic rocks are markedly anhydrous, which means biotite and hornblende are rare, and they commonly contain fayalite, indicating extreme iron enrichment. Examples include the granophyres of the Skaergaard intrusion (Wager and Brown, 1967), and the expansive, iron-rich granitic rocks that cap the Bushveld intrusion (Map 9.1; Vantongerren, Mathez, and Kelemen, 2010).

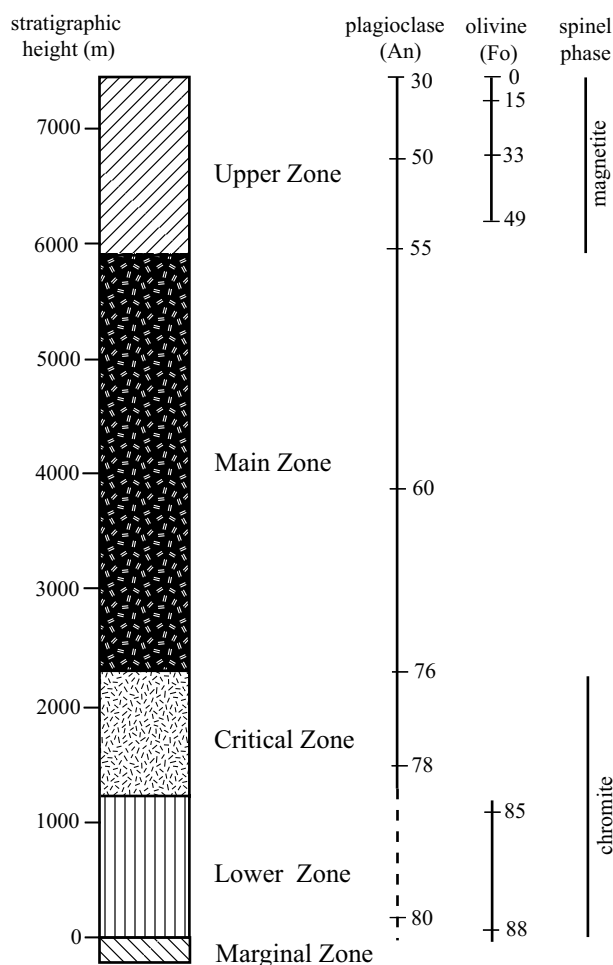


Figure 9.3 Stratigraphic cross-section across the Bushveld complex showing the variation in olivine and plagioclase compositions. After Atkins (1969).

9.2.4 Tectonic Environments of LMIs

The major tectonic environments established for the formation of layered mafic intrusions include 1) rifting environments, 2) deep portions of volcanoes, and 3) astroblems.

Rifting environments. Some layered mafic intrusions are clearly associated with continental rifts. Perhaps the best example is the Duluth intrusion, which intruded the coeval flood basalts of the Keweenaw rift (Green and Fitz, 1993). Another example is the Dufek intrusion, which was emplaced in the Jurassic when Gondwana began to rift apart.

Other LMIs are not associated with continental extension. The Great Dyke of Zimbabwe is a distinctly tabular body more than 500 kilometers long. Although dikes are commonly interpreted to indicate rifting, the Great Dyke was emplaced at a time when there is no known local

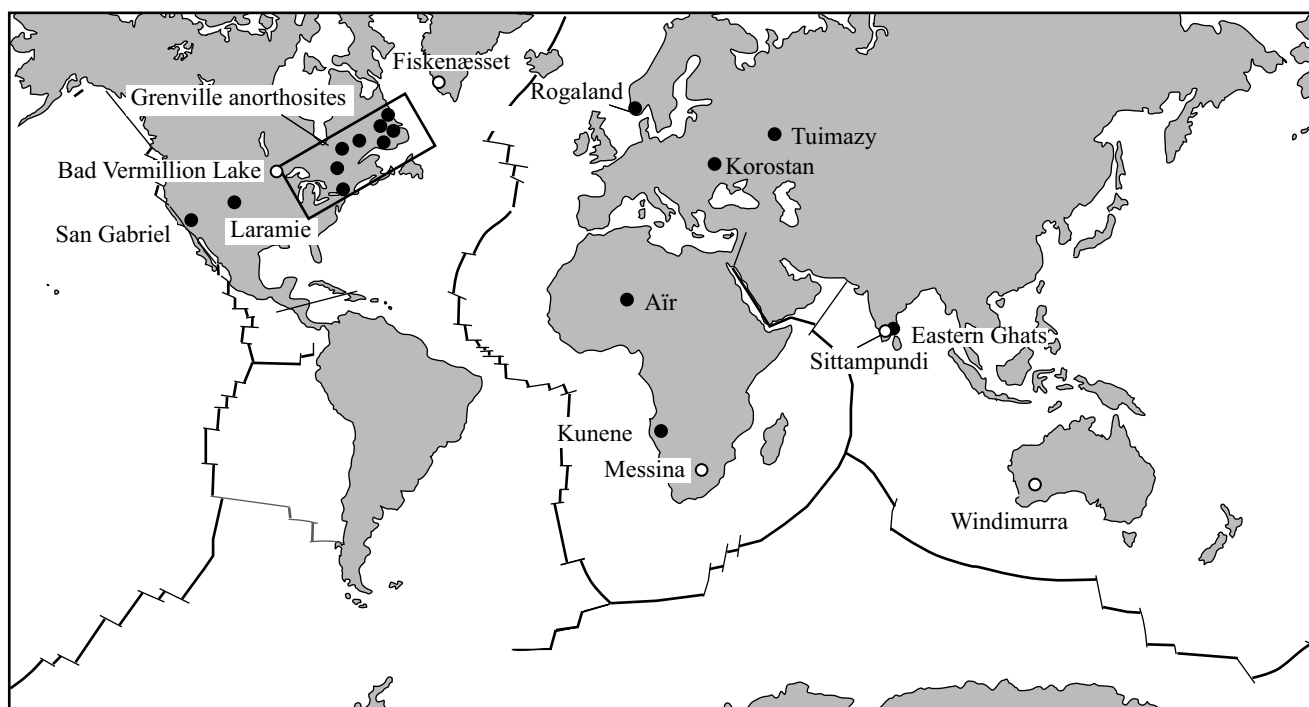
rifting event (Oberthür et al., 2002). Other large mafic intrusions, including the Bushveld and Stillwater intrusions, contain magma emplaced on a scale similar to that of flood basalts, but there is no clear geologic evidence that either formed in a rifting environment.

Plutons beneath volcanoes. Some smaller layered intrusions, including Skaergaard, Rum (in Scotland), and Duke Island, probably formed within a magma chamber beneath a volcano. Both Skaergaard and Rum represent basaltic volcano-plutonic complexes associated with the Tertiary opening of the Atlantic Ocean, and therefore are rift related. The Duke Island intrusion, which lacks iron enriched silicates and contains early magnetite crystallization, is of calc-alkalic affinity and probably formed at the base of an arc volcano. Frost and Lindsley (1992) list several other mafic intrusions that likely formed beneath arc volcanoes. Although technically these calc-alkalic intrusions form in the magmatic arc-type environments discussed in Chapter 7, they are included here because their structure and layering is similar to that of other layered mafic intrusions.

Astroblems. There is very strong evidence that the Sudbury intrusion, which hosts the world's largest nickel deposit, formed as the result of a meteorite impact approximately 1.85 billion years ago (Faggart and Basu, 1985). Evidence for this includes the fact that the area beneath the intrusion is highly brecciated and includes shatter cones – rocks deformed into cone-shaped, nested shears – a feature found only in meteorite impacts. Furthermore, the intrusion is blanketed by fallback breccia deposited following the impact. Finally, Sudbury is the only quartz-bearing layered mafic intrusion (Naldrett et al., 1970), suggesting its parent melt formed from a mixture of mafic, mantle-derived melt and felsic, crustal melt. Because Sudbury has been successfully explained as an astroblem, some petrologists argue that the Bushveld and Stillwater, layered mafic intrusions of uncertain origin, may also have formed by a similar process. It is important to note that neither of these contains the overwhelming evidence seen in the Sudbury intrusion for an extraterrestrial trigger for the magmatism.

9.3 Anorthosites and Related Rocks

Anorthosite is a rock composed of 90 percent or more plagioclase. Anorthosite layers up to several meters thick



Map 9.3 Worldwide distribution of massif anorthosites (filled circles) and Archean anorthosites (open circles). The box outlines an area encompassing the Grenville anorthosites; the names of the individual Grenville anorthosites are given in Map 9.4.

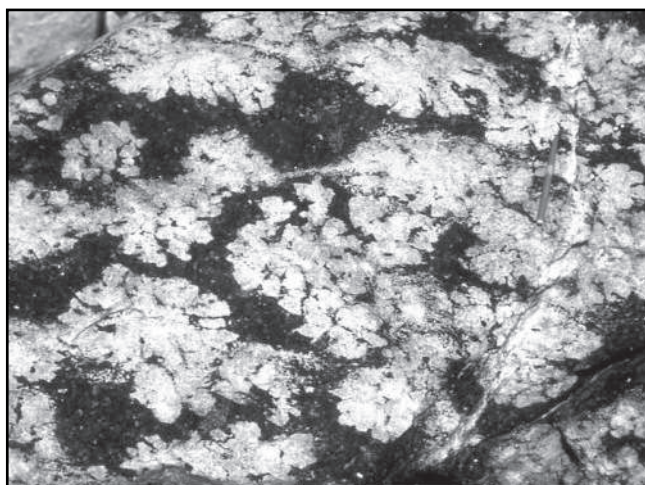


Figure 9.4 Photo showing agglomeration of coarse plagioclase grains in leucogabbro, a texture common in Archean anorthosites. The pencil in the upper right is fifteen centimeters long. Fiskenæsset intrusion, west Greenland. Photo by John Myers.

are found in most layered mafic intrusions (Figure 9.1C). In addition, anorthosite occurs in two types of intrusions that may occur on a batholithic scale. These intrusions, which are compositionally and texturally distinct,

are called **Archean** and **massif anorthosites** (Map 9.3; Tables 9.2 and 9.3).

9.3.1 Archean Anorthosites

Archean anorthosites consist of clusters of plagioclase megacrysts ($\sim\text{An}_{85\pm5}$) that may be one to five centimeters in diameter surrounded by a matrix of mafic material of basaltic composition (Figure 9.4). They generally form small dike- and sill-like bodies, but the largest, such as Fiskenæsset and Windimurra, outcrop over areas of more than 100 km² (Ashwal, 1993). Perhaps the best-studied Archean anorthosite is the Fiskenæsset intrusion in west Greenland (Myers, 1976; Polat et al., 2011). Although the intrusion has been intensely deformed and metamorphosed to amphibolite (and locally granulite) facies, studies in low-strain zones where cumulate textures survive have allowed geologists to construct a reasonable stratigraphy for the intrusion (Figure 9.5). From the base upward the stratigraphy consists of dunite → peridotite → pyroxenite → gabbro → leucogabbro → anorthosite. The primary melt probably resembled that supplying modern arc magmas, as indicated by the presence of magnetite in the peridotites and primary hornblende in the

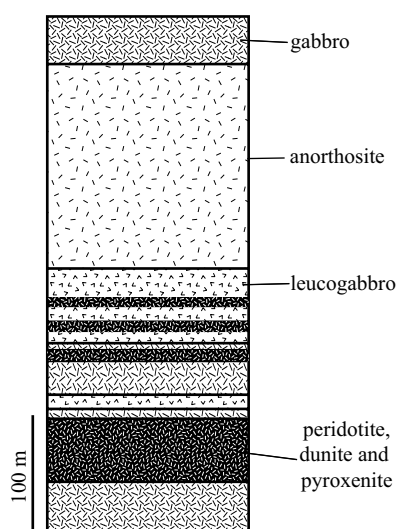


Figure 9.5 Schematic cross section of the Fiskensæset intrusion. Modified after Myers (1976).

gabbro (Polat et al., 2011) (attributes shared with the Duke Island intrusion; Section 9.2.2). Archean anorthosites are assumed to have formed by shallow-level intrusion of dikes and sills of basaltic magma carrying a slurry of plagioclase crystals. Subsequent differentiation formed the ultramafic horizons (Polat et al., 2011). The exact tectonic environment is uncertain because, as the name implies, Archean anorthosites are restricted to Archean shields; no Phanerozoic example has yet been discovered.

9.3.2 Massif Anorthosites

Massif anorthosite intrusions are batholith-sized plutons composed almost entirely of plagioclase. These differ from Archean anorthosites in that they are composed almost entirely of relatively sodic plagioclase (An_{40-50}) and lack ultramafic units. These anorthosite bodies have been emplaced as domed intrusions that may cover an area thousands of km^2 (see Table 9.2). To distinguish them from Archean anorthosites, this kind of anorthosite intrusion is called **massif anorthosite**. Ore deposits associated with massif anorthosite include Fe-Ti oxides, nickel, copper, and cobalt (Box 9.2).

Massif anorthosite plutons also are different from layered mafic intrusions in several ways. First, massif anorthosite intrusions are dominated by anorthosite and rarely contain rocks with less than 90 percent plagioclase. In addition to lacking ultramafic units, gabbroic rocks are unabundant. Second, although some massif anorthosite

Table 9.2 Differences between Archean and Massif Anorthosites

Age	Entirely Archean	Mostly Proterozoic
Plag comp	ca. An_{85}	ca. An_{50}
Size	Small, generally < 100 km^2 ; largest is 2,200 km^2	Large, largest is 17,000 km^2
Shape	Sill-like	Domal
Associate rocks	Gabbro, peridotite, pyroxenite	Monzonite, syenite

intrusions are strongly layered, such as the Laramie anorthosite complex (Scoates, Lindsley, and Frost, 2010), many are not. Finally, massif anorthosites are mostly restricted to the Proterozoic, with only a few rare occurrences in the Archean or Phanerozoic (Table 9.3).

The Laramie Anorthosite Complex. In North America, Proterozoic massif anorthosites are exposed in a band extending from northeastern Canada to the southwestern United States. They are part of the mid-Proterozoic igneous event that led to the emplacement of granitic rocks across all of the southwestern and central United States and extending into northeastern Canada and Fennoscandia (Map 9.4). Unlike many of the Grenville anorthosite complexes, the Laramie anorthosite complex (LAC) in southeastern Wyoming was not subsequently metamorphosed, and therefore preserves the relationships between massif anorthosite and coeval granitic intrusions. The LAC, which crops out over an area of 800 km^2 in the southern Laramie Range, was emplaced across the Cheyenne belt, a major crustal suture that separates Archean rocks of the Wyoming Province to the north from Proterozoic rocks to the south (Map 9.4).

The Laramie anorthosite complex consists of three anorthositic intrusions, three syenitic to monzonitic intrusions, and a number of smaller intrusions of leucogabbro and ferrodiorite (Map 9.5; Frost et al., 2010; Lindsley et al., 2010; Scoates et al., 2010). The earliest intrusion, the Poe Mountain anorthosite, has an average plagioclase composition of An_{45} . Plagioclase in the Chugwater anorthosite averages around An_{55} , and plagioclase from the Snow Creek anorthosite ranges from An_{45} to An_{55} . Each of these three anorthositic plutons forms a broad dome in

BOX 9.2 | ORE DEPOSITS ASSOCIATED WITH ANORTHOSITE COMPLEXES

Fe-Ti oxides: Because the floor of anorthosite complexes is rarely exposed, massif anorthosite intrusions lack the chromium and platinum group ore deposits commonly associated with layered mafic intrusions. However, anorthosite massifs do contain concentrations of Fe-Ti oxide ore similar to the concentrations of magnetite found in the upper levels of LMIs (see Box 9.1). These ore bodies are associated with late leucogabbroic rocks where they form concentrations near the floor of the leucogabbro or as dike-like bodies intruding the underlying anorthosite. The Fe-Ti oxide bodies in anorthosite are poorer in vanadium and richer in titanium than similar bodies associated with LMIs. The Tellnes deposit in south Norway, which is associated with the Rogaland anorthosite, is the largest hard-rock titanium deposit in the world.

Nickel, Copper, and Cobalt: Geologists had assumed that, like Cr and PGE deposits, base¹ metal deposits associated with anorthosites were left behind deep in the crust during the initial crystallization of an anorthosite intrusion. That assumption was proved wrong by the 1992 discovery of giant nickel deposits at Voisey's Bay. The Voisey's Bay deposit occurs in an early troctolite intrusion within the Nain anorthosite suite. Evidently, before olivine crystallization could deplete Ni from the melt, assimilation of country rock drove the melt toward sulfide saturation (Amelin et al., 2000). The sulfide minerals are concentrated in constrictions of the magma conduit, forming one of the largest Ni deposits in the world.

¹ Base metals, which include iron, nickel, copper, and lead, are so called because they are inexpensive, in contrast to precious metals such as silver and gold.

which stratigraphically deeper layers of the intrusion are encountered as one moves inward from the margin of the intrusion. For each intrusion only a portion of the dome is preserved; the rest has been truncated by later intrusions or by ca. 65 Ma Laramide faulting that produced the uplift in which the rocks are exposed. The rocks of the Laramie anorthosite complex display a complete range in textures from clearly magmatic textures similar to those seen in layered mafic intrusions to the highly deformed and recrystallized textures that record deformation related to emplacement typical of most massif anorthosites.

At high structural levels in the Poe Mountain anorthosite, the anorthosite and associated leucogabbro exhibit igneous layering manifested by differing abundances of plagioclase and pyroxene (Figure 9.6). The rocks have typical igneous textures with tabular plagioclase and interstitial pyroxene and olivine (c.f. Figure 1.7a). At lower structural levels the rocks become more plagioclase rich and more deformed (Scoates, Lindsley, and Frost, 2010).

Intergrown equant grains replace the tabular plagioclase. Undeformed igneous textures are less common in the Chugwater anorthosite, even at higher structural levels, and are rare in the Snow Creek anorthosite.

Two later monzonitic plutons, the Sybille monzosyenite and the Maloin Ranch pluton, were intruded along the flanks of the anorthosite domes (Kolker et al., 1991; Scoates et al., 1996). A third monzonitic body, the Red Mountain pluton (Anderson, Frost, and Frost, 2003), intruded the Sybille monzosyenite in the northeastern part of the complex. The Sybille, Maloin, and Red Mountain plutons are inferred to have formed from residual, anorthositic liquids, with minor to moderate crustal contamination (Kolker et al., 1991; Scoates et al., 1996; Anderson, Frost, and Frost, 2003).

Origin of Massif Anorthosite. Two observations from experimental work provide insight into understanding the origin of massif anorthosites. One, as pressure increases, plagioclase in equilibrium with augite becomes more

Table 9.3 Major Anorthosite Complexes

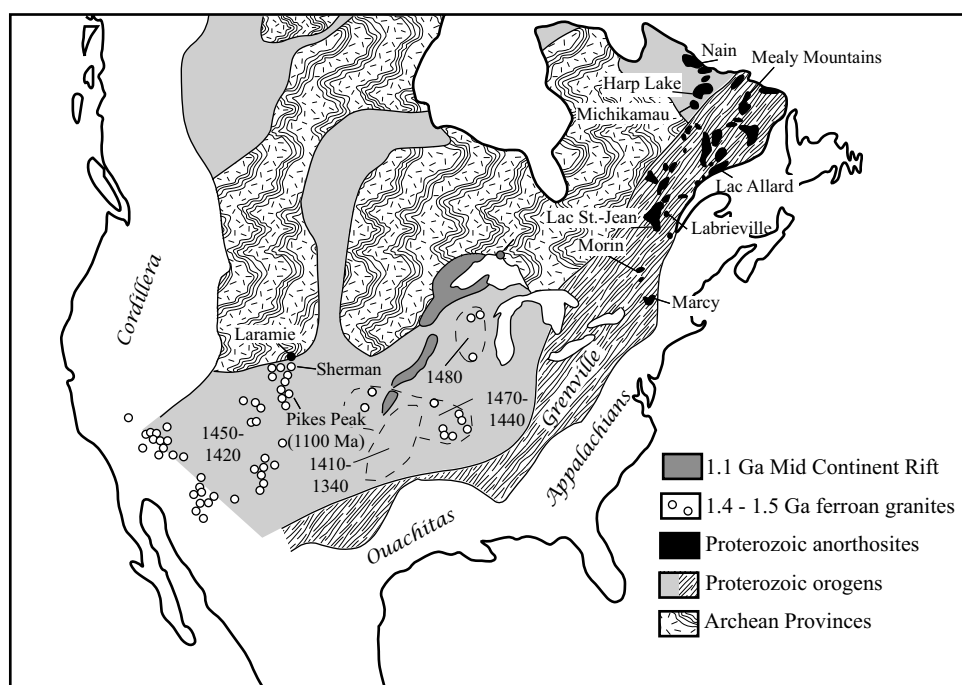
Pluton	Location	Age (Ma)	Area (Km ²)	Ref
Archean anorthosites				
Windimurra	Western Australia	~2700	2,200	1
Fiskenæsset	Greenland	2970	500	1, 2
Bad Vermillion Lake	Ontario, Canada	~2750	100	1
Messina	South Africa	3358	~100	1, 3
Sittampundi	India	2935	~30	1, 4
Massif anorthosites				
Lac Saint-Jean	Quebec	1150	17,000	1
Kunene	Angola	1371	15,000	5
Harp Lake	Labrador, Canada	1460	10,000	1
Nain	Labrador, Canada	1305	7,000	1
Duluth	Minnesota, USA	1130	6,000	1
Lac Allard	Quebec, Canada	1120	5,500	1
Marcy	New York, USA	1155	3,000	6
Mealy Mtns.	Labrador, Canada	1646	2,600	1
Morin	Quebec, Canada	1160	2,500	1
Korostan	Russia	Ca. 1800	2,185	1
Michikamau	Labrador, Canada	1450	2,000	1
Tuimazy	Russia	2570	1,800	1
Laramie	Wyoming, USA	1435	800	7
Rogaland	Norway	930	580	8
Air	Niger	430	475	1
Labrieville	Quebec, Canada	1010	250	9
San Gabriel	California, USA	1200	250	1
Eastern Ghats	India	1500–800	Many small intrusions	10

1 = Ashwal (1993); 2. Polat and colleagues (2011); 3. Zeh and colleagues (2010); 4. Bhaskar Rao and colleagues (1996); 5. Mayer and colleagues (2004); 6. McLelland and colleagues (2004); 7. Frost and colleagues (2010); 8. Schärer and colleagues (1996); 9. Owens and colleagues (1994); 7. Vijaya Kumar and colleagues (2007).

sodic. Two, high-pressure conditions restrict the crystallization field for plagioclase. These observations have led to the conclusion that the Archean anorthosites, with calcic plagioclase, probably crystallized at shallow levels in the crust, and that the relatively sodic plagioclase in the massif anorthosite formed at deeper crustal levels. The most widely accepted model for the formation of massif anorthosite involves a two-stage process (Longhi and Ashwal, 1985). First, basaltic magma, probably tholeiitic in composition, ponded near the base of the crust. Olivine and pyroxene crystallized in this deep-level magma chamber, just as they do in layered mafic intrusions. This stage of crystallization is recorded in high-Al pyroxenes, which occur as xenocrysts and enclaves in many anorthosites around the world (Charlier et al., 2010). The second stage involved the injection of the residual, feldspathic magma produced by crystallization in the deep magma chamber into a second, mid-crustal level magma chamber, leaving the ultramafic cumulates behind. Plagioclase crystals accumulated in this second chamber, trapping variable amounts of interstitial melt and resulting in thick sequences of layered anorthositic cumulates. These relatively buoyant plagioclase-rich cumulates and interstitial melt tended to rise diapirically, producing large-scale domal structures. Deformation was accommodated by varying degrees of recrystallization of plagioclase and may have led to local mobilization of interstitial melt. The interstitial melt and residual melt produced during extensive fractionation of plagioclase form the minor Fe-Ti oxide, ferrodiorite, and gabbroic dikes that intrude most of the massif anorthosite plutons. The monzonitic rocks may represent a portion of residual liquids produced during crystallization of the anorthositic cumulates, which were then variably contaminated by crustal wall rocks (Scoates et al., 1996).

9.4 Ferroan Granites

Anorthosite massifs are commonly associated, both in time and space, with distinctive, Fe-rich granites. Many massif anorthosite complexes include plutons of these granites, such as in the Laramie anorthosite complex (Map 9.5), but there are also large batholiths of Fe-rich granites that completely devoid of anorthosite. These ferroan granites are distinct from granites found in Cordilleran batholiths. Not only are they more iron rich, they are also more



Map 9.4 Geologic map showing the Archean and Proterozoic provinces of North America and the distribution of Proterozoic massif anorthosites and ferroan granites. Age ranges of ferroan rocks given in millions of years.

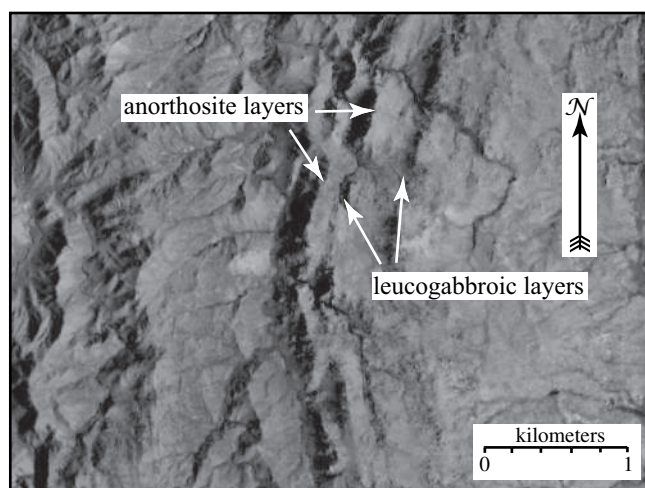


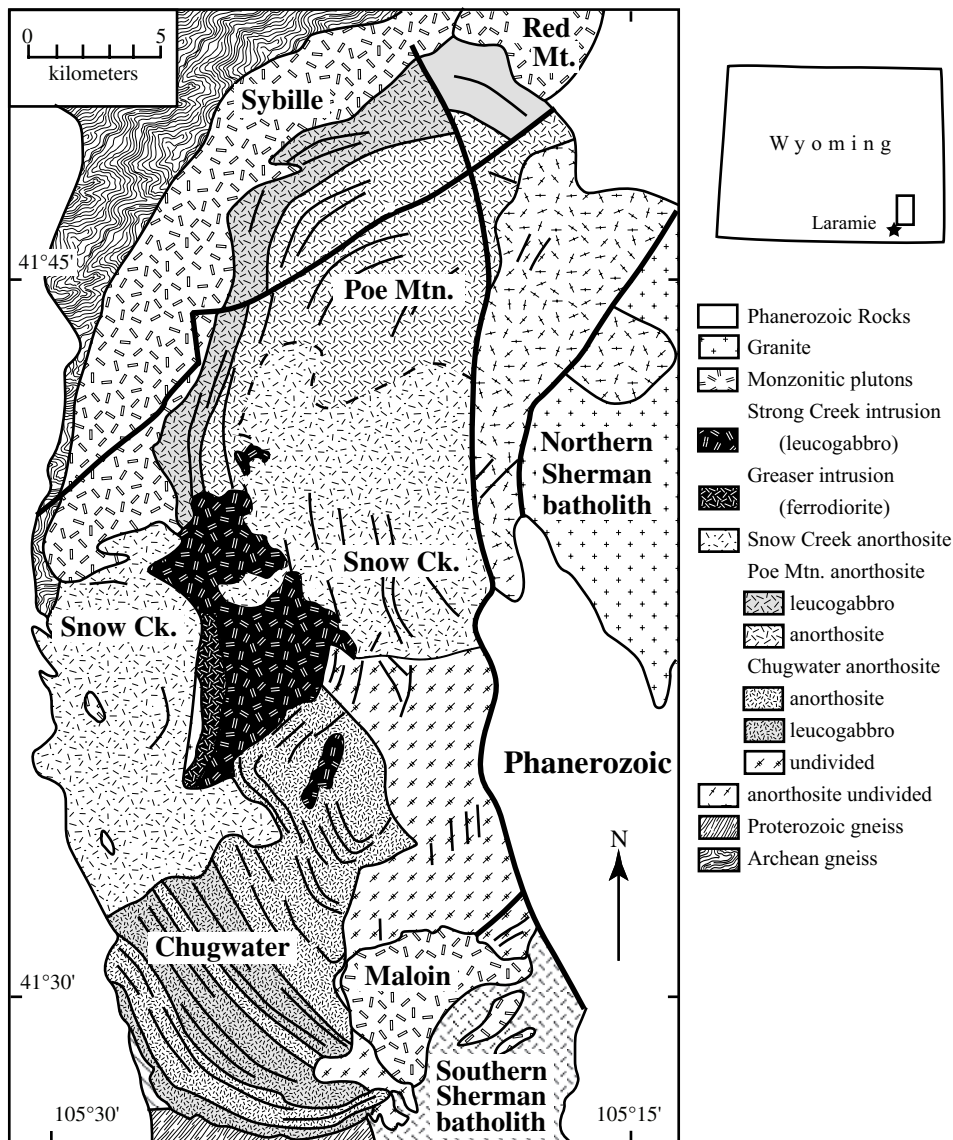
Figure 9.6 Google Earth image showing layering in the Poe Mountain anorthosite. Light-colored anorthosite layers tend to weather in relief, whereas darker leucogabbroic layers tend to erode from low topography.

potassic and usually contain much more potassium feldspar than plagioclase, giving them a distinctly pink color. Many of the ferroan granites are anhydrous, containing fayalite and clinopyroxene rather than biotite or hornblende. These granites were originally called “anorogenic granites” (Loiselle and Wones, 1979) because they were not associated with compressive structures or subduction.

Subsequently, a greater variety of tectonic environments have been proposed for these rocks’ formation and the term has been shortened to “A-type granites.” A-type granites have a broad range of geochemical characteristics yet are united by their iron-rich compositions (Frost and Frost, 2013). Because the differences in composition reflect different geologic environments of formation, we have proposed that instead of “A-type” they be called **ferroan** granites (Frost and Frost, 2011). Ferroan granites are more reduced than other granite types. This is indicated mineralogically by the common presence of fayalite, the fact that magnetite is rare or absent in these rocks, and that ilmenite is the main Fe-Ti oxide. Iron is present mainly as Fe^{2+} dissolved into the silicates. Common emplacement temperatures are 900°C or higher, well above the water-saturated solidus for granite. The major fluid species was probably CO_2 rather than H_2O .

9.4.1 The Pikes Peak Batholith

A classic example of ferroan granite is the Pikes Peak batholith, a 1.1 Ga pluton in central Colorado (Map 9.6). As is typical of ferroan granites, the Pikes Peak batholith is not zoned. Rather it is dominated by rather coarse-grained, pink granite. Relatively mafic rocks, ranging in composition from gabbro to monzonite or syenite, are present locally but they are not distributed around the margins of



Map 9.5 Geologic map of the Laramie anorthosite complex. Inset shows its location within Wyoming, USA. Box indicates the area shown in Figure 9.6. Modified after Frost et al. (2010).

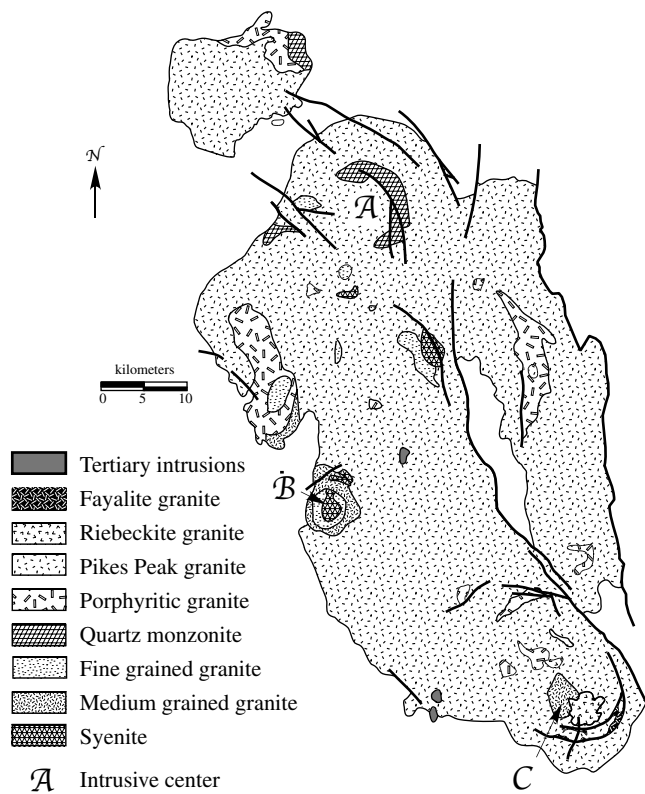
the plutons as is common in zoned Cordilleran plutons (c.f. Map 7.5). Although feldspar fabrics in the Pikes Peak batholith indicate it was emplaced through three intrusive centers, the overwhelming impression one gets from Map 9.6, and from ferroan granites in the field, is their large-scale homogeneity.

9.4.2 The Composition of Ferroan Granites

Ferroan granites, as exemplified by Pikes Peak, are compositionally similar to rhyolites derived from differentiation of basalt (Figure 9.7; see Cedar Butte in Figure 8.4). They are ferroan, and alkalic to alkali-calcic. Also shown in Figure 9.7 are the Nebo granite, which caps the Bushveld

intrusion, and the Red Mountain and Sybille plutons, which are associated with the Laramie anorthosite complex. Figures 9.7 and 8.4 show that the granitic rocks generated by extreme differentiation of basaltic rock tend to be ferroan, alkalic, and metaluminous. However, portions of both the Nebo and the Pikes Peak granite are peraluminous. This leads to the question: What makes a granitic melt peraluminous?

It is clear that crystallization of olivine, pyroxene, and Fe-Ti oxides, none of which contain Al_2O_3 , will increase alumina in the residual melt, which is why the aluminum saturation index for most suites tends to increase with increasing silica. However, since all feldspars have an ASI



Map 9.6 Geologic map of the Pikes Peak batholith. Modified after Scott and colleagues (1978), Bryant, McGrew, and Wobus (1981), and Hutchinson (1976).

= 1.0, it is impossible for fractional crystallization to drive melt compositions to peraluminous compositions. The closer the melts get to $ASI = 1.0$, the more feldspar crystallizes. There is no fractional crystallization process that can push the melt to aluminum saturation indices that lie beyond feldspar saturation. Experimental petrology shows that peraluminous melts can only be produced by melting rocks that contain minerals with an $ASI > 1.0$. The classic example is muscovite, which has an ASI of 2.5 to 3.0 and which melts at low temperatures (see Figure 4.11B). Thus, partial melting of a pelitic rock containing muscovite will produce peraluminous melts. Nominally biotite ($K(Fe,Mg)_3Si_3AlO_{10}(OH)_2$) has an ASI of 1.0; this is the consequence of its formula, which has an equal number of potassium and aluminum atoms. However, most natural biotites have excess aluminum substituting for Mg, Fe, and Si by the substitution $Al_2 \rightleftharpoons (Mg,Fe)Si$. For this reason, partial melting of tonalitic biotite granites and gneisses can also produce peraluminous melts. Because

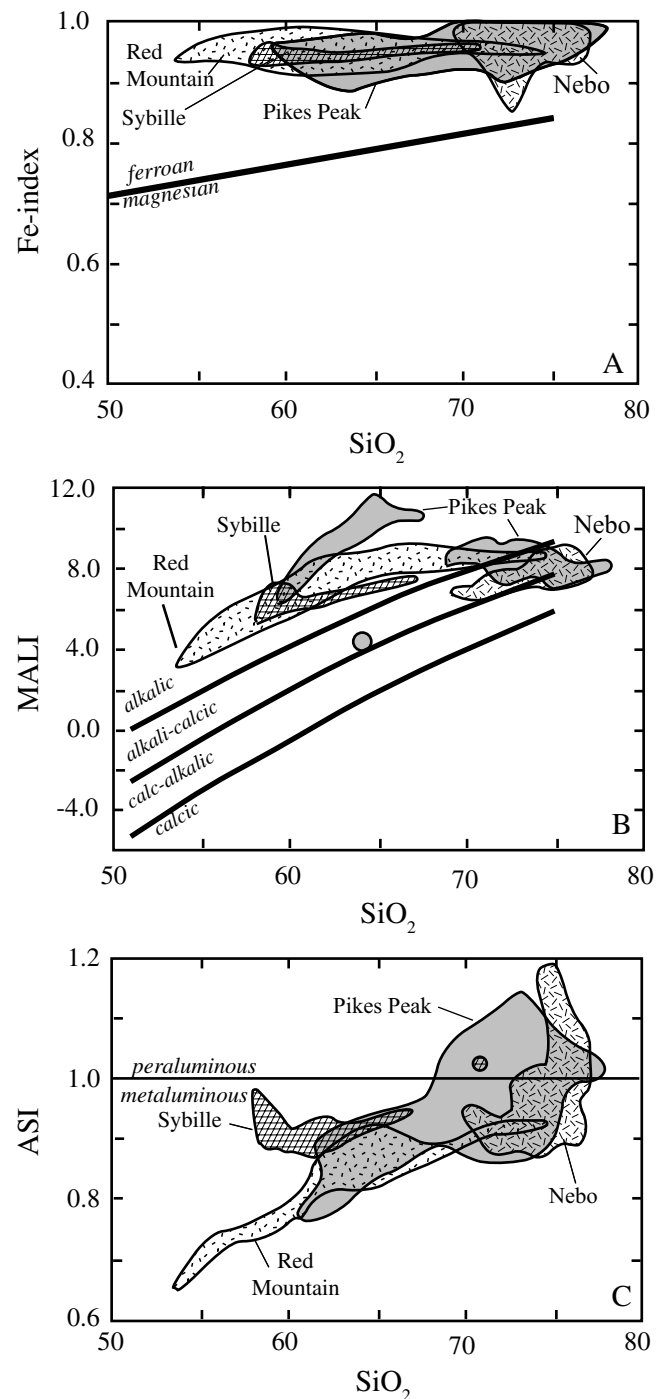


Figure 9.7 Geochemical characteristics of ferroan granites associated with mafic intrusions and anorthosites. Data from Anderson, Frost, and Frost (2003), Barker and colleagues (1975), Kleeman and Twist (1989), Smith and colleagues (1999), and Scoates and colleagues (1996).

the excess alumina for these melts resides in biotite and biotite is one of the first minerals to melt, initial melts generated from tonalitic gneisses will be peraluminous; the ASI of these melts will decrease with increasing degree of melting (Frost and Frost, 2011).

The extremely high $\text{FeO}/(\text{FeO}+\text{MgO})$ ratio of these granites indicates that, like the Yellowstone rhyolites, they are largely derived from residual melts produced by partial melting or differentiation of basalt. However, those portions of the Nemo and Pikes Peak granites that are weakly peraluminous must have assimilated a certain amount of crustal melt. This is not surprising considering that the high magmatic temperatures from which these granites were derived almost certainly melted adjacent wall rock.

9.5 Alkaline Complexes

Alkaline intrusions make up an extremely small volume compared to other rocks described in this chapter; they contain minerals uncommon in any other environment,

and they are graced with rock names obscure even to most geologists. As a result, the study of alkaline complexes has traditionally been an aspect of petrology with few devotees. However, the proliferation of cell phones, computers, flat panel televisions, and a variety of clean energy technologies has changed this picture entirely. These devices and technologies contain permanent magnets, lighting phosphors, and other components that use rare earth elements (REEs), which has led to an increased demand for these and other relatively scarce elements (Box 9.3). REEs are concentrated in alkaline intrusions and as a result, economic geologists now study alkaline intrusions as sources for these metals. Alkaline intrusions are found in ancient rifts, such as in the Gardar province, as well as in areas where rifting is not obvious, as in the Kola peninsula (Map 8.3).

9.5.1 Geology of the Ilimaussaq Intrusion

The Ilimaussaq intrusion serves as a good example of an alkaline pluton for two reasons. First, its tectonic context

BOX 9.3 | ENRICHMENT OF RARE METALS IN ALKALINE PLUTONS

Because of their use in a number of “green” energy technologies, including wind turbines, electric vehicles, photovoltaic cells, and fluorescent lighting, there is an increasing demand for rare earth elements (REEs) and other scarce metals, including In, Ga, Te, Li, and Y. Alkaline intrusions are a major source for many of these metals. For example, the Ilimaussaq intrusion hosts one of the richest REE deposits in the world, where the lujavrite contains more than one percent total rare earths (Bailey et al., 2001). Alkaline rocks are enriched in these rare metals by the same process that causes layered mafic intrusions to be enriched in chromium, nickel, copper, and platinum group elements – igneous fractionation. PGEs, Cr, and Ni have extremely large partition coefficients between mineral and melt (or between silicate melt and sulfide melt) and concentrate early in the fractionation history of an igneous system, such as in layered mafic intrusions. In contrast, elements such as the REEs have extremely low partition coefficients between mineral and melt. These elements concentrate by orders of magnitude in the residual melt if sufficient fractionation has taken place (see Figure 4.13).

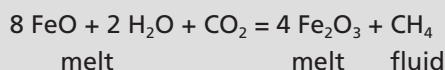
Extreme enrichments in rare metals in an igneous system are the result of two features. First, the bulk D for the rare metals between melt and the crystallizing phase must remain low throughout the crystallization history of a rock. Second, igneous fractionation must proceed until only a very small fraction of melt remains. In most igneous rocks zircon concentrates REEs, particularly the heavy REEs, so once zircon begins to crystallize out of a melt, the bulk D between melt and the crystallizing phases becomes greater than one. At this point these heavy metals behave compatibly and their concentration in the residual melt decreases with increasing fractional crystallization. This effect is observed in the

(continued)

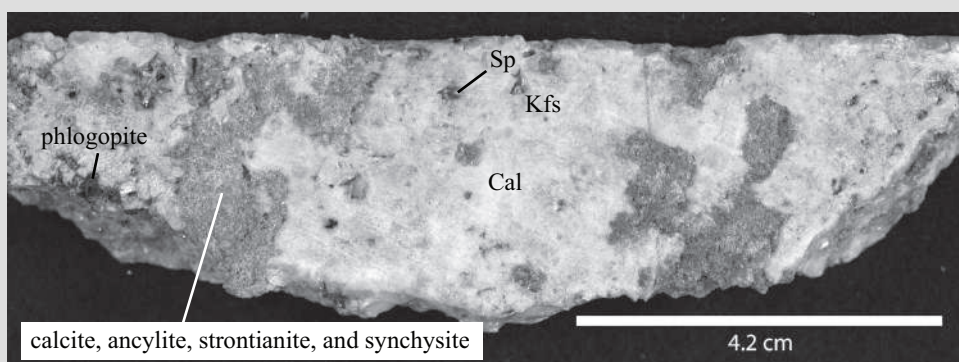
BOX 9.3 (CONT.)

Red Mountain pluton, where zircon saturation occurred at around 60 percent SiO₂ and fractional crystallization after this point depleted Zr (as well as REEs, Hf, and Ta) from the melt (Figure 4.14). Zircon has high solubility in alkaline melts (Linnen and Keppler, 2002), which inhibits crystallization of zircon in alkaline melts. If zircon does not crystallize, then the bulk D for REEs remains near zero, allowing them to be enriched in the residual melt. Eventually the zirconium concentration becomes so high that eudialyte, the Na-Zr silicate, crystallizes instead of zircon.

The other feature that enriches REEs in alkaline rocks is that alkaline melts continue crystallizing (and hence differentiating) down to very low temperatures. Most granitic magmas solidify at around 650°C to 700°C (see Figure 3.3). However, the alkaline melt at Ilimaussaq may have remained molten to temperatures well below 600°C (Markl, 2001). Alkaline rocks are rich in elements such as Li, F, Na, Be, and B that are known to flux silicate melts to relatively low temperature. The reason alkaline rocks crystallize to such low temperatures is complex and is related to the Na-rich composition of the melt. Because highly sodic rocks contain more Na₂O than feldspars can accommodate, the extra Na₂O must be taken up by amphiboles (riebeckite or arfvedsonite) and pyroxenes (aegerine), in which NaFe³⁺ substitutes for MgFe²⁺. Iron in the parent magma is likely to be ferrous, as in the augite syenite in the Ilimaussaq intrusion. The excess oxygen necessary to convert the ferrous iron to ferric iron likely sources from H₂O and CO₂ bound in the melt structure (Markl, Marks, and Frost, 2010). The reaction is:



The depletion of water from the melt to make ferric iron and methane means that, unlike typical granitic magmas, the alkaline magmas never reach water saturation; they become saturated in CH₄-rich fluids instead. Indeed, CH₄-rich fluid inclusions are common in alkaline rocks (Konnerup-Madsen and Rose-Hansen, 1982). Because water never evolves during fractionation of alkaline intrusions, elements such as Li, F, Na, Be, and B remain in the melt rather than being fractionated into the fluid. This allows alkaline melts to fractionate down to lower T, thus increasing the REE content of the residual liquid.



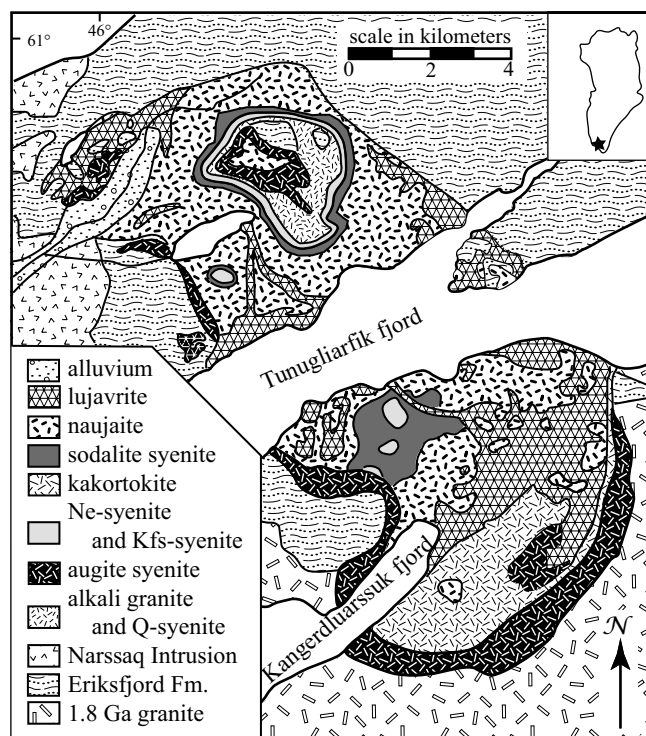
Box 9.3 Rare earth element ore from the Bear Lodge alkaline igneous complex, Wyoming. The sample is composed of >50 percent calcite (Cal). The primary rare earth element has been replaced with dendritic ancylite (SrCe(CO₃)₂(OH)·H₂O), fibrous aggregates of synchysite (Ca(Ce,La,Nd,Y,Gd)(CO₃)₂F), and parisite, with interstitial hematite, strontianite, barite, celestine, calcite, and sulfides. Galena, pyrite, sphalerite (Sp), phlogopite, and moderately to strongly altered potassium feldspar (Kfs) are disseminated throughout the sample. Photo courtesy of Danielle Olinger and Rare Earth Resources, Ltd.

is clear and both intrusive and extrusive rocks compose the complex: it is intruded into coeval rift-related sediments and alkaline lava flows (the Eriksfjord formation in Map 9.7). Second, it is the most alkaline intrusion in the world and also the host of one of the largest known deposits of rare metals. However, there are hurdles to understanding the crystallization of the Ilimaussaq intrusion, namely, the bizarre minerals that comprise the intrusion

and the even more bizarre names to the rocks. In addition to containing common minerals any geologist should know, including alkali feldspar, sodalite, nepheline, and aegerine, the Ilimaussaq contains two rock-forming minerals rarely found except in alkaline rocks: eudialyte and arfvedsonite. Eudialyte is a complex sodium-zirconium silicate that forms in sodium-rich rocks in place of zircon. Arfvedsonite is a highly sodic amphibole with the formula $\text{Na}_3\text{Fe}^{2+}_4\text{Fe}^{3+}\text{Si}_8\text{O}_{22}(\text{OH})_2$. In this amphibole, sodium fills both Ca site (as in riebeckite) and the vacant site (as in hornblende). The charge balance is maintained by ferric iron substituting for ferrous iron.

Although some of the rock units in the Ilimaussaq intrusion are named using mineralogical naming terminology (see Figure 1.1), the three most important units do not and are nearly unpronounceable to an English speaker unfamiliar with the Nordic alphabet (in which J is pronounced “ya”). These three terms are based more on textural features than mineralogy. Kakortokite is a layered nepheline syenite containing nepheline, alkali feldspar, arfvedsonite, and eudialyte. Naujaite is a sodalite syenite that consists of euhedral crystals of sodalite surrounded by crystals of alkali feldspar, arfvedsonite, and eudialyte. Lujavrite is an arfvedsonite- or aegerine-rich nepheline syenite.

The Ilimaussaq intrusion is nearly completely rimmed by augite syenite (Map 9.7 and Figure 9.8), which is a syenite that is neither quartz nor nepheline bearing. This grades inward to nepheline syenites and various other K-feldspar-rich syenites. The main portion of the pluton consists of the sequence kakortokite, naujaite, and lujavrite. These rocks comprise the original magma chamber for the intrusion. During the crystallization



Map 9.7 Geologic map of the Ilimaussaq intrusion. Inset shows its location in Greenland. Modified after Ferguson (1964).

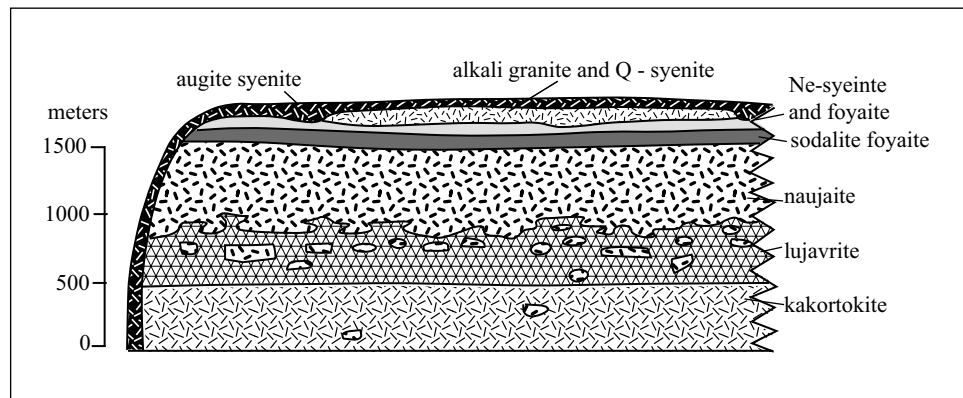


Figure 9.8 Schematic cross-section of the Ilimaussaq intrusion. Modified after Andersen, Bohse, and Steinfeldt (1981).

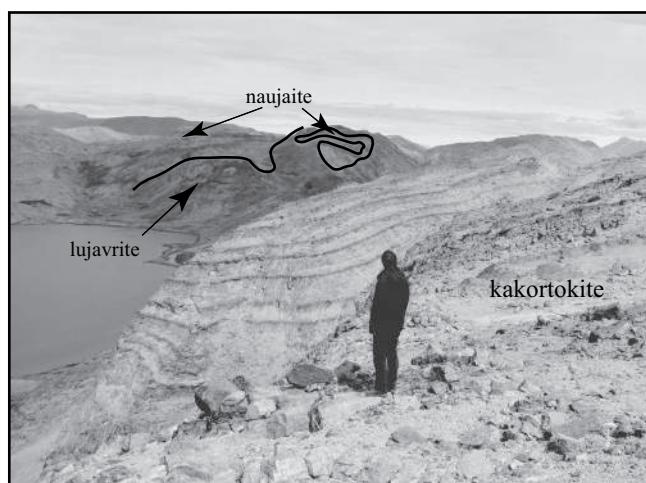


Figure 9.9 Photo of the Ilimaussaq intrusion taken on the southeast shore of Kangerdluarssuk fjord looking northeast. Kakortokite composed of cumulus minerals on the floor of the complex in the foreground, naujaite is the sodalite-rich floating cumulates in the background, and lujavrite is the horizon sandwiched between the two.

of the pluton-dense crystallizing phases, eudialyte and arfvedsonite accumulated on the floor of the chamber,

interlayered with alkali feldspar, and formed the layered kakortokites (see Figure 9.9). At the same time, sodalite grains, which were less dense than the melt, floated to the top of the chamber, where they were cemented together with eudialyte, arfvedsonite, and alkali feldspar, forming the naujaite. From time to time blocks of the naujaite broke off the roof of the intrusion and fell into the residual melt and sometimes were incorporated into the kakortokites. The residual melt eventually crystallized to make the lujavrite.

In addition to the aforementioned differentiation of the Ilimaussaq intrusion by fractional crystallization processes, at least two other magmatic processes were involved in forming the complex. First, limited assimilation of the lower crust is implicated in the formation of the peralkaline granite. Second, evidence that the rocks of the complex interacted with late-stage gaseous and aqueous fluids is preserved in late-stage pegmatites and hydrothermal veins (Marks et al., 2004). These fluids are implicated in the enrichments in U, Th, REE, and Be found in Ilimaussaq and other alkaline plutons (see Box 9.3).

Summary

Intraplate magmatism involves a complex assortment of magma types, both extrusive and intrusive. The wide variety of intraplate magmatism is caused by different compositions of mafic magmas that can be produced during mantle melting, the extent to which they interact with the crust, and the various depths at which they differentiate. The formation of this diversity of igneous rocks is summarized schematically in Figure 9.10.

- Partial melts of the mantle are implicated in the formation of intraplate magmatism. As shown in Figure 9.10, the melts generated from the mantle may range from tholeiite to highly alkaline in composition, depending on the composition of the mantle melted and the depth and extent of melting. Abundant melting produces tholeiitic melts, which may be emplaced as flood basalts or may pond at relatively shallow levels to produce a layered mafic intrusion.
- Differentiation of diverse parent magmas at various depths in the crust also is a factor in the diversity of intraplate magmatism (Figure 9.10).
 - Ponding of the melt at the base of the crust may produce feldspar-rich, crystal-laden magmas that ascend to form anorthositic intrusions.
 - Differentiation of the mafic melts in LMIs or anorthosite complexes will lead to the production of syenite, which will further differentiation to produce ferroan granite.
 - Transitional basalts, those that are sodium rich but not necessarily alkaline, may differentiate to produce peralkaline granites and alkali basalts, or basanites will differentiate to produce nepheline syenite.

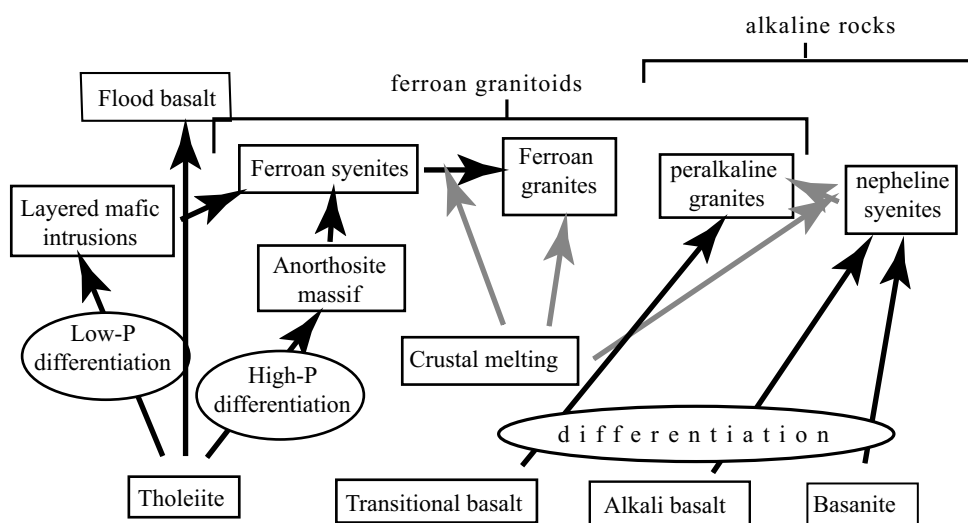


Figure 9.10 Flow sheet showing how the range of rock types found in intracontinental magmatism are related. Modified after Frost and Frost (2011).

- Throughout the differentiation process the mantle melts may interact with crustal melts (Figure 9.10). Small degrees of melting of crustal rocks may produce ferroan granite. Alternatively, assimilation of crustal melts by syenitic melts produced by differentiation of tholeiites may also make ferroan granite. Mixing of crustal melts with nepheline syenite melts can produce peralkaline granites.

Questions and Problems

Problem 9.1. Summarize the tectonic environments in which layered mafic intrusions may form and give an example of each.

Problem 9.2. a) Referring to Figure 2.17, identify several different sequences of layering that might develop in layered mafic intrusions by the crystallization of a basaltic parent. (Note that the figure shows one such sequence starting with basalt liquid composition Y.)

b) Compare these to the stratigraphic section through the Fiskensæset intrusion shown in Figure 9.5

- Can the layering in the Fiskensæset intrusion be explained by any of the crystallization sequences you identified in 2a)?
- Under what circumstances might a layer of dunite be followed by a layer of pyroxenite?
- How might the pure anorthosite layer be formed?

Problem 9.3. What are the differences between Archean and massif anorthosites?

Problem 9.4. How do ferroan granites like the Pikes Peak granite (Map 9.6, Figure 9.7) differ from continental arc plutons such as the Tuolumne intrusion (Figures 7.5 and 7.8 and Map 7.5)?

Further Reading

Ashwal, L. D., 1993, *Anorthosites*. Springer-Verlag, New York.

Frost, C. D., and Frost, B. R., 2011, On ferroan (A-type) granites: Their compositional variability and modes of origin. *Journal of Petrology* 52, 39–53.

Wager, L. R., and Brown, G. M., 1967, *Layered igneous rocks*. W.H. Freeman and Company, San Francisco.

Winter, J.D., 2010, *Principles of igneous and metamorphic petrology*, 2nd ed., Prentice Hall, New York, Chapter 12.

Chapter 10

Interpretation of Granitic Rocks

10.1 Introduction

Granitic rocks are the most abundant rocks in continental crust and geologists have developed many ways to classify them. This text has relied heavily on the geochemical classification of Frost and colleagues (2001), but it is important that petrology students understand other classification schemes are in use. This chapter begins with a summary of the other classification schemes for granitic rocks: 1) the mineralogical classification, 2) a classification based on the presence or absence of magnetite, and 3) an “alphabet” classification based on the inferred origin of the granites.

The chapter continues with a discussion of granitic rocks from continental collisions. They are compositionally distinct from the Cordilleran and ferroan granites discussed in previous chapters. A summary of the four geochemical types of granitic rocks, noting the compositional characteristics of each type and showing how the compositional changes are manifested in the mineralogy of the granitic rocks concludes the chapter.

10.2 Classification of Granitic Rocks

10.2.1 Mineralogical Classification

The mineralogical classification discussed in Chapter 1.1, which is the simplest of the classifications for granitic rocks, is based on modal proportions of quartz, plagioclase, and alkali feldspars. The advantage of this classification is that it can be readily applied in the field and it is simple to use. The major drawback is that it ignores compositional variations apart from those that affect the feldspar compositions. Thus mafic and felsic rocks may plot in the same field even if they have significantly different chemical compositions. Furthermore, the classification cannot address the presence or absence of minor phases, such as muscovite, which may convey significant petrologic information.

10.2.2 Classification Based on Opaque Oxides

A second classification scheme for granites is based on the presence of magnetite. Most granites contain magnetite but some do not. This has led to the classification of granites in terms of the occurrence or absence of magnetite (Ishihara, 1977). Magnetite contains Fe^{3+} ; therefore magnetite will be present in relatively oxidized rocks and absent in relatively reduced ones. **Magnetite granites** are relatively oxidized granites that contain magnetite and ilmenite as the major oxides, whereas **ilmenite granites** are relatively reduced and contain ilmenite as the only Fe-Ti oxide. One reason granites may lack magnetite relates to the composition of the magma source. Partial melting of pelitic rocks produces magma that crystallizes peraluminous, ilmenite granites. Since pelitic rocks contain graphite, and graphite is a reducing agent, magnetite will not be stable in these magmas. The advantage of this classification scheme is that it is simple; one can classify granites by measuring their magnetic susceptibility. In fact aeromagnetic surveys map the distribution of magnetite and ilmenite granites over a wide terrain. The disadvantage is that the classification scheme telescopes the whole range of granite compositions into two categories and hence overlooks the chemical complexity of granitic rocks.

10.2.3 Alphabetic Classification

Chappell and White (1974) developed an alternate classification scheme that emphasizes the origin of granites.

For obvious reasons it is sometimes referred to as the alphabetic classification. The major types of granites in this classification are:

I – type (I = igneous): Metaluminous granites that are typically magnetite bearing. I-type granites are inferred to be produced by differentiation of andesite or partial melting of an igneous source.

S – type (S = sedimentary): These peraluminous granites are typically magnetite free. These are inferred to be produced by partial melting of pelitic rocks. Hence S-type granites are assumed to come from a sedimentary source.

A – type (A = anorogenic): These are granites not associated with an obvious penetrative contractional orogeny. They are compositionally distinct from I-type granites, being almost exclusively ferroan and higher in K, REEs, and Zr. They are inferred to be produced by partial melting or fractional crystallization of mafic rocks.

Even though this classification scheme is widely used, many petrologists look upon it with disfavor because it is genetically dependent. It assumes petrologists know what rocks melted to make the granite. However, it turns out that peraluminous granites don't only come from melting of sedimentary rocks; they can form from small degrees of melting of a tonalite (Skjerlie and Johnston, 1993; Patiño Douce, 1997). Similarly, melting of an immature greywacke can form granite that is compositionally "I-type." An ideal classification scheme depends only on the features seen in the rock, not on inferred origin. For these reasons the alphabetic classification of granites is slowly falling out of favor.

10.2.4 Geochemical Classification

A number of major element indices of differentiation were presented in Chapter 4.4, and these have been used in Chapters 7, 8, and 9 to identify the processes by which magmas evolve. However, these indices are also useful in classifying granitic rocks. The classification scheme of Frost and colleagues (2001) and Frost and Frost (2008) relies on four geochemical indices to classify granitic rocks. The indices, which are reviewed later in this chapter, are based on the major element abundances in the rock analyses and include:

Fe-index $(\text{FeO} + 0.9 \cdot \text{Fe}_2\text{O}_3) / (\text{FeO} + 0.9 \cdot \text{Fe}_2\text{O}_3 + \text{MgO})$:

This index measures the iron-magnesium ratio of the ferromagnesian silicates. **Ferroan** rocks have either undergone extensive fractional crystallization of olivine and pyroxene and minor magnetite fractionation or formed by minor melting of crustal rocks. **Magnesian** rocks have undergone early crystallization of magnetite, which suppressed iron enrichment.

Modified Alkali-Lime Index (MALI) $(\text{Na}_2\text{O} + \text{K}_2\text{O} - \text{CaO})$:

This index monitors the compositions of the feldspars in the rock. This is modified after the alkali-lime index of Peacock (1931) and involves four classes. In order of increasing alkalinity these are **calcic**, **calc-alkalic**, **alkali-calcic**, and **alkalic**.

Aluminum saturation index (ASI) (molecular $\text{Al} / ((\text{Ca} - 1.67 \cdot \text{P}) + \text{Na} + \text{K})$): This index compares the amount of Al, Ca, Na, and K in the rock to the amounts needed to make feldspars. Phosphorous is included because small amounts of apatite are present in rocks and the calcium in apatite is not available for incorporation into feldspars. This index determines whether a rock is **metaluminous**, in which case it has more Ca, Na, and K than feldspars consume, or **peraluminous**, in which case the rock has excess Al. Peraluminous rocks contain aluminous minerals including muscovite, garnet, sillimanite, and cordierite.

Alkalinity Index (AI) (molecular $\text{Al} - \text{Na} + \text{K}$): This index determines the balance between aluminum and alkalis (Na + K). A rock that contains excess Al may be metaluminous or peraluminous (see the ASI index). A rock with excess Na + K is **peralkaline** and will contain Na-pyroxene and Na-amphibole.

Using these four indices, Frost and colleagues (2001) described fourteen chemical varieties of granitic rocks, which fall into four distinct tectonic environments. Chapters 7 and 9 examined granitic rocks formed in two of these tectonic environments. Cordilleran-type granites form in arc environments and are characterized by magnesian compositions dictated by early crystallization of magnetite. In contrast, ferroan granites are characteristic of rifting environments, where they form by partial melting or extreme differentiation of basaltic magma. This section describes the other two types of granite, both of

which occur during continental collision. *Peraluminous leucogranites* may form as tectonic decompression brings hot rocks to shallow crustal levels. After collision, the base of the thickened crust may delaminate as the lower portion of it sinks into the mantle. Mantle lithosphere rising into the space vacated by delaminated crust may melt, causing the formation of “post-tectonic” or *Caledonian granites*. Granites are associated with a number of different ores (Box 10.1).

10.3 Peraluminous Leucogranites

Many orogenic belts contain small plutons of leucogranite emplaced during the height of deformation. These granites are silica rich and are composed mostly of quartz and feldspars (and hence are *leucocratic*) with only a small amount of muscovite, garnet, or biotite. These rocks are distinctly peraluminous and hence are termed **peraluminous leucogranites**. Some peraluminous leucogranites may also contain sillimanite, cordierite, or tourmaline as important phases. Peraluminous leucogranites form by decompression melting in a manner analogous to the process that forms basaltic melts at a spreading center. In a mountain belt where the crust has been tectonically thickened, deeply buried rocks may get much hotter than is necessary to melt H_2O -saturated granite (Figure 10.1). However, because high-grade metamorphism leaves rocks H_2O undersaturated, little melt, if any, is produced when the water-saturated granite melting curve is crossed. However, above the temperature of the granite solidus, several **dehydration melting** reactions can produce substantial amounts of granitic melt. If deep, relatively hot rocks are brought to shallower levels by tectonic activity, either by thrusting or extension, then the rocks in the lower plate will experience rapid decompression (heavy arrow in Figure 10.1), causing the rocks to undergo one or two important melt-producing reactions: muscovite + plagioclase + quartz = sillimanite + K-spar + melt, and biotite + plagioclase + sillimanite + quartz = K feldspar + garnet + melt. This process of **decompression melting** is analogous to melting reactions at mid-ocean ridges, although in crustal rocks decompression melting involving rocks that contain muscovite, plagioclase, sillimanite, biotite, and quartz will take place at much lower temperatures than melting of the mantle at a mid-ocean ridge.

BOX 10.1 | ORE DEPOSITS AND GRANITES

Granitic rocks commonly are enriched in incompatible elements, including metals that form important ore deposits. The ore deposits found in a granite pluton are closely tied to their composition and, to a lesser extent, the tectonic environment of the intrusion. For example, porphyry copper deposits (discussed in Box 7.2) occur in subduction-related settings. Other ore deposits hosted in granites yield tin, tungsten, and gold.

Tin: Tin (Sn) is present in biotite and muscovite as a trace element in abundances up to 1,000 ppm (Eugster, 1985). Because Sn is present as a minor component in magnetite and sphene, it will be disseminated rather than building up in the magma to ore concentrations unless those minerals have not crystallized. Both magnetite and sphene are destabilized by reducing conditions. Thus tin granites are typically peraluminous granites formed by melting of aluminous metasedimentary rocks, which are reducing because of the presence of graphite. Tin granites can form in arc settings if assimilation



Box 10.1 Old Faithful Geyser, Yellowstone National Park, Wyoming. The hydrothermal system driven by Yellowstone magmatism is analogous to those that form epithermal gold deposits. It was likely a thermal environment like this that led to the formation of the Comstock Lode.

(continued)

BOX 10.1 (CONT.)

of oxidized continental crust is not involved. They may also form in rift settings (Eugster, 1985). Tin granites are not widespread, but instead concentrate in certain belts, including the Cornwall area of Great Britain, Bolivia, and Malaysia. Although cassiterite, the major ore for tin, may crystallize out as a magmatic mineral in granites, most of the ore zones for tin granites represent reaction zones between the fluids evolved late during the crystallization of the granite and the host rock.

Tungsten: Tungsten (W) behaves geochemically like tin. Tungsten deposits, like tin deposits, are found in granites formed from melting of W-bearing sedimentary rocks (Yidou, 1995). Although some tungsten deposits occur as veins within granites, the richest deposits occur in **skarns**, reaction zones between granite and surrounding carbonates. Major tungsten districts include the McKenzie Mountains on the Yukon-Northwest Territory boundary of Canada (Rasmussen et al., 2011) and in southern China (Yidou, 1995).

Gold: Gold (Au) deposits in granite include Bonanza-type epithermal deposits. These deposits, as exemplified by the high-grade vein deposits associated with the Comstock Lode in Nevada, are deposited by low-temperature hydrothermal fluids associated with shallow-level granitic plutons. (The term *epithermal* means veins formed at 50–200°C.) During circulation of hydrothermal fluids, gold is leached from the country rock (commonly rhyolitic or dacitic lavas) and is deposited when the fluids boil. The locality type of this deposit is the Comstock Lode, which produced 258 tons of gold out of a vein system that extends for more than three miles. The Comstock Lode formed as the result of granitic magmatism that occurred during Miocene rifting of western North America (Vikre, 1989). It is likely that the geothermal processes that formed this deposit are similar to those in Yellowstone today (Box 10.1). It is important to note that epithermal deposits are not restricted to any given plate tectonic environment, but can occur in both rifting and arc environments. A good example of an epithermal deposit currently in the process of forming is the Volcan Gelaras, in Columbia, which Goff and colleagues (1994) calculate emits 500 to 5,000 tons of SO₂ and 0.5 kilograms of Au per day.

10.3.1 Himalayan Leucogranites

The best-known example of peraluminous leucogranite comes from the Himalaya, where small leucogranite bodies were emplaced into the highest-grade portion of the area during peak metamorphism (Figure 10.2). Peraluminous leucogranites are common in other regions of the world, and include the Harney Peak granite in the Black Hills of South Dakota (Nabelek, Russ-Nabelek, and Denison, 1992) and the leucogranites of Brittany in France (Strong and Hamer, 1981). One of the best studied of the Himalayan leucogranites is the Manaslu granite (Le Fort, 1981) (Map 10.1). We note three distinctive features of the Manaslu granite. First, compared to the continental arc batholiths, it occupies a relatively small volume. Second, the body has a sheet-like form

oriented parallel to the structural grain of the Himalaya. Third, the granite is compositionally homogenous. Unlike continental arc batholiths, it contains no granodiorite or more mafic components. The absence of these components is consistent with the theory that these leucogranites are a product of crustal melting due to tectonic thickening, and that no mantle heat source, and hence no mafic melts, are involved.

10.3.2 Geochemistry of Peraluminous Leucogranites

Because of their restricted high silica contents (above 70 percent SiO₂), peraluminous leucogranites plot in a small field on MALI and the iron enrichment index

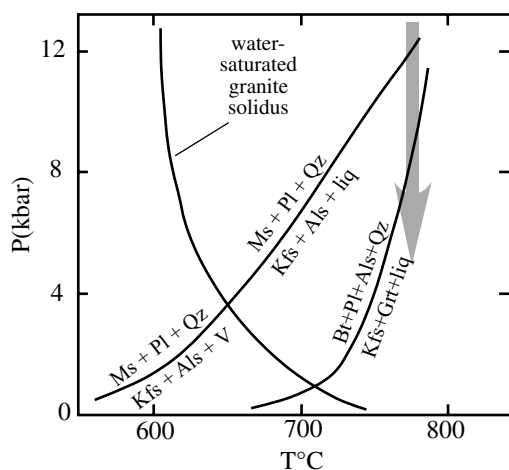


Figure 10.1 P-T diagram showing the relation between the water-saturated granite solidus and **two common** dehydration melting curves for pelitic rocks. Heavy grey arrow shows a possible P-T path followed in continental crust that has been tectonically thickened and then rapidly decompressed by extension. From Clarke (1992).

plots (Figure 10.3). They span the range from magnesian to ferroan and from calcic to alkalic. Part of this variation occurs because the melt is dominated by silica and aluminum. This means MALI and iron enrichment parameters are very sensitive to small changes in the abundances of Na_2O , K_2O , CaO , FeO , and MgO . The change from ferroan to magnesian may reflect changes in degree of melting from the source. Because iron is fractionated into the melt over magnesium, initial melts will tend to be ferroan, whereas progressive melting will enrich the melt in magnesium over iron. The differences in MALI appear to reflect differences in water pressure in the source region. In areas of low water pressure, melting is restricted to the micas, and the resulting melt is relatively enriched in K_2O over CaO and Na_2O . Higher water pressure allows more plagioclase to melt along with the mica resulting in more calcic melts. Thus early melts should be relatively calcic and, as water is depleted from the source, the later melts should become increasingly alkalic. In addition to crustal thickening, the insulating effect of overriding plate, radioactive heat production within the crust, and shear strain heating near large crustal shear zones may contribute to the higher temperatures required for dehydration melting

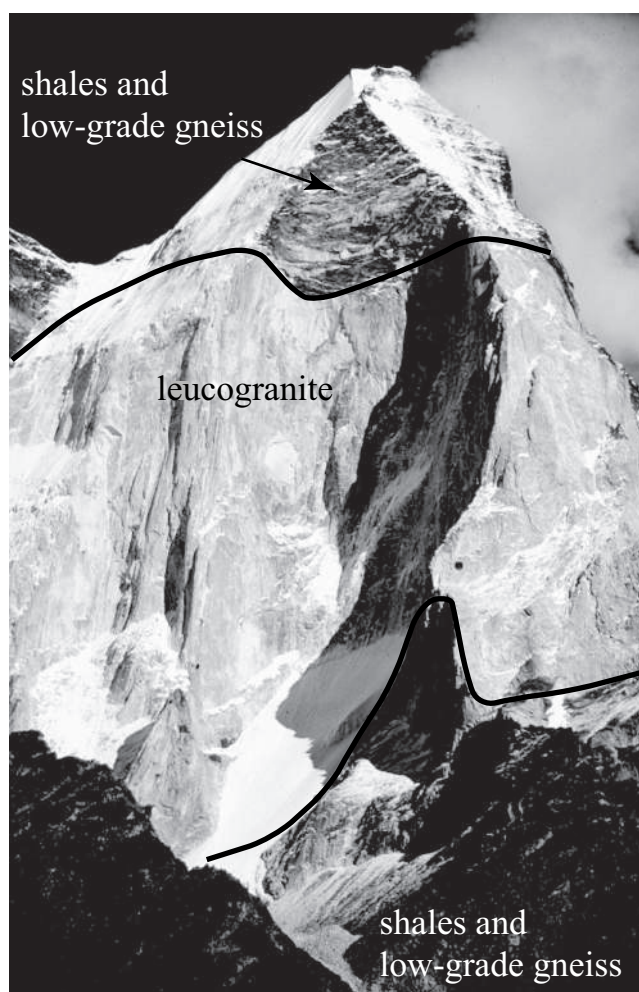
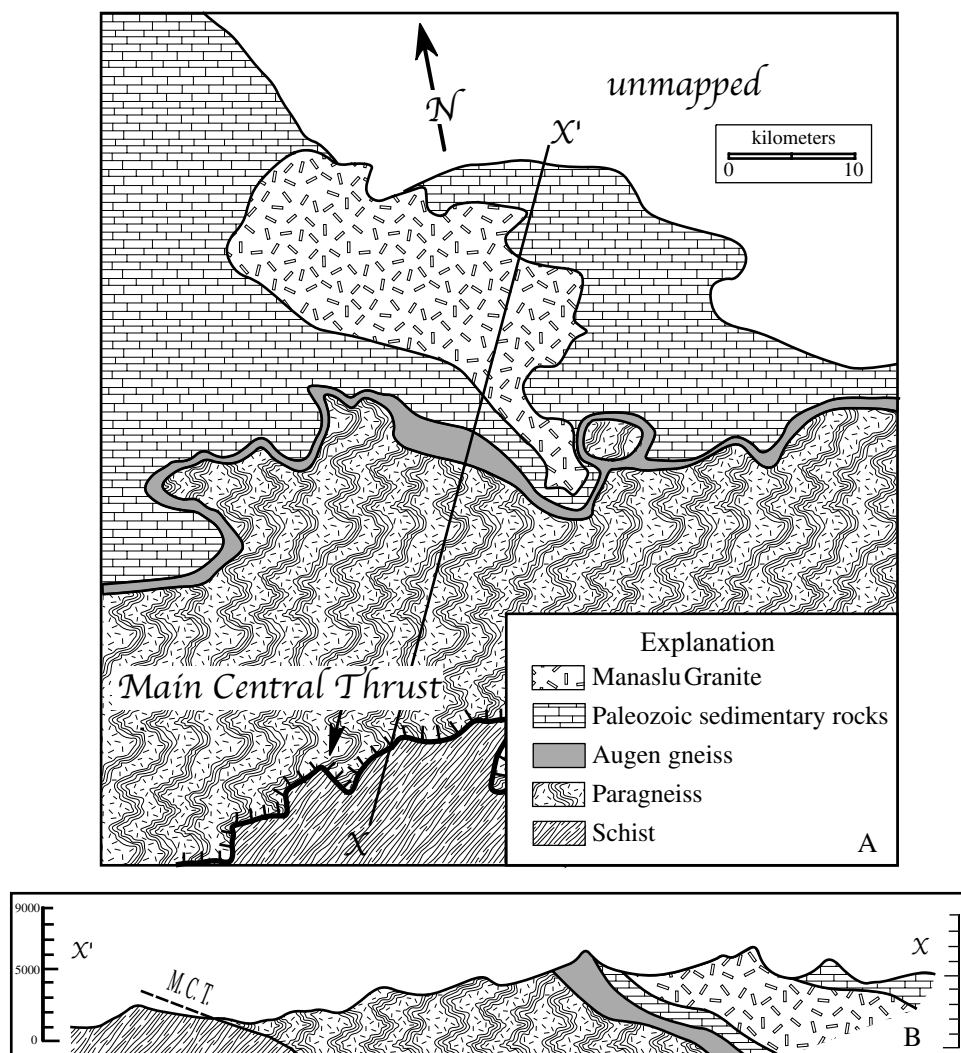


Figure 10.2 South face of Bhagirtahi III, showing fifteen-hundred-meter-thick tourmaline-garnet and two-mica bearing leucogranite sill, Garhwal Himalaya, North India. The high-grade layered gneisses below contain kyanite and/or sillimanite, whereas the rocks above are low-grade shales locally with andalusite. Photo by Mike Searle.

(Strong and Hamner, 1981; Patiño Douce, Humphreys, and Johnston, 1990).

10.4 Caledonian Granites

Early geologists studying the geology of Great Britain recognized a suite of granitic rocks emplaced late in the history of the Caledonian orogeny. The Caledonian orogeny involved the collision of two continents, Europe and North America, during the Ordovician to Early Devonian. During the final stages of this orogeny, a



Map 10.1 Geologic map of the Manaslu granite after Colchen, Le Forte, and Pecher (1980). Inset at bottom gives cross-section along the line X-X', modified from Pecher (1989).

number of relatively small granitic plutons intruded the metamorphosed Precambrian rocks of northwestern Scotland (Map 10.2). These granites have been termed “post-orogenic” because they were emplaced late in the Caledonian orogeny around twenty million years after Laurentia (North America) collided with Baltica (Europe) (Atherton and Ghani, 2002). The term *Caledonian granite* is preferred in this text because this description carries no tectonic implications.

10.4.1 The Etive Granite

An example of Caledonian granite is the Etive granite of Scotland (Map 10.3). The map of the Etive granite shows several features characteristic of many Caledonian granites. First, like the Tuolumne pluton (Map 7.5), it is zoned

with mafic units located on the margin and more evolved rocks in the center. Second, it locally intrudes the volcanic rocks exposed in Glen Coe that were erupted as part of the Etive magmatic event. Although portions of the Sierra Nevada batholith contain roof pendants of coeval volcanic rocks, most plutons in the Sierra Nevada, including Tuolumne, intrude other plutonic rocks; their coeval volcanic rocks have eroded away. The presence of volcanic rocks associated with the Caledonian granites is a manifestation of the fact that the Caledonian granites tend to form small, isolated plutons (Map 10.2) rather than coalescing into the giant batholiths, like the Cordilleran granites. Third, the Etive granite contains a substantial volume of true granite, unlike the Tuolumne, which is dominantly granodiorite (Map 10.3).

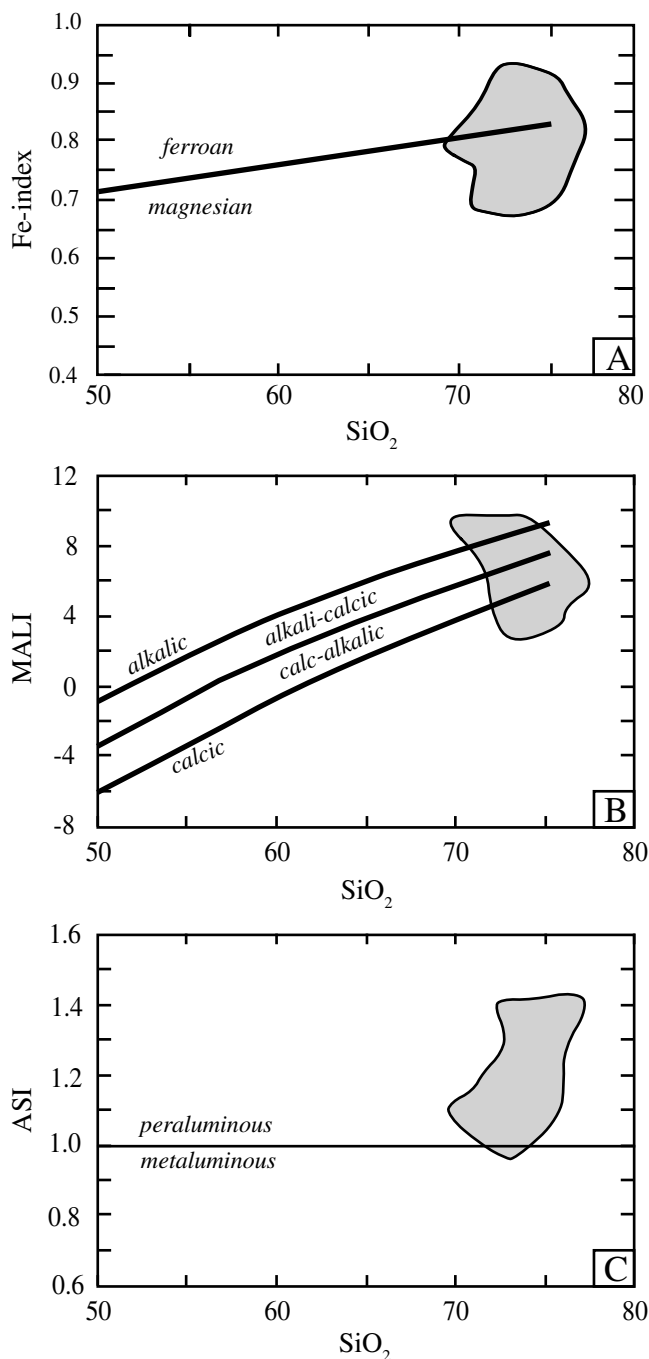
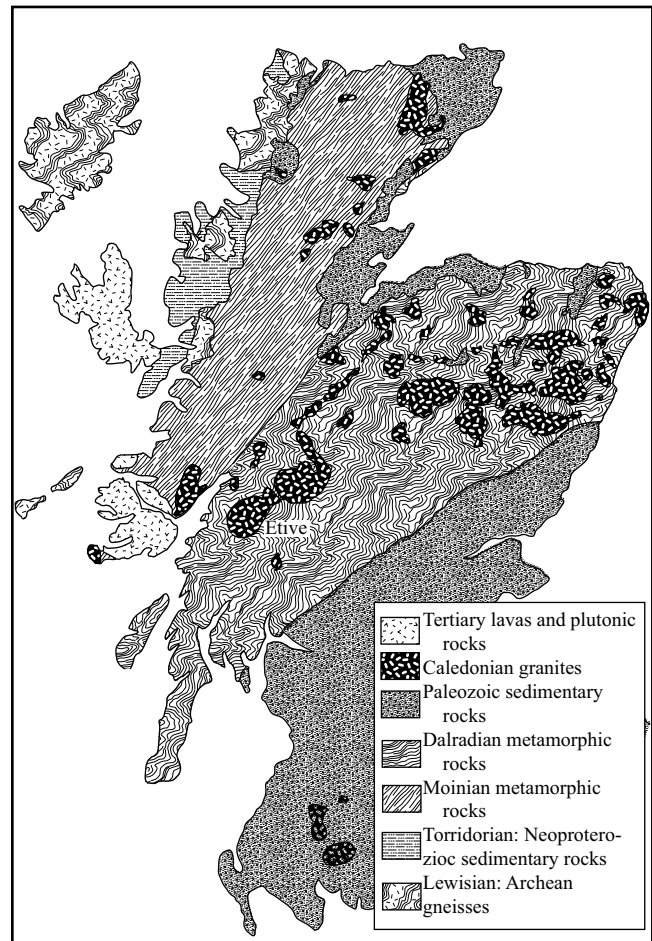


Figure 10.3 Chemical characteristics of peraluminous leucogranites (Frost et al., 2001).

10.4.2 Geochemistry and Origin of Caledonian Granites

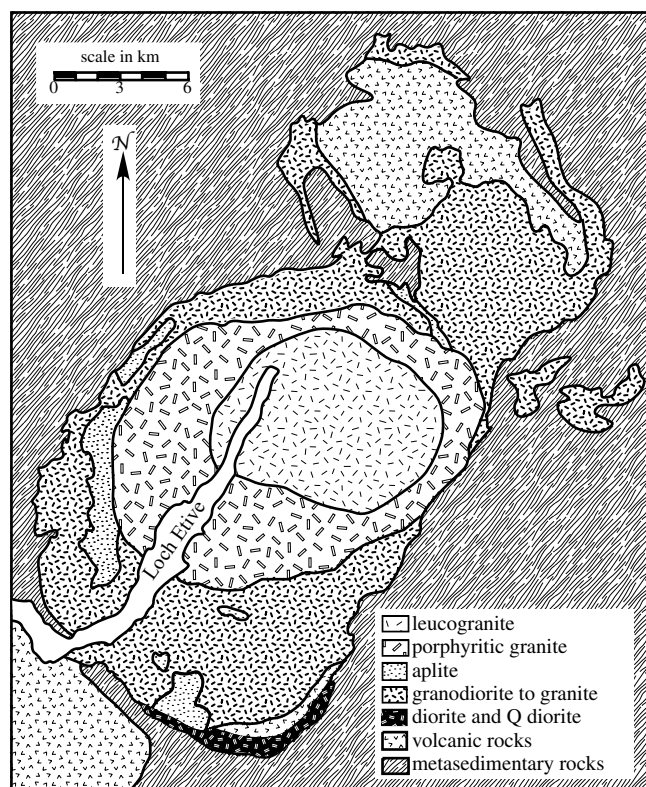
Chemically, the Etive granite is distinct from the Cordilleran granites (Figure 10.4). Whereas both are magnesian, the Etive granite is more potassic. On the MALI diagram (Figure 10.4B), the Etive granite is mainly



Map 10.2 Geologic map of Scotland showing the locations of the Caledonian granites.

alkali-calcic, rather than calc-alkalic or calcic. Possible equivalents to these post-collisional granites related to the Caledonian orogeny include Cenozoic volcanic bodies found in the Tibetan Plateau (Arnaud et al., 1992). Continent-continent collision zones, including the Caledonides and Himalaya, produce dramatically thickened crust.

Caledonian granites like the Etive are thought to form through the process of **crustal delamination**. In areas of continental collision, the base of the thickened lithosphere metamorphoses at very high pressures, producing very dense rocks. These rocks are denser than the mantle beneath them and therefore may delaminate and sink into the mantle (Bird, 1979). Hot asthenospheric mantle moves upward to replace the delaminated lithosphere and undergoes decompression melting. These melts intrude, heat, and partially melt the crust, ultimately producing the



Map 10.3 Geologic map of the Etive granite after Frost and O'Nions (1985).

plutons we see as Caledonian granites. This model could explain why the Caledonian granites occupy a smaller volume than do the Cordilleran batholiths. The Sierra Nevada formed above a subduction zone in a magmatic event that was active for more than eighty million years. During this time, individual plutons were continuously intruded, eventually forming a coalescing mass. In contrast, the delamination episode following the Caledonian orogeny was probably relatively short-lived, and hence there may have been insufficient time to produce the interlocking plutons overlying continental magmatic arcs.

10.5 Review of the Four Major Granite Types

As noted previously, petrologists recognize four distinct environments in which granites are generated. In order of decreasing volume of magma produced these include the magmatic arc (or Cordilleran-type) granites, inter-continental rift (or ferroan granites), post-collisional (or Caledonian-type) granites, and leucogranites (or Himalayan-type granites) formed from continental

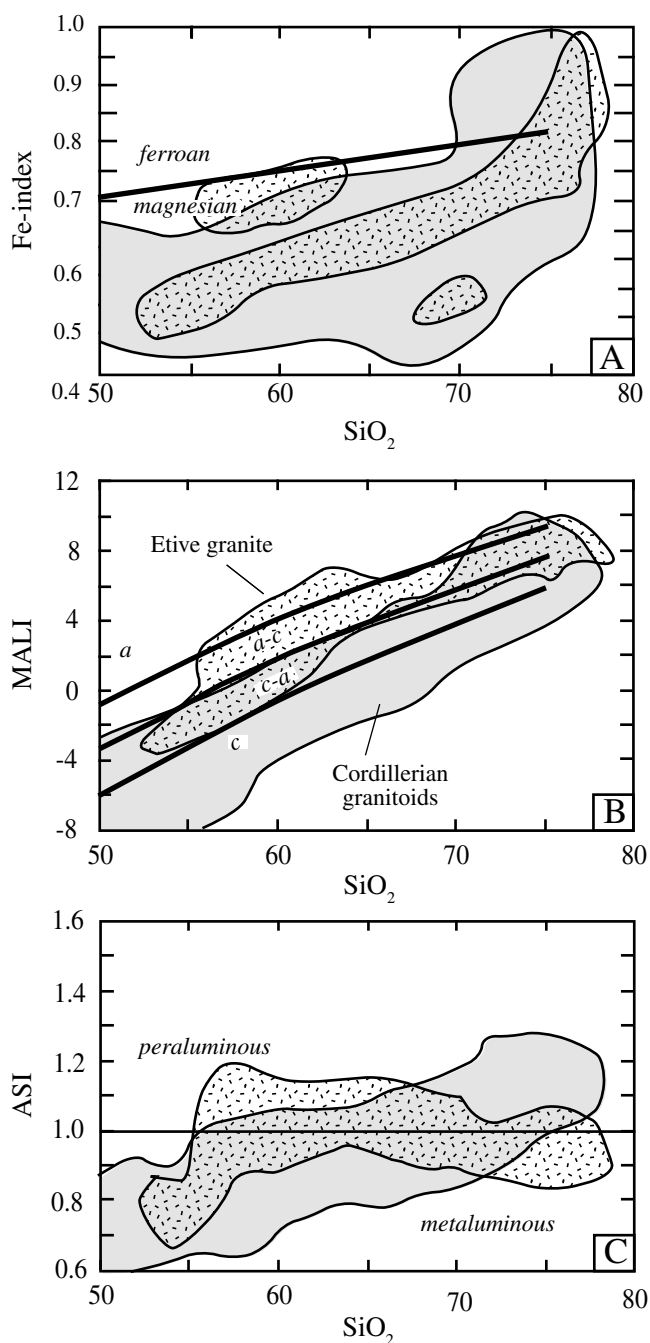


Figure 10.4 Comparison of the chemical characteristics of Caledonian-type Etive granite (stippled area) with Cordilleran granites (shaded area) (Data for Etive from Frost and O'Nions, 1985; data for Cordilleran granites from Frost and colleagues, 2001).

collisions (Table 10.1). For the most part, these granite groups are geochemically distinct (Figure 10.5), which allows geologists to assign a tectonic context to ancient granitic rocks even in a situation lacking other geologic evidence. Cordilleran granitic rocks tend to be magnesian

Table 10.1 The Four Major Granitic Rock Types in Order of Decreasing Relative Abundance

Granite Type	Tectonic Environment	Composition Type	Other Names
Cordilleran	magmatic arcs	magnesian calc-alkalic and calcic granitic rocks	Calc-alkalic, I-type
Ferroan	intercontinental rifts	ferroan alkali-calcic to calc-alkalic granitic rocks	Anorogenic or A-type granites
Caledonian	post-collisional orogens	magnesian alkali-calcic granitic rocks	
Himalayan	continent-continent collision zones	peraluminous leucogranites	S-type

and calcic to calc-alkalic. They are magnesian because of early magnetite crystallization and relatively calcic since they are intruded into the roots of an arc where the crustal rocks are basaltic or andesitic, and hence poor in K-feldspar. Ferroan granites are iron rich because they contain significant portions of melt that has undergone extensive fractional crystallization in reducing conditions. They range from alkalic to calc-alkalic depending on how much crustal material has been assimilated. Caledonian granites are magnesian and alkali-calcic to alkalic. Their relatively high potassium content probably reflects deep, basaltic sources for these granitic rocks because, as was argued in Chapter 7, deeper melting produces higher K-content in arcs. Finally, peraluminous leucogranites are silica-rich, peraluminous, and their geochemistry ranges widely in both the Fe-index and the modified alkali-lime index.

Although the compositional trends outlined here are generally applicable, there is quite an overlap in the fields of the various geochemical families. This is particularly evident at high silica contents where a significant population of Caledonian and Cordilleran granites are ferroan and a significant population of the ferroan granites are calc-alkalic. A good explanation for this overlap is that the silica-rich magmas for all groups probably contain a significant amount of crustal-derived melt, as indicated by the fact that many Cordilleran, ferroan, and Caledonian granitic rocks with high silica are peraluminous. Mixing of crustal melts into the fractionation trend of Cordilleran, ferroan, or Caledonian magmas will produce the overlapping compositions shown in Figure 10.5. Some pegmatites formed from fluid-rich, siliceous magmas contain strategic metals and industrial minerals (Box 10.2).

Because of their geochemical differences, these four granite types follow distinct trends on a Q-A-P diagram (Figure 10.5). As noted in Chapter 7, Cordilleran batholiths, being relatively rich in CaO, follow trends characterized by an increase in quartz and only moderate increases

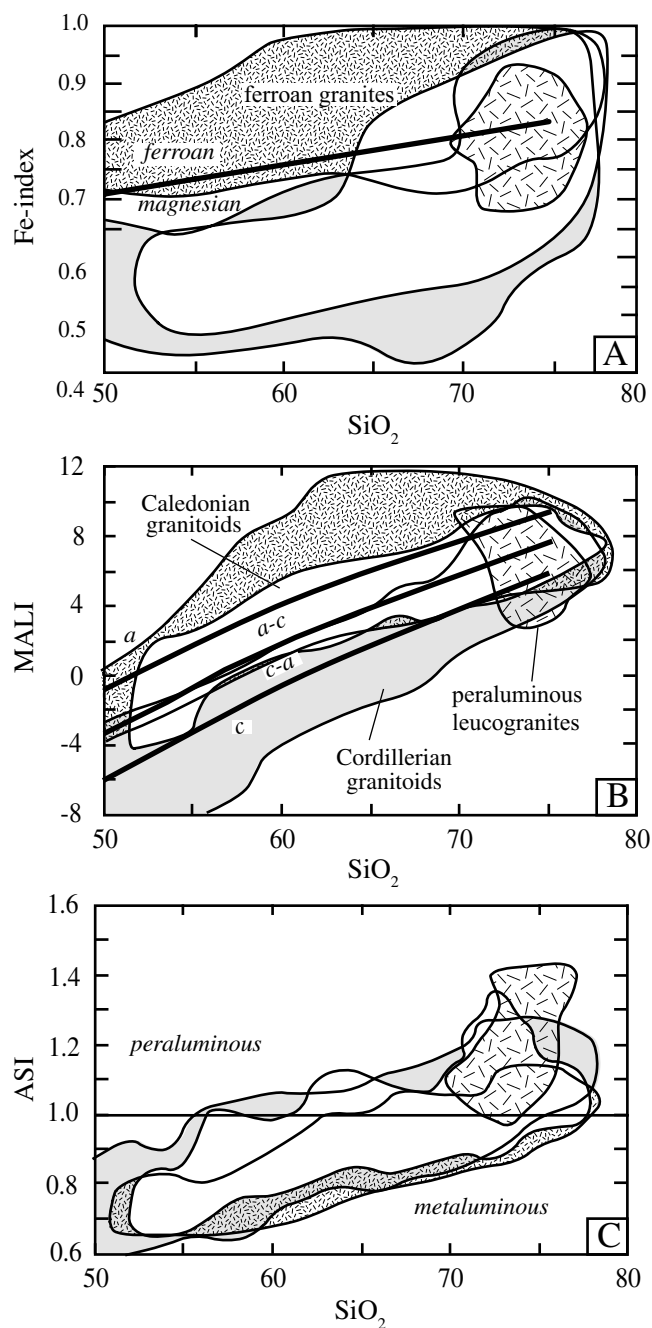


Figure 10.5 Comparison of the geochemical characteristics of peraluminous leucogranites, Caledonian granites, ferroan granites, and Cordilleran granites (Frost and colleagues, 2001).

BOX 10.2 | GRANITE PEGMATITES

Pegmatites are coarse-grained dikes or segregations that usually have a granitic composition. Most form from fluid-rich granitic magma enriched in elements that are not incorporated into rock-forming minerals during crystallization of a pluton. A small fraction of the world's pegmatites contain uncommon minerals, including gem-quality beryl, tourmaline, topaz, spodumene, and spessartine. Pegmatites are also important sources of industrial minerals and strategic metals.

Some of the most spectacular gemstones occur in cavities in the coarse interior of pegmatites. Crystallization of feldspars and quartz from granitic magma enriches the residual melt in elements that are excluded from those minerals. Water and other volatiles may exsolve from the melt as crystallization continues or as the magma ascends to lower pressure. Minerals growing in the volatile-rich cavities may develop into beautifully euhedral, gem-quality crystals (Simmons et al., 2012).

The feldspars, quartz, micas, and Li-pyroxene in pegmatites are important industrial minerals. Most feldspar is used for ceramics and glass manufacture, but it is also used as a filler in paint and plastic and as an abrasive in household cleansers. Quartz is important in the manufacture of all types of glass. High-purity quartz is used in a number of industrial applications, supplying a high thermal stability filler. In



Box 10.2 Gigantic crystals of spodumene are exposed in the walls of the Etta Mine, Keystone, South Dakota. The molds of two large spodumene crystals in this photo are more than ten meters long and their thickness approaches one meter. The mine was opened in 1883 as a mica mine, and spodumene was mined from 1898 to 1959. This photo appeared in a 1916 USGS report by Schaller (1916). USGS photo library image file: /html/lib/btch368/btch368j/btch368z/swt00066.jpg.

(continued)

BOX 10.2 (CONT.)

the past, mica from pegmatites was used as window material, particularly in stoves and ovens. Now it is used in coatings, lubricants, and fillers. Spodumene is used in ceramics, and is also an important source of lithium, a strategic metal that is in growing demand for batteries and pharmaceuticals (Glover, Rogers, and Barton, 2012).

In addition to providing a source of Li, pegmatites host other strategic metals including beryllium, tantalum, cesium, and rare earth elements. The strategic metals in a pegmatite appear to correlate to the type of granite with which the pegmatite is associated. Peraluminous granites that have incorporated metamorphosed juvenile sedimentary rocks tend to form pegmatites enriched in Li, Cs, Ta, B, P, and F. Ferroan granites are associated with pegmatites rich in rare earth elements, Nb, U, and Th. In contrast, Cordilleran and other arc granites are largely devoid of pegmatites (Cerny, London, and Novák, 2012).

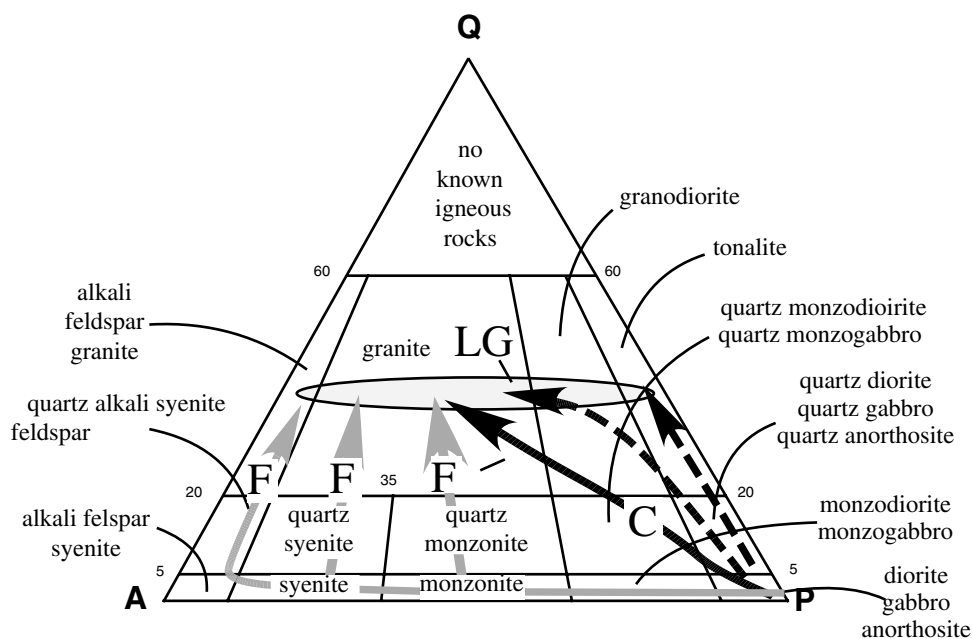


Figure 10.6 QAP diagram showing the differentiation path followed by various granite types. Dashed lines = granites of Cordilleran batholiths, C = Caledonian granites, F = ferroan granites, and LG = peraluminous leucogranites.

in potassium feldspar (dashed lines in Figure 10.6). The dominant rock type in these intrusions is tonalite or granodiorite. Himalayan-type granites (i.e., peraluminous leucogranites) have high quartz content but show a range in feldspar composition, from nearly pure albite (i.e., leucotonalite) to nearly pure microcline (i.e., alkali feldspar granite) (stippled field in Figure 10.6). Because Caledonian plutons are more alkalic than Cordilleran plutons, they contain granitic rocks that follow a more potassic path during differentiation (path C in Figure 10.6). The end product

is abundant granite rather than granodiorite, and the less-differentiated portions may contain quartz monzodiorite and monzogabbro rather than quartz diorite and gabbro. Ferroan granites may follow a range of paths, depending on the alkali content of the parent basalt from which they differentiated and the extent of crustal assimilation (gray arrows in Figure 10.6; Frost and Frost, 2013). A tholeiitic host trend from monzonite to granite, whereas progressively more alkalic hosts follow paths involving syenite or even alkali feldspar syenite.

Summary

- Granites may be classified according to a number of schemes:
 - The mineralogical classification is based on the proportion of quartz, alkali feldspar, and plagioclase;
 - The classification based on opaque oxides evaluates the presence or absence of magnetite and reflects the oxidation state of the magma;
 - The alphabetic classification emphasizes the inferred origin of the granite, whether from igneous sources (I-type), sedimentary sources (S-type), or formed in an anorogenic environment (A-type); and
 - The major element geochemical classification discriminates groups of granites based on four indices, including the Fe-index, modified alkali-lime index, aluminum saturation index, and alkalinity index.
- Peraluminous leucogranites are high-silica granites formed by partial melting of continental crust, commonly in continent-continent collision zones. Granitic melt is produced by dehydration melting of metamorphosed crustal rocks brought to high temperature by processes that may include crustal thickening, radioactive heating, and frictional heating. Coeval mafic rocks are not associated with peraluminous leucogranites.
- Caledonian granites are alkali-calcic, magnesian granites that post-date collisional events. They may be related to crustal delamination. Ascending mantle may melt by decompression and interact with the crust to form these relatively small, compositionally zoned plutons and associated volcanic rocks.
- The compositional differences between peraluminous leucogranites, Caledonian granites, ferroan granites, and Cordilleran granites reflect their magma sources and subsequent differentiation.

Questions and Problems

Problem 10.1. What is the difference between “granite” and “granitic rock”? Do any of the four types of granitic rock suites described in this chapter consist solely of granite?

Problem 10.2. Explain the trend to more peraluminous compositions with increasing silica shown in Figure 10.5.

Problem 10.3. What tectonic environment may produce granites with the greatest involvement of continental crust? Which may produce granites with the least involvement of continental crust? Explain.

Problem 10.4. Using the maps of granitic intrusive complexes in Chapters 9 and 10 as a guide, what tectonic environments appear to produce the largest volumes of granitic rocks? Why is this so?

Further Reading

- Barbarin, B., 1999, A review of the relationships between granitoid types, their origins and their geodynamic environments. *Lithos*, 46, 605–26.
- Clarke, D. B., 1992, *Granitoid rocks*. Chapman and Hall, London.
- Pitcher, W. S., 1997, *The nature and origin of granite*. Chapman and Hall, London.
- Whitney, J. A., 1988, The origin of granite: The role and source of water in the evolution of granitic magmas. *Geological Society of America Bulletin*, 100, 1886–97.

Chapter 11

Introduction to Metamorphic Petrology

11.1 Introduction

Metamorphic petrology studies rocks that recrystallized in the solid state within Earth's crust or, rarely, within the upper mantle. In most instances, recrystallization of rocks within the crust involves deformation, because deformation enhances mineral reactions by introducing strain energy and by opening pathways for fluid movement. As such, metamorphic petrology overlaps with the field of structural geology. Many ore deposits form from hydrothermal fluids at temperatures well below those of igneous activity. Consequently, the study of the reactions between these ore fluids and the country rocks can be included within the realm of metamorphic petrology.

As with igneous petrology, metamorphic petrology involves the study of the mineralogy of metamorphic rocks.¹ Metamorphic petrologists use the minerals present in a metamorphic rock to determine what its parent was (i.e., the **protolith**) and to estimate the conditions of metamorphism. Unlike igneous petrology, metamorphic petrology does not rely heavily on whole rock geochemistry. Whereas variations in chemistry may provide important information about the origin and evolution of igneous rocks, chemical variations in metamorphic rocks merely change the relative abundance of minerals in the rock and provide very little information about metamorphic conditions. For example, a basaltic rock metamorphosed at moderate grades will have the assemblage hornblende – plagioclase, regardless of whether the parent rock was an alkali basalt, tholeiite, or andesite, but the relative proportions will vary with the composition of the rock. This portion of the text first shows how petrologists use mineral associations to estimate conditions of metamorphism. It then describes in detail the mineralogical changes that occur with increasing metamorphism in rocks derived from basalt, peridotite, shale, and carbonates. Finally, the discussion closes with a chapter on the tectonic environments of metamorphism.

This chapter introduces terms important to the discussion of metamorphism and metamorphic rocks. The next chapter (Chapter 12) approaches metamorphic rocks through the interpretation of metamorphic phase diagrams and petrogenetic grids. After these tools are introduced, Chapter 13 discusses the metamorphism of mafic rocks and metamorphic facies. Metamorphic facies, which establish the relative temperature and pressure conditions of metamorphism, were introduced long before petrologists had the ability to quantify

temperatures and pressures from metamorphic mineral compositions. Chapter 14 covers **thermobarometry** – the quantitative estimate of metamorphic conditions and describes the P and T conditions that constitute metamorphism. After this the text describes how pressure, temperature, and fluid composition affect the metamorphism of major protoliths, starting with peridotites, which are chemically the simplest (Chapter 15). Subsequently more complex systems are discussed, such as pelitic rocks (Chapter 16). Attention then turns to how mineral assemblages, especially those in calc-silicate rocks, monitor fluid composition (Chapter 17). Finally, the text describes environments where various types of metamorphism are found and the tectonic significance of various types of metamorphic belts (Chapter 18).

11.2 The Scope of Metamorphism

Sedimentary rocks usually contain minerals such as clays and carbonates that contain substantial volatiles (H_2O or CO_2) incorporated in their structures. As a result, volatile-bearing rocks are stable only in low-temperature environments. Should these rocks be subjected to higher temperatures, be it by sedimentary or tectonic loading or by intrusion of magmas, these low-temperature minerals will react by releasing all or part of their volatile constituents. In a similar manner, should igneous rocks, which typically are dominated by anhydrous minerals, interact with fluids after solidification from the melt, new minerals will form that are more stable in lower-temperature, hydrous conditions. Thus, in the core of any orogenic belt where sedimentary and igneous rocks have been deformed at particular temperatures and pressures, the rocks present will be those that equilibrated in the solid state at metamorphic temperatures and pressures. Understanding how these reactions occur and how the fabric and mineralogy of metamorphic rocks reflect the conditions under which the rocks formed is the field of metamorphic petrology.

To provide a simple definition, *metamorphism* is the recrystallization of a rock at conditions below those of the liquidus. At low temperatures, metamorphism merges with the process known as **diagenesis**, which are the changes that occur during cementation of sedimentary rocks. Diagenesis involves reactions in the pore space of sedimentary rocks, with little or no participation of the clastic grains. For the sake of simplicity, the boundary between diagenesis and metamorphism can be described to lie

at those conditions where the clastic grains significantly participate in the mineral reactions. At high temperatures, metamorphism overlaps with igneous processes at conditions where melts are generated. The process of partial melting of rocks is called **anatexis**. The melts generated by this process are true igneous rocks, while the residue left behind after extraction of the melt, a rock known as the **restite**, is a metamorphic rock. The rock is metamorphic because the minerals in a restite, although they may have been in equilibrium with the melt, did not crystallize directly from it.

11.3 Types of Metamorphism

Several types of metamorphism have been recognized out of the continuum of subsolidus reactions that occur in the crust. The most common types are regional, contact, burial, dynamic, and hydrothermal metamorphism.

11.3.1 Regional Metamorphism

Regional metamorphism is metamorphism on a regional extent. It is usually related to orogeny and accompanying deformation. A geologic traverse across the Alps, Himalaya, or the Canadian Rockies would reveal metamorphic rocks in the core of the ranges where rocks were subjected to deformation and metamorphism at the time the mountains were forming. Similarly, a traverse inland from the coast of California would document rocks deformed and metamorphosed during accretion of sediments along the west coast of North America in the Mesozoic. The metamorphic terrain in these areas is typical of the scale of regional metamorphism.

11.3.2 Contact Metamorphism

Intrusion of magmas into the crust brings heat to mid- or upper-crustal levels. This heat contact metamorphoses in the country rock adjacent to the intrusion. Contact metamorphism is localized to the area adjacent to the intrusion. At high crustal levels, rocks that have undergone contact metamorphism are not deformed, but in deep environments the rocks may be deformed and contact metamorphism may grade into regional metamorphism.

11.3.3 Burial Metamorphism

At increasing depth within a deep sedimentary basin the temperature and pressure increases simply because of regional heat flow. The study of the effect of heating on the

diagenesis of sedimentary rocks in deep basins is key to the understanding the origin petroleum, but if the basin is deep enough the temperature exceeds those of petroleum generation and enters the realm of metamorphism. Areas that have undergone burial metamorphism typically have been subjected to the lowest grades of metamorphism and have not been deformed.

11.3.4 Dynamic Metamorphism

Most rocks in Earth's crust are not in equilibrium with the temperature and pressure conditions at which they now reside. Most granitic crust contains assemblages that equilibrated at temperatures of 600°C or more. Although the rocks may now be at shallower depth and lower temperature, most areas will show no sign of reacting to lower-temperature minerals (i.e., undergoing **retrograde metamorphism**). Because the crust is generally dry, there commonly is no water available to react and produce low-temperature hydrous assemblages. However, during deformation of deep crustal rocks, hydrous fluids migrate into deformation zones and interact with the fine-grained minerals in protolith. The consequence is dynamic metamorphism, a localized zone of retrograde metamorphism that may extend from a shear zone several meters into the surrounding undeformed rocks.

11.3.5 Hydrothermal Metamorphism

In many geologic environments, the presence of magma near the surface of Earth leads to the circulation of hot water through the upper crust, which triggers hydrothermal (i.e., hot water) metamorphism. The water reacts with the original rock-forming minerals, such as feldspars, pyroxenes, and amphiboles, to make micas and clays. Commonly this type of metamorphism is associated with the deposition of sulfide ore minerals to make hydrothermal ore deposits. Good examples of areas where hydrothermal processes are taking place today are the mid-ocean ridges or the thermal features of Yellowstone National Park.

11.4 Basic Goals of Metamorphic Petrology

In general a petrologist will ask three questions about a metamorphic rock:

- 1) **What was the protolith?** (i.e., what were the parent rocks?)

Were they igneous or sedimentary rocks and what kind of igneous and sedimentary rocks were they?

- 2) **What were the conditions of metamorphism?**

At what temperature and pressure did the metamorphic rock crystallize?

What was the composition of the fluid present at the time of crystallization?

Was the metamorphism isochemical? (i.e., did the rock change composition during metamorphism?) Were major chemical components added to or extracted from the rock in a process called **metasomatism**?

- 3) **What was the structural history of the rock?**

Is the rock undeformed or was it subjected to **penetrative deformation**, deformation that affects the rock at all scales?

If it was deformed, did the deformation take place before, during, or after the metamorphic minerals crystallized?

Petrologists use the textures and fabric of the rock and the minerals present to answer these questions. The mineralogy gives clues to the nature of the protolith and is the major feature used to determine the conditions of metamorphism, whereas the textures and fabric of the rock give information relevant to answering all three of these questions.

11.5 Identification of Protolith

11.5.1 Rocks of Clearly Sedimentary Parentage

The first question a petrologist asks with regard to the protolith is whether the parent rock was sedimentary or igneous. In weakly metamorphosed rocks where the original igneous or sedimentary textures and structures of the rock are readily recognized, this question is readily answered. In high-grade rocks, where the original textures and structures commonly have been obliterated, the petrologist must infer whether the protolith was sedimentary or igneous from the mineralogy of a rock. The distinction between an igneous or sedimentary protolith will be difficult in high-grade rocks if the original sediment was immature. In an active tectonic environment, igneous minerals in a rock are disaggregated by mechanical weathering and are incorporated in sediments with

Table 11.1 *Clearly Sedimentary Protoliths*

Rock type	Characteristics	Parent rock
Quartzite	90–100% quartz	Quartz arenite, chert
Quartzose	> 60% quartz	Sandstone
Pelitic	abundant micas and quartz Al-rich silicates (garnet, Al_2SiO_5 , staurolite), graphite	Shale or mudstone
Semi-pelite, psammite	abundant micas and quartz few Al-silicates	Impure sandstones
Carbonate	abundant calcite or dolomite Ca-Mg silicates: tremolite, diopside	Limestone or dolomite
Iron formation	Magnetite, hematite, quartz Fe-rich silicates, carbonates or sulfides.	Iron formation
Mn-formation	Mn-rich silicates, oxides, or carbonates	Mn-rich chert

little chemical weathering or change in composition. Such immature sediments, if subjected to high-grade metamorphism, may be chemically indistinguishable from a metamorphic equivalent of the igneous source rock.

In a mature sedimentary environment, however, intense weathering is an effective agent of chemical differentiation. The original minerals of the rock react to form clay, quartz, and iron oxides, while sodium and calcium, and to a lesser extent magnesium, ions go into solution. In a continental margin environment these weathering products are deposited as quartz sandstone (**psammite**), shale (**pelite**), carbonate (limestone and dolomite), and evaporites, depending on the sedimentary environment. These sedimentary rocks are so chemically distinctive they can be recognized even after the highest grades of metamorphism (Table 11.1).

The most characteristic feature of metamorphosed mature sediments is that they tend to be quartz-rich and feldspar-poor. Quartz contents ranges from 100 percent in quartzites to less than 50 percent in pelitic rocks; plagioclase and microcline are not abundant in either. As quartz abundance decreases, the abundances of micas, biotite, and muscovite, which represent the original clay components of the protolith, increase, leading to a gradation from quartzose, through psammitic, to pelitic protolith. The psammitic protolith can be recognized because it has moderately abundant quartz and micas but only minor feldspar. Psammitic rocks are often garnet-bearing,

but the presence of other aluminous minerals, such as the aluminosilicates, staurolite, or cordierite, mark the rock as pelitic rather than psammitic.

Another important mineral in many sedimentary rocks is carbonate, mainly calcite and dolomite. Metamorphosed limestones, dolomites, and marls are distinguished by high CaO and MgO and low SiO_2 and FeO. In low- and medium-grade rocks these rocks are identified by the presence of calcite and dolomite. In high-grade rocks, however, dehydration reactions may have removed the carbonates. In such rocks a carbonate-rich protolith can be identified by Ca- and Mg-bearing minerals such as wollastonite, diopside, forsterite, and tremolite. In marls, where the protolith contained abundant clay as well as carbonate, the calcareous identity of the protolith is marked by the presence of Ca-rich minerals such as grossular and epidote.

As with carbonates, other chemical sediments are compositionally distinct and their metamorphic equivalents are easily recognized. Evaporites are rarely preserved in the metamorphic record because the salts are easily dissolved in the metamorphic fluids. Iron formations are distinctive by the interlayering of quartz-rich horizons with zones richer in iron silicates, iron oxides, or iron sulfides. Manganese-formations, which are rich in Mn-oxides or pink Mn-silicates, are metamorphosed equivalents of Mn-cherts and, hence, record metamorphosed deep-water sediments.

Table 11.2 *Igneous Protoliths or Protoliths of Uncertain Parentage*

Rock type	Characteristics	Parent rock
Igneous protoliths		
Ultramafic	Virtually no feldspars, abundant olivine, pyroxenes, amphiboles, or serpentine	Mantle peridotite Ultramafic cumulates
Alkaline	Presence of feldspathoids or sodic pyroxenes and Na-amphiboles	Alkaline lava Nepheline syenite
Protoliths of Uncertain Parentage		
Mafic	Plagioclase + quartz < mafic minerals	Basalt, gabbro, andesite, diorite Immature sandstone Calcareous shale
Quartzo-feldspathic	Quartz + feldspars > mafic minerals	Dacite, rhyolite, granitic rock, arkose, Immature sandstones

11.5.2 Rocks of Clearly Igneous Parentage

Because most igneous rock compositions occur in both immature sediments and igneous rocks, there are few definitively igneous protoliths (Table 11.2). The most important of these select few is the peridotitic protolith. Olivine is easily hydrated to serpentine and serpentine does not persist in a detrital environment. True, there are some spectacular olivine beach sands in Hawaii, but in a sedimentary basin such sands would be hydrated to serpentine, which subsequently reacts with any detrital quartz to make talc. Thus there is no immature sedimentary equivalent to the peridotitic protolith. The presence of olivine- and serpentine-rich rocks therefore indicates that the protolith was either a fragment of the mantle or cumulate peridotites from the base of a layered mafic intrusion. As with peridotites, alkaline rocks do not form immature sediments. Nepheline is more easily weathered than albite, so silica-deficient alkaline rocks are rarely present as sedimentary equivalents. Thus the rare occurrences of alkaline gneisses may be interpreted as metamorphosed alkaline intrusions.

11.5.3 Rocks of Uncertain Parentage

Many sedimentary rocks and igneous rocks have similar geochemical compositions. When metamorphosed, it is difficult to distinguish a sedimentary from igneous protolith. Nevertheless, the metamorphic rocks can be categorized into two broad protoliths: mafic and quartzo-feldspathic (Table 11.2).

Mafic metamorphic rocks broadly classify as basaltic, although andesitic compositions may also be present. These rocks are often called metabasites, and are identified by subequal amounts of mafic minerals (amphiboles or, more rarely, pyroxene) and plagioclase (or metamorphic equivalents). Rocks where feldspars and quartz are more abundant than amphiboles or pyroxene are called quartzo-feldspathic.

11.6 Determination of Metamorphic Conditions

In addition to preserving information about protolith, the mineral assemblage of a rock also may record the conditions of metamorphism, including temperature and pressure of formation and fluid composition present at the time the rock formed. There are four levels of sophistication in this approach: two consider stability of minerals and their assemblages and two others, facies analysis and thermobarometry, combine chemical and environmental variables to deduce metamorphic regime.

11.6.1 Stability Range of Single Minerals

Many metamorphic minerals, such as the aluminosilicate (Al_2SiO_5) polymorphs, have a limited range of P-T conditions over which each is stable. These minerals' occurrence constrains the conditions at which the rock equilibrated.

11.6.2 Stability of Mineral Assemblages

Petrologists can get a more precise estimate of metamorphic conditions by determining the mineral association that was stable in the rock when metamorphism peaked. An association of minerals interpreted to have equilibrated during metamorphism is known as an **assemblage**. Careful study of a suite of rocks may reveal that two or more assemblages are related by a common chemical reaction. The trace of this reaction on a map (or in the field) is known as an **isograd**.

11.6.3 Metamorphic Facies

Metamorphic facies are defined by mineral assemblages repeatedly associated in rocks of varying age and in many places around the globe. Whereas a given mineral assemblage or reaction is applicable only to a specific rock composition, metamorphic facies include all possible protoliths. The facies designation developed into a coarse classification system for metamorphic conditions widely used to describe regional metamorphism.

11.6.4 Thermobarometry

During the past century, technological advances in metamorphic petrology have enabled precise chemical measurements of metamorphic minerals. These data are incorporated into thermodynamic datasets to obtain quantitative estimates of temperature and pressure stability for many mineral assemblages. This field, thermobarometry, transformed metamorphic petrology from a qualitative description of relative stability conditions of mineral assemblages to an essential tool in the modern study of orogenesis.

11.7 Metamorphic Textures

To determine the metamorphic history of a rock, petrologists use metamorphic textures, both as they are observed in hand sample and in thin section. In addition to providing key information about the deformation history of a rock, the texture of a metamorphic rock infers information about the protolith and thus, the rock's metamorphic history. Geologists recognize two types of textures: primary textures, or features formed with the protolith, and secondary textures, those that formed during metamorphism or deformation.

11.7.1 Primary Textures

Primary textures formed during the deposition of sedimentary rocks or during the crystallization of igneous rocks. Some of these textural features survive to surprisingly high metamorphic grades, especially when the texture involves variations in bulk composition.

Sedimentary Textures. One of the most distinctive features of sedimentary rocks is bedding. Following metamorphism, bedding manifest as compositional layering (Figure 11.1A). Especially in a high-grade gneiss, compositional layering may be an important indication of a sedimentary protolith. This guideline is not infallible because a thick greywacke that originally was very poorly bedded may become metamorphosed to a quartzofeldspathic gneiss without layers. Conversely, intense deformation of a homogeneous granite may produce a strongly layered gneiss because the deformation may be focused in high-strain zones that become rich in mica. To determine if gneissic layering is of sedimentary origin, look for thin quartzose, calcareous, or pelitic layers, which are indicative of bedding planes from previously sedimentary rocks.

Many sedimentary textures are destroyed during metamorphism. Cross-bedding is often obliterated because the quartz in the rock recrystallizes at relatively low metamorphic grades. On the other hand, if fine hematite grains blanket the original cross-bedded surfaces, the hematite-decorated cross-bedding may survive to moderate metamorphic grades. Similarly, pebbles in a conglomerate may survive to moderate metamorphic grades, particularly if the pebbles were distinctly different in composition from the matrix (Figure 11.1B, C). The most robust sedimentary feature in metamorphism is graded bedding (Figure 11.1A) because graded bedding involves variations in bulk composition. The lower portion of the graded bed may be quartzose, but the thin, upper layer, which originally consisted of clay, will be pelitic. Because the clay-rich horizons are far more reactive during metamorphism, the clay-rich upper portion of a graded bed may become a relatively coarse-grained pelitic layer, whereas the underlying quartz-rich layer remains relatively fine grained, producing **reverse graded bedding**.

Igneous textures. One of the most important igneous textures that can survive a wide range of metamorphic conditions is tabular feldspar (Figure 11.2A). When crystallizing from a melt, both plagioclase and K-feldspar will

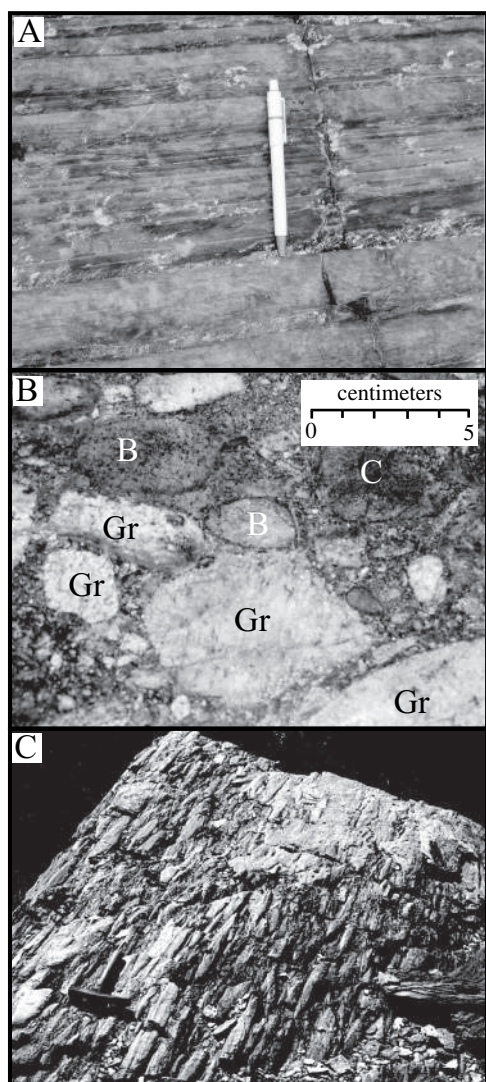


Figure 11.1 Relict sedimentary textures in metamorphic rocks. (A) Turbidite metamorphosed to greenschist facies shows relict graded bedding. Pencil indicates inverted stratigraphic-up direction. Yellowknife, Northwest Territories, Canada. (B) Conglomerate metamorphosed to greenschist facies containing clasts indicated as Gr=metamorphosed granite and granitic gneiss, B=epidotized basalt, and C=chert. (C) Deformed pebble conglomerate from the Raft River Mountains, Utah. Photo by Arthur W. Snoke.

grow as tabular plates that are elongate along the c-axis and flattened along the b-axis. A typical texture in gabbro is shown in Figure 1.7A, wherein tabular plagioclase is surrounded by irregularly shaped pyroxene. Tabular potassium feldspar also commonly occurs as large phenocrysts, in granitic rocks. Tabular feldspars do not grow

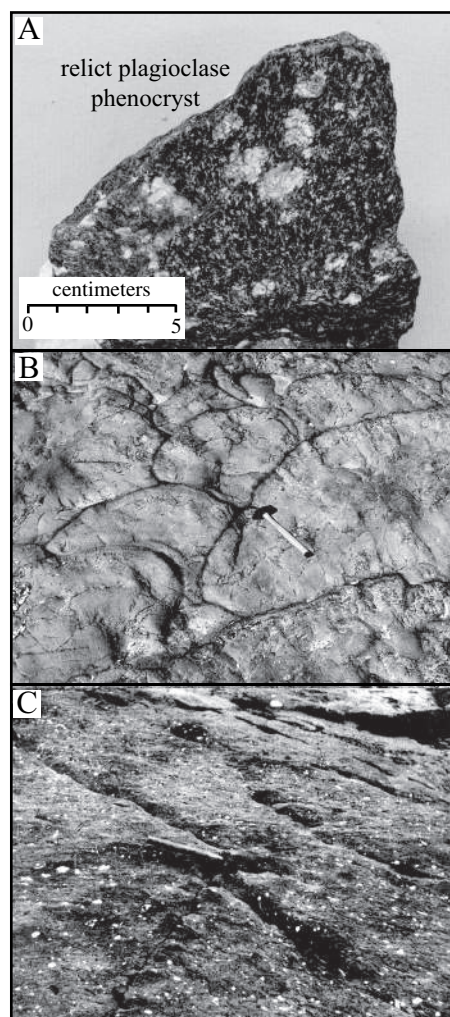


Figure 11.2 Relict igneous textures in metamorphic rocks. (A) Porphyritic diabase metamorphosed in amphibolite facies showing relict plagioclase phenocrysts. From the Laramie Mountains, Wyoming. (B) Greenschist facies pillow basalts from the Smartville ophiolite, northern Sierra Nevada, California. Photo by Arthur W. Snoke. (C) Weakly metamorphosed basalt containing calcite-filled amygdules. Photo from USGS photographic library image Bastin ES 112.

in metamorphic rocks, where surrounding crystals constrain their shape (Figure 11.3A). Thus the existence of tabular feldspars in a metamorphic rock is clear evidence of an igneous precursor. Relict tabular plagioclase allows geologists to recognize an amphibolite as a metadiabase (Figure 11.2A) or metagabbro, and relict tabular plagioclase or potassium feldspar may provide the key in identifying a quartzo-feldspathic gneiss as an **orthogneiss** (a gneiss derived from an igneous parent) rather than a **paragneiss** (a gneiss derived from a sedimentary parent).

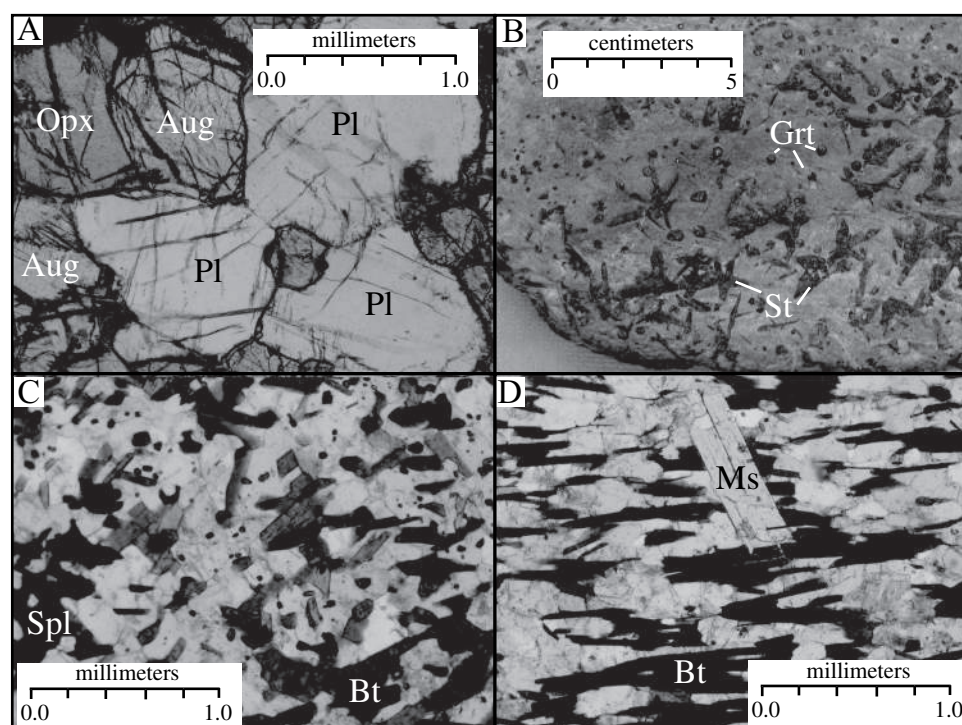


Figure 11.3 Textures in metamorphic rocks. (A) Photomicrograph in plane-polarized light (PPL) showing relations between pyroxene and plagioclase in granulite from southwestern Montana. Note how grains meet at triple boundaries with angles approximating 120° , a texture distinctly different from igneous textures shown in Figure 1.7A, B. (B) Porphyroblasts of garnet (Grt) and staurolite (St) in mica schist from near Taos, New Mexico. (C) Photomicrograph in PPL showing randomly oriented biotite (Bt) from cordierite-corundum-spinel (Spl) – plagioclase-K-feldspar hornfels adjacent to the Laramie anorthosite complex, Wyoming. Light-colored matrix consists of intergrown cordierite, plagioclase, and K-feldspar. Corundum is not shown. (D) Photomicrograph in PPL showing biotite with strong preferred orientation from southern Ontario, Canada. Also present is muscovite (Ms) growing across the foliation defined by the biotite. Matrix consists of quartz and plagioclase.

Another igneous feature likely to survive to high grades of metamorphism are pillow structures that form when basaltic lava is quickly chilled in a subaqueous environment (see Figure 1.7). Pillows survive to high grades of metamorphism because the quickly chilled rims of the pillows are very glassy and are more susceptible to alteration by seawater than the crystalline pillow core. This alteration, which may result in the leaching of alkalis or the oxidation of iron, produces rims compositionally distinct from cores. Because of this compositional difference, pillows can be recognized even in highly metamorphosed and deformed rocks (Figure 11.2B).

Another igneous feature that may survive to moderate grades of metamorphism are vesicles that form on the upper portions of lava flows. In low and medium grades of metamorphism these empty pockets fill with zeolite, calcite, epidote, or prehnite. These minerals form light-colored, rounded spots in a metabasalt called **amygdules**

(Figure 11.2D). Amygdules, though important for determining the metamorphic assemblages in weakly metamorphosed rocks, seldom survive above medium grades of metamorphism.

11.7.2 Metamorphic Textures

Petrologists can use the texture of metamorphic rocks to determine if solid-phase recrystallization took place in a static environment or whether deformation was occurring when the rocks crystallized. Petrologists recognize two broad textures to metamorphic rocks: 1) static textures in which minerals grew without deformation or after deformation had ceased, and 2) tectonic textures in which deformation controlled the distribution and shape of minerals in the rock.

Static Textures. Static textures are characterized by equant and polygonal mineral grains that tend to intersect at triple boundaries separated by three, 120° angles

(Figure 11.3A). This angle, called the **dihedral** angle, is governed by the surface energy of the minerals, which, simply put, is how easily minerals form crystal faces. In a mineralogically simple rock, such as quartzite or dunite where all grains have the same surface energy, the intersections are uniformly 120° ; in polyminerologic rocks the intersections tend to deviate slightly from 120° because each mineral has slightly different surface energy. Some minerals, such as micas, that have strong cleavage will not form the 120° grain boundaries because grain boundaries trend along the cleavage planes of the mineral.

Although euhedral feldspars are indicative of an igneous texture, euhedral crystals can also form in metamorphic rocks. In metamorphic rocks, minerals bounded by crystal faces are called **porphyroblasts** (Figure 11.3B). Porphyroblasts grow by reactions that consume the surrounding matrix and the minerals that make porphyroblasts, such as garnet, staurolite, and aluminosilicates, tend to have low surface energies that favor the formation of rational crystal faces.

Granoblastic textures, such as those shown in Figure 11.3A, are common in metamorphic rocks that have undergone heating without deformation, as in a contact aureole around an igneous intrusion. Usually these rocks are so fine-grained that individual grains are indistinguishable in hand sample. However, the presence of an intimately intergrown crystal network is indicated by a fine-grained rock that resists breaking with a hammer and often breaks along conchoidal fractures. Such a fine-grained rock is called a **hornfels**. The term *hornfels* is entirely a texture term; it may be modified by an compositional adjective such as *pelitic*, *mafic*, or *ultramafic*.

Tectonic textures. If a rock has deformed, the minerals align in a preferred orientation. During deformation, minerals tend to rotate, grow, or nucleate so that they are oriented in a position that most readily accommodates the strain. Thus, unlike in rocks with static textures, minerals in deformed rocks exhibit **preferred orientation**. Figure 11.3C shows an example of a hornfels where the biotite has no preferred orientation; the elongate biotite grains have many possible orientations. This chaos is in contrast to the schist shown in Figure 11.3D, where all the biotite grains are parallel, indicating a strong preferred orientation in response to strain.

The distribution of minerals in a rock and their type of preferred orientation produces several macroscopic textural features. Deformed metamorphic rocks contain

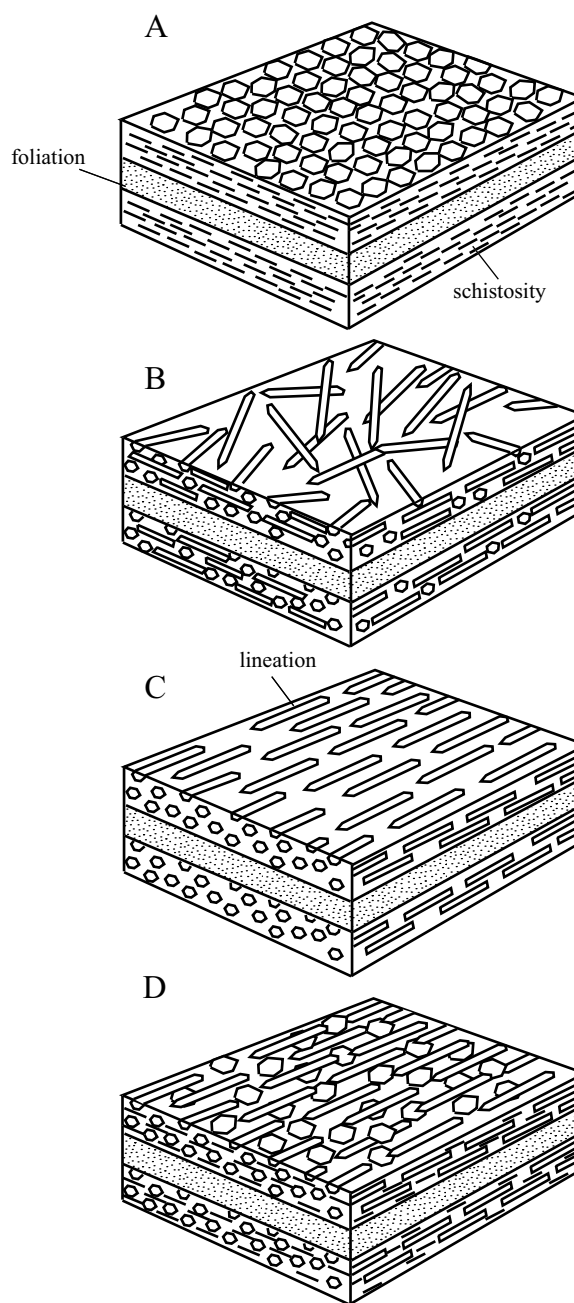


Figure 11.4 Illustrations comparing the relationship between schistosity, foliation, and lineation in metamorphic rocks. (A) Rock with foliation and schistosity. (B) Rock with foliation and weak schistosity marked by preferred orientation of tabular minerals. (C) Rock with foliation and lineation, but no schistosity. (D) Rock with foliation, schistosity, and lineation.

three types of fabric: **foliation**, **schistosity**, and **lineation** (Figure 11.4). *Foliation* is a term to describe any planar feature in a rock, including primary layering, such as bedding, or a secondary planar feature caused by deformation. *Schistosity* describes planar features defined by preferred

orientation of platy or tabular minerals. *Lineation* is a linear feature that may form by preferred orientation of tabular minerals or by intersection of foliation planes. Figure 11.4A illustrates a rock that contains two foliations, a primary bedding plane and schistosity parallel to that bedding. The schistosity is caused by the strong preferred orientation of micas and is recognizable in hand sample because the rocks split along parallel planes mirroring the parallel arrangement of platy mineral crystals. When mica defines schistosity, reflections off the mica cleavage identify the schistose surface. Rocks dominated by less platy minerals, such as feldspars, will not break along the plane of the preferred orientation; in such rocks the texture is called **gneissosity**. Gneissic foliation need not be parallel to the schistosity, as it is in Figure 11.4A; it may be oblique or several sets of foliation may intersect primary foliation at different angles.

Figure 11.4B illustrates a rock with foliation and weak schistosity defined by an elongate mineral (an amphibole) that has its c-axes all lying in the same plane. The c-axes are not parallel so the rock does not display lineation. If the c-axes of the tabular minerals all lie in the same plane and are all pointed in the same direction, then the rock has a lineation (Figure 11.4C). The rock in Figure 11.4C has a foliation and a lineation, but not schistosity. Figure 11.3C provides an example of a lineation defined by relict pebbles stretched into elongate shapes. Finally, if a rock contains both platy minerals, such as mica, and tabular minerals, such as sillimanite, it can develop foliation, schistosity, and lineation (Figure 11.4D). In this book these structural features are defined such that a student can interpret hand samples of metamorphic rocks. The tectonic relations between foliation, schistosity, and lineation is treated more exhaustively in the field of structural geology.

11.8 Naming a Metamorphic Rock

Compared to igneous petrology, naming metamorphic rocks is relatively straightforward. Most metamorphic rock names list of the minerals present, usually in order of decreasing abundance, followed by a rock term that describes the appearance of the rock (Table 11.3). Geologists usually do not prefix the names “slate” or “phyllite” with minerals because these rocks are typically

Table 11.3 Common Rock Names for Metamorphic Rocks

Rock	Characteristics
Structural terms conventionally prefixed by mineral names	
Granofels	Relatively coarse grained rock with equant grains
Hornfels	Massive, fine-grained rock that breaks with a conchoidal fracture
Slate	Very fine-grained rock with a perfect planar cleavage
Phyllite	Fine-grained rock with a silky luster on the cleavage surface
Schist	A strongly schistose rock
Gneiss	Foliated metamorphic rock dominated by feldspars
Rock names that imply a mineral assemblage and protolith	
Greenschist	A foliated mafic rock with actinolite as the major amphibole
Greenstone	A massive mafic rock with actinolite as the major amphibole
Amphibolite	A mafic rock with hornblende as the major amphibole
Blueschist	A mafic rock with sodic amphibole as the major amphibole
Granulite	A mafic rock containing orthopyroxene and clinopyroxene
Eclogite	A mafic rock containing clinopyroxene and garnet
Marble	A rock dominated by calcite and dolomite
Serpentine	An ultramafic rock containing serpentine as the major mineral

so fine-grained that detailed determination of their mineralogy is not practical without X-ray techniques.

An example of a rock name in this classification scheme is quartz-plagioclase-biotite-muscovite-garnet-kyanite schist. If a very small amount of a mineral, say staurolite, was present in this rock, we could call it a staurolite-bearing quartz-plagioclase-biotite-muscovite-garnet-kyanite schist. This cumbersome scheme is often simplified by omitting some of the most common phases. For example, since most schists contain quartz, plagioclase, biotite, and muscovite, the rock named here can also be described as a staurolite-bearing garnet-kyanite schist.

Only a small population of metamorphic rock names exists, many of which apply to mafic rocks and carry an implication of protolith deduced from the metamorphosed assemblage (Table 11.3). These rock names need not be prefixed by any mineral, but the addition of a mineral prefix is often used,

particularly if the prefix provides important information about the metamorphic conditions of the rock. These rock terms are discussed in detail in subsequent chapters that describe how mineral assemblages vary with increasing metamorphic grade for different protoliths.

Summary

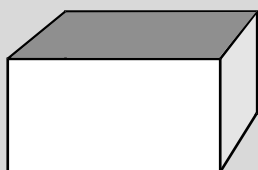
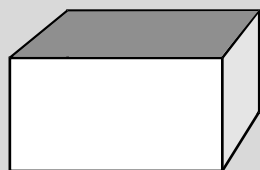
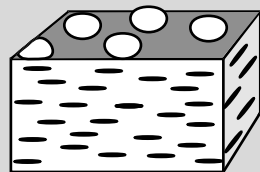
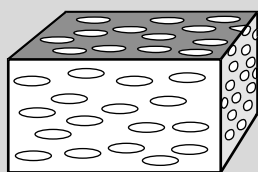
- Metamorphism involves the crystallization or recrystallization of a rock in the solid state and occurs under a range of conditions from diagenesis to the beginning of melting.
- The most common types of metamorphism are:
 - **Regional metamorphism**
 - **Contact metamorphism**
 - **Burial metamorphism**
 - **Dynamic metamorphism**
 - **Hydrothermal metamorphism**
- Metamorphic petrology endeavors to answer three fundamental questions:
 - What was the metamorphic protolith?
 - What were the conditions under which it formed?
- What do metamorphic indicators imply about the structural history of the rock?
- Clearly sedimentary protoliths include
 - **Pelitic** (metamorphosed shale)
 - **Psammitic** (metamorphosed sandstone)
 - **Quartzose**
 - **Carbonate**
- The only common clearly igneous protolith is *ultramafic*
- Protoliths that may have either an igneous or sedimentary source include:
 - **Mafic**
 - **Quartzo-feldspathic**
- Metamorphic conditions can be inferred from:
 - The stability of a single mineral

- The stability of mineral assemblages
- Metamorphic facies
- Thermobarometry
- Metamorphic textures encode evidence about whether a rock was metamorphosed in a static environment or whether it was deformed during metamorphism in a tectonic environment.
- Metamorphic textures also assist protolith determination whether igneous or sedimentary.

Questions and Problems

Problem 11.1. What process marks the high-temperature limit of metamorphism? The lower-temperature and pressure limit of metamorphism? Which limit is easier to define?

Problem 11.2. List the minerals *in order of decreasing abundance* found in a staurolite-bearing quartz-plagioclase-biotite-muscovite-garnet-kyanite schist.



Problem 11.3. How does one distinguish rocks affected by contact metamorphism from those affected by regional metamorphism?

Problem 11.4. What information is used to determine the conditions of metamorphism?

Problem 11.5. What are the diagnostic minerals for the following protoliths?

- pelitic
- metasedimentary
- mafic
- peridotitic

Further Reading

- Fettes, D. and Desmons, J. (eds.), 2007, *Metamorphic rocks: A classification and glossary of terms. Recommendations of the International Union of Geological Sciences Subcommittee on the systematics of metamorphic rocks*, Cambridge University Press, Cambridge, UK.
- Miyashiro, A., 1994, *Metamorphic petrology*. Oxford University Press, Oxford, UK.
- Vernon, R. H., and Clarke, G. L., 2008, *Principles of metamorphic petrology*. Cambridge University Press, Cambridge, UK.
- Winter, J. W., 2010, *An introduction to igneous and metamorphic petrology*, 2nd ed., Prentice Hall, New York, Chapter 21.
- Yardley, B. W. D., 1989, *An introduction to metamorphic petrology*. Longman, Essex, UK.

Notes

- 1 A review of igneous and metamorphic minerals is found in Appendix 1.

Chapter 12

Interpretation of Metamorphic Phase Diagrams

12.1 Introduction

Phase diagrams and chemographic projections are so prevalent in metamorphic petrology that it is rare to find a paper in this discipline that does not contain one. Phase diagrams provide information about the stability fields of mineral assemblages with respect to pressure, temperature, and fluid composition. **Chemographic projections** graphically depict mineral compositions and when used in combination with phase diagrams, help visualize what mineral assemblages occur together at given metamorphic conditions of temperature and pressure. Chemographic projections also aid determination of whether a group of minerals could represent a stable assemblage or whether they must be related by a reaction relationship. Because phase diagrams and chemographic projections are ubiquitous in metamorphic petrology, understanding them is a critical background necessary to master this field of geology.

This chapter details how these graphical approaches can be used to understand the stability of mineral assemblages in rocks. The discussion begins with simple two-component systems and advances to systems with three or more components. The basic rules outlined in this chapter extend to natural rocks, most of which are chemically complex. These rules will be used throughout the rest of the book, which discusses the metamorphism of various protoliths, each of which differs in composition, as can be depicted on different chemographic projections.

12.2 A Little History

The first study that tried to make sense of the mineral relations found in metamorphic rocks was that of George Barrow (1893, 1912), who recognized six metamorphic zones based on the mineral assemblages found in pelitic schists of the Scottish Highlands. Barrow's classification worked well in pelitic rocks but had little relevance to other rock compositions. A few years later, Finnish petrologist Pentti Eskola (1915, 1920) introduced the concept of metamorphic facies, which identified broader categories of mineral assemblages that described metamorphic conditions. At about the same time, the German school of petrologists, headed by Paul Niggli, established a classification of metamorphic rocks based on depth (epizone = shallow, low grade; mesozone = moderate depths, medium grade; katazone = deep level, high grade; Grubenmann and Niggli, 1924). Throughout the twenties and thirties, the German school held sway with the result that metamorphic facies did not gain acceptance until Francis Turner's classic 1948 text on metamorphism. Today the Germanic classification system is all but forgotten except for the term *epizonal*, which is usually applied to plutonic rocks, despite a proposal to revive it in a slightly different form by Winkler (1976).

Beginning in the late fifties and continuing today, metamorphic petrologists have been concerned with determining the relative stabilities of mineral assemblages in various protoliths. The diagrams produced by such studies are known as **petrogenetic grids**. The grids are thermodynamically reasoned and corroborated by high-temperature, high-pressure experimental work. For pelitic rocks, the petrogenetic grids were established by students at Harvard University under J. B. Thompson in the fifties and sixties (see Albee, 1965). Grids for meta-peridotites were developed in the sixties and seventies by B. W. Evans and V. Trommsdorff (see Evans, 1977). Grids for carbonate rocks were developed in the seventies by many workers, including Metz and Trommsdorff (1968) and Skippen (1971).

Although petrologists have long known that metamorphic mineral assemblages preserve information about the composition of the attendant fluid phase, the quantitative use of mineral assemblages for this purpose didn't become important until the explosion of metamorphic petrology in the late 1960s and 1970s. At present, many

studies estimate metamorphic fluid composition, considering this variable as important as pressure or temperature of formation. Among the fluid species petrologists commonly evaluate in metamorphic rocks are H₂O, CO₂, CH₄, sulfur, and oxygen.

The development of the electron microprobe in the mid-1960s revolutionized petrology. Not only did this instrument provide the data necessary to better constrain the petrogenetic grids in P-T space and to determine the composition of the fluid phase, it also led to the development of the disciplines **geothermometry** and **geobarometry** (these terms are often combined to form the name **thermobarometry**). These disciplines use thermodynamics and mineral equilibria to quantify the pressure and temperature conditions of crystallization. Although a detailed treatment is beyond the scope of this book, an introduction to thermobarometry is presented in Chapter 14. This text shows that for many bulk compositions careful use of petrogenetic grids can constrain metamorphic conditions nearly as well as thermobarometry. The evolution of petrogenetic grids and thermobarometry does not necessarily make metamorphic facies obsolete, but it does mean the facies designation is best used in a regional context or as a field term. When dealing with metamorphic rocks on a small scale, it is more helpful to determine conditions, if possible, from petrogenetic grids or thermobarometry.

The development of analytical instruments, including the Super High Resolution Ion Microprobe (SHRIMP) in the 1980s (Compston, Williams, and Meyer, 1984; Williams, 1998) and the laser ablation ICP-MS in the 1990s (Storey, Jeffries, and Smith, 2004), that allow for spatial analysis of minerals and determination of their age and chemical composition led to the development of metamorphic geochronology – the use of accessory minerals to date metamorphic and deformation events. Geochronology is one of the active fields of research in metamorphism today (see, for example, Vance, Müller, and Villa (2003) and promises to provide geologists closer constraints on the duration of tectonic events.

12.3 Use of Chemographic Projections

Sometimes it is possible to write a reaction between all the phases in a particular metamorphic rock. If so, the assemblage is univariant and the reaction traces a line on

a phase diagram or an isograd on a geologic map. Most of the time, however, rocks contain assemblages of higher variance. It is important to find ways to treat multivariant assemblages so it is possible to visualize the pressure, temperature, or fluid compositions that control them. Divariant assemblages are easy to understand in a system with one component, such as the system Al_2SiO_5 , for these assemblages consist of only one phase (Figure 2.1). In systems with more components, however, it becomes progressively more difficult to recognize divariant assemblages merely through inspection. In complex systems, chemographic projections make it possible to recognize divariant assemblages and to find their stability fields in a phase diagram. In chemographic projections, mineral compositions are expressed graphically and the graphical relationship between minerals determines whether they are in a reaction relationship.

12.3.1 Chemographic Projections in a Two-Component System

Consider a hypothetical two-component system consisting of the components $a - b$ and the phases $V = a$, $W = a_2b$, $Y = ab_2$, and $Z = b$ (Figure 12.1; note the convention that components are written in lower case letters, whereas phases are written in capitals). With a little bit of work with pencil and paper, you can show that this system contains the following univariant reactions:



These reactions could potentially intersect at an invariant point, as in Figure 12.2. The diagram in Figure 12.2 is called a **topology**. It shows the arrangement of reactions around an invariant point but does not locate the reactions in P-T space.

Even with a quick glance at Figure 12.2 one can determine where three-phase assemblages such as $W-V-Z$ are stable, since each three-phase assemblage is marked by one of the reactions listed previously. The problem comes when one has a divariant assemblage or suite of divariant assemblages. For example, where would the assemblages WY and YV be stable? This question is answered by locating chemographic diagrams for this system (i.e., Figure 12.1) in each of the divariant fields. Realize that



Figure 12.1 Chemography for the two-component system $a-b$ with phases V, W, Y, Z . The topology for this system is shown in Figures 12.2 and 12.3.

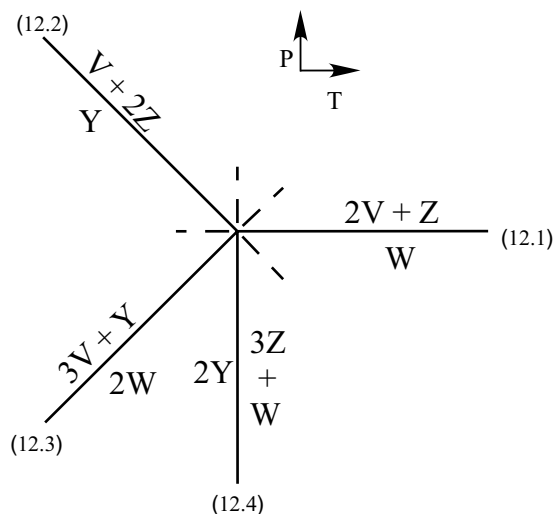


Figure 12.2 Topology for the hypothetical two-component system $a-b$ shown in Figure 12.1.

each reaction is an expression of a change in chemography: two phases react to form one phase (or one phase breaks down to form two others; chemographically they are equivalent). The chemographic expression of a reaction is the appearance (or disappearance) of the product phase on the segment of line that lies between the two reactant phases. For example, consider the reaction (12.1) in Figure 12.2. On the high-pressure side of this reaction, phases $V + Z$ are stable; this means there is a line running from V to Z with no intervening phases. On the low-pressure side of this reaction, W has appeared. Chemographically this means that on this side of the reaction point, W lies between V and Z . Consequently the stable two-phase assemblages in this field are VW and WZ . This is shown in Figure 12.3. Using this rule it is possible to fill in all the rest of the divariant fields in Figure 12.3 with chemographic projections that indicate what two-phase assemblage is stable in each field. With this information added to Figure 12.3, it becomes straightforward to answer the question raised earlier about where WY and YV are stable.

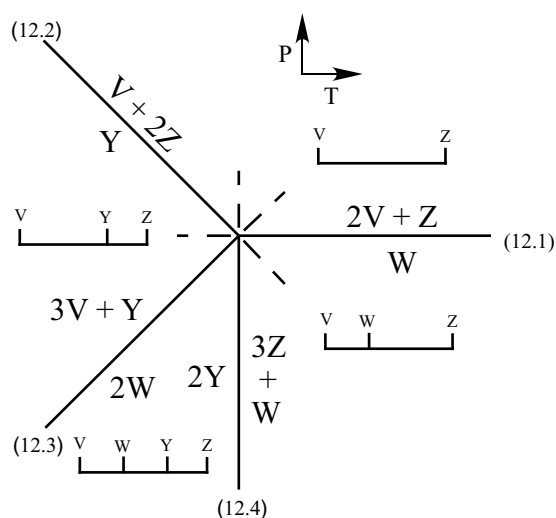


Figure 12.3 Topology for the hypothetical two-component system a-b shown in Figure 12.1., with divariant assemblages identified using chemographic projections.

12.3.2 Chemographic Projections in a Three-Component System

Now consider a hypothetical three-phase system x, y, z containing the phases: $A = x$, $B = xz$, $C = yz$, $D = y$, and $E = x_2yz$. Again, after a little work with a pencil and paper it is possible to balance the following reactions:



The divariant assemblages for a three-component system are expressed chemographically using an equilateral triangle that has one component at each apex. The chemography for the three-component system in question is shown in Figure 12.4. (For rules governing the construction of this figure, see Section 2.3)

Figure 12.5 presents a topology showing how these reactions could be related. The four-phase assemblages make up the five univariant reactions in this system. Chemographic projections are used to determine where three-phase or two-phase assemblages are stable in this system. The chemographic representation of a divariant assemblage in a three-component system is a triangle that has as its apices the three stable phases. Figure 12.6

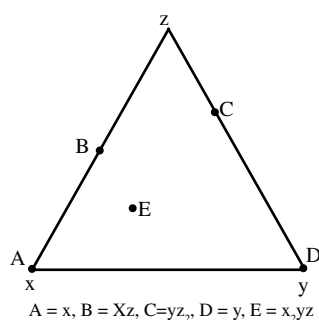


Figure 12.4 Chemographic diagram for a hypothetical three-component system x - y - z .

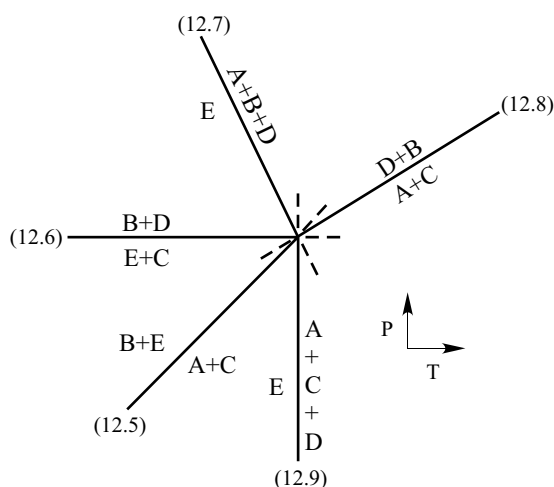


Figure 12.5 Topology for the hypothetical three-component system x - y - z .

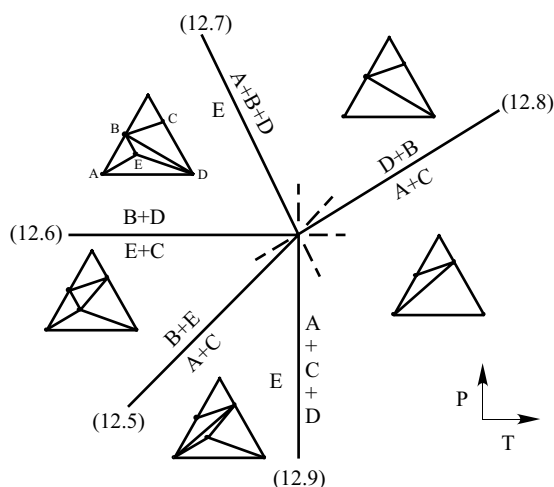


Figure 12.6 Topology for the hypothetical three-component system x - y - z , with divariant assemblages identified using chemographic projections.

provides an illustration of how a topology of a three-phase system is interpreted using chemographic projections.

Consider the field outlined by reactions (12.5) and (12.6) in Figure 12.6. From reaction (12.6) ($4B + 3D = 2E + C$) one can see that the tie line E-C is stable, and from reaction (12.5) ($3A + C = B + E$) it is evident that the tie line B-E is stable. Having established two tie lines, how does one fill in the rest of the triangle? Note that if reaction (12.6) operated on a bulk assemblage with abundant D and small amounts of B, B would be consumed by this reaction, leaving some D remaining along with the products of E + C. This implies that in the divariant field between reactions (12.5) and (12.6) there must be a tie line from E to D. Similar reasoning concerning reaction (12.5) implies that there must be a tie line from E to A. Thus the divariant field between reactions (12.5) and (12.6) contains the following assemblages: B-C-E, C-E-D, A-B-E, and A-E-D.

Once one has determined the divariant assemblages present in one field, the relations in other fields are determined by performing the operation implied by each univariant reaction. For example, in crossing reaction (12.6), the tie line from E to C is broken and a tie line from B to D forms instead. This leads to the chemography shown in the divariant field between reactions (12.6) and (12.7). Note that all the other tie lines shown in the field between reactions (12.5) and (12.6) are unchanged. What happens when one goes from the field bounded by reactions (12.6) and (12.7) to that bounded by (12.7) and (12.8)? Reaction (12.7) says that E reacts out to form A + B + D. Chemographically, that means E disappears within the triangle A-B-D. Since E has disappeared, the tie lines from E to A, B, and D disappear also (Figure 12.6).

A careful study of Figure 12.6 reveals two types of reactions. One type has two or more phases on each side of a reaction. The chemographic representation of this reaction is a quadrilateral in which two tie lines have an interior intersection (e.g., reaction (12.6) in Figure 12.6). This type of reaction is known as a **tie line flip** reaction. When a reaction such as this occurs, all the phases remain intrinsically stable; it is merely the stable *assemblages* that change. The second type of reaction occurs when only one phase occurs on either side of the reaction. The chemographic representation of this type of reaction is a triangle with an interior phase (e.g., reaction {(12.7)} in Figure 12.6). A reaction such as this is called a **terminal** reaction. In

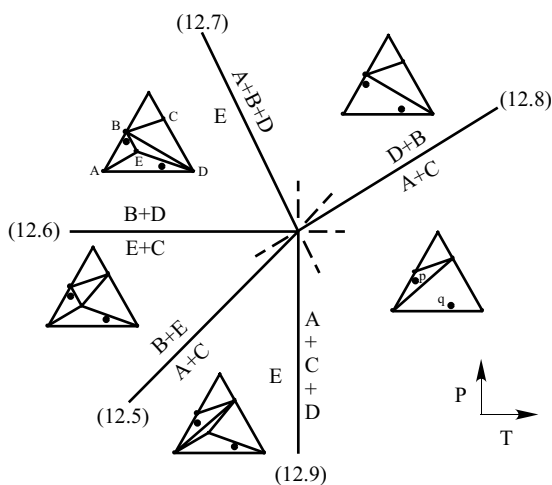


Figure 12.7 Same topology as Figure 12.6 showing the assemblages found in two hypothetical bulk compositions, p and q.

crossing a terminal reaction, a phase destabilizes in all bulk compositions.

Rarely are minerals consumed by terminal reactions. Most of the time, metamorphic reactions involve tie line flip reactions. As an example, consider the stability of chlorite. Chlorite is a common mineral in low-grade metamorphism of most protoliths; it disappears with increasing metamorphic grade. However, chlorite is not restricted to low metamorphic temperatures. Chlorite disappears because, with increasing temperatures, tie line flip reactions restrict its occurrence to increasingly limited bulk compositions. The terminal reaction for chlorite (chlorite = olivine + orthopyroxene + spinel) occurs at temperatures around 700°C, which means that in ultramafic rocks chlorite may be stable up to very high grade metamorphism.

In addition to indicating the stable phases in a given divariant field, chemographic projections also show the assemblage present in a rock of a given bulk composition. To understand this concept, consider Figure 12.7, which shows the same topology as that given in Figure 12.6 along with the chemographic diagrams for the compositions of two hypothetical rocks, p and q. Rock p has a composition very close to mineral B, whereas rock q has a composition that lies close to the A-D tie line. In the divariant field bounded by reactions (12.7) and (12.8), both bulk compositions will have the same assemblage: A-B-D. Rock p will have a lot of B and only a small amount of A and D,

whereas rock *q* will have mostly *D* and *A* and only minor amounts of *B*. As reaction (12.8) ($D + B = A + C$) proceeds, each assemblage behaves differently. Mineral *D* will be depleted from rock *p*, which is dominated by mineral *B*, whereas mineral *B* will be depleted first from rock *q*. These relations are shown in the chemographic projection in the field bounded by reactions (12.8) and (12.9), where composition *p* lies in the triangle *A*-*C*-*B*, whereas composition *q* lies in the field *A*-*C*-*D*. The reader is encouraged to determine the assemblages for these bulk compositions in the other fields in Figure 12.7 as an exercise.

12.3.3 Chemographic Projections in Systems with Four and More Components

In a system with four components, the phases can be expressed using a three-dimensional tetrahedron, but in systems of five or more components it is not possible to display relations chemographically because it requires more than three dimensions. There are two ways to handle this problem. One way is to explore the system in *n*-dimensional vector space using matrix algebra. In other words, the problem is addressed mathematically rather than graphically. This approach, while useful, will not be addressed in this text. The other way is to use projections. The extra dimensions of a complex system can be eliminated by assuming that one or more phases are always present in an assemblage. By projecting from the common phases it is possible to reduce a multidimensional chemography to a triangular chemographic projection. Such diagrams are called **pseudoternary projections** and are used precisely like the chemographic diagrams described for a three-component system. The difference is that these projections only depict reactions that contain the projecting phases. Crossing a reaction that does not contain all the projecting phases does not change the relations shown on the projection. Pseudoternary projections have been used previously in this text to discuss basalt melting and the chemistry of MORB, where relations were projected from plagioclase onto the olivine-clinopyroxene-quartz triangle (Figures 5.5 and 6.5).

Figure 12.8 illustrates a projection from a triangular chemography to a binary one. Figure 12.8A shows chemographic relations in the system $\text{MgO-SiO}_2\text{-H}_2\text{O}$. If one assumes that H_2O is always present during metamorphism of a serpentinite, we can show the same information on a linear chemography projected from H_2O

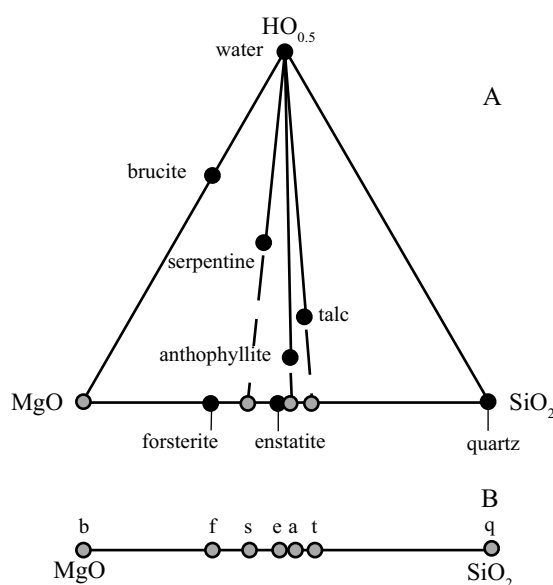


Figure 12.8 A. Chemography for the system $\text{MgO-SiO}_2\text{-H}_2\text{O}$ showing projection from H_2O to the MgO-SiO_2 plane. Dark points plot mineral compositions, gray points are projection points. B. Pseudobinary projection from H_2O for the same system.

(Figure 12.8B). The coordinates used in the ternary projection are obtained by taking the ratio of each of the three cations (Mg, Si, H) to the total number of cations ($\text{Mg} + \text{Si} + \text{H}$). Similarly the coordinates used in the projection from H_2O are obtained by taking the ratio of each of two cations (Mg and Si) to the sum of these two ions (Table 12.1). As long as H_2O is involved in a reaction, the binary and ternary chemographies show the same information (Figure 12.8A), although all reactions will appear as terminal reactions on the binary system. Indeed, they are terminal if H_2O is always in excess.

Ternary projections have strict rules in application to topologies and phase diagrams. If the plot of an assemblage on a chemographic diagram produces crossing tie lines or has a phase lying within a triangle outlined by three other phases, then it is clear there is a reaction relationship among the phases. There is, however, another type of projection that doesn't have such a strict application, but which is nevertheless very handy in understanding mineral relations in chemically complex rocks. This is the ACF projection of Eskola (1920). This is a projection from quartz, plagioclase, and orthoclase onto a plane defined by $A = (\text{Al}_2\text{O}_3 + \text{Fe}_2\text{O}_3 - \text{Na}_2\text{O} - \text{K}_2\text{O})$, $C = \text{CaO}$, and

Table 12.1 Coordinates for Phases in the System $MgO-SiO_2-H_2O$

Phase	Formula	MgO : SiO ₂ : H ₂ O	MgO : SiO ₂
Anthophyllite	Mg ₇ Si ₈ O ₂₂ (OH) ₂	0.41:0.47:0.12	0.47:0.53
Brucite	Mg(OH) ₂	0.33:0.0:0.67	1.0:0
Enstatite	MgSiO ₃	0.5:0.5:0	0.5:0.5
Forsterite	Mg ₂ SiO ₄	0.67:0.33:0	0.667:0.33
Quartz	SiO ₂	0:1:0	0:1.0
Serpentine	Mg ₃ Si ₂ O ₅ (OH) ₄	0.33:0.222:0.44	0.6:0.4
Talc	Mg ₃ Si ₄ O ₁₀ (OH) ₂	0.33:0.44:0.22	0.43:0.57
Vapor	H ₂ O	0:0:1.0	

F = (FeO + MgO) (Figure 12.9). Since this projection is from feldspars, the A coordinate involves subtraction of Na₂O and K₂O to account for aluminum that would be bound in the feldspars. Eskola (1920) used these ACF diagrams to

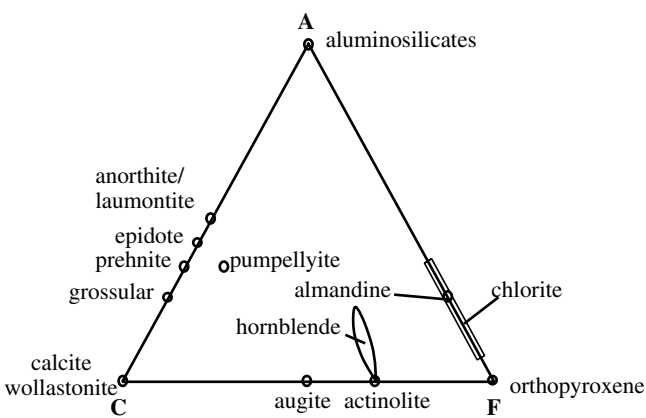


Figure 12.9 ACF diagram plotting common metamorphic minerals.

define metamorphic facies, painting a rough picture of the reactions involved in metamorphism. However, because of the large number of other components in natural rocks that are not considered in ACF projections, they cannot be used strictly to define mineral reactions.

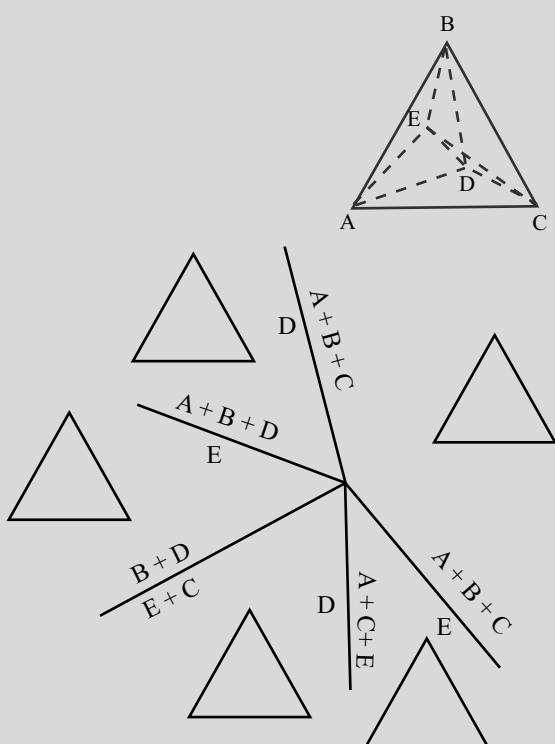
Summary

- Chemographic projections assist in visualizing what phases are stable in divariant fields of a phase diagram.
- The chemographic projection of a two-component system is a line. A reaction is indicated by the appearance or disappearance of a phase between two other phases on this line.
- In a three-component system, the chemographic projection is a triangle.
- Two type of reactions are recognized in three-component (or higher) systems:
 - In a tie line flip reaction, all phases remain stable; the reaction is simply manifested by a change in assemblage.
 - In a terminal reaction, one phase reacts away.
- In a four-component or higher system, relations can be shown by projection from one or more phases assumed present in all reactions.

Questions and Problems

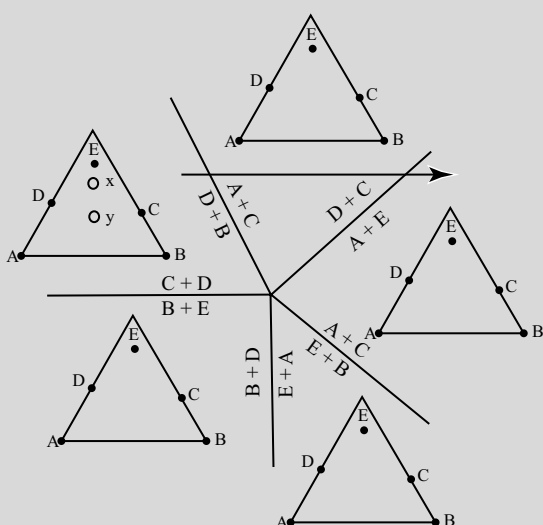
Problem 12.1. Show that for typical metamorphic rocks, the phase rule can be expressed as $\Phi = C$. You may wish to refer to Chapter 2, where the phase rule is introduced. Under what circumstances might $\Phi > C$?

Problem 12.2. The following questions refer to the figure below.



1. Fill in the triangles showing the assemblages in each divariant field.
2. Label which reactions are tie line flip reactions and which are terminal reactions.

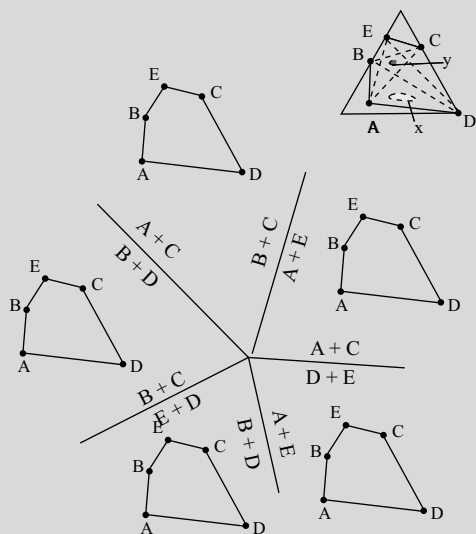
Problem 12.3. Answer the following questions, referring to the figure below.



1. Indicate the stable assemblages present in each of the divariant fields below by filling in the appropriate tie lines on the chemographic triangles.

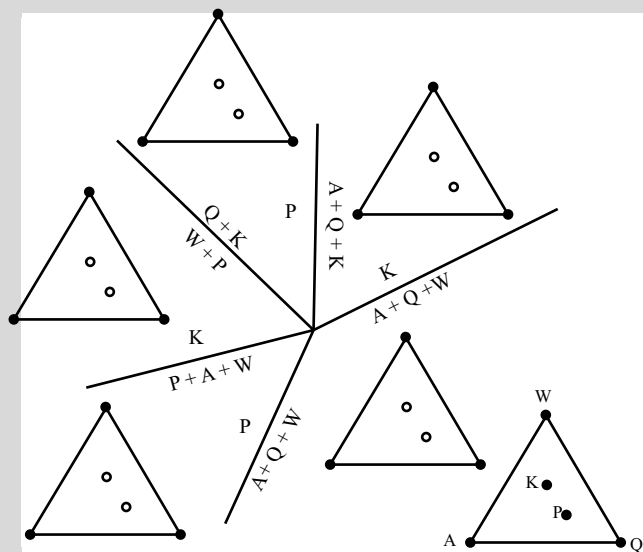
- For each reaction note whether it is a tie line flip reaction or a terminal reaction.
- Which of the two bulk compositions, x or y, is more sensitive to changes in temperature along the path indicated by the arrow?

Problem 12.4. The following questions refer to the diagram below.



- Fill in the chemographic triangles showing the stable assemblages in each field.
- Given rocks (X and Y) with two distinct bulk compositions (see plot below), note what assemblages are found in these rocks in each divariant field.
- Which bulk composition is the most sensitive monitor of metamorphic conditions? Explain your answer.

Problem 12.5. Below is a topology for a portion of the system Al_2O_3 - SiO_2 - H_2O , which is projected onto the triangle Al_2SiO_5 - SiO_2 - H_2O . The phases involved are A = andalusite (Al_2SiO_5), K = kaolinite ($\text{Al}_2\text{Si}_2\text{O}_5(\text{OH})_4$), P = pyrophyllite ($\text{Al}_2\text{Si}_4\text{O}_{10}(\text{OH})_2$), Q = quartz, W = water.



1. Indicate the stable assemblages present in each of the divariant fields by filling in the appropriate tie lines on the chemographic triangles.
2. For each reaction note whether it is a tie line flip reaction or a terminal reaction.

Further Reading

.....

Ernst, W. G., 1976, *Petrologic phase equilibria*, San Francisco, W.H. Freeman.

Thompson, J. B., Jr., 1982a. Composition space: An algebraic and geometric approach. In *Characterization of metamorphism through mineral equilibria*, ed. J. M. Ferry. *Reviews in Mineralogy*, 10, 1–31.

Thompson, J. B., Jr., 1982b. Reaction space: An algebraic and geometric approach. In *Characterization of metamorphism through mineral equilibria*, ed. J. M. Ferry. *Reviews in Mineralogy*, 10, 33–52.

Chapter 13

Metamorphic Facies and the Metamorphism of Mafic Rocks

13.1 Introduction

In the late nineteenth and early twentieth centuries, petrologists found it challenging to characterize the conditions of metamorphism because they lacked the thermodynamic data that today allow researchers to calculate the pressures and temperatures of metamorphism. Metamorphic facies, which were formulated by Eskola (1915), remain useful, even though their P-T conditions were initially very poorly defined. Indeed, metamorphic facies were simply defined as “a series of mineral assemblages that are found repeatedly associated in time and space” (Eskola, 1915). The definitions naturally carried an implication about the temperature and pressure conditions of metamorphism, but at the time petrologists had no way to specify these conditions. For example, they recognized that, with increasing metamorphic grade, actinolite turns into hornblende, and that at even higher grades hornblende breaks down to orthopyroxene and augite, but researchers had no way to assign absolute temperatures and pressures to these assemblages.

This chapter details the mineral changes that occur in mafic rocks with increasing temperature and pressure and how these produce the assemblages that define the various facies of metamorphism. The next chapter covers how petrologists use thermodynamics to characterize the pressure and temperature limits to metamorphism. That chapter also discusses the pressure and temperature conditions that characterize the facies discussed in this chapter.

Table 13.1 *Metamorphic Facies as Defined by Mineral Assemblages in Mafic Rocks*

Metamorphic Facies	Ferromagnesian Minerals	Ca-Al silicates
Zeolite	chlorite	zeolites, (prehnite), (epidote)
Prehnite-Pumpellyite	chlorite	epidote, pumpellyite, (prehnite)
Lawsonite-Albite-Chlorite	chlorite	lawsonite
Greenschist	actinolite	epidote, (plagioclase)
Blueschist	Na-amphibole, chlorite, almandine	epidote, lawsonite
Amphibolite	hornblende, (garnet)	plagioclase, (epidote)
Granulite	orthopyroxene, augite, (garnet)	plagioclase
Eclogite	omphacite, almandine (in garnet)	grossular (in garnet)

13.2 Definition of Metamorphic Facies

ACF diagrams, as noted in the previous chapter, can graphically depict the assemblages in metamorphic rocks because they can accommodate a wide range in bulk compositions, including pelitic, mafic, and calc-silicate rocks (Figure 13.1). Eskola (1915) defined metamorphic facies based on the assemblages found in mafic rocks, which have bulk compositions that lie in the middle of the ACF triangle (Figure 13.1; Table 13.1). Because of its bulk composition, a given assemblage in mafic rocks defines the tie lines within the ACF triangle and thus constrains assemblages in protoliths of other bulk compositions. The protolith of metamorphosed mafic rocks (also called **metabasites**) is basalt or gabbro. These rocks consist mainly of plagioclase (usually around An_{60-80}), and the mafic minerals (pyroxene and olivine). A good way to remember the mineralogy that characterizes the individual metamorphic facies is to consider what minerals substitute for the primary minerals from a gabbro in each metamorphic facies. To examine the mineral assemblages that define these facies this chapter first discusses the mineral changes that occur in mafic rocks during prograde metamorphism.

13.3 Facies of Regional Metamorphism

In the original definition, Eskola distinguished between facies formed in areas of regional metamorphism (Figure 13.2) and facies formed at low pressures due to metamorphism by shallow igneous intrusions that is, facies of contact metamorphism. Because the assemblages

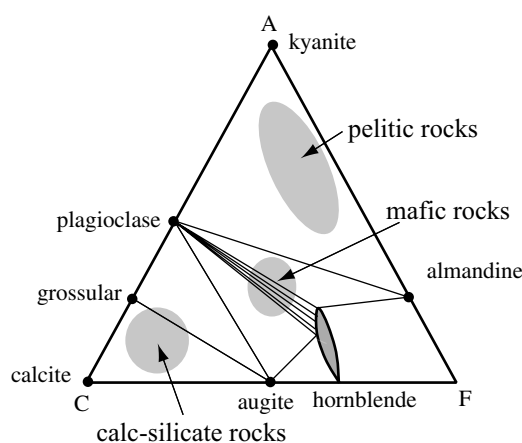


Figure 13.1 ACF diagram for mineral stabilities at amphibolite facies showing the approximate fields where pelitic, mafic, and calc-silicate rocks occur.

found in mafic rocks are essentially the same regardless of pressure and because the boundary between regional and contact metamorphism in P-T space is very poorly defined, this text focuses on the facies of regional metamorphism. Contact metamorphism is discussed briefly in Section 13.4.

13.3.1 Greenschist Facies

In most metamorphic belts the lowest-grade metamorphism encountered is greenschist facies. This name reflects the fact that under these metamorphic conditions mafic rocks contain minerals that tend to give them a greenish color in hand sample. Chief among these minerals is actinolite, although epidote and chlorite are also commonly present (Figure 13.3). Under greenschist

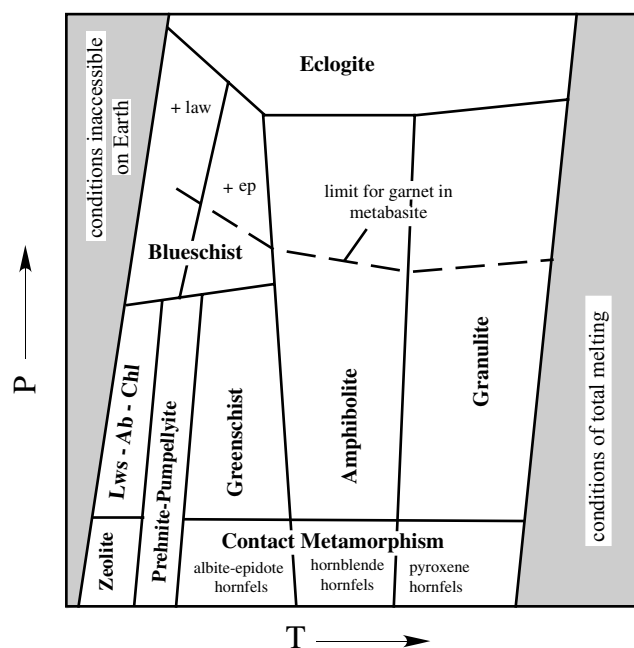


Figure 13.2 Approximate P-T stabilities for the metamorphic facies.

facies, plagioclase is usually nearly pure albite, although at low pressures a somewhat more calcic plagioclase may be present (Starkey and Frost, 1990). Because epidote and chlorite are distinctly silica poor (both have 35 percent SiO_2 or less), the formation of these minerals has a tendency to release silica. Consequently, quartz is common in greenschists and their nonfoliated counterparts, greenstones, even though the igneous protolith almost certainly did not contain quartz. Common accessory minerals include sphene, muscovite (or phengite), and biotite. At low pressures, greenschist rocks may contain oligoclase or even andesine coexisting with epidote, while high-pressure, low-temperature greenschists may contain pumpellyite. Pumpellyite-bearing rocks are sometimes considered as belonging to a separate facies, the pumpellyite-actinolite facies.

13.3.2 Blueschist Facies

With increasing pressure, actinolite disappears as the major amphibole and a sodic amphibole appears in its stead. The sodic amphibole turns the rock blue, hence the term *blueschist*. With increasing pressure, the first blue amphibole to appear is crossite, an amphibole that contains nearly as much ferric iron as alumina, and consequently has a deep purple color in thin section. With

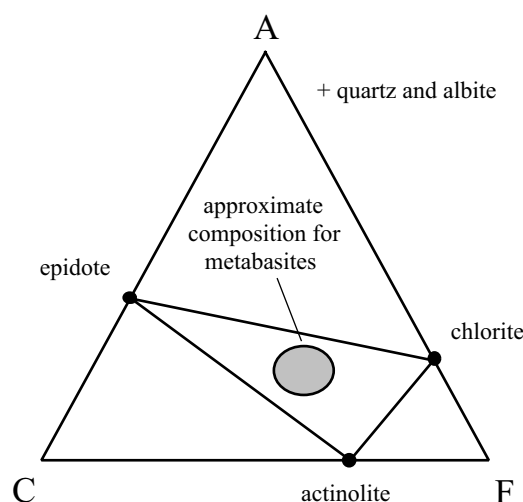


Figure 13.3 ACF diagram showing the stable assemblages in mafic rocks in greenschist facies.

increasing pressure, the ferric iron content decreases and alumina increases, with the result that glaucophane stabilizes and the color of the amphibole becomes pale lavender in thin section.

Blueschist facies was originally defined as the glaucophane-lawsonite schist facies, and some authors (e.g., Turner, 1968) prefer to restrict the facies to those assemblages that contain high-pressure phases such as lawsonite and to relegate crossite-bearing assemblages to greenschist facies. A broader interpretation is advocated by Evans and Brown (1987) whereby blueschist facies is defined as conditions where metabasites contain any blue amphibole. Evans (1990) identifies two subfacies of blueschist facies, depending on the Ca-Al silicate present. Lawsonite blueschists occur at relatively low temperatures and relatively high pressures, whereas epidote blueschists occur at higher temperatures and lower pressures (see Figure 13.1). At the highest pressures of blueschist facies, a jadeite pyroxene may form from albite; this marks the beginning of the transition to eclogite facies. Other minerals potentially present in mafic rocks in blueschist facies include pumpellyite, almandine garnet, rutile, aragonite, and stilpnomelane. Because the amphibole in blueschist facies has a high Na-content the mineral assemblages for blueschist facies are not easily expressed on an ACF projection, where sodium is not a participating component.

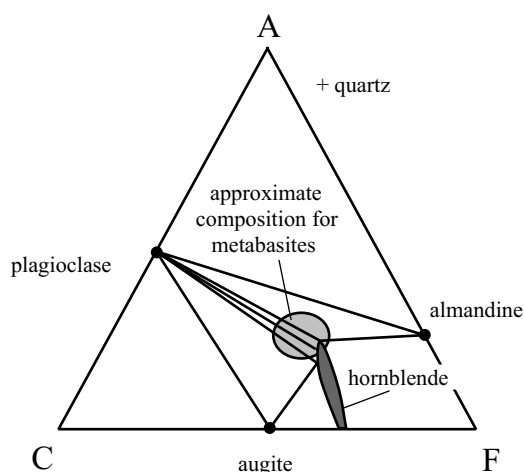


Figure 13.4 ACF projection showing mineral relationships in mafic rocks in amphibolite facies.

13.3.3 Amphibolite Facies

Subjecting weakly metamorphosed metabasites to increasing temperature allows more aluminum to substitute in the tetrahedral site of the amphiboles, causing both actinolite and glaucophane to change to hornblende. The appearance of hornblende in a mafic rock defines the amphibolite facies. Because the substitution of aluminum in hornblende is also accompanied by ferric iron, the color of the amphibole in hand sample changes from green to black. In thin section, hornblende has a brownish color in plane-polarized light (PPL). In addition to changes in amphibole composition, increasing temperature stabilizes Ca in the plagioclase and causes the disappearance of epidote. Because hornblende has such a variable composition, amphibolites are classic high-variance rocks (meaning they have many degrees of freedom), and the diagnostic assemblage is simply hornblende + plagioclase (Figure 13.4). Those amphibolites that are relatively more calcic than typical basalt may contain diopside, while those that are relatively less calcic may contain chlorite, garnet, or more rarely, cummingtonite.

Although amphibolites are renowned for their high variance, some mineralogic characteristics indicate where in amphibolite facies the rocks formed. One feature is the pleochroism of the hornblende. Hornblende pleochroism apparently is dependent on the amount of Fe^{3+} and TiO_2 it contains. These minor components usually increase with increasing temperature. Consequently, hornblende from

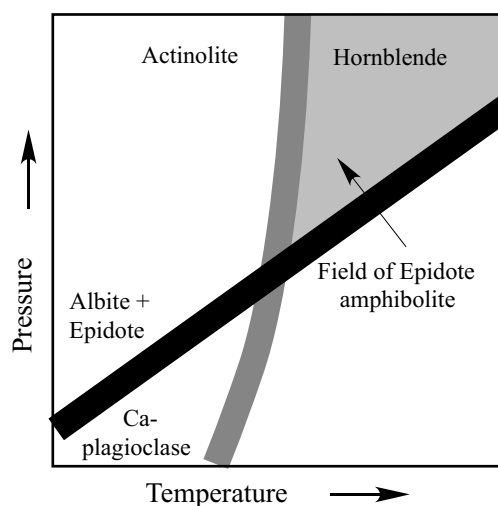


Figure 13.5 Schematic diagram comparing the P-T stabilities of anorthite-forming and hornblende-forming reactions.

high-temperature amphibolite facies has olive-brown to brown pleochroism, while hornblende from low-temperature amphibolite facies will have green pleochroism with a hint of olive brown. Hornblende from high-pressure, low-temperature amphibolites (i.e., those from grades slightly higher than that of blueschist) will have a distinct bluish tone to its pleochroism. Two other indicators of metamorphic conditions in amphibolite facies are the presence of epidote or garnet. Although the reactions governing the transition from actinolite to hornblende and the reaction of albite + epidote to calcic plagioclase are not well defined, petrologists recognize they are not parallel on a P-T plot (Figure 13.5). As a consequence, in low-pressure amphibolites, epidote disappears from the rock before hornblende forms, while in high-pressure rocks, epidote can survive into amphibolite facies. Such rocks are known as epidote amphibolites and indicate relatively high pressure.

At high pressures, the anorthite component of plagioclase ($\text{CaAlSi}_2\text{O}_8$) reacts to grossular ($\text{Ca}_3\text{Al}_2\text{Si}_3\text{O}_{12}$) in garnet. Thus at high pressures, generally above five or six kilobars, a calcic almandine garnet appears in amphibolites (Figure 13.6). Garnet amphibolites are good indicators of relatively high pressure of metamorphism. In many samples, such as that shown in Figure 13.6, the garnet is rimmed by plagioclase. This texture indicates the rock underwent decompression late in its metamorphic history with the result that the grossular component of the garnet reacted to plagioclase.

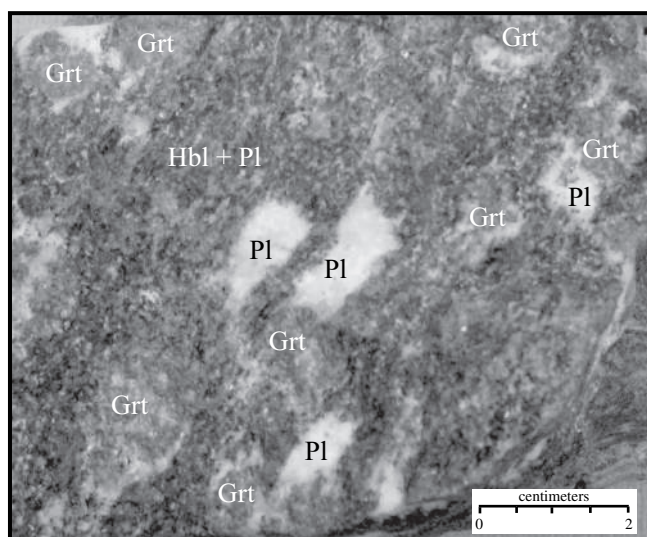


Figure 13.6 Photograph of a garnet amphibolite with plagioclase rims (Pl) around the garnet (Grt). The plagioclase probably formed from calcium released from the garnet during decompression. From near Mica Dam, British Columbia, Canada.

13.3.4 Very Low-Temperature Metamorphism

Before mafic igneous rocks can form equilibrium mineral assemblages in low-grade metamorphism, they must undergo hydration. Many weakly metamorphosed mafic rocks are marked by the survival of the primary igneous minerals. Indeed, augite in particular seems resistant to low-temperature hydration. Zeolite and prehnite-pumpellyite facies were originally defined from mineral assemblages in sedimentary protoliths, where hydration of the original igneous mineralogy occurs more readily than in igneous rocks (Coombs, 1954, 1960). Many of the subsequent studies of very low-temperature metamorphic changes in mafic rocks have been made in the amygdaloidal portions of basaltic flows.

Zeolite facies. Zeolite facies is defined by the presence of zeolites, of which there are a bewildering variety. Zeolites are tectosilicates that are analogous to feldspars, but because of their open lattice they accommodate structural water. Near the upper temperature limit of zeolite facies, the most common zeolite is laumontite. In some areas of high heat flow (i.e., relatively low pressure and high temperature), wairakite, a mineral with the same composition as laumontite but with less H_2O , may also occur. Other minerals in zeolite facies include calcite, albite, quartz, chlorite, epidote, prehnite, and pumpellyite (Figure 13.7A).

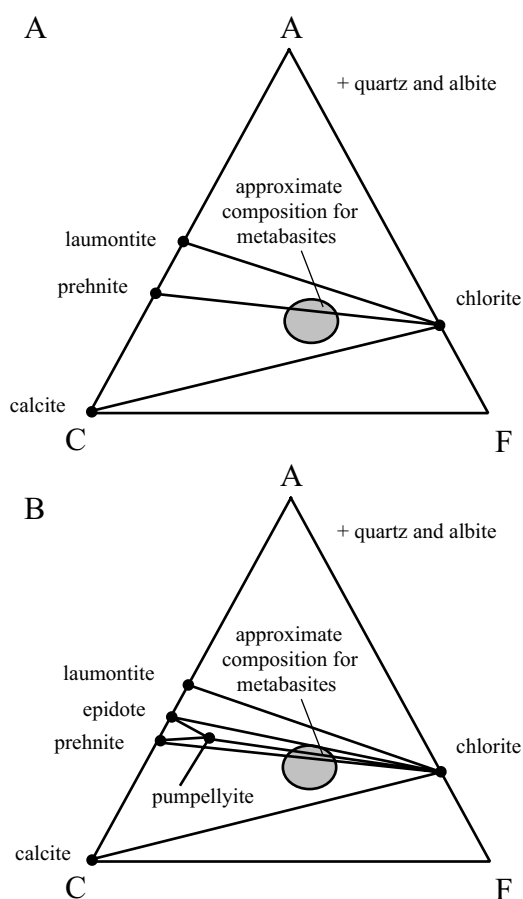


Figure 13.7 ACF diagrams showing mineral relations in weakly metamorphosed mafic rocks. A. zeolite facies. B. prehnite-pumpellyite facies.

Prehnite-Pumpellyite facies. The reactions that eliminate laumontite from mafic rocks are those that produce the assemblage chlorite-epidote-quartz (Frost, 1980) (Figure 13.7B). Prehnite or pumpellyite are also likely to be present (Figure 13.7B). Actinolite is distinctive by its absence. It is important to note that in some bulk compositions laumontite and wairakite may survive into prehnite-pumpellyite facies. If they do so, however, they will not occur with prehnite and pumpellyite. The high-pressure limits of prehnite-pumpellyite facies are poorly defined. The facies is probably transitional into blueschist facies, since pumpellyite is found in some blueschists. The transition from prehnite-pumpellyite facies to greenschist facies is marked by the appearance of actinolite and the disappearance of prehnite and pumpellyite. At low pressures, pumpellyite disappears

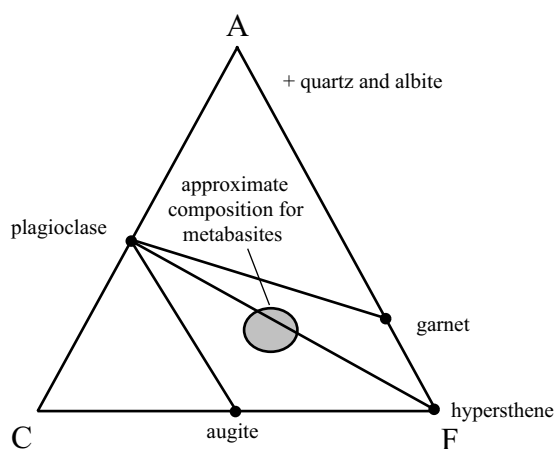


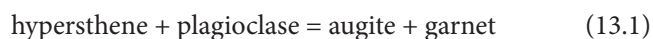
Figure 13.8 ACF diagram showing mineral relations in mafic rocks in granulite facies.

at lower temperatures than does prehnite, resulting in a narrow temperature range where prehnite and actinolite coexist. At high pressures, there is a stability field for pumpellyite and actinolite.

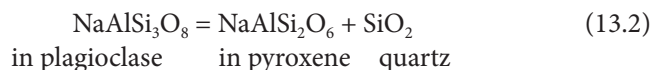
Lawsonite-Albite-Chlorite facies. A separate facies distinguished by the assemblage lawsonite-albite-chlorite may exist, a possible high-pressure equivalent to zeolite facies (Coombs, Nakamura, and Vuagnat, 1976). This facies lies at temperatures below those of prehnite-pumpellyite facies and at pressures below those of blueschist facies. Lawsonite-albite-chlorite facies is indicative of very low temperatures and high pressures of metamorphism and is found in only a few locations, such as on Crete, where subduction of a cold slab is postulated to have occurred (Theye, Seidel, and Vidal, 1992).

13.3.5 Granulite Facies

Granulite facies is marked by the breakdown of hornblende to hypersthene and augite (Figure 13.8). Because hornblende can assume a number of compositions, this reaction takes place over a range of temperatures, with the result that most granulites contain both hornblende and its breakdown products, pyroxenes. Mafic granulites are mineralogically very simple. At relatively low pressures, the assemblage is orthopyroxene-clinopyroxene-plagioclase +/- hornblende. In some rocks olivine may also occur. At higher pressures (above about six kilobars), garnet is typically present as well. At even higher pressures, orthopyroxene reacts out by the reaction:



resulting in the high-pressure assemblage garnet-clinopyroxene-plagioclase. The plagioclase in this assemblage gets progressively more sodium rich with increasing pressure as the anorthite component reacts to grossular in garnet. With increasing pressure, the albite component of plagioclase reacts to jadeite by the reaction:



The jadeite component in this reaction dissolves into the clinopyroxene. As reaction (13.2) progresses, plagioclase abundance decreases. The rock becomes an eclogite when plagioclase has been consumed.

13.3.6 Eclogite Facies

As pressure increases, the anorthite component of plagioclase dissolves into garnet and the albite component dissolves into pyroxene. Thus, at very high pressures rocks of basaltic composition are made up of dominantly garnet and omphacite (Na-rich augite), both of which show extensive solid solution. A rock with this assemblage is known as an eclogite. Other common phases likely to occur in eclogite include kyanite, phengite, and rutile. As shown in Figure 13.1 eclogite facies lies on the high-pressure side of blueschist, amphibolite, and granulite facies.

Eclogites occur in two high-pressure environments. One is at low-temperatures in subduction zones associated with blueschists. In some fossil subduction zones, such as in the Alps, where Europea partially subducted under Africa, the transition from blueschist facies to eclogite facies can be observed in the field (Figure 18.5). The other environment for eclogite lies at high temperatures, where they are associated with granulites. Such eclogites are found in continental collisions, at the base of crustal cross-sections, continental-scale thrust faults that expose deep crust, and as xenoliths sampled from the lower crust by alkali basalts.

13.4 Facies of Contact Metamorphism

Contact metamorphism can be considered a separate facies, which occupies the low-pressure fields in Figure 13.1. Contact metamorphic facies are designated

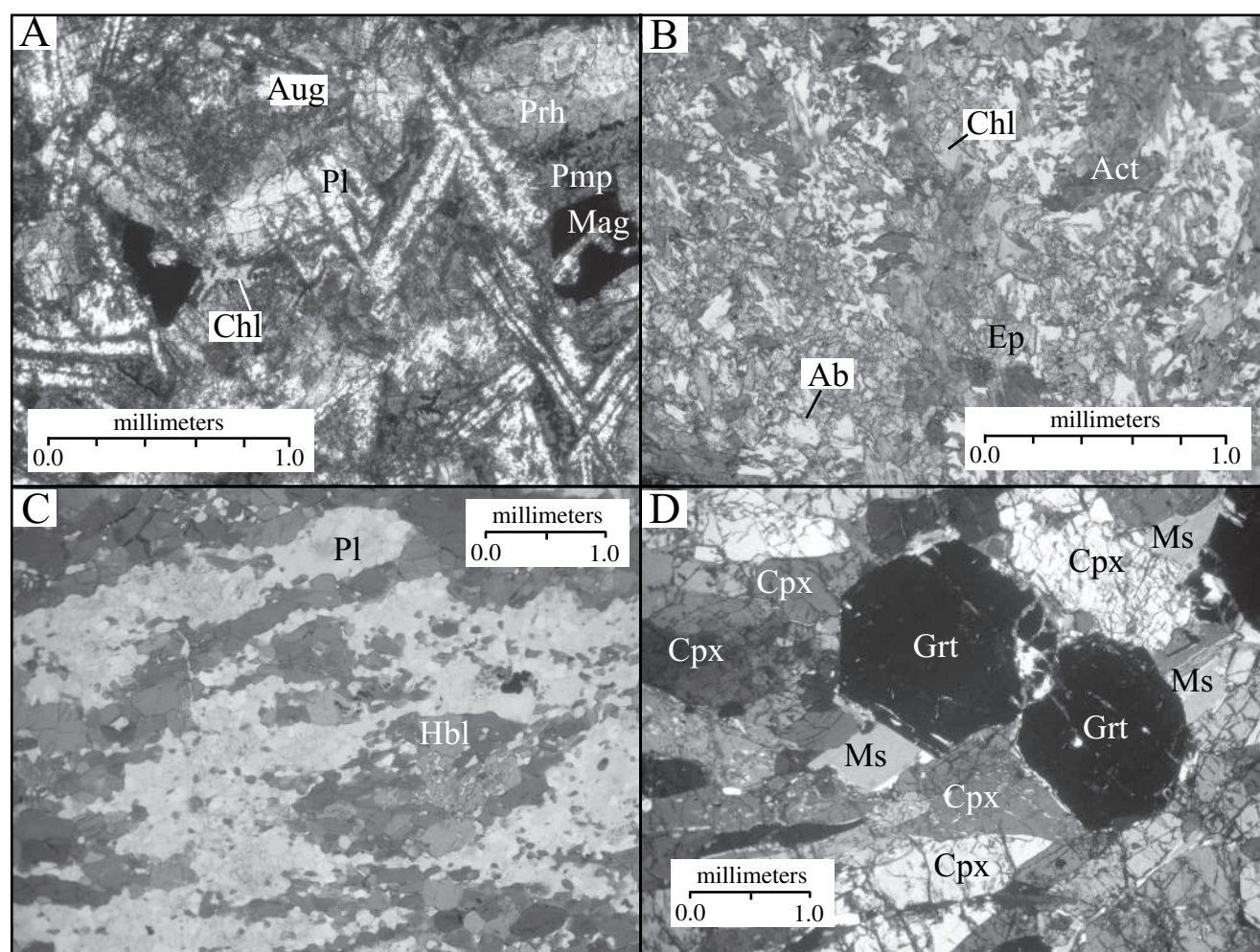


Figure 13.9 Photomicrographs showing textures typical of metabasic rocks. (A) Metabasalt in prehnite-pumpellyite facies in PPL. Note that the basaltic texture is still evident. The tabular plagioclase (Pl) is albite with clusters of pumpellyite on the margin. Primary augite (Aug) and Ti-magnetite (Mag) are still present locally. Other metamorphic minerals include prehnite (Prh), pumpellyite (Pmp), and chlorite (Chl). From the Karmusteen volcanoes, Vancouver Island, Canada. (B) Greenschist containing actinolite (Act), epidote (Ep), chlorite (Chl), and albite (Ab) in PPL. Note that the albite (white in this figure) is arranged in clusters, which might be relict from primary plagioclase. From the Ligurian Alps, Italy. (C) Amphibolite containing hornblende (Hbl) and plagioclase (Pl) in PPL. The rock has a relict diabasic texture similar to the matrix in Figure 11.1C. In thin section the plagioclase maintains a suggestion of tabular shape, but it has recrystallized into a matrix of small grains. From the Laramie Range, Southeastern Wyoming. (D) Eclogite containing garnet (Grt), omphacite (Cpx), and muscovite (Ms) in XPL. Sesia zone, Italian Alps.

by the same mineral assemblages as facies of regional metamorphism, but the contact metamorphic environment is recognized on the basis of textural features and field relations rather than by mineral assemblages. The contact metamorphic facies shown in Figure 13.1 include **albite-epidote hornfels**, essentially similar to greenschist; **hornblende hornfels**, equivalent to a low-pressure amphibolite facies; and **pyroxene-hornfels**, which has the assemblages of low-pressure granulite facies.

13.5 Textural Changes during Metamorphism

Weakly metamorphosed mafic rocks commonly preserve relicts of the primary igneous texture, including tabular plagioclase and blocky crystals of Fe-Ti oxides (Figure 13.9A). The extent to which the igneous textures survive depends on the deformation history of a rock, but these relict textures may present in rocks metamorphosed

Original Minerals	Zeolite Facies	Prehnite-Pumpellyite Facies	Greenschist
Orthopyroxene Augite	Chlorite	Pumpellyite	Actinolite
Olivine	Chlorite	Chlorite	Chlorite
Anorthite	Laumontite	Prehnite Epidote	Epidote
Albite	Albite Analclime at v. low T	Albite	Albite
Other	± Quartz ± Calcite	± Quartz ± Calcite	± Quartz

Table 13.2 Diagram Showing the Changes in Mineralogy in Mafic Rocks at Very low T

to moderate grades, which allows a geologist to characterize a mafic rock as a metabasalt, metadiabase, or a metagabbro. Figure 13.9B shows a metabasalt from greenschist facies that retains a subtle hint of tabular feldspar. The tabular shape is partially obscured because the Ca component of the feldspar has reacted to epidote and is only recognized by considering the shape of the colorless areas in the figure (which are mostly small grains of albite). Figure 13.8C shows a thin section of a metadiabase similar to that shown in Figure 11.1C, which shows white plagioclase grains in hand sample. In thin section, it is clear these plagioclase grains have recrystallized into a mosaic of fine grains. In the eclogite shown in Figure 13.8D there is no trace of the original igneous texture. However, a relict gabbroic texture may be found in some eclogites as displayed by the large-scale distribution of garnet, clinopyroxene, and rutile.

13.6 Mafic Mineral Assemblages at Increasing Temperature and Pressure

Rather than memorizing a series of assemblages, a preferable way to understand metamorphism of mafic rocks is to follow the mineralogical changes with increasing temperature and pressure. The unmetamorphosed mafic protolith consists of plagioclase, pyroxenes, and perhaps olivine. These minerals contain the chemical components redistributed during metamorphism. – an albite component (Na, Al), an anorthite component (Ca, Al), and a

ferromagnesian component (Ca, Mg, Fe). Because metamorphism covers a wide range of pressure and temperature conditions, they are summarized in three tables. Table 13.2 covers the mineralogical changes that occur from zeolite to greenschist facies, Table 13.3 covers the changes that occur with increasing temperature from greenschist facies to granulite facies, and Table 13.4 covers the changes that occur with increasing pressure from greenschist to blueschist facies.

13.6.1 Relations at Very Low Temperatures

At low temperatures and pressures, the stable plagioclase is albite (although note that at the very lowest temperatures, the albite component may be present as a zeolite, analclime) (Table 13.2). In zeolite facies, the Ca-Al component of plagioclase is present as laumontite, in prehnite-pumpellyite facies it occurs as prehnite, and in greenschist facies it occurs in epidote. Some of the Ca released by the breakdown of anorthite may occur in calcite, which is common in zeolite and prehnite-pumpellyite facies, but less so in greenschist facies. The major host to Fe and Mg in zeolite facies is chlorite; the Al in chlorite probably is derived from the breakdown of anorthite, which has more Al than other Ca-Al silicates. In prehnite-pumpellyite facies, the Fe and Mg may also be hosted in pumpellyite (which also contains considerable Ca and Al). In greenschist facies, pumpellyite is replaced by actinolite, producing the common greenschist assemblage albite-epidote-chlorite-actinolite. Because some of the minerals

Original Minerals	Greenschist Facies	Amphibolite Facies	Granulite Facies
Orthopyroxene Augite	Actinolite	olive → brown Hornblende Al	Orthopyroxene Hornblende Augite
Olivine	Chlorite		Olivine (v. hi T)
Anorthite Al	Epidote	Plagioclase	Plagioclase
Albite	Albite	(transition is P-dependent)	
Other	± Quartz	± Quartz ± Garnet (at high P)	± Quartz ± Garnet (at high P)

Table 13.3 Diagram Showing the Changes in Mineralogy in Mafic Rocks with Increasing T

Original Minerals	Greenschist Facies	Blueschist Facies	Eclogite Facies
Orthopyroxene Augite	Actinolite	deep purple → lavender increasing P Na-amphibole	
Olivine	Chlorite	Na (low P) → (high P) Garnet	Garnet
Anorthite Al	Epidote	Epidote Lawsonite (hi P, low T)	Epidote (low T)
Albite	Albite	Na Pyroxene	Na Pyroxene
Other	± Quartz	± Quartz	± Quartz ± Kyanite ± Muscovite

Table 13.4 Diagram Showing the Changes in Mineralogy in Mafic Rocks with Increasing P at Low T

in low-grade metabasites are silica poor (especially chlorite), quartz may be present in all these assemblages.

13.6.2 Relations at Low Pressure with Increasing Temperature

At low pressures, increasing temperature causes Al to dissolve into the actinolite, making hornblende. The appearance of hornblende marks the entry into amphibolite facies. At approximately the same temperature, epidote begins to break down, releasing CaO that dissolves into the plagioclase (Table 13.3). The epidote-out reaction is

more strongly pressure dependent than the hornblende-forming reaction, with the result that epidote may be present in high-pressure amphibolites. Garnet may also be present in high-pressure amphibolites. Hornblende breaks down by the reaction hornblende = orthopyroxene + clinopyroxene + plagioclase, so the appearance of pyroxenes in amphibolites marks the upper limit of amphibolite facies. The presence of augite in a mafic rock doesn't necessarily indicate amphibole breakdown because clinopyroxene may be present in relatively calcic amphibolites even at relative low temperature. For this reason

the beginning of granulite facies is marked by the appearance of orthopyroxene. Hornblende changes its composition as it breaks down, becoming increasingly enriched in refractory elements such as Ti, Fe^{3+} , and F. This change in composition allows hornblende to persist to very high temperature in granulite facies. As in amphibolites, high-P granulites may contain garnet.

13.6.3 Relations at Low Temperature with Increasing Pressure

At low temperatures, increasing pressure causes actinolite to accommodate more Na (Table 13.4). The appearance of Na-bearing amphiboles with a bluish color (and pleochroism) marks the low-pressure limits of blueschist facies. Such low-pressure blueschists have a similar mineralogy

to greenschist (Na-amphibole-Ab-Ep-Chl), except for the appearance of Na-amphibole rather than actinolite. Increasing pressure causes garnet to form from chlorite. At still higher pressures and somewhat lower temperatures, lawsonite forms from epidote. Finally, at still higher pressures, albite reacts to the jadeite component of pyroxene. This produces the assemblage for high-pressure blueschists of glaucophane-garnet-clinopyroxene-epidote. With increasing temperature or pressure, the amphibole breaks down, producing the assemblage garnet-clinopyroxene-epidote, distinctive of low-T eclogite facies. High-T eclogite facies lacks epidote. As discussed in Section 13.3.5, high-temperature eclogites form from granulites as increasing pressure drives plagioclase components (anorthite and albite) into garnet and pyroxene.

Summary

A useful way to understand metamorphic facies in mafic rocks is to consider the ferromagnesian minerals present or absent:

- **Amphibole-bearing facies.** Three metamorphic facies contain amphibole as a critical phase.
 - In greenschist (or the albite-epidote hornfels) facies the amphibole is actinolite.
 - In amphibolite (or hornblende hornfels) facies the amphibole is hornblende.
 - In blueschist facies the amphibole is sodic amphibole.
- **Amphibole-free facies.** Five metamorphic facies do not contain amphibole as a critical phase, although some relict amphibole may be present.
 - In granulite facies, hornblende is in the act of breaking down to orthopyroxene and clinopyroxene.
 - In eclogite facies, the stable minerals are omphacite (Na-rich augite) and garnet. Minor amounts of sodic amphibole may be present at low temperatures.
 - In prehnite-pumpellyite facies, assemblages including chlorite and pumpellyite appear instead of actinolite.
 - In zeolite facies, assemblages including chlorite and laumontite (\pm prehnite, laumontite or calcite) appear instead of actinolite.
 - In albite-chlorite-lawsonite facies, albite-lawsonite and chlorite are present instead of actinolite.

Questions and Problems

Problem 13.1. What minerals give the green color to rocks in greenschist facies? What minerals are responsible for the blue that gives the name to blueschist facies?

Problem 13.2. From the assemblages below, give the metamorphic conditions as precisely as the assemblage allows. (For example, the assemblage clinopyroxene-garnet-epidote would be in low-temperature eclogite facies.) Explain how you reached your conclusion.

- A. glaucophane-garnet-albite-lawsonite
- B. albite-epidote-actinolite-chlorite
- C. hornblende-plagioclase-garnet
- D. hornblende-orthopyroxene-clinopyroxene-plagioclase
- E. clinopyroxene-garnet-orthopyroxene-plagioclase

Problem 13.3. Below are lists of minerals that occur in a series of mafic rocks. For each list determine if the assemblage could represent an equilibrium assemblage and if so, identify the facies to which it belongs. If it is not an equilibrium assemblage, determine what minerals are out of equilibrium and to what facies the rest of the minerals belong.

- A. hornblende-plagioclase-garnet-prehnite
- B. orthopyroxene-augite-hornblende-plagioclase
- C. augite-plagioclase-garnet-chlorite
- D. omphacite-garnet-glaucophane
- E. prehnite-chlorite-epidote-quartz

Further Reading

- Bucher, K. and Frey, M., 2002, *Petrogenesis of metamorphic rocks*. Springer, Heidelberg, Chapter 9.
- Cooper, A. F., 1972, Progressive metamorphism of metabasic rocks from the Haast Schist group of southern New Zealand. *Journal of Petrology*, 13, 457–92.
- Evans, B. W., 1990, Phase relations of epidote-blueschists. *Lithos*, 25, 3–23.
- Philpotts, A. R. and Ague, J. J., 2009, *Principles of igneous and metamorphic petrology*. Cambridge University Press, Cambridge, UK, Chapter 16.
- Winter, J. D., 2010, *Principles of igneous and Metamorphic Petrology*, 2nd ed., Prentice Hall, New York, Chapter 25.
- Yardley, B. W. D., 1989, *An introduction to metamorphic petrology*, Longman, Essex, UK, Chapter 4.

Chapter 14

Thermobarometry and the Conditions of Metamorphism

14.1 Introduction

Metamorphic facies provide a qualitative estimate of the conditions of metamorphism based on changes in mineral assemblages over inferred changes in temperature and pressure. Information from metamorphic facies can be quantified using experimental petrology, which provides pressure and temperature information on the mineral reactions that produce the assemblages characteristic of the metamorphic facies. Additional quantification comes from **thermobarometry**, which are calculations based on mineral chemistry that produce reasonably precise estimates of temperature and pressure for metamorphic rocks. The rise of thermobarometry as a field of petrology over the past forty years has been driven by two parallel developments. One was the invention of the electron microprobe in the late 1960s, which allowed petrologists to obtain complete chemical analyses of minerals on the scale of microns. The other was the extraction of thermodynamic data (both for end members and for solid solutions) for minerals from experimental studies of phase equilibria. Petrologists can now apply thermodynamics to the compositions of minerals present in an equilibrium assemblage to estimate the conditions at which the assemblage formed.

Many of the details of the thermobarometric calculations are beyond the scope of this text. This chapter introduces thermobarometry and how the approach provides quantitative information about metamorphic conditions. It then describes how the results of thermobarometry constrain the conditions of the metamorphic facies discussed in Chapter 13. The chapter ends with a discussion of the limits of metamorphism.

14.2 Review of Thermodynamics

14.2.1 Free Energy

The key variable in thermodynamics is **free energy** (G), which is the energy produced by a chemical reaction that is available to do work. The free energy for a reaction is defined as:

$$\Delta G = \Delta H - T\Delta S \quad (14.1)$$

where Δ refers to the difference in the thermodynamic function between the products and reactants, H refers to **enthalpy**, and S represents **entropy**. *Enthalpy* is the heat released (or consumed) by a reaction due to the breaking of bonds and the formation of new bonds. *Entropy* is the heat tied up in the bonds of the various phases involved in the reaction. Reaction (14.1) says the amount of energy released by a reaction is equal to the amount of energy released when the bonds of the product minerals are reorganized to form the bonds of the product minerals minus the amount of heat consumed (or produced) by changing the configuration of the elements within the mineral structures.

If the ΔG in reaction (14.1) is less than zero, then the free energy of the reactants is greater than that of the products and the reaction can proceed spontaneously, evolving heat in the process. If ΔG is greater than zero, the reaction cannot proceed unless further heat is added to the system. If ΔG equals zero, the products and reactants of the reaction are in equilibrium. This does not mean that nothing is happening in the reaction; it merely means that the rate of the reaction producing the products from the reactants is the same as the rate producing the reactants from the products.

14.2.2 Effect of Changes in Pressure and Temperature on ΔG

How free energy changes with respect to pressure and temperature is given by equation (14.2):

$$dG = -SdT + VdP \quad (14.2)$$

where V refers to volume.

If we are dealing with a reaction, as we usually are in metamorphic petrology, equation (14.2) becomes:

$$d\Delta G = -\Delta SdT + \Delta VdP \quad (14.3)$$

At equilibrium, equation (14.3) becomes:

$$0 = -\Delta SdT + \Delta VdP \quad (14.4)$$

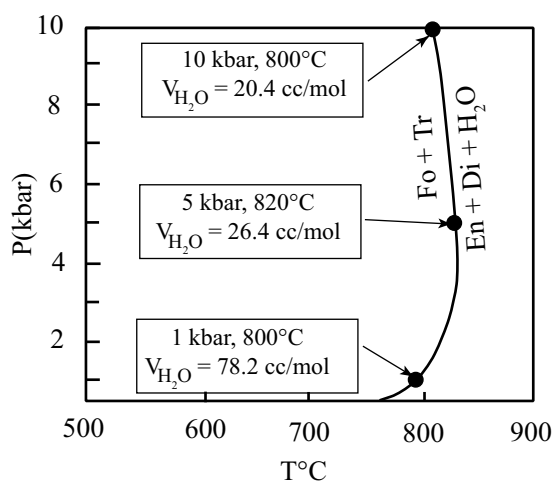


Figure 14.1 P-T diagram showing how the decrease in the molar volume of H_2O affects the slope of the dehydration reaction olivine + tremolite = enstatite + diopside + H_2O . Data from Burnham, Holloway, and Davis (1969).

rearranging gives:

$$\Delta VdP = \Delta SdT \quad (14.5)$$

$$dP/dT = \Delta S/\Delta V \quad (14.6)$$

Equation (14.6) is called the **Clausius-Clapeyron equation** and it indicates that the slope of a reaction in a P-T diagram is dependent on the ratio of $\Delta S/\Delta V$ of the reaction.

The Clausius-Clapeyron equation explains why dehydration reactions on a P-T diagram generally have an increasing slope with increasing P . Water released by dehydration reactions has a large volume at low pressures (see Figure 3.4), leading to a large denominator in equation (14.6) and a correspondingly low positive slope in P-T space. As pressure increases, the ΔV also decreases, and the slope, as governed by equation (14.6), becomes progressively steeper. At very high pressures some dehydration reactions, such as the reaction shown in Figure 14.1, have a negative slope.

14.2.3 The Equilibrium Constant

The expression for the equilibrium constant, also known as the **law of mass action**, is the key step in determining pressure and temperature of metamorphism from mineral analyses. Consider an equilibrium:

$$nA + mB = pC + qD \quad (14.7)$$

where A, B, C, and D are phases and n, m, p, and q are stoichiometric coefficients of those phases in the reaction. The equilibrium expression for this reaction is:

$$K = \frac{\alpha_A^n \alpha_B^m}{\alpha_C^p \alpha_D^q} \quad (14.8)$$

where a_i = the activity of phase I, a point discussed in detail later in this chapter. The equilibrium constant is related to the free energy of reaction (14.7) by the following expression:

$$\ln K = \frac{-\Delta G}{RT} \quad (14.9)$$

where R = the gas constant. Substituting equation (14.1) into equation (14.9):

$$\ln K = \frac{-\Delta H}{RT} + \frac{\Delta S}{R} \quad (14.10)$$

On a plot of $\ln K$ versus $1/T$, equation (14.10) yields a straight line with a slope of $-\Delta H$ and an intercept of $\frac{\Delta S}{R}$. Assuming that temperature is fixed, and substituting equation (14.3) into equation (14.9), yields:

$$\ln K = \frac{-\Delta V}{RT} \quad (14.11)$$

Finally, combining equations (14.10) and (14.11) gives the basic equation for thermobarometry:

$$\ln K = \frac{-\Delta H}{RT} + \frac{\Delta S}{R} - \frac{\Delta V}{RT} \quad (14.12)$$

14.2.4 Activity-composition Relations

The key to using mineral analyses to calculate thermometry or barometry lies in evaluating the activity of a component in the mineral. The simplest definition of activity is the “effective concentration” of a component in a solution. If a solution is ideal, the activity is the same as the mole fraction (X_i). As noted in Section 12.3.1, X_i is defined as the number of moles of component i divided by the total number of moles of components in solution. Calculating mole fraction is somewhat more complex when dealing with a solid solution, such as the olivine from New Caledonia given in Table 14.1. Table 14.1 contains two parts. The upper portion gives the analysis for olivine in terms of weight percent oxide. The lower portion of the

Table 14.1 Analysis of Olivine from New Caledonia

SiO ₂	40.75
Al ₂ O ₃	0.00
FeO	8.70
MnO	0.11
NiO	0.37
MgO	50.22
CaO	0.02
Total	100.17
Cation proportions on a basis of four oxygens	
Si	0.994
Al	0.000
Fe	0.177
Mn	0.002
Ni	0.007
Mg	1.825
Ca	0.000
total	3.006
X _{Mg}	0.911
Mg/(Mg+Fe)	0.907
X _{Fe}	0.089
Fe/(Fe+Mg)	0.088

table gives the cation proportions of the olivine that is normalized to four oxygens, which is the number of oxygens in the olivine formula.

In calculating the mole fraction of forsterite in this olivine, one can neglect silica because Mg and Fe (and minor amounts of Ni and Mn) substitute for each other only on the octahedral sites in olivine. Silica fills the tetrahedral site in olivine regardless of how much Fe or Mg is present in the octahedral sites. Mole fraction of Mg (X_{Mg}) is then calculated as the cation ratio $Mg/(Mg+Fe+Mn+Ni)$. Because, in the vast majority of silicates, Fe and Mg are the major cations in the octahedral site many people equate X_{Mg} with $Mg/(Mg+Fe)$. For the olivine listed in Table 14.1, these two ratios are nearly equivalent. Because there are two sites for Mg in olivine, the activity of Mg_2SiO_4 in olivine (assuming an ideal solution) is given by X_{Mg}^2 , which

means that (assuming ideality) the activity of Mg_2SiO_4 in this olivine is 0.82.

Unfortunately, solution of individual ions into mineral structures is rarely ideal. Some energy is required or evolved when various ions substitute for each other in a site. To convert mole fraction to activity, one uses the *activity coefficient* (γ). Thus, in real solutions activity becomes:

$$a_i = X_i \gamma_i \quad (14.13)$$

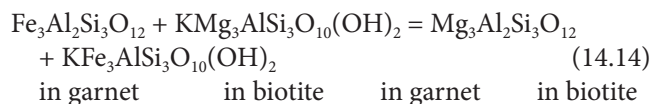
Activity coefficients must be determined empirically for each mineral. Most modern thermobarometry programs have these determinations built into the calculation; the inputs for such programs usually are the mole fractions of various components.

14.3 Thermobarometers

Equation (14.2) implies that a chemical reaction that has a relatively low ΔV and a high ΔS will be highly temperature dependent and therefore makes a good thermometer, whereas a reaction with a relatively low ΔS and high ΔV will be pressure dependent and accordingly will make a good barometer. As the field of thermobarometry developed in the 1970s and decades following a series of reactions were calibrated as thermometers and barometers.

14.3.1 Geothermometry

Ion-exchange thermometry. The main type of reaction for geothermometry is an ion-exchange reaction. This reaction type involves the exchange of two ions (usually Fe and Mg) in two phases. A classic example of this is the distribution of Fe and Mg between garnet and biotite. This reaction can be written as:



Because garnet and biotite appear on both sides of the reaction, the ΔV of this reaction will be small, making a perfect thermometer. Garnet strongly favors Fe over Mg (Figure 14.2) so that at 450°C biotite with even a moderate amount of Fe will coexist with a very Fe-rich garnet. As temperature increases, the tie lines between garnet and biotite increasingly steepen as garnet can accommodate more Mg. Consider the bulk composition of a rock that

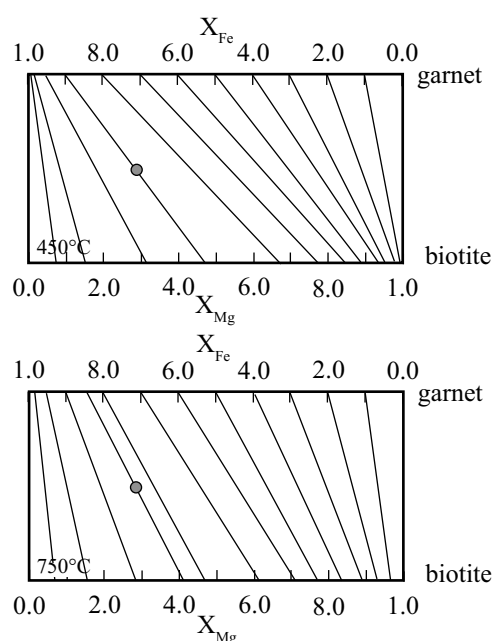


Figure 14.2 Diagram showing how the Fe and Mg contents of biotite and garnet vary as a function of T. (A) relations at 450°C, (B) relations at 750°C. Gray circle gives the hypothetical bulk composition of a rock. See text for details. Calculations from the data of Ferry and Spear (1978).

contains equal amounts of garnet and biotite and a bulk composition of $X_{\text{Fe}} = 0.70$, which is represented by the gray point in Figure 14.2. At 450°C this rock will contain a garnet with $X_{\text{Fe}} = 0.90$ coexisting with a biotite with $X_{\text{Fe}} = 0.52$. At 750° the same rock will contain garnet with $X_{\text{Fe}} = 0.84$ and biotite with $X_{\text{Fe}} = 0.59$.

The tie lines in Figure 14.2 were calculated using the garnet-biotite thermometer of Ferry and Spear (1978). More recent formulations of the thermometer have incorporated various solution models and are more complex than that derived by Ferry and Spear (1978). However, Figure 14.2 shows graphically how the garnet-biotite tie lines change orientation with increasing temperature. By measuring the composition of coexisting biotite and garnet and knowing how the orientations of the tie lines change with temperatures, one can determine the temperature at which these minerals last equilibrated.

Solvus thermometry. A special type of ion exchange thermometer involves the equilibrium between two phases on either side of a solvus. For example, calcite and dolomite are compositionally distinct at low temperatures but with increasing temperature, more Mg can be

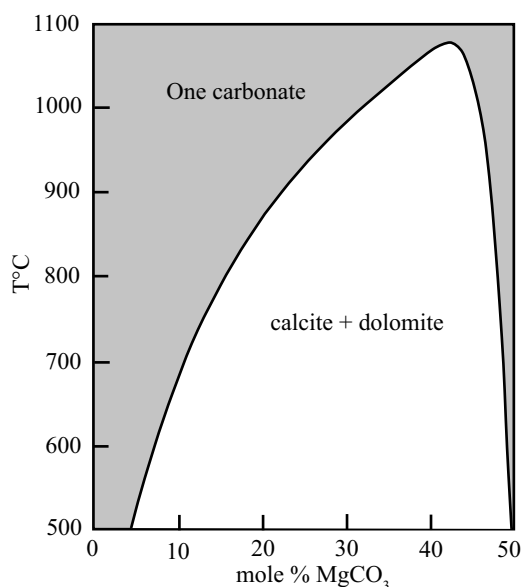
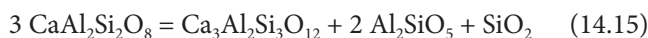


Figure 14.3 Calcite – dolomite solvus after Goldsmith and Heard (1961).

accommodated in the calcite structure until at temperatures around 1,100°C, there is but a single carbonate with the composition $(\text{Ca,Mg})\text{CO}_3$ (Figure 14.3). Figure 14.3 shows that the Mg content in calcite that coexists with dolomite is a sensitive thermometer. From the composition of calcite coexisting with dolomite, this solvus can be used to determine the temperature at which the two minerals last equilibrated. Theoretically, the Ca content of dolomite may also serve as a thermometer, however because the limb of the solvus is so steep on the dolomite side, the Ca content of dolomite is not as sensitive to temperature changes as is the Mg content of calcite.

14.3.2 Geobarometry

Reactions that are good barometers are those that involve large changes in volume and do not involve volatiles, because as shown in Figure 14.1, dehydration reactions have steep slopes in P-T space. A good example of a barometer is the reaction:



in plagioclase in garnet kyanite quartz

The equilibrium constant for this reaction (assuming quartz and kyanite are pure phases) is:

$$K = \frac{\alpha_{\text{grs}}^{\text{gar}}}{(\alpha_{\text{An}}^{\text{plag}})^3} \quad (14.16)$$

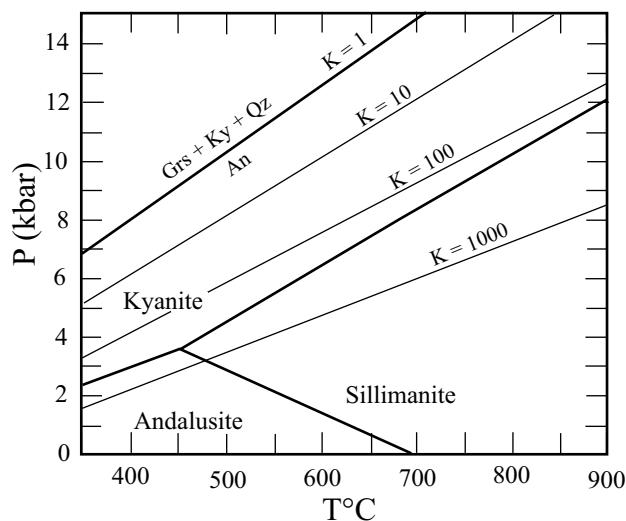


Figure 14.4 Location of the equilibrium anorthite = grossular + kyanite + quartz and isopleth lines showing the displacement of this equilibrium in systems with plagioclase and garnet solid solutions. After Koziol and Newton (1988).

Assuming that $\alpha_{\text{An}}^{\text{plag}} = X_{\text{Ca}}^{\text{plag}}$ and, because there are three atoms of Ca in a formula unit of grossular, $\alpha_{\text{grs}}^{\text{gar}} = (X_{\text{Ca}}^{\text{gar}})^3$ equation (14.16) becomes:

$$K = \frac{(X_{\text{Ca}}^{\text{gar}})^3}{(X_{\text{Ca}}^{\text{plag}})^3} \quad (14.17)$$

Reaction (14.15) has many properties that make it an ideal geobarometer. First, it has a relatively flat slope in P-T space (Figure 14.4). Second, garnet and plagioclase have a wide range of solid solution, which means the assemblage garnet-plagioclase-kyanite (or sillimanite or andalusite) is widespread assemblage in pelitic rocks. At low pressures, where K is large, garnet will have very little Ca and plagioclase will be relatively calcic. With increasing pressure, Ca will be transferred from plagioclase to garnet until at high pressures, the garnet will be relatively calcic and the plagioclase will be sodic. The barometer determined by reaction (14.15) is called the GASP barometer (for Garnet-Aluminosilicate-Silica-Plagioclase). However, because the reaction of the anorthite component of plagioclase to form the grossular component into garnet with increasing pressure is a common petrologic process, there are many barometers in addition to GASP that rely on the distribution of Ca between plagioclase and garnet.

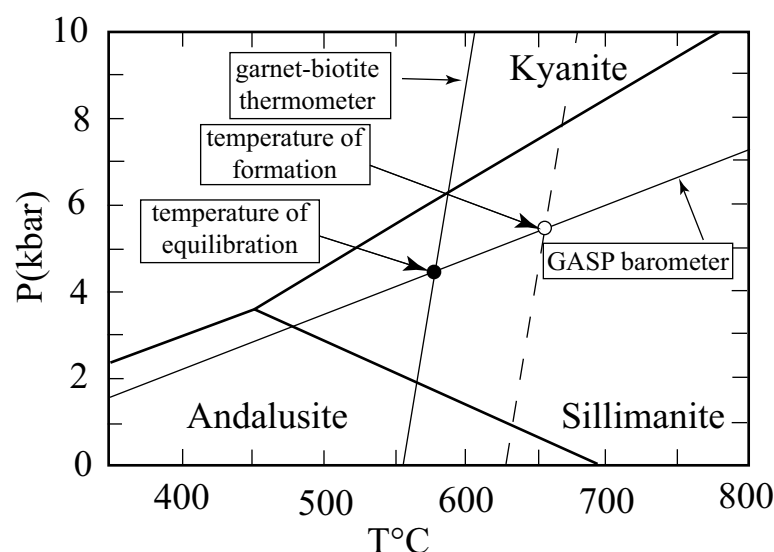


Figure 14.5 Thermobarometry from an assemblage sillimanite-garnet-biotite-plagioclase-quartz. Filled circle gives conditions of final equilibrium. Open circle gives possible conditions of formation followed by Fe-Mg exchange between garnet and biotite.

Because barometers involve reactions that transfer a component from one phase to another, they are called **mass-transfer reactions**. As a mass-transfer reaction (such as reaction {14.15}) proceeds under conditions of increasing pressure there is volumetrically less plagioclase in the rock and more garnet. This differs substantially from ion-exchange reactions, such as reaction (14.14). As reaction (14.14) proceeds with increasing temperature that amount of garnet and biotite remains the same, but Fe in garnet is exchanged for Mg in biotite.

14.3.3 Thermobarometry

Because thermometers have a steep slope and barometers have a gentle slope, the intersection of a thermometer and a barometer should provide a unique determination of the temperature and pressure at which an assemblage equilibrated. Figure 14.5 shows the results from a hypothetical assemblage of sillimanite-garnet-biotite-plagioclase-quartz. Analyses of garnet and plagioclase from this sample provide the location of the GASP barometer whereas analyses of biotite and garnet provide a temperature from the garnet biotite thermometer. The intersection of these two curves (filled circle at 550°C and 4.5 kilobars in Figure 14.5) is the point where the assemblage last equilibrated.

The problem with this approach is that, particularly at temperatures of upper amphibolite and granulite facies, mineral equilibria in a rock tend to reset on cooling. Thermometers that involve simple ion exchange tend

to reset readily and may freeze in at temperatures significantly below those at which the assemblage formed. Barometers, in contrast, involve dissolution of components from plagioclase, for example, and reprecipitation of those components in garnet. This is a much more complex process, and these types of equilibria tend to freeze in at much higher temperatures than ion-exchange equilibria. Thus, it is impossible to tell, without additional information, whether the garnet-sillimanite-biotite-plagioclase-quartz shown in Figure 14.5 actually formed at 550°C and 4.5 kilobars or whether it formed at a higher temperature and pressure (such as 650°C and 5.5 kilobars shown by the open circle in Figure 14.5) and the ion exchange reactions continued to reset as the rock cooled (Frost and Chacko, 1989).

One way to deal with this uncertainty is to determine the equilibrium conditions for a rock using all the possible equilibria in an assemblage (Berman, 1991). For example, given the assemblage Opx-Cpx-Grt-Pl-Qz, and using Fe- and Mg- end members of these solid solutions, Berman (1991) recognized eleven equilibria (Table 14.2). Note that some reactions (reactions 6, 8, and 4) involve simple exchange between Fe and Mg end members and are thermometers, and others (reactions 2, 5, 9, 11) involve equilibria between grossular and anorthite and are barometers. Other equilibria involve a mixture of ion-exchange and mass transfer reactions. To show the utility of his multi-equilibria approach, Berman calculated the P-T location of these eleven equilibria using the compositions of the

Table 14.2 *Equilibria in the Assemblage Opx-Cpx-Gar-Plag-Qz¹*

1. $\text{Qz} + \text{Di} + \text{Alm} = \text{An} + \text{En} + \text{Prp}$
2. $3 \text{Qz} + \text{Grs} + 2 \text{Alm} = 3 \text{An} + 6 \text{Fs}$
3. $3 \text{Qz} + 3 \text{Di} + 4 \text{Alm} = 3 \text{An} + 12 \text{Fs} + \text{Prp}$
4. $\text{Alm} + 3 \text{Di} = \text{Grs} + 3 \text{Fs} + 3 \text{En}$
5. $\text{Qz} + \text{Grs} + 3 \text{En} = \text{An} + 2 \text{Di}$
6. $\text{Alm} + 3 \text{En} = \text{Prp} + 3 \text{Fs}$
7. $\text{Qz} + \text{Prp} + \text{Di} = \text{An} + \text{En}$
8. $2 \text{Alm} + 3 \text{Di} = \text{Prp} + \text{Grs} + 6 \text{Fs}$
9. $3 \text{Qz} + \text{Prp} + 2 \text{Grs} = 3 \text{An} + \text{Di}$
10. $\text{Prp} + 3 \text{Di} = \text{En} + \text{Grs}$
11. $3 \text{Qz} + 2 \text{Prp} + \text{Grs} = 3 \text{An} + 6 \text{En}$

¹ Mineral abbreviations used in this text are defined in Table A.1.

texturally earliest assemblage in the rock (Figure 14.6A). All the equilibria intersect in a small area around 800°C and ten kilobars. When he used the composition of early phases mixed with the compositions of later-formed phases in the rock, which were clearly not in equilibrium with the earlier minerals, he obtained no common intersection (Figure 14.6B).

One can use Berman's (1991) multi-equilibria process to obtain an estimate of the original equilibrium conditions for an assemblage by back calculating to take the retrograde Fe-Mg exchange into account. Pattison and colleagues (2003) took a series of granulites and adjusted the Fe-Mg contents of the phases until the equilibria among the minerals intersected at a single point. When they did this they found that granulites formed at temperatures around 800°C, rather than the 700°C commonly recorded in the reset thermometers.

14.4 Conditions of Metamorphism

The results of experimental petrology and thermobarometry have allowed petrologists to determine the temperatures and pressures where the various facies boundaries lie (Figure 14.7). The boundaries in Figure 14.7 are shown in dashed lines because the locations of the reactions that determine the facies boundaries are very strongly dependent on bulk rock composition (Green and Ringwood, 1972; Evans, 1990). Despite this inherent uncertainty,

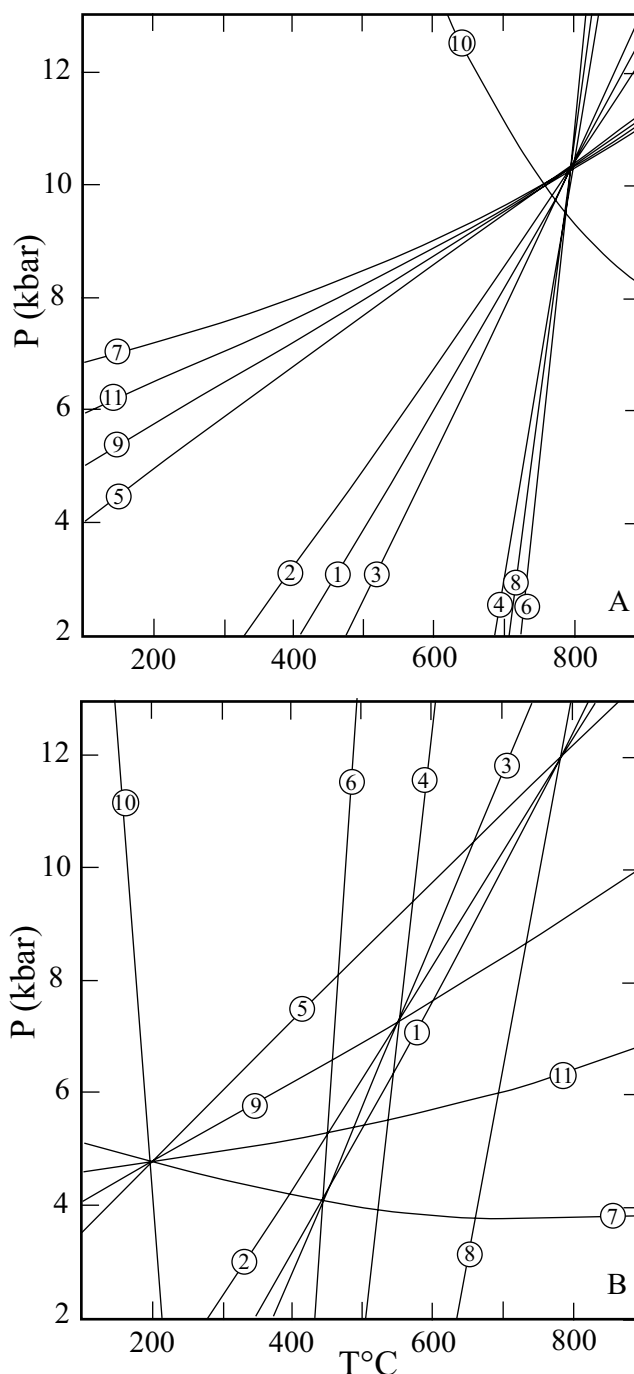


Figure 14.6 P-T diagrams showing multi-equilibria thermometry of a granulite with the assemblage orthopyroxene-clinopyroxene-garnet-plagioclase-quartz. (A) Calculations using the compositions of texturally early phases. (B) Calculations using compositions of a mixture of texturally early and young phases. Data from Berman (1991). Numbers refer to reactions given in Table 14.2.

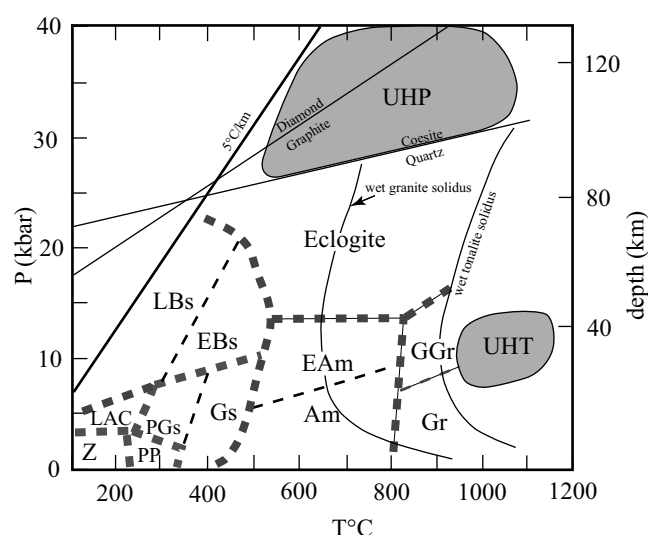


Figure 14.7 P-T conditions of metamorphism showing the conditions for UHP and UHT metamorphism and the approximate conditions for the metamorphic facies. Am = amphibolite, EAm = epidote amphibolite, EBs = epidote blueschist, LBs = lawsonite blueschist, Gr = granulite, GGr = garnet granulite, Gs = greenschist, PGs = pumpellyite greenschist, PP = prehnite-pumpellyite, LAC = lawsonite-albite-chlorite, Z = zeolite. Data from Evans (1990), Green and Ringwood (1972), Harley (1998), Liou, Maruyama, and Cho (1987), Liou and colleagues (2004), and Moody, Meyer, and Jenkins (1983).

Figure 14.7 gives a good indication of where the various metamorphic facies lie in P-T space.

14.4.1 The Pressure and Temperature Conditions for the Metamorphic Facies

In Figure 14.7 the low-temperature limit for metamorphism is set at the geothermal gradient of 5°C/km since rare examples of cold subduction have assemblages indicating metamorphism under these geothermal gradients (Ravana et al., 2010). At low pressures and temperatures, metamorphism grades into diagenesis. Zeolites, particularly laumontite, are common diagenetic minerals in sandstones (Noh and Boles, 1993). Indeed in some locations diagenesis extends to temperatures around 200°C, well into the field of zeolite facies (Helmold and Van de Kamp, 1984). The boundary between diagenesis and metamorphism is poorly defined. One reasonable distinction between the two is that diagenesis involves deposition of material in the pores of a sandstone, whereas metamorphic reactions involve a substantial participation of the grains as well.

The low-temperature limit for zeolite facies is difficult to constrain because zeolite stability is strongly dependent on the fluid composition. Zeolites may not appear at all if the fluid is too rich in CO₂. Even moderate amounts of CO₂ in the fluids causes kaolinite + calcite to form instead of laumontite (Frost, 1980). In many low-grade terrains, metasediments contain the assemblage clay-calcite-quartz; zeolites are never encountered. Some zeolite assemblages, especially those in which analcime has replaced albite, have formed at temperatures as low as 125°C (Miron, Neuhoﬀ, and Amthauer, 2012). The high-temperature limits of zeolite facies are marked by the disappearance of zeolites from basaltic rocks. Frost (1980) argues these conditions coincide with the formation of the epidote-chlorite-quartz tie line (Figure 13.7B) at temperatures around 250°C.

Prehnite-pumpellyite facies is stable from around 250°C to around 300–350°C, where actinolite appears, marking the transition to greenschist facies. The high-temperature limit to greenschist facies is around 400–450°C. The high-pressure limit, of greenschist facies, where it is bounded by blueschist facies, is around six kilobars. The high-temperature limit of blueschist facies, where, like greenschist facies, it is bounded by amphibolite facies, is somewhat higher than the high-temperature limit of greenschist facies, perhaps 450–500°C. The high-pressure limit of blueschist facies, where it transitions to eclogite facies, is strongly temperature and composition dependent and ranges from ten to twenty kilobars.

Amphibolite facies covers the whole range of conditions from ca. 400–500°C to 800°C. The cores of many metamorphic terrains are marked by areas of abundant granite, usually intermixed with various types of metamorphic rocks. These field relations indicate the high-grade areas were flooded with granitic melt. In most of these areas, hornblende has remained stable in mafic rocks and is present in many of the surrounding granites. Thus, in most environments amphibolite facies extends into the realm of igneous crystallization. This is consistent with experimental studies (Figure 14.8), which show that when $P_{H_2O} = P_{total}$ hornblende begins to break down to pyroxenes at temperatures around 800°C. Thermometry indicates that granulites may equilibrate at 700°C, although Pattison and colleagues (2003) argue this temperature is due to resetting of the thermometers and that the low-temperature limit to granulite metamorphism is around

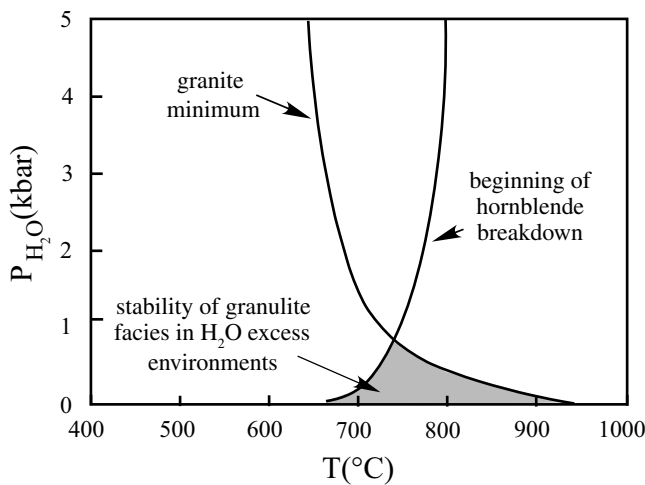


Figure 14.8 Comparison of the P-T conditions for granite minimum melt (Luth, Jahns, and Tuttle, 1964) and the beginning of hornblende breakdown (Spear, 1981).

the 800°C indicated by experimental studies. The transition from amphibolite to eclogite facies at high pressure is rarely preserved in nature. Figure 14.7 shows the transition occurs somewhere around twelve to fourteen kilobars, although this limit is poorly constrained.

Figure 14.8 shows that when $P_{H_2O} = P_{total}$ pyroxenes are stable with a granitic melt only at very low pressures. From this, it is evident that granulite facies requires unusually anhydrous conditions for formation. The cause of these anhydrous conditions was the subject of intense debate throughout the 1980s. Some authors maintain that granulites display evidence of pervasive CO_2 streaming from the mantle (Collerson and Fryer, 1978); others believe the dehydration is a natural consequence of crustal melting (Brown and Fyfe, 1970), while others argue granulite metamorphism is associated with the passage of dry magmas through the lower crust (Frost and Frost, 1987; Figure 14.9). The theory of CO_2 streaming is partially constructed on the conclusion from thermobarometry that granulites form at relatively low temperatures (ca. 700°C). If this is true, then something external, such as the addition of CO_2 , is needed to suppress the temperature of hornblende dehydration. The observation by Pattison and colleagues (2003) that the lower temperature limits of granulite facies is closer to 800°C obviates the need for anhydrous fluids to suppress amphibole stability, meaning the theories of Brown and Fyfe (1970) and Frost and Frost (1987) are more likely to be true. This suggests granulite

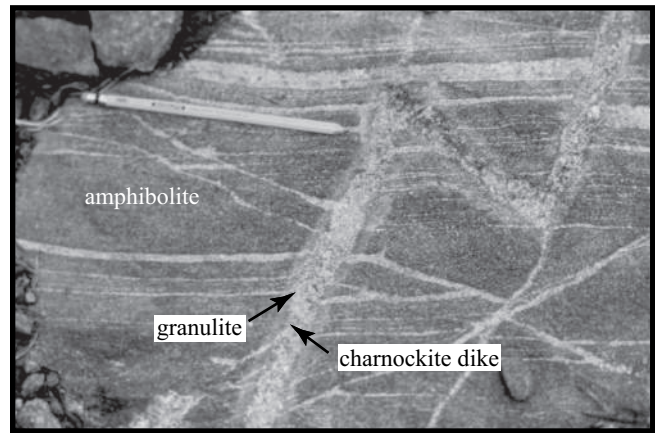


Figure 14.9 Photograph of charnockite dike in amphibolite in the Wind River Range, Wyoming. Intrusion of anhydrous charnockitic magma dehydrated the adjacent amphibolite, producing a granulite facies selvage along the margins of the dike. On a larger scale, this process may be responsible for the formation of granulite terrains.

mineral assemblages formed under unusually hot conditions in the lower and middle crust likely in response to igneous activity.

The lower pressure limits to eclogite facies are shown in Figure 14.7 to lie between fifteen and twenty kilobars, although there is a great uncertainty in this. Because mafic rocks have a wide range in composition, the lower pressure limit of eclogite facies will occur at different pressure for different mafic rocks. Depending on the bulk composition of the rock, the lower limit of eclogite facies lies between twelve and twenty kilobars (De Paoli, Clarke, and Daczko, 2012).

14.4.2 The Upper Temperature Limits to Metamorphism and Migmatites

The upper temperature limit of metamorphism lies at the wet tonalite solidus, where basaltic rocks melt to make tonalite magma. Most metamorphic terrains lie at temperatures below this, but a few record temperatures of metamorphism in excess of 1,000°C. This extreme condition has been called ultra-high-temperature (UHT) metamorphism and indicates heating of the lower crust by either basaltic melts or diapiric emplacement of hot asthenosphere (Harley, 1998).

Even at temperatures well below those of high- and ultra-high-temperature metamorphism, rocks will begin to melt. In fact, most rocks in UHT terranes are refractory

rocks from which granitic melt has already been extracted. These rocks are called **restites**. Most melting takes place under conditions of upper amphibolite facies where rocks contain water. Subjection of high-T metasedimentary rocks, mostly biotite-rich psammitic and pelitic schists, to decompression can produce considerable magma through dehydration melting (see Figure 10.1). If the granitic melt is segregated into large bodies it will produce leucogranites, such as the Himalayan granite discussed in Chapter 10. If the melt is not efficiently segregated from the restite, melting produces a **migmatite**.

A migmatite is a “mixed rock” that contains granite, or granitic gneiss, interlayered with a more mafic gneiss (Figure 14.10). The granitic layers are called **leucosome** (for light layer) and the more mafic layers are called **melanosome** (for dark layer) (Mehnert, 1968). The leucosome usually is granitic, since this rock melts at the lowest temperature, but it may range in composition from granite to tonalite. The melanosome may range from pelitic, wherein it will contain biotite and Al-rich silicates such as garnet, cordierite, or sillimanite, to psammitic, wherein it will contain mainly biotite as the ferromagnesian silicate, although hornblende and garnet may be present.

A key question when interpreting a migmatite is whether the rock represents a closed system, in which the leucosome and melanosome separated from the protolith through melting or metamorphic segregation, or whether the leucosome represents granitic material injected from an external source. In most migmatite localities this is difficult to determine because no sample of the unmelted protolith survives. In some localities a melting reaction that relates the leucosome (i.e., the melt) with the melanosome (i.e., the restite) is apparent (Milord, Sawyer, and Brown, 2001), but in most migmatites the reaction relationship is unclear. In many occurrences of migmatite it is difficult to tell whether the leucosome was extracted from the melanosome, even through the use of chemical analyses. One helpful feature is the presence of a **mafic selvage**, a concentration of mafic minerals (mostly biotite and hornblende) on the contact between the melanosome and the leucosome, such as in Figure 14.10. The presence of a mafic selvage indicates that at least some portion of the leucosome was derived from the melanosome, leaving a selvage of mafic minerals behind.

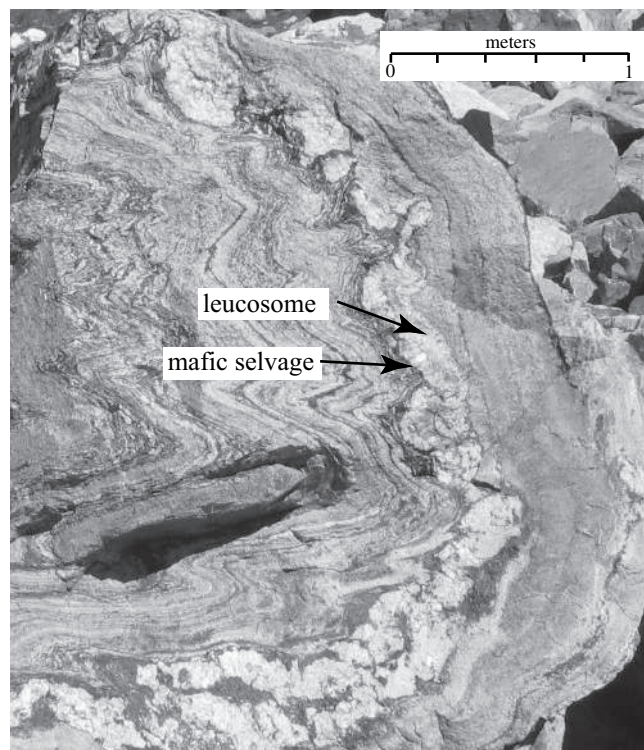


Figure 14.10 Photograph of migmatitic paragneiss, Teton Range, Wyoming. The existence of a mafic selvage around the leucosome indicates that at least some of the granitic material in the leucosome was extracted from the host rock.

14.4.3 Upper Pressure Limit of Metamorphism

The upper pressure limit on metamorphism is mostly determined by the preservation of ultra-high-pressure (UHP) rocks. UHP rocks almost certainly represent fragments of continental crust that were subducted to mantle depths during continental collisions and were tectonically exhumed because of the inherent buoyancy of continental crust (Liou et al., 2004). Fragments of rocks subjected to pressures within the coesite stability field are present in many orogenic belts. Most of these UHP rocks were metamorphosed at pressures of twenty to forty kilobars, but some rocks preserve evidence of pressures around sixty kilobars (Nimis and Trommsdorff, 2001). The presence of rocks evincing UHP metamorphism is a dramatic indication of the dynamic nature of Earth's crust. Without the presence of rocks containing relict coesite there would be little indication that crustal rocks could be subducted to depths of 120 kilometers or more and then return to the surface to tell their stories (see Box 14.1).

BOX 14.1 | THE DYNAMIC EARTH

Since the plate tectonic revolution in the 1970s geologists have known that Earth is a highly dynamic planet. All students of introductory geology learn that crust is continually consumed at subduction zones and replenished at mid-ocean ridges. More recently metamorphic petrology has shown just how dynamic the process of subduction and continental collision is. The first hint was the discovery of coesite in whiteschists from the western Alps (Chopin, 1984). Coesite is a high-pressure polymorph of quartz only stable at pressures of more than twenty-five kilobars (Figure 14.7). Coesite is now known in many high-P terrains from the Caledonian orogeny in Norway (Janak, Ravana, and Kullerud, 2012), in various mobile belts in China (Han et al., 2011; Liu et al., 2011), and in the Himalaya (Mukherjee and Sachan, 2009). The presence of coesite-bearing eclogites means portions of mountain belts must have been exhumed from depths of nearly 100 kilometers. Similar high pressures are reported from eclogites on the Zermatt-Saas ophiolite (Bucher and Grapes, 2009), but these are trivial compared to the possible sixty-kilobar pressures estimated for garnet peridotite inclusions in the Alps (Nimis and Trommsdorff, 2001). Together, these petrologic observations indicate that crustal material can be carried to depth of 100 kilometers (or more) and exhumed rapidly enough that the mineral record of these conditions is preserved.

Summary

.....

- **Thermobarometry** involves the use of thermodynamics to determine the temperatures and pressures at which mineral assemblages last equilibrated.
- **Thermometers** are reactions that involve very small changes in volume over a range of temperatures. Good thermometers include
 - **Ion-exchange thermometers** in which ions such as Fe and Mg are exchanged between two minerals
 - **Solvus thermometers**
- **Barometers** are reactions that involve large volume changes over a range of pressures.
- Combining a thermometer and a barometer should give the temperature and pressure at which an assemblage crystallized, unless the ion-exchange thermometer re-equilibrated on cooling.
- Thermometry shows that the temperature conditions of metamorphism ranges from around 200°C to more than 900°C.
- Barometry shows that, whereas most metamorphism occurs at pressures less than eight kilobars, some high-pressure rocks may have formed at pressures of twenty-five kilobars or more.

Questions and Problems

.....

Problem 14.1. How does a modern approach to determining metamorphic conditions compare to Eskola's metamorphic facies approach? What are the advantages and disadvantages of each?

Problem 14.2. What kinds of reactions make the best thermometers?

Problem 14.3. What kind of reaction makes a good barometer?

Problem 14.4. What is the difference between mass-transfer and ion-exchange reactions?

Problem 14.5. Referring to Figure 14.4, determine whether ΔG for the reaction $An = Grs + Ky + Q$ positive or negative at 600°C and ten kilobars.

Problem 14.6. What is a migmatite? What does it tell the geologist about the metamorphic conditions?

Further Reading

.....

Berman, R. G., 1991, Thermobarometry using multi-equilibrium calculations: a new technique, with petrological applications. *Canadian Mineralogist*, 29, 833–55.

Ernst, W. G., 1976, *Petrologic phase equilibria*, San Francisco, W.H. Freeman.

Powell, R. and Holland, T. J. B., 2008. On thermobarometry. *Journal of Metamorphic Geology*, 26, 155–79.

Chapter 15

Metamorphism of Peridotitic Rocks

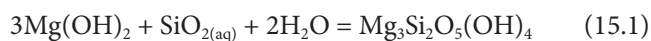
15.1 Introduction

Most peridotitic rocks originally formed as portions of the upper mantle and oceanic crust. During interaction with seawater on the sea floor or during tectonic events occurring at subduction zones, metaperidotite, originally composed of olivine and pyroxenes, may be wholly or partially converted to serpentine $[(\text{Mg,Fe})_3\text{Si}_2\text{O}_5(\text{OH})_4]$. Prograde metamorphism initiates a series of mineralogical changes in these serpentinites that make them effective markers of metamorphic conditions. Thus, although metamorphosed serpentinites and peridotites make up only a small portion of most metamorphic belts, their significance is greater than their abundance might suggest. Because their very existence in a sequence indicates those rocks incorporated ultramafic material, either from the mantle or from the cumulate horizon of a layered mafic intrusion, the presence of metaperidotite provides clues about the geologic history of the rock sequence within which it lies. In addition, metaperidotite mineral assemblages are very useful in estimating the temperature of metamorphism. Last, because peridotites are chemically simple rocks, they are a good protolith to illustrate how mineral assemblages can estimate metamorphic conditions.

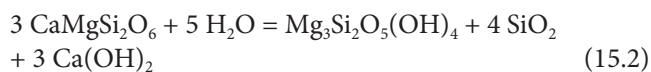
15.2 The Process of Serpentinization

The processes by which mantle peridotites become serpentinites must be discussed before describing the metamorphism of serpentinite. The description of oceanic magmatism in Chapter 7 noted how faulting commonly exposes peridotites on the sea floor. Those peridotites exposed on or within a few kilometers of the sea floor react with seawater to form serpentinite. Serpentinization plays a major role in modifying the rheology of the oceanic crust, defines an important geochemical process on the sea floor, and produces the most reducing, alkaline fluids of any natural environment on Earth.

When, at low temperatures, peridotites can access water, either by exposure on the sea floor or in other tectonic environments, these rocks undergo serpentinization. The modal mineralogy of the peridotite controls the products of low-temperature metamorphism. If the original rock consisted of more than 58 volume percent olivine, as is typical of most peridotites, the first products of hydration are serpentine and brucite. If, on the other hand, the protolith was a pyroxenite with less than 58 volume percent olivine, the hydrated rock consists of serpentine + talc. Although peridotites and serpentinites have a relatively simple chemical composition – they can be well constrained by the system CaO-MgO-FeO-SiO_2 – the process of serpentinization is complex. Part of this complexity comes from the fact that, given a source of silica, brucite ($\text{Mg,Fe}(\text{OH})_2$) will react to make serpentine (Frost and Beard, 2007) by reaction (15.1):



The silica needed for this reaction can come from many sources, including alteration of orthopyroxene within the peridotite or alteration of plagioclase in associated gabbro. Another source of silica is from hydration of diopside in peridotite to make serpentine (reaction (15.2)):



This reaction produces abundant silica from the conversion of brucite to serpentine, and it also produces abundant $\text{Ca}(\text{OH})_2$. Calcium hydroxide is a strong base, which explains why hydration of peridotite produces alkaline fluids (which may reach pH of twelve). When these Ca-bearing fluids encounter a rock that is not ultramafic, the Ca reacts with this rock to form a **rodingite**. No matter

whether the protolith to rodingite was basalt or gabbro, pelitic rocks or granite, the minerals formed are the same: grossular, epidote, prehnite, and other Ca-Al silicates. Although in some ways rodingites are petrologic oddities, they provide important clues that help petrologists reconstruct the tectonic history of an area. In high-grade metamorphic terrains, they may provide the only evidence that the metaperidotites with which they are associated were once serpentinites.

Serpentinization almost always involves the magnetite formation. Since almost all the iron in olivine is ferrous, magnetite formation requires significant oxidation. This may seem strange, given the extremely reducing nature of serpentinite. The exact process by which magnetite is formed is still a matter of considerable debate, but the significant consequence is that the fluids released from serpentinites create some of the most reducing conditions on Earth. Early in Earth's history, the reducing conditions in serpentinizing environments may have been conducive to the synthesis of reduced organic compounds that combined to produce the earliest lifeforms (Russell, Hall, and Martin, 2010).

Serpentinization causes a 40 to 50 percent increase in the volume of the rock, which may affect ocean floor bathymetry in areas underlain by serpentinites. Because this large volume change becomes a volume *decrease* when serpentinite breaks down during metamorphism in subduction zones, some petrologists propose that some deep-focus earthquakes could be caused by dehydration of serpentinite in subduction zones (Dobson, Meredith, and Boon, 2002).

15.3 Prograde Metamorphism of Serpentinite: Reactions in the System $\text{CaO-MgO-SiO}_2\text{-H}_2\text{O}$

Serpentine is a mineral group that includes chrysotile, lizardite, and antigorite. Serpentine group minerals consist of interlayered tetrahedral ($(\text{Si}_2\text{O}_5)^{2-}$) and octahedral ($\text{Mg}_3(\text{OH})_6$) sheets. Charge balance is maintained because two of the oxygen atoms in the tetrahedral sheet substitute for two OH ions in the octahedral sheet. However, the two sheets are not the same size; the octahedral sheet is somewhat larger than the tetrahedral sheet. This misfit can be accommodated in three ways. One way is for the misfit to spread throughout the structure, producing the mineral **lizardite**. Another way is for the misfit to accommodate by

Table 15.1 Reactions Occurring during Metamorphism of Peridotitic Rocks

Reaction	No
17 Ctl = 3 Brc + Atg ¹	(15.3)
Atg + 20 Brc = 34 Fo + 51 H ₂ O	(15.4)
Atg + 8 Di = 18 Fo + 4 Tr + 27 H ₂ O	(15.5)
Atg = 18 Fo + 4 Tlc + 27 H ₂ O	(15.6)
4 Fo + 9 Tlc = 5 Ath + 4 H ₂ O	(15.7)
2 Fo + 2 Ath = 9 En + 2H ₂ O	(15.8)
2 Fo + 2Tlc = 5 En + H ₂ O	(15.9)
2En + Tlc = Ath	(15.10)
Fo + Tr = 3 En + 2Di + H ₂ O	(15.11)
Tc + Mgs = 4 Fo + 5 CO ₂ + H ₂ O	(15.12)
3 Mgs + 2 Q + H ₂ O = Tlc + 3 CO ₂	(15.13)
Atg + 20 Mgs = 34 Fo + 31 H ₂ O + 20 CO ₂	(15.14)
17 Tlc + 45 Mgs + 45 H ₂ O = 2 Atg + 45 CO ₂	(15.15)
Brc + CO ₂ = Mgs + H ₂ O	(15.16)

¹ Capitani and Mellini (2004) give the composition of antigorite as Mg_{2.82}Si₂O₅(OH)_{3.64}. Multiplying by seventeen yields the composition Mg₄₈Si₃₄O₈₅(OH)₆₂, which was used in balancing reactions on this table.

curvature of the sheet, making a fiber, the mineral form of **chrysotile**. The third way is for the structure to modulate such that some areas have the octahedral sheet pointing up and others have it pointing down. When the sheets flip, a certain amount of the brucite sheet is omitted to make it better fit to the shape of the tetrahedral sheet, making the mineral **antigorite**, which is not, strictly speaking, a polymorph of serpentine because it is slightly more silica rich (Capitani and Mellini, 2004).

Because antigorite is also slightly less hydrous than lizardite or chrysotile, it is the high-temperature phase. The formation reaction is chrysotile (or lizardite) = brucite + antigorite (reaction (15.3) in Table 15.1). One of the first metamorphic effects recognizable in serpentinites is the replacement of lizardite by antigorite. Although it is difficult to distinguish serpentine polymorphs in thin section, antigorite has a clearly bladed appearance (though it is very fine-grained), whereas lizardite does not (compare Figures 15.1A and 15.1B).

Most of the mineralogical changes encountered during metamorphism of peridotitic rocks can be modeled

using the system CaO-MgO-SiO₂-H₂O. Although Al₂O₃ and FeO are present, they do not affect the basic petroge- netic relationships. The mineral reactions encountered in the system CaO-MgO-SiO₂-H₂O at low and medium tem- peratures of metamorphism are listed in Table 15.1, and the occurrence of these reactions in P-T space is shown in Figure 15.2. All phase diagrams in this chapter, includ- ing Figure 15.2, were calculated from the thermody- namic data of Berman (1988). The mineralogical changes encountered in the system CaO-MgO-SiO₂-H₂O are con- trolled by dehydration reactions that have steep slopes on a P-T diagram. As a result, metaperidotites are very sensitive indicators of changes in metamorphic temper- ature but are generally poor indicators of metamorphic pressure. Notice that in the pure Mg system, anthophyl- lite in metaperidotites is restricted to pressures below six kilobars (reaction {15.8}). Furthermore, the reaction of olivine + talc to enstatite + H₂O (reaction {15.9}) has a slightly negative slope. At very high pressures (around fifteen kilobars), the reaction trace intersects antigorite = forsterite + talc + H₂O, truncating the stability field for talc in metaperidotites. The reaction of antigorite directly to forsterite + enstatite may rarely occur deep in subduc- tion zones, but it is only recognized at one location in the world (Padrón-Navarta and colleagues, 2011). The dis- cussion in this chapter therefore focuses on relations at crustal pressures shown in Figure 15.2.

The chemography of peridotitic rocks can be represented by projecting from H₂O, assuming the system is hydrated throughout reaction, onto the system CaO-MgO-SiO₂ (Figure 15.3). Since all reactions of interest occur within the triangle defined by brucite (or periclase)-diopside- quartz (see assemblage **a**, Figure 15.3), only that part of the system defined by the triangle brucite-diopside-quartz is shown for the other assemblages. Primary peridotites have a relatively restricted composition and will consist mostly of olivine with lesser amounts (10–20 percent) of enstatite and diopside. The limited range of composition means there will be only one divariant assemblage stable in metaperidotites at any given temperature. These assem- blages (labeled **a** through **h**) are shown in Figure 15.2 and again in Figure 15.3 as gray fields.

At low temperatures, the stable phases in a serpentinite include chrysotile (or lizardite), brucite, and diopside (assemblage **a**, Figure 15.3). The brucite may be cryptic, meaning it may not be visible in thin section and can only be distinguished by X-ray diffraction. The diopside

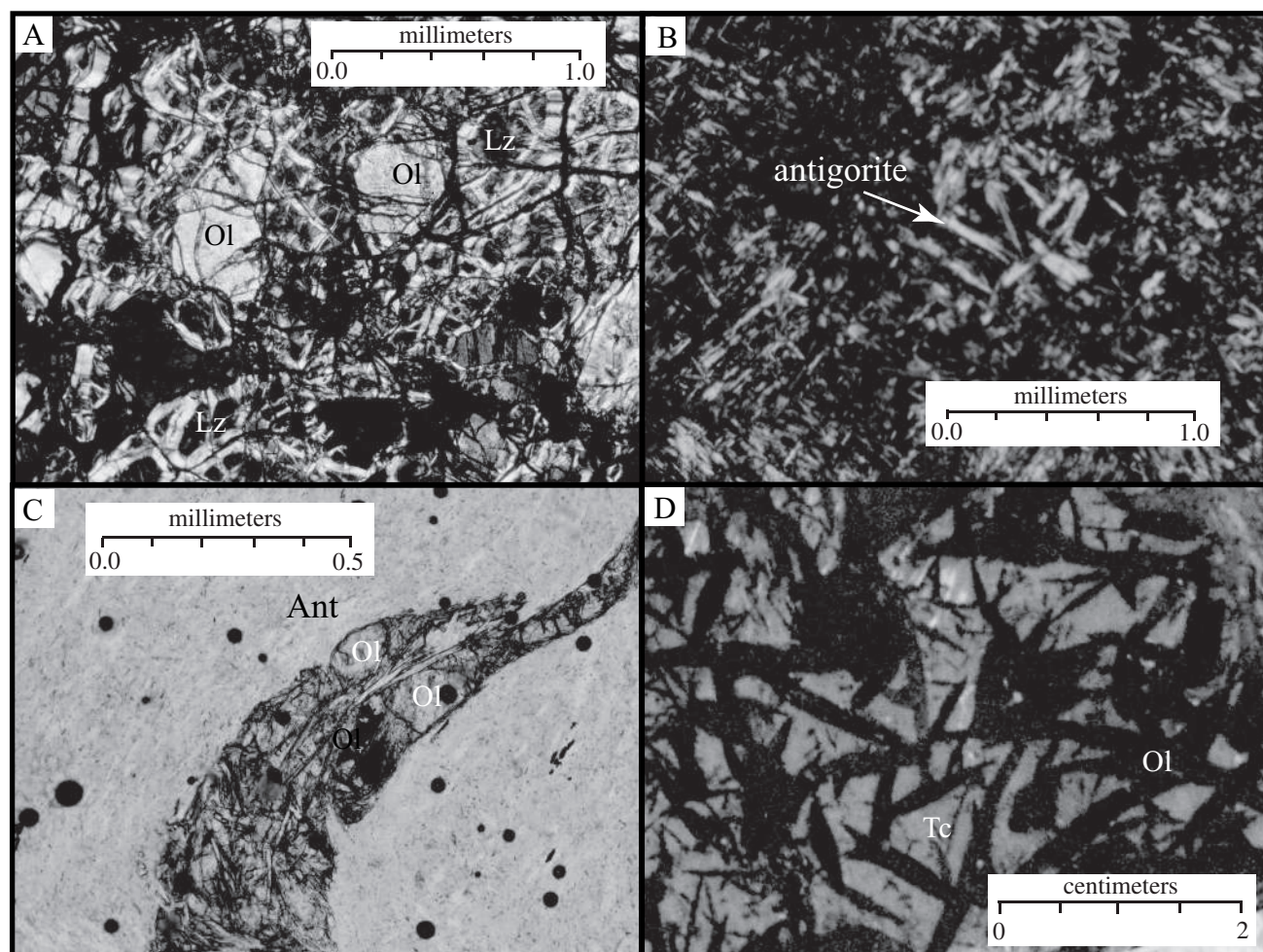


Figure 15.1 Photographs and photomicrographs of textures in metaperidotites. (A) Photomicrograph in XPL showing lizardite pseudomorphs after olivine. Notice onion-skin texture of the lizardite pseudomorphs. Paddy-Go-Easy pass, Central Cascades, Washington. (B) Photomicrograph in XPL showing antigorite serpentinite. Notice how the antigorite is acicular. Paddy-Go-Easy pass, Central Cascades, Washington. (C) Photomicrograph in XPL of olivine (Ol) in equilibrium with antigorite (Atg) from the Zermatt-Saas area, Swiss Alps. Black circles are bubbles in the mounting epoxy. (D) Photograph of elongate olivine crystals, showing characteristic “jack-straw” texture, in olivine-talc rocks, central Cascades, Washington

may be relict after the primary diopside in the rock, although stable metamorphic diopside may be present as well. As noted earlier, the first change observed during prograde metamorphism is the change from chrysotile or lizardite to antigorite (reaction {15.3}). Brucite may appear at this point, since antigorite is slightly more siliceous than chrysotile or lizardite. Although this reaction is shown as a line in Figure 15.1, its location in P-T space is poorly constrained. Furthermore, the reaction is apparently very sluggish, since detailed X-ray studies show that chrysotile persists in some rocks to olivine-bearing grades.

Olivine appears in metaperidotites by the model reaction antigorite + brucite = forsterite + H₂O (reaction {15.4}), leading to the assemblage antigorite-olivine-diopside (assemblage c, Figure 15.3). Texturally the olivine produced by this reaction is distinct from relict olivine. Generally it has rational boundaries with antigorite (i.e., the boundary is parallel to 001 plane in antigorite) (Figure 15.1C). If olivine grains impinge each other during growth they will form typical 120° grain boundaries, the dihedral angle, without any crystallographic evidence of serpentine. Such a texture is exceedingly unlikely in rocks containing relict olivine and serpentine.

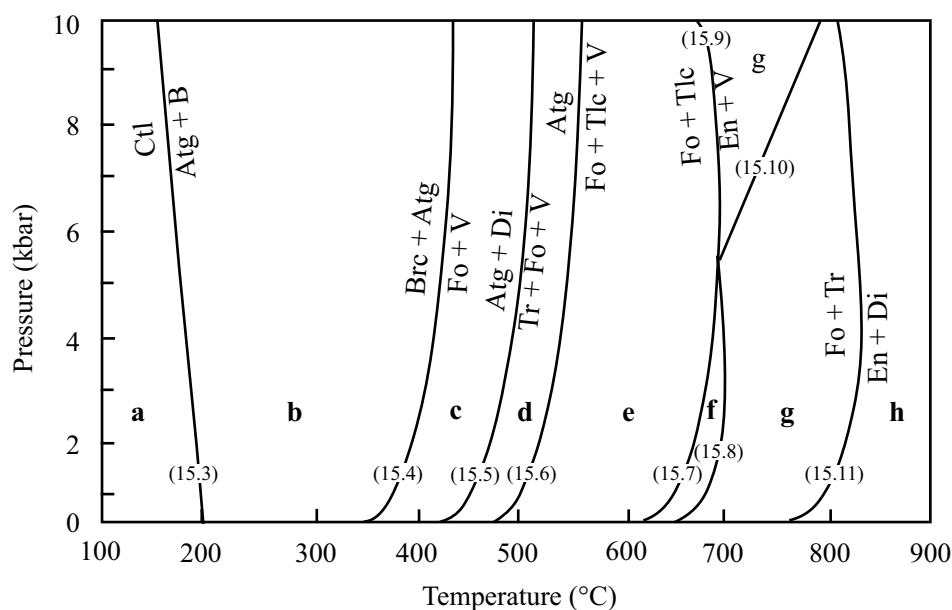


Figure 15.2 P-T diagram showing mineral stabilities in the system CaO-MgO-SiO₂-H₂O. Numbers refer to reactions listed in Table 15.1.

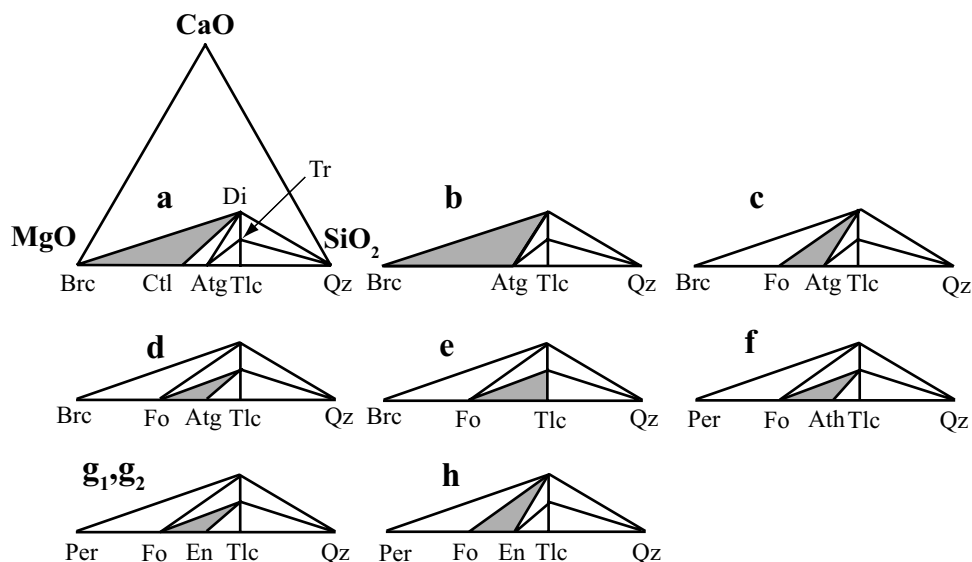


Figure 15.3 Chemographic projections showing assemblages in the divariant fields in Figure 15.2. Stippled areas show assemblages in metaperidotites. Ath = anthophyllite, Atg = antigorite, Brc = brucite, Ctl = chrysotile, En = enstatite, Di = diopside, Per = periclase, Qz = quartz, Tlc = talc, Tr = tremolite.

The next change encountered with increasing metamorphic grade involves the disappearance of diopside by the reaction diopside + antigorite = forsterite + tremolite + H₂O (reaction {15.5}), forming the assemblage antigorite-olivine-tremolite (assemblage **d**, Figure 15.3). Note that this reaction not only produces tremolite, but also increases the amount of olivine relative to antigorite. Antigorite disappears at a slightly higher metamorphic grade by the reaction antigorite = forsterite + talc +

H₂O (reaction {15.6}). In metaperidotites, this reaction produces the assemblage olivine-talc-tremolite (assemblage **e**, Figure 15.3). In some metamorphic rocks, olivine forming by this reaction will be distinctively elongate (Figure 15.1D). Some workers have mistaken reaction (15.6) for the reaction that marks the first appearance of olivine. However, in a typical metaperidotite, olivine appears by reaction (15.4) at temperatures almost 100°C lower than those marked by reaction (15.6). Indeed, given

a typical protolith (80 percent olivine, 10 percent enstatite, and 10 percent diopside), at temperatures just below those of reaction (15.6), the rock will have 68 percent olivine, 16 percent tremolite, and only 16 percent antigorite. Thus, the dehydration of serpentine to peridotite is not a single step that releases large amounts of H_2O at a given temperature, but rather a process that takes place over a temperature span of 100°C .

In the pure system, the assemblage olivine-talc-tremolite is limited at high temperatures by the reaction forsterite + talc = anthophyllite + H_2O (reaction {15.7}) or, at higher pressures by the reaction forsterite + talc = enstatite + H_2O (reaction {15.9}). Reaction (15.7) produces the assemblage olivine-anthophyllite-tremolite (assemblage **f**, Figure 15.3). Because most metaperidotites in this temperature range contain tremolite, it is important to distinguish anthophyllite from tremolite in thin section. The easiest way to accomplish this is to search for amphiboles with the highest birefringence. In grains with this orientation, the petrographer looks nearly down the Y index and, therefore, the b crystallographic axis. In such an orientation, anthophyllite will have parallel extinction, whereas tremolite will have extinction of about 15° .

At temperatures slightly higher than those of reaction (15.7), anthophyllite reacts out by reaction (15.8), anthophyllite + forsterite = enstatite + H_2O , producing the assemblage olivine-enstatite-tremolite (assemblages **g1** and **g2**, Figure 15.3). This is the same assemblage that would be produced by reaction (15.10) at higher pressures. Finally, at somewhat higher temperatures, tremolite + forsterite reacts to form diopside by reaction (15.11). This produces the ultramafic assemblage olivine-enstatite-diopside, (assemblage **h**, Figure 15.3), which is the same as that of the mantle protolith for metaperidotites.

15.4 Role of Minor Components

15.4.1 Iron

The preceding section described reactions in metaperidotites assuming they were composed solely of CaO , MgO , SiO_2 , and H_2O . The average peridotite contains $X_{\text{Fe}} \sim 0.1$, so it is important to consider the effect that small amounts of iron have on the reactions shown in Figure 15.2. This question can be addressed using two simple chemical principles. The first is that chemical species, such as iron and magnesium, are seldom distributed evenly between

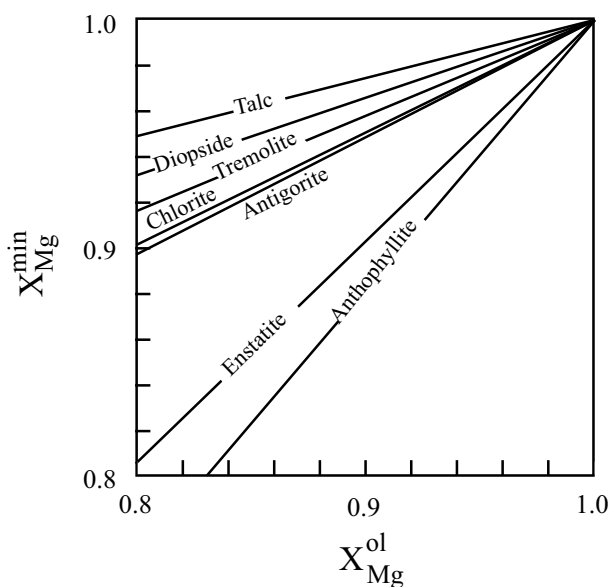


Figure 15.4 Diagram showing the relation between X_{Mg} of olivine and X_{Mg} of other silicates. Data from Trommsdorff and Evans (1974).

phases. Some minerals have structural sites that are more suitable for magnesium, which is a slightly smaller ion, than for iron. Consequently, there is a distribution of iron and magnesium between coexisting silicates in natural systems, with the result that X_{Mg} ($\text{Mg}/(\text{Mg}+\text{Fe})$) is different for different minerals in a rock. Figure 15.4 shows a plot of X_{Mg} for various silicates in metaperidotites compared to X_{Mg} of coexisting olivine. From this diagram it is evident that anthophyllite is always more iron rich than olivine, while enstatite is only slightly more magnesian. Talc, diopside, tremolite, chlorite, and antigorite are considerably more magnesian than coexisting olivine, with talc the most magnesian mineral found in metaperidotites.

The second chemical principle, Le Chatelier's Principle, explains the significance of this iron distribution. Le Chatelier's Principle states that a chemical equilibrium responds to any disturbance by trying to undo the effects of that disturbance. To see how this operates, consider the reaction talc = enstatite + quartz + H_2O . Figure 15.4 shows that enstatite accepts iron more readily than does talc. If a small amount of iron is added to this system, Le Chatelier's Principle indicates the reaction will adjust itself to counter the effects of this addition. Because enstatite can accept iron more readily than can talc, enstatite stabilizes, driving the reaction talc = enstatite + quartz + H_2O to lower temperatures.

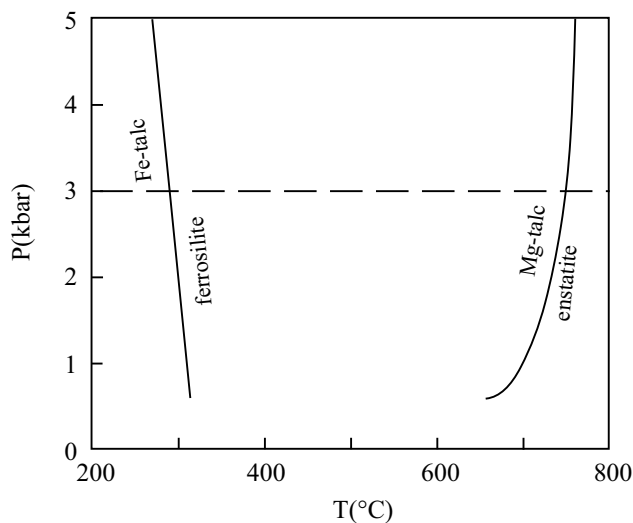


Figure 15.5 P-T diagram comparing the breakdown of Mg-talc with Fe-talc. The dashed line is the pressure at which the isobaric section in Figure 15.6 is constructed.

The addition of FeO to the system $\text{CaO-MgO-SiO}_2\text{-H}_2\text{O}$ has another effect, as indicated by the phase rule. Because FeO dissolves into the silicate phases without producing a new phase, the addition of FeO also adds an additional degree of freedom in all reactions. This means that a reaction, which is univariant in the pure system $\text{MgO-SiO}_2\text{-H}_2\text{O}$, is divariant in the system containing FeO. This increase in variance means the reaction can only be used to estimate temperature when pressure is known and X_{Mg} can be determined.

To see how this works, consider again the reaction $\text{talc} = \text{orthopyroxene} + \text{quartz} + \text{H}_2\text{O}$. Figure 15.5 shows the P-T conditions at which both pure magnesium and pure iron reactions occur (this example is for illustrative purposes; however, the pure iron reaction is metastable and iron amphiboles would form instead of orthopyroxene and iron-rich talc). As indicated previously, because of the strong tendency for iron to favor orthopyroxene, the iron end member of the reaction lies at a lower temperature than does the magnesium end member. In a natural system containing both iron and magnesium, talc must break down at some temperature between the extremes shown in Figure 15.5. A helpful way to visualize the effect of composition on talc breakdown is to display relations on a T- X_{Mg} diagram constructed at fixed pressure (i.e., isobaric conditions) (Figure 15.6). At the pressure of three kilobars, iron-talc breaks down at 292°C and magnesium-talc

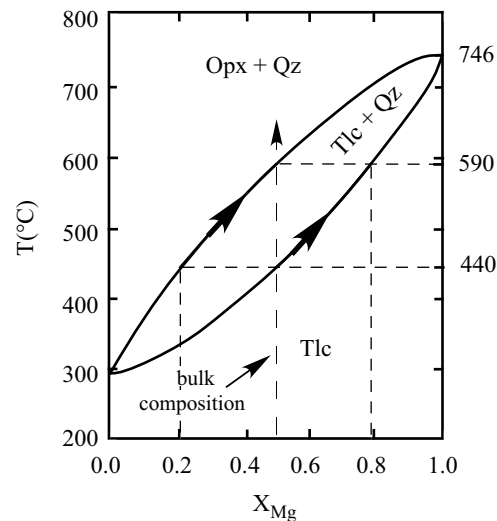


Figure 15.6 Isobaric T- X_{Mg} diagram for the reaction $\text{talc} = \text{orthopyroxene} + \text{quartz} + \text{H}_2\text{O}$ at 3 kbar.

breaks down at 746°C. Between these two temperatures, a loop that represents the reaction in the Fe-Mg bearing system. The two curves on this projection show the compositions of talc and enstatite in equilibrium with quartz at any given temperature. Because orthopyroxene is always more iron rich than coexisting talc, it is clear that the high iron curve represents the composition of orthopyroxene, while that at higher magnesium represents the talc composition.

Figure 15.6 can be used to understand how reactions take place in natural, divariant, or even multivariant systems. Consider metamorphism of a hypothetical assemblage consisting of talc having $X_{\text{Mg}} = 0.5$ (with or without quartz). When the temperature reaches 440°C, talc begins to break down and produces a small amount of orthopyroxene with composition $X_{\text{Mg}} = 0.2$. As temperature increases, talc will continue to break down and both talc and orthopyroxene become richer in magnesium. The reaction ceases at 590°C, when the final amounts of talc are consumed. At this temperature, orthopyroxene has the composition $X_{\text{Mg}} = 0.5$ while the last talc to disappear has the composition $X_{\text{Mg}} = 0.8$.

In this example, the assemblage orthopyroxene – quartz – talc would be stable over a temperature range of 150°C, and hence it would not be a sensitive indicator of metamorphic grade. The addition of Fe affects the P-T stability fields of mineral assemblages in metaperidotites, but it is not an extreme effect because ultramafic rocks are

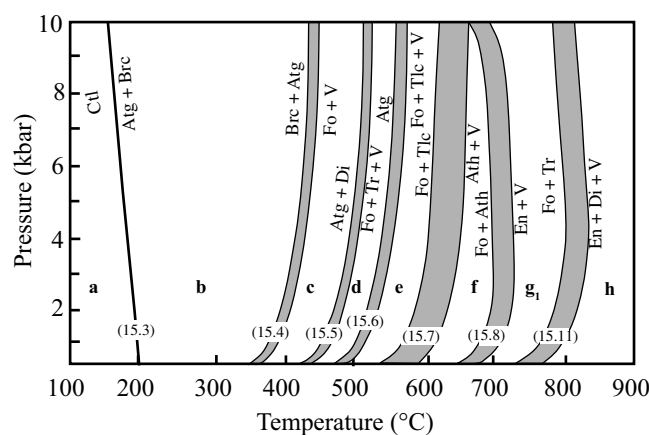


Figure 15.7 P-T diagram showing the divariancy of reactions in natural metaperidotites due to the presence of iron.

very magnesian. The composition of olivine from nearly all metaperidotites falls in the range of $X_{Mg} = 0.85\text{--}0.95$ (although the range within each individual metaperidotite body is much smaller). The effects of this range in olivine composition on the phase relations of the ultramafic system are shown in Figure 15.7. Except for the stability field for the assemblage olivine-anthophyllite (assemblage f), the effects are minor. The largest change has been the expansion of the field for the assemblage olivine + anthophyllite at the expense of olivine + talc and, to a lesser extent, olivine + enstatite. This is a reflection of the fact that iron is far more compatible with anthophyllite than with talc or enstatite.

15.4.2 Aluminum

In discussing mineral assemblages in low and medium metamorphic grades, the role of aluminum has not been considered because the aluminous phase, chlorite, is stable throughout this temperature range. At higher temperatures, however, chlorite breaks down to make cordierite or spinel (Figure 15.8). Figure 15.8 predicts that cordierite is the stable aluminous phase in metaperidotites at low pressures. Cordierite, however, is very rare in metaperidotites (Arai, 1975) because of the relatively high Cr content of metaperidotites. Spinel is very receptive to Cr, and therefore Le Chatelier's Principle predicts that in natural systems, the reaction enstatite + spinel = forsterite + cordierite lies at very low pressures and that a Cr-bearing spinel is stable in metaperidotites at almost all pressures.

As a result of the wide stability range of spinel, in most metaperidotites the reaction that eliminates chlorite from

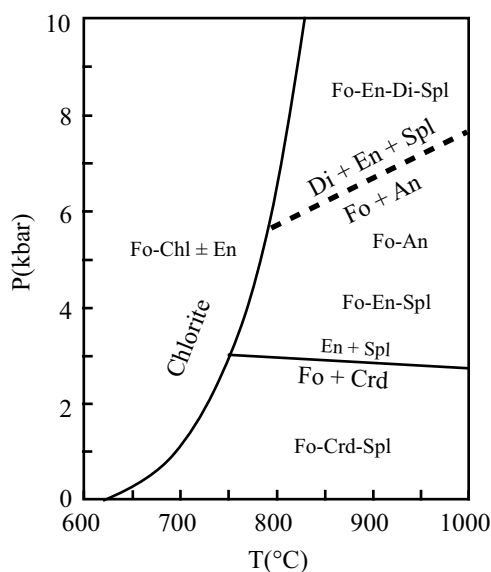


Figure 15.8 P-T diagram showing important reactions in high-temperature peridotites. An = anorthite, Chl = chlorite, Crd = cordierite, Spl = spinel, other abbreviations as in Table 15.1.

the rock is chlorite = forsterite + enstatite + spinel + H_2O . This occurs at temperatures slightly above those for the appearance of enstatite in the Al-free system. When chlorite breaks down, the calcic-amphibole in the metaperidotite becomes hornblende rather than tremolite. Because metaperidotites are markedly poor in elements such as ferric iron and titanium that produce the pleochroism in hornblende from mafic rocks, the hornblende in most metaperidotites is colorless.

Figure 15.8 also predicts that plagioclase, not spinel, is stable in metaperidotites at pressures below about six kilobars. However, like cordierite, plagioclase is destabilized by the presence of Cr in the spinel. Consequently, plagioclase is found in metaperidotites only in low-pressure environments. There are two environments where plagioclase peridotites form. One is in low-pressure contact metamorphic environments, where the plagioclase has formed from complex reactions involving spinel, hornblende, or chlorite (see Frost, 1976). The other environment is in suboceanic mantle that has been infiltrated by basaltic melt at relatively shallow crustal depths (i.e., at low pressures), a process known as "refertilization." Calculations by Müntener and colleagues (2010) suggest that plagioclase peridotites can host up to 12 percent of MORB-like melt compared to depleted peridotites.

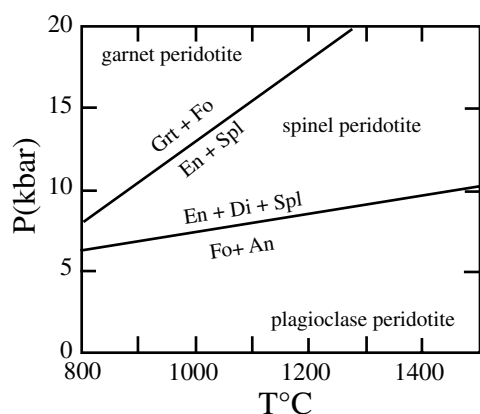


Figure 15.9 Phase diagram showing the stability fields of garnet, spinel, and plagioclase in high-T peridotites, based on experimental results of Kushiro and Yoder (1966), Danckwerth and Newton (1978), and O'Neill (1981).

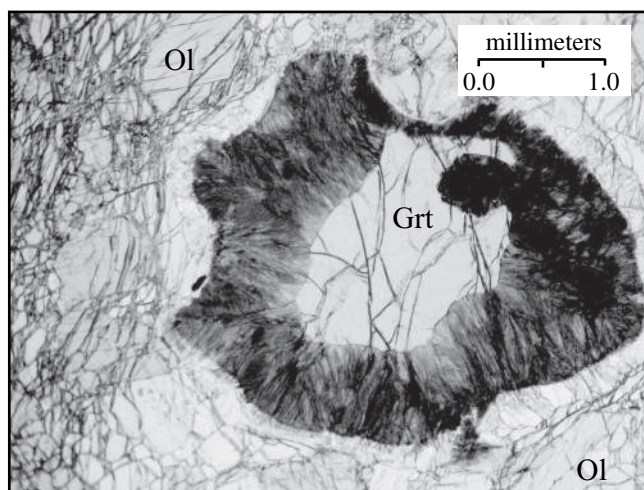


Figure 15.10 Photomicrograph in PPL of garnet in a garnet peridotite. Note the garnet is rimmed by a dark halo of spinel and orthopyroxene produced by decompression. From Alpe Arami, Swiss Alps.

Such “refertilized” peridotites have been recognized in the mantle sections of ophiolites from around the world (Müntener et al., 2010).

At mantle pressures (ca. fifteen to twenty kilobars), spinel plus orthopyroxene react to make garnet (Figure 15.9). The garnet produced by this reaction is pyrope but contains a substantial grossular component. These reactions produce a twofold division to the mantle. At low pressures, the peridotites of the mantle contain spinel, whereas at high pressure garnet is the aluminous phase instead (Figure 15.9). Although garnet peridotites

Table 15.2 Relationship between Metamorphic Facies and Mineral Assemblages in Metaperidotites

Facies	Assemblage
zeolite	lizardite/chrysotile
prehnite-pumpellyite	serpentinites
“low” greenschist	antigorite-brucite-diopside
blueschist	antigorite-brucite-diopside
“high” greenschist	antigorite-forsterite-diopside
“low” eclogite	antigorite-forsterite-diopside
amphibolite	tremolite-bearing metaperidotite
hornblende hornfels	tremolite-bearing metaperidotite
pyroxene hornfels	plagioclase lherzolite
granulite	spinel lherzolite
“high” eclogite	garnet lherzolite

Source: After Evans (1977)

are considered a major component in the deep mantle, this assemblage is not commonly found in the crust. In most garnet peridotites exposed in the crust, the garnet is haloed by fine-grained spinel and orthopyroxene, which formed as the hot mantle was exhumed to lower pressures (Figure 15.10). The division of the mantle into spinel and garnet peridotites is geologically important for two key reasons. First, because garnet is denser than spinel, garnet peridotites have a higher seismic velocity than do spinel peridotites. Second, garnet has a greater affinity for rare earth elements, which means magmas derived from the garnet peridotite field will have a different REE pattern from those derived from the spinel field.

15.5 Metaperidotites and Metamorphic Facies

It is evident from Figures 15.2 and 15.8 that mineral assemblages in metaperidotites are more sensitive indicators of temperature than are the metamorphic facies. However, since the metamorphic facies classification is so widely used in the literature, it is important to relate the assemblages found in metaperidotites with the metamorphic facies. This is done in Table 15.2.

The transition from chrysotile to antigorite is approximately equivalent to the boundary between prehnite-

pumpellyite and greenschist or blueschist facies. The assemblage antigorite-diopside (with brucite or olivine) is found in greenschist, blueschist, and even low-temperature eclogite facies, making most serpentinites a poor indicator of metamorphic pressure. The appearance of tremolite in metaperidotites marks the transition to amphibolite facies. The transition to granulite facies is more difficult to determine. Evans (1977) places it at the reaction tremolite + forsterite = enstatite + diopside + H_2O . These indicators of amphibolite and granulite facies in metaperidotites are similar to those in mafic rocks. In metaperidotites, the presence of tremolite marks amphibolite facies, whereas the assemblage orthopyroxene-clinopyroxene-olivine marks granulite facies. Finally, one must note the correspondence of high-temperature eclogite facies with the garnet peridotite assemblage.

15.6 Role of CO_2 in Metamorphism of Peridotites

Up to now it has been assumed that the fluid phase present during metamorphism of serpentinites is pure H_2O . In the absence of any evidence to the contrary, this is a reasonable assumption. Dehydration of serpentinite produces 12 weight percent H_2O . This large amount of H_2O would overwhelm any other fluid species originally present in the rock and drive the fluid toward H_2O saturation. However, many metaperidotites, particularly serpentinites, contain carbonate, clear evidence that at least some CO_2 must have been present in the fluid. Metaperidotites emplaced into metasedimentary sequences commonly show evidence of CO_2 infiltration from the country rock. Alternatively, the parent rock may have been a carbonate-bearing serpentinite from the sea floor, in which case the CO_2 was produced by reactions with primary carbonate material. In either instance, it is important to consider both H_2O and CO_2 as volatile species. Carbon dioxide has only limited solubility in water under surface conditions, as any soda or beer drinker knows. This is because of the great difference between the properties of water, a liquid, and gaseous CO_2 .

Under increasing temperatures, water behaves more and more like a gas. As shown on the phase diagram for the system H_2O in Figure 15.11, at low pressures and temperatures, H_2O can exist as two distinct phases, liquid and vapor. Increasing temperature or decreasing

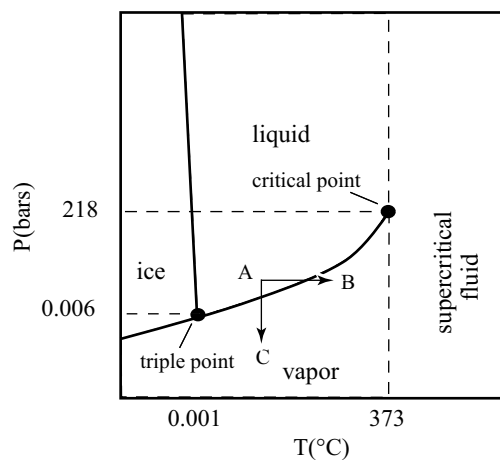


Figure 15.11 P-T diagram for the system H_2O showing the relation between liquid, vapor, and supercritical fluid. Axes are not to scale.

pressure can cause a liquid to boil (see paths A-B and A-C, Figure 15.11). Boiling involves an abrupt increase in the volume of H_2O with the appearance of a vapor phase, and marks the phase boundary between vapor and liquid. As temperature increases, the volume difference between the vapor phase and the liquid phase gets progressively smaller until no distinction can be made between the two phases. This point is known as the **critical point** and it marks the termination of the phase boundary between liquid and vapor. At temperatures above the critical point, both pressure and temperature can change to a great extent without observing a discontinuity in the properties of H_2O (see, for example, point X in Figure 15.11). Under such conditions, H_2O is said to exist as a **supercritical fluid**. The critical point for H_2O is at 373°C and 218 bars. Thus, over most of the metamorphic temperature range, H_2O will exist as a supercritical fluid, the density of which approaches that of liquid water at surface conditions. Thus, when metamorphic petrologists speak of “water,” they generally mean an H_2O -rich supercritical fluid.

A T-diagram X_{CO_2} (Figure 15.12) shows that at temperatures below 270°C there is limited solubility of CO_2 in H_2O . For example, at 200°C the aqueous fluid can dissolve only 8 percent CO_2 while the vapor coexisting with this fluid contains 86 percent CO_2 and 14 percent H_2O (see dashed lines in Figure 15.12). As temperature increases, CO_2 becomes increasingly soluble in H_2O until at temperatures above 280°C there is complete solubility between H_2O and CO_2 . Up to about five kilobars, the

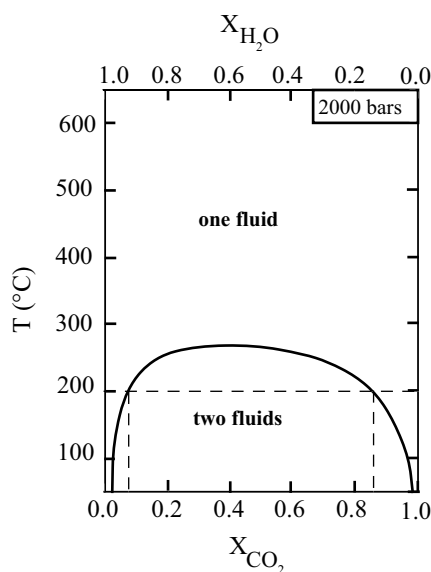


Figure 15.12 T-X diagram showing the mutual solubilities of H₂O and CO₂. Data from Todheide and Frank (1963).

solvus is only weakly dependent on pressure, meaning that in the pure system, CO₂ and H₂O are completely miscible in medium- and high-grade metamorphic environments. Of course the fluid in metamorphic rocks is seldom pure H₂O. Metamorphic fluids probably contain variable amounts of soluble species, the most abundant of which is NaCl. Sodium chloride is highly soluble in aqueous fluids, but it is nearly insoluble in CO₂. Consequently, the presence of NaCl in fluids will expand the H₂O-CO₂ solvus to higher temperatures. If the brines are saline enough, the H₂O-CO₂ solvus may extend up to temperatures where granitic rocks melt. For the time being, this point will be ignored and relations will be discussed as if the fluids involved in metamorphosed peridotites were pure H₂O + CO₂.

The addition of CO₂ to the ultramafic system adds another degree of freedom to most reactions, for as with Fe, carbon dioxide does not produce an additional phase but dissolves into one of the phases already present. To take this extra degree of freedom into account, phase relations are shown on an isobaric T-X_{CO₂} diagram. For the sake of simplicity, relations in the system MgO-SiO₂-H₂O-CO₂ will be discussed (Figure 15.13); the phase diagram is far more complex in the calcium-bearing system (Trommsdorff and Evans, 1977), but the general relations are the same.

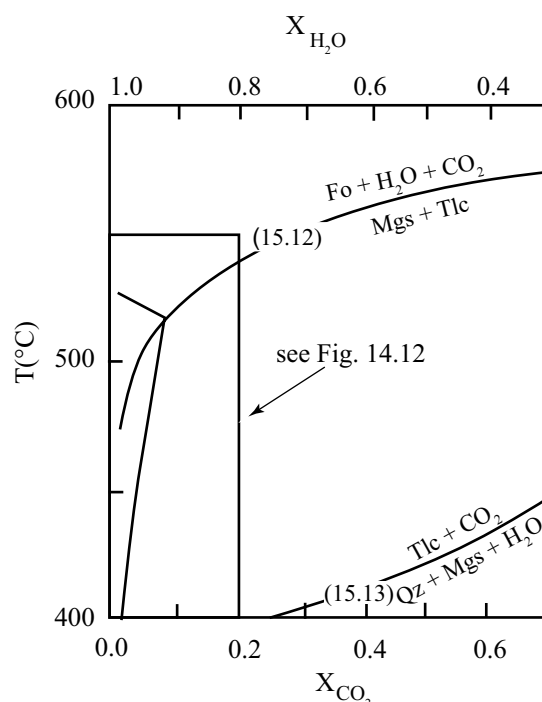


Figure 15.13 T-X diagram showing mineral relations in the system MgO-SiO₂-H₂O-CO₂ at three kilobars. Thick lines show the upper stability of carbonate in metaperidotite. Numbers refer to reactions listed on Table 15.1.

The important feature about phase relations in the system MgO-SiO₂-H₂O-CO₂ is that the X_{CO₂} of the fluid with which olivine is stable is very dependent on temperature. At a temperature near 600°C, olivine may coexist with a fluid containing more than 80 mole percent CO₂, whereas at 500°C olivine reacts to magnesite if the fluid has more than 2 percent CO₂. Low-temperature relations are shown in detail in Figure 15.14. A very important observation to draw from Figure 15.14 is that antigorite and brucite are stable only in fluids that contain small amounts of CO₂. The fact that small amounts of CO₂ in the fluid stabilize carbonates means that the assumption made in the first part of this chapter about P_{H₂O} being equal to P_{total} is quite reasonable in any rock containing serpentine but no carbonate.

Figure 15.14 shows that, at low temperature, influx of fluid containing even a small amount of CO₂ into a serpentinite will produce carbonate-bearing assemblages. At low temperatures (ca. 400°C), increasing X_{CO₂} will produce the following sequence of stable assemblages in metaperidotite: antigorite-brucite, antigorite-magnesite, and talc-magnesite. At somewhat higher temperatures (480°C and 3,000 bars), the stable assemblages will be antigorite-forsterite,

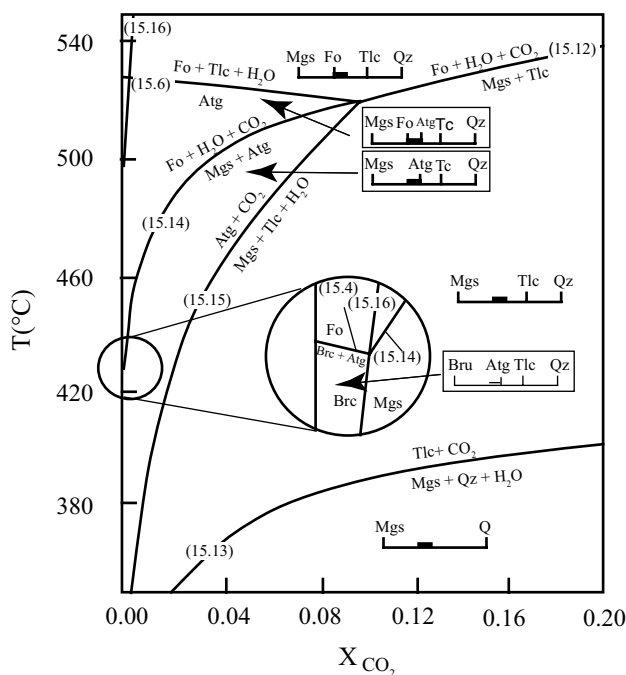


Figure 15.14 T-X diagram showing mineral relations in the system $\text{MgO-SiO}_2\text{-H}_2\text{O-CO}_2$ at three kilobars and low temperatures. Atg = antigorite, Bru = brucite, Fo = forsterite, Mgs = magnesite, Qz = quartz, Tc = talc.

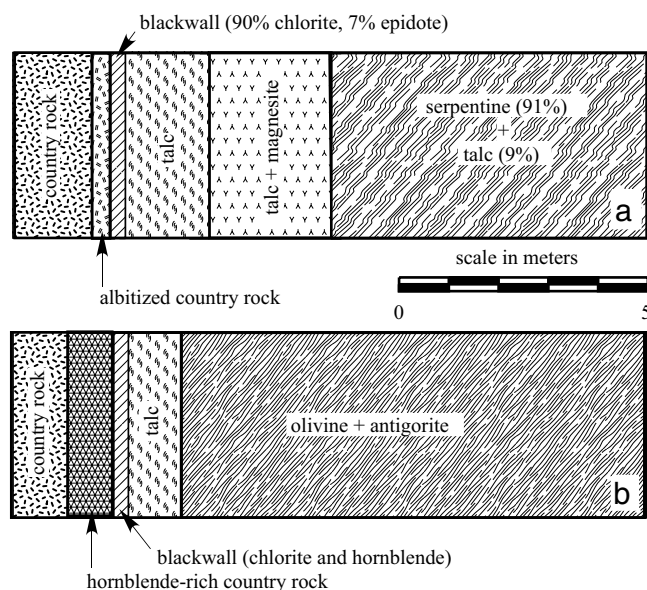


Figure 15.15 Diagrams showing meta-somatic zones found at the margin of metaperidotite bodies. A. greenschist facies (Chidester, 1962). B. amphibolite facies (Sandiford and Powell, 1986).

antigorite-magnesite, and talc-magnesite. For both temperatures at very high X_{CO_2} , the assemblage magnesite-quartz may be encountered (see Figure 15.14). Zoning due to infiltration of CO_2 -bearing fluid is commonly found in metaperidotites, with talc-magnesite along the outer margin of the metaperidotitic body where X_{CO_2} was likely to have been relatively high, and antigorite-magnesite or antigorite-forsterite found in the core, where CO_2 -bearing fluids did not penetrate (Figure 15.15).

15.7 Metasomatism of Peridotites

Metaperidotite bodies that display evidence of CO_2 metasomatism commonly show margins subjected to metasomatism of other chemical species. Because metaperidotite bodies exposed on the continents are chemically very different from the rocks that surround them, huge chemical gradients are developed at the margins. This results in intense metasomatism involving the movement of chemical species into and out of ultramafic bodies. Although such zoning patterns are highly variable, they have many things in common. Figure 15.15 shows schematically two examples of metasomatized metaperidotite described in the literature and Figure 15.16 shows an example of a metasomatic reaction zone in the field.

Figure 15.15a shows a reaction sequence formed at greenschist grade. The inner zone of this body has the assemblage serpentine-talc with serpentine making up more than 91 percent of the assemblage. This rock could have undergone slight SiO_2 metasomatism or it might represent a pyroxene-rich protolith. Outward from this is a zone of talc + magnesite, precisely what one would predict to form from CO_2 metasomatism (Figure 15.14). Further outward is a zone of monomineralic talc (such a rock is also known as steatite or soapstone). To make such a rock from a metaperidotite requires addition of SiO_2 . This suggests the steatite marks an area of SiO_2 metasomatism. Talc is commonly found in low-grade metamorphosed peridotites because of both SiO_2 and CO_2 metasomatism. Although the presence of talc is commonly thought to indicate low-temperature metamorphism of metaperidotite, this is a misconception, because in **isochemically** metamorphosed peridotitic rocks talc appears only in middle amphibolite facies.

Figure 15.15B shows a reaction sequence formed at amphibolite grade. Many details differ between this

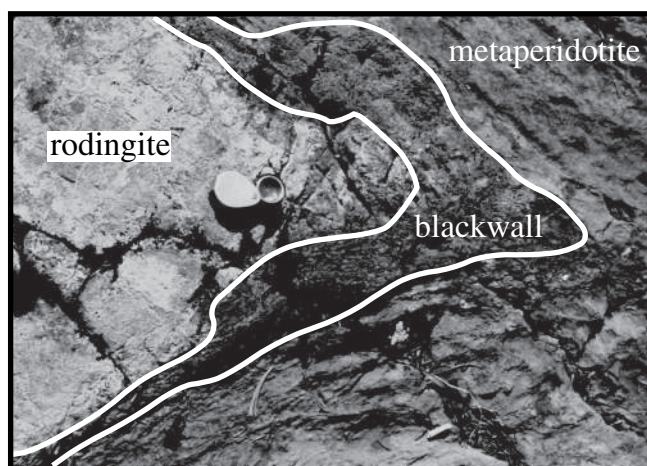
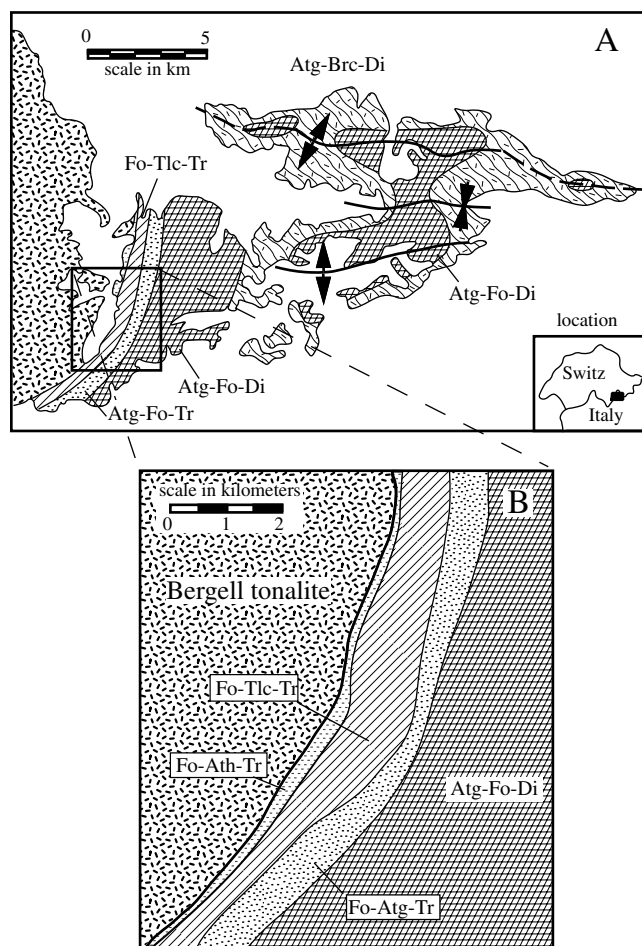


Figure 15.16 Metasomatic blackwall zone between metagabbro (now rodingite) and metaperidotite. Paddy-Go-Easy pass, Central Cascade Range, Washington.

reaction sequence and that shown in Figure 15.15A, but two aspects are similar. One is the presence of soapstone, marking silica metasomatism, and the other is the presence of an external blackwall zone. Blackwall zones are common around metaperidotite at most metamorphic grades. Depending on metamorphic grade and the nature of the country rock, they may contain chlorite, actinolite or hornblende, or phlogopite. The high variance of blackwall rocks makes them of limited value in determining the metamorphic grade of an ultramafic body. However, in many terrains the original peridotitic rocks have undergone such a high degree of digestion that only the blackwall mineralogies remain. In such a situation, the occurrence of blackwall is important because it alerts a petrologist to the fact that at some point in its history the blackwall was a peridotite.

Figure 15.16 provides a good example of the persistence of metasomatic zones adjacent to peridotites to high metamorphic grades. This figure shows a block of metagabbro that reacted with metaperidotite during serpentinization. Calcium moving out of the peridotite during serpentinization (as described in Section 15.2) altered the gabbro to a pale green rodingite, while Al_2O_3 moving out of the metagabbro altered the surrounding serpentinite to chlorite-rich blackwall. Long after these metasomatic reactions took place the rocks underwent metamorphism that converted the serpentinite back to peridotite. However, the presence of the gabbro that has been altered to rodingite and a surrounding blackwall demonstrates the existence of a previous serpentinization event.



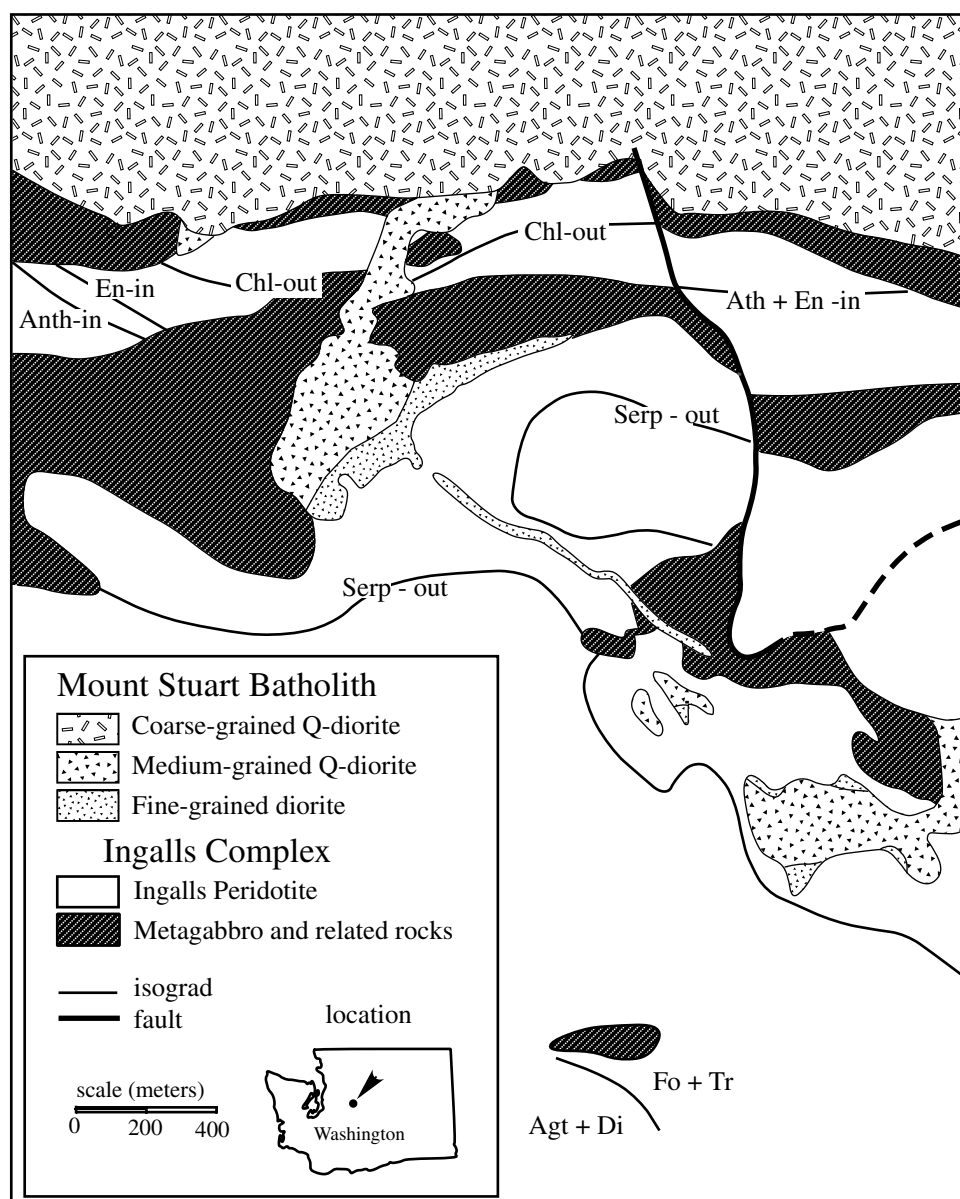
Map 15.1 Metamorphic geology of the Val Malenco area of Italy and Switzerland. (A) The regional and contact metamorphic isograds, (B) Detailed map of the contact aureole. Modified after Trommsdorff and Evans (1974) and Peretti (1988).

15.8 Examples of Metaperidotites in the Field

Because metaperidotites are so sensitive to changes in temperature, mineral assemblages in metamorphosed serpentinites make ideal monitors for the thermal structure of areas that have undergone regional or contact metamorphism. Two classic areas are described in this section.

15.8.1 Malenco Serpentinite

Perhaps the best examples of metaperidotite come from the Malenco serpentinite in the Swiss and Italian Alps (Map 15.1). The Malenco serpentinite is a slab of the



Map 15.2 Geologic map of the contact aureole at Paddy-Go-Easy pass, Central Cascades, Washington (after Frost, 1975).

Tethian ocean floor that originally stood between Africa and Europe and that was thrust onto the European continent during the Alpine orogeny. The thrusting was associated with upper greenschist grade metamorphism. This regional metamorphism produced two assemblages exposed in Val Malenco: antigorite-brucite-diopside, and antigorite-olivine-diopside. The isograd that separates these assemblages, antigorite + brucite = olivine + H_2O , has an irregular distribution across the serpentinite body (Map 15.1A). The distribution of the isograds reflects the late-stage folding of the Malenco serpentinite, with the higher temperature assemblages occupying cores

of anticlines and the lower grad assemblages lying in synclines.

During the waning stages of the Alpine orogeny, the western margin of the Malenco serpentinite was intruded by the Bergell tonalite. This intrusion produced a contact aureole that overprinted the regional isograds in the Malenco serpentinite. The aureole measured from the contact to the tremolite-in isograd measures about two kilometers wide. If the westernmost boundary of the antigorite-brucite-diopside zone is considered part of the contact metamorphism, then the aureole is five kilometers wide. The highest-grade assemblage in the Bergell aureole

is forsterite-anthophyllite-tremolite, which, according to Figure 15.8, would be indicative of temperatures of around 650°C.

15.8.2 Ingalls Peridotite

The contact aureole produced by the intrusion of the Mount Stuart batholith into the Ingalls peridotite serves as a good comparison to the aureole around the Bergell tonalite. The Ingalls peridotite lies in the central Cascades in Washington state and is part of the complex series ophiolites emplaced onto the western portion of North America during the late Mesozoic. The Ingalls peridotite was extensively serpentinized during emplacement, though in many places the primary mantle assemblage (olivine-orthopyroxene-augite-chromite) persists. It has been intruded and metamorphosed by the Cretaceous Mount Stuart batholith; the aureole is best exposed where it crosses the Wenatchee Mountains at Paddy-Go-Easy Pass (Frost, 1975) (Map 15.2). Here the highest metamorphic assemblage encountered is forsterite-enstatite-tremolite-spinel, which at approximately 700°C, is much hotter than in the Bergell aureole (Map 15.1). The quartz diorite of the Mount Stuart batholith had similar magmatic

temperature to the Bergell tonalite, so the difference in metamorphic grade in the two aureoles does not reflect differences in the temperatures of the intruding magma.

One clue to the cause for the higher temperatures recorded in the aureole at Paddy-Go-Easy pass lies in the complex shapes of the isograds. Unlike the aureole around the Bergell tonalite (cf. Map 15.1), where the isograds are relatively planar, the isograds at Paddy-Go-Easy pass form irregular patterns that extend for kilometers away from the contact of the main batholith. The irregular isograd pattern reflects the complex intrusive history of the Mt. Stuart batholith in this area. The first intrusive event was the emplacement of isolated dioritic plutons and dikes that dehydrated the serpentinite to the assemblage olivine-talc-tremolite and that caused the irregular shape to the serpentine-out isograd. As a result of these early intrusions, the main stage of Mt. Stuart batholith was emplaced into a country rock that was already hot and partially dehydrated. This meant that in the high-grade portions of the aureole the contact metamorphism produced the reactions $\text{olivine} + \text{anthophyllite} = \text{enstatite} + \text{H}_2\text{O}$ and $\text{chlorite} = \text{forsterite} + \text{enstatite} + \text{spinel} + \text{H}_2\text{O}$. Neither reaction is present in the Bergell aureole.

BOX 15.1 | PETROLOGY AND GEOPHYSICS

Although they are generally studied separately, petrology and geophysics are actually sister sciences. Geophysics uses information including seismic velocity, density, magnetic susceptibility, and electrical potential to infer the structure and composition of the crust and mantle. Interpretation of the geophysical data requires petrologic information that links geophysical properties to particular rock types and structures. Similarly petrology can tell geologists what minerals, rocks, and structures are present on the surface of Earth, but geologists must rely on geophysical techniques to project these materials to depth with any degree of accuracy. Nowhere is this more evident than in the study of the oceanic mantle.

During flow within the mantle, olivine crystals assume a preferred orientation. Depending on physical conditions, several types of olivine orientation are possible, but it is common for the b-axis of olivine to lie normal to the foliation plane while the a- and c-axes lie within the plane. Olivine is an orthorhombic mineral, and like light waves, the velocity of seismic waves within olivine also vary with crystallographic orientation. The maximum P-wave velocity lies in the plane of the a-axis, whereas the minimum P-wave velocity lies parallel to the b-axis. Therefore, if the mantle has an olivine fabric in which the b-axis lies normal to the foliation, then the seismic waves will travel faster in the plane of the foliation than across it. This property is called **seismic anisotropy** and is a common property of the mantle. By studying the olivine fabrics in peridotites exposed in ophiolites, petrologists and geophysicists can model the seismic

(continued)

BOX 15.1 (CONT.)

anisotropy those rocks would have had in the mantle (Salisbury and Christensen, 1985). By studying the rocks directly, petrologists also can determine what processes may produce changes in mantle anisotropy (Vauchez and Garrido, 2001; Michibayashi, Ina, and Kanagawa, 2006).

Serpentine has a distinctly lower density, lower seismic velocity, and higher magnetic susceptibility than the parent mantle peridotite. This means zones of serpentinized mantle should be readily imaged by geophysical surveys (Schroeder, John, and Frost, 2002). Because of the low seismic velocity of serpentine relative to fresh olivine, Kamimura and colleagues (2002) interpreted low velocity in the mantle wedge above the Izu-Bonin subduction zone, which is in the western Pacific south of Japan, to be caused by serpentinization due to dewatering of the subducting slab. In addition, Jung (2011) argues the trench-parallel seismic anisotropy seen in the mantle wedge above many trenches is produced by serpentine with a strong preferred orientation.

Summary

.....

- Serpentinization of peridotites, which occurs mostly on the sea floor, produces fluids that are highly reducing and very alkaline.
- Prograde metamorphism of serpentinites is marked by the following assemblages:
 - For assemblages with serpentine: brucite → olivine + diopside → olivine + tremolite
 - For assemblages with olivine: antigorite + diopside → antigorite + tremolite → talc + tremolite → anthophyllite + tremolite → enstatite + tremolite → enstatite + diopside.
- At low temperatures, the presence of even minor amounts of CO₂ in the fluid produces carbonate: calcite, dolomite, or magnesite.
- At granulite grade, the aluminous phase in lherzolites is a monitor of pressure: anorthite = low pressure, spinel – moderate pressure (six to twelve kilobars), garnet > twelve kilobars.

Questions and Problems

.....

Problem 15.1. Is serpentinization a metamorphic process? Explain why or why not.

Problem 15.2. Number the following ultramafic assemblages in order of increasing grade:

- a. Antigorite-brucite-diopside-chlorite

- b. Serpentine-forsterite-tremolite-chlorite
- c. Forsterite-enstatite-tremolite-spinel
- d. Forsterite-talc-tremolite-chlorite

Problem 15.3. Number the following assemblages in order of increasing pressure:

- a. Forsterite-enstatite-diopside-garnet
- b. Forsterite-enstatite-diopside-anorthite
- c. Forsterite-enstatite-diopside-spinel

Problem 15.4. Below is a list of minerals in a series of rocks. For each rock determine if the association could represent a stable assemblage. If it cannot be a stable assemblage, what mineral in the list is out of equilibrium?

- a. Forsterite-Opx-Cpx-serpentine
- b. Forsterite-serpentine-talc-chlorite
- c. Serpentine-forsterite-magnesite-talc
- d. Forsterite-Opx-Cpx-chlorite-garnet

Problem 15.5. Why do many geologists believe life probably began in sea floor vents derived from serpentinizing fluid?

Problem 15.6. To what metamorphic facies do the following assemblages belong? (Note there may not be a unique answer to some questions.)

- a. Antigorite – brucite – diopside – chlorite
- b. Forsterite – Opx – Cpx – garnet
- c. Forsterite – anthophyllite – tremolite – chlorite
- d. Forsterite – Opx – Cpx – spinel

Problem 15.7. Why is monomineralic talc more commonly associated with metasomatism rather than regional metamorphism of ultramafic rocks?

Further Reading

- Bucher, K. and Frey, M., 2002, *Petrogenesis of metamorphic rocks*. Springer, Heidelberg, Chapter 5.
- Evans, B. W., 1977, Metamorphism of alpine peridotite and serpentinite. *Annual Reviews of Earth and Planetary Sciences*, 5, 647–52.
- Winter, J. D., 2010, *Principles of igneous and metamorphic petrology*, 2nd ed. Prentice Hall, New York, 635–44.

Chapter 16

Metamorphism of Pelitic Rocks

16.1 Introduction

Perhaps the most sensitive protolith to changes in temperature and pressure during metamorphism is pelitic schist. In addition, pelitic rocks (i.e., metamorphosed shales) are widespread in most orogenic belts. Therefore many studies use pelitic schists to map out geographic variations in metamorphic conditions and the pressure and temperature history of orogenic belts. However, pelitic rocks are a chemically complex system composed of at least ten components: Na_2O - K_2O - CaO - FeO - Fe_2O_3 - MgO - Al_2O_3 - TiO_2 - SiO_2 - H_2O . Because of this chemical complexity, pelitic rocks can crystallize into a bewildering array of mineral assemblages, making the study of pelitic rocks appear daunting. A major breakthrough in metamorphic petrology occurred in 1957 when J. B. Thompson showed how to project this complex system onto two-dimensional chemographic diagrams (Thompson, 1957). These diagrams have been used ever since to characterize the mineral assemblages and reactions that govern metamorphism of pelitic rocks. This chapter endeavors to present the array of assemblages found in pelitic rocks in a systematic way so that the student is introduced to how these assemblages can be used to monitor changes in temperature and pressure within a mountain belt.

This chapter first discusses the difference between continuous and discontinuous reactions and how they are represented in chemographic diagrams. It then discusses the derivation of chemographic diagrams for pelitic systems and how to use them to characterize metamorphic assemblages in pelitic rocks. Finally, the chapter discusses how mineral assemblage in pelitic rocks can be used to characterize changes of temperature and pressure.

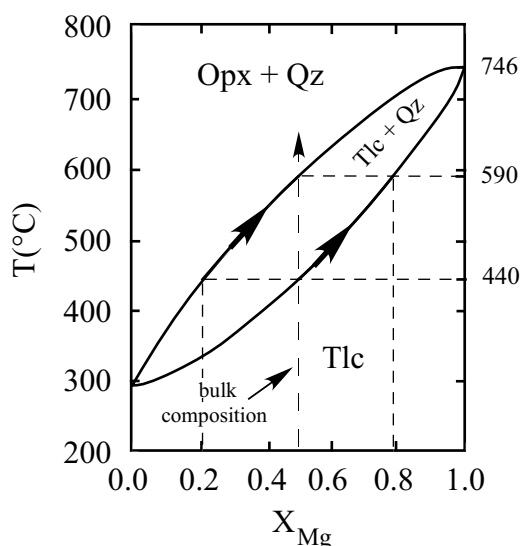


Figure 16.1 Isobaric T-X diagram showing the breakdown of talc to orthopyroxene + quartz (reproduction of Figure 14.5).

16.2 Chemographic Projections for Pelitic Systems

16.2.1 Chemographic Projections for Continuous Reactions

The description of reactions in metaperidotites presented in Chapter 15 made the simplifying assumption that variations in Fe and Mg could be neglected because metaperidotites are invariably very magnesian (X_{Mg} ($\text{Mg}/(\text{Mg}+\text{Fe})$) = 0.9). This assumption does not hold for pelitic rocks because they are characterized by a wide range in X_{Mg} . To construct chemographic projections for pelitic rocks, it is necessary to understand how to show continuous reactions (i.e., reactions involving changes in X_{Mg} as well as changes in P and T) graphically.

As noted in the previous chapter, the presence of additional components introduces additional degrees of freedom to any reaction. For example, Section 15.3.1 observed that in ultramafic rocks the addition of Fe to the Mg end member system results in a reaction such as talc = orthopyroxene + quartz + H_2O occurring over a range of temperatures (Figure 14.5; reproduced as Figure 16.1). Such a reaction is known as a **continuous reaction**. We can show this reaction chemographically on a projection from H_2O onto the FeO-MgO- SiO_2 plane of the FeO-MgO- SiO_2 - H_2O tetrahedron, resulting in an MgSiO_3 - FeSiO_3 - SiO_2 diagram (Figure 16.2). On this chemographic projection

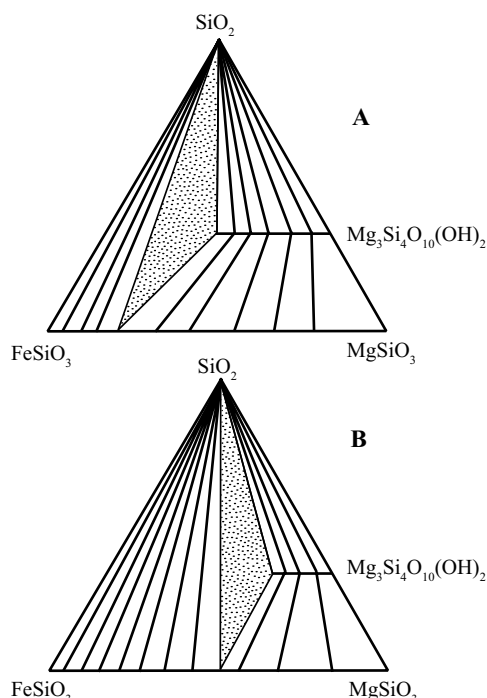


Figure 16.2 Isobaric, isothermal FeSiO_3 - MgSiO_3 - SiO_2 chemographic projections displaying the continuous nature of the reaction talc = enstatite + quartz + H_2O . Stippled fields show composition range where talc, enstatite, and quartz coexist with an aqueous fluid. (A) $T = 440^\circ\text{C}$. (B) $T = 590^\circ\text{C}$.

the minerals present do not have a fixed composition. Rather, they occur as lines with a fixed $\text{SiO}_2/(\text{FeO} + \text{MgO} + \text{SiO}_2)$ ratio. For example, the Mg end member composition of talc, $\text{Mg}_3\text{Si}_4\text{O}_{10}(\text{OH})_2$, lies on a point between the SiO_2 and MgSiO_3 apices of the triangle. The addition of Fe moves the composition into the triangle, defining a horizontal line representing talc compositions. Tie lines in this figure show compositions of talc and enstatite that coexist (and also tie lines of talc or enstatite that coexist with quartz). In actuality there are an infinite number of tie lines possible, but for the sake of clarity only a few are shown in Figure 16.2. Figure 16.2A shows the relations at 440°C , just at the point where, as described in the previous chapter, talc with a composition $X_{\text{Mg}} = 0.5$ begins to react to orthopyroxene. As shown in Figure 16.1, at this temperature talc with X_{Mg} less than 0.5 no longer is stable, so the line indicating talc composition terminates at $X_{\text{Mg}} = 0.5$. Figure 16.1 also tells us that talc with this composition coexists with an orthopyroxene with $X_{\text{Mg}} = 0.2$; in the chemography this is the line connecting talc ($X_{\text{Mg}} = 0.5$) with orthopyroxene ($X_{\text{Mg}} = 0.2$). Since both talc and

orthopyroxene in this assemblage coexist with quartz, the assemblage is represented by the stippled triangle on the chemographic diagram in Figure 16.2. This triangle is a chemographic representation of the assemblage that occurs within the reaction loop on Figure 16.1, namely talc, orthopyroxene, and quartz.

On the kind of diagram depicted in Figure 16.2, where one or more phases exhibits a solid solution, there are two types of fields. The two-phase field is marked by tie lines between two phases and represents a high-variance assemblage (i.e., the Fe/Mg ratio of the silicates may vary over a wide range without changing the assemblage). The second is a three-phase field such as the one marked by the stippled field in Figure 16.2A. The additional phase means this field displays one fewer degree of freedom. This decrease in variance is indicated by the fact that the X_{Mg} of each phase in a three-phase field is fixed. The three-phase field in a chemographic triangle is thus a representation of a continuous reaction. With increasing temperature the three-phase field changes location in the chemographic triangle. For example, with increasing temperature the three-phase triangle in Figure 16.2A migrates toward higher Mg values, as indicated in Figure 16.1. This temperature dependence is seen in Figure 16.2B, which depicts phase relationships at 590°C, the temperature at which the last trace of the talc in the original assemblage has been consumed.

Because most metamorphic reactions involve devolatilization, the three-phase triangles may propagate either toward the Fe-rich side of diagram or the Mg-rich side, depending on whether Fe or Mg is incorporated preferentially in the hydrous phase. Figure 16.3 shows the two possible chemographies for continuous reactions. Figure 16.3A shows a situation where the three-phase field has migrated toward the short legs of the triangle (i.e., toward phase A). Phase A_1 is incorporated within the new triangle A_2 -B-C, meaning the continuous reaction is $A = B + C + \text{H}_2\text{O}$. In Figure 16.3B, the three-phase field has migrated toward the long leg of the triangle (i.e., away from phase A). This implies the reaction has an opposite sense, namely $B + C = A + \text{H}_2\text{O}$.

In addition to continuous reactions, chemographic projections with solid solution can define tie line flip and terminal reactions. These reactions are distinct from the continuous reactions, and are referred to as **discontinuous** reactions because they occur at a fixed temperature and pressure. A discontinuous reaction occurs when two

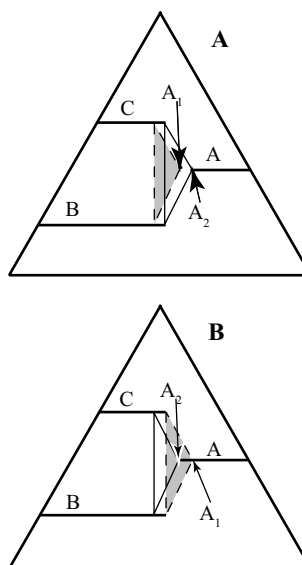


Figure 16.3 Diagram showing the behavior of chemographic projections in continuous reactions. (A) shows the behavior of the three-phase field in a system where the reaction is $A_1 = B + C + A_2 + \text{H}_2\text{O}$. (B) shows the same for the reaction $B + C + A_1 = A_2 + \text{H}_2\text{O}$. Dashed tie lines = T_1 , solid lines = T_2 , where $T_1 < T_2$.

continuous reactions intersect. An example in Figure 16.4 shows four hypothetical solid solutions: A, B, C, and D. At temperatures below T_1 the two-phase field B-D is stable and we have the three-phase fields A-B-D and B-C-D. If with increasing temperature the three-phase field A-B-D migrates to the right and the three-phase field B-C-D migrates toward the left, the two-phase field B-D will shrink. If this happens, then at some temperature, taken as T_1 in Figure 16.4A, the two-phase field shrinks to a single tie line. At this temperature the compositions of A, B, C, and D are fixed and the discontinuous tie line flip reaction $B + D = A + C$ will occur. Increasing temperature causes the two-phase field A + C to expand while the three-phase field A-C-D migrates left and A-B-C migrates right.

A similar sequence produces discontinuous terminal reactions, as indicated in Figure 16.4B. This shows four hypothetical solid solutions with mineral D lying in the triangle defined by phases A, B, and C. At temperatures below T_1 the stable assemblages are A-C-D, A-B-D, and B-C-D. With increasing temperature the three-phase field of A-C-D migrates toward right while the three-phase field A-B-D migrates left. The result is that the compositional range for D shrinks. At T_1 the compositional field for D has shrunk to a point, the compositions of A, B, C,

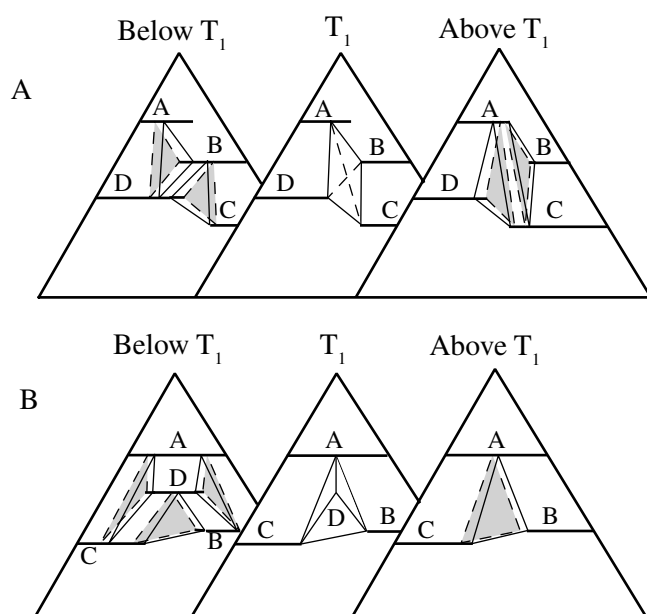


Figure 16.4 Diagram showing the relation between continuous reactions and discontinuous reaction. Stippled areas show the location of the three-phase fields at temperatures a small increment above the temperature given in each diagram. (A) shows a tie line flip reaction, and (B) shows a terminal reaction.

and D are fixed, and the terminal reaction $D = A + B + C$ (+ H_2O) takes place. With further increases in temperature above T_1 this system will have a continuous reaction involving the three-phase field A-B-C.

16.2.2 AFM Projections for Pelitic Rocks

As observed earlier, the metamorphic reactions in pelitic rocks are complex because of the number of components in the pelitic system. This complexity is manifested by the many continuous reactions in pelitic rocks. Representing pelitic mineral assemblages and continuous reactions on chemographic projections is possible by making the following simplifying assumptions (Thompson, 1957):

- 1) the variations in Na_2O and CaO are fixed by the presence of plagioclase in the rock,
- 2) variations of TiO_2 and Fe_2O_3 are controlled by the presence of magnetite and ilmenite in the rock,
- 3) variation in SiO_2 is controlled by the presence of quartz in the rock, and
- 4) $P_{H_2O} = P_{total}$

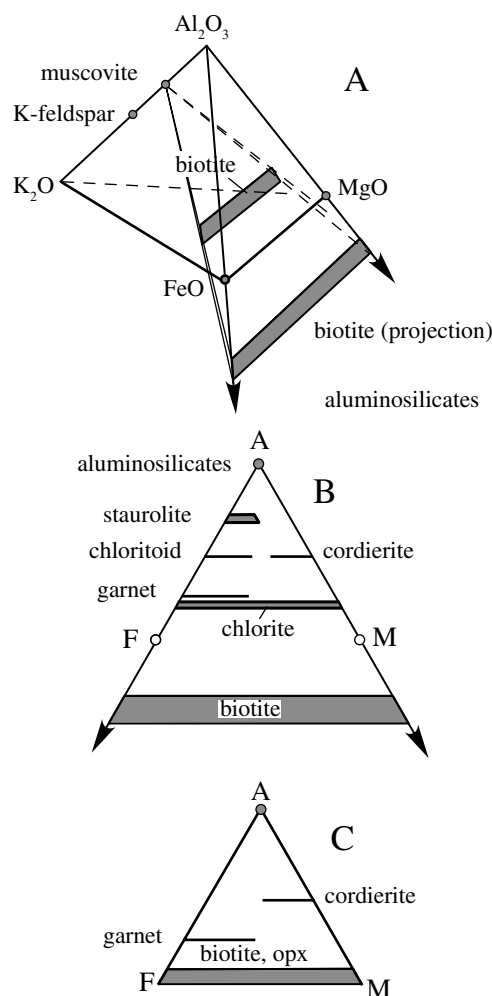


Figure 16.5 Construction of the AFM projection for metapelitic compositions. (A) The K_2O - FeO - MgO - Al_2O_3 tetrahedron showing the projection from muscovite to the FeO - MgO - Al_2O_3 plane. (B) AFM projection showing where common minerals plot when projected from muscovite. (C) AFM projection showing where common minerals plot when projected from orthoclase.

In this way, the ten-component system Na_2O - K_2O - CaO - FeO - MgO - Al_2O_3 - Fe_2O_3 - TiO_2 - SiO_2 - H_2O can be reduced to K_2O - FeO - MgO - Al_2O_3 and can be displayed in three dimensions as a tetrahedron (Figure 16.5).

Because a three-dimensional figure is cumbersome, this chemography is commonly projected into two dimensions. Most minerals in pelitic rocks are potassium free (i.e., garnet, staurolite, aluminosilicates, chlorite, cordierite) and can be expressed in terms of the system FeO - MgO - Al_2O_3 - SiO_2 - H_2O . In a projection from quartz

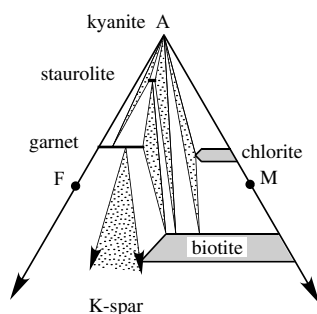


Figure 16.6 A typical AFM projection from muscovite for middle amphibolite facies (kyanite zone). Stippled areas show the three-phase fields.

and H_2O these minerals will lie on the $FeO-MgO-Al_2O_3$ plane. Thus the best projection would be from a K-rich phase onto the $FeO-MgO-Al_2O_3$ plane. Such a chemography is achieved by AFM diagrams, which project from muscovite or from potassium feldspar (Thompson, 1957). Because at all except the highest metamorphic grades, muscovite, rather than orthoclase, is the stable potassium phase in pelitic schists, petrologists use a muscovite projection for most metamorphic conditions. On an AFM projection from muscovite, one plots the following:

$$A = (Al - 3K)/(Al - 3K + Fe + Mg)$$

$$F = Fe/(Al - 3K + Fe + Mg)$$

$$M = Mg/(Al - 3K + Fe + Mg)$$

In this calculation, subtracting three times the moles of K from the number of moles of Al accounts for the projection from muscovite ($KAl_3Si_3O_{10}(OH)_2$), which has three moles of Al for each mole of K. For a projection from orthoclase ($KAlSi_3O_8$) $A = (Al - K)/(Al - K + Fe + Mg)$. By inspection of these expressions, it is evident that those minerals that do not contain K will plot on the Fe-Mg-Al face of the K-Al-Fe-Mg tetrahedron and their position will be unaffected by the choice of projection, either from muscovite or K-feldspar. K-bearing phases, such as biotite, will be projected onto the Fe-Mg-Al plane (Figure 16.5A).

Because the AFM projection includes a plane involving Fe and Mg, the AFM projection will have properties similar to the projection described for the system $FeO-MgO-SiO_2$; the diagrams will depict both continuous and discontinuous reactions. AFM projections can be used to visualize mineral reactions if the distribution of Fe and

Mg between common pelitic phases is known. Mineral analyses from many rocks show that the tendency to accept iron relative to magnesium is: hercynite (spinel) > garnet > chloritoid > staurolite > orthopyroxene > biotite > chlorite > cordierite. Figures 16.5B and 16.5C show where the typical pelitic minerals plot on AFM projections from muscovite and orthoclase, respectively. Figure 16.6 shows the tie lines between coexisting minerals for a projection from muscovite for conditions in middle amphibolite facies.

16.3 Progressive Metamorphism of Pelitic Rocks: Barrovian Metamorphism

16.3.1 The Protolith: The Mineralogy of Shale

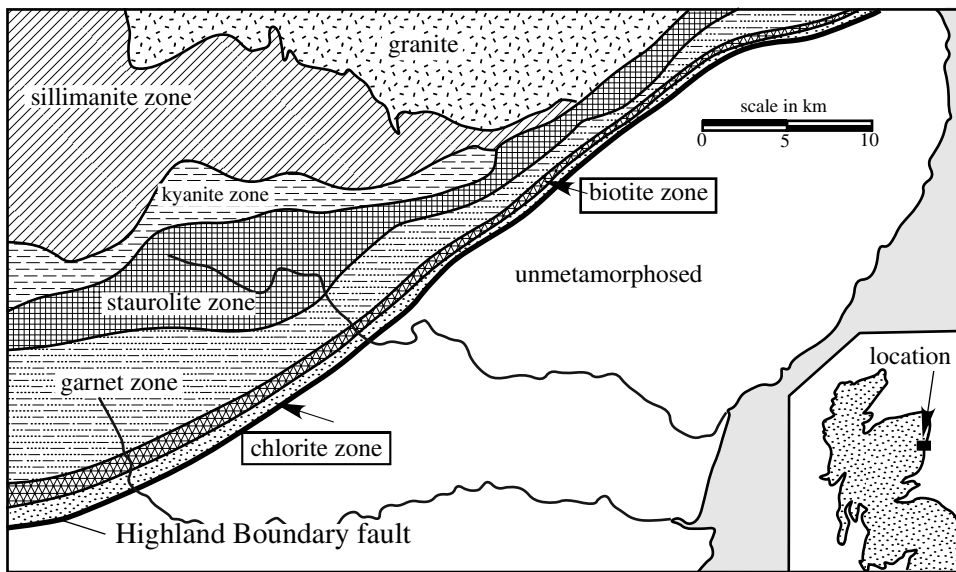
The protolith for pelitic schists is typically shale. Prior to metamorphism, shales consist of kaolinite, montmorillonite, carbonate, usually ankerite ($Ca(Fe,Mg)(CO_3)_2$), and very fine-grained detrital quartz and feldspar. Shales range in color from red to black, recording the presence or absence of graphite and the oxidation state of the iron. Red shales are rich in hematite, whereas black shales are rich in organic matter. Organic matter reduces any iron in the rock so that it is present as pyrite, rather than hematite.

16.3.2 Low-Grade Metamorphism of Pelitic Rocks

The reactions by which these protolith minerals react to form the mineral assemblages diagnostic of greenschist facies are complex and not well known, largely because weakly metamorphosed pelitic rocks are fine grained. Many of the low-grade minerals, such as kaolinite, illite, pyrophyllite, and muscovite look the same in thin section; usually they are grouped under the general term “sericite.” Consequently, mineral assemblages in low-grade pelitic rocks can be inferred only by X-ray diffraction techniques with a scanning electron microscope.

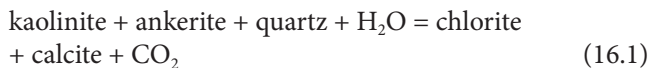
From studies of weakly metamorphosed pelitic rocks we can infer that prograde metamorphism of these rocks involves the following reactions:

1. *Disappearance of montmorillonite:* Montmorillonite (a complex clay with Na or Ca in the interlayer site) disappears early in diagenesis with chlorite and illite forming at its expense. Montmorillonite is usually gone by middle zeolite facies.



Map 16.1 Map showing the distribution of metamorphic zones in southeastern Scotland as defined by assemblages in pelitic rocks. Modified from Barrow (1893).

2. *Formation of chlorite*: Chlorite forms at grades around those of zeolite facies. The formation reactions are not well known. One reaction may involve the breakdown of montmorillonite, another reaction is probably:



3. *Formation of illite*: Illite can be thought of as closely related to muscovite. Muscovite has the composition $\text{KAl}_2\text{Si}_3\text{AlO}_{10}(\text{OH})_2$. As the formula indicates, muscovite contains tetrahedral aluminum substituting for silica. The charge imbalance produced by this substitution is accommodated by the substitution of K between the layers of the phyllosilicate. At low temperatures, the substitution of Al for silica is not energetically favored, so the formula for the potassic phyllosilicate becomes $\text{K}_{(1-x)}\text{Al}_2\text{Si}_{(2+x)}\text{Al}_x\text{O}_{10}(\text{OH})_2$; this mineral is illite. Illite probably forms by reactions between detrital orthoclase and kaolinite and appears in lowest zeolite facies. With increasing grade illite, becomes increasingly enriched in Al and K. In the process, illite approaches muscovite in composition and by greenschist facies muscovite appears in its stead.

As a result of these three reactions, by the beginning of greenschist facies the mineral assemblage in pelitic rocks has become muscovite, chlorite, quartz, and detrital feldspar (mostly albite and orthoclase). Other phases may be pyrophyllite ($\text{Al}_2\text{Si}_4\text{O}_{10}(\text{OH})_2$), the Na mica paragonite,

the Ca mica margarite, carbonates, graphite, Fe-Ti oxides, and pyrite or pyrrhotite.

16.3.3 Barrovian Metamorphism of Pelitic Schists

One of the first studies of the metamorphism of metapelitic rocks was undertaken in the southern Highlands of Scotland, where George Barrow introduced the concept of metamorphic zones (1893). Barrow studied the Dalradian Supergroup, an Eocambrian-Cambrian sequence of sediments with minor volcanic rocks. During the Devonian Caledonian orogeny this group of rocks was metamorphosed to grades ranging from greenschist to upper amphibolite facies. The southeastern margin of this metamorphic belt is marked by the Highland Boundary fault, which juxtaposes weakly metamorphosed Dalradian metasedimentary rocks against unmetamorphosed Devonian sedimentary rocks (Map 16.1).

The Dalradian rocks just north of the fault are slates that preserve much of their sedimentary structure. Within a short distance from the Highland Boundary fault the rocks increase in grade to become garnet bearing and change from phyllite to schist. Transecting farther northwest the metamorphic grade increases from garnet, through staurolite and kyanite to become sillimanite bearing; a sequence now known as Barrovian metamorphism. There is an area in the eastern portion of the region where the kyanite-bearing rocks disappears and the staurolite-bearing rocks

abuts directly against those with sillimanite. A decrease in pressure to the northeast, which would eliminate kyanite as a participating phase, could cause the observed variation in mineralogy. Another possibility is that it simply reflects how rocks in this region lacked the proper composition to form kyanite, crystallizing staurolite instead.

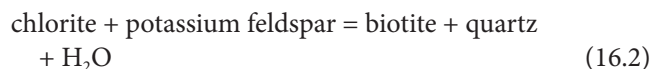
Barrow (1893) recognized three metamorphic zones in the Dalradian Supergroup, and Tilley (1925) later identified three more low-grade zones (Map 16.1). These zones were defined in terms of the first appearance of key minerals. With increasing grade, the zones are:

chlorite
biotite
garnet
staurolite
kyanite
sillimanite

Until the appearance of the AFM projection (Thompson, 1957), these zones were the basis for describing and comparing the metamorphism of pelitic schist. It is, therefore, reasonable to start the discussion of pelitic schists by showing how the Barrovian metamorphic zones are expressed in terms of AFM projections.

Biotite Zone. As described earlier, metamorphism of pelitic rocks to lower greenschist grade results in the common assemblage muscovite-chlorite-quartz. The reaction between the chlorite and the biotite zone is shown in AFM diagrams on Figure 16.7. In relatively aluminous rocks, the common assemblage also contains pyrophyllite. Because of the optical similarity of muscovite and pyrophyllite it is usually impossible to distinguish between the two without detailed X-ray analysis. In rocks that are less aluminous, the common assemblage contains potassium feldspar. Although the stable potassium feldspar at this grade is microcline, in many rocks the K-feldspar present is detrital orthoclase.

Increasing grade leads to the appearance of biotite by the model reaction:



This reaction cannot easily be balanced because chlorite in weakly metamorphosed pelitic rocks has a highly

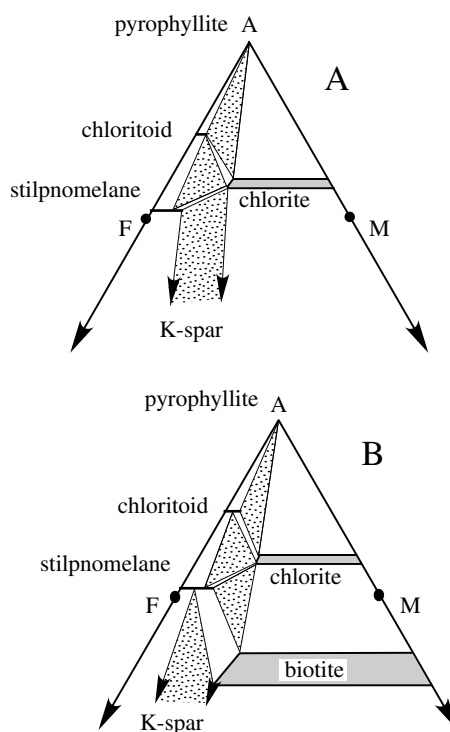


Figure 16.7 AFM projections showing transition from the chlorite zone (A) to the biotite zone (B).

variable composition. The aluminous assemblage with pyrophyllite is not changed by this reaction. The less aluminous assemblage is, however, replaced by the assemblage muscovite-quartz-chlorite-biotite, the dominant assemblage in the biotite zone because most pelitic rocks contain biotite. Reaction (16.2) is important because it marks the disappearance of K-feldspar from pelitic rocks. As shown later in this chapter, only at the very highest limits of amphibolite facies does K-feldspar appear again.

Very iron-rich rocks at biotite grade may contain stilpnomelane, an Fe-Mg phyllosilicate that looks like biotite but is more siliceous, less potassic, and more hydrous. Because of its iron- and water-rich composition stilpnomelane is restricted to iron-rich bulk compositions and low temperatures of metamorphism.

Garnet Zone. The first appearance of garnet in pelitic rocks is not well understood. Because garnet and chlorite have roughly the same Mg/Al ratio, the reaction can be written:



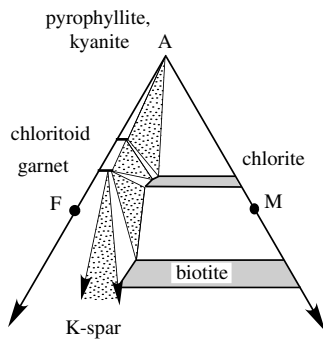


Figure 16.8 AFM projection for the garnet zone.

The first garnet to appear in pelitic rocks, however, is rich in Mn as well as iron. Thus, the garnet-in reaction must also involve a Mn-bearing phase, typically ilmenite. As metamorphic grade increases above the garnet-in isograd, the Mn content of garnet decreases. This decrease is often seen in individual garnets, which are commonly zoned, and have cores rich in Mn and rims rich in Fe. The variable Mn content of garnet cannot be shown on an AFM projection because MnO is a minor component that is not included in the AFM projection.

The AFM projection for rocks in the garnet zone is shown in Figure 16.8. Garnet first appears on the iron-rich side of the projection. The most common assemblage in this zone is muscovite-quartz-garnet-chlorite-biotite. Rocks with high Fe and low Al contents may have the assemblage muscovite-quartz-garnet-biotite-K-feldspar. Rocks with this assemblage are not truly pelitic because pelitic rocks necessarily contain aluminous minerals other than (or in addition to) garnet. Rocks that do not contain these aluminous minerals are called *semi-pelitic*.

In highly aluminous rocks, the assemblage is muscovite-quartz-garnet-chlorite-pyrophyllite (or kyanite). Pyrophyllite dehydrates to kyanite + quartz in this temperature range. As noted earlier, because biotite is common in pelitic rocks, pyrophyllite-bearing assemblages are not common. However, it is important to note that in aluminous quartzites, which may have originally been deposited as quartz + kaolinite, kyanite may appear in greenschist facies.

Staurolite Zone. The staurolite zone is marked by the first appearance of staurolite in biotite-bearing pelitic rocks. In aluminous compositions, the reaction that leads

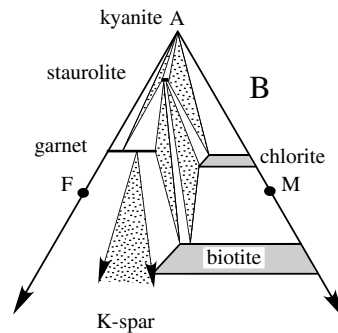
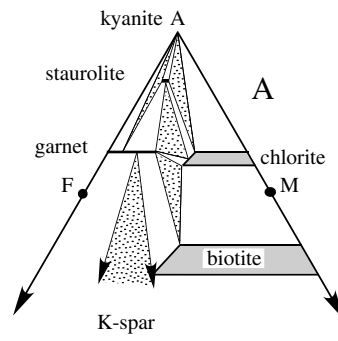
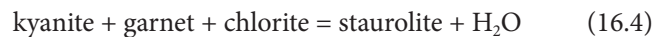
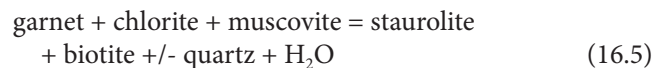


Figure 16.9 AFM projections showing the transition from the garnet to the staurolite zones. (A) upper garnet zone, and (B) staurolite zone.

to the first appearance of staurolite is likely something like (Figure 16.9A):



In most pelitic rocks, where biotite is common, the reaction that produces the appearance of staurolite in pelitic schists is (Figure 16.9B):



In modeling this reaction (or any other reaction based upon AFM chemographies) note that, apart from muscovite, biotite is the only K-bearing phase in pelitic rocks. Thus, to balance any reaction, muscovite, which is a projection point, must occur on the opposite side of a reaction from biotite. It is not often easy to determine merely by inspection on which side of the reaction quartz occurs. However, since the system is inferred to have excess quartz, it doesn't matter on which side of the reaction quartz occurs.

Kyanite Zone. The first appearance of kyanite in biotite-bearing pelitic rocks results from the reaction:



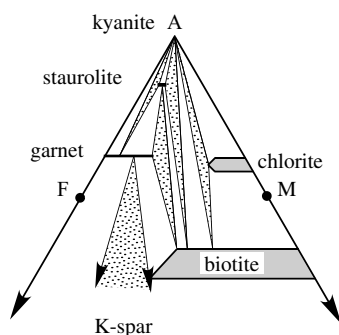
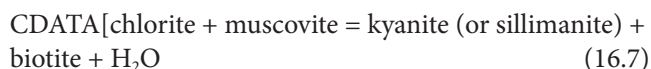


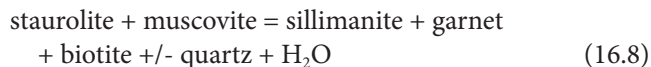
Figure 16.10 AFM projection for the kyanite zone.

The AFM projection resulting after this reaction has occurred is shown in Figure 16.10. This tie line flip reaction represents the disappearance of chlorite from many pelitic rocks. With increasing metamorphic grade, the stability field of chlorite shrinks to progressively higher Mg compositions, first by discontinuous reactions, and then by the continuous reaction (16.7). In a few rare rocks, Mg-rich chlorite may coexist with sillimanite:



In most terrains, therefore, chlorite disappears from pelitic rocks when the Mg/Fe ratio required to stabilize chlorite becomes higher than the Mg/Fe ratio found in the rocks themselves.

Sillimanite Zone. The transition from the kyanite zone to the sillimanite zone in the type area for Barrovian metamorphism evidences two mineralogic changes. Not only is there a change from kyanite to sillimanite as the major aluminosilicate, there is also the disappearance of staurolite by the reaction:



The AFM projection resulting from this reaction is shown in Figure 16.11A, and it illustrates that assemblages in high-grade metapelites are comparatively simple; the dominant assemblage is muscovite-quartz-biotite-sillimanite-garnet. Interesting, the two minerals often considered diagnostic of pelitic rocks, garnet and aluminosilicates, don't coexist until the higher grades of amphibolite facies.

Although Barrow did not recognize a grade of metamorphism higher than sillimanite, later workers discovered that at higher grades of metamorphism muscovite disappears by the reaction:

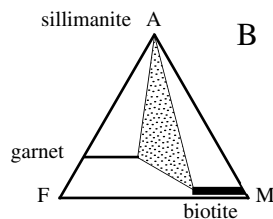
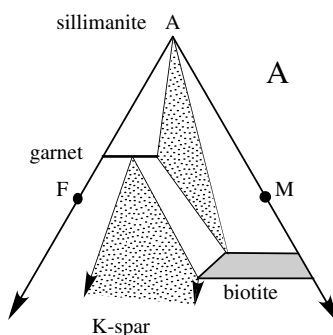


Figure 16.11 AFM projections for the sillimanite zone. (A) with muscovite, (B) with orthoclase.



In a Barrovian sequence, this reaction is often called the **second sillimanite isograd**. This isograd marks the reappearance of potassium feldspar in pelitic rocks and the disappearance of muscovite. The assemblages in rocks crystallizing at metamorphic temperatures above those of reaction (16.9) must be shown on K-feldspar projections, rather than muscovite projections (compare Figure 16.11B with Figure 16.11A).

At pressures below about four kilobars, the second sillimanite reaction proceeds without melting, but above four kilobars the potassium feldspar produced by the reaction resides in a granitic melt (Figure 16.12A). As noted in Section 10.3, this kind of a reaction is called dehydration melting and crossing these reactions through decompression can produce significant amounts of crustal melt. In some areas it is possible to use the mineral assemblage in the melted zones to identify the reaction involved in the melting. For example, the rock in Figure 16.12B contains large garnets surrounded by K-feldspar halos. The K-feldspar halos likely represent crystallized granitic melt and implicate the reaction that formed this texture as: biotite + sillimanite + quartz + plagioclase = garnet + melt.

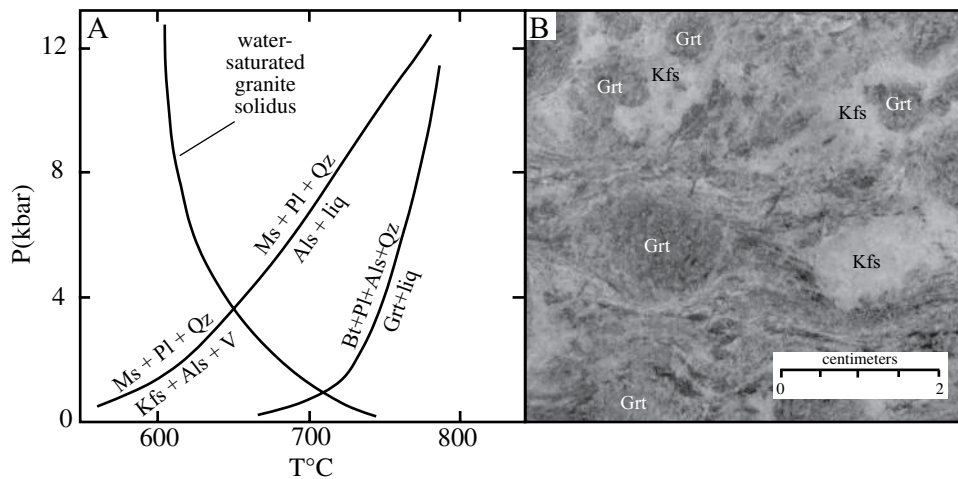


Figure 16.12 (A) P-T diagram showing two dehydration melting curves in pelitic rocks and a possible path followed during decompression melting (reproduction of Figure 10.1). (B) photomicrograph of pelitic gneiss that underwent melting via the reaction biotite + plagioclase + sillimanite + quartz = garnet + melt. From central Massachusetts.

16.4 Comparison between Barrovian and Other P-T Conditions for Metamorphism of Pelitic Rocks

For years after Barrow's work in Scotland, Barrovian metamorphism was considered typical for pelitic rocks. Developments after World War II showed that, rather than being common, Barrovian metamorphism indicated unusually high pressures. A prograde metamorphic sequence occurring at a slightly lower pressure would have the same sequence of zones as in Barrovian metamorphism, except that andalusite would be present rather than kyanite. At even lower pressures, cordierite is found in metapelitic rocks. Rocks with the assemblage cordierite and staurolite are restricted to pressures of three to four kilobars. At yet lower pressures, staurolite destabilizes and prograde reactions involve garnet, cordierite, andalusite, and sillimanite.

16.4.1 Correlation of Barrovian Zones to Metamorphic Facies

Zeolite and Prehnite-Pumpellyite: As noted previously, mineral reactions in low-grade pelitic rocks are not well defined. In general pelitic rocks metamorphosed at subgreenschist conditions contain abundant clays, mostly illite.

Greenschist: Greenschist facies corresponds to the chlorite and biotite zones of pelitic rocks.

Amphibolite: Most of the reactions described in the Barrovian sequence occur in amphibolite facies. Indeed, it is because pelitic rocks are so reactive in amphibolite facies

that they are especially useful in subdividing the pressure and temperature conditions of amphibolite facies.

Granulite: Granulite facies can be divided into two assemblages (Figure 16.13). At pressures below about ten kilobars, the distinctive granulite assemblage is: K-spar – garnet – cordierite +/- biotite +/- orthopyroxene. At around ten kilobars, the garnet-cordierite tie line breaks, forming tie lines between orthopyroxene and sillimanite instead. At twelve to fourteen kilobars, the diagnostic assemblage becomes orthopyroxene – kyanite. A good example of a granulite assemblage (although it comes from a contact aureole) is the assemblage cordierite – orthopyroxene – biotite – K-feldspar – plagioclase shown in Figure 16.14A.

Blueschist: The distinctive feature about blueschist metamorphism of pelitic rocks is the lack of biotite. Garnet is present and some Fe-rich rocks may have stilpnomelane. In addition, chloritoid, which has a rather limited stability at low pressures, is much more common in blueschist facies (Figures 16.14B and 16.15). Sodic amphibole may also be present, but it is not shown on an AFM projection because Na, which is usually incorporated in albite, is a projection point.

Eclogite: Pelitic rocks metamorphosed in low temperature eclogite facies are similar to those in blueschist facies, with chlorite, phengite, and quartz being dominant. Until the 1980s, the existence of pelitic rocks in high-temperature eclogite facies was unknown. Discoveries of unusual pelitic rocks known as *whiteschists* (Chopin, 1981) has led to the recognition that pelitic rocks have been metamorphosed under conditions consistent with

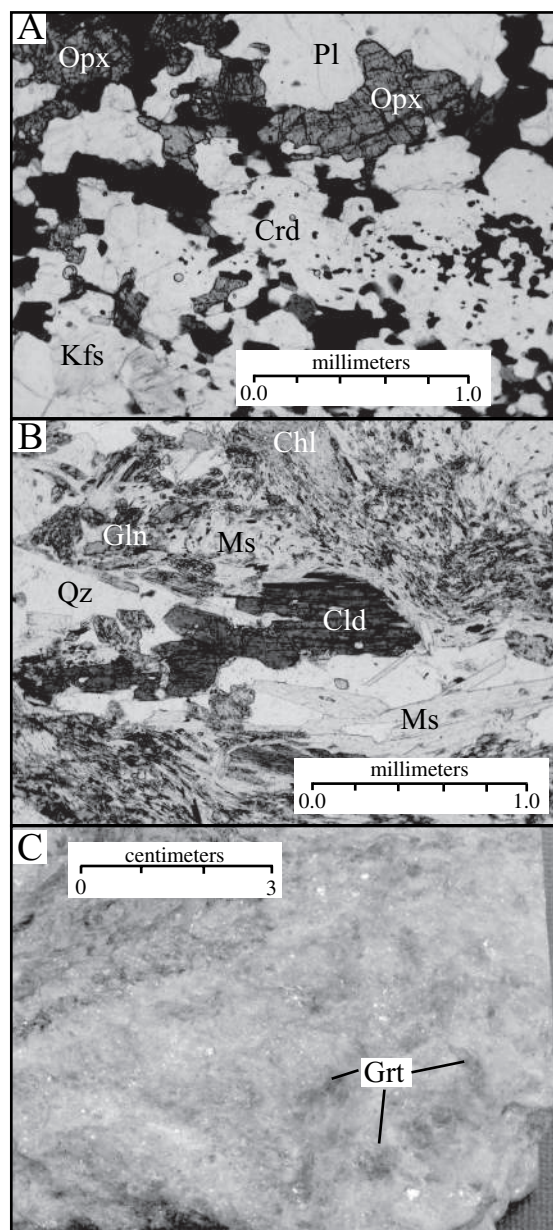


Figure 16.13 Photographs and photomicrographs of pelitic rocks in blueschist, granulite, and whiteschist facies. (A) Photomicrograph in PPL of pelitic rock in blueschist facies containing chlorite (Chl), chloritoid (Cld), glaucophane (Gln), muscovite (Ms), and quartz (Qz). Note the total lack of biotite. From the Bering Peninsula, Alaska. (B) Photomicrograph in PPL of a pelitic rock in granulite (pyroxene hornfels) facies containing cordierite (Crd), K-feldspar (Kfs), Opx, and Plagioclase (Pl). Contact aureole of the Laramie anorthosite complex, southeast Wyoming. (C) Photograph of whiteschist containing pale pink garnet in a matrix of muscovite, kyanite, and quartz. From Casa Parigia, Italian Alps.

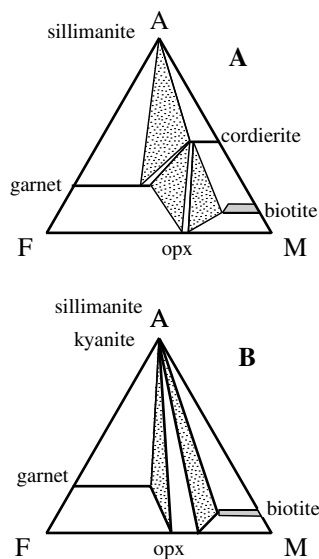


Figure 16.14 AFM projections for pelitic rocks in granulite facies. (A) (left) relatively low P; (B) (right) relatively high pressure.

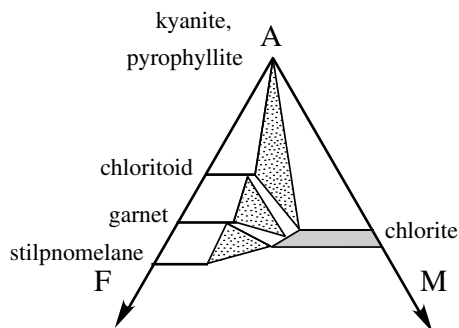


Figure 16.15 AFM projection for common pelitic assemblages in blueschist facies.

high-temperature eclogite facies. The distinctive feature of whiteschists is the instability of both biotite and chlorite. Instead, the assemblage kyanite and talc are stable (Figure 16.16). In addition there is Mg-rich garnet, which in some localities contains inclusions of coesite, the high-pressure polymorph of silica, indicative of pressures in excess of twenty-four kilobars.

16.4.2 Pressure Information from Pelitic Schists

Barrovian metamorphic zones provide one way to understand how assemblages in pelitic rocks function with temperature. To visualize the effect of pressure on phase

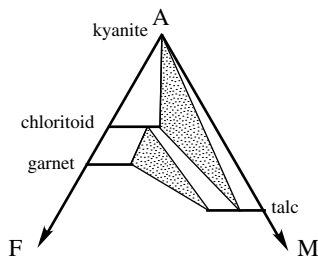
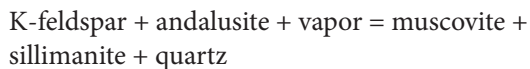


Figure 16.16 AFM projections for mineral assemblages in whiteschist (i.e., eclogite-facies pelitic rocks).

relations in pelitic rocks, petrologists use **bathograds** (Carmichael, 1978; Pattison, 2001). Ordinary isograds are dependent on both pressure and temperature and, hence, it is not possible to know in a prograde terrain whether the increasing metamorphism is a function merely of increasing temperature or of increases in both temperature and pressure. A bathograd, on the other hand, consists of two intersecting isograds and, therefore, depends only on pressure. The bathograd net as modified by Pattison (2001) is constructed by combining the aluminosilicate – in reaction (16.6), in the staurolite-out reaction (16.8), and in the muscovite-out reaction (16.9) that defines the aluminosilicate triple point (Figure 16.17). Reactions (16.6), (16.8), and (16.9) intersect the kyanite-sillimanite and the andalusite-sillimanite reactions. As a result, there are five intersections defined as bathograds, and these bathograds define six *bathozones*, which are regions in P-T space delimited by the reactions between the bathograds.

Bathozone 1: At the lowest pressure (below about three kilobars), quartz + muscovite react to form K-feldspar while andalusite is still stable. Thus the assemblage andalusite – K-feldspar (Figure 16.18A) is diagnostic of the low pressure bathozone. Cordierite is common in such regimes, while staurolite is very rare. Bathograd 1 is marked by the intersection of the muscovite-out reaction (16.9) with the andalusite-sillimanite phase boundary. This bathograd is defined by the reaction:



At higher pressures (about three kilobars), muscovite + quartz react to sillimanite + K-feldspar rather than to andalusite. The assemblage muscovite-quartz-sillimanite-K-feldspar is not particularly diagnostic of pressure because it can occur in bathozones 2, 3, 4, or 5.

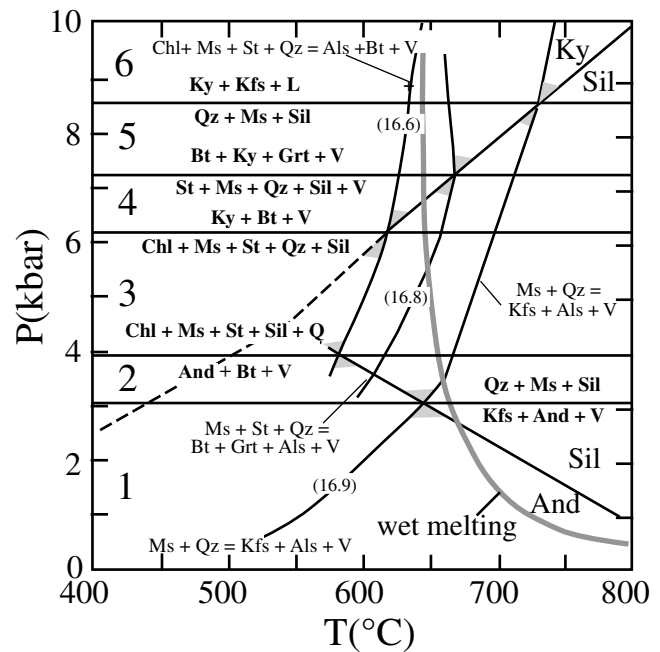


Figure 16.17 P-T diagram showing the location of bathograds and bathozones. Shaded areas represent where the phase assemblages on either side of the bathograd are stable. And = andalusite, Bi = biotite, Chl = chlorite, Grt = garnet, Ky = kyanite, Kfs = K-feldspar, l = liquid, (granitic melt), Ms = muscovite, Qz = quartz, Sil = sillimanite, St = staurolite, V = vapor. After Pattison (2001).

Bathozone 2: Bathozone 2 is defined as a terrain in which andalusite and biotite are stable at low grades and sillimanite and muscovite are stable at higher grades. At low pressures this is bounded by bathograd 1, whereas at high pressures it is bounded by the reaction of chlorite + staurolite to muscovite + biotite + sillimanite. Cordierite may be present in rocks from this zone, but it will be restricted to bulk compositions that have a relatively high Mg/(Fe + Mg) ratio.

Bathozone 3: Bathozone 3 is marked by the breakdown of the assemblage muscovite + staurolite + chlorite to sillimanite + biotite (i.e., the sillimanite-bearing version of reaction {16.16}). Andalusite is not stable with biotite in this bathozone.

Bathozone 4: In bathozone 4, staurolite + chlorite reacts to kyanite + biotite so that there is a stability field for kyanite + biotite at grades below those where sillimanite appears. At the higher temperatures indicative of bathozone 4, staurolite + muscovite react to garnet + biotite + sillimanite. In other words reaction (16.6) occurs in the presence of kyanite, whereas reaction (16.8) occurs in the

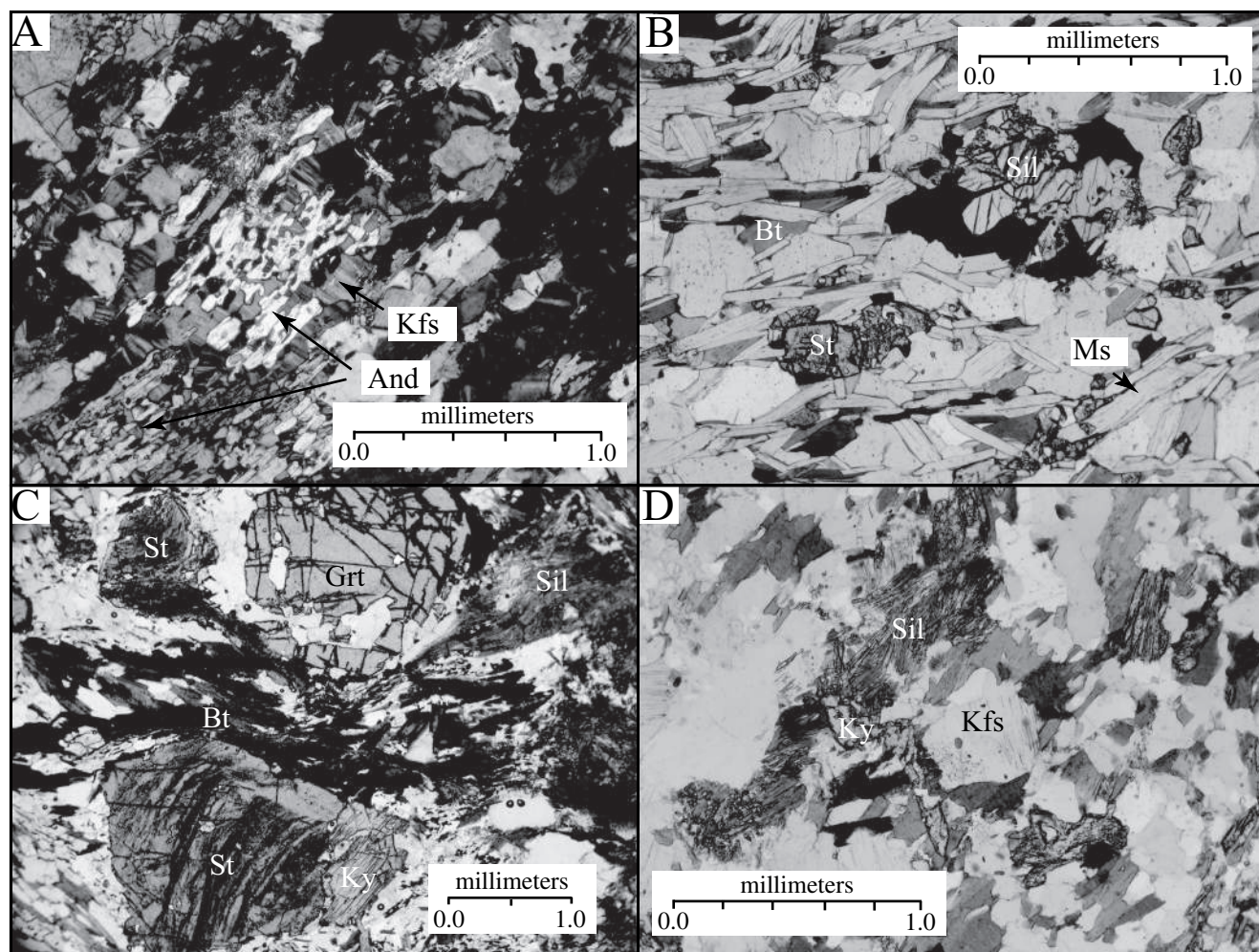


Figure 16.18 Photomicrographs of pelitic rocks from a range of bathozones. (A) Photomicrograph in XPL showing coexisting andalusite and K-feldspar, indicative of bathozone 1 and pressures of three kilobars or below. Contact aureole of the Laramie anorthosite complex, southeastern Wyoming. (B) Photomicrograph in PPL of the assemblage biotite-muscovite-staurolite-sillimanite indicating bathozones 3 or 4, pressures of four to seven kilobars. Grenville province of southern Ontario, Canada. (C) Photomicrograph in PPL of pelitic schist with the assemblage biotite (Bt)-Muscovite-garnet (Grt)-kyanite (Ky)-staurolite (St) with late sillimanite (Sil). This assemblage is indicative of bathozone 5 or pressures of 7 to 8.5 kilobars. Central Laramie Mountains, Wyoming. (D) Photomicrograph in PPL of the assemblage Kyanite (Ky)-K-feldspar (Kfs) with late sillimanite. This assemblage is diagnostic of pressures in excess of 8.5 kilobars. From the Grenville of southern Ontario, Canada.

presence of sillimanite. The assemblage biotite-muscovite-staurolite-sillimanite (Figure 16.18B) is stable in this bathozone and in bathozone 3. In bathozone 3 the assemblage lies upgrade of assemblages containing muscovite-chlorite-staurolite, whereas in bathozone 4 it lies upgrade of a zone where kyanite is stable.

Bathozone 5: In bathozone 5, staurolite + muscovite break down to garnet-kyanite-biotite. Figure 16.8C shows the assemblage garnet-staurolite-kyanite-biotite. Muscovite is not present in this rock, so it is evident this

lithology crossed reaction (16.8) with the depletion of muscovite. This is the relationship found in Barrovian metamorphism.

Bathozone 6: Bathozone 6 is marked by the coexistence of kyanite and K-feldspar (Figure 16.18D) and occurs at pressures above those where the muscovite breakdown reaction (reaction (16.9)) crosses the kyanite-sillimanite boundary. In H_2O -saturated systems, upon which the bathograd classification is predicated, this reaction accompanies partial melting, so bathozone 6 is defined by

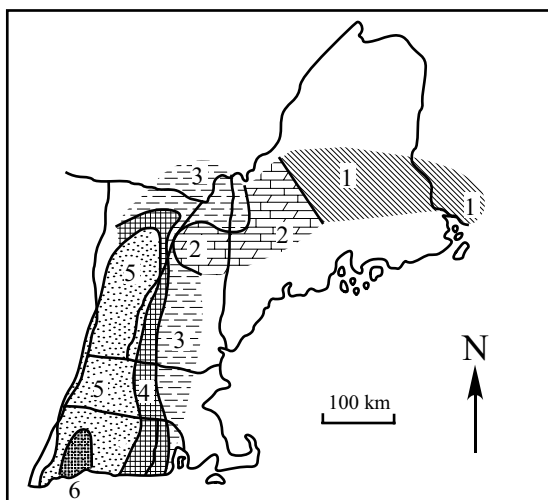


Figure 16.19 Bathozones (numbered) in New England (after Carmichael, 1978).

kyanite-bearing migmatites and is indicative of pressures greater than nine kilobars.

The validity of the bathograd classification is debatable because variations in water pressure or changes in bulk composition might allow chlorite, muscovite, or staurolite to survive to slightly higher temperatures in one rock than they do in another. Such variations in the staurolite-out and the muscovite-out reactions necessarily add a degree of uncertainty to the pressures ascribed to the various bathograds. However, they do not decrease the utility of the bathograd or bathozone concept when it is applied on a regional scale. For example, a bathozone map of the northern Appalachians (Carmichael, 1978) (Figure 16.19) shows a distinct, north-south trending high-pressure area defined by bathozones 5 and 6. The high-pressure zone probably marks the area of crustal thickening produced by the Taconic orogeny.

Summary

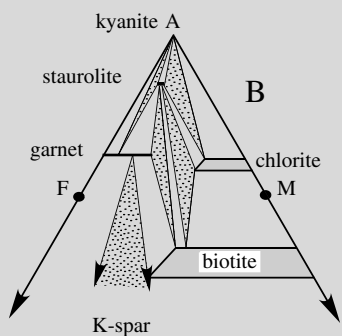
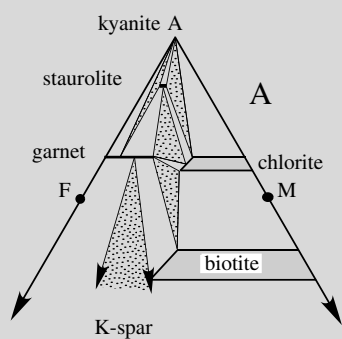
- In complex systems like pelitic rocks both **continuous** and **discontinuous** reactions take place.
 - **Continuous reactions** take place over a range of temperatures as the compositions of the participating minerals change.
 - **Discontinuous reactions** occur when the compositions of the minerals are fixed by the appearance of another mineral. There are two types of discontinuous reactions, as discussed in Chapter 12:
 - **Tie line flip reactions**
 - **Terminal reactions**
- A chemical description of the system of pelitic rocks requires at least ten components. To portray this system on the AFM chemographic projections requires a number of simplifying assumptions.
- Low-temperature metamorphism of shale involves:
 - The formation of illite; with increasing temperature illite becomes muscovite.
 - The formation of chlorite
- There are seven Barrovian zones that indicate progressive metamorphism of shale: chlorite, biotite, garnet, staurolite, kyanite, and sillimanite. The chlorite and biotite zones occur in greenschist facies. The garnet, staurolite, kyanite, and sillimanite zones are found in amphibolite facies.
- At low pressures, andalusite appears in place of kyanite and cordierite appears in place of staurolite.
- At the upper temperature limits of amphibolite facies, muscovite breaks down to sillimanite + K-feldspar and pelitic rocks begin to melt.
- Bathozones are one way to monitor the variation of pressure in pelitic terranes:
 - Bathozone 1 = coexisting andalusite + K-feldspar

- Bathozone 2 = staurolite coexisting with andalusite
- Bathozone 3 = staurolite + muscovite + chlorite breakdown to sillimanite + biotite
- Bathozone 4 = staurolite appears in the presence of kyanite but breaks down in the presence of sillimanite
- Bathozone 5 = staurolite breaks down in the presence of kyanite
- Bathozone 6 = muscovite breaks down in the presence of kyanite (i.e., kyanite + K-feldspar are stable.)

Questions and Problems

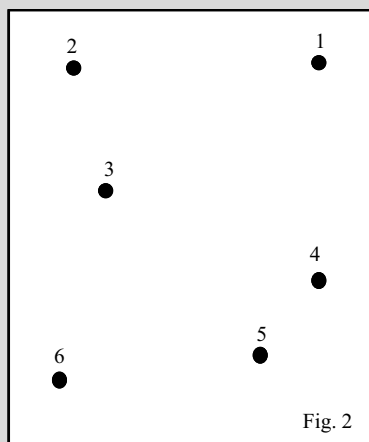
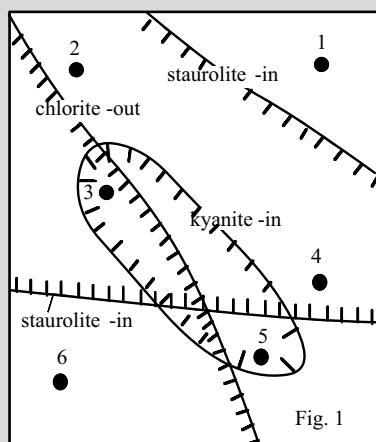
Problem 16.1. The following questions refer to Figure 16.9, reproduced below:

- For the following assemblages (each has both muscovite and quartz) note whether it is stable in Figure A, Figure B, both Figure A and B, or neither Figure A or B:
 - garnet-staurolite-biotite _____
 - staurolite-kyanite-biotite _____
 - garnet-biotite-chlorite _____
 - kyanite-chlorite-staurolite _____
 - biotite-kyanite-chlorite _____
- What is the reaction that separates diagram A and diagram B?



Problem 16.2. Buffo, a budding metamorphic petrologist, has asked you to help him with a mapping project. He has collected a number of samples of pelitic schists and has done the petrology on them but the isograd map he has produced (Figure 1, isograds have the ticks on the high-grade side) is downright confusing. He hasn't a clue as to what to do next. Please help him out! Below is a list of assemblages he found and a map showing where the samples were collected.

1. Plot each assemblage on an AFM projection.
2. Determine the reactions that relate the various assemblages (hint: there is only one!)
3. Plot the location of the reaction on the map (Figure 2) as an isograd.



4. Explain why Buffo had things so very wrong.
 1. quartz-muscovite-biotite-garnet
 2. quartz-muscovite-biotite-staurolite-chlorite
 3. quartz-muscovite-biotite-staurolite-kyanite
 4. quartz-muscovite-biotite-staurolite-chlorite
 5. quartz-muscovite-biotite-kyanite-chlorite
 6. quartz-muscovite-biotite-garnet
5. Plot the following assemblages on AFM diagrams (assume all have muscovite and quartz:
 1. biotite-staurolite-kyanite
 2. biotite-kyanite-chlorite
 3. biotite-cordierite-garnet
 4. biotite-andalusite-cordierite
6. Below is a list of minerals found in a series of rocks. For each rock determine the bathozone and relative pressures at which the assemblage formed.

1. Biotite-K-feldspar-kyanite-garnet-plagioclase-quartz
 2. Biotite-muscovite-andalusite-staurolite-plagioclase-quartz
 3. Biotite-muscovite-kyanite-staurolite-garnet-plagioclase-quartz
 4. Biotite-muscovite-staurolite-sillimanite-garnet-quartz
 5. Biotite-muscovite-andalusite-K-Feldspar-garnet-quartz
7. Determine to what metamorphic facies the mineral assemblages listed below belong. Constrain the P-T conditions further, if possible:
1. Chlorite-muscovite-K-feldspar-plagioclase-quartz
 2. Muscovite-talc-kyanite-plagioclase-quartz
 3. Biotite-muscovite-staurolite-kyanite-plagioclase-quartz
 4. Biotite-K-feldspar-sillimanite-garnet-plagioclase-quartz
 5. Biotite-K-feldspar-garnet-cordierite-plagioclase-quartz

Further Reading

.....

Bucher, K. and Frey, M., 2002, *Petrogenesis of metamorphic rocks*. Springer, Heidelberg, Chapter 7.

Philpotts, A. R. and Ague, J. J. , 2009, *Principles of igneous and metamorphic petrology*, 415–64.

Winter, J. D., 2010, *Principles of igneous and metamorphic petrology*, 2nd ed., Prentice Hall, New York, 607–32.

Yardley, B. W. D., 1989, *An introduction to metamorphic petrology*, Longman Scientific and Technical, London, 60–90.

Chapter 17

Metamorphism of Calcareous Rocks and the Role of Fluids in Metamorphism

17.1 Introduction

Chapters 13, 15, and 16 described how the mineral assemblages in mafic, ultramafic, and pelitic rocks estimate the temperature and pressure of metamorphism. In addition to indicating temperature and pressure, mineral assemblages in metamorphic rocks can monitor fluid composition. In the previous chapters, the metamorphic fluid phase was implied to consist entirely of H_2O . This approximation was valid because most metamorphic reactions in mafic, ultramafic, and pelitic rocks involve dehydration of hydrous silicates; carbonates are uncommon in these rock types. Chapter 15 did mention the role of fluid composition in altering carbonate-bearing serpentinites because small amounts of CO_2 in the fluid are sufficient to produce carbonate in serpentinite. However as long as carbonate is absent in serpentinites, assuming the major fluid species is H_2O provides a reasonable simplification. In discussing the metamorphism of carbonates, however, CO_2 is a fluid phase of critical importance because reactions in these assemblages produce (or consume) both H_2O and CO_2 .

This chapter discusses the mineral assemblages that form during progressive metamorphism of a dolomitic limestone that originally contained minor quartz and how the assemblages found in these rocks reflect changes in temperature and in fluid composition. It then shows how mineral assemblages can be used to monitor changes in other fluid compositions, including oxygen, sulfur, and pH.

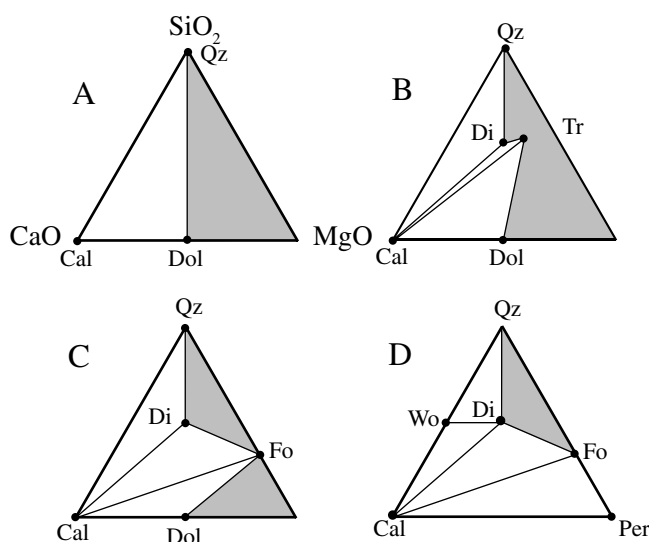


Figure 17.1 Ternary diagrams showing the minerals that form in impure dolomitic limestones during metamorphism. Gray areas are compositionally inaccessible in sedimentary rocks. A. Composition range in the protolith. B. Mineral assemblage in low-amphibolite facies. C. Mineral assemblages in upper-amphibolite facies. D. Mineral assemblages in high-grade contact aureoles.

17.2 Metamorphism of Impure Dolomitic Marble

Before considering the role of fluids, consider first the mineralogic changes that accompany increasing temperature in a carbonate rock that originally consisted of calcite, dolomite, and quartz (Figure 17.1). Because the protolith has the assemblage calcite-dolomite-quartz, the bulk composition for these rocks occupies only half of the CaO-MgO-SiO₂ triangle (Figure 17.1A). There are a few bedded magnesite deposits in the world that may have sedimentary origin, but they are very unusual. Most natural sediments do not have bulk compositions with an Mg/(Mg+Ca) ratio greater than 0.5; in other words, magnesium in the protolith is usually tied up in dolomite. In Figure 17.1, all areas whose assemblages are inaccessible because of this compositional restriction are shaded.

In mafic, ultramafic, and pelitic protoliths, increasing metamorphic grade progressively dehydrates the silicates. In metamorphosed carbonate rocks, however, increasing metamorphism produces reactions between the silicates and the carbonates that release mostly CO₂. These

reactions drive Ca and Mg from the carbonate minerals into the silicates. As a result, progressive metamorphism of impure dolomitic marbles produces Ca-Mg silicates with decreasing amounts of silica. As metamorphic grade increases, these minerals are: talc, tremolite, diopside, forsterite, wollastonite, and periclase. Wollastonite also forms at the lowest grade of a sequence of Ca-silicates that occur in marbles that have been metamorphosed at extremely high-grade temperatures (i.e., ~ 1000°C). These minerals also show a trend of decreasing silica content with increasing metamorphic grade, but because this sequence is uncommon it won't be considered further.

In some metamorphic terrains, talc is the first silicate to form during metamorphism of impure dolomitic limestones (Tilley, 1948), and with increasing metamorphic grade talc reacts with calcite to form tremolite. In many terrains, talc does not occur at all and tremolite forms directly from dolomite + quartz. In amphibolite facies, tremolite may dehydrate to diopside (Figure 17.1B). Diopside is the highest-grade silicate found in many metamorphosed carbonates, but in silica-poor marbles, forsterite forms by a reaction between dolomite and tremolite or diopside (Figure 17.1C).

In upper amphibolite and granulite facies conditions, where no hydrous minerals present in metamorphosed carbonates, three assemblages are possible depending on the relative amount of silica (Figure 17.1C). In relatively siliceous rocks the assemblage is calcite-quartz-diopside. Although these rocks may be considered relatively siliceous, the protolith did not necessarily have high quartz content; it merely had a high quartz/dolomite ratio. Because all the magnesium in the rock is contributed by dolomite, if the abundance of dolomite was low then quartz remains after dolomite depletes. Rocks with slightly higher dolomite/quartz ratio in the protolith have the assemblage calcite-diopside-forsterite, whereas those that have the highest dolomite/quartz ratio have the assemblage calcite-dolomite-forsterite. Figures 17.1B and C illustrate an important concept in metamorphosed siliceous dolomites: if a Mg-bearing silicate is stable, be it tremolite, diopside, or forsterite, then quartz and dolomite are incompatible. Thus in a carbonate rock that contains Mg silicates and quartz it is quite likely that all carbonate is calcite, and dolomite is not present.

At extremely high temperatures, usually in contact metamorphic environments, two additional minerals appear,

periclase and wollastonite. They both indicate very high temperatures and usually low pressures but these two oddities are mutually exclusive (Figure 17.1D). Wollastonite forms in quartz-excess rocks by the reaction:



whereas periclase forms in dolomite excess rocks by the reaction:



It is exceedingly common for the periclase, formed by reaction (17.2), to hydrate to brucite during cooling.

This sequence of minerals applies to metamorphism of dolomitic limestones that contained only quartz as a major noncarbonate mineral. Dolomitic limestones that originally contained other detritus, such as kaolinite, plagioclase, K-feldspar, or Fe-Ti oxides, may also contain spinel, scapolite, grossular, phlogopite, or sphene.

17.2.1 Stability of Metamorphic Assemblages in T-X Space

Although the general variability of mineral assemblages in impure dolomitic limestones during prograde metamorphism was an early observation in metamorphic petrology (Bowen, 1940), detailed mineral relations weren't understood until isobaric T- X_{CO_2} diagrams were developed several decades later (Greenwood, 1967; Skippen, 1974). Inspection of Table 17.1 shows some reactions in metamorphosed siliceous dolomites consume H_2O and release CO_2 , some release CO_2 and do not involve H_2O , and others release various proportions of both CO_2 and H_2O . These reactions cannot be shown on a P-T diagram without somehow fixing the fluid composition. One approach is to hold pressure constant to show relations on an isobaric T- X_{CO_2} diagram (Figure 17.2). Because the reactions in Table 17.1 evolve (or consume) variable amounts of CO_2 and H_2O they produce a complex pattern in Figure 17.2.

Figure 17.2 illustrates how individual mineral assemblages in impure metamorphosed dolomites may be stable over a wide temperature range, depending on the composition of the fluid. Figure 17.2 indicates that if the CO_2 content of the fluid is high enough, tremolite, which is a hydrous mineral, is never stable and prograde metamorphism produces first diopside and then forsterite. If the fluid is water rich, then all the occurrence of all reactions

Table 17.1 Mineral Reactions in Impure Dolomitic Marbles

Reaction	Number
$\text{CaCO}_3 + \text{SiO}_2 = \text{CaSiO}_3 + \text{CO}_2$	17.1
$\text{CaMg}(\text{CO}_3)_2 = \text{MgO} + \text{CaCO}_3 + \text{CO}_2$	17.2
$5 \text{ Dol} + 8 \text{ Qz} + \text{H}_2\text{O} = \text{Tr} + 3 \text{ Cal} + 7 \text{ CO}_2$	17.3
$\text{Dol} + 2 \text{ Qz} = \text{Di} + 2 \text{ CO}_2$	17.4
$3 \text{ Cal} + 2 \text{ Qz} + \text{Tr} = 5 \text{ Di} + \text{H}_2\text{O} + 3 \text{ CO}_2$	17.5
$3 \text{ Cal} + \text{Tr} = \text{Dol} + 4 \text{ Di} + \text{H}_2\text{O} + \text{CO}_2$	17.6
$3 \text{ Dol} + \text{Di} = 4 \text{ Cal} + 2 \text{ Fo} + \text{CO}_2$	17.7
$11 \text{ Dol} + \text{Tr} = 13 \text{ Cal} + 8 \text{ Fo} + \text{H}_2\text{O} + 9 \text{ CO}_2$	17.8
$5 \text{ Cal} + \text{Tr} = 11 \text{ Di} + 2 \text{ Fo} + 3 \text{ H}_2\text{O} + 5 \text{ CO}_2$	17.9
$3 \text{ Dol} + \text{Kfs} + \text{H}_2\text{O} = \text{Phl} + 3 \text{ Cal} + 3 \text{ CO}_2$	17.10
$5 \text{ Phl} + 6 \text{ Cal} + 24 \text{ Qz} = 3 \text{ Tr} + 5 \text{ Kfs} + 6 \text{ CO}_2 + 2 \text{ H}_2\text{O}$	17.11
$5 \text{ Tr} + 6 \text{ Cal} + \text{Ksp} = \text{Phl} + 12 \text{ Di} + 6 \text{ CO}_2 + 2 \text{ H}_2\text{O}$	17.12

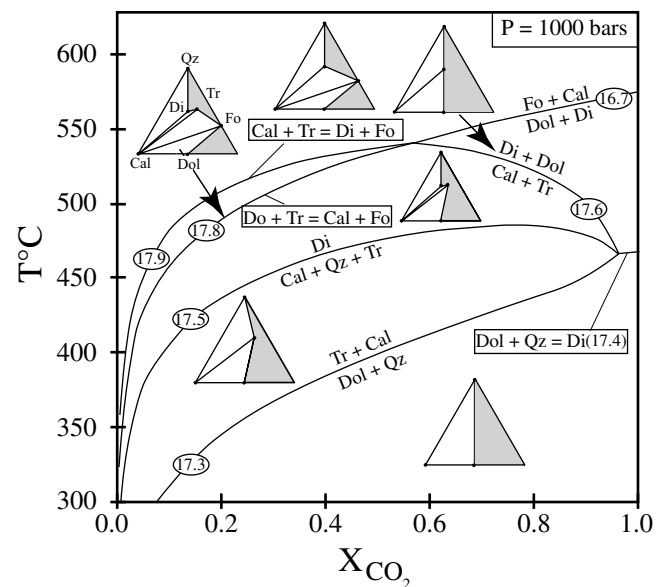


Figure 17.2 T-X diagram showing mineral stabilities during metamorphism of impure dolomitic marbles. Numbers indicate reactions on Table 17.1.

is constrained a very small temperature range. Not only did the introduction of T- X_{CO_2} diagrams allow petrologists to understand the controls on mineral assemblages during metamorphism of impure carbonates, they also provided a tool to monitor how fluid composition in metamorphosed carbonates changed during metamorphism.

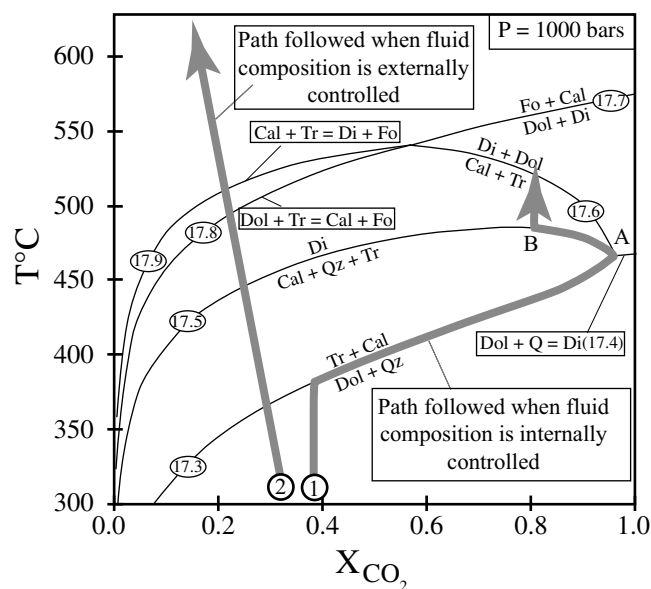


Figure 17.3 T-X diagram showing the paths followed during 1) internal control of fluid composition (buffering) and 2) external control of fluid composition (infiltration). Numbers indicate reactions on Table 17.1.

Two end members are recognized for the behavior of the fluid during metamorphism. In one end member the fluid is internally controlled, or **buffered**. In this instance, fluid is entirely generated by the devolatilization reactions, producing a small volume of fluid relative to the volume of rock. In this situation, the fluid composition follows the paths dictated by the mineral reactions, and is thought of as a “rock-dominated” fluid (path 1 in Figure 17.3). For example, consider a rock containing Dol-Qz-Tr-Cal. As temperature increases, the fluid follows a reaction path along $\text{Dol} + \text{Qz} = \text{Tr} + \text{Cal}$ to a point where the reaction intersects another reaction, $\text{Dol} + \text{Qz} = \text{Di}$ (Figure 17.3) (point A in Figure 17.3). At this point either dolomite or quartz will be depleted from the rock thereby initiating a new reaction governed by the minerals that remain in the rock. Figure 17.3 assumes that dolomite is depleted at invariant point A and the fluid follows reaction (17.5). Once the fluid attains the composition that marks the maximum stability of a reaction (point B in Figure 17.3), one of the phases becomes depleted from the reaction. The fluid composition remains unaffected by changes in T unless another reaction is reached.

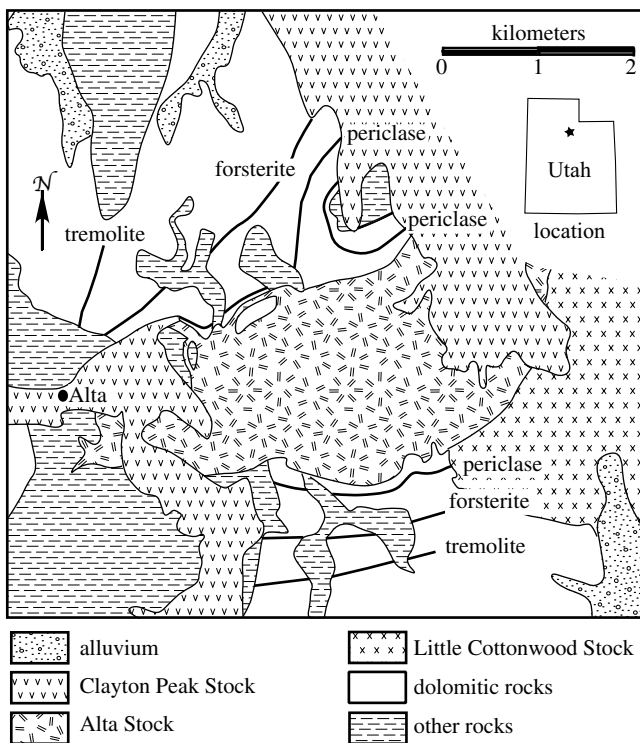
The other end member for metamorphic fluid behavior involves external control of fluid composition, or **infiltration**. In this instance there is a large volume of fluid

relative to the volume of rock and the fluid composition is controlled by an external reservoir. The fluid path then tracks the boundary between the composition of the fluid in the rock and the composition of the fluid in the reservoir (path 2, Figure 17.3). Because of the proportionately large volume of externally derived fluid, the X_{CO_2} will change little during interaction with the fluids in the rock. As a result, most fluid paths cross the reaction curves at a high angle and the individual reaction assemblages occupy only a small temperature ranges. For example, in Figure 17.3, rocks undergoing metamorphism with an internally controlled fluid composition (path 1) will have the stable assemblage Dol-Qz-Cal-Tr over a temperature range of 75°C. In contrast rocks undergoing metamorphism during infiltration will have the same assemblage over a much more limited temperature range as they cross the reaction boundary.

17.2.2 Examples of How Mineral Assemblages Can Monitor Fluid Flow in Aureoles

Two examples illustrate how the mineral assemblages can be used to monitor fluid flow in metamorphosed carbonates. The first is the contact aureole around the Alta stock (Map 17.1). The Alta stock is one of a series of Tertiary plutons that intruded Paleozoic sedimentary rocks in the Wasatch Mountains east of Salt Lake City, Utah. The country rock largely consists of impure dolomitic marbles, making this locale an ideal area to study the effect of contact metamorphism on carbonaceous rocks. Moore and Kerrick (1976) recognize three isograds in the area – tremolite-in, forsterite-in, and periclase-in. The lower-grade isograds parallel the intrusive contact with the stock, suggesting they record a simple thermal gradient. In contrast, the periclase zone forms a long arm extending more than a kilometer north of the intrusive contact. The distribution of the periclase zone suggests either that this arm of the zone outlines an area of extremely high heat flow or a place where the roof of the Alta stock lies just below the present erosional surface.

Low variance assemblages (i.e., assemblages with many phases) are rare in the aureole, suggesting the fluid composition was externally controlled. The occurrence of periclase further indicates this fluid relation, because this mineral is restricted to very water-rich conditions (Figure 17.4). From the mineral assemblages, Moore and Kerrick (1976) inferred that the distal portion of



Map 17.1 Map of the contact aureole of the Alta stock in Utah, showing the tremolite-, forsterite-, and periclase-in isograds. Modified after Moore and Kerrick (1976).

the aureole fluids were internally buffered and the fluids became enriched in CO_2 as a reaction such as akin to (17.3) proceeded (Figure 17.4). In contrast, the occurrence of periclase near the contact of the stock indicates the fluid was very water rich proximal to intrusion. The water-rich fluid most likely sourced from the magma of the Alta stock, because extensive skarns (massive calc-silicate rocks with grossular, epidote, and pyroxene) developed along the contact between the dolomitic marbles and the stock. Between the distal portion of the stock, where Dol-Qz-Tr-Cal were stable, and the areas near the granite contact, the fluid was externally controlled by water infiltrating out of the granite (Figure 17.4), as indicated by the manifestation of the forsterite-in isograd as a single line, rather than a band, as would be indicated by buffering.

The map of the contact aureole around the Marysville stock in Montana (Rice, 1977) (Map 17.2) looks similar to the aureole around the Alta stock. In detail, however, evidence for very different processes occurring in the two aureoles is readily apparent. The Marysville stock is a small Cretaceous pluton emplaced into the Proterozoic Helena dolomite. Unlike the highly irregular periclase-in isograd

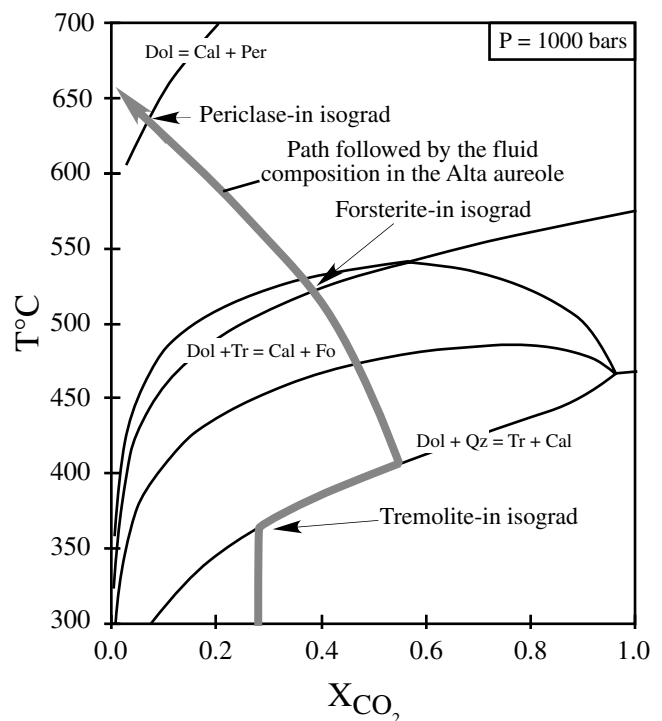
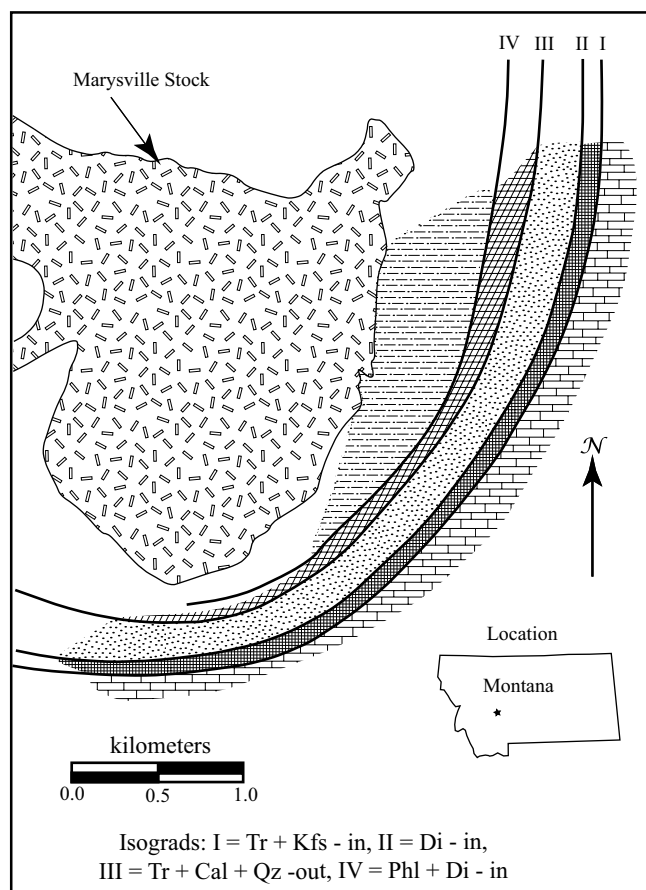


Figure 17.4 Isobaric T-X diagram showing the fluid path followed in the contact aureole of the Alta stock. Modified after Moore and Kerrick (1976).

in the Alta aureole, the isograds around the Marysville stock are parallel to the contact. In addition, although the isograds around the Alta stock are easily designated by the appearance of different minerals, the isograds in the Marysville stock are much more complex and must be designated by the appearance or disappearance of full mineral assemblages. This complexity indicates the fluid was internally buffered in the Marysville stock. The Helena dolomite contains detrital K-feldspar alongside quartz, so the phase diagram summarizing the mineral reactions in the Marysville aureole (Figure 17.5) is slightly more complex than the phase diagram for calcite-dolomite-quartz (Figure 17.2), but the buffering process is the same in both depictions. During metamorphism in the aureole of the Marysville stock, the fluid in the distal portion of the aureole was buffered by the reaction dolomite + K-feldspar = phlogopite + calcite (reaction {17.10}) until it hit invariant point I, where tremolite appears with K-feldspar. The fluid was buffered along the reaction $\text{Dol} + \text{Qz} = \text{Tr} + \text{Cal}$ until it reached invariant point II, where diopside appeared. Subsequently the fluid was buffered along reaction (17.6) until the assemblage $\text{Tr} + \text{Cal} + \text{Qz}$ was depleted from the



Map 17.2 Geologic map of the contact aureole around the Marysville stock, Montana, USA. Modified after Rice (1977).

rock (isograd III) (at an $X_{\text{CO}_2} = 0.75$) because both reaction (17.5) and reaction (17.12) have a maximum at $X_{\text{CO}_2} = 0.75$. Therefore, no change in the fluid occurred during reaction (17.12), which produced the assemblage phlogopite + diopside (isograd IV).

17.3 Buffering of other Fluid Components

Water and CO_2 are not the only fluids that may be buffered by mineral assemblages in metamorphic rocks. If a reaction involving a fluid species can be defined by the minerals seen in a rock, then those mineral assemblages buffered the fluid. An example is given by the reaction zone that exists around the sulfide ore bodies in Ducktown, Tennessee (Nesbitt and Kelly, 1980). The ore bodies, consisting mainly of pyrrhotite and pyrite with minor chalcopyrite, sphalerite, and magnetite, are hosted in a metagreywacke schist with the assemblage

Table 17.2 Reactions around the Ducktown Ore Body

Reaction	No.
$\text{Fe}_3\text{O}_4 + 3 \text{S}_2 = 3 \text{FeS}_2 + 2 \text{O}_2$	17.13
$2 \text{FeS}_2 = 2 \text{FeS} + \text{S}_2$	17.14
$2 \text{TiO}_2 + 2 \text{FeS} = 2 \text{FeTiO}_3 + \text{S}_2$	17.15
$\text{CO}_2 = \text{C} + \text{O}_2$	17.16

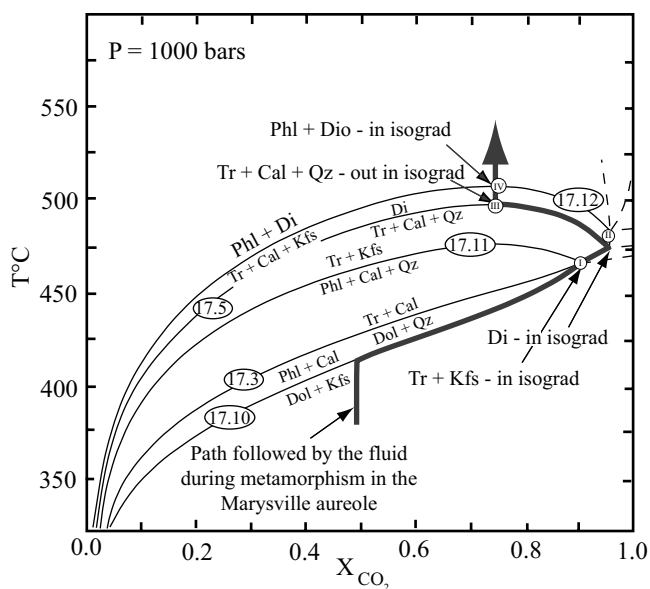


Figure 17.5 Isobaric T-X diagram showing the path followed by the fluid during metamorphism in the Marysville stock. Modified after Rice (1977).

quartz-plagioclase-biotite-muscovite-ilmenite-graphite. Metamorphism is inferred to have occurred at six kilobars and 550°C (Nesbitt and Kelly, 1980). Traversing a distance of 100 meters from the ore body into the country rock, the following changes are observed: first magnetite disappears, then rutile appears, then pyrite disappears, then ilmenite replaces rutile, and finally graphite appears (Figure 17.6). The appearance of rutile reflects change in bulk composition; the other changes are governed by the reactions listed on Table 17.2. It is clear from the reactions in this table that gradients in sulfur and oxygen cause the mineralogic changes observed around this ore body.

Evaluating how these fluid components change necessitates modifying the techniques used in thermobarometry. For example, consider reaction (17.13) from Table 17.2. If

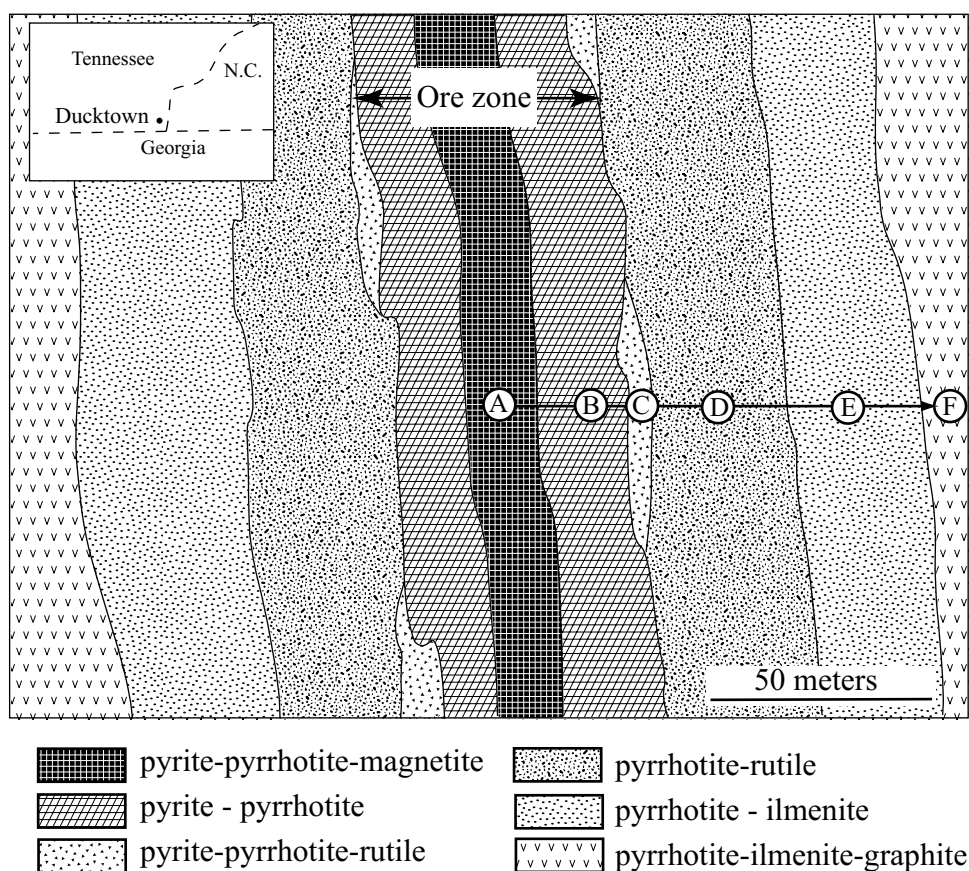


Figure 17.6 Sketch map of the opaque mineral assemblages surrounding the ore body at Ducktown, Tennessee. Arrow connects assemblages found in a traverse from the ore zone into the country rock schist. Letters refer to the assemblages noted on Figure 17.7. Modified from Nesbitt and Kelly (1980).

we assume magnetite and pyrite are pure phases, the equilibrium constant for this reaction becomes:

$$K_{16.10} = \frac{P_{O_2}^2}{P_{S_2}^3} \quad (17.17)$$

In petrology, we use fugacity (f) in place of partial pressure. One can think of fugacity as the thermodynamic pressure a gas exerts in a system. For ideal gases $P = f$, and for real gases $P \cdot \gamma = f$, where γ is a correction factor to account for the deviation from ideality. Substituting f for P and taking the log of both sides of equation (17.17) gives:

$$\log K_{16.10} = 2 \log f_{O_2} - 3 \log f_{S_2} \quad (17.18)$$

From Chapter 12:

$$\log K = \frac{-\Delta G}{2.303RT} \quad (17.19)$$

Equation (17.19) augments the reactions on Table 17.2, and the alongside the free energies of the mineral phases

in the reactions (which can be obtained from thermodynamic databases referred to in Chapter 13), can be used to calculate the stabilities of assemblages involving magnetite, pyrite, pyrrhotite, ilmenite, rutile, and graphite as they function with the fugacities of sulfur and oxygen (Figure 17.7). Figure 17.7 shows how the assemblages recorded around the Ducktown ore body reveal a decrease in both oxygen and sulfur fugacity from the core of the ore body to the surrounding graphitic schist.

Because sulfide ore bodies contain limited quantities of hydrous phases, it is likely that the source for the fluid involved in this reaction was the surrounding schist. The schist surrounding the Ducktown ore body contains the assemblage quartz-Kfs-biotite-muscovite-ilmenite-pyrrhotite-graphite with minor staurolite and garnet. Mineral reactions involving these phases produced an aqueous fluid $X_{CO_2} = 0.15$ (Nesbitt and Kelley, 1980) that infiltrated the ore body. Reactions between this fluid and the ore produced the chemical gradients seen in Figure 17.7.

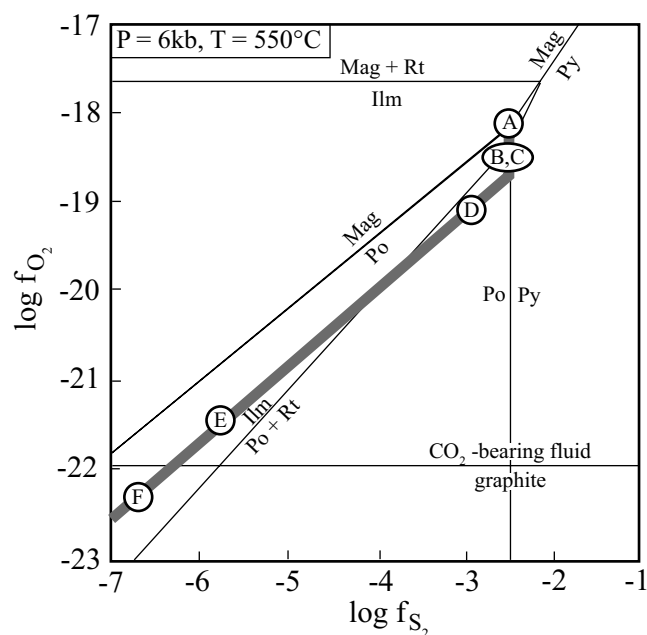
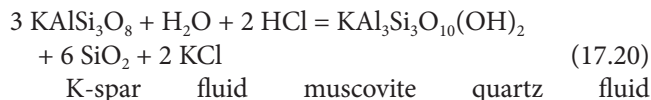


Figure 17.7 Plot of the $\log f_{S_2}$ vs $\log f_{O_2}$ showing the variation of fluid composition adjacent to the ore body at Ducktown, Tennessee. Letters refer to the assemblages noted on Figure 17.6. Modified from Nesbitt and Kelly (1980).

17.4 Buffering of pH

Although understanding the reactions between a rock and an infiltrating fluid is integral to metamorphic petrology, it is also important in the field of economic geology. Many ore deposits form via reactions between a hydrothermal fluid and the country rock. Economic geologists study these alteration reactions around ore deposits as a way to understand the composition of the fluid that deposited the ore, including its pH. Rocks have the ability to buffer the pH of the fluid moving through them. A good example of a buffering reaction is:



This reaction is balanced using HCl and KCl rather than H^+ and K^+ because at metamorphic temperatures HCl is highly associated (rather than disassociated, as it is at low temperature).

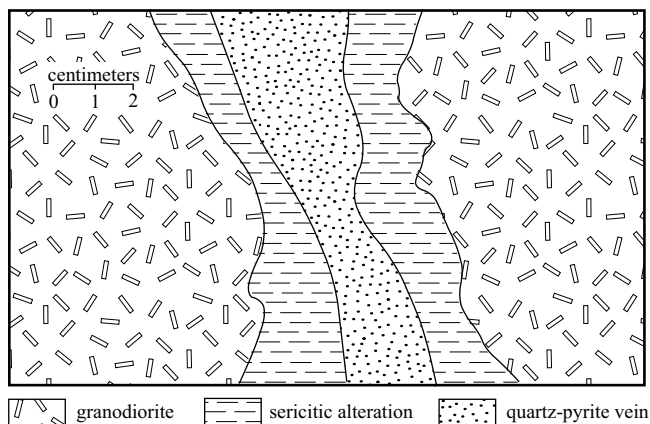


Figure 17.8 Sketch of alteration around a quartz-pyrite vein in granodiorite from porphyry copper deposit in Ajo, Arizona. Based on descriptions from Meyer and Hemley (1967).

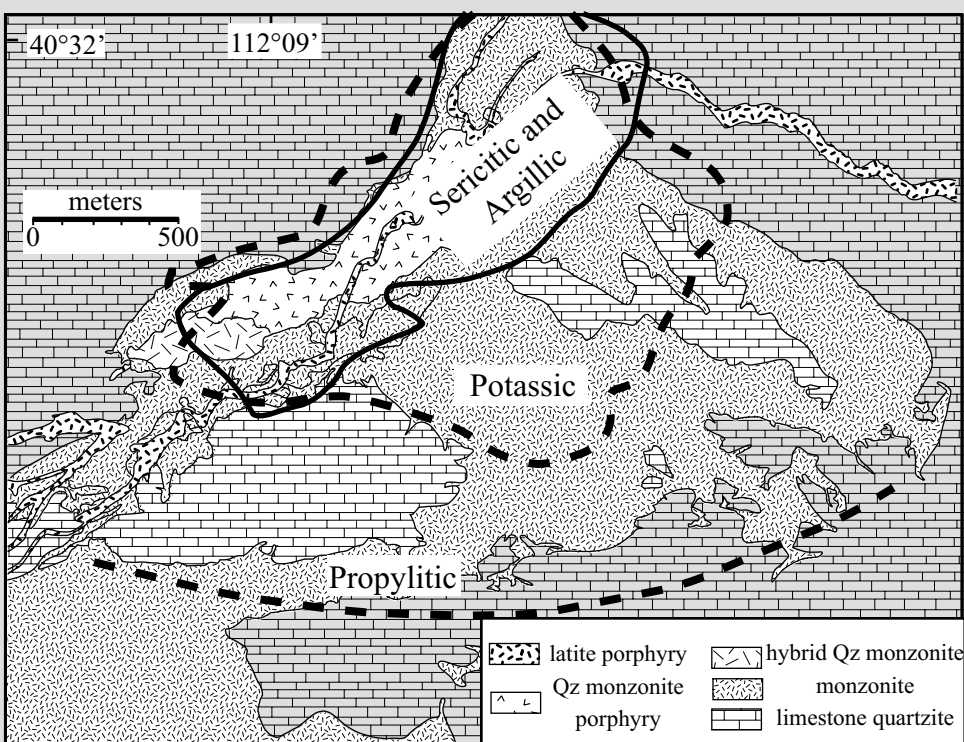
Figure 17.8 shows alteration around a quartz-pyrite vein in a granodiorite from a porphyry copper deposit in Ajo, Arizona. Between the quartz diorite and the vein is a zone where the rock has been sericitized, in other words, the feldspar has been converted to fine-grained muscovite by a reaction similar to reaction (17.20). The sericite halo around the quartz vein suggests the vein was deposited by fluids relatively rich in HCl. Because Fe was probably transported in the fluid as FeCl_2 , it is likely the reactions that altered the wall rock also utilized some of the Cl that was complexing the iron, causing pyrite to precipitate.

Neutralization reactions like this are important in economic geology because metals, sulfur, and Cl behave incompatibly during crystallization of granitic melts. The fluid liberated late in the crystallization of granitic melts will be acidic (or at very least Cl-rich) and sulfidic. Because metals are moderately soluble when they complex with Cl, these fluids will also be laden with metals. When these fluids interact with surrounding rocks the reactions neutralize the fluid, altering the original mineralogy from potassium feldspar to muscovite or clay and, simultaneously depositing metal sulfides. Hydrothermal alteration similar to that shown in Figure 17.8 may cover areas of many square kilometers (Box 17.1). Geologists searching for ore deposits carefully map areas of hydrothermal alteration, because this alteration is commonly the clue that an ore deposit is hidden at depth.

BOX 17.1 | HYDROTHERMAL ORE DEPOSITS AND HYDROTHERMAL ALTERATION

Many ore deposits are formed when metals are deposited from hot aqueous fluids, commonly referred to as *hydrothermal fluids*. There are many classes of hydrothermal ore deposits. Some, like porphyry copper deposits (see Box 7.1), form from fluids derived directly from igneous intrusions. In others, such as those associated with black smokers (Box 6.1), igneous intrusions provide the heat for the fluids, but the fluids are derived mostly from seawater or groundwater. Still other deposits derive from the circulation of groundwater: the heat involved is not magmatic; it is geothermal. The formation of all of these deposits is associated with wall-rock alteration, referred to as *hydrothermal alteration*. Economic geologists study hydrothermal alteration because it provides important information about the formation of the ore, including the composition of the fluid that deposited the ore, the reactions that could have caused the deposition of the ore, and the temperature at which the deposition occurred.

The most common type of hydrothermal alteration is the kind found around porphyry copper deposits (Box 7.2) and epithermal gold deposits (Box 10.1). These types of alteration indicate the movement of acidic fluids through granitic rocks. With increasing acidity the alteration assemblages include:



Box 17.1 Geologic map of the area around the Bingham ore body in Utah showing the alteration around the ore body. Modified from Parry et al., 2002.

(continued)

BOX 17.1 (CONT.)

Propylitic: alteration to chlorite, epidote, calcite, and other minerals indicative of greenschist facies in relatively neutral fluids;

Potassic: alteration to K-feldspar and biotite, indicative of neutral fluids or relatively acidic fluids at high T;

Sericitic: muscovite-rich alteration indicative of acidic conditions; and

Argillic: clay-rich alteration indicative of highly acidic conditions.

These altered rocks often form on a regional scale, as indicated by the alteration around the Bingham ore body in Utah (Box 17.1), and thus provide helpful clues in the exploration of ore bodies.

Fluids that are not particularly acidic or fluids interacting with rocks other than granitic rocks can alter in ways other than the types listed above. Chief among these are:

Silicic: Because silica is highly soluble at temperatures above 300°C, silicic alteration can simply indicate extensive movement of fluid through the rock with attendant deposition of quartz.

Chloritic: Chloritic alteration occurs mostly in mafic rock. Leaching of alkalis by acidic fluids will leave behind Fe, Mg, and Al, which will manifest as chlorite.

Carbonate: This kind of alteration contains large amounts of calcite or dolomite, which indicates the fluid contained CO₂. (Figures 15.13 and 17.2 show that at low temperature, it is not necessary for the fluid to have contained large amounts of CO₂ to form carbonate.)

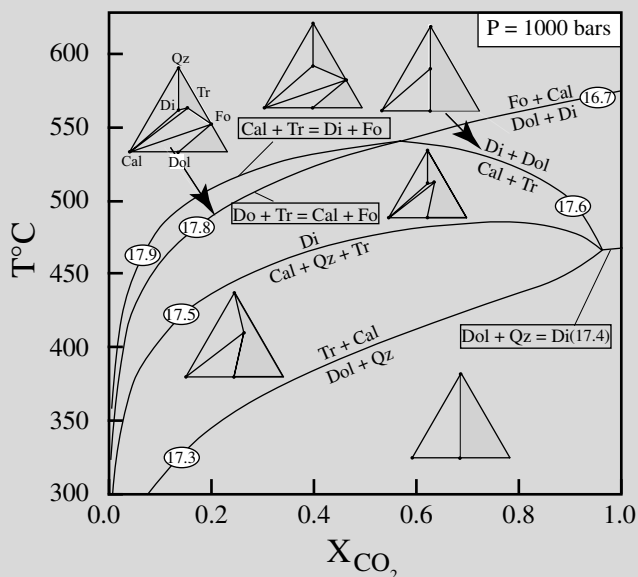
Summary

.....

- Metamorphosed calcareous rocks give petrologists information on the composition of the ambient fluid, as well as the temperature of metamorphism.
- There are two end members for the behavior of fluid during metamorphism:
 - When fluids are **buffered**, or **internally controlled**, their compositions are controlled by the mineral reactions in the rocks. Such rocks usually have a comparatively large number of minerals present.
 - When fluids are **infiltrated**, or **externally controlled**, the mineral assemblages are governed by the composition of the fluid. Such rocks usually have a relatively small number of minerals present.
- A rock was buffering the fluid composition if one can write a reaction among the phases present using fluid species as the only unknown. In some areas, these reactions can monitor the flow of fluids.
- Rocks buffer pH, which is an important process in the formation of ore deposits.

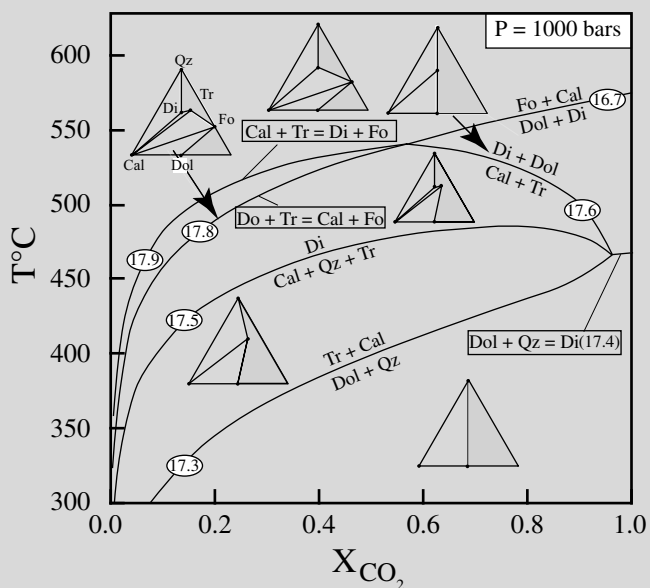
Questions and Problems

Problem 17.1. A metamorphic aureole in impure dolomitic marble records the prograde assemblages listed below. Was the fluid internally or externally controlled during this metamorphism? Show the likely path on Figure 17.2.



- Calcite-dolomite-tremolite-quartz
- Calcite-dolomite-diopside-tremolite-quartz
- Calcite-tremolite-diopside-quartz
- Calcite-diopside-quartz

Problem 17.2. A metamorphic aureole in impure dolomitic marble records the prograde assemblages listed below. Was the fluid internally or externally controlled during this metamorphism? Show the likely path on Figure 17.2.



- a. Calcite-dolomite-tremolite-quartz
- b. Calcite-tremolite-quartz
- c. Calcite-diopside-quartz

Problem 17.3. What type of alteration formed at Ajo, Arizona? Consult Box 17.1 for a brief description of the types of alteration.

Further Reading

.....

Bucher, K. and Frey, M., 2002, *Petrogenesis of metamorphic rocks*. Springer, Heidelberg, Chapters 6 and 8.

Rose, A. W. and Burt, D. M., 1979, Hydrothermal alteration. In *Geochemistry of Hydrothermal Ore Deposits*, 2nd ed., ed. H. L. Barnes. John Wiley & Sons, New York, 173–235.

Winter, J. D., 2010, *Principles of igneous and metamorphic petrology*, 2nd ed. Prentice Hall, New York, 635–44.

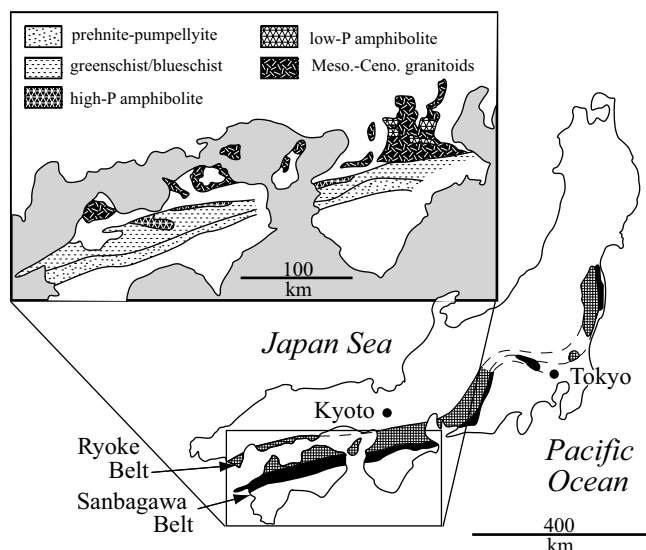
Yardley, B. W. D., 1989, *An introduction to metamorphic petrology*, Longman, Essex, UK, Chapter 5, 126–46.

Chapter 18

Regional Occurrence and Tectonic Significance of Metamorphic Rocks

18.1 Introduction

Over the past four decades, metamorphic petrology has become a significant tool for unraveling the thermal history of mountain belts. The conditions of metamorphism of a given sequence of rocks provide important clues about the tectonic environment in which these rocks formed. There are four major tectonic environments for regional metamorphism: (1) along convergent plate margins; (2) in continent-continent collisions; (3) in rifting terrains; and (4) on the sea floor. In addition, we recognize two metamorphic environments where the tectonic causes are variable or debatable: (5) metamorphism forming granulite terrains and (6) metamorphism in Precambrian shields. This chapter summarizes metamorphism in these environments.



Map 18.1 Paired metamorphic belts from the island of Honshu, Japan. Inset shows the increase in metamorphic grade in the blueschist belt toward the continent. Modified after Miyashiro (1973).

18.2 Metamorphism along Convergent Plate Margins

In 1961, Akiho Miyashiro wrote a seminal paper that related metamorphic conditions to tectonic environment. In this paper he recognized that a consistent association of metamorphic belts exists in the circum-Pacific region. On the ocean-ward side of the continent is a high-pressure belt, commonly metamorphosed to blueschist facies. Examples of these high-pressure belts include the Sanbagawa belt of Japan (Map 18.1), the Franciscan belt of California, and the Shuksan belt of the North Cascades. Inland from this belt on the continent side and commonly in fault contact with these high-pressure rocks is a low-pressure, high-temperature metamorphic belt. The Ryoke belt of Japan (Map 18.1) and the Sierra Nevada of California are examples of these inboard belts. Miyashiro (1961) called this phenomenon **paired metamorphic belts**. Although initially the cause of this association was unclear, the advent of the theory of plate tectonics recognized that the blueschist belts represent fossil subduction zones and the coeval low-pressure belts are deeply eroded magmatic arcs.

18.2.1 Characteristics of Low-Temperature, High-Pressure Belts

Lithologically, low-temperature, high-pressure belts have clearly oceanic affinities. These are dominated by mafic

volcanic rocks, and serpentinites are common. Where metasedimentary rocks are present, they are greywackes; mature sediments, such as metapelites, quartzites, and marbles, are scarce or absent. Granitic rocks also are notable for their absence. In some terrains, such as the Franciscan complex in California, metagreywacke, metabasalt, and serpentinite are intermixed on an outcrop scale. Such a scrambled mixture of rocks is known as **mélange**, an association interpreted to result from subduction. Mélanges are by no means typical of all blueschist terrains; some of these terrains have lithologic packages that are relatively coherent and mappable on a regional scale.

The lowest-grade rocks in a high-pressure belt are commonly in prehnite-pumpellyite facies, though in some terrains, such as the Otago belt in New Zealand, zeolite facies occur. The lowest-grade rocks are found on the oceanward side of the belts, and they grade into blueschist facies and even locally into epidote amphibolite facies, toward the continent (Map 18.1). The highest-grade rocks coincide with the major tectonic break that marks the contact between the high-pressure belt and the adjacent low-pressure belt.

18.2.2 Characteristics of Low-Pressure, High-Temperature Belts

Unlike the high-pressure belt, granitic rocks dominate the low-pressure belt and typically intruded at the peak of metamorphism. Mature metasedimentary rocks are common while metavolcanic rocks and serpentinites are rare. Metapelitic rocks contain andalusite or cordierite at lower grades and sillimanite at higher grades, indicative of low-pressure metamorphism. Unlike the high-pressure belts, there is no simple isograd pattern in the low-pressure belts. Rather, large areas of the low-pressure belts typically consist of isolated blocks of relatively high-grade metamorphic rocks intermixed with granitic rocks. Lower-grade metamorphism occurs only in areas away from the voluminous granites.

18.2.3 Tectonic Interpretation

Paired metamorphic belts represent the remnants of subduction zone – magmatic arc associations (Oxburgh and Turcotte, 1971). The high-pressure belt includes the subducted and metamorphosed oceanic plate and associated sedimentary rocks. Because of their oceanic origin, these rocks illustrate why mafic plutonic rocks are so common in high-pressure belts whereas mature sediments are rare.

The subduction of this cold, wet slab into the mantle causes the geotherms around it to be strongly suppressed. As the cold slab descends to higher pressure conditions, the rocks recrystallize within the blueschist facies. These low-temperature, high-pressure conditions are not normally attained elsewhere in Earth's crust.

Melting triggered by subduction results in the magmatic arc rocks landward of the subduction zone. Movement of magmas into and through the crust transports heat to shallow crustal depths, elevating the geotherms and inducing the low-pressure, high-temperature metamorphism that is diagnostic of the low-pressure zones. The melt bodies in a magmatic arc tend to coalesce into batholiths, leaving the metamorphosed country rock as isolated pendants. The batholiths, which are dominated by granodiorite, tend to have Cordilleran-type geochemical characteristics typical of continental magmatic arcs (c.f. Chapter 7).

18.3 Metamorphism in Continental Collisions

During the early part of the twentieth century, Barrovian metamorphism was considered the “typical” type of prograde metamorphism. However, studies of metamorphism after the Second World War led to the realization that Barrovian metamorphism was the exception rather than the rule. The high pressure of the Barrovian sequence indicated a significant amount of the crust had to be eroded off to expose them, but a more precise understanding of their tectonic evolution didn't emerge until the 1980s.

Thermal modeling showed rocks should follow a “clockwise P-T-t (pressure-temperature-time) path” during continent-continent collisions (England and Thompson, 1984; Thompson and England, 1984) (Figure 18.1). Such a path can be divided into three stages. First, continental overthrusting increases pressure without much increase in temperature, producing blueschist- and possibly eclogite-facies metamorphism. The second stage involves nearly isobaric heating as the deep rocks slowly adjust to the insulating effect of the overlying thrust pile. This results in an overprints of the blueschist metamorphism with high-T, high-P (Barrovian) metamorphism. Finally, the third stage involves relatively rapid uplift of the rocks because of either erosion or tectonic exhumation. Some heating may continue early in this stage, but as the rocks get closer

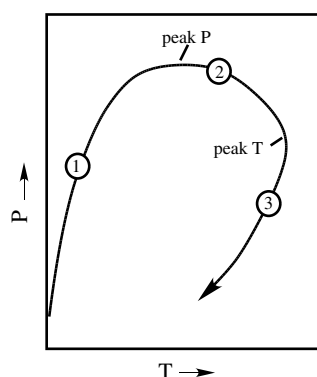


Figure 18.1 P-T diagram showing the clockwise path followed in a metamorphic terrain during continental over-thrusting. Three stages in the path are labeled, 1 = rapid burial by thrusting, 2 = heating, 3 = uplift due to interaction between erosion and isostasy (after England and Thompson, 1984).

to the surface the cooling rate increases until any fluids in the rocks are consumed by retrogressive reactions. Once the fluids have been consumed metamorphic reactions will cease. The uplift during this stage may be recorded in some rocks as decompressive reactions (such as sillimanite after kyanite and cordierite after garnet) or as minor retrogression. However, most of the cooling path may not be recorded in the rocks at all.

The concept of the clockwise P-T-t path introduces a critical question: Just what do the P-T conditions are recorded in Barrovian metamorphism? As shown in Figure 18.1, in a clockwise P-T-t path, the maximum pressure is likely reached before the maximum temperature. As noted earlier, metamorphic reactions likely cease once the rocks start cooling after reaching maximum temperature because water is no longer evolved by metamorphic reactions. Thus, the P-T conditions recorded in a rock are likely those of the maximum temperature. However, in many rocks relicts of earlier, higher-pressure assemblages might survive and, in addition, minor retrograde and decompressive effects might be present.

The concept of a clockwise P-T-t path has influenced the way petrologists interpret the metamorphic assemblages encountered in continental collisions. Petrologists used to take the suite of metamorphic assemblages that record a series of metamorphic grades across a terrain and attribute their P-T conditions to a “fossil” geothermal gradient. It is now known that this inference is fallacious. The rocks from the high-grade portion of a metamorphic terrane (path A in Figure 18.2) will have followed a very

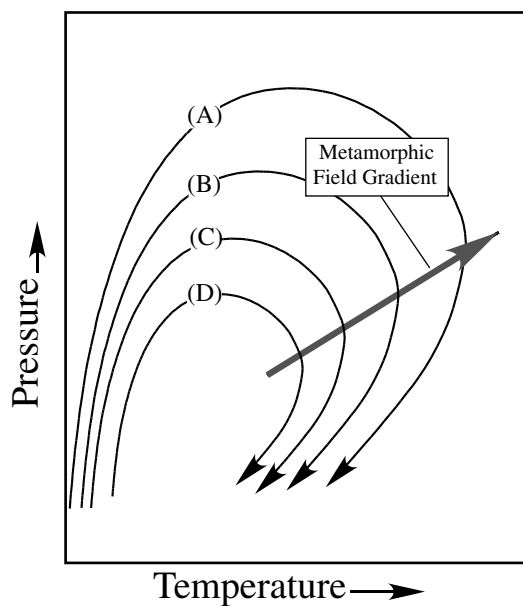


Figure 18.2 A comparison between the assemblages recorded in metamorphic terrane (the metamorphic field gradient) and the P-T path followed by the rocks during metamorphism. A, B, C, D = localities in a metamorphic belt in order of increasing grade.

different P-T-t path from those in the low-grade portion of the terrains (path D, Figure 18.2). A gradient defined by the highest temperature in each path (i.e., the temperature where metamorphic reactions would have ceased) defines a P-T path none of the other rocks in the terrain actually followed. The curve connecting the P-T conditions recorded across a terrain is now known as the **metamorphic field gradient**. As shown in Figure 18.2, the metamorphic field gradient may outline the maximum pressures and temperatures recorded across a terrain, but it does not reflect a fossil geothermal gradient.

18.3.1 Examples of Continental Collisions

Barrovian metamorphism is recognized in most collisional orogens. The type locality is the Caledonide belt of Scotland and Ireland and its continuation north into Norway and south into New England (Map 16.1). In the Caledonides most of the early high-pressure assemblages have been obliterated by the later high-temperature metamorphism. Evidence for relict blueschist metamorphism survives in only a few areas of low-grade metamorphism in Vermont (Laird and Albee, 1981) and in Ireland (Gray and Yardley, 1979).

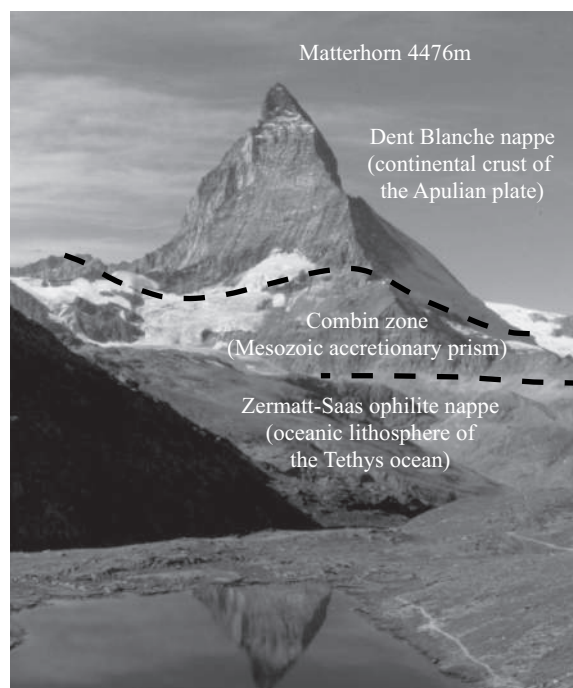
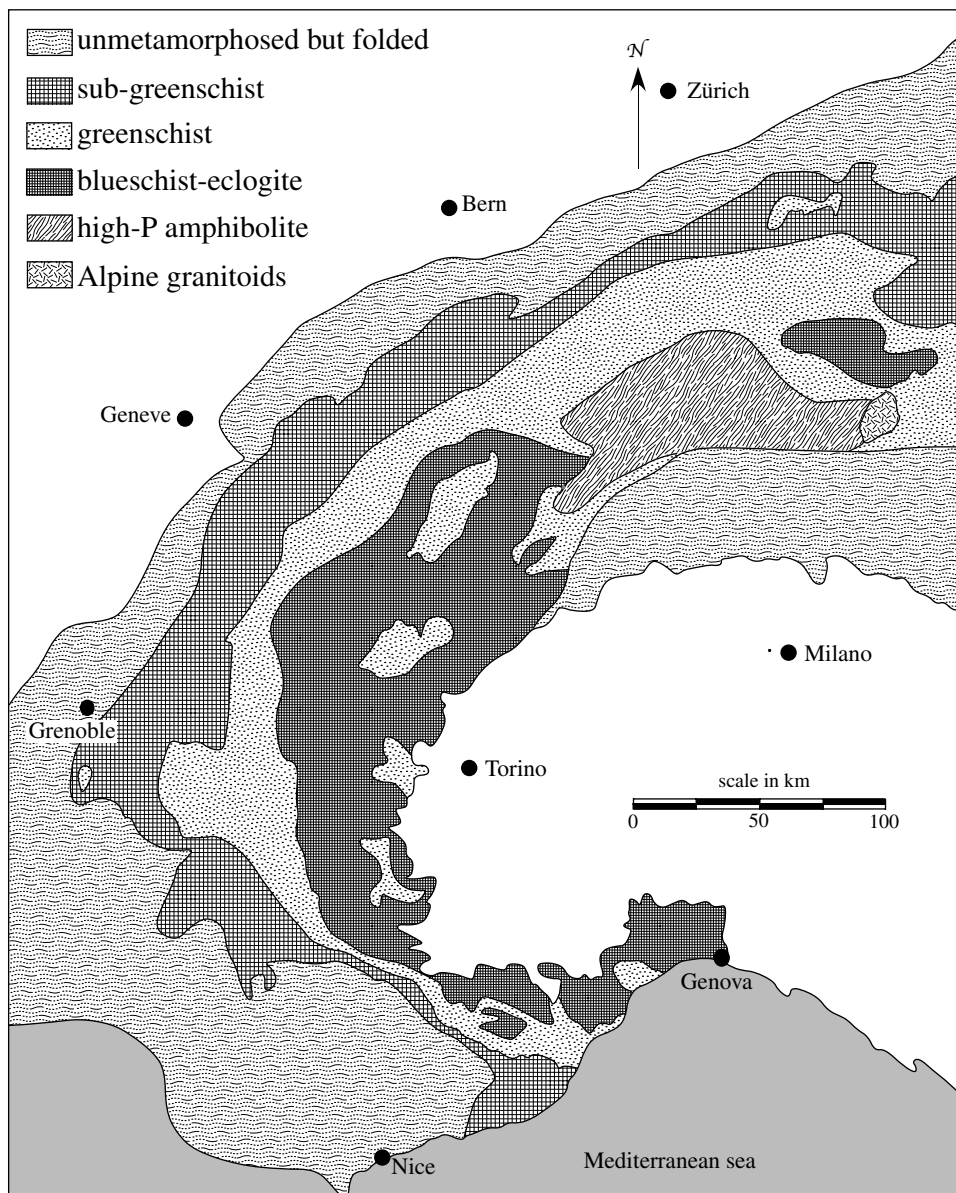


Figure 18.3 Structure of the Alpine orogeny as exemplified by exposures on the Matterhorn.

Perhaps the best example of a continental collision is in the Alps, where the early high-pressure metamorphism has been extensively preserved. The Alps formed when Europe subducted beneath the Apulian plate, a microplate consisting mostly of Italy that was trapped between the European and African plate. A series of ophiolites represents the remnants of the Tethyan sea floor that lay between the two continents. Structural relations for the construction of the Alps are beautifully exposed on the Matterhorn, where the upper portions of the mountain consist of continental crust of the Apulian plate, whereas the base of the mountain contains rocks of the Zermatt-Saas ophiolite (Figure 18.3). The Zermatt-Saas ophiolite contains metagabbros that locally record eclogite facies metamorphism at 600°C and twenty-five kilobars (Bucher and Grapes, 2009), indicating the rocks had been subducted to depths of more than ninety kilometers.

The Alps have undergone two distinct metamorphic events. The earlier blueschist or locally eclogite event, as preserved in the Zermatt-Saas ophiolite, is known as Eoalpine metamorphism and occurred during the tectonic stacking of cold crust during the continental collision. A later Barrovian metamorphic event occurred in a rather restricted area (Map 18.2). Berger and colleagues (2011)



Map 18.2 Map of rocks recording the Alpine metamorphism in the Western Alps. Modified after Frey and colleagues (1974).

contented Barrovian metamorphism was associated with tectonic emplacement of hot, high-pressure rocks to shallower levels late in the Alpine orogeny. Outside the high-P, high-T belt, Alpine Barrovian metamorphism is recorded only as isolated zones of retrogression. The metamorphic map of the Alps, therefore records mostly the effect of the underthrusting during the Eoalpine metamorphism. This event is recorded by an increase in metamorphic grade from zeolite facies to high-pressure blueschist or eclogite facies along an eastward line from Grenoble toward Torino (Figure 18.3).

18.4 Metamorphism in Rifting Terrains

One of the major revolutions in structural geology in the 1970s and 1980s was the recognition that extension plays a major role in the development of many structural belts. This observation was accompanied by a recognition that high-grade metamorphism can be associated with rifting environments. In areas undergoing active extension, the thinning of the crust, the emplacement of hot asthenosphere at the base of the crust, and the intrusion of magmas into the crust produces high-grade metamorphic environments. It

has been postulated that some low-pressure (i.e., pressures of five to six kilobars) granulites can form in such a manner (Wickham and Oxburgh, 1985). Rifting necessarily precedes the opening of any ocean, and hence is a part of the mountain building cycle. When the ocean basin closes again, the high-grade metamorphic rocks produced by the earlier rifting event may be emplaced into a metamorphic and structural belt formed through compressive tectonics. The Hercynian granulites of the Pyrenees and the Alps, both of which were tectonically excavated during the Alpine orogeny (Sills, 1984; Wickham and Oxburgh, 1985) are examples of granulite terrains that predate the compressional terrains in which they are exposed. Similarly the Proterozoic granulites of Norway were emplaced into the Scandinavian shield during the Caledonian orogeny (Bingen, Davis, and Austrheim, 2001).

18.5 Sea Floor Metamorphism

The basalts emplaced at the mid-ocean ridges during sea floor spreading are clearly out of equilibrium with the ocean water that surrounds them. Through time the basalts hydrate in reactions with ocean water. These reactions are the driving-force for sea floor metamorphism. Unfortunately, the sea floor is covered by several kilometers of water, limiting the view of the processes that occur there. Indeed, until the 1970s the concept of sea floor metamorphism was essentially unknown. However, aided by a large number of ODP and IODP drill holes and the observations of ophiolites, which as discussed in Chapter 7 are considered fragments of sea floor thrust on to the continental crust, petrologists over the past few decades have outlined a general model of the processes governing sea floor metamorphism.

For a few million years after emplacement of fresh basaltic magma, the new ocean crust lies above the thermal anomaly marked by the spreading center. This hot area acts as a driving force for the circulation of hot seawater through fractures in the ocean crust. This circulation has a significant effect on the sea floor. Not only do the rocks alter by hydration reactions, they also undergo significant metasomatism. Magnesium and sodium are added to the rocks and transition metals (Fe, Mn, Cu, and Zn) are removed. These transition metals are re-precipitated on the sea floor as “black smokers,” sulfide-rich hydrothermal deposits (McCaig et al., 2007) (see Box 6.1).

The effect of seawater circulation into the ocean crust may be recorded in ophiolites. Where complete sections of ophiolites are exposed, a general gradient in metamorphism punctuates through the section. The upper portion of the ophiolites, occupied by pillow basalts, is highly altered. The degree of alteration varies; the metamorphic grade is prehnite-pumpellyite, or more rarely zeolite facies. The influence of circulating fluid is indicated by the common occurrence of veins. Not uncommonly these rocks record a range of metamorphic conditions; for example, host rocks containing prehnite-pumpellyite facies assemblages may be cut by zeolite facies veins. This relation documents the cooling of the circulating fluids as the crust migrates away from the mid-ocean ridge heat source. Further down in the ophiolite section, generally in the sheeted dike horizon, the metamorphic grade increases to greenschist facies. In the gabbroic section, the metamorphism is seen as late hornblende growth indicative of amphibolite facies, although commonly the lower portions of the gabbros are unaltered.

The same sequence of metamorphic assemblages has been documented in drill holes drilled into fast-spreading oceanic crust. The deep IODP hole 1256D, for example, contains clay as major alteration mineral in the upper portion of the hole (Teagle et al., 2011). Somewhere between 1,000 and 1,200 meters below the sea floor the clay gives way first to greenschist assemblages and then to amphibolite facies a few hundred meters lower. The alteration occurs mostly in veins rather than pervasively as is typical in ophiolites. However, the crust penetrated by hole 1256D is only fifteen million years old. As the crust ages one would expect that the alteration would become more pervasive.

Two other deep drill holes in the ocean crust (745B and 1309D) were drilled into slow-spreading crust, where deep oceanic crust was tectonically exhumed during spreading (Dick et al., 2000; Blackman et al., 2011). Hole 745B comes from crust that is twelve million years old; hole 1309D is only about two million years old. These drill holes exhibit a different style of metamorphism than the drill hole in fast-spreading oceanic crust. The alteration pattern in both holes is very complex (Figure 18.5). In both of them, the assemblages occur as isolated veins in otherwise relatively fresh rock. In both holes high-grade assemblages, such as granulite in 1309D, occur high in the hole, and low-grade assemblages, such as clay and zeolites, are more

prevalent toward the bottom. This inversion reflects the fact that the different metamorphic assemblages occurred at different times. The formation of the oceanic core complexes into which both hole 745B and 1309D were drilled involved deformation while the crust was still hot. The granulite facies assemblages seen locally in the upper portion of 1309D formed during these extensional events. The rocks in the lower part of the core were also hot at this time, but they were not subjected to deformation and hence did not develop metamorphic textures indicative of granulite metamorphism. After tectonic exhumation, the upper portion of the crust cooled rapidly. The low-grade metamorphism documented in the lower portions of holes 745B and 1309D are assemblages produced by reactions taking place at the time the holes were drilled.

Most ophiolites appear to be fragments of young crust thrust onto the continents within a few. No ophiolites have been identified that are composed of oceanic crust more than 100 million years old. It is likely that the circulation of seawater through the ocean crust continues throughout the life of that crust, with the water penetrating progressively deeper as the crust cools and moves away from the spreading center. If this is true, metamorphic zones should migrate downward through the crust with time, with lower amphibolite facies rocks (i.e., serpentinites) possibly forming the upper mantle in the oldest regions of the sea floor. Such a correlation of increased metamorphic grade with age of oceanic crust is suggested by the magnetic anomalies in Cretaceous oceanic crust, which are best explained by having a contribution from magnetite in serpentinized (or partially serpentinized) mantle (Dyment, Arkani-Hamed, and Ghods, 1997).

18.6 Granulite Terrains

As discussed in Chapter 13, granulite facies metamorphism is not only hot, but it requires unusually dry conditions for formation. Because of its high temperature, granulite facies metamorphism is intimately tied to igneous activity (Frost and Frost, 1987). Key to the discussion of granulites is the way CO_2 and H_2O behave in melts. As discussed in Chapter 4, H_2O is very soluble in silicate melts, and any silicate melt moving through the crust will extract H_2O either as a fluid or incorporated in crustal melts. In contrast, CO_2 is most soluble in mafic melts and its solubility is strongly dependent on pressure. The intrusion of mafic melt deep

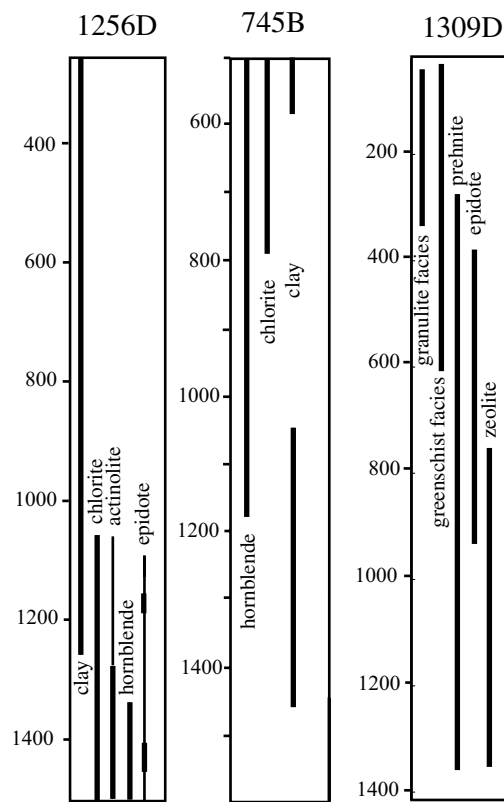


Figure 18.4 Metamorphic alteration in IODP holes 1256D, 745B, 1309D. Locations for these holes are given in Figure 7.2. Sources of data as in Figure 7.3.

in the crust will evolve CO_2 as it crystallizes and melts the crust around it. Thus the evolution of CO_2 from the mafic melt and the extraction of H_2O into both the mafic melt and any crustal melt tends to dehydrate the country rock.

Figure 18.4 shows a magmatic environment where mafic melt has been emplaced into the lower crust and induces crustal melting. Relations such as those shown in Figure 18.4 are most likely found in rifting environments, but extensive interaction of mafic melts with crustal rocks is also found in arc environments, although relations may be slightly different than those shown in Figure 18.5. There are four regions where granulite mineral assemblages may form:

- 1) *Mafic melt injected near the base of the crust and later deformed.* Mafic melts crystallize to clinopyroxene-orthopyroxene-plagioclase (\pm olivine). If a gabbro with this assemblage is subjected to deformation and recrystallization, it will become a mafic granulite without ever having had a hydrated protolith.

- 2) *Melting of the crust around the mafic melts.* Injection of mafic melt into the lower crust will dehydrate the country rock as H_2O is extracted into melt. Movement of these crustal melts to shallower crustal levels will result in dehydration of the source region.
- 3) *CO_2 – metasomatism around mafic melts (and hot granitic melts).* Crystallization of mafic melts evolves CO_2 , and if this fluid invades the country rock, this rock will undergo granulite metamorphism because of the lowered water activity.
- 4) *The lower portion of granitoid plutons.* In many granitoids, pyroxenes are early-crystallizing phases; these convert to hornblende or biotite as the granite approaches water saturation. If the original granitic melt moves to higher crustal levels, bringing the hydrous fluids with them, they leave behind pyroxene-bearing granitoids. These types of plutons are called **charnockites**; if charnockites become deformed they become felsic granulites.

Granulites formed in these four environments are sampled in various geologic environments. Chief among these are: (1) as xenoliths in basaltic rocks, (2) in crustal cross sections, (3) in areas subjected to extensive hot granitic magmatism.

1. *Xenoliths from basaltic rocks.* Some basaltic volcanoes carry fragments of the crust through which they have traveled, and many of these crustal xenoliths are mafic granulites (Rudnick and Taylor, 1987). These granulites probably came from metamorphosed and deformed gabbros emplaced at or near the base of the crust.

2. *Crustal cross-sections.* Large fragments of lower continental crust may be tectonically exposed by thrust faulting and transpressional faulting. The rocks deep in these crustal cross-sections lie in granulite facies. Some granulites in these cross-sections have been metamorphosed at pressures as high as ten kilobars, indicating these are indeed lower crustal rocks. Others record lower pressures indicative of granulites that formed during rifting events (Percival et al., 1992).

3. *Charnockite terrains.* In some areas, the crust has been invaded by one or more hot-dry granitic plutons (i.e., charnockites). The heat and CO_2 from these plutons have metamorphosed the surrounding country rock to granulite facies (Frost and Frost, 1987).

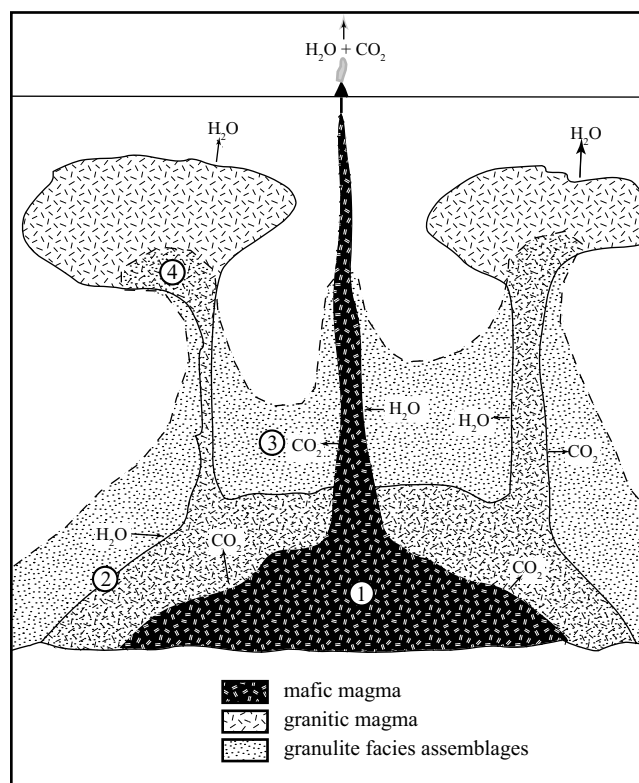
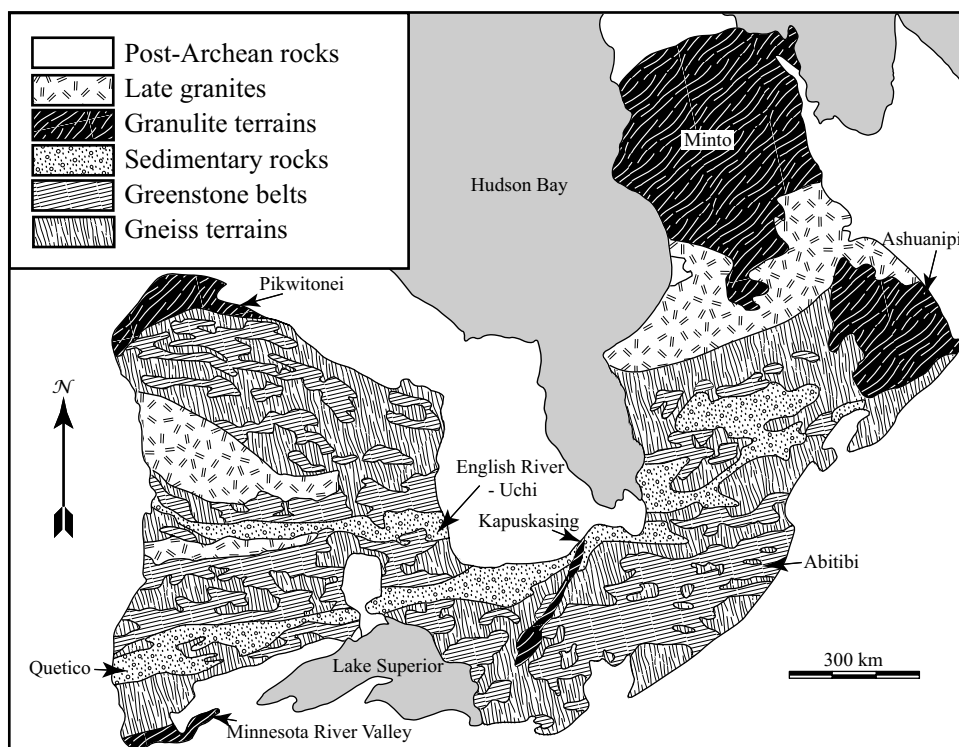


Figure 18.5 Environments of granulite metamorphism: (1) crystallization of mafic magma to become gabbro, (2) dehydration during melting of granite, (3) metamorphism associated with CO_2 fluxing from mafic magma, and (4) crystallization of felsic magma to form pyroxene-bearing felsic rocks. Modified after Frost and Frost (1987).

The Superior province in central Canada exposes a large terrain of metamorphic rocks and contains five major granulite terrains (Figure 18.5), which represent two of the three environments of granulite metamorphism. The Pikwitonei and Kapuskasing are crustal cross-sections that form the core of fault blocks thrust northwestward during the 1.8 Ga Trans-Hudson orogeny. Metamorphic pressures of the Pikwitonei increase from three kilobars to nine kilobars as one moves northwestward across the block (Mezger, Bohlen, and Hanson, 1990). Similarly, the granulites in the Kapuskasing block record nine-kilobar pressures, which is distinct from the four to six kilobar pressures in amphibolite facies rocks to the west of the block (Percival and McGrath, 1986). In contrast, the Minto and Ashuanipi blocks both show pressures of six to six and a half kilobars and contain a mixture of granulite-facies metamorphic rocks and charnockitic plutons (Percival, 1991,



Map 18.3 Distribution of terrains within the Superior province, with the granulite terrains labeled. After Thurston (2002).

Percival et al., 1992), indicating the granulites in these terrains formed during intrusion of hot, dry magmas. Metamorphism in the Minnesota River is also relatively low P (4.5–7.5 kilobars), suggesting granulites here too were produced by magmatic processes (Moecher et al., 1986).

18.7 Metamorphism in Archean Terrains

Precambrian shields are large terrains composed mostly of metamorphic rocks that form the cores of all continents. In many areas, the Archean shield rocks are surrounded by Proterozoic orogenic belts. The tectonic and metamorphic style of the Proterozoic is generally similar to that of the Phanerozoic, but that of the Archean is markedly different. A good example is in the Superior province, the largest Archean craton in the world (Map 18.3). The Superior province consists of four types of metamorphic terrains: (1) granulite terrains, (2) greenstone belts, (3) gneiss terrains, and (4) metasedimentary belts. As noted in the previous section, the granulite terrains represent either deep crustal rocks that have been tectonically exhumed or terrains of hot and dry magmatism. The rest of the province contains individual blocks of greenschist-

facies metabasalts and related rocks (greenstone belts) interspersed within quartzofeldspathic gneiss. The greenstone belts are separated by east-west trending belts of supracrustal rocks (Map 18.3).

It is possible that the low-grade Archean metamorphic terrains (i.e., those that are not in granulite facies) formed by plate tectonic processes similar to those occurring in Earth today. However, because the nature of Archean tectonism is still a matter of considerable debate, this chapter considers the metamorphism of Archean terrains a separate topic.

The elongate metasedimentary belts, which run for thousands of kilometers across the province, appear to represent sedimentary basins that formed between the various greenstone-gneiss blocks. The metasedimentary rocks are immature lithic-rich sandstones that appear to have come from a volcanic source region (Percival, 1989). They appear similar to sedimentary rocks found in modern accretionary prisms, which are composed of marine sediment scraped off the down-going oceanic plate at convergent margins. However, the metamorphic conditions and the pattern of metamorphism of the metasedimentary belts in the Superior province do not match the conditions found in modern accretionary prisms. Both the Quetico

and the English River-Uchi belts in the Superior province were metamorphosed at low pressures (Thurston and Breaks, 1978, Percival, 1989). Pressure is generally three to five kilobars, although pressure in the Quetico belt gets as high as six kilobars near the Kapuskasing uplift. Andalusite and cordierite are common throughout; kyanite is found locally. Temperature increases from the margins of the belts, where it may be as low as 450°C, toward the middle where it is more than 700°C, and locally it reaches granulite conditions (Thurston and Breaks, 1978, Percival, 1989). Percival (1989) suggests the Quetico belt was an accretionary prism trapped in a dextral transpressional boundary between two continental blocks and that thickening of the sedimentary package in the core of the belt produced melting. Movement of these melts to shallow level brought the heat necessary for the high-grade metamorphism.

The continental blocks on either side of the metasedimentary belts consist of irregularly shaped greenstone belts within gneiss terrains. These two rock types are present in most exposed Archean cratons and there is considerable debate as to their origin.

18.7.1 Greenstone Belts

Greenstone belts are sequences of relatively weakly metamorphosed supracrustal rocks. As the name implies, greenstone belts generally contain green-colored amphiboles, typically hosted in greenschist to amphibolite facies mafic volcanic rocks. In addition, most greenstone belts also contain significant amounts of immature sediments, mostly greywacke, with minor amounts of iron formation. Within any given greenstone belt, the proportion of volcanic rocks relative to the sedimentary rocks tends to decrease with stratigraphic height. In addition, at higher stratigraphic levels, the volcanic rocks tend to become more felsic and the sedimentary rocks incorporate more detritus from continental sources. Greenstone belts, such as the Abitibi in Quebec and Ontario (Figure 18.5), are economically important because they host large deposits of base and precious metals.

Greenstone belts generally occur as isolated and irregularly shaped synformal basins infolded between granitic batholiths or gneiss domes. Classic examples of greenstone belts occur in the Pilbara craton of northwestern Australia where, because of the lack of vegetation

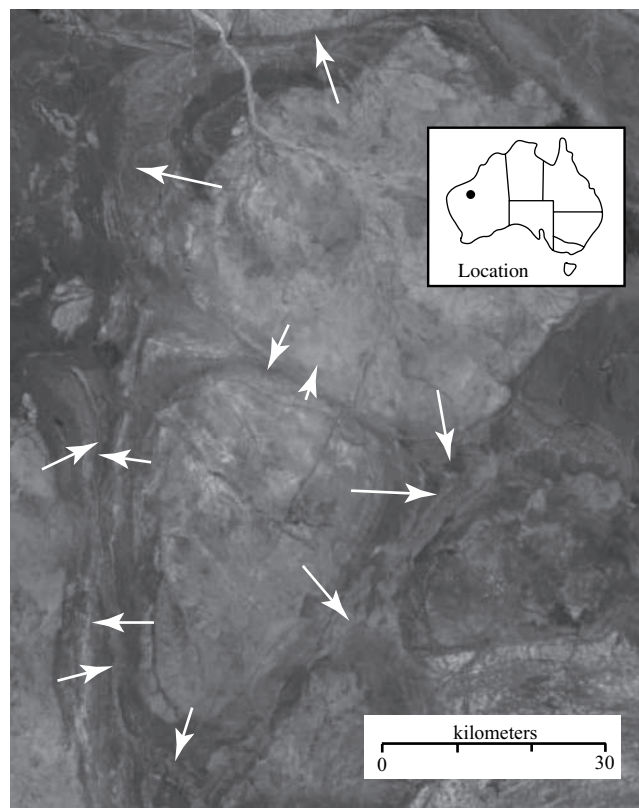
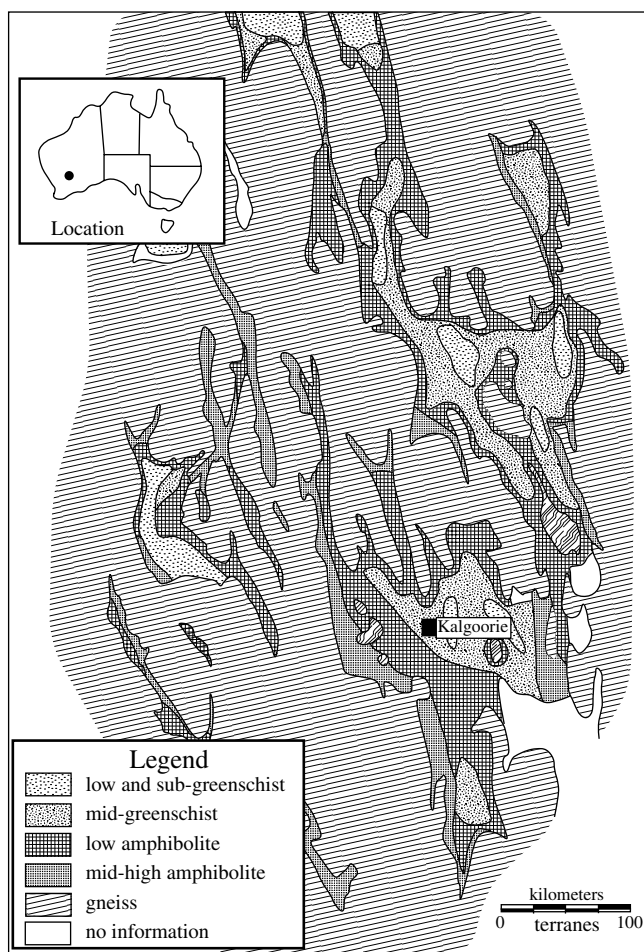


Figure 18.6 Google Earth image of gneiss terranes (light) and greenstone belts (dark) in the Pilbara craton of northwestern Australia. Arrows indicate the dip direction of the foliations in the gneiss and in the greenstone. Structural trends after Van Kranendonk and colleagues (2002).

in the area, the structure is evident in satellite images (Figure 18.6). Metamorphic grade in greenstone belts, for example in the Abitibi (Jolly, 1978) and in the greenstone belts in the Yilgarn craton of Australia (Archibald et al., 1978), tends to increase as one moves outward from the core of the synforms (Map 18.4). The lowest grade recorded is often greenschist facies, although prehnite-pumpellyite facies is found in some greenstone belts. The margins of the belts are usually in amphibolite facies. Pressure is moderate to low, commonly around three to four kilobars; certainly no blueschists have been found in the Precambrian.

18.7.2 Gneiss Terrains

Gneiss terranes commonly surround greenstone belts. These terrains consist dominantly of quartzo-feldspathic gneisses, the composition of which ranges from tonalite to granite. Fragments of metasedimentary rocks are



Map 18.4 Distribution of metamorphic facies in the Eastern Goldfields subprovince of the Yilgarn Archean province. After Binns, Gunthorpe, and Groves (1976).

commonly interfolded in these gneisses. These metasedimentary rocks usually have a mature composition, with metapelitic rocks, quartzites, marbles, and iron formations usually represented. Metamorphic grade is typically amphibolitic and, unlike the greenstone belts, where some changes in metamorphic grade are recognized on a regional scale, many gneiss belts have a uniform metamorphic grade over many thousands of square miles.

18.7.3 Tectonic Interpretation of Archean Metamorphic Belts

There are some similarities between the greenstone belt-gneiss belt metamorphic suite and Phanerozoic paired metamorphic belts. Both greenstone belts and blueschist terrains are dominated by mafic volcanic rocks of sea floor affinity. However, greenschist terranes lack any evidence of high-pressure metamorphism. Furthermore, the metamorphic grade increases in both directions outward from the core of the synforms that characterize greenstone belts, rather than being unidirectional in fossil subduction zones (compare Map 18.1 to Map 18.4). In addition, greenstone belts form roughly circular synformal bodies, as opposed to the markedly linear nature of blueschist terranes, and have a tendency to grade toward volcanic and sedimentary rocks of a continental affinity at their tops. For this reason, skeptics maintain that, if greenstone-gneiss terranes represent paired metamorphic belts, then plate tectonics operated on different scales and resulted in different thermal regimes in the Archean than it does today.

Smithies, Champion, and Cassidy (2003) postulate that the Archean greenstone-gneiss terrains formed by melting of over-thickened oceanic plateau in a manner unlike any tectonic process found on Earth today. In their theory, plate tectonics did not operate on the early Earth and ocean floor basalts were erupted from relatively fixed vents, producing thick accumulations of basalt. Because the Archean Earth had a higher heat flow than modern Earth, the base of these basalt plateau eventually became hot enough to melt, producing a tonalitic magma. Magma intruded the basalt pile and left remnants as deep synforms between the tonalitic plutons. This theory of formation explains the shapes of the greenstone belts and the pattern of metamorphic assemblages they show. If the tonalitic magmatism produced both plutons and extrusive rocks, it would also explain why the greenstone belts include more felsic lavas in the higher stratigraphic levels.

Summary

- **Paired metamorphic belts** are found in convergent boundaries. Blueschist belts lie on the oceanward side of continents, and low-P, high-T belts lie inboard.
- The blueschist (and locally low-P eclogite) facies metamorphic belts record the location of a fossil subduction zone.

- Low-P, high-T metamorphism is commonly associated with Cordilleran-type batholiths.
- **Barrovian metamorphism** is associated with continental collisions and is characterized by a **clockwise P-T-t path** that involves:
 - Low-T, high P metamorphism during continental collision.
 - Increasing T at high P as the thermal structure of the crust adjusts.
 - Decreasing P at high T as the metamorphic belt is unroofed by erosion or tectonic processes.
- Metamorphism in rifting environments is characterized by low-P granulite facies.
- **Sea floor metamorphism** occurs as the fresh oceanic crust hydrates in reactions with the ocean floor. This hydration continues as long as the ocean crust is in contact with seawater and may reach into the mantle in old crust.
- **Granulite metamorphism** records extremely high temperatures and probably forms by reactions between the crust and through-going magmas. Granulites may be exposed in:
 - Crustal cross-sections
 - Areas of extensive high-T magmatism
 - Xenoliths of lower crust
- Archean terrains contain two types of metamorphic belts not common in Phanerozoic environments.
 - **Greenstone terrains.** Greenstone belts are tightly folded synformal structures that usually expose weakly metamorphosed rocks (prehnite-pumpellyite or zeolite facies) in the cores of the folds and amphibolite facies on the margins.
 - **Gneiss terrains.** Gneiss terrains surround the greenstone belts and contain orthogneiss with enclaves of supracrustal rocks in amphibolite facies.

Questions and Problems

1. Consider rocks with the following assemblages. What was the likely protolith for each rock? What kinds of conclusions can be drawn about the tectonic environments in which the rocks formed?
 - a. biotite-muscovite-andalusite-plagioclase-quartz
 - b. orthopyroxene-clinopyroxene-plagioclase-garnet-quartz
 - c. muscovite-chlorite-garnet-glaucophane-quartz.
 - d. biotite-muscovite-kyanite-garnet-plagioclase-quartz
 - e. prehnite-pumpellyite-chlorite-albite-quartz
2. In what ways are greenstone belts similar to blueschist terrains and in what way are they different? What evidence suggests it might be a mistake to equate the two?

3. What are the requirements for the formation of a granulite terrain? In what geologic environments might granulite terrains form?
4. In what way is sea floor metamorphism different from other types of metamorphism? What features would you look for in a metamorphic terrain to determine if the metamorphism formed on the sea floor?
5. What characteristics would you look for in a suite of metamorphic rocks to determine if they underwent burial metamorphism?

Further Reading

.....

Card, K. D., 1990, A review of the Superior province on the Canadian Shield, a product of Archean accretion. *Precambrian Research*, 48, 99–156.

Miyashiro, A., 1975, *Metamorphism and metamorphic belts*. John Wiley & Sons, New York, 327–425.

Yardley, B. W. D., 1989, *An introduction to metamorphic petrology*, Longman Scientific and Technical, London, 187–216.

Appendix: Review of Mineralogy

A.1 Introduction

An important skill necessary to the mastery of igneous and metamorphic petrology is the ability to recognize minerals in hand sample and thin section. Most mineralogy texts follow the system pioneered by James Dana in his 1848 book *The Manual of Mineralogy* whereby minerals are discussed in order of increasing chemical complexity. In this scheme, native elements are discussed first, then oxides, then carbonates, and finally silicates. This appendix reviews minerals in a different order, one that emphasizes the major rock-forming minerals found in igneous and metamorphic rocks. First, the leucocratic minerals that dominate rocks from gabbro through granite and most metamorphic rocks are described: feldspars, quartz, feldspathoids, and carbonates. Next, ferromagnesian minerals are reviewed, then the minerals common in metamorphic rocks, including the Al-rich minerals and Ca-Al silicates. Finally, the reader will find a description of minerals that occur in minor abundance in most rocks: opaque minerals and accessory minerals.

A.2 Leucocratic Rock-forming Minerals

A.2.1 Quartz

Quartz (SiO_2) is the most common mineral in Earth's crust. As such it is common in many igneous and metamorphic rocks. It is usually found as anhedral grains that make up the framework of the rock. The hexagonal crystal shape that is diagnostic in drusy quartz is rarely exhibited when quartz crystallizes in a rock, although euhedral quartz may be an early crystallizing phase in some siliceous volcanic rocks or in some quartz veins.

Hand Sample and Optical Properties. Quartz in hand sample has gray color, greasy luster, conchoidal fracture, and lack of cleavage. It is identified in thin section by its uniaxial (+) optic sign, its low birefringence, and its low relief. Other features that readily identify quartz in thin

section include: 1) undulatory extinction, 2) lack of alteration, and 3) common occurrence of fluid inclusions.

1) *undulatory extinction*: At high temperatures (above ca. 350°C), quartz is very easily deformed by crystal-plastic flow. Any quartz-bearing rock that is even slightly deformed above these temperatures will show the effects of this deformation by development of undulatory extinction. This means extinction sweeps across a grain as the microscope stage is rotated, instead of the whole grain going to extinction at the same time.

2) *lack of alteration*: Other low-relief, low-birefringence minerals that can be confused with quartz (feldspars, nepheline, or cordierite) alter easily at low temperatures. Even a small amount of alteration will make these crystals cloudy in plane-polarized light. In contrast, quartz is particularly resistant to alteration and remains clear.

3) *fluid inclusions*: Because silica is highly soluble at high temperatures, fractures in quartz (even on a micron scale) tend to be quickly healed by re-precipitation of silica. Often, during this healing process, micro-sized bubbles of the ambient fluid are left behind as fluid inclusions. In many rocks, trails of fluid inclusions cutting the quartz are common features. In some rocks the inclusions are so fine that, except at the highest powers, they look like dust. Fluid inclusions are rare in feldspars or nepheline, so any low-relief mineral with fluid inclusions is likely quartz. Beware, however, apatite, which typically forms only tiny grains, may trap fluid inclusions, and can look like quartz. However, apatite has much higher relief than quartz.

A.2.2 Feldspars and Feldspathoids

The feldspars are the most common mineral group. Few indeed are the rocks that do not contain a feldspar; many common rocks contain two. The feldspar group consists of three end members – albite (Ab, $\text{NaAlSi}_3\text{O}_8$), anorthite (An, $\text{CaAl}_2\text{Si}_2\text{O}_8$), and orthoclase (Or, KAlSi_3O_8) – arranged into two solid solutions, plagioclase (Ab-An) and alkali feldspars (Ab-Or) (Figure A.1). Only a limited amount of Ca

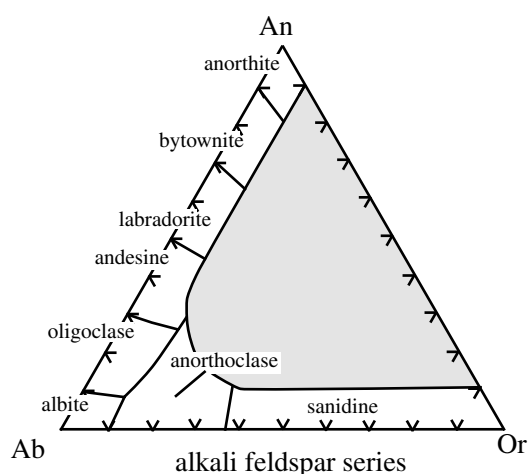


Figure A.1 The system Ab-An-Or showing the names of the various feldspars. (After Deer, Howie, and Zussman, 1963.) Mineral abbreviations as on Table 2.1.

can substitute for K so any rock with a bulk composition that plots in the shaded portion of Figure A.1 contains two feldspars, both a plagioclase and an alkali feldspar.

In hand sample, the feldspars are white, gray, pink, or black in color, distinguishable from quartz, which is glassy and gray. In distinguishing the feldspars from one another, it is helpful to look for twinning and exsolution. Plagioclase feldspar characteristically shows albite twins, which appear as striations parallel to the (010) plane. K-feldspar shows only the Carlsbad twin, which forms a single twin, usually in the middle of a feldspar lath. Alkali feldspars in slowly cooled rocks may contain fine, usually irregularly shaped, exsolution blebs of plagioclase. These exsolved alkali feldspars are called *perthites*. When the plagioclase dominates in an exsolved feldspar, it is called *antiperthite*.

Plagioclase Series

The plagioclase series is one of the most important groups of igneous minerals; almost all igneous rocks contain plagioclase of some composition. Plagioclase is a solid solution between *albite* (Ab) ($\text{NaAlSi}_3\text{O}_8$) and *anorthite* (An) ($\text{CaAl}_2\text{Si}_2\text{O}_8$) (These and other mineral abbreviations are listed in Table A.1.). The solution series has been broken into compositional ranges, each of which has been assigned a mineral name. (Figure A.1). Apart from labradorite, which locally shows iridescence and andesine, most of these names are nearly obsolete because the microprobe allows petrologists to determine the exact composition of plagioclase. Thus, instead of using mineral names, modern

Table A.1 Abbreviation for minerals

Mineral	Abbreviation	Mineral	Abbreviation
actinolite	Act	lawsonite	Lws
albite	Ab	leucite	Lct
andalusite	And	lizardite	Lz
anorthite	An	magnesite	Mgs
anthophyllite	Ath	magnetite	Mag
antigorite	Atg	moscovite	Ms
augite	Aug	nepheline	Nph
biotite	Bt	olivine	Ol
brucite	Brc	orthoclase	Or
calcite	Cal	orthopyroxene	Opx
chrysotile	Ctl	periclase	Per
chlorite	Chl	phlogopite	Phl
chloritoid	Cld	pigeonite	Pgt
clinopyroxene	Cpx	plagioclase	Pl
cordierite	Crd	prehnite	Prh
diopside	Di	pumpellyite	Pmp
dolomite	Dol	pyrite	Py
enstatite	En	pyrope	Prp
epidote	Ep	pyroxene	Px
fayalite	Fa	pyrrhotite	Po
ferrosilite	Fs	quartz	Qz
forsterite	Fo	rutile	Rt
garnet	Grt	sillimanite	Sil
glaucophane	Gln	sphalerite	Sp
grossular	Grs	spinel	Spl
hedenbergite	Hd	staurolite	St
hornblende	Hbl	talc	Tlc
hypersthene	Hyp	tremolite	Tr
ilmenite	Ilm	water vapor	V
k-feldspar	Kfs	wollastonite	Wo
kyanite	Ky		

petrologists designate plagioclase composition by the mole fraction (i.e., mole percent) of An or Ab. For example, a plagioclase with the composition ($\text{Na}_{0.4}\text{Ca}_{0.6}\text{Al}_{1.6}\text{Si}_{2.4}\text{O}_8$) can be expressed either as An_{60} or Ab_{40} .

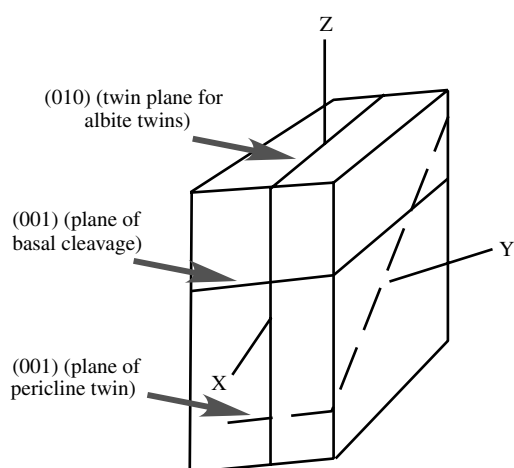


Figure A.2 Crystallographic sketch of plagioclase showing the orientation of albite twins (010), the basal cleavage (001), and pericline twins (which form on a rhombic section).

Calcic plagioclase tends to be found in mafic rocks, such as basalt and gabbro, whereas sodic plagioclase is more common in granodiorite and granite. It is common in igneous rocks for plagioclase to be tabular, elongate along the c-axis, and to show euhedral zoning (Plate 2.3). If the core of the plagioclase is more calcic than the rim, then the zoning is called *normal zoning* (because this is the pattern one would expect to form during cooling of an igneous melt). If the core is more sodic than the rim, the zoning is called *reverse zoning*. Igneous plagioclase may show alternating normal and reverse zoning; such zoning is called *oscillatory zoning*.

The diagnostic feature of plagioclase, both in hand sample and thin section, is its twinning (Figure A.2). The most common twin in plagioclase is the albite twin; this has the (010) plane for its twin plane. In plagioclase the albite twin is *polysynthetic*, which means that usually multiple albite twins are present in a given plagioclase crystal. Plagioclase may also show Carlsbad and pericline twins. Carlsbad twins have the same twin plane as albite twins but a feldspar crystal can have only one Carlsbad twin. Pericline twins are twinned along a plane that is oblique to Z and X but parallel to Y. When viewed down the a-axis, pericline twins are parallel to the 001 cleavage plane. In plagioclase, pericline twins are not polysynthetic.

Plagioclase in metamorphic rocks, unlike igneous plagioclase, is generally equant; it is never tabular. Tabular plagioclase forms when it grows unconstrained in a melt. Thus the existence of tabular plagioclase in a metamorphic rock is a clear indication that the rock had an igneous

protolith. Metamorphic plagioclase may be untwinned and it is rarely zoned.

Optical Properties: Plagioclase of all compositions has similar optical properties. All are triclinic, have low birefringence (usually first-order gray), and have diagnostic tabular twinning on (010) (albite twinning). Compositions from albite to anorthite are accompanied by changes in relief and changes of optic orientation.

1) *changes in relief:* Albite and oligoclase have low negative relief, andesine and labradorite have low positive relief, and bytownite and anorthite have moderate positive relief.

2) *changes of optic orientation:* The optic orientation of plagioclase changes as a function of composition, which means plagioclase grains with different compositions will have different extinction angles. This is important because it provides a technique for estimating plagioclase composition in thin section called the X-normal method.

The X-normal method: This way to estimate plagioclase composition under the microscope requires that you find a plagioclase crystal oriented normal to the X-axis. In these crystals, the extinction angle will help identify the plagioclase composition. The easiest approach to finding an appropriately oriented crystal is to look for twin planes that are razor sharp and for crystals in which the twins on either side of the twin plane have the same birefringence (Figure A.3A). However, crystals with these characteristics can be oriented at any angle normal to the (010) plane. To be certain of a crystal orientation normal to the X, the petrographer must identify a section perpendicular to (001). Fortunately, plagioclase has two features that lie along (001), the (001) cleavage and the pericline twin (narrow twins that lie at high angles to the albite twins). A section in which the albite twin *and* the (001) cleavage or the pericline twin plane both are razor sharp is a section oriented normal to X.

Another property of the section normal to (010) is that the alternating twins will show symmetrical extinction; one set will go to extinction with a certain rotation clockwise and the other set will go to extinction with the same rotation counter-clockwise (Figures A.3B and C). To determine the anorthite content of plagioclase in a thin section, the petrographer finds a grain that shows the proper orientation and then measures the angle of extinction clockwise and counter-clockwise for the twin lamellae. They should agree to within 5°. If the results are not exactly the same (but within 5°), then average them and, using Figure A.4, read off the anorthite composition. There

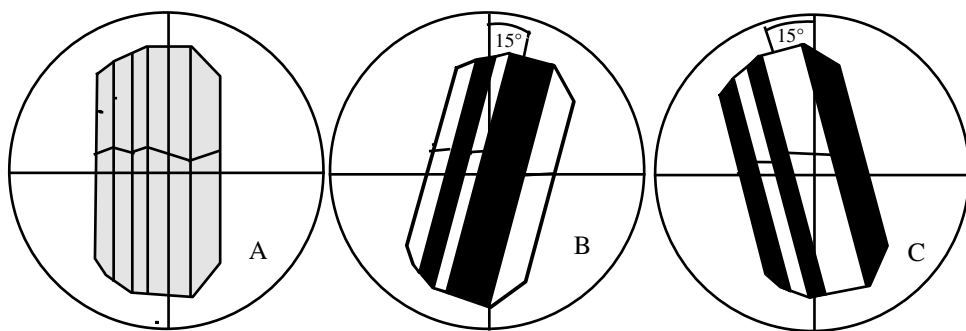


Figure A.3 Figure showing what a plagioclase grain would look like when oriented normal to X. Both (010) cleavage and the albite twin plane are razor sharp and both sets of twins show the same birefringence (A). The twins will go to extinction with the same amount of rotation clockwise (B) and counter-clockwise (C). Using the chart shown on Figure 2.4, the composition of this plagioclase can be identified as An_{32} .

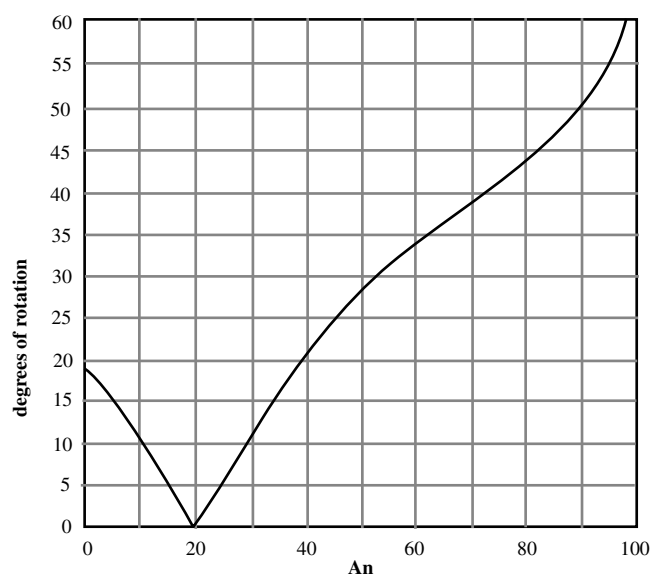


Figure A.4 Graph showing the relation between plagioclase composition and rotation angle to extinction when looking down the X-axis. From Heinrich (1965).

is one slight complication with Figure A.4 – for rotations of 0–20° there are two possible compositions. For example, the plagioclase with an extinction angle of 10° could have the composition of either An_4 or An_{28} . The correct value can be determined from the relief of the plagioclase against quartz or epoxy. Remember that plagioclase with $An < 20^\circ$ has low negative relief, while plagioclase with $An > 20^\circ$ has positive relief. Thus if the plagioclase in question has an extinction angle of 10° and negative relief it is An_4 ; if it has positive relief it is An_{28} .

Because extinction angle changes with composition, one can easily determine whether plagioclase in a rock

is zoned. Unzoned plagioclase will have uniform extinction, such as plagioclase shown in Figure A.3. In zoned plagioclase extinction will sweep across the grain, and in oscillatory-zoned plagioclase the zoning will be seen as light and dark bands running parallel to the margins of the grain.

Alkali Feldspars

Alkali feldspars are those that are solid solutions of $NaAlSi_3O_8$ and $KAlSi_3O_8$ with minor amounts of $CaAl_2Si_2O_8$ (Figure A.5). In igneous rocks the phase relations among the alkali feldspars depend on the temperature of the magma. In many igneous environments magmas solidify at temperatures higher than the top of the solvus between $NaAlSi_3O_8$ and $KAlSi_3O_8$ (Figure A.5A). In these *hypersolvus* granites only a single feldspar crystallizes. Igneous melts that contain abundant water, fluorine, or boron may remain molten until temperatures below those of the alkali feldspar solvus (Figure A.5B). In such *subsolvus* granites, two alkali feldspars – an Ab-rich feldspar and an Or-rich feldspar – crystallize directly from the melt.

K-feldspar. There are three polymorphs of potassium feldspar ($KAlSi_3O_8$): *sanidine*, *orthoclase*, and *microcline*. The differences between them are determined by the extent to which Al and Si are ordered on the tetrahedral site. Sanidine, the disordered alkali feldspar, is found in rapidly cooled volcanic rocks (see a in Figure A.5A). Orthoclase may occur in some volcanic rocks or in relatively quickly cooled plutonic rocks (b in Figure A.5A). The ordered feldspar, microcline occurs in slowly cooled plutonic rocks (c in Figure A.5A).

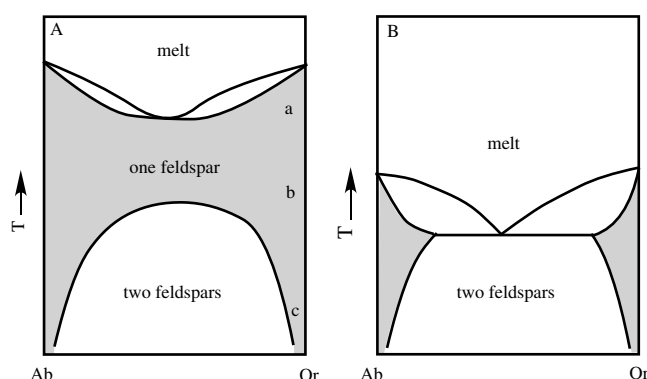


Figure A.5 Schematic phase diagrams for the alkali feldspars. A. Phase relations for anhydrous magmas that solidify at relatively high temperatures. a = stability region for sanidine, b = stability for orthoclase, c = stability for microcline. B. Phase relations for magmas with H_2O that crystallize at lower temperatures.

Optical Properties: All potassium feldspars have low negative relief (relief is always lower than coexisting albite) and low birefringence, with maximum colors of first-order gray.

Microcline is completely ordered and is triclinic. Like the triclinic plagioclase feldspars it shows abundant twinning. Carlsbad, albite, and pericline twins are all present, although only the albite and pericline twins occur as multiple twins. Unlike plagioclase, where albite twins are dominant and pericline twins are rare, the albite and pericline twins in microcline are present in equal abundance. Furthermore, they are repeated on a fine scale, giving microcline a pattern of cross-hatched or “tartan” twinning under crossed polars. Because microcline occurs in slowly cooled rocks, it is usually nearly pure $KAlSi_3O_8$. The sodium expelled from the structure commonly forms inclusions with the microcline. This structure, microcline containing exsolution blobs of albite, is called *perthite*. This exsolution is commonly seen in thin section, and in some rocks it is coarse enough to be recognized in hand sample.

Orthoclase and **sanidine** are progressively more disordered and are monoclinic. Because they are monoclinic, they cannot show albite and pericline twins; only Carlsbad twins may be present. Both sanidine and orthoclase are biaxial (-); $2V$ is a function of degree of ordering. $2V$ ranges from 40° to 70° for orthoclase; K-feldspar with $2V$ less than 40° is called sanidine. Orthoclase may show exsolution of albite, but sanidine never does.

Sanidine, being a high-temperature, disordered form of K-feldspar, is found mainly in volcanic rocks and usually contains considerable amounts of dissolved $NaAlSi_3O_8$. It is recognized by its lack of twinning and low $2V$.

Anorthoclase. Anorthoclase, $(Na,K)AlSi_3O_8$, is a high-temperature alkali feldspar that, like sanidine, occurs only in volcanic rocks. Indeed, one might consider it a sodic variant of sanidine (Figure A.1). Most samples of anorthoclase also contain more than 5 mole percent $CaAl_2Si_2O_8$. Like plagioclase, anorthoclase is triclinic, but unlike plagioclase, the pericline twins are equally as abundant as albite twins, much as they are in microcline. However, unlike microcline the twins in anorthoclase are repeated on an extremely fine scale, giving the anorthoclase a felted appearance in thin section. It also is easy to distinguish anorthoclase from microcline because anorthoclase only occurs in volcanic rocks and microcline is found only in plutonic rocks.

Feldspathoids

Feldspathoids are minerals characteristic of igneous rocks that are so poor in silica that quartz is not present and feldspars are destabilized. These rocks will contain nepheline ($NaAlSiO_4$) or sodalite ($Na_8Al_6Si_6O_{24}Cl_2$) in place of or in addition to albite ($NaAlSi_3O_8$) and perhaps leucite ($KAlSi_2O_6$) in place of K-feldspar. They are very rarely found in metamorphic rocks.

Nepheline. Nepheline ($NaAlSiO_4$) is the most common feldspathoid. It substitutes for albite in silica-undersaturated, sodic rocks. In hand sample it looks similar to quartz, being greasy gray with no cleavage. With a hardness of 5.5 to 6, it is softer than quartz. In thin section it looks like quartz and untwinned feldspars, with low birefringence and low negative relief. Unlike feldspars it is uniaxial. Nepheline can be distinguished from quartz by the fact that it is uniaxial (-) whereas quartz is uniaxial (+). Nepheline, like feldspars, is easily altered. One common alteration product is cancrinite, a complex hydrated tectosilicate similar in many respects to zeolites. Cancrinite is pink in hand sample. In thin section it is colorless with moderate 1° birefringence. Alteration of nepheline to cancrinite is a diagnostic feature in hand sample and thin section.

Leucite. Leucite ($KAlSi_2O_6$), the potassic feldspathoid, is not nearly as abundant as nepheline. Leucite is a common mineral in potassic, alkaline magmas. At high

temperatures, leucite is cubic and crystallizes into diagnostic hexoctahedra phenocrysts. On cooling the structure inverts to tetrahedral. This is accommodated by the formation of twins in the original hexoctahedra. Leucite has such low birefringence that it looks isotropic; sometimes the twins can only be seen by inserting the first-order plate. This is because the eyes are much more sensitive to minor changes in blue than minor changes in black.

Sodalite. Sodalite ($\text{Na}_8\text{Al}_6\text{Si}_6\text{O}_{24}\text{Cl}_2$) is chemically equivalent to 6 nepheline + 2 NaCl, which indicates it is likely to be found in alkaline intrusions also rich in chlorine. In a few localities sodalite is deep blue in hand sample. Because those localities have supplied geology labs for years, many people assume this is a diagnostic feature of sodalite. However, sodalite can assume a wide variety of colors from bluish gray to green to yellow. In some rocks sodalite has a distinct cubic shape; in others it is anhedral. In thin section it is identified by its isotropic nature and moderate negative relief. The only mineral with similar properties is fluorite, but fluorite is characterized by octahedral cleavage.

A.2.3 Carbonates

In addition to all the silicates discussed previously, the other important framework-forming minerals found in metamorphic (and much more rarely in igneous) rocks are the carbonates. Carbonates form the framework of metamorphic rocks derived from some metasedimentary hosts, but there are also igneous rocks, known as carbonatites, that also are composed mostly of carbonates. There is a large number of carbonates, but only those listed in Table A.2 are commonly rock-forming minerals. Of these, the first four have similar crystal structure and optical properties. They form in the hexagonal system and have distinct rhombohedral cleavage. They have similar optical properties and are difficult to distinguish in thin section. All are uniaxial (-) and have extreme birefringence and thus are pearly white under crossed nicols. Calcite, dolomite, and magnesite have one index of refraction, n , that is lower than 1.53. Therefore, on rotation the relief of those grains that have the c-axis near the plane of the thin section goes from low negative to high positive. On rotation of the stage, therefore the relief changes dramatically. This phenomenon is known as “twinkling.”

There is no easy way to distinguish among these minerals in thin section. This is a problem because calcite and dolomite commonly occur together in

Table A.2 Carbonate Minerals Commonly Found in Metamorphic Rocks

Mineral	Composition
Calcite	CaCO_3
Dolomite-ankerite	$\text{CaMg}(\text{CO}_3)_2 - \text{CaFe}(\text{CO}_3)_2$
Magnesite	$\text{Mg}(\text{CO}_3)$
Siderite	$\text{Fe}(\text{CO}_3)$
Aragonite	CaCO_3

metamorphosed limestones and dolomites; calcite, dolomite, and magnesite may coexist in carbonatized metaperidotites; and calcite, ankerite, and siderite may occur together in iron formations. Numerous staining techniques are used to distinguish the carbonates. Here are a few ways calcite, dolomite, magnesite, and siderite can be distinguished.

- Dolomite, since it may contain small amounts of iron, may be somewhat turbid or stained by iron oxide in thin section, whereas calcite will not have such stains.
- Dolomite tends to be more idioblastic than the other carbonates.
- Siderite can be distinguished from calcite by its relief, which is higher than quartz in all orientations.

Another carbonate, aragonite occurs in shells, fresh deep-water sediments, and in high-temperature, low-pressure metamorphosed rocks. Superficially it looks like calcite. It has a similar extreme birefringence and it twinkles on rotation of the stage. However, aragonite is orthorhombic and therefore it lacks the rhombohedral cleavage of calcite. Furthermore, aragonite gives a biaxial figure rather than a uniaxial one.

A.3 Ferromagnesian Minerals

A.3.1 Olivine

Olivine is made up of two major end members: forsterite (Mg_2SiO_4) and fayalite (Fe_2SiO_4). Mg-rich olivine melts at a higher temperature than Fe-rich olivine, thus forsteritic olivine is usually found in the mantle or in igneous rocks directly extracted from the mantle, whereas Fe-rich olivine

is found in evolved rocks such as fayalite-granites or fayalite-rhyolites. Mg-rich olivine is also found in metamorphosed magnesian rocks, such as serpentinites or impure marbles, whereas fayalite may be found in metamorphosed Fe-rich rocks such as iron formations. Over most of its composition range olivine is incompatible with quartz; pyroxenes form instead of olivine and quartz. However, because the iron-rich pyroxene ferrosilite is not stable at crustal pressures, fayalite can be present along with quartz in granites. Olivine is usually a nearly pure Fe-Mg solution, with only minor amounts of other elements. Forsteritic olivine may contain as much as 1 percent NiO and fayalite olivine may contain up to several percent MnO. Unlike plagioclase, olivine rarely preserves zoning.

In hand sample olivine typically has a green or yellow-green color. The color of olivine is a rough indication of its Fe/(Fe+Mg) ratio. Pure forsterite (such as forsterite in metamorphosed impure dolomitic marbles) may be white, and increasingly iron-rich olivine may range from honey yellow through brown to black. Regardless of its color, olivine has a distinct glassy luster and lacks cleavage. Mg-rich olivine weathers to a pale reddish brown; the rock name *dunite* alludes to this color. Iron-rich varieties weather to a rusty brown surface. Olivine is orthorhombic, but because olivine crystals are usually anhedral and show no cleavage, the crystallographic system can only be recognized where olivine occurs as phenocrysts in volcanic rocks.

In thin section olivine is distinguished by its high relief, which increases with iron content. It is colorless (though very Fe-rich olivine may be slightly yellow), has high birefringence, and lacks cleavage. Mg-rich olivines are recognized by their positive optic sign and very high 2V, and fayalitic olivines by their negative optic sign and a 2V of around 50–60°. Olivine is distinguished from pyroxenes by its higher relief, lack of cleavage, higher birefringence (3° compared to 2° for pyroxenes) and often anhedral habit.

Olivine is easily altered and this alteration is often helpful in identifying the presence of olivine (if it hasn't obliterated the olivine entirely). Magnesian olivine alters to serpentine, which may occupy grain boundaries or cracks. More iron-rich olivine (Fo₈₀ or less) will form a red-brown isotropic material known as *iddingsite*. Iddingsite is a mixture of clay, chlorite, and goethite and like serpentine, commonly forms on grain boundaries and cracks in olivine.

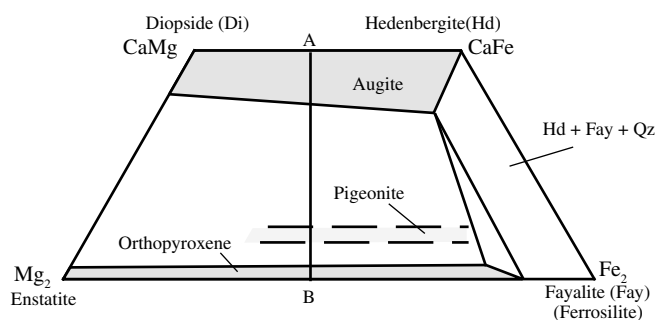


Figure A.6 Diagram showing the approximate composition ranges for the three pyroxene quadrilateral solution series. A-B shows the line of section displayed as a T-X diagram in Figure A.7. Mineral fields from Lindsley and Frost (1992).

A.3.2 Pyroxenes

Pyroxenes are among the most common minerals in igneous rocks, second only to the feldspar group minerals. They are particularly important in igneous petrology because the composition of pyroxenes in a rock can tell the petrologist a lot about the crystallization conditions of that rock. Pyroxenes also occur in metamorphic rocks; in most bulk compositions they are indicative of high temperatures.

Pyroxenes have the general formula XYZ_2O_6 , where:

X = 6–8 coordinated cations that occupy the M2 site, which includes the larger cations like Ca and Na, in addition to Fe²⁺, Mg, or Mn;

Y = octahedrally coordinated cations that occupy the M1 site, which includes Fe, Mg, Ti, Al, and Mn; and

Z = tetrahedrally coordinated cations in the T site such as Si or Al.

The pyroxenes can be divided into two major series:

1. *quadrilateral pyroxenes*: These are pyroxenes with the general formula $(Ca,Fe,Mg)(Fe,Mg)Si_2O_6$. The quadrilateral pyroxenes are so named because their composition can be projected onto a quadrilateral with the apices $CaMgSi_2O_6$, $CaFeSi_2O_6$, $Mg_2Si_2O_6$, and $Fe_2Si_2O_6$ (Figure A.6). The majority of naturally occurring pyroxenes occur in this family.
2. *sodic pyroxenes*: These are pyroxenes that contain Na substituting for calcium and include relatively uncommon pyroxenes such as jadeite and aegirine.

Quadrilateral Pyroxenes

The quadrilateral pyroxenes have the following end members:

Diopside	$\text{CaMgSi}_2\text{O}_6$	(Di)
Hedenbergite	$\text{CaFeSi}_2\text{O}_6$	(Hd)
Enstatite	$\text{Mg}_2\text{Si}_2\text{O}_6$	(En)
Ferrosilite	$\text{Fe}_2\text{Si}_2\text{O}_6$	(Fs)

The quadrilateral pyroxenes can be divided into three solid solution series (Figure A.6). Along the bottom of the pyroxene quadrilateral are the Ca-poor pyroxenes, which form a solid solution between enstatite and ferrosilite. Because all of these are orthorhombic, they are called orthopyroxenes (Opx). As noted earlier, Fe-rich Opx is not stable at low pressures; fayalite is found instead.

Along the top of the quadrilateral are the Ca-rich pyroxenes, which form a solid solution between diopside and hedenbergite. Intermediate members are called augite or ferroaugite. The incorporation of the relatively large Ca ion distorts the pyroxene lattice, hence Ca-rich pyroxenes have lower symmetry than Ca-poor pyroxenes. The Ca-rich pyroxenes are all monoclinic. In the middle of the quadrilateral is the Ca-poor clinopyroxene series, pigeonite.

To understand how the three solution series (augite, pigeonite, and orthopyroxene) are related, consider relations on a T-X slice across the quadrilateral (Figure A.7). Several features are key to understanding these minerals. One is that pigeonite is a high-temperature phase that, on cooling, inverts to a mixture of orthopyroxene and augite. The second is that at high temperatures augite and pigeonite have the same structure, in fact, if temperatures are high enough the two merge to form *sub-calcic augite*. The third is that the Ca content of pyroxene in the assemblages augite-pigeonite, pigeonite-Opx, and augite-Opx is a sensitive function of temperature. This makes quadrilateral pyroxenes important geothermometers.

The inversion of pigeonite to orthopyroxene + augite does not occur at a fixed temperature; rather it is strongly dependant on iron content of the pyroxene. For the pure Mg system, the inversion temperature is above the melting temperature of rocks, so pure Mg pigeonite is not found in nature, whereas for iron-rich pyroxenes the inversion occurs around 850°C (Figure A.8). At 800°C and three kilobars pigeonite is not stable at all and the assemblage

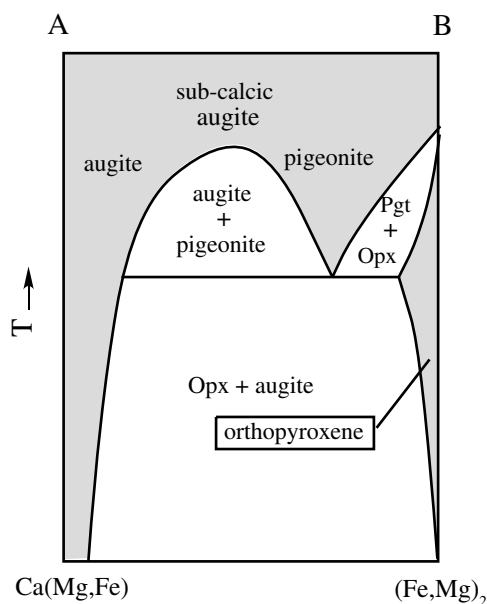


Figure A.7 Schematic T-X diagram showing the phase relations between augite, pigeonite, and orthopyroxene along section A-B in Figure A.6.

Opx-augite occurs across the pyroxene quad, except for the most iron-rich compositions where olivine + augite + quartz occur instead. Since metamorphic rocks rarely attain temperatures as high as 850°C, this means pigeonite is mostly an igneous mineral; it is absent in all but the most iron-rich, high-temperature metamorphic rocks. At 900°C and three kilobars there is a small stability field for pigeonite in iron-rich compositions. By 1,000°C the pigeonite stability field has expanded and there is a narrow composition range where pigeonite + augite react to form a single clinopyroxene, sub-calcic augite. The stability fields for both pigeonite and sub-calcic augite expand to more magnesian compositions with increasing temperature, as shown by the isothermal section at 1,100°C in Figure A.8.

In hand specimen, pyroxenes may be distinguished from amphibole (almost exclusively hornblende in igneous rocks) on the basis of cleavage (90° as opposed to 120°) and on the basis of color. Whereas hornblende always appears black on the weathered surface, in magnesium-rich rocks such as gabbros, clinopyroxene is green and orthopyroxene is brown. In more iron-rich rock, both ortho- and clinopyroxenes weather brown in color. In thin section pyroxenes are colorless with high relief and high birefringence. They have a distinct (110) cleavage that, when looking down the c-axis, intersects at approximately 90° angles. Augite is

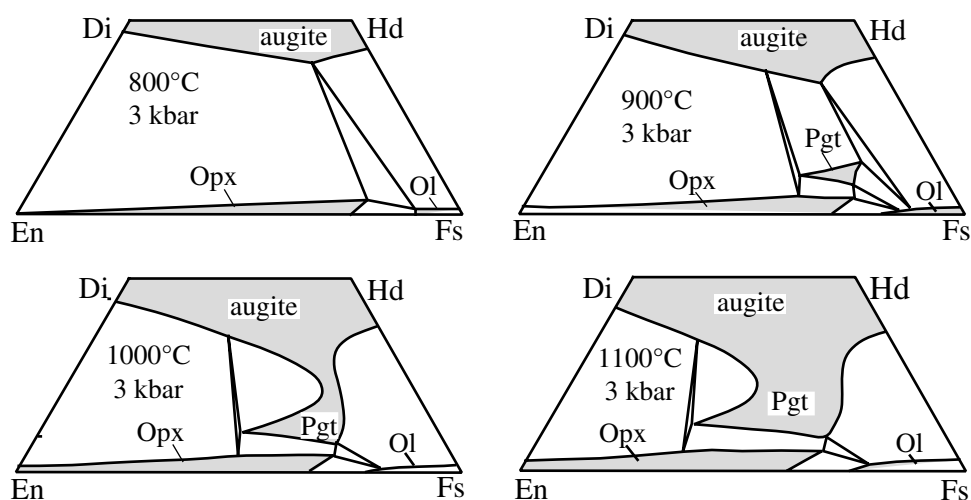


Figure A.8 Isothermal sections of the pyroxene quad at 800°, 900°, 1000°, and 1100°C showing how the pigeonite stability field expands with increasing temperature. Modified from Lindsley and Frost (1992).

monoclinic, (+) with a 2V of about 45°, and the angle between the c-axis and gamma is equal to about 45°. Pigeonite looks like augite, except it has a smaller 2V (0–36°). Both have second-order birefringence. Orthopyroxene is told from clinopyroxene by its lower birefringence (usually low first order) and parallel extinction.

Pyroxenes in quickly cooled rocks, such as volcanic or hypabyssal rocks, may retain their high-temperature compositions, but pyroxenes in plutonic rocks will change composition as the rocks cool. Usually this is accommodated by exsolution. The exsolution textures produced in this process provide important keys to the composition of the original pyroxene (Figure A.9)

For example, an orthopyroxene host with fine lamellae of augite (sometimes the lamellae are so fine that they appear only as lines in thin section) indicates that at high temperature this mineral was orthopyroxene that had incorporated only small amounts of CaO (Figure A.9A). If, however, an orthopyroxene contains abundant augite lamellae, then at high temperature this orthopyroxene incorporated a lot of CaO. Exsolution usually takes place along specific crystallographic orientations. In pyroxene the most common exsolution planes are roughly parallel to (100) or (001). Sometimes both orientations of lamellae can be seen. If, as in Figure A.9B, these orientations intersect at an angle *other* than 90°, then the exsolution took place when the mineral was a monoclinic pyroxene, rather than an orthopyroxene. In other words, this is perfect evidence that the pyroxene formed as pigeonite, exsolved augite as it cooled, and then inverted to orthopyroxene. If the exsolved pyroxene consisted of an augite host with orthopyroxene exsolution

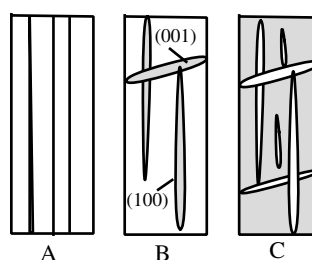
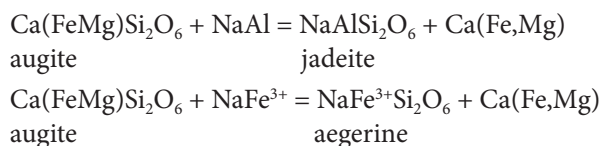


Figure A.9 Sketches of exsolution textures in pyroxenes. A. Orthopyroxene with narrow lamellae of augite. B. Orthopyroxene with wide lamellae of augite (inverted pigeonite). C. Augite host with exsolution of orthopyroxene.

(as in Figure A.9C), then the original pyroxene was augite with a certain amount of orthopyroxene dissolved in it. If the exsolution lamellae are particularly abundant, then the original pyroxene may have been a sub-calcic augite.

Sodic Pyroxenes

In addition to the quadrilateral pyroxenes, the other important pyroxene group is the sodic pyroxenes, which contain Na substituting for Ca. Since Na is univalent and Ca is divalent, this substitution must occur coupled with substitution of a trivalent ion for a divalent ion. The most common substitutions are:



The compositions of the non-quadrilateral pyroxenes can be shown on a triangular diagram (Figure A.10), in which

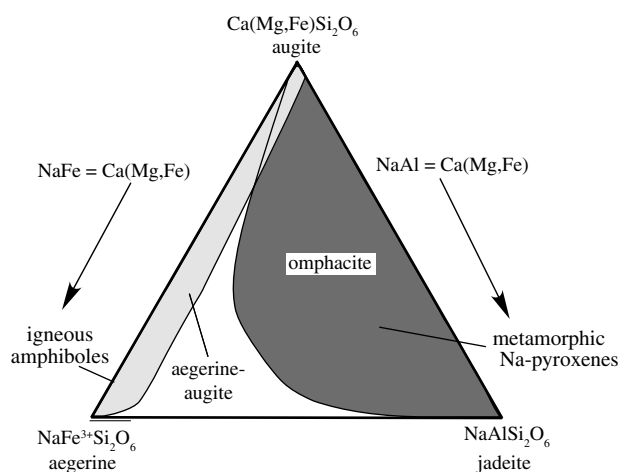
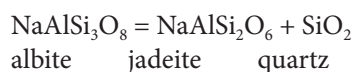


Figure A.10 Compositional range of sodic pyroxenes in igneous rocks and in metabasites. Compiled from data in Deer, Howie, and Zussman (1978).

the jadeite-aegerine solid solution is shown across the base of the triangle, and compositions with Ca, Mg, and Fe in the M2 site lie closer to the apex.

Jadeite. Jadeitic pyroxenes are restricted to high pressures. With increasing pressure, the relatively open structure of albite becomes unstable relative to the denser pyroxene structure and we get the reaction:



Pyroxenes formed at low pressure and in equilibrium with plagioclase will have relatively low jadeite component, whereas those at increasingly higher pressures will have progressively more of the jadeite component. Pyroxenes of intermediate composition between augite and jadeite are known as *omphacite*. Omphacitic pyroxenes have many properties similar to calcic pyroxenes. They have a slightly higher 2V and a pale green, non-pleochroic color. These two properties are diagnostic. Pure jadeite may be fibrous with low anomalous birefringence. It may be confused with clinozoisite, which has a higher relief.

Aegerine (or acmite). The aegerine solid solution typically occurs in igneous rocks enriched in sodium. If there is more Na in a rock than can be accommodated in feldspars, the excess Na becomes incorporated in pyroxene as the aegerine component. Compositions intermediate between augite and aegerine are known as *aegerine-augite*.

As ferric iron is added to augite the pleochroism increases from colorless in augite to deep green in aegerine. Increasing ferric iron also changes 2V and optic

sign; augite is (+) with $2V = 45^\circ$, aegerine-augite has 2V around 90° , and aegerine is (-) with 2V around $60\text{--}70^\circ$. Aegerine and aegerine-augite may occur with quartz in alkalic granites, but they are more commonly associated with nepheline.

A.3.3 Amphiboles

Amphiboles are double-chain silicates that contain OH as part of the structure. Because of this they are more stable at lower temperatures and consequently they are more common in metamorphic environments than in igneous ones. Amphiboles have the basic formula $A X_2 Y_5 Z_8 O_{22} (OH)_2$, where:

A = The “vacant” site. It is so called because it is vacant in amphiboles such as tremolite, anthophyllite, and glaucophane. It is a large eight-fold site that can accommodate Na or K.

X = This is a large six-fold site that can accommodate Ca, Fe, or Mg. Na is often found in this site in high-pressure environments.

Y = This is a small six-fold site that accommodates Fe^{2+} and Mg, and also ferric iron, Ti, and Al (such aluminum in octahedral coordination is known as Al^{IV}).

Z = tetrahedral site. This site is usually filled with Si, but at high temperatures variable amounts of Al (Al^{VI}) may also be present.

The amphiboles can be divided into three series:

- 1) *the quadrilateral amphiboles*, which consist of amphiboles containing Ca, Fe, and Mg but with only minor amounts of Al substituting for Si. They are analogous to the quadrilateral pyroxenes.
- 2) *the sodic amphiboles*, in which Na substitutes for Ca of actinolite. This series is analogous to the sodic pyroxenes.
- 3) *hornblende*, a calcic amphibole that contains significant amounts of Al in the tetrahedral site. There is no analogous mineral in the pyroxenes.

Quadrilateral Amphiboles

The quadrilateral amphiboles, like the quadrilateral pyroxenes, are composed of Ca, Fe, and Mg. They have the following end members:

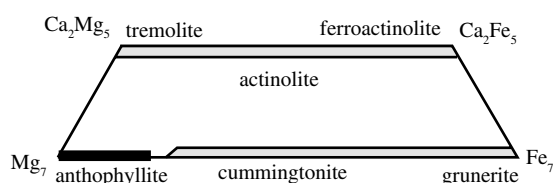


Figure A.11 Diagram showing the composition range of the quadrilateral amphiboles.

Tremolite	$\text{Ca}_2\text{Mg}_5\text{Si}_8\text{O}_{22}(\text{OH})_2$
Actinolite	$\text{Ca}_2\text{Fe}_5\text{Si}_8\text{O}_{22}(\text{OH})_2$
Anthophyllite	$\text{Mg}_7\text{Si}_8\text{O}_{22}(\text{OH})_2$
Grunerite	$\text{Fe}_7\text{Si}_8\text{O}_{22}(\text{OH})_2$

These form three solid solution series, the tremolite-actinolite series, the cummingtonite-grunerite series, and the orthoamphibole series (Figure A.11). There is only limited solid solution between the tremolite-actinolite series and the low-Ca amphiboles.

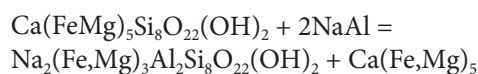
Tremolite-Actinolite series. Minerals in this series occur exclusively in metamorphic rocks. Tremolite is found in weakly to moderately metamorphosed siliceous marbles and in metaperidotites up to very high grades of metamorphism. Actinolite is found in weakly metamorphosed mafic rocks and gives way to hornblende with increasing metamorphic grade. Both tremolite and actinolite are recognized by their acicular habit. Tremolite is colorless in marbles but may be dark colored (dark green to black) in metaperidotites because the rock itself has a dark color. Actinolite is a deep green color; this causes rocks containing abundant actinolite (such as greenschists) to be colored green. Both minerals are biaxial (-) with 2V near 85° and a second-order birefringence. Both are monoclinic with a maximum extinction angle relative to the *c* crystallographic axis of 10 to 20°. Tremolite is colorless and distinguished from diopside (with which it may be associated) by its optically (-) character and its lower angle of extinction. Actinolite is pleochroic green and has a higher relief than chlorite but a lower relief than pumpellyite, two green minerals with which it might be confused.

Ca-free amphiboles. Ca-free amphiboles form two solution series, an orthorhombic and a monoclinic series. The orthorhombic series is magnesian and consists of *anthophyllite* and an aluminous anthophyllite called *gedrite*. The aluminum-poor anthophyllite is most commonly found in

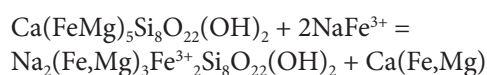
metaperidotites while *gedrite* is found in medium-grade metamorphosed pelitic rocks and in metamorphosed, hydrothermally altered, mafic rocks. The monoclinic series extends from $\text{Fe}/(\text{Fe}+\text{Mg}) = 0.4$ to $\text{Fe}/(\text{Fe}+\text{Mg}) = 1.0$. The relatively magnesian end of this series is called *cummingtonite*, whereas the iron-rich end is called *grunerite*. Cummingtonite is the only quadrilateral amphibole that may occur in igneous rocks; it is found in some dacitic tuffs. Grunerite is found mostly in metamorphosed iron formations. Anthophyllite in metaperidotites is identified by its acicular habit, although in hand sample it is impossible to distinguish it from tremolite. In other rock types, low-calcium amphibole can be identified by its acicular nature and honey-brown color. In thin section anthophyllite and *gedrite* are colorless to pale brown with high relief and high birefringence. They are the only amphiboles that have parallel extinction. Both have a high 2V; anthophyllite is biaxial (-) and *gedrite* is biaxial (+).

In hand sample cummingtonite has the same acicular habit and brownish color as *gedrite*. Grunerite in iron formations tends to be pale green and acicular. In thin section, minerals of the cummingtonite-grunerite series are colorless to pale green or brown in color. They have high birefringence and an inclined extinction similar to that of tremolite. The diagnostic character of these amphiboles is the presence of polysynthetic twins on {100}. The 2V of this series changes as a function of iron content, with the result that the relatively magnesian portion of the series (i.e., cummingtonite) is optically (+) while the iron-rich portion (grunerite) is optically (-).

Sodic amphiboles. Sodic amphiboles have two types of substitution:



tremolite-actinolite glaucophane



tremolite-actinolite riebeckite

As was true of the NaAl-bearing pyroxenes, the NaAl amphibole, glaucophane, is restricted to metamorphic rocks. The NaFe^{3+} amphiboles are important minerals in sodic rocks.

Glaucophane-crossite series. Sodic amphiboles are diagnostic of low temperature and high-pressure

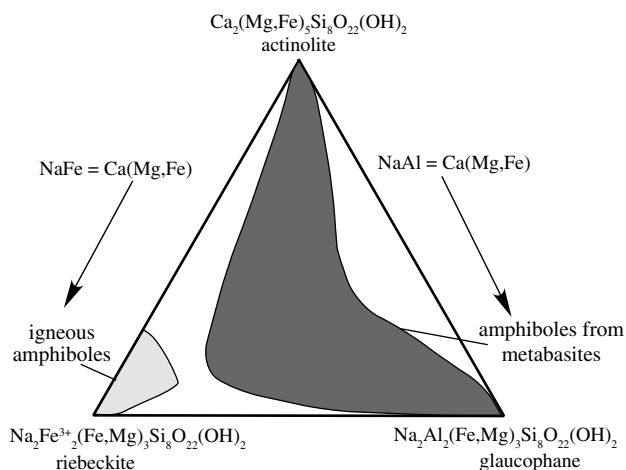


Figure A.12 Diagram showing the composition range of sodic amphiboles in igneous and metamorphosed mafic rocks. Fields defined by data from Brown (1974) and Deer, Howie, and Zussman (1997).

metamorphism, where a complete solid solution series from actinolite to glaucophane may be stable. Minerals intermediate in this series are called *crossite* (Figure A.12). They are found most commonly in mafic rocks, but may also occur in metapelitic rocks and more rarely in metamorphosed impure carbonates. With increasing pressure the stable amphibole in mafic rocks is first actinolite, then crossite, and finally glaucophane.

The distinctive blue color of sodic amphiboles makes them easy to identify both in hand sample and in thin section. No other minerals have the amphibole habit and the blue-lavender-purple pleochroism of the sodic amphiboles. Because of its lower ferric iron content glaucophane generally has a less intense pleochroism than does crossite.

Riebeckite. Riebeckite is most easily identified in thin section by its intense blue or purple pleochroism. In some rocks the color is so intense that only on the thin edges of grains can one see that the grain is translucent and not opaque. Riebeckite is most common in alkaline rocks, where it is commonly associated with aegirine. It is also found in some weakly metamorphosed iron formations. In highly sodic rocks a substitution of NaFe^{2+} for Fe^{3+} in riebeckite produces *arfvedsonite* $\text{NaNa}_2(\text{Fe,Mg})_4\text{Fe}^{3+}\text{Si}_8\text{O}_{22}(\text{OH})_2$. There is a complete solid solution between riebeckite and arfvedsonite and they are optically very similar. Therefore we may consider both part of a riebeckite family.

Hornblende

Hornblende is an amphibole that has one to two atoms of Al substituting for silica; rarely does a hornblende have more than two atoms of Al in the tetrahedral site. Substitution of trivalent Al for tetravalent Si produces a charge imbalance that can be satisfied through the substitution of Na (or K) in the A site or Al for (Fe,Mg). The two simplest exchange operations involve:

- 1) $\text{Si} = \text{NaAl}$ or (NaAlSi_{-1}) . In this substitution Al substitutes for Si in the tetrahedral site while Na moves into the vacant site. The resulting amphibole is called *edenite* with the formula $\text{NaCa}_2(\text{Fe,Mg})_5\text{Si}_7\text{AlO}_{22}(\text{OH})_2$.
- 2) $\text{Al}_2 = (\text{Fe,Mg})\text{Si}$ or $(\text{Al}_2(\text{Fe,Mg})_{-1}\text{Si}_{+1})$. In this substitution the charge imbalance produced by substituting Al for Si is accommodated by substituting Al for divalent Fe or Mg. The resulting mineral end member (*tschermakite*) has the formula: $\text{Ca}_2(\text{Fe,Mg})_4\text{AlSi}_7\text{AlO}_{22}(\text{OH})_2$.
- 3) A combination of these two substitutions leads to the *pargasite* end member, $\text{NaCa}_2(\text{Fe,Mg})_4\text{AlSi}_6\text{Al}_2\text{O}_{22}(\text{OH})_2$.

Tschermakite is a hypothetical end member since there are no amphiboles known that do not have Na or K in the A site. However, a plot of the number of Al and Na+K atoms per formula unit of amphibole can accommodate the composition of almost all natural amphiboles (Figure A.13). The substitution of Al for Si in the tetrahedral site is an important thermometer because it reflects increasing temperature of formation.

The substitution of Al into the tetrahedral site of amphibole requires a second, coupled substitution. Of the many possibilities, the most important optically are the substitution of Ti and Fe^{3+} for octahedral Al. Both of these elements have a strong coloring effect, thus as Ti and ferric iron increase in a hornblende the color becomes more intense. This tends to make hornblende black rather than green in hand sample. In thin section, low-temperature hornblende tends to have green pleochroism, whereas high temperature hornblende tends to be intensely colored in brown or red. Sodic hornblende, wherein Na has substituted for some of the Ca, has been found in some alkaline rocks. It is identified as a hornblende with a touch of blue to its pleochroism.

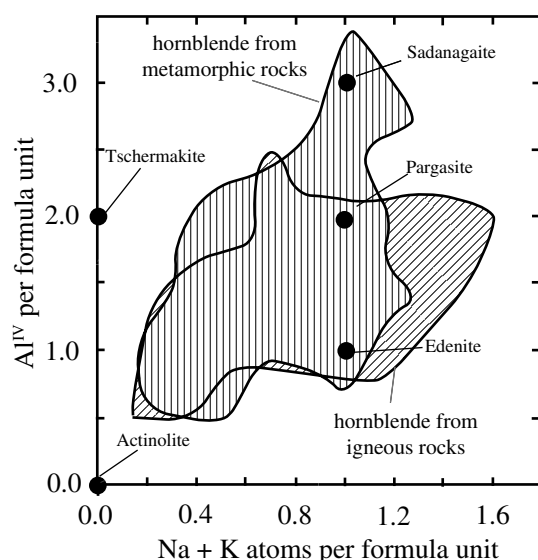


Figure A.13 Diagram showing the compositional range of hornblende from igneous and metamorphic rocks. Fields defined by data from Deer, Howie, and Zussman (1997).

A.3.4 Phyllosilicates

Like amphiboles, phyllosilicates contain considerable water. As a result they are most stable at lower temperatures and are more common in metamorphic rocks than in igneous rocks. They can occur in metamorphic rocks of all compositions and are important indicators of metamorphic grade.

Serpentine

Although commonly referred to as a single mineral, serpentine is actually a complex mineral group involving the phases *chrysotile*, *lizardite*, and *antigorite*. Chrysotile and lizardite have compositions approaching the ideal formula of $\text{Mg}_3\text{Si}_2\text{O}_5(\text{OH})_4$ although lizardite may contain a small amount of aluminum. Antigorite has a distinctly more siliceous composition, which can be modeled by the formula $\text{Mg}_{48}\text{Si}_{34}\text{O}_{85}(\text{OH})_{62}$. The serpentine minerals are the hydration products of peridotites. Chrysotile and lizardite, the low-temperature forms of serpentine, are formed at temperatures ranging from those of surface conditions to those of low-grade metamorphism. Antigorite, being somewhat less hydrous than the other two serpentine minerals, is a mineral of medium-grade metamorphism.

Serpentine is pale green and waxy in hand sample. It is colorless to pale green in thin section, has

low birefringence (1° gray) and is generally very fine grained. Generally it is impossible to obtain optic figures on serpentine. The only mineral with which serpentine can be confused is chlorite. However, the chlorite that occurs in metaperidotites is length fast while serpentine is length slow. Although it is impossible to distinguish between the three serpentine types with certainty without the use of X-ray diffraction, one can often make a fairly good guess at the serpentine type from their microscopic textures. Antigorite, being the high-temperature form, generally has a fairly strongly developed micaceous habit, whereas chrysotile is markedly fibrous. Lizardite may assume a range of habits from nearly isotropic aggregates to moderately coarse-grained sheets. Usually, however, it doesn't have the tabular, interlocking habit of antigorite.

Greenalite

Greenalite is an iron analog of serpentine that occurs in weakly metamorphosed iron formations. It forms green to brown, fine-grained aggregates that commonly preserve sedimentary textures. The grains are so small that they may look isotropic under crossed-nicols. The only mineral that looks similar to greenalite is glauconite, which has similar habit of occurrence but is distinguished by its high birefringence.

Talc

Talc is usually very close to the end member composition $\text{Mg}_3\text{Si}_4\text{O}_{10}(\text{OH})_2$. Small amounts of ferrous iron may be present, but most talc contains 90 percent or more of the Mg end member. Talc is a common mineral in metamorphosed peridotites. It is found less commonly in metamorphosed impure dolomites and is also a diagnostic mineral for the rare high-pressure metapelitic rock known as whiteschist.

Talc is easily distinguished in hand sample because of its soapy feel. It is also possible to determine if talc is present in small concentrations in a rock by feeling the head of the hammer after hitting the rock. If the head feels soapy, talc is present. In thin section talc is a colorless mica with high (3°) birefringence. It may be mistaken for muscovite or phlogopite, but it has a higher birefringence than either. Muscovite usually has a higher 2V and, except in the most magnesian environments, phlogopite has a pale pleochroism.

Minnesotaite

Minnesotaite is an iron analog of talc that forms in metamorphosed iron formations. It is optically similar to talc, although it is usually very fine grained and may have faint yellow pleochroism. Its association with iron formations is diagnostic. The only other fibrous mineral in iron formations is grunerite, which, unlike minnesotaite, does not have parallel extinction.

Chlorite

Although it does not have the same structure as serpentine, the simplest way to think of the composition of chlorite is as a mineral with a serpentine base $(\text{Mg,Fe})_6\text{Si}_4\text{O}_{10}(\text{OH})_8$ that has a certain amount of Al substituting for Si and (Mg,Fe). The amount of aluminum substitution is variable, so it is difficult to write a simple formula for this mineral, but most chlorites have compositions near that of clinocllore $(\text{Mg,Fe})_5\text{Al}(\text{Si}_3\text{Al})\text{O}_{10}(\text{OH})_8$. Chlorite is a widespread mineral in low-grade rocks, where it can be found in serpentinites, metamorphosed pelitic rocks, mafic rocks, and impure dolomitic limestones. The stability of chlorite shrinks with increasing metamorphic grade, but in rocks of appropriate composition, specifically metaperidotites and magnesian metapelitic schists, chlorite may survive to upper amphibolite grades.

Chlorite is green and micaceous in hand sample. Unlike serpentine, which is extremely fine grained, individual grains of chlorite are commonly recognizable in hand sample. In thin section it is told by its micaceous habit, colorless to green pleochroism, and low birefringence. The birefringence is commonly anomalous, with blue and brown appearing in place of first-order gray. The only minerals chlorite is likely to be confused with are serpentine and green biotite. The chlorite found in serpentinites is length fast whereas coexisting serpentine is length slow. Chlorite is distinguished from green biotite by its low and anomalous birefringence.

Micas

Micas are phyllosilicates that contain alkali ions, usually K^+ , more rarely Na^+ and Ca^{2+} , between the silicate sheets. The extra charge from the alkalis is accommodated by substitution of Al for Si in the tetrahedral site. The interlayer alkali ions stabilize the phyllosilicate structure to higher temperature, with the result that some micas, including biotite and muscovite, are stable in igneous rocks.

Biotite. The biotite series is made up of the end members *phlogopite* $\text{KMg}_3\text{AlSi}_3\text{O}_{10}(\text{OH})_2$ and *annite* $\text{KFe}_3\text{AlSi}_3\text{O}_{10}(\text{OH})_2$. In addition to a Fe-Mg substitution, there is substitution of Al and Ti for Fe and Mg in the octahedral sites. Phlogopite is optically distinct from the rest of the biotite series and, therefore, it is often categorized as a separate mineral from the more iron-rich biotites. This is not true for annite, which looks like any other iron-bearing biotite.

Biotite is identified by its micaceous habit, brown, red-brown, or, rarely, green pleochroism, and high birefringence. Green biotite might be confused with chlorite, from which it is distinguished by high birefringence. Phlogopite has similar properties to those of biotite except that it is weakly colored in thin section. Very magnesian phlogopite may be totally colorless, but most samples of phlogopite have pale tan pleochroism. There is, of course, complete gradation between the optical properties of phlogopite and those of biotite, but the convention is that one vibration direction in phlogopite is colorless whereas in biotite it is pale brown or pale green. Phlogopite is told from muscovite by its small 2V (near 0) and from talc by lower birefringence.

Phlogopite, being a magnesian biotite, is restricted to Mg-rich rocks, such as metaperidotites and impure dolomitic limestones. The rest of the biotite series is widespread in occurrence. Biotite is a dominant mineral in metapelitic schists but it is also found in metamorphic mafic rocks (metabasites) and in quartzofeldspathic gneisses. Biotite is stable over a wide range of metamorphic grades and in most rock types it can survive to the highest temperatures of metamorphism. It is also found in a wide variety of igneous rocks, where it may be stabilized by high Ti and F contents.

Muscovite. Muscovite has the general formula $\text{KAl}_2(\text{AlSi}_3\text{O}_{10})(\text{OH})_2$. High-T muscovite may have compositions close to this model formula, but muscovite from low-temperature metamorphic rocks commonly deviates significantly from this composition. In many metamorphic rocks, particularly those formed at low pressures or low temperatures, there are more than three silicon atoms per formula unit. This substitution of Si for Al in the tetrahedral site is accommodated by substitution of Fe and Mg for Al in the octahedral site. Such an iron and magnesium-bearing muscovite is known as *phengite*. Muscovite is common in metapelitic rocks and in other metamorphic

rocks derived from sediments that contained significant amounts of clay. It occurs over a wide range of metamorphic grades but breaks down to K-feldspar at the higher grades by the reaction:



muscovite K-feldspar melt fluid

Muscovite is not as widespread in igneous rocks as biotite because, as indicated by the reaction above, it only forms in rocks that have more Al_2O_3 than is necessary to make feldspars. Most granitic rocks are not that aluminous and thus contain biotite but lack muscovite.

Muscovite is identified in hand sample by its lack of color. In thin section it is colorless with high birefringence and a 2V (-) of 30–45°. Phengite is a muscovite with a small 2V. Muscovite is distinguished from phlogopite by a higher 2V and from talc by a lower birefringence.

Paragonite. Paragonite $\text{NaAl}_2(\text{AlSi}_3\text{O}_{10})(\text{OH})_2$ is a sodium mica that may occur in weakly metamorphosed pelitic rocks or in low-temperature, high pressure metamorphosed basalts. Paragonite has the same optical properties as muscovite and can be rarely distinguished optically. It is usually safe to assume that the major white mica in a low-grade rock is muscovite, but X-ray methods are required to distinguish whether small amounts of paragonite are also present.

A.4 Aluminum-excess Minerals

Aluminum excess minerals are found in rocks where $\text{Al} > \text{Na} + \text{K} + 2\text{Ca}$ (in moles). Another way of saying this is that there is more aluminum than required to make feldspars. Such a situation is characteristic of metapelitic rocks, where Na and Ca have been removed by weathering but may also be found in other rock types subjected to hydrothermal alteration.

A.4.1 Aluminosilicates (Andalusite, Kyanite, and Sillimanite)

The aluminosilicates have the formula Al_2SiO_5 and are quite pure, with only minor substitution by Fe^{3+} and Mn^{3+} . The stability fields of these minerals are related by a phase diagram (Figure A.14), with andalusite the low-pressure polymorph, kyanite stable at high pressures, and sillimanite stable at high temperatures. The triple point, at which all three phases are stable, is at approximately 4.5 kilobars and 550°C (Pattison, 1992).

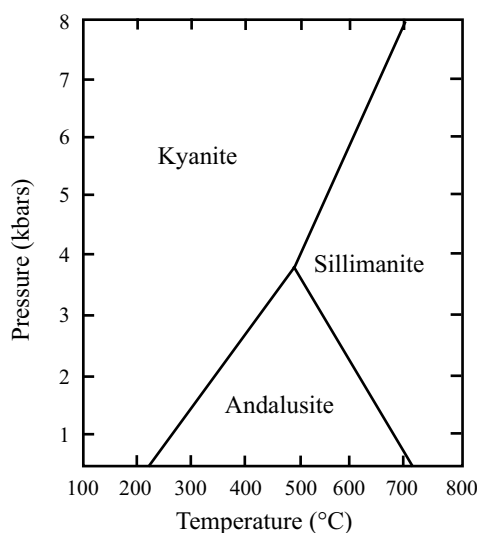


Figure A.14 Phase diagram showing the P-T stabilities of the aluminosilicate minerals. Data from Pattison (1992).

Andalusite

Andalusite typically forms tabular orthorhombic porphyroblasts that may be colorless, pale pink, or, rarely, pale green in hand sample. A common diagnostic feature is an accumulation of carbonaceous matter on the edges of the nearly square cross-section. This leads a cross-section that looks like a cross; a mineral known as *chiastolite*. In thin section the mineral has low birefringence, medium relief, and high 2V (-). Andalusite is distinguished from sillimanite by lower birefringence and a general tabular morphology. In andalusite, cleavage is either weak or missing. Rarely andalusite shows pale pink pleochroism that may be zoned.

Sillimanite

Sillimanite is typically seen in hand sample as fine, white, fibrous mats called fibrolite. Its optical properties include orthorhombic crystal form, 2° birefringence, high relief, and low 2V(+). In the lowest-grade metamorphic rocks in which it is stable, sillimanite forms fine-grained fibrous mats and individual crystals cannot be distinguished even in thin section. These fibrous mats are length slow and are distinctive because nothing similar occurs in metapelitic schists. At higher grades sillimanite may be coarser, but is usually more acicular than either andalusite or kyanite. It is told from both by higher birefringence, a distinctive cross-section when looking down the c axis, and low 2V.

Kyanite

In hand sample, kyanite is identified by its tabular shape. It is often white in color, but it commonly has touches of blue (hence its name); indeed gem-quality kyanite is deep blue. Kyanite is triclinic and is distinctive because it has two hardnesses. Parallel to the *c*-axis it has a hardness of five, and normal to the *c*-axis it is seven. Thus a knife will scratch kyanite parallel to the *c* axis but not normal to it. Optical properties include high relief, middle first-order birefringence, and high 2V(-). Kyanite is distinctive because it has the highest relief of any of the aluminosilicates and is the only one with inclined extinction. Caution is warranted, however, because in some orientations the extinction angle is only 2°. It also has a perfect (100) cleavage with a strong (001) parting. When present, the parting will distinguish it from andalusite and sillimanite.

A.4.2 Garnets

Garnets have the general formula $A_3B_2Si_3O_{12}$ where A = +2 ion and B = +3 ion. There are two major series of rock-forming garnets:

1. *Aluminum garnets* with various divalent ions in the A site. The major end members are:

A site	B site	
Mg	Al	pyrope
Fe	Al	almandine
Mn	Al	spessartine

This series is often referred to as *pyralspite* garnets.

2. *Calcic garnets* with various trivalent ions in the B site. Major end members are:

A site	B site	
Ca	Al	grossular
Ca	Fe ³⁺	andradite

This series is often referred to as *grandite* garnets.

In upper and middle crustal environments, the grandite and pyralspite garnets have two distinct types of occurrence. Pyralspites are found in metapelitic schists and, at higher pressures, in metabasites. Pyrope is not stable at low pressures. In olivine-bearing rocks, the assemblage enstatite + spinel occurs instead, and in quartz-bearing rocks,

the assemblage cordierite + enstatite replaces pyrope. Grandites occur in metamorphosed and metasomatized marbles. The stability of garnet is strongly expanded by an increase in pressure to the extent that in lower crustal rocks and under mantle conditions there is a complete solid solution between grandites and pyralspites. Garnets from high-pressure environments will contain considerable amounts of Ca, Mg, and Fe.

Pyralspite garnets are recognized as equant red crystals that are commonly porphyritic and that may reach sizes on the order of centimeters. Grandite garnets are commonly xenoblastic and may range in color from colorless or pale yellow to black. In thin section garnets are isotropic with very high relief ($n = 1.7$ to 1.9). Calcic garnets may have anomalous low first-order birefringence. Pyralspite garnets are usually pale pink in transmitted light, while grandites can vary from colorless (for Al-rich varieties) to deep orange (for Fe³⁺-rich varieties).

A.4.3 Staurolite

Staurolite has the formula $(FeMg)_2Al_5Si_4O_{22}(OH)_2$, with iron usually more abundant than magnesium. The most important minor element in staurolite is ZnO, which may be present in abundances up to several weight percent. Staurolite is a relatively high-pressure mineral. It is more commonly found associated with kyanite than with andalusite. Staurolite is identified as tabular brown crystals that may form phenocrysts up to centimeters in size. In thin section, staurolite has high relief and low first-order birefringence. Staurolite is easily identified by its distinctive yellow pleochroism. It is usually poikiloblastic.

A.4.4 Cordierite

Cordierite is a cyclosilicate with the composition $(Mg,Fe)_2Al_4Si_5O_{18}$. Magnesium is generally more abundant than iron. Although the formula does not include water, cordierite almost invariably contains small amounts of H₂O and more rarely CO₂ and SO₂ in the broad channels defined by the rings of silica tetrahedra. Because of its open structure, cordierite is a large-volume mineral favored by low pressure. It is a common mineral in contact metamorphic environments and is also found in low-pressure regional metamorphic terranes. Cordierite is found with andalusite and sillimanite but only very rarely with kyanite. It is characteristically a medium- to high-

temperature mineral and also is found in some granites and rhyolites.

In low-grade occurrences cordierite may form anhedral porphyroblasts that produce a knotty appearance to the rock. Such rocks are commonly known as spotted schists or spotted hornfels. In higher-grade rocks, cordierite occurs as a matrix-forming mineral. Gem-quality cordierite is deep blue in color with no cleavage, a greasy luster, and a conchoidal fracture; it looks very much like quartz. A cordierite-rich rock is identified by its greasy luster and bluish color on a fractured surface. In thin section cordierite looks very much like feldspar. It is biaxial (either (+) or (-)), has low relief (either positive or negative) and gray birefringence. It may be impossible to distinguish from orthoclase and untwinned plagioclase. Cordierite from high-grade rocks may be twinned. When these twins are triangular-shaped, like slices of a pie, they are diagnostic. Cordierite is easily altered. Thus the presence of a pale yellow, non-pleochroic chlorite along grain boundaries or fractures is diagnostic of cordierite. Another distinguishing feature of cordierite is the presence of yellow pleochroic halos around uranium-bearing inclusions such as zircon or monazite. These are a reflection of oxidation of iron in the cordierite due to radiation damage from uranium decay. Since feldspars and quartz do not contain iron, zircons included in these minerals do not show pleochroic halos.

A.4.5 Chloritoid

Chloritoid is a tabular mineral with the formula $(\text{Fe,Mg})_2\text{Al}_4\text{Si}_2\text{O}_{10}(\text{OH})_4$. Iron is generally more abundant than magnesium. Chloritoid is common in low-grade metapelites. In iron-rich rocks it may be the first porphyroblastic phase to appear with prograde metamorphism. Its stability extends into medium grades of metamorphism; rarely it is found with sillimanite. Similarly, its stability seems to expand with pressure, since it is found rather widely in high-pressure terranes and does not occur at all in contact metamorphic environments. In hand sample chloritoid is recognized as a tabular green-to-gray porphyroblast with brittle fracture. In thin section its optical properties are distinctive. It has a green-to-gray pleochroism and low, frequently anomalous birefringence. It is commonly twinned normal to the c-axis. It is told from chlorite by higher relief and twinning.

A.5 Ca-Al Silicates

Under many conditions of metamorphism the calcic plagioclase, anorthite, is not stable and another Ca-Al silicate occurs instead. For weakly metamorphosed mafic rocks the identity of the Ca-Al mineral is an important indicator of metamorphic grade.

A.5.1 Clinozoisite-Epidote

Zoisite and clinozoisite have the formula $\text{Ca}_2\text{Al}_3(\text{SiO}_4)_3(\text{OH})$. Epidote is a variant of this mineral in which up to a third of the aluminum is replaced by ferric iron. Epidote is the major “anorthite substitute” mineral in metamorphic rocks. It occurs in a wide variety of protoliths at a wide range of metamorphic grades. Its stability increases with pressure to the extent that epidote is a stable igneous mineral at pressures of around ten kilobars. The iron-poor varieties are found dominantly in metamorphosed or metasomatized carbonate rocks.

Zoisite and clinozoisite are white to pink in hand sample, while epidote is a distinctive yellow-green. The color is reminiscent of that of pistachio nuts, hence the name pistachite that is often given to epidote. In thin section the minerals have high relief ($n = 1.70 - 1.78$) and anomalous birefringence (blue in place of first-order gray). Other properties are dependent on Fe content. Clinozoisite is (+) with $2V = 14-90^\circ$. It is colorless with low 1° birefringence. Epidote is (-) with $2V = 64-89^\circ$. It has colorless to yellow pleochroism and up to 2° birefringence. It is the change from optically positive to optically negative character that marks the boundary between clinozoisite and epidote.

A.5.2 Prehnite

Prehnite has the formula $\text{Ca}_2\text{Al}_2\text{Si}_3\text{O}_{10}(\text{OH})_2$ with up to half the aluminum replaced by ferric iron. Prehnite is diagnostic of very low-grade metamorphism. It is found most frequently in weakly metamorphosed basalts, commonly as an amygdale filling. It occurs more rarely as cement in sandstones.

In hand specimen prehnite is white to green in color and, if massive, may show a botryoidal surface. When it is an amygdale filling, prehnite shows a distinctive radiating crystal shape. In thin section it is colorless with high relief and high birefringence. It is optically (+) with a high $2V$ (although low $2V$ varieties are known). It is distinguished

from epidote, with which it may occur, by lower relief and lack of pleochroism.

A.5.3 Pumpellyite

Pumpellyite has the formula $\text{Ca}_2(\text{Mg,Fe})\text{Al}_2\text{Si}_3\text{O}_{11}(\text{OH})_2 \cdot \text{H}_2\text{O}$. There is a wide range of substitution of ferrous iron for magnesium and ferric iron for aluminum. Like prehnite, pumpellyite is found in very low-grade metamorphic rocks. The stability of pumpellyite seems to be favored by increasing pressure, for unlike prehnite, pumpellyite is sometimes found coexisting with sodic amphiboles.

In hand sample pumpellyite is recognized by its needle-like habit and dark green color. Its optical properties include high relief, biaxial (+) with 2V ranging from 10° to 85° , and anomalous first- to second-order birefringence. In most occurrences pumpellyite has a deep green pleochroism, but very Mg-rich pumpellyite may be colorless to pale yellow and difficult to distinguish from epidote. It is distinguished from chlorite by higher relief and generally deeper pleochroism.

A.5.4 Lawsonite

Lawsonite has the formula $\text{CaAl}_2\text{Si}_2\text{O}_7(\text{OH})_2 \cdot \text{H}_2\text{O}$ and in most rocks it shows little chemical variability. It is a high-pressure, low-temperature mineral that commonly occurs with sodic amphiboles. Lawsonite is orthorhombic, biaxial (+) with a high 2V and moderate to high first-order birefringence. Lamellar twinning on {101} is common. Lawsonite is distinguished from zoisite and clinozoisite by its higher birefringence and lack of anomalous birefringence.

A.5.5 Laumontite

Laumontite ($\text{CaAl}_2\text{Si}_4\text{O}_{12} \cdot 4\text{H}_2\text{O}$) is one of many zeolites. Zeolites form a complex mineral group that is stable at very low temperatures, in the range of diagenesis and the lowest temperatures of metamorphism. Because it is the most stable at high temperatures and elevated pressures, laumontite is the zeolite most likely to be encountered in metamorphic rocks. Laumontite is found both as amygdulites and veins in weakly metamorphosed basalts (where it is studied by metamorphic petrologists) and also as cement in sandstones (where it is studied by sedimentary petrologists).

In thin section laumontite is colorless with low negative relief and low first-order birefringence. It is biaxial

(-) with a small to moderate 2V. It is found with other low-temperature Ca-Al silicates (prehnite, pumpellyite, and epidote). Its negative relief and occurrence is distinctive.

A.6 Oxide, Sulfide, and other Nominally Opaque Phases

A.6.1 Fe-Ti Oxides (Magnetite and Ilmenite)

Most igneous rocks contain one or both of the most common Fe-Ti oxides, *magnetite* and *ilmenite*. Both of these minerals are complex solid solutions that have a wide range of stability. Magnetite is a spinel mineral with the formula $\text{Fe}^{2+}\text{Fe}^{3+}_2\text{O}_4$. It commonly is found to be nearly pure, but at high temperatures it forms the end member of a mineral series that shows complete solid solution with ulvöspinel (Fe_2TiO_4). Ilmenite has the formula FeTiO_3 and at high temperatures it has complete solid solution with hematite (Fe_2O_3). In most igneous and metamorphic rocks the ferrous-ferric iron ratio in these minerals monitors the fugacity (partial pressure) of oxygen in the rocks.

Magnetite can be distinguished from ilmenite because it is magnetic. If the grains are large enough, ilmenite can be recognized by its perfect (001) cleavage. Since both magnetite and ilmenite are opaque phases, they are difficult to distinguish in thin section. Ilmenite may have a platy morphology and magnetite may form octahedra, but in many samples the grains are intergrown and show no distinct crystal form.

A.6.2 Other Spinel Minerals

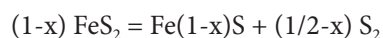
Chromite ($(\text{Fe,Mg})\text{Cr}_2\text{O}_4$) is common in ultramafic to basaltic rocks. In hand sample it is identified as a black mineral that is frequently octahedral and is non-magnetic. In thin section it is isotropic, brown to nearly black in color. It is commonly the first mineral to crystallize in basalts and often found as inclusions in olivine.

Green spinel ($(\text{Fe,Mg})\text{Al}_2\text{O}_4$) is absent from quartz-bearing rocks because green spinel + quartz = cordierite (unless it is stabilized by considerable Zn). It is commonly found intergrown with magnetite gabbros, in which it has exsolved out of magnetite during cooling. It is also found as a metamorphic mineral in partially melted metapelitic rocks, in gabbroic rocks that have undergone high-

pressure and high-temperature metamorphism, and in impure, dolomitic marbles (in these rocks the spinel may be pale to colorless).

A.6.3 Fe Sulfides

Pyrite (FeS_2) and pyrrhotite ($\text{Fe}_{(1-x)}\text{S}$) may occur in minor amounts in many igneous and metamorphic rocks. Just as the Fe-Ti oxides monitor oxygen fugacity in rocks, the Fe sulfides monitor the sulfur fugacity. With increasing temperature, or at low sulfur fugacities, pyrite breaks down to pyrrhotite by the reaction:



This relationship indicates that, whereas pyrite may be stable in some relatively low-temperature rocks such as granites, pyrrhotite is the only sulfide found in high-temperature rocks such as basalt and gabbro.

Because they are opaque phases, pyrite and pyrrhotite cannot be distinguished from each other (or from oxides) in thin section. If an opaque phase in a thin section is large enough, sometimes it can be identified as a sulfide by examining the thin section with a hand lens and looking for light reflecting off the surface of the section.

A.6.4 Graphite

Graphite is an important constituent phase in many metamorphic rocks, where it forms by thermal decomposition of organic matter. In igneous rocks, where it is found only rarely, it forms by abiotic processes. A good way to determine whether a rock contains graphite is to hit the rock with a hammer and rub the hammerhead on your hand. Dark streaks on your hand will indicate the presence of graphite, even if only a small amount is present in the rock. Graphite can sometimes be distinguished in thin section as tabular flakes that have a “ragged” shape.

A.6.5 Rutile

Rutile (TiO_2) is a common oxide mineral in metapelitic rocks and metabasites. Rutile also is the major titanium-bearing mineral in eclogites. In addition, it is commonly found as a detrital mineral in sandstones. In hand sample, it is typically reddish brown with adamantine luster and forms acicular and prismatic crystals. In thin section it is identified by its uniaxial (+) character and high birefringence (though this can be masked by the strong color of the mineral).

A.7 Accessory Minerals

Accessory minerals are minerals present in low abundance in most igneous rocks. The most important of these are zircon, sphene, apatite, and monazite. These minerals can be geochronometers because they contain minor amounts of uranium. They are rarely visible in hand specimen, but are found in most igneous and metamorphic rocks.

A.7.1 Zircon

Zircon (ZrSiO_4) is an important mineral because it is one of the few that can accommodate zirconium. Thus zircon crystallizes out late in the evolution of many igneous rocks, and as it does, it incorporates uranium from the melt. As a result zircon is one of the most important minerals for geochronology. Although it occurs in most rock types, it is rarely seen in hand sample because of its low abundance. In thin section zircon is tetragonal with high relief and high birefringence. It is uniaxial (+), but rarely do you find grains large enough to give an interference figure. A diagnostic feature of zircon is that as the U or Th it contains decays, it causes radiation damage to adjacent crystals. The radiation tends to oxidize the iron in surrounding ferromagnesian silicates. Thus most zircon grains included in biotite or hornblende are surrounded by dark pleochroic haloes showing the extent of radiation damage.

A.7.2 Sphene (or Titanite)

Although ilmenite (FeTiO_3) is the major Ti-bearing mineral in most igneous rock, sphene (CaTiSiO_5) is common in many plutonic rocks of intermediate composition (diorites, granodiorites, and some granites). It is also found in many metamorphic rocks. In hand sample, sphene is identified as small red to yellow grains with a distinct lozenge shape. In thin section it is recognized by its high relief and extreme birefringence. It has a birefringence similar to that of calcite, but unlike calcite, the relief doesn't vary on rotation. Sphene can accommodate small amounts of uranium and is an important mineral for dating both igneous and metamorphic rocks.

A.7.3 Apatite

Apatite ($\text{Ca}_5(\text{PO}_4)_3(\text{F},\text{OH},\text{Cl})$) is one of the few minerals that can accommodate phosphorous. As a result it is

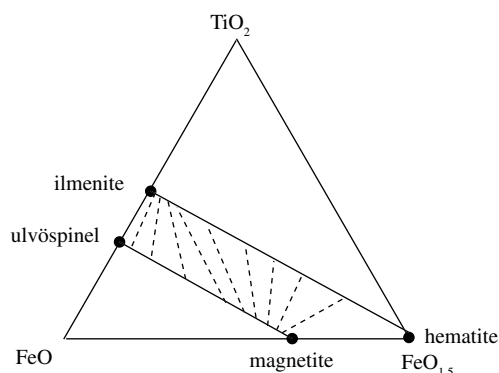


Figure A.15 Diagram showing the composition relations between the ilmenite and magnetite solid solutions at magmatic temperatures. Dashed tie lines show the approximate compositions of coexisting phases. Modified after Lindsley (1991).

present in small quantities in almost every igneous rock. Apatite is uniaxial (-) and forms small rods that have low 1° birefringence (usually gray) and moderate relief. When looking down the c-axis, apatite forms small hexagonal grains that appear isotropic. Apatite can accommodate uranium but diffusion is fast enough in apatite that it has relatively low closure temperature, which means that any age obtained from U-Pb dating of apatite will give the time the rock cooled through that temperature, instead of the time the rock formed.

Summary

The major minerals in igneous rocks are relatively few, and include quartz, feldspars, nepheline, olivine, pyroxenes, amphibole (mainly hornblende), and micas. Because igneous differentiation enriches the melt in H_2O , in Na over Ca, and in Fe over Mg, there is a consistent change in mineralogy and mineral composition during differentiation. This change is summarized by Bowen's reaction series (Figure A.16). Although it is an oversimplification, Bowen's reaction series gives a first-order description of how the mineralogy of the crystallizing assemblage changes during the evolution of igneous magmas. The ferromagnesian side of the series consists of olivine, pyroxene, and, if the rock is hydrous, hornblende and biotite. The feldspar side of the series consists of plagioclase that initially is calcic and becomes progressively enriched in sodium. At some point in the differentiation history K-feldspar joins plagioclase in the crystallization history, and quartz is one of the last minerals to begin crystallizing.

Metamorphic minerals tend to be far more complex than igneous minerals. However there are two simple rules for the stability of metamorphic minerals:

1. Dense minerals, such as garnet, are favored at high pressure.
2. The more hydrous a mineral is, the lower its likely temperature of stability.

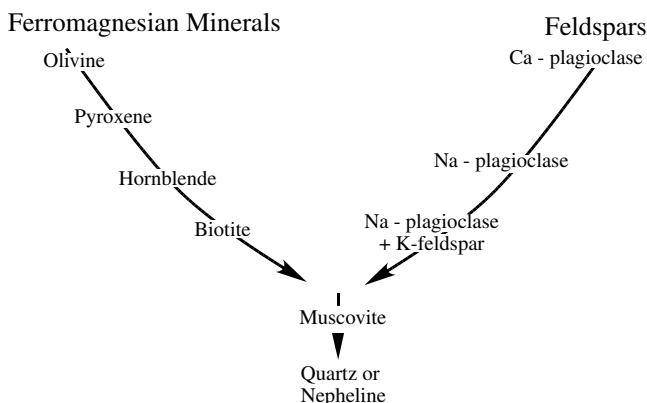


Figure A.16 Bowen's reaction series showing the minerals that will crystallize during differentiation of a basaltic magma.

A.7.4 Monazite

Monazite ($CePO_4$) is a phosphate mineral that is rarer than apatite, but is relatively common in metapelite schists and in some granitic rocks. It is an important mineral for dating metamorphic rocks. Monazite is rarely seen in hand sample, but in thin section it forms small tabular grains that are distinctly yellow and have a pleochroic halo. Monazite is distinguished from zircon by its yellow color, but if the grains are fine enough, it may be difficult to tell whether a given pleochroic halo surrounds zircon or monazite.

References

- Albee, A. L., 1965, A petrogenetic grid for the Fe-Mg silicates of pelitic schists. *American Journal of Science*, 263, 512–36.
- Amelin, Y., Li, C., Valeev, O., and Naldrett, A. J., 2000, Nd-Pb-Sr isotope systematics of crustal assimilation in the Voisey's bay and Mushuau Intrusions, Labrador, Canada. *Economic Geology*, 95, 815–30.
- Andersen, S. G., Bohse, H., and Steenfelt, A., 1981, A geological section through the southern part of the Ilimaussaq intrusion. Rapport. *Grønlands Geologiske Undersøgelse*, 103, 39–42.
- Anderson, I. C., Frost, C. D., and Frost, B. R., 2003, Petrogenesis of the Red Mountain pluton, Laramie anorthosite complex, Wyoming: Implications for the origin of A-type granites. *Precambrian Research*, 124, 243–67.
- Anonymous, 1972, Penrose Field Conference on ophiolites. *Geotimes*, 17, 24–25.
- Arai, S., 1975, Contact metamorphosed dunite-harzburgite complex in the Chugoku District, western Japan. *Contributions to Mineralogy and Petrology*, 52, 1–16.
- Archibald, N. J., Bettenay, L. F., Binns, R. A., Groves, D. I., and Gunthorpe, R. J., 1978, The evolution of Archaean greenstone terrains, Eastern Goldfields Province, Western Australia. *Precambrian Research*, 6, 103–31.
- Arnaud, N. O., Vidal, P., Tapponnier, P., Matte, P., Deng, W. M., 1992, The high K₂O volcanism of northwestern Tibet: Geochemistry and tectonic implications. *Earth and Planetary Science Letters*, 111, 351–67.
- Ashwal, L. D., 1993, *Anorthosites*. Springer-Verlag, New York.
- Atherton, M. P. and Ghani, A. A., 2002, Slab breakoff: A model for Caledonian, Late Granite syn-collisional magmatism in the orthotectonic (metamorphic) zone of Scotland and Donegal, Ireland. *Lithos*, 62, 65–85.
- Atkins, F. B., 1969, Pyroxenes of the Bushveld Intrusion, South Africa. *Journal of Petrology*, 10, 222–49.
- Bailey, J. C., Gwozdz, R., Rose-Hanses, J., and Sørensen, H., 2001, Geochemical overview of the Ilimaussaq alkaline complex, South Greenland. *Geology of Greenland Survey Bulletin*, 190, 35–53.
- Baksi, A. K., 2010, Comment to “Distribution and geochronology of the Oregon Plateau (USA) flood basalt volcanism: The Steens Basalt Revisited” by M. E. Brueseke et al. *Journal of Volcanology and Geothermal Research*, 196, 134–38.
- Barberi, F., Ferrara, G., Santacrocis, R., Treuil, M., and Varet, J., 1975, A transitional basalt – pantellerite sequence of fractional crystallization, the Boina centre (Afar Rift, Ethiopia). *Journal of Petrology*, 16, 22–56.
- Barker, F., Wones, D. R., Sharp, W. N., and Desborough, G. A., 1975, The Pikes Peak batholith, Colorado Front Range, and a model for the origin of gabbro-anorthosite-syenite-potassic granite suite. *Precambrian Research*, 2, 97–160.
- Barrow, G., 1893, On an intrusion of muscovite-biotite gneiss in the southeastern highlands of Scotland, and its accompanying metamorphism. *Geological Society of London Quarterly Journal*, 49, 330–58.
- Barrow, G., 1912, On the geology of Lower Dee-side and the southern highland border. *Proceedings of the Geologists' Association*, 23 (5), 274–90.
- Barry, T. L., Self, S., Kelley, S. P., Reidel, S., Hooper, P., and Widdowson, M., 2010, New ⁴⁰Ar/³⁹Ar dating of the Grande Ronde lavas, Columbia River Basalts, USA: Implications for duration of flood basalt eruption episodes. *Lithos*, 118, 213–22.
- Basaltic Volcanism Study Project, 1981, *Basaltic volcanism on the terrestrial planets*. Pergamon Press, Inc., New York.
- Bateman, P. C. and Chappell, B. W., 1979, Crystallization, fractionation, and solidification of the Tuolumne intrusive series, Yosemite National Park, California. *Geological Society of America Bulletin* 90, 465–82.
- Batiza, R., 1982, Abundances, distribution and sizes of volcanoes in the Pacific Ocean and implications for the origin of non-hot spot volcanoes. *Earth and Planetary Science Letters*, 60, 195–206.
- Beard, J. S. and Day, H. W., 1988, Petrology and emplacement of reversely zoned gabbro-diorite plutons in the Smartville complex, northern California. *Journal of Petrology*, 29, 965–95.
- Berger, A., Schmid, S. M., Engi, M., Bosquet, R., and Wiederker, M., 2011, Mechanisms of mass and heat transport during Barrovian metamorphism: A discussion based on field evidence from the Central Alps (Switzerland/northern Italy). *Tectonics*, 30, TC1007, doi 10.1029/2009TC002622, 2011.
- Berman, R. G., 1988, Internally-consistent thermodynamic data for minerals in the system Na₂O-K₂O-CaO-MgO-FeO-Fe₂O₃-Al₂O₃-SiO₂-TiO₂-H₂O-CO₂. *Journal of Petrology* 29, 445–522.
- Berman, R. G., 1991, Thermobarometry using multi-equilibrium calculations: A new technique, with petrological applications. *Canadian Mineralogist*, 29, 833–55.

- Bhaskar Rao, Y. J., Chetty, T. R. K., Janardhan, A. S., and Gopalan, K., 1996, Sm-Nd and Rb-Sr ages and P-T history of the Archean Sittampundi and Bhavani layered meta-anorthosite complexes in Cauvery shear zone, South India: Evidence for Neoproterozoic reworking of Archean crust. *Contributions to Mineralogy and Petrology*, 125, 237–50.
- Bianchini, G., Beccaluva, L., and Siena, F., 2008, Post-collisional and intraplate Cenozoic volcanism in the rifted Apennines/Adriatic domain. *Lithos*, 101, 125–40.
- Bingen, B., Davis, W. J., and Austrheim, H., 2001, Zircon U-Pb geochronology in the Bergen arc eclogites and their Proterozoic protoliths, and implications for the pre-Scandian evolution of the Caledonides in western Norway. *Geological Society of America Bulletin*, 113, 640–49.
- Binns, R. A., Gunthorpe, R. J., and Groves, D. I., 1976, *Metamorphic patterns and development of greenstone belts in eastern Yilgarn Block, Western Australia*. John Wiley & Sons, New York.
- Bird, P., 1979, Continental delamination and the Colorado Plateau. *Journal of Geophysical Research*, 84, 7561–71.
- Blackman, D. K., Ildefonse, B., John, B. E., Ohara, Y., Miller, D. J., Abe, N., Abratis, M., Andal, E. S., Andreani, M., Awaji, S., Beard, J. S., Brunelli, D., Charney, A., Chirstie, D. M., Collins, J., Delacour, A. G., Delius, H., Drouin, M., Einaudi, F., Escartin, J., Frost, B. R., and thirty-two others, 2011, Drilling constraints on lithospheric accretion and evolution at Atlantis Massif, Mid-Atlantic Ridge 30°N. *Journal of Geophysical Research*, 116, B07103, doi 10.1029/2010JB007931.
- Boria, E. and Conticelli, S., 2007, Mineralogy and petrology of associated Mg-rich ultrapotassic, shoshonitic, and calc-alkaline rocks: The Middle Latin valley, monogenetic volcanos, Roman Magmatic Province, Southern Italy. *Canadian Mineralogist*, 45, 1443–69.
- Boudier, F. and Nicolas, A., 2011, Axial melt lenses at oceanic ridges – A case study in the Oman ophiolite. *Earth and Planetary Science Letters*, 304, 313–25.
- Bowen, N. L., 1913, The melting phenomena of the plagioclase feldspars. *American Journal of Science*, 4th ser. 35, 577–99.
- Bowen, N. L., 1915, The crystallization of haplobasaltic, haplodioritic, and related magmas. *American Journal of Science* 4th ser. 40, 161–85.
- Bowen, N. L., 1940, Progressive metamorphism of siliceous limestone and dolomite. *Journal of Geology*, 48, 225–74.
- Bowen, N. L., 1945, Phase equilibria bearing on the origin and differentiation of alkaline rocks. *American Journal of Science*, 243A, 75–89.
- Bowen, N. L. and Andersen, O., 1914, The binary system MgO-SiO₂. *American Journal of Science* 37, 487–500.
- Bowen, N. L. and Schairer, J. F., 1935, The system MgO-FeO-SiO₂. *American Journal of Science* 5th ser. 29, 151–217.
- Brotzu, P., Morbidelli, L., and Piccirillo, E. M., 1983, The basanite to peralkaline phonolite suite of the Pilo-quaternary Nyambeni multicenter volcanic range (East Kenya Plateau). *Neues Jahrbuch fur Mineralogy, Abhandlungen*, 147, 253–80.
- Brown, E. H., 1974, Comparison of the mineralogy and phase relations of blueschists from the North Cascades, Washington, and greenschists from Otago, New Zealand. *Geological Society of America Bulletin*, 85, 333–44.
- Brown, G. C. and Fyfe, W. S., 1970, The production of granitic melts during ultrametamorphism. *Contributions to Mineralogy and Petrology*, 28, 310–18.
- Brown, G. C. and Mussett, A. E., 1981, *The inaccessible earth*. Allen and Unwin, London.
- Brown, G. M., Holland, J. G., Sigurdsson, H., Tomblin, J. F., and Arculus, R. J., 1977, Geochemistry of the Lesser Antilles volcanic island arc. *Geochimica et Cosmochimica Acta*, 41, 785–801.
- Brueseke, M. E., Heizler, M. T., Hart, W. K., and Mertzman, S. A., 2007, Distribution and geochronology of the Oregon Plateau (USA) flood basalt volcanism: The Steens Basalt Revisited. *Journal of Volcanology and Geothermal Research*, 161, 187–214.
- Bryan, S. E., Riley, T. R., Jerram, D. A., Stephens, C. J. and Leat, P. T., 2002, Silicic volcanism: An undervalued component of large igneous provinces and volcanic rifted margins. In *Volcanic Rifted Margins, Geological Society of America Special Paper* 362, eds. M. A. Menzies, S. L. Klemperer, C. J. Ebinger, and J. Baker, pp. 97–118.
- Bryant, B., McGrew, L. S., and Wobus, R. A., 1981, Geologic map of the Denver 1° by 2° quadrangle, north-central Colorado. United States Geologic Survey Miscellaneous Investigations Map I-1163, scale 1:250,000.
- Buchan, K. L., Goutier, J., Hamilton, M. A., Ernst, R. E., and Matthews, W. A., 2007, Paleomagnetism, U-Pb geochronology, and geochemistry of Lac Esprit and other dyke swarms, James Bay area, Quebec and implications for Paleoproterozoic deformation of the Superior Province. *Canadian Journal of Earth Sciences*, 44, 643–64.
- Bucher, K. and Grapes, R., 2009, The eclogite-facies Allalin Gabbro of the Zermatt-Saas ophiolite, Western Alps: A record of subduction zone hydration. *Journal of Petrology*, 50, 1405–42.

- Burnham, C. W., 1979, The importance of volatile constituents. In *The Evolution of Igneous Rocks, 50th anniversary perspectives*. Princeton University Press, Princeton, NJ, 439–82.
- Burnham, C. W., Holloway, J. R., and Davis, N. F., 1969, Thermodynamic properties of water to 1,000°C and 10,000 bars. *Geological Society of America Special Paper* 132.
- Camp, V. E., 1995, Mid-Miocene propagation of the Yellowstone mantle plume head beneath the Columbia River basalt source region. *Geology*, 23, 435–38.
- Capitani, G. and Mellini, M., 2004, The modulated crystal structure of antigorite: The m=17 polysome, *American Mineralogist*, 89, 147–58.
- Carmichael, D. M., 1978, Metamorphic bathozones and bathograds: A measure of the depth of post-metamorphic uplift and erosion on the regional scale. *American Journal of Science*, 278, 769–97.
- Carmichael, I. S. E., 1964, The petrology of Thingmuli, a Tertiary volcano in eastern Iceland. *Journal of Petrology*, 5, 435–60.
- Cawthorn, R. G., Ellam, R. M., Ashwal, L. D., and Webb, S. J., 2012, A clinopyroxenite intrusion from the Plianesberg Alkaline Province, South Africa, *Precambrian Research*, 198–99, 25–36.
- Chappell, B. W. and White, A. J. R., 1974, Two contrasting granite types. *Pacific Geology*, 8, 173–74.
- Charlier, B., Duchesne, J. C., Vander Auwera, J., Storme, J.-Y., Marquill, R., and Longhi, J., 2010, Polybaric fractional crystallization of high-alumina basalt parental magmas in the Egersund-Ogna Massif-type anorthosite (Rogalandm, SW Norway) constrained by plagioclase and high-alumina orthopyroxene megacrysts. *Journal of Petrology*, 51, 2515–46.
- Chidester, A. H., 1962, Petrology and geochemistry of selected talc-bearing ultramafic rocks and adjacent country rocks in north-central Vermont. *U.S. Geological Survey Professional Paper*, P345.
- Chopin, C., 1981, Talc-phengite: A widespread assemblage in high-grade pelitic blueschists of the Western Alps. *Journal of Petrology*, 22, 628–50.
- Chopin, C., 1984, Coesite and pure pyrope in high-grade blueschists of the Western Alps – A 1st record and some consequences. *Contributions to Mineralogy and Petrology*, 86, 107–18.
- Christiansen, E. and McCurry, M., 2007, Contrasting origins of Cenozoic silicic volcanic rocks from the western Cordillera of the United States. *Bulletin of Volcanology*, 70, 251–67.
- Christiansen, R. L., Lowenstern, J. B., Smith, R. B., Heasler, H., Morgan, L. A., Nathenson, M., Mastin, L. G., Muffler, P., and Robinson, J. E., 2007, Preliminary assessment of volcanic and hydrothermal hazards in Yellowstone National Park and vicinity. *U.S. Geological Survey Open-file Report* 2007–1071.
- Christiansen, R. L. and Peterson, D. W., 1981, Chronology of the 1980 eruptive activity. In *The 1980 eruptions of Mount St. Helens, Washington*, eds. P. W. Lipman and D. R. Mullineaux. *USGS Professional Paper* 1250, 17–30.
- Clarke, D. B., 1992, *Granitoid rocks*. Chapman and Hall, London.
- Cochran, J. R., 2008, Seamount volcanism along the Gakkel Ridge, Arctic Ocean. *Geophysical Journal International*, 174, 1153–73.
- Coffin, M. F. and Eldholm, O., 1992, Volcanism and continental break-up; a global compilation of large igneous provinces. In *Magmatism and causes of continental break-up*. *Geological Society Special Publications*, 68, 17–30.
- Colchen, M., LeFort, P., and Pecher, A., 1980, *Carte geologique Annapurna-Manaslu-Ganesh, Himalaya du Nepal 1/200.000*. Centre National de la Recherche Scientifique, Paris.
- Collerson, K. D. and Fryer, B. J., 1978, The role of fluids in the formation and subsequent development of early continental crust. *Contributions to Mineralogy and Petrology*, 67, 151–67.
- Compston, W., Williams, I. S., and Meyer, C., 1984, U-Pb geochronology of zircons from Lunar Breccia 73217 using a Sensitive High Mass-Resolution Ion Microprobe. Proceedings of the Fourteenth Lunar and Planetary Science Conference, Part 2. *Journal of Geophysical Research*, pp. B525–B534.
- Coombs, D. S., 1954, The nature and alteration of some Triassic sediments from Southland, New Zealand. *Transactions of the Royal Society of New Zealand*, 82, 65–109.
- Coombs, D. S., 1960, Lawsonite metagraywackes in New Zealand. *American Mineralogist*, 45, 454–55.
- Coombs, D. S., Nakamura, Y., and Vuagnat, M., 1976, Pumpellyite-actinolite facies schists of the Taveyanne Formation near Loeche, Valais, Switzerland. *Journal of Petrology*, 17, 440–71.
- Corliss, J. B., Dymond, J., Gordon, L. I., Edmond, J. M., Von Herzen, R. P., Ballard, R. D., Green, K., Williams, D., Bainbridge, A., Crane, K., and Van Andel, T. H., 1979, Submarine thermal springs on the Galapagos Rift. *Science*, 203, 1073–83.

- Corticelli, S., D'Antonio, M., Pinarelli, L., and Civetta, L., 2002, Source contamination and melt heterogeneity in the genesis of Italian potassic and ultrapotassic volcanic rocks: Sr-Nd-Pb isotope data from Roman Province and southern Tuscany. *Mineralogy and Petrology*, 74, 189–222.
- Cox, K. G., 1980, A model for flood basalt volcanism. *Journal of Petrology*, 21, 629–50.
- Cox, K. G., Bell, J. D., and Pankhurst, R. J., 1979, *The interpretation of igneous rocks*. George Allen and Unwin, London.
- Crisp, J. A., 1983, Rates of magma emplacement and volcanic output. *Journal of Volcanology and Geothermal Research*, 20, 177–211.
- Cross, W., Iddings, J. P., Pirsson, L. W., and Washington, H. S., 1902, A quantitative chemicominalogical classification and nomenclature of igneous rocks. *Journal of Geology*, 10, 555–690.
- Danckwerth, P. A. and Newton, R. C., 1978, Experimental determination of the spinel peridotites to garnet peridotites reaction in the system $\text{MgO-Al}_2\text{O}_3\text{-SiO}_2$ in the range of 900°–1100°C and Al_2O_3 isopleths of enstatite in the spinel field. *Contributions to Mineralogy*
- Dawson, J. B., 1967, A review of the geology of kimberlite. In *Ultramafic and related rocks*, ed. P. J. Wyllie. John Wiley & Sons, New York, pp. 241–51.
- Dawson, J. B. and Smith, J. V., 1988, Metasomatised and veined upper-mantle xenoliths from Pello Hill, Tanzania: Evidence for anomalously-light mantle beneath the Tanzanian sector of the East African Rift Valley. *Contributions to Mineralogy and Petrology*, 100, 510–27.
- Deer, W. A., Howie, R. A., and Zussman, J., 1963, *Rock-Forming Minerals. Volume 4, Framework silicates*. John Wiley & Sons, New York.
- Deer, W. A., Howie, R. A., and Zussman, J., 1978, *Rock-Forming Minerals. Volume 2A, Single-Chain silicates*, 2nd Ed. John Wiley & Sons, New York.
- Deer, W. A., Howie, R. A., and Zussman, J., 1997, *Rock-Forming Minerals. Volume 2B, Double-Chain silicates*, 2nd ed. The Geological Society, London.
- De Paoli, M. C., Clarke, G. L., and Daczko, N. R., 2012, Mineral equilibrium modeling of the granulite-eclogite transition: Effects of whole-rock composition on metamorphic facies type-assemblages. *Journal of Petrology*, 53, 949–70.
- Dick, H. J. B., Natland, J. H., Alt, J. C., Bach, W., Bideau, D., Gee, J. S., Haggas, S., Hertogen, J. G. H., Hirth, G., Holm, P. M., Ildefonse, B., Iturrino, G. J., John, B. E., Kelley, D. S., Kikawa, E., Kingdon, A., LeRoux, P. J., Maeda, J., Meyer, P. S., Miller, D. J., Naslund, H. R., Niu, Y.-L., Robinson, P. T., Snow, J., Stephen, R. A., Trimby, P. W., Worm, H.-U., and Yoshinobu, A., 2000, A long in situ section of the lower ocean crust: Results of ODP, *Earth and Planetary Science Letters*, 179, 31–51.
- DiRenzo, V., Di Vito, M. A., Arienzo, I., Carandente, A., Civetta, L., D'Antonio, Giordano, F., Orsi, G., and Tonarini, S., 2007, Magmatic history of Somma-Vesuvius on the basis of new geochemical and isotopic data from a deep borehole (Camalodoli della Torre). *Journal of Petrology*, 48, 753–84.
- Dobson, D. P., Meredith, P. G., and Boon S. A., 2002, Simulation of subduction zone seismicity by dehydration of serpentine. *Science*, 298, 1407–10.
- Duke, J. M., 1988, Magmatic segregation deposits of chromite. In *Ore Deposit Models, Geoscience Canada Reprint series 3*, eds. R. G. Roberts and P. A. Sheanhan, pp. 133–43.
- Dyment, J., Arkani-Hamed, J., and Ghods, A., 1997, Contribution of serpentinized ultramafics to marine magnetic anomalies at slow and intermediate spreading centres: Insights from the shape of the anomalies. *Geophysics Journal International*, 129, 691–701.
- Dzurisin, D., Koyanagi, R. Y., and English, T. T., 1984, Magma supply and storage at Kilauea volcano, Hawaii, 1956–1983. *Journal of Volcanology and Geothermal Research*, 21, 177–206.
- Eby, G. N., 1985, Montereian Hills II. Petrography, major and trace element geochemistry and strontium isotopic chemistry of the eastern intrusions: Mounts Shefford, Brome, and Megantic. *Journal of Petrology*, 26, 418–48.
- Elthon, D., 1989, Pressure of origin of primary mid-ocean ridge basalts. In *Magmatism in the Ocean Basins*, eds. A. D. Saunders and M. J. Norry. *Geological Society Special Publications*, 42, 125–36.
- England, P. C. and Thompson, A. B., 1984, Pressure-temperature-time paths of regional metamorphism I. Heat transfer during the evolution of regions of thickened continental crust. *Journal of Petrology*, 25, 894–928.
- Eskola, P., 1915, On the relations between the chemical and mineralogical composition in the metamorphic rocks of the Orijärvi region. *Bulletin de la Commission géologique de Finlande*, 44, 1–107; English summary 109–45.
- Eskola, P., 1920, The mineral facies of rocks. *Norsk Geologisk Tidsskrift*, Bd 6, 143–94.

- Evans, B. W., 1977, Metamorphism of alpine peridotite and serpentinite. *Annual Reviews of Earth and Planetary Sciences*, 5, 397–447.
- Evans, B. W., 1990, Phase relations of epidote-blueschists. *Lithos*, 25, 3–23.
- Evans, B. W. and Brown, E. H., 1987, Blueschists and eclogites, *Geological Society of America Memoir*, 164.
- Faggart, B. E., Jr. and Basu, A. R., 1985, Origin of the Sudbury Complex by meteoritic impact: Neodymium isotopic evidence. *Science*, 230, 436–39.
- Faure, G., 1986, *Principles of isotope geology*, 2nd ed. John Wiley & Sons, New York.
- Ferguson, J., 1964, Geology of the Ilimaussaq alkaline intrusion, south Greenland. *Bulletin Grølands Geologiske Undersøgelse*, 39.
- Ferry, J. M. and Spear, F. S., 1978, Experimental calibration of the partitioning of Fe and Mg between biotite and garnet. *Contributions to Mineralogy and Petrology*, 66, 113–17.
- Fisher, R. V., 1966, Rocks composed of volcanic fragments. *Earth-Science Reviews*, 1, 287–98.
- Fodor, R. V., Frey, F. A., Bauer, G. R., and Clague, D. A., 1992, Ages, rare-earth element enrichment, and petrogenesis of tholeiitic and alkali basalts from Kahoolawe Island, Hawaii. *Contributions to Mineralogy and Petrology*, 110, 442–62.
- Forsyth, D. W., 1977, The evolution of the upper mantle beneath mid-ocean ridges. *Tectonophysics*, 38, 89–118.
- Frey, F. A. and Clague, D. A., 1983, Geochemistry of diverse basalt types from Loihi Seamount, Hawaii: Petrographic implications. *Earth and Planetary Science Letters*, 66, 337–55.
- Frey, M., Hunziker, J. C., Frank, W., Bocquer, J., Dal Piaz, G. V., and Niggli, E., 1974, Alpine metamorphism of the Alps, a review. *Schweizerische Mineralogische und Petrographische Mitteilungen*, 54, 247–90.
- Frost, B. R., 1975, Contact metamorphism of serpentinite, chloritic blackwall, and rodingite at Paddy-Go-Easy Pass, Central Cascades, Washington. *Journal of Petrology*, 16, 272–313.
- Frost, B. R., 1976, Limits to the assemblage forsterite-anorthite as inferred from peridotite hornfels, Icicle Creek, Washington. *American Mineralogist*, 61, 732–50.
- Frost, B. R., 1980, Observations on the boundary between zeolite facies and prehnite-pumpellyite facies. *Contributions to Mineralogy and Petrology*, 73, 365–73.
- Frost, B. R., Arculus, R. J., Barnes, C. G., Collins, W. J., Ellis, D. J., and Frost, C. D., 2001, A geochemical classification of granitic rock suites. *Journal of Petrology*, 42, 2033–48.
- Frost, B. R. and Beard, J. S., 2007, On silica activity and serpentinization, *Journal of Petrology*, 48, 1351–68.
- Frost, B. R. and Chacko, T., 1989, The granulite uncertainty principle: Limitations on thermobarometry in granulites. *Journal of Geology*, 97, 435–50.
- Frost, B. R. and Frost, C. D., 1987, CO₂, melts, and granulite metamorphism. *Nature*, 327, 503–506.
- Frost, B. R. and Frost, C. D., 2008, A geochemical classification for feldspathic rocks. *Journal of Petrology*, 49 (11), 1955–69.
- Frost, B. R. and Lindsley, D. H., 1992, Equilibria among Fe-Ti oxides, pyroxenes, olivine and quartz. 2. Applications. *American Mineralogist*, 77, 1004–20.
- Frost, B. R. and Touret, J. L. R., 1989, Magmatic CO₂ and saline melts from the Sybille Monzosyenite, Laramie anorthosite complex, Wyoming. *Contributions to Mineralogy and Petrology*, 103, 178–86.
- Frost, C. D. and Frost, B. R., 1997, Reduced rapakivi-type granites: The tholeiite connection. *Geology*, 25, 647–50.
- Frost, C. D. and Frost, B. R., 2011, On ferroan (A-type) granites: Their compositional variability and modes of origin. *Journal of Petrology*, 52, 39–53.
- Frost, C. D., Frost, B. R., Chamberlain, K. R., and Edwards, B. R., 1999, Petrogenesis of the 1.43 Ga Sherman batholith, SE Wyoming: a reduced, rapakivi-type anorogenic granite. *Journal of Petrology*, 40, 1771–802.
- Frost, C. D., Frost, B. R., Chamberlain, K. R., and Hulsebosch, T. P., 1998, The Late Archean history of the Wyoming Province as recorded by granitic magmatism in the Wind River Range, Wyoming. *Precambrian Research*, 89, 145–73.
- Frost, C. D., Frost, B. R., Lindsley, D. H., Chamberlain, K. R., Swapp, S. M., and Scoates, J. S., 2010, Geochemical and isotopic evolution of the anorthositic plutons of the Laramie anorthosite complex: Explanations for variations in silica activity and oxygen fugacity of massif anorthosites. *Canadian Mineralogist*, 48, 925–46.
- Frost, C. D. and O’Nions, R. K., 1985, Caledonian magma genesis and crustal recycling. *Journal of Petrology*, 26, 515–44.
- Frost, C. D. and Snoke, A. W., 1989, Tobago, West Indies, a fragment of a Mesozoic oceanic island arc: Petrochemical evidence. *Journal of the Geological Society of London*, 146, 953–64.
- Gill, R., 2010, *Igneous rocks and processes: A practical guide*. Wiley-Blackwell, Oxford.
- Goldsmith, J. R. and Heard, H. C., 1961, Subsolidus phase relations in the system CaCO₃ – MgCO₃. *Journal of Geology*, 69, 45–74.

- Grant, J. A., 1985, Phase equilibria in low-pressure partial melting of polytic rocks. *American Journal of Science*, 285, 409–35.
- Gray, J. R. and Yardley, B. W. D., 1979, A Caledonian blueschist from the Irish Dalradian, *Nature*, 278, 736–37.
- Green, D. H. and Ringwood, A. E., 1969, The origin of basalt magmas. In *The Earth's crust and upper mantle*, *Geophysical Monograph*, pp. 489–95.
- Green, D. H. and Ringwood, A. E., 1972, A comparison of recent experimental data on the gabbro-garnet granulite-eclogite transition. *Journal of Geology*, 80, 277–88.
- Green, J. C. and Fitz, T. J. III, 1993, Extensive felsic lavas and rheognimbrites in the Keweenaw Midcontinent Rift plateau volcanics, Minnesota: Petrographic and field recognition. *Journal of Volcanology and Geothermal Research*, 54, 177–96.
- Greenwood, H. J., 1967, Wollastonite: Stability in H₂O-CO₂ mixtures and occurrence in a contact-metamorphic Aureole near Salmo, British Columbia, Canada. *American Mineralogist*, 52, 1769–80.
- Grove, T. L., Baker, M. B., Price, R. C., Parman, S. W., Elkins-Tanton, L.T., Chatterjee, N., and Müntener, O., 2005, Magnesian andesite and dacite lavas from Mt. Shasta, northern California: Products of fractional crystallization of H₂O-rich mantle melts. *Contributions to Mineralogy and Petrology*, 148, 542–65.
- Grove, T. L. and Bryan, W. B., 1983, Fractionation of pyroxene-phyric MORB at low pressure; an experimental study. *Contributions to Mineralogy and Petrology*, 84, 293–309.
- Grubenmann, U. and Niggli, P., 1924, *Die Gesteinsmetamorphose*, 3rd and revised edition of *Die Kristallinen schiefer*, I. Allgemeiner Teil. Gebrüder Borntraeger, Berlin, 368–413.
- Halliday, A. N., Fallick, A. E., Dickin, A. P., Mackenzie, A. B., Stephens, W. E., and Hildreth, W., 1983, The isotopic and chemical evolution of Mount St. Helens. *Earth and Planetary Science Letters*, 63, 241–56.
- Harker, A., 1909, *The natural history of igneous rocks*. Macmillan, New York.
- Harley, S. L., 1998, On the occurrence and characterization of ultrahigh-temperature crustal metamorphism. *Geological Society London Special Publication* 138, 81–107.
- Harpp, K. S., Wirth, K. R., and Korich, D. J., 2002, Northern Galapagos Province: Hotspot-induced, near-ridge volcanism at Genovesa Island. *Geology*, 30, 399–402.
- Hawkins, J. and Melchior, J., 1983, Petrology of basalts from Loihi Seamount, Hawaii. *Earth and Planetary Science Letters*, 66, 356–68.
- Heinrich, E. W., 1965, *Microscopic identification of minerals*. McGraw-Hill, New York.
- Hekinian, R., 1982, *Petrology of the ocean floor*. Elsevier, Amsterdam.
- Helmold, K. P. and Van de Kamp, P. C., 1984, Diagenetic mineralogy and controls on albitization and laumontite formation in Paleogene arkoses, Santa Ynez Mountains, California. In *Clastic Diagenesis*. *American Association of Petroleum Geologists Memoir* 37, eds. D. A. McDonald and R. C. Surdam, pp. 239–76.
- Hess, P. C., 1989, *Origins of igneous rocks*. Harvard University Press, Cambridge, MA.
- Hildreth, E. W., 1979, The Bishop Tuff: Evidence for the origin of compositional zonation in silicic magma chambers. In *Ash-flow tuffs*. *Geological Society of America Special Paper* 180, eds. C. E. Chapin and W. E. Elston, pp. 43–76.
- Hildreth, E. W., Halliday, A. N., and Christiansen, R. L., 1991, Isotopic and chemical evidence concerning the genesis and contamination of basaltic and rhyolitic magma beneath the Yellowstone Plateau volcanic field. *Journal of Petrology*, 32, 63–137.
- Himmelberg, G. R. and Ford, A. B., 1976, Pyroxenes of the Dufek Intrusion. *Journal of Petrology*, 17, 219–43.
- Holdaway, M. J., 1971, Stability of andalusite and the aluminum silicate phase diagram. *American Journal of Science*, 271, 97–131.
- Hooper, P. R., 2000, Chemical discrimination of Columbia River basalt flows. *Geochemistry, Geophysics, Geosystems*, 1, doi: 10.1029/2000GC000040.
- Hooper, P. R., Camp, V. E., Reidel, S. P., and Ross, M. E., 2007, *The origin of the Columbia River flood basalt province: Plume versus non plume models*. *Geological Society of America Special Paper* 470, 635–68.
- Hooper, P. R. and Swanson, D. A., 1990, The Columbia River Basalt Group and associated volcanic rocks of the Blue Mountains province. In *Geology of the Blue Mountains region of Oregon, Idaho, and Washington: Cenozoic geology of the Blue Mountains region*. *USGS Professional Paper* 1437, 63–99.
- Hooper, P. R. and Hawkesworth, C. J., 1993, Isotopic and geochemical constraints on the origin and evolution of the Columbia River basalt, *Journal of Petrology*, 34, 1203–46.
- Hopson, C. A., 2008, Geologic map of Mount St. Helens, prior to the 1980 eruption. *United States Geological Survey Open-File Report* 2002–468.
- Hutchinson, R. M., 1976, Granite-tectonics of Pikes Peak batholith. *Professional Contributions of the Colorado School of Mines*, 8, 32–43.

- Irvine, T. N., 1974, Petrology of the Duke Island ultramafic complex, Southeastern Alaska. *Geological Society of America Memoir* 138.
- Irvine, T. N. and Baragar, W. R. A., 1971, A guide to the classification of the common volcanic rocks. *Canadian Journal of Earth Sciences*, 8, 523–48.
- Irwin, W. P. and Coleman, R. G., 1974, Ophiolites and ancient continental margins. In *The geology of continental margins*, eds. C. A. Burk and C. L. Drake. Springer-Verlag, New York, pp. 921–31.
- Ishihara, S., 1977, The magnetite-series and ilmenite-series granitic rocks. *Mining Geology*, 27, 293–305.
- Johnson, R. W., Mackenzie, D. E., and Smith, I. E. M., 1978, Volcanic rock associations at convergent plate boundaries: Re-appraisal of the concept using case histories from Papua New Guinea. *Geological Society of America Bulletin*, 89, 96–106.
- Jolly, W. T., 1978, Metamorphic history of the Archean Abitibi Belt, *Geological Survey of Canada Paper* 78–10, 63–78. *Journal of Petrology*, 52, 2047–78.
- Kamimura, A., Kasahara, J., Shinohara, M., Hino, R., Shiobara, H., Gujie, G., and Kanazawa, T., 2002, Crustal structure study at the Izu-Bonin Subduction zone around 31°N: Implications of serpentinized materials along the subduction plate boundary. *Physics of the Earth and Planetary Interiors*, 132, 105–29.
- Karson, J. A., 1998, Internal structure of oceanic lithosphere; a perspective from tectonic windows. In *Faulting and magmatism at mid-ocean ridges*, Geophysical Monograph 106, 177–218.
- Kerr, A. C., 2004, Oceanic plateaus. In *Treatise on Geochemistry*, vol. 3, *The Crust*, eds. H. D. Holland and K. K. Turekian. Elsevier, Amsterdam, pp. 537–65.
- Kerr A. C., Tarney J., Marriner G. F., Nivia A., and Saunders A. D., 1997, The Caribbean-Colombian Cretaceous igneous province: The internal anatomy of an oceanic plateau. In *Large Igneous Provinces; Continental, Oceanic and Planetary Flood Volcanism*, American Geophysical Union Monograph 100, eds. J. J. Mahoney and M. Coffin., pp. 45–93.
- Kistler, R. W. and Peterman, Z. E., 1973, Variations in Sr, Rb, K, Na, and initial $^{87}\text{Sr}/^{86}\text{Sr}$ in Mesozoic granitic rocks and intruded wall rocks in central California. *Geological Society of America Bulletin*, 84, 3489–512.
- Kistler, R. W. and Peterman, Z. E., 1978, Reconstruction of crustal blocks of California on the basis of initial strontium isotopic compositions of Mesozoic granitic rocks. *USGS Professional Paper* 1071.
- Kleeman, G. J. and Twist, D., 1989, The compositionally zoned sheet-like granite pluton of the Bushveld Complex: Evidence bearing on the nature of A-type magmatism. *Journal of Petrology*, 30, 1383–414.
- Kolker, A., Frost, C. D., Hanson, G. N., and Geist, D. J., 1991, Nd, Sr and Pb isotopes in the Maloin Ranch Pluton, Wyoming: Implications for the origin of evolved rocks at anorthosite margins. *Geochimica et Cosmochimica Acta*, 55, 2285–97.
- Konnerup-Madsen, J. and Rose-Hansen, J., 1982, Volatiles associated with alkaline igneous rift activity; fluid inclusions in the Ilimaussaq Intrusion and the Gadar granitic complexes (South Greenland). *Chemical Geology*, 37, 79–93.
- Koziol, A. M. and Newton, R. C., 1988, Redetermination of the anorthite breakdown reaction and improvement of the plagioclase-garnet-Al₂SiO₅-quartz geobarometer. *American Mineralogist*, 73, 216–23.
- Kushiro, I. and Yoder, H. S., Jr., 1966, Anorthite-forsterite and anorthite-enstatite reactions and their bearing on the basalt-eclogite transformation. *Journal of Petrology* 7, 377–362.
- Kurth-Velz, M., Sassen, A., and Galer, J. G., 2004, Geochemical and isotopic heterogeneities along an Island Arc-spreading ridge intersection: Evidence from the Lewis Hills, Bay of Islands ophiolite, Newfoundland. *Journal of Petrology*, 45, 615–68.
- Laird, J. and Albee, A. L., 1981, High-pressure metamorphism in mafic schist from northern Vermont. *American Journal of Science*, 281, 97–126.
- LeBas, M. J., LeMaitre, R. W., Streckeisen, A., and Zanettin, B. A., 1986, Chemical classification of volcanic rocks based on the total alkali-silica diagram. *Journal of Petrology*, 27, 745–50.
- LeBas, M. J. and Streckeisen, A. L., 1991, The IUGS systematics of igneous rocks. *Journal of the Geological Society*, 148, 825–33.
- Le Fort, P., 1981, Manaslu leucogranite; a collision signature of the Himalaya, a model for its genesis and emplacement. *Journal of Geophysical Research*, 86, 10545–10, 568.
- LeMaitre, R. W., Bateman, P., Dudek, A., Keller, J., Lemeyre, M., LeBas, P. A., Sabin, P. A., Schmid, R., Sørensen, H., Streckeisen, A., Wooley, A. R., and Zanettin, B., 1989, *A classification of igneous rocks and glossary of terms*. Blackwell Scientific Publishers, Oxford, UK.
- Lindsley, D. H., 1991, Experimental studies of oxide minerals. *Reviews in Mineralogy*, 25, 69–106.
- Lindsley, D. H. and Frost, B. R. 1992, *Equilibria among Fe-Ti oxides, pyroxenes, olivine, and quartz: Part I. Theory*. *American Mineralogist*, 77, 987–1003.

- Lindsley, D. H., Frost, B. R., Frost, C. D., and Scoates, J. S., 2010, Petrology, geochemistry, and structure of the Chugwater anorthosite, Laramie Anorthosite complex, S.E. Wyoming, U.S.A. *Canadian Mineralogist*, 48, 887–923.
- Linnen, R. L. and Keppler, H., 2002, Melt composition control of Zr/Hf fractionation in magmatic processes. *Geochimica et Cosmochimica Acta*, 66, 3293–301.
- Liou, J. G., Maruyama, S., and Cho, M., 1987, Very log-grade metamorphism of volcanic and volcanoclastic rocks – mineral assemblages and mineral facies. In *Low Temperature Metamorphism*, ed. M. Frey. Blackie, London, pp. 59–113.
- Liou, J. G., Tsujimori, T., Zhang, R. Y., Katayama, I., and Maruyama, S., 2004, Global UHP metamorphism and continental subduction/collision: The Himalayan model. *International Geology Review*, 46, 1–27.
- Loiselle, M. C. and Wones, D., 1979, Characteristics and origin of anorogenic granites. *Geological Society of America Abstracts with Programs*, 11, 468.
- Longhi, J. and Ashwal, L. D., 1985, Two-stage models for lunar and terrestrial anorthosites: Petrogenesis without a magma ocean. Proceedings of the 15th Lunar and Planetary Science Conference, Part 2. *Journal of Geophysical Research*, 90 (supplement): C571–C584.
- Luth, W. C., Jahns, R. H., and Tuttle, O. F., 1964, The granite system at pressures of 4 to 10 kilobars. *Journal of Geophysical Research*, 69, 759–73.
- MacDonald, G. A., 1968, Composition and origin of Hawaiian lavas. *Geological Society of America Memoir*, 116, 477–522.
- MacKenzie, D., 1984, The generation and compaction of partially molten rock. *Journal of Petrology*, 25, 713–65.
- MacKenzie, D. and O’Nions, R. K., 1991, Partial melt distributions from inversion of rare earth element concentrations. *Journal of Petrology*, 32, 1021–91.
- Manning, C., 2004, The chemistry of subduction-zone fluids. *Earth and Planetary Science Letters*, 223, 1–16.
- Markl, G., 2001, A new type of silicate liquid immiscibility in peralkaline nepheline syenites (lujavrites) of the Ilimaussaq complex, South Greenland. *Contributions to Mineralogy and Petrology*, 141, 458–72.
- Markl, G., Marks, M. A. W., and Frost, B. R., 2010, On the controls of oxygen fugacity in the generation and crystallization of peralkaline melts. *Journal of Petrology*, 51, 1831–47.
- Marks, M., Vennemann, T., Siebel, W., and Markl, G., 2004, Nd-, O-, and H-isotopic evidence for complex, closed-system fluid evolution of the peralkaline Ilimaussaq intrusion, south Greenland. *Geochimica et Cosmochimica Acta*, 68, 3379–95.
- Marsh, B. D. and Carmichael, I. S. E., 1974, Benioff zone magmatism. *Journal of Geophysical Research*, 79, 1196–206.
- Mason, B. G., Pyle, D. M., and Oppenheimer, C., 2004, The size and frequency of the largest explosive eruptions on Earth. *Bulletin of Volcanology*, 66, 735–48.
- Mayer, A., Hofmann, A. W., Sinigoi, S., and Morais, E., 2004, Mesoproterozoic Sm-Nd and U-Pb ages for the Kunene anorthosite complex of SW Angola. *Precambrian Research*, 133, 187–206.
- McBirney, A. R., 1993, *Igneous petrology*. Jones and Bartlett Publishers, Boston, MA.
- McBirney, A. R., 2007, *Igneous petrology*, 3rd ed. Jones and Bartlett, Boston.
- McBirney, A. R. and Williams, H., 1969, Geology and petrology of the Galapagos Islands. *Geological Society of America Memoir* 118.
- McCaig, A., Cliff, R. A., Escartin, J., Fallick, A. E., and MacLeod, C. J., 2007, Oceanic detachment faults focus very large volumes of black smoker fluids. *Geology*, 35, 935–38.
- McCurry, M., Hayden, K. P., Morse, L. H., and Mertzman, S., 2008, Genesis of post-hotspot, A-type rhyolite of the Eastern Snake River Plain volcanic field by extreme fractional crystallization of olivine tholeiite. *Bulletin of Volcanology*, 70, 361–83.
- McLelland, J. M., Bickford, M. E., Hill, B. M., Clechenko, C. C., Valley, J. W., and Hamilton, M. A., 2004, Direct dating of Adirondack massif anorthosite by U-Pb SHRIMP analysis of igneous zircon: Implications for AMCG complexes. *Geological Society of America Bulletin*, 116, 1299–317.
- McMillan and Panteleyev, 1988, Porphyry copper deposits., In *Ore deposit models*, eds. R. G. Roberts and P. A. Sheahan. Geoscience Canada Reprint Series 3, pp. 45–58.
- Mehnert, K. R., 1968, *Migmatites and the origin of granitic rocks*. Elsevier, New York.
- Meshesha, D., Shinjo, R., Matsumura, R., and Chekol, T., 2011, Metasomatized lithospheric mantle beneath Turkana depression in southern Ethiopia (the East Africa Rift): geochemical and Sr-Nd-Pb isotopic characteristics. *Contributions to Mineralogy and Petrology*, 162, 889–907.
- Metz, P. and Trommsdorff, V., 1968, On phase equilibria in metamorphosed siliceous dolomites. *Contributions to Mineralogy and Petrology*, 18, 305–309.

- Meyer, C. and Hemley, J. J., 1967, Wall rock alteration. In *Geochemistry of Hydrothermal Ore Deposits*, ed. H. L. Barnes. Hold, Reinhart and Winston, New York, pp.176–235.
- Mezger K., Bohlen, S. R., and Hanson, G. A., 1990, Metamorphic history of the Archean Pikwitonei granulite domain and the Cross Lake subprovince, Superior Province, Manitoba, Canada. *Journal of Petrology*, 31, 483–517.
- Michibayashi, K., Ina, T., and Kanagawa, K., 2006, The effect of dynamic recrystallization on olivine fabric and seismic anisotropy; insight from a ductile shear zone, Oman ophiolite. *Earth and Planetary Science Letters*, 244, 695–708.
- Miller, R. B., Miller, J. S., and Paterson, S. R., 2005, Pluton emplacement and magma chamber processes: Insights from the Tuolumne Intrusive Suite. *Geological Society of America Abstracts with Programs* 37 (4), 38.
- Milord, I., Sawyer, E. W., Brown, M., 2001, Formation of diatexite migmatite and granite magma during anatexis of semi-pelitic metasedimentary rocks: An example from St. Malo, France. *Journal of Petrology*, 42, 487–505.
- Miron, G. D., Neuhoff, P. S., and Amthauer, G., 2012, Low-temperature hydrothermal metamorphic mineralization of island-arc volcanics, South Apuseni Mountains, Romania, *Clays and Clay Minerals*, 60, 1–17.
- Mitchell, R. H., 1986, *Kimberlites: Mineralogy, geochemistry, and petrology*. Plenum Press, New York.
- Mitchell, R. H. and Bergman, S. C., 1991, *Petrology of lamproites*. Plenum Press, New York.
- Miyashiro, A., 1961, Evolution of metamorphic belts. *Journal of Petrology*, 2, 277–311.
- Miyashiro, A., 1973a, *Metamorphism and Metamorphic Belts*. John Wiley & Sons, New York.
- Miyashiro, A., 1973b, The Troodos complex was probably formed in an island arc. *Earth and Planetary Science Letters*, 19, 218–81.
- Miyashiro, A., 1974, Volcanic rocks series in island arcs and active continental margins. *American Journal of Science*, 274, 321–55.
- Miyashiro, A., 1975, Classification, characteristics, and origin of ophiolites. *Journal of Geology*, 83, 249–81.
- Moecher, D. P., Perkins, D., III, Leier-Englehardt, P. J., and Medaris, L. G. Jr., 1986, Metamorphic conditions of the late Archean high-grade gneisses, Minnesota River valley, U.S.A., *Canadian Journal of Earth Sciences*, 23, 633–45.
- Mohriak, W. U., Rosendahl, B. R., Turner, J. P., and Valente, S. C., 2002, Crustal architecture of South Atlantic volcanic margins. In *Volcanic rifted margins*, *Geological Society of America Special Paper* 362, eds. M. A. Menzies, S. L. Klemperer, C. J. Ebinger, and J. Baker, pp. 159–202.
- Moody, J. B., Meyer, D., and Jenkins, J. E., 1983, Experimental characterization of the greenschist/amphibolite boundary in mafic systems. *American Journal of Science*, 283, 48–92.
- Moore, J. N. and Kerrick, D. M., 1976, Equilibria in siliceous dolomites of the Alta aureole, Utah, *American Journal of Science*, 276, 502–24.
- Moores, E. M., 1982, Origin and emplacement of ophiolites. *Reviews of Geophysics and Space Physics*, 20, 735–60.
- Morse, S. A., 1970, Alkali feldspars with water at 5 kb pressure. *Journal of Petrology*, 11, 221–51.
- Morse, S. A., 1980, Kiglapait geochemistry. II. Petrography. *Journal of Petrology*, 20, 394–410.
- Muir, I. D. and Tilley, C. E., 1957, Contributions to the petrology of Hawaiian basalts 1. The picroite-basalts of Kilauea. *American Journal of Science*, 255, 241–53.
- Müntener, O., Manatschal, G., Desmurs, L., and Pettke, T., 2010, Plagioclase peridotites in ocean-continent transitions: Refertilized mantle domains generated by melt stagnation in the shallow mantle lithosphere. *Journal of Petrology*, 51, 255–94.
- Myers, J. S., 1976, Channel deposits of peridotite, gabbro and chromitite from turbidity currents in the stratiform Fiskensætt anorthosite complex, southwest Greenland. *Lithos*, 9, 281–91.
- Nabelek, P. I., Russ-Nabelek, C., and Denison, J. R., 1992, The generation and crystallization conditions of the Proterozoic Harney Peak Leucogranite, Black Hills, South Dakota, USA: Petrologic and geochemical constraints. *Contributions to Mineralogy and Petrology*, 173–91.
- Naldrett, A. J., Bray, J. G., Gasparri, E. L., Podolsky, T., Rucklidge, J. D., 1970, Cryptic variation and the petrology of the Sudbury nickel irruptive. *Economic Geology*, 65, 122–55.
- Nash, W. P., Carmichael, I. S. E., and Johnson, B. W., 1969, The mineralogy and petrology of Mount Suswa, Kenya. *Journal of Petrology*, 10, 409–39.
- Neal, C. R., Mahoney, J. J., Kroenke, L. W., Duncan, R. A., and Petterson, M. G., 1997, The Ontong Java Plateau. In *Large igneous provinces; continental, oceanic and planetary flood volcanism*, American Geophysical Union Monograph 100, eds. J. J. Mahoney and M. Coffin, pp. 183–216.
- Nesbitt, B. E. and Kelly, W. C., 1980, Metamorphic zonation of sulfides, oxides, and graphite in and around the orebodies at Ducktown, Tennessee. *Economic Geology*, 75, 1010–21.

- Newhall, C. G., Hendley, J. W., and Stauffer, P. H., 1997, The cataclysmic 1991 eruption of Mount Pinatubo, Philippines, U.S. *Geological Survey Fact Sheet 113–97*, [http://pubs.usgs.gov/fs/1997/fs113–97/](http://pubs.usgs.gov/fs/1997/fs113-97/) accessed August 28, 2012.
- Newhall, C. G., and Self, S., 1982, The volcanic explosivity index (VEI): An estimate of explosive magnitude for historical volcanism. *Journal of Geophysical Research*, 87, 1231–38.
- Nikogosian, I. K. and van Bergen, M. J., 2010, Heterogeneous mantle sources of potassium-rich magmas in central-southern Italy: Melt inclusion evidence from Roccamonfina and Ernici (mid Latina Valley). *Journal of Volcanology and Geothermal Research*, 197, 279–302.
- Nimis, P. and Trommsdorff, V., 2001, Revised thermobarometry of Alpe Arami and other garnet peridotites from the Central Alps. *Journal of Petrology*, 42, 103–15.
- Nockolds, S. R. and Allen, R., 1956, The geochemistry of some igneous rock series – III. *Geochimica et Cosmochimica Acta*, 9, 34–77.
- Noh, J. H. and Boles, J. R., 1993, Origin of zeolite cements in the Miocene sandstones, North Tejon oil fields, California. *Journal of Sedimentary Petrology*, 63, 248–60.
- Oberthür, T., Davis, D. W., Blenkinsop, T. G., and Höhndorf, A., 2002, Precise U-Pb mineral ages, Rb-Sr and Sm-Nd systematics for the Great Dyke, Zimbabwe – constraints on late Archean events in the Zimbabwe craton and Limpopo belt. *Precambrian Research*, 113, 293–305.
- O'Connor, J. M., Stoffers, P., Wijbrans, J. R., and Worthington, T. J., 2007, Migration of widespread long-lived volcanism across the Galapagos Volcanic Province: Evidence for a broad hotspot melting anomaly? *Earth and Planetary Science Letters*, 263, 339–54.
- O'Neill, H. St. C., 1981, The transition between spinel lherzolite and garnet lherzolite, and its use as a geobarometer. *Contributions to Mineralogy and Petrology* 77, 185–94.
- Osborn, E. F. and Tait, D. B., 1952, The system diopside-forsterite-anorthite. *American Journal of Science*, Bowen volume, part 2, 413–33.
- Owens, B. E., Dymek, R. F., Tucker, R. D., Brannon, J. C., and Podosek, F. A., 1994, Age and radiogenic isotopic composition of a late- to post-tectonic anorthosite in the Grenville Province: The Labrieville massif, Quebec. *Lithos*, 31, 189–206.
- Oxburgh, E. R. and Turcotte, D. L., 1971, Origin of paired metamorphic belts and crustal dilation in island arc regions. *Journal of Geophysical Research*, 76, 1315–27.
- Parsons, I., 1978, Feldspars and fluids in cooling plutons. *Mineralogical Magazine*, 42, 1–17.
- Patiño Douce, A. E., 1997, Generation of metaluminous A-type granites by low-pressure melting of calc-alkaline granitoids, *Geology*, 25, 743–46.
- Patiño Douce, A. E., Humphreys, E. D., and Johnston, A.D., 1990, Anatexis and metamorphism in tectonically thickened continental crust exemplified by the Sevier hinterland, western North America. *Earth and Planetary Science Letters*, 97, 290–315.
- Pattison, D. R. M., 1992, Stability of andalusite and sillimanite and the Al_2SiO_5 triple point: Constraints from the Ballachulish aureole, Scotland. *Journal of Geology*, 100, 432–46.
- Pattison, D. R. M., 2001, Instability of Al_2SiO_5 “triple-point” assemblages in muscovite+biotite+quartz-bearing metapelites, with implications. *American Mineralogist*, 86, 1414–22.
- Pattison, D. R. M., Chacko, T., Farquhar, J., and McFarlane, C. R. M., 2003, Temperatures of granulite-facies metamorphism: Constraints from experimental phase equilibria and thermobarometry corrected for retrograde exchange. *Journal of Petrology*, 44, 867–900.
- Peacock, M. A., 1931, Classification of igneous rock series. *Journal of Geology*, 39, 54–67.
- Peacock, S. M., 1991, Numerical simulation of subduction zone pressure-temperature-time paths; constraints on fluid production and arc magmatism. In *The behavior and influence of fluids in subduction zones. Philosophical Transactions of the Royal Society of London, Series A: Mathematical and Physical Sciences*, 335, 341–53.
- Pearce, J. A., Harris, N. B. W. and Tindle, A. G., 1984, Trace element discrimination diagrams for the tectonic interpretation of granitic rocks. *Journal of Petrology* 25, 956–83.
- Pearce, J. A., Lippard, S. J., and Roberts, S., 1984, Characteristics and tectonic significance of supra-subduction zone ophiolites. *Geological Society of London Special Publication* 16, 77–94.
- Pearce, J. A. and Peate, D. W., 1995, Tectonic implications of the composition of volcanic arc magmas. *Annual Review of Earth and Planetary Sciences*, 23, 251–85.
- Pecher, A., 1989, The metamorphism in the Central Himalaya. *Journal of Metamorphic Geology*, 7, 31–41.

- Percival, J. A., 1989, A regional perspective of the Quetico metasedimentary belt, Superior Province, Canada. *Canadian Journal of Earth Science*, 26, 677–93.
- Percival, J. A., 1991, Granulite-facies metamorphism and crustal magmatism in the Ashuanipi Complex, Quebec-Labrador. *Journal of Petrology*, 32, 1261–97.
- Percival, J. A., Fountain, D. M., and Salisbury, M. H., 1992, Exposed crustal cross sections as windows on the lower crust. In *Developments in geotectonics 23, continental lower crust*, eds. D. M. Fountain, R. Arculus, and R. W. Kay, Elsevier, Amsterdam, pp. 317–62.
- Percival, J. A. and McGrath, P. H., 1986, Deep crustal structure and tectonic history of the northern Kapuskasing uplift of Ontario: An integrated petrological-geophysical study. *Tectonics*, 5, 553–72.
- Percival, J. A., Mortensen, J. K., Stern, R. A., Card, K. D., and Bégin, N. J., 1992, Giant granulite terranes of northeastern Superior Province: The Ashuanipi complex and Minto block. *Canadian Journal of Earth Science*, 29, 2287–308.
- Perkins, M. E. and Nash, B. P., 2002, Explosive silicic volcanism of the Yellowstone hotspot: The ash fall tuff record. *Geological Society of America Bulletin*, 114, 367–81.
- Peretti, A., 1988, Occurrence and stabilities of opaque minerals in the Malenco serpentinite (Sondrio, northern Italy), PhD dissertation, Swiss Federal Institute of Technology, Zürich.
- Petford, N., 2009, Which effective viscosity? *Mineralogical Magazine*, 73, 167–91.
- Petterson, M. G., Neal, C. R., Mahoney, J. J., Kroenke, L. W., Saunders, A. D., Babbs, T. L., Duncan, R. A., Tolia, D., and McGrail B., 1997, Structure and deformation of north and central Malaita, Solomon Islands: Tectonic implications for the Ontong Java Plateau – Solomon arc collision, and for the fate of oceanic plateaus. *Tectonophysics* 283, 1–33.
- Pettijohn, F. J., 1975, *Sedimentary rocks*, 3rd ed., Harper and Row, New York.
- Pfaff, K., Krumrei, T., Marks, M., Wenzel, T., Rudolf, T., and Markl, G., 2008, Chemical and physical evolution of the “lower layered sequence” from the nepheline syenitic Ilimaussaq intrusion, South Greenland: Implications for the origin of magmatic layering in peralkaline felsic liquids. *Lithos*, 106, 280–96.
- Philpotts, A. R. and Ague, J. J., 2009, *Principles of igneous and metamorphic petrology*, 2nd ed., New York: Cambridge University Press, Cambridge.
- Polat, A., Fryer, B. J., Appel, P. W. U., Kalvig, P., Kerrich, R., Dilek, Y., and Yang, Z., 2011, Geochemistry of anorthositic differentiated sills in the Archean (~2970 Ma) Fiskensæset Complex, SW Greenland: Implications for parental magma compositions, geodynamic setting, and secular heat flow in arcs. *Lithos*, 123, 50–72.
- Premo, W. R. and Loucks, R. R., 2000, Age and Pb-Sr-Nd isotopic systematics of plutonic rocks from the Green Mountain magmatic arc, southeastern Wyoming. *Rocky Mountain Geology*, 35, 51–70.
- Rabinowicz, M. and Toplis, M. J., 2009, Melt segregation in the lower part of the partially molten mantle zone beneath an oceanic spreading centre: Numerical modeling of the combined effects of shear segregation and compaction. *Journal of Petrology*, 50, 1071–106.
- Ravana, E. J. K., Andersen, T. B., Jolivet, L., and De Capitani, C., 2010, Cold subduction and the formation of lawsonite eclogite – constraints from prograde evolution of eclogitized pillow lava from Corsica. *Journal of Metamorphic Geology*, 28, 381–95.
- Ren, Z-Y, Hanyu, T., Miyazaka, T., Chang, Q., Kawabata, H., Takahashi, T., Hirahara, Y., Nichols, A. R. L., and Tatsumi, Y., 2009, Geochemical differences of the Hawaiian shield lavas: Implications for melting process in the heterogeneous Hawaiian plume. *Journal of Petrology*, 50, 1553–73.
- Rice, J. M., 1977, Progressive metamorphism of impure dolomitic limestone in the Marysville aureole, Montana. *American Journal of Science*, 277, 1–24.
- Rosenthal, A., Foley, S. F., Pearson, D. G., Nowell, G. M., and Tappe, S., 2009, Petrogenesis of strongly alkaline primitive volcanic rocks at the propagating tip of the western branch of the East African Rift. *Earth and Planetary Science Letters*, 284, 236–48.
- Rudnick, R. L. and Taylor, S. R., 1987, The composition and petrogenesis of the lower crust, a xenolith study. *Journal of Geophysical Research*, 92, 13981–4005.
- Russell, M. J., Hall, A. J., and Martin, W., 2010, Serpentinization as a source of energy at the origin of life. *Geobiology*, 8, 355–71.
- Ryan, M. P., Koyangi, R. Y., and Fiske, R. S., 1981, Modeling the three-dimensional structure of macroscopic magma transport systems: Application to Kilauea volcano, Hawaii. *Journal of Geophysical Research*, 86, 7111–29.
- Salisbury, M. H., and Christiansen, N. I., 1985, Olivine fabrics in the Bay of Islands Ophiolite; implications for oceanic mantle structure and anisotropy. *Canadian Journal of Earth Sciences*, 22, 1757–66.

- Sandiford, M. and Powell, R., 1986, Deep crustal metamorphism during continental extension: Modern and ancient examples. *Earth and Planetary Science Letters*, 79, 151–8.
- Sawka, W. N., Chappell, B. W., and Kistler, R. W., 1990, Granitoid compositional zoning by side-wall boundary layer differentiation: Evidence from the Palisade Crest intrusive suite, central Sierra Nevada, California. *Journal of Petrology*, 31, 519–53.
- Scarfe, C. M., 1973, Viscosity of basic magmas at varying pressure. *Nature Phys. Sci.*, 241, 101–102.
- Schairer, J. F. and Bowen, N. L., 1956, The system $\text{Na}_2\text{O}-\text{Al}_2\text{O}_3-\text{SiO}_2$. *American Journal of Science*, 254, 129–95.
- Schärer, U., Wilmar, E., and Duchesne, J.-C., 1996, The short duration and anorogenic character of anorthosite magmatism: U-Pb dating of the Rogaland complex, Norway. *Earth and Planetary Science Letters*, 139, 335–50.
- Schroeder, T., John, B., and Frost, B. R., 2002, Geologic implications of seawater circulation through peridotite exposed at slow-spreading mid-ocean ridges. *Geology*, 30, 367–70.
- Scoates, J. S. and Friedman, R. M., 2008, Precise age of the platiniferous Merensky reef, Bushveld Complex, South Africa, but the U-Pb zircon chemical abrasion ID-TIMS technique. *Economic Geology*, 103, 465–71.
- Scoates, J. S., Frost, C. D., Mitchell, J. N., Lindsley, D. H., and Frost, B. R., 1996, Residual-liquid origin for a monzonite intrusion in a mid-Proterozoic anorthosite complex: The Sybille intrusion, Laramie anorthosite complex, Wyoming. *Geological Society of America Bulletin*, 108, 1357–71.
- Scoates, J. S., Lindsley, D. H., and Frost, B. R., 2010, Magmatic and structural evolution of an anorthositic magma chamber: The Poe Mountain intrusion, Laramie Anorthosite Complex, Wyoming. *Canadian Mineralogist*, 48, 851–55.
- Scott, G. R., Taylor, R. B., Epis, R. C., and Wobus, R. A., 1978, Geologic map of the Pueblo 1° by 2° quadrangle, south-central Colorado. United States Geological Survey Miscellaneous Investigations Map 1–1022, scale 1:250,000.
- Shand, S. J., 1943, *The eruptive rocks*, 2nd ed. John Wiley & Sons, New York.
- Shaw, D. M., 2006, *Trace elements in magma: A theoretical treatment*. Cambridge University Press, Cambridge.
- Sills, J., 1984, Granulite facies metamorphism in the Ivrea Zone, N.W. Italy. *Schweizerische Mineralogische und Petrographische Mitteilungen*, 64, 169–91.
- Singer, B. S., Myers, J. D., and Frost, C. D., 1992, Mid-Pleistocene lavas from the Segum volcanic center, central Aleutian arc: Closed-system fractional crystallization of basalt to rhyodacite. *Contributions to Mineralogy and Petrology*, 110, 87–112.
- Skippen, G. B., 1971, Experimental data for reactions in siliceous marbles. *Journal of Geology*, 79, 457–81.
- Skippen, G. B., 1974, An experimental model for low pressure metamorphism of siliceous dolomitic marble. *American Journal of Science*, 274, 487–509.
- Skjerlie, K. P. and Johnston, A. D., 1993, Fluid-absent melting behavior of an F-rich tonalitic gneiss at mid-crustal pressures: Implications for the generation of anorogenic granites. *Journal of Petrology*, 34, 785–815.
- Smith, D. R. and Leeman, W. P., 1993, The origin of Mount St. Helens andesites. *Journal of Volcanology and Geothermal Research*, 55, 271–303.
- Smith, D. R., Noblett, J., Wobus, R. A., Unruh, D., Douglass, J., Beane, R., Davis, C., Goldman, S., Kay, G., Bustavson, B., Saltoun, B., and Steward, J., 1999, Petrology and geochemistry of late-stage intrusions of the a-type mid-Proterozoic Pikes Peak batholith (Central Colorado, USA): Implications for petrogenetic models. *Precambrian Research*, 98, 271–305.
- Smithies, R. H., Champion, D. C., and Cassidy, K. F., 2003, Formation of the Earth's early Archean continental crust. *Precambrian Research*, 127, 89–101.
- Snoke, A. W., Rowe, D. W., Yule, D. J., and Wadge, G., 2001, Petrologic and structural history of Tobago, West Indies; a fragment of the accreted Mesozoic oceanic arc of the southern Caribbean. *Geological Society of America Special Paper* 354.
- Sørensen, H., 1974, Introduction. In *The alkaline rocks*, ed. H. Sørensen. John Wiley & Sons, New York, pp. 1–11.
- Spear, F. S., 1981, An experimental study of hornblende stability and compositional variability in amphibolite. *American Journal of Science*, 281, 697–734.
- Spera, F. J. and Bergman, S. C., 1980, Carbon dioxide in igneous petrogenesis: I. *Contributions to Mineralogy and Petrology*, 74, 55–66.
- Stakes, D. S., Shervais, J. W., and Hopson, C. A., 1984, The volcanic-tectonic cycle of the FAMOUS and AMAR valleys, Mid-Atlantic Ridge (36°47'N): Evidence from basalt glass and phenocryst compositional variations for a steady state magma chamber beneath the valley midsections, AMAR 3. *Journal of Geophysical Research*, 89, 6995–7028.
- Starkey, R. J. and Frost, B. R., 1990, Low-grade metamorphism of the Karmutsen Volcanics, Vancouver Island, British Columbia. *Journal of Petrology*, 31, 167–95.

- Stern, C. R. and de Wit, M. J., 2003, Rocas Verdes ophiolites, southernmost South America: Remnants of progressive stages of development of oceanic-type crust in a continental margin back-arc basin. In *Ophiolites in earth history*, eds. Y. Dilek and P. T. Robinson. Geological Society of London Special Publication, London.
- Stillitoe, R. H., 2010, Porphyry Copper Systems. *Economic Geology*, 105, 3–41.
- Streckeisen, A., 1976, To each plutonic rock its proper name. *Earth-Science Reviews*, 12, 1–33.
- Streckeisen, A., 1980, Classification and nomenclature of volcanic rocks, lamprophyres, carbonatites and melilitic rocks: IUGS Subcommission on the systematics of igneous rocks. *Geologische Rundschau*, 69, 194–207.
- Strong, D. F. and Hamner, S. K., 1981, The leucogranites of southern Brittany: Origin by faulting, frictional shearing, fluid flux, and fractional melting. *Canadian Mineralogist*, 19, 163–76.
- Storey, C. D., Jeffries, T. E., and Smith, M., 2004, Common lead-corrected laser ablation ICP-MS U–Pb systematics and geochronology of titanite. *Chemical Geology*, 227, 37–52.
- Swanson, D. A., Casadevall, T. J., Dzurisin, D., Holcomb, R. T., Newhall, C. G., Malone, S. D., and Weaver, C. S., 1985, Forecasts and predictions of eruptive activity at Mount St. Helens, USA. *Journal of Geodynamics*, 3, 397–423.
- Swanson, D. A., Wright, T. L., Hooper, P. R., and Bentley, R. D., 1979, Revisions in stratigraphic nomenclature of the Columbia River basalt group. *U.S. Geological Survey Bulletin*, 1457–G.
- Tate, M. C., Norman, M. D., Johnson, S. E., Fanning, C. M., and Anderson, J. L., 1999, Generation of tonalite and trondjemite by subvolcanic fractionation and partial melting in the Zarza intrusive complex, western Peninsular Ranges Batholith, northwestern Mexico. *Journal of Petrology*, 40, 983–1010.
- Taylor, S. R., 1975, *Lunar science: A post-Apollo view*. Pergamon Press, New York.
- Teagle, D. and others, 2011, Integrated Ocean Drilling Program Expedition 335 preliminary report: Superfast Spreading Rate Crust 4: Drilling gabbro in intact ocean crust formed at a superfast spreading rate: April 13–June 3. *Preliminary Report of the Integrated Ocean Drilling Program*, 335.
- Theye, T., Seidel, E., and Vidal, O., 1992, Carpholite, sudoite, and chloritoid in low-grade high-pressure metapelites from Crete and the Peloponnese, Greece. *European Journal of Mineralogy*, 4, 487–507.
- Thompson, A. B. and England, P. C., 1984, Pressure-temperature-time paths of regional metamorphism II: Their inference and interpretation using mineral assemblages in metamorphic rocks. *Journal of Petrology*, 25, 929–55.
- Thompson, J. B., 1957, The graphical analysis of mineral assemblages in pelitic schists. *American Mineralogist*, 42, 842–58.
- Thurston, P. C., 2002, Autochthonous development of the Superior Province greenstone belts. *Precambrian Research*, 115, 11–36.
- Thurston, P. C. and Breaks, F. W., 1978, Metamorphic and tectonic evolution of the Uchi-English River subprovince. *Canadian Geologic Survey Paper* 78–10, 49–62.
- Tilley, C. E., 1925, Metamorphic zones in the southern Highlands of Scotland. *Quarterly Journal of the Geological Society of London*, 81, 100–12.
- Tilley, C. E., 1948, Earlier stages in the metamorphism of siliceous dolomites. *Mineralogical Magazine*, 28, 272–76.
- Tilling, R. I., 1989, Volcanic hazards and their mitigation: progress and problems. *Reviews of Geophysics*, 27, 237–69.
- Todheide, K. and Frank, E. U., 1963, Das Zweiphasengebiet und die Kritische Kurve in Sys Cokendioxiid-Wasser bis zu Drucken von 3500 bar. *Zeitschrift Physische Chemie Nenefolge*, 37, 388–401.
- Trommsdorff, V. and Evans, B. W., 1974, Alpine metamorphism of peridotitic rocks. *Schweizerische Mineralogische und Petrographische Mitteilungen*, 54, 333–52.
- Trommsdorff, V. and Evans, B. W., 1977, Antigorite-ophicarbonates; phase relations in a portion of the system CaO–MgO–SiO₂–H₂O–CO₂. *Contributions to Mineralogy and Petrology*, 60, 39–56.
- Turner, F. J., 1948, Mineralogical and structural evolution of the metamorphic rocks. *Geological Society of America Memoir*, 30.
- Turner, F. J., 1968, *Metamorphic Petrology, Mineralogical and Field Aspects*. McGraw Hill, New York.
- Vance, D., Müller, W., and Villa, I. M., 2003, Geochronology: Linking the isotopic record with petrology and textures. *Geological Society Special Publication* 220.
- Van Kranendonk, M. J., Hickman, A. H., Smithies, R. H., Nelson, D. R., and Pike, G., 2002, Geology and tectonic evolution of the Archean North Pilbara terrain, Pilbara craton, *Western Australia*. *Economic Geology*, 97, 695–732.
- Vantongeren, J. A., Mathez, E. A., and Kelemen, P. B., 2010, A felsic end to Bushveld differentiation. *Journal of Petrology*, 51, 1891–912.

- Varne, R., Brown, A. V., and Faloon, T., 2000, Macquarie Island: Its geology, structural history, and the timing and tectonic setting of its N-MORB to E-MORB magmatism. In *Ophiolites and oceanic crust: New insights from field studies and the Ocean Drilling Program. Geological Society of America Special Paper 349*, eds. Y. Dilek, E. M. Moores, D. Elthon, and A. Nicolas, pp. 53–64.
- Vauchez, A. and Garrido, C., 2001, Seismic properties of an asthenospherized lithospheric mantle; constraints from lattice preferred orientations in peridotites from the Ronda Massif. *Earth and Planetary Science Letters*, 192, 235–49.
- Vermaak, C. F. and Von Gruenewaldt, G., 1981, Guide to the Bushveld excursion (28th of June to the 4th of July, 1981). *Geological Society of South Africa*, Marshalltown, South Africa.
- Vernon, R. H., 2004, *A practical guide to rock microstructures*. Cambridge University Press, Cambridge.
- Vijaya Kumar, K., Frost, C. D., Frost, B. R., and Chamberlain, K. R., 2007, The Chimakurti, Errakonda, and Uppalapadu plutons, Eastern Ghats belts, India: An unusual association of tholeiitic and alkaline magmatism. *Lithos*, 97, 30–57.
- Voordouw, R., Gutzmer, J., and Beukes, N. J., 2009, Intrusive origin for Upper Group (UG1, UG2) stratiform chromitite seams in the Dwars River area, Bushveld Complex, South Africa. *Mineralogy and Petrology*, 97, 75–94.
- Wager, L. R. and Brown, G. M., 1967, *Layered igneous rocks*, W.H. Freeman and Company, San Francisco, CA.
- Watson, E. B. and Harrison, T. M., 1983, Zircon saturation revisited; temperature and composition effects in a variety of crustal magma types. *Earth and Planetary Science Letters*, 64, 295–304.
- West, H. B., Garcia, M. O., Gerlach, D. C., and Romano, J., 1992, Geochemistry of tholeiites from Lanai, Hawaii. *Contributions to Mineralogy and Petrology*, 112, 520–42.
- Whitney, J. A., 1988, The origin of granite: The role and source of water in the evolution of granitic magmas. *Geological Society of America Bulletin*, 100, 1886–97.
- Willemse, J., 1969, The vanadiferous magnetic iron ore of the Bushveld igneous complex. *Economic Geology Monograph 4*, 187–208.
- Wilkinson, J. F. G. and Hensel, H. D., 1988, The petrology of some picrites from Mauna Loa and Kilauea volcanoes, Hawaii, *Contributions to Mineralogy and Petrology*, 98, 326–245.
- Wickham, S. M. and Oxburgh, E. R., 1985, Continental rifts as a setting for regional metamorphism. *Nature*, 318, 330–34.
- Williams, I. S., 1998, U-Th-Pb geochronology by ion microprobe. In *Applications of microanalytical techniques to understanding mineralizing processes*, eds. M. A. McKibben, W. C. Shanks III, and W. I. Ridley. *Reviews in Economic Geology*, 7, 1–35. Wilson, M., 1989, *Igneous petrogenesis: A global tectonic approach*. Unwin Hyman, London.
- Winkler, H. G. F., 1976, *Petrogenesis of metamorphic rocks*. (English Editor, E. Froese). Springer-Verlag, New York. Wright, T. L., 1984, Origin of Hawaiian tholeiite: A mesomatic model. *Journal of Geophysical Research*, 89, 3233–52.
- Yardley, B. W. D., 1989, *An introduction to metamorphic petrology*, Longman Scientific and Technical, London.
- Yoder, H. S. and Tilley, C. E., 1962, Origin of basalt magmas; an experimental study of natural and synthetic rock systems. *Journal of Petrology*, 3, 342–529.
- Zeh, A., Gerdes, A., Barton, J., and Klemd, R., 2010, U-Th-Pb and Lu-Hf systematics of zircon from TTGs, leucosomes, meta-anorthosites, and quartzites of the Limpopo Belt (South Africa): Constraints for the formation, recycling and metamorphism of Paleoproterozoic crust. *Precambrian Research*, 179, 50–68.
- Zen, E.-A., 1988, Phase relations of peraluminous granitic rocks and their petrogenetic implications. *Annual Review of Earth and Planetary Sciences*, 16, 21–52.

Index



- aa**, 9, 10
 abbreviation, mineral, 264
 Abitibi belt, Canada, 258
 Absaroka Mountains, Wyoming, USA, 102
 absarokaite, 102
 accessory mineral, 99, 182, 281–282
 accretionary prism, 257
 ACF diagram. *See* chemographic projection
 acmite*, 272
 actinolite*, 272
 activity coefficient, 194
 adiabat, 68
 adiabatic decompression. *See* decompression melting
 aegerine*, 272
 aeromagnetic survey, 15, 145
 AFC (assimilation with fractionation crystallization), 44
 AFM diagram, 100, 223, 224, 226, 227, 228, 230, 231
 Ajo, Arizona, 244
 albite, 264
 albite*, 263, 264
 albite thermal barrier. *See* phase diagram, thermal barrier
 albite-epidote hornfels, 186
 Aleutian island arc, Alaska, USA., 89, 92–93, 97, 101, 102, 103
 alkali lime index. *See* modified alkali lime index (MALI)
 alkaline
 gneiss, 161
 intrusion, 124, 138, 161
 magmatism, 116, 117
 volcanism, 121
 alkalinity index (AI), 56, 118, 146
 peralkaline, 56
 allanite, 99
 almandine*, 278
 Alpe Arami, Switzerland, 211
 alphabet classification. *See* granite
 Alpine orogeny, 107, 185, 216, 252, 254
 Alps Mountains, Europe, 158, 201, 211, 252, 253
 Alta stock, Utah, USA, 240, 241
 aluminosilicate, 21, 149, 160, 161, 277
 P-T diagram, 19
 triple point, 19, 231
 aluminum saturation index (ASI), 55–56, 81, 114, 117, 119, 137, 146, 153
 metaluminous, 55, 80, 115, 145
 peraluminous, 55, 114, 136, 145, 155
 aluminum-excess minerals, 277–280
 amphibole*, 272
 hornblende*, 274
 quadrilateral, 272, 273
 sodic, 274
 amphibolite, 186, 199
 amphibolite facies, 131, 163, 183, 198, 200, 212, 214, 224, 238, 250, 254
 correlation to Barrovian zone, 229
 amygdale, 163, 164, 279
 analcime, 187, 198
 anatexis, 158. *See* partial melting
 ancylite, 139
 andalusite*, 277
 Andes Mountains, South America, 91
 andesine*, 264
 andesite, 8, 40, 51, 91, 94, 98, 100, 103, 105, 145
 andradite*, 278
 anhedral grain, 7, 9, 43, 263
 ankerite, 224
 annite*, 276
 anorogenic granite. *See* granite
 anorthite*, 263, 264
 anorthite-diopside, 22
 anorthoclase*, 267
 anorthosite, 3, 5, 41, 58, 124, 127, 131, 135
 anorthosite complex, 132, 134
 Archean, 124, 131
 massif, 124, 131, 132, 135
 anthophyllite*, 272
 anticline, 216
 antigorite, 205, 206, 207, 275
 apatite*, 281
 Appalachian Mountains, USA, 233
 Apulian plate, 252
 aragonite*, 268
 arc, 129, 148
 batholith, continental, 95–97, 148
 island and continental magma series, 104
 K₂O variability, 100, 101
 magmatism, 104
 in paired metamorphic belt, 250
 petrography, 97–99
 plutonic complex, 91, 93–94, 102
 relation to large mafic intrusions, 130
 structure, 91
 volcano, continental, 94–95
 arfvedsonite, 116, 140, 274
 argillic alteration, 246
 Arrhenius equation, 40
 ash, volcanic, 11, 12, 90, 113
 assemblage, mineral, 162, 170, 171, 197, 220, 252
 Barrovian metamorphic, 226
 calcareous, 213, 239, 240
 equilibrium, 191
 granulite, 255
 mafic, 181, 187–189
 opaque, 243
 pelitic, 224, 232
 ultramafic, 205, 207, 208, 211
 astrobleme, 130
 A-type granite. *See* granite
 augite*, 270, 271, 272
 sub-calcic, 270
 aureole, 165, 215, 216, 230, 232, 238, 240, 241, 242
 Australia rift zone, 107
 autolith, 9, 15, 105
 Azores, 83
 back-arc, 70, 74, 91
 Baikal rift, Siberia, Russia, 107
 Baltica, 150
 Bandolier, New Mexico, USA, 12
 Barrovian metamorphism, 224–228, 251, 252
 basalt, 10, 39, 54, 79, 94, 98, 109, 163, 181
 alkali, 66, 83, 115, 121, 155
 chemistry and petrography, 66–67
 classification, 66
 differentiation, 49, 110, 129
 ferro-, 80, 100, 116
 from hot spot volcanism, 81
 nepheline, 8, 115
 olivine, 40
 pressure effect on melting, 69
 tetrahedron, 66
 tholeiitic, 83, 99, 108, 112, 134
 tholeiitic versus alkali, 66, 69–70, 115
 basanite, 66, 115
 base metal deposit, 133
 Basin and Range province, USA, 107
 bathograd, 231
 batholith, 8, 14, 91, 95, 102, 124, 217, 251
 bathozone, 231–233
 Bay of Islands, Canada, 74
 Bear Lodge alkaline complex, Wyoming, USA, 139
 bedded magnesite deposits, 238
 bedding, sedimentary, 162, 165
 Benioff zone, 88, 91, 92, 101
 Bergell tonalite, European Alps, 216
 Bering peninsula, Alaska, 230
 beryl, 154
 beryllium, 155
 bimodal volcanism, 112–115
 Bingham mine, Utah, USA, 91, 245, 246
 biotite*, 276
 biotite zone, 226
 Bishop Tuff, 43
 Black Hills, South Dakota, USA, 55, 148
 black smoker, 84, 254
 blackwall zone, 214, 215
 block, volcanic, 10, 96
 Blue Mountains, Oregon, USA, 9
 blueschist, 182
 blueschist belt, 250
 blueschist facies, 182, 198, 212, 230, 250, 251
 correlation to Barrovian zone, 229
 Boina volcano, Afar region, Africa, 116, 117
 bomb, volcanic, 10
 Bonanza-type gold deposit. *See* gold deposits
 boundary layer fractionation, 43, 44
 Bouvet Island, South Atlantic, 109
 Bowen's reaction series, 282
 brecciation, breccia, 93, 120, 130
 brine, 213
 Brittany leucogranites, France, 148
 bulk assimilation, 44
 bulk distribution coefficient. *See* distribution coefficient

- buoyancy fracturing, 41
 Bushveld intrusion, South Africa, 125, 127, 128, 129, 130
 bytownite*, 265
- cacrinite*, 267
 calcite*, 268
 calcite-dolomite thermometer, 195
 calcium-aluminum silicate, 279–280
 calc-silicate rock, 181, 241
 caldera, 38, 92, 94, 112, 113
 Caledonian orogeny, 149, 201, 225, 254
 Caledonide belt, Europe, 252
 Cameroon volcanic line, Africa, 107
 carbonate alteration, 246
 carbonates, 104, 120, 148, 160, 171, 195, 212, 213, 238, 268
 carbonatite, 5, 116
 Caribbean plateau, 81
 Casa Parigia, Italy, 230
 Cascade Mountains, North America, 94, 95, 100, 206, 217
 Cascade trend. *See* iron enrichment index (Fe-index)
 cassiterite, 148
 celestine, 139
 cesium, 155
 charnockite, 2, 5, 199, 256
 terrane, 256
 chemical gradient, 214
 chemographic projection, 170, 171–176, 205, 220
 ACF diagram, 175, 176, 181, 182, 183, 184, 185
 continuous reaction, 221, 222, 223
 discontinuous reaction, 222, 223
 divariant, 173, 207
 four-component, 175
 pelitic system, 221–224
 pseudobinary, 175
 pseudoternary, 175
 ternary, 238
 three-component, 173
 tie line, 198
 two-component, 172
 univariant, 172
 chert, 73, 160, 163
 Cheyenne belt, Wyoming, USA, 132
 chiasolite*, 277
 chilled margin, 9, 14
 chlorite*, 276
 chlorite zone, 226
 chloritic alteration, 246
 chloritoid*, 279
 chondritic meteorite, 58, 67
 chromite, 126, 127, 128, 280
 podiform, 84, 125
 stratiform, 84, 125
 chrysotile, 205, 275
 CIPW norm, 48
 Clausius-Clapeyron equation, 192
 cleavage, 165, 166
 clinozoisite*, 279
 clockwise P-T-t (pressure-temperature-time) path, 251
- CO₂
 effect on melting temperature, 68
 effect on polymerization and viscosity, 38
 and ferroan granite, 135
 and melt evolution, 38–39, 120, 255
 in metamorphism, 171, 198, 199, 212, 237, 256
 solubility, 213
 Coast Range batholith, Canada, 91
 coesite. *See* UHP rocks
 Columbia River basalts, USA, 109, 110, 111
 chemistry, 110
 relation to Snake River Plain-Yellowstone, 108, 109–112
 units, 109
 columnar jointing, 9, 10
 comendite, 56
 compatible trace element, 48, 57, 58
 component, thermodynamic, 19, 172, 221
 composite volcano, 92
 Comstock Lode, Nevada, USA, 147, 148
 conchoidal fracture, 165, 263, 279
 conglomerate, 163
 congruent melting, 24
 constructive plate margin, 70
 contact aureole. *See* aureole
 continental arc magmatism, 89, 105
 continental collision, 185, 201, 251, 252
 continental overthrusting, 67, 72, 251, 254
 continental rifting, 107, 108, 130
 continuous reaction, 221, 222, 223
 convergent margin, 75, 88, 89, 104–105, 144
 metamorphism, 250
 copper deposits. *See* porphyry
 cordierite*, 278
 Cordilleran batholith, 91, 95–97, 102, 134, 146
 cotectic. *See* phase diagram
 Craters of the Moon, Idaho. *See* Snake River Plain, Idaho, USA
 critical point, 212
 cross bedding, 162
 crossite*, 273
 crustal cross-section, 256
 crustal delamination, 146, 151
 cummingtonite*, 273
 cumulate, 7, 9, 93, 99, 126, 128, 131, 141
 Curaçao, Netherlands Antilles, 10
- dacite, 8, 54, 94, 98, 103, 148
 Dalradian Supergroup, Scotland, UK, 225
 daughter isotope, 60
 Deccan traps, India, 108
 decompression melting, 68, 70, 79, 81, 146
 decompression reaction, 183
 deep basin, 159
 Deep Sea Drilling Project (DSDP), 72, 77
 degrees of freedom. *See* variance
 dehydration melting, 104, 146, 149, 229, 256
 dehydration reaction, 192, 195, 199, 204, 205, 212, 228, 238
 delamination. *See* crustal delamination
 Denver International Airport, Colorado, USA, 15
 destructive plate margin, 70
 diabase, 163
- diagenesis, 158, 198
 diamond, 120
 diatreme, 120
 differentiation, 67, 99
 diffusion, 29
 dihedral angle, 165
 dike, 8, 9, 13, 14, 15, 41, 94, 111, 120
 sheeted, 74, 254
 swarm, 14, 15, 41
 diopside*, 270
 diorite, 54, 91, 99
 ferro-, 132
 monzo-, 155
 discontinuous reaction, 222, 223
 discrimination diagram, 59
 distribution coefficient
 divariant, 172
 dolomite*, 268
 drusy quartz, 263
 Ducktown, Tennessee, USA, 242, 243, 244
 Dufek intrusion, Antarctica, 127, 130
 Duke Island, Alaska, USA, 99, 129
 Duluth intrusion, Minnesota, USA, 125,
 See also Keweenaw basalts, North America
 dunite, 25, 93, 131, 165
- Earth structure, 67
 asthenosphere, 67, 104, 151, 253
 core-mantle boundary, 81
 crust, thickness of oceanic and continental, 67, 82
 geophysical evidence, 67, 74, 78, 82, 91, 92, 217
 lithosphere, 82, 88, 104, 120
 lithospheric mantle, 67, 104
 lower mantle, 68
 mesosphere, 68
 upper mantle, 67, 68, 81, 104
 earthquake, 82, 88, 91, 92, 95, 204
 East African rift, 69, 107, 116, 117, 118, 121
 East Pacific Rise (EPR), 74, 75
 Eastern Goldfields sub-province, Australia, 259
 eclogite, 186
 eclogite facies, 182, 185, 189, 198, 199, 201, 212, 231, 251, 252
 correlation to Barrovian zone, 229
 edenite*, 274
 El Teniente mine, Chile, 91
 electron microprobe, 171, 191, 264
 enclave, 15, 51, 86, 134
 English River – Uchi belt, Canada, 258
 enstatite*, 270
 enthalpy, 192
 entropy, 192
 Eoalpine metamorphism, 252
 epidote*, 279
 epidotization, 163
 epithermal alteration, 147, 148
 epizone, 171
 equilibrium constant, 192, 243
 equilibrium crystallization, 21, 42
 albite-silica, 26
 anorthite-diopside, 23
 forsterite-fayalite, 27
 forsterite-silica, 24

- olivine-anorthite-diopside, 30
 equilibrium melting, **21**, **42**
 anorthite-diopside, 23
 forsterite-fayalite, 28
 forsterite-silica, 25
 equilibrium, thermodynamic, 98, 162, 192, 195, 196
 escape tectonics, 107
 Eskola classification. *See* metamorphic, facies, grade; Barrovian metamorphism
 Etendeka flood basalt, Namibia and Angola, 109
 Etive granite, Scotland, UK, 150, 152
 Etta mine, South Dakota, USA, 154
 eudialyte, 139, 140
 euhedral grain, 7, 9, 140, 154, 165
 eutectic. *See* phase diagram
 evaporite, 160
 exhumation, 200, 255
 experimental petrology, **2**, 133, 171, 211
 exsolution texture, 99, 264, 267, 271
 anitperthite, 264
 perthite, 264
 in pyroxene, 271
 extensional faulting, 75
 extinction angle, 266, 270
 Eyjafjallajökull volcano, Iceland, 85, 90
- facies, grade, 171
 FAMOUS valley, 80, *See also* Mid-Atlantic Ridge (MAR)
 fault bounding, 73
 fayalite*, 268
 feldspar*, 263, 264
 alkali*, 266, 267
 plagioclase*, 264, 265, 266
 feldspathoid*, 263, 267
 feldspathoid silica saturation index (FSSI), 56, 118
 Fennoscandia, 132
 ferroaugite*, 270
 ferromagnesian silicates, 31, 98, 99, 181, 187, 189
 ferrosilite*, 270
 Fe-Ti oxides, 76, 99, 100, 103, **133**, 145, 186, 280
 fiamme, **12**
 fibrolite, 277
 Fiji, 98
 filter pressing, **21**, **42**
 Fiskensætt anorthosite complex, Greenland, 131, 132
 flood basalt, 108, 109, 112, *See also* large igneous province (LIP)
 petrography and chemistry, 111
 flow segregation, **42**
 fluid
 externally controlled (infiltrated), 91, 121, 214, 240
 internally controlled (buffered), 91, 240
 fluid inclusion, 263
 fluid-rock ratio, 240
 fluorine poisoning, 85
 foliation, 164, 165, 217, 258
 fore-arc, 91
 forsterite*, 268
- fractional crystallization, **21**, 31, 42, 51, 57, 58, 74, 104, 110, 118, 124, 141
 anorthite-diopside, 23
 forsterite-fayalite, 27, 28
 forsterite-silica, 25
 olivine-anorthite-diopside, 30
 fractional melting, **21**, 42
 anorthite-diopside, 23
 forsterite-fayalite, 28
 forsterite-silica, 25
 Franciscan complex, California, USA, 250
 free energy (Gibbs), **192**, 243
 freezing point, depression, 22, 30
 Frost pyroxenite, 127
 fugacity, 243, 244, 280
- gabbro, 4, 9, 54, 99, 126, 127, 131, 163, 181, 254, 256
 classification, 5
 leuco-, **4**, 131, 132, 133, 135
 mela-, **4**, 93
 monzo-, 155
 in ophiolite, 74
 oxide, 78
 Gakkel ridge, Arctic Ocean, 74, 75
 Galapagos Islands, 79, 81, 99, 100, 109
 Gangotri glacier, Garhwal Himalaya, India, 149
 Gardar province, 138
 garnet*, 278
 garnet zone, 226, 227
 garnet-biotite thermometer, 194
 GASP barometer, 195
 gedrite*, 273
 gemstone, 154
 geobarometry, 171, 195
 geochemistry, 104, 111, 114, 153
 isotope, **2**
 major element, **2**, 79, 145
 trace element, **2**, **47**, 56–59, 78, 118
 whole rock, 157
 geochronology, **60**, 171
 geothermal gradient, 68, 198
 fossil, 251
 geothermal heat, 245
 geothermometry, **171**, 194
 Gibbs free energy. *See* free energy (Gibbs)
 glass
 manufacturing, 154
 volcanic texture, 7, 8, 12, 79
 glaucophane*, 273
 Glomar Challenger, 77
 gneiss, 162, 163
 ortho-, **163**
 para-, **163**
 quartzo-feldspathic, 257
 terrane, 258
 gneissosity, **166**
 gold deposits, 147, 148
 Gondwana, 108, 130
 graded bedding, 163
 reverse, **162**
 grandite garnets*, 278
 granite, 9, 52, 54, 55, 99, 102, 145, 148, 149, 153, 163, 198
 alphabet classification, 135, 145
- Caledonian-type, 149, 151, 152, 153, 155
 Cordilleran-type, 146, 152, 153, 155, 251
 dehydration melting, 256
 ferroan, 124, 134–138, 146, 152, 153, 155
 granitoid, 129, 155
 hypersolvus, 266
 magnetite and ilmenite, **145**
 in metamorphism, 200, 250
 mineralogy and petrology, 145–146
 minimum melt, 199
 peralkaline, 141
 peraluminous leucogranite (Himalayan-type), **146**, 148, 149, 150, 151, 152, 153, 155
 subsolvus, 266
 tin, 147
 volcanic arc (VAG), 59
 within plate (WPG), 59
 granoblastic texture, **165**
 granodiorite, 9, 15, 54, 91, 95, 99, 102
 granophyre, 99, 129
 granulite, 254
 granulite facies, 131, 164, 185, 189, 197, 199, 212, 230, 238, 255, 256
 correlation to Barrovian zone, 229
 granulite terrane, 249, 254, 255, 257
 graphite, 145, 147, 224, 281
 Great Dyke, South Africa, 125, 130
 green spinel*, 280
 greenalite*, 275
 greenschist, 186
 greenschist facies, 163, 181, 182, 187, 198, 212, 214, 225
 correlation to Barrovian zone, 229
 greenstone belt, 257, 258
 Grenada, Lesser Antilles, 98, 101
 Grenoble, France, 253
 Grenville anorthosite complexes, North America, 131, 132
 Grenville province, Ontario, Canada, 232
 greywacke, 145, 162, 250, 258
 grossular garnet*, 278
 groundwater, 245
 grunerite*, 272, 273
 guyot. *See* seamount
- H₂O, 12, 38, 96, 154, 184
 effect on melting temperature, 38, 68, 99, 128, **146**, 149
 effect on polymerization and viscosity, 37
 and melt evolution, 28, 37–38, 104, 149, 255
 in metamorphism, 171, 175, 176, 192, 237
 phase diagram, 212
 in serpentinization, 204
 solubility, 213
 Harker diagram, 49–51, 53, 58
 Harney Peak granite. *See* Black Hills, South Dakota, USA
 harzburgite, 68
 Hawaii-Emperor chain, 68, 69, 82–83
 Kilauea, 10, 82, 90
 Loihi, 81, 83
 Mauna Kea and Mauna Loa, 82
 relation to hot spot, 82, 107
 heat capacity, 39
 heat of fusion, 39, 44

- hedenbergite*, 270
 Helena dolomite, 241
 Hercynian granulites, 254
 hercynite, 224
 high pressure belt. *See* paired metamorphic belt
 Highland Boundary fault, Scotland, UK, 225
 Himalaya Mountains, 158, 201
 Himalayan leucogranite, 148, 200
 Himalayan orogeny, 107
 Honshu, Japan, 250
 hornblende*, 275
 hornfels, 164, 165, 230
 hornblende, 186
 Hortavær complex, Norway, 44
 hot spot, 68, 70, 79, 81
 Hudson Bay, Canada, 15
 hyaloclastite, 11
 hydration reaction, 254
 hydrofracturing, 91
 hydrothermal alteration, 244, 254
 hydrothermal cell, 39
 hydrothermal fluid, 84, 99, 141, 148, 159, 244
- Iceland, 79, 99, 109
 icelandite, 100
 iddingsite, 120
 ideal gas, 243
 ideal solution, 193
 idioblastic texture, 268
 igneous
 classification, plutonic, 3–5, 145
 classification, preliminary, 3
 classification, volcanic and hyperabyssal, 6, 7, 11, 12
 petrogenesis, 2
 petrography, 2
 petrology, 1, 2
 structures, 8–15, 126, 148
 textures, 5–8, 9, 124, 162, 163
 Ilimaussaq intrusion, Greenland, 127, 128, 138–141
 ilmenite*, 280, 282
 immiscible fluid, 43
 incompatible trace element, 48, 57, 66, 69, 79, 125, 147
 incongruent melting, 24
 industrial minerals, 124, 138, 154
 Ingalls peridotite, Washington, USA, 217
 Integrated Ocean Drilling Program (IODP), 75, 76, 77, 79, 254, 255
 International Union of Geological Sciences (IUGS), 1, 2, 3, 4, 5, 6, 7, 48
 intrusions, 15
 ion-exchange reaction, 196
 ion-exchange thermometry, 194
 iron enrichment index (Fe-index), 54–55, 79, 81, 99, 100, 102, 114, 116, 117, 119, 137, 146, 148, 153
 ferroan, 111, 115
 magnesian, 100, 153
 iron formation, 160, 258, 259
 island arc, 89, 92
 magmatism, 89, 101, 104
 volcano, 92–93
- isograd, 162, 216, 231, 240, 241, 250
 second sillimanite, 228
 isopleth line, 195
 isostasy, 251
 isotope geochemistry, 59–61, 105, 114, 115, 118
 radioactive, 60, 83, 103
 Iszu – Bonin subduction zone, western Pacific, 218
- jack-straw texture, 206
 jadeite, 182, 185, 271
Joides Resolution, 77
 Juan de Fuca plate, 109
- Kaiserstuhl, Germany, 8
 kakortokite, 140, 141
 Kalapana Gardens subdivision, Hawaii, USA, 85
 Kangerdluarssuk fjord, Greenland, 141
 Kapuskasing block, Canada, 256
 Karmusten volcanics, Vancouver Island, Canada, 186
 Karoo basalts, South Africa, 108
 katazone, 171
 Katmai, Alaska, USA, 96
 Kerguelen plateau, 81
 Keweenaw basalts, North America, 108
 Kiglapait intrusion, Canada, 129
 kimberlite, 41, 119, 120
 kinetics, 206
 Kola, 138
 komatiite, 5
 Krakatoa, Indonesia, 96
 KREEP basalt (lunar), 57–59
 Kurile island arc, 89
 kyanite*, 277
 kyanite zone, 224, 227, 228
- labradorite*, 264
 Lake Owen complex, Wyoming, USA, 99
 lamellae, 271
 lamproite, 119, 120
 lamprophyre, 5
 lapilli, 11
 Laramide orogeny, 133
 Laramie anorthosite complex, Wyoming, USA, 15, 41, 43, 132, 136, 164, 230, 232
 Chugwater intrusion, 132
 Maloin Ranch pluton, 133
 Red Mountain pluton, 50, 51, 53, 54, 58, 133, 139
 Sybille monzosyenite, 133
 Laramie Mountains, Wyoming, USA, 50, 59, 163, 186, 232
 large igneous province (LIP), 81, 108
 laser ablation, 171
 laumontite*, 280
 Laurentia, 150
 lava dome, 12, 13, 14, 95, 96
 lava tube, 95
 law of mass action, 192
 lawsonite*, 280
 lawsonite-albite-chlorite facies, 185
 layered mafic intrusion (LMI), 99, 124, 126–130
 mineralogic variability, 126, 128
- stratigraphy, 131
 tectonic environment, 130
 Le Chatelier's principle, 208
 Lesser Antilles, Caribbean, 89, 98, 101
 leucite*, 267
 Leucite Hills, Wyoming, USA, 120
 leucocratic minerals, 263–268
 leucosome, 200
 lever rule, 19–20
 lherzolite, 67, 68, 69, 78
 depleted, 68
 fertile, 68, 104
 Ligurian Alps, Italy, 186
 limestone, 238
 lineation, 165
 liquidus, 22, 27, 29, 39, 103, 158
 lithium, 155
 lizardite, 205, 206, 275
 Long Valley caldera, California, USA, 43
 low-pressure belt. *See* paired metamorphic belt
 lujavrite, 138, 140, 141
- Macquarie Island, South Pacific, 74
 mafic minerals, 268–277
 mafic selvage, 199, 200
 magma, 36
 ascent, 40–41, 79, 99, 120, 154
 assimilation and contamination, 41, 44, 52, 104, 105, 110, 111, 124, 141, 147
 chamber, 82, 99, 104, 111, 113, 128
 density, 40, 141
 differentiation, 48
 environment of magmagenesis, 70, 104–105, 111
 exsolution of aqueous fluid, 91, 148
 isotopic composition, 60, 105
 mass transfer, 108
 mixing, 44, 51, 52, 103, 119, 124
 oxygen fugacity, 55, 100, 139, 145, 147
 in paired metamorphic belts, 251
 temperature, 39
 viscosity, 39–40, 95, 96
 magmatic differentiation, 42–44, 79, 99, 100, 112, 126
 continental arc, 103
 mid-ocean ridge, 78
 oceanic, 100
 magnetic anomaly, 255
 magnetite*, 280, 282
 major elements, 86, 99, 111, 119, 145,
 See also oxides
 Malenco serpentinite, European Alps, 215
 manganese (Mn) formation, 160
 mantle, 42, 68, 78, 86, 88, 104, 111, 120, 217
 composition, 67, 121
 convection, 68
 isotopic composition, 105
 melting, 68–69, 104, 121
 olivine fabric, 217
 peridotite, 204
 plume. *See* (hot spot)
 protolith, 208
 xenocryst, 98
 xenolith, 121

- marble, 238–242, 250
 Marianas island arc, 89
 marl, 160
 Marysville stock, Montana, USA, 241, 242
 mass extinction, 86
 mass fractionation, **60**
 massive sulfide deposit. *See* volcanogenic massive sulfide (VMS)
 mass-transfer reaction, **196**
 Matterhorn, Switzerland, 252
 McKenzie Mountains, Yukon-Northwest Territory, Canada, 148
 megacryst, 131, 163
 mélange, **250**
 melanosome, **200**
 mesozone, 171
 metabasalt, 163, 164, 186, 187
 metabasite, 161, **181**, 188, 272
 metaconglomerate, 162, 163
 metadiabase, 163, 187
 metagabbro, 215
 metamorphic
 conditions, 161, 180, 197–200
 facies, grade, 162, 171, 176, 182, 211, 226, 238, 259
 field gradient, 252
 fluid, 171, 238–242
 inversion, 254
 nomenclature, 166, 167
 petrology, 157
 textures and fabric, 159, 162–166, 186, 197, 206
 metamorphism, **158**
 in Archean terranes, 257, 259
 burial, 158
 contact, 158, 185, 215, 238
 in continental collision, 185, 251
 dynamic, 159
 in granulite terranes, 255
 hydrothermal, 159
 isochemical, 159, **214**
 prograde, 203, 204
 regional, 158, 181–185, 215, 216, 249
 retrograde, 159, 197, 253
 in rifting terranes, 253
 seafloor, 254
 metapelite, 250
 metaperidotite, 171, 203, 205, 206, 210, 211, 213, 214, 215
 metasedimentary belt, 257
 metasedimentary rock, 104, 200, 212, 250
 metasomatism, **121**, **159**, 214, 215, 256
 of peridotite, 214
 mica*, 276
 Mica Dam, British Columbia, Canada, 184
 microcline*, 266, 267
 Mid-Atlantic ridge (MAR), 74, 75, 76, 79
 mid-ocean ridge, 75, 109, 146, 159, 254
 Mid-Ocean Ridge Basalt (MORB), 67, **78**, 83, 104, 111
 composition, 59, 78–80
 E-MORB, 79, 111
 interaction with mantle, 77, 79
 N-MORB, 79, 111
 pressure effect on melting, 79
 migmatite, 200
 minnesotaite*, 275
 minor elements, 47
 mobile belts, 201
 modal mineralogy, 4, 5, 6, 48, 204
 mode, **48**
 modified alkali lime index (MALI), 53–54, 81, 102, 114, 116, 117, 119, 137, 148, 153
 alkalic, 54, 66, 80, 91, 114, 117, 136, 153
 alkali-calcic, 66, 80, 98, 100, 101, 114, 136, 151, 153
 calc-alkalic, 54, 66, 80, 91, 98, 100, 101, 102, 121, 130, 153
 calcic, 54, 66, 97, 100, 102, 153
 Moho, 67, 74
 monazite*, 281
 Mont Pelée, Martinique, 12
 monzonite, 50, 54, 134, 155
 Mount Pinatubo, Philippines, 90, 96
 Mount Saint Helens, Washington, USA, 12, 14, 90, 94–95, 97, 100, 101, 103, 105
 Mount Somma caldera, Italy, 119
 Mount Stuart batholith, Washington, USA, 217
 Mount Vesuvius, Italy, 11, 118, 119
 Mullen Creek complex, Wyoming, USA, 99
 muscovite*, 276
 myrmekite, 99

 Nain anorthosite complex, Canada, 133
 naujaite, 140, 141
 Nebo granite, South Africa, 136
 nepheline*, 267
 network-forming ions, **36**, 37, 40
 network-modifying ions, **36**, 37, 40, 90
 Neuberg Peak, Antarctica, 127
 neutralization reaction, 244
 Nevado del Ruiz, Columbia, 90
 New Caledonia, 193
 New Hebrides island arc, 89
 norite, 4
 norm, **48**
 normal zoning, 264
 normative mineralogy, 66, 83, 115, 119, 145,
 See also CIPW norm
 nucleation, 6, 165
 Nyambeni, Kenya, 116, 117
 Nyiragongo, Congo, 90, 116, 117

 Ocean Drilling Program (ODP), 77, 254
 ocean floor bathymetry, 204
 ocean island, 82
 volcano, **80**, 82–83
 Ocean Island Basalt (OIB), 67, **78**, 111
 ocean plateau, *See also* large igneous province, 81, 82
 oceanic spreading center, 68
 fast, 74, 75, 78, 254
 rate, 75
 slow, 74, 75
 ultra-slow, 74, 75
 off-ridge magmatism, **78**, 80–81
 Ok Tedi mine, Papua New Guinea, 91
 Ol Doinyo Lengai, Tanzania, 116

 Old Faithful geyser, Wyoming, USA, 147
 olivine*, 268
 pressure effect on melting, 78
 Oman ophiolite, 74
 omphacite*, 272
 Ontong-Java plateau, 83–86
 opaque mineral, 280
 ophiolite, 67, 72, 73–78, 84, 254
 optical mineralogy, 2, 187
 ore deposit, association with
 hydrothermal alteration, 245–246
 ore deposits, occurrence in
 anorthosite complexes, 133
 astrobleme, 130
 granite, 155
 layered mafic intrusions, 125
 oceanic crust, 84
 ore fluid, 157
 Oregon plateau. *See* Columbia River basalts, USA
 orthoclase*, 263, 264, 266, 267
 orthogneiss, **163**
 orthopyroxene*, 270, 271
 Otago belt, New Zealand, 250
 oxide mineral, 280
 oxides, 3, 19, 48, 193

 Paddy-Go-Easy pass, Washington, USA, 206, 215, 216, 217
 pahoe-hoe, **9**, 10
 paired metamorphic belt, 250
 high-pressure, 250, 252
 low-pressure, 250
 pantellerite, 56
 paragneiss, **163**, 200
 paragonite*, 277
 Paraná plateau, Brazil, 108
 parent isotope, **60**
 pargasite*, 274
 parisite, 139
 partial melting, 31, 42, 57, 67, 74, 78, 79, 86, 115, 121, 145
 assimilation of, **44**
 partition coefficient, 57, 138
 Peacock classification. *See* modified alkali lime index (MALI)
 pegmatite, 7, 57, 141, 154–155
 Pele, 85
 pelite, pelitic, **160**, 229, 232
 chemographic projection, 221–224
 pendant, 251
 penetrative deformation, **159**
 Peninsular Ranges batholith, North America, 91
 Penrose Conference, 73
 peralkaline, 115
 periclase zone, 240
 peridotite, 5, 67, 76, 120, 128, 131
 garnet, 201, 211
 high temperature, 210, 211
 metamorphic protolith, 161, 203
 in ophiolite, 74
 refertilized, 210
 peritectic. *See* phase diagram
 petrogenetic grid, 171

- petrographic microscope, 48
 pH
 alkaline (basic) fluids, 204
 buffering, 244
 phase diagram, 170
 binary, 20, 21–29
 cotectic, **30**, 78
 divariant, 19, 20, 22
 eutectic, 21, **22**, 25, 29, 30, 68, 69, 78, 79
 invariant, 19
 peritectic, **24**, 30
 pseudoternary, 30, 69, 78
 P-T diagram, 19, 38, 39, 149, 192, 197, 205, 207, 209, 210, 211, 212, 229, 251, 277
 ternary, 20, 21, 29–31, 68, 69
 thermal barrier, **26**, 31, 67, 118
 T-X diagram, 22, 23, 24, 25, 26, 27, 28, 209, 213, 214, 221, 239, 240, 241, 242, 269, 270
 univariant line, 19, 22
 phase rule, 19–20, 209
 phase, thermodynamic, **19**, 172, 192
 equilibria, 191
 phengite*, 276
 phenocryst, 7, 8, 9, 78, 79, 97, 99, 111, 163
 Philippine Institute of Volcanology and Seismology, 96
 phlogopite*, 276
 phonolite, 40, 67, 116
 phyllite, 225
 phyllosilicate*, 274
 pigeonite*, 270, 271
 Pikes Peak batholith, Colorado, USA, 135, 137
 Pikwitonei block, Canada, 256
 Pilbara craton, Australia, 258
 pillow basalt, **9**, 10, 73, 163, 164, 254
 plagioclase effect, 118
 plane of critical silica undersaturation, **66**
 plane of silica saturation, **66**
 plate tectonic revolution, 201, 249
 platinum group elements (PGEs), 125, 133
 pleochroism, 66, 183, 189, 210
 Pliny the Younger, 11, 119
 pluton, plutonic, **8**, **14**, 91, 95, 141, 150
 charnockitic, 256
 epizonal, 171
 point-counting, 48
 polymerization, polymers, 37, 40
 aqueous fluids, 104
 CO₂, 38
 silica, 36
 polythermal projection, 29
 Pompeii, Italy, 11, 119
 porphyroblast, porphyroblastic, 164, **165**
 porphyry, **8**, 9
 copper deposit, 91, 147, 244, 245
 potassic alteration, **246**
 Precambrian shield, 249, 257
 precious metal, 258
 preferred orientation, 164, 165, 217, 218
 prehnite*, 279
 prehnite-pumpellyite facies, 184, 186, 187, 198, 212, 254
 correlation to Barrovian zone, 229
 primary texture, 162
 propylitic alteration, **246**
 protolith, **157**, 159, 167, 187
 calcareous, 239
 granitic, 200
 igneous, 161
 mafic, 161
 quartzo-feldspathic, 161
 sedimentary, 159, 160, 162, 220, 224, 237
 ultramafic, 204
 psammite, psammitic, **160**, 200
 pseudomorphs, 206
 pumice, **11**, 12, 96
 pumpellyite*, 279
 pumpellyite-actinolite facies, 182
 pyralisite garnets*, 278
 Pyre Peak, Alaska, USA, 92
 Pyrenees, Europe, 254
 pyrite*, 280
 pyroclastic rocks, **5**, **8**, 11
 pyrometer, 39
 pyrope*, 278
 pyroxene*, 269, 271
 clino-, 270
 ortho-, 270
 quadrilateral, 55, 269
 sodic, 269, 271, 272
 pyroxene-hornfels, **186**
 pyroxenite, **5**, 9, 93, 128, 131, 204
 pyrrhotite*, 280
 QAPF diagram, classification, 3, 4, 102, 145, 153, 155
 quadrilateral reaction, 174
 quartz*, 263
 quartzite, 160, 165, 250
 Quetico belt, Canada, 257
 Raft River Mountains, Utah, USA, 163
 rapakivi texture, 43
 rare earth elements (REEs), 42, 56, 138, 155
 in alkaline intrusions, 138–139
 diagram, **58**
 in garnet, 211
 in lunar samples, 59
 Rayleigh fractionation, 57
 reaction rim, 43, 99, 164, 183, 184, 211, 228
 Red Sea, 107, 116
 refertilization, 210
 residual melt, 26
 resorbed crystal, **43**, **44**, 66
 restite, **158**, **200**
 retrogressive reactions, 251
 reverse zoning, 265
 rheology, 204
 Rhine graben, Europe, 107
 rhyolite, 39, 40, 51, 54, 79, 99, 100, 112, 148
 melt viscosity, 40
 peralkaline, 116
 riebeckite, 116, 140, 274
 rift zone, 148, *See also* continental rifting
 Rio Grande rift, North America, 107
 Rocas Verdes, Chile, 74
 Rocky Mountains, North America, 158
 rodingite, **204**, 215
 Rogaland anorthosite complex, Norway, 133
 Roman province, Italy, 69, 118, 119, 121
 Rum intrusion, Scotland, UK, 127, 130
 rutile*, 281
 Ryoke belt, Japan, 250
 Ryuku island arc, 89
 San Miguel Regla, Hidalgo, Mexico, 10
 sanidine*, 266, 267
 Scandinavian shield, 254
 scanning electron microscope (SEM), 224
 schist, 164, 225, 243
 schistosity, 165
 scoria, **11**
 Scotia island arc, South Atlantic, 89
 seamount, **80**
 seawater, 104, 164, 254
 sedimentary texture, 162, 163
 Segum. *See* Aleutian island arc, Alaska, USA
 seismic anisotropy, **217**
 seismograph, 96
 selvage. *See* mafic selvage
 semi-pelitic rocks, 227
 sericite, sericitization, 224, 244
 sericitic alteration, **246**
 serpentine*, 275
 serpentine polymorphs, 205
 serpentinite, serpentinitization, 73, 120, 175, 204–208, 250
 role of aluminum, 210
 role of iron, 208
 Sesia zone, Italy, 186
 shale, 2, 149, 220, 224
 shatter cone, 130
 shear segregation, 42
 shear zone, 159
 Sherman batholith, Wyoming, USA, 43, 49, 50, 52, 54, 59
 Lincoln granite, 51, 52, 59
 Sherman granite, 51, 52, 54, 59
 Shiprock, New Mexico, USA, 14
 Shuksan belt, Cascade Mountains, North America, 250
 Siberian traps, Russia, 109
 Sierra Nevada batholith, California, USA, 14, 91, 95, 98, 102, 105, 150
 Tuolumne pluton, 53, 54, 55, 95–97, 98, 101, 102, 150
 silicate
 octahedral site, 36, 37, 204
 tetrahedral site, 36, 37, 183, 204, 225
 silicic alteration, **246**
 sill, **8**, **14**, 149
 sillimanite*, 277
 sillimanite zone, 228
 Skaergaard intrusion, Greenland, 9, 128
 Skaergaard trend. *See* iron enrichment index (Fe-Index)
 skarn, **148**, 241
 slate, 225
 Smartville ophiolite, California, USA, 99, 163
 Smoky Buttes, Montana, USA, 120
 Snake River Plain, Idaho, USA, 10, 107, 109, 112, 114, 117, *See also* Yellowstone hot spot, USA
 soapstone. *See* steatite
 sodalite*, 267, 268

- solid solution, 20, 27, 185, 195, 222, 263, 270, 272
 partial, 29
 solidus, 27, 68, 112, 135, 149
 CO₂, 39
 dry, 37, 39
 sub-, 99
 Solomon Islands, 81, 89
 solvus, 29, 195, 213, 266
 solvus thermometry, 194
 Soufrière volcano, St. Vincent, 8
 Southwest Indian ridge, 76
 spessartine*, 278
 sphene*, 281
 St. Helena, 83
 St. Kitts and Nevis, 100
 static texture, 164
 staurolite*, 278
 staurolite zone, 227
 steatite, 214
 Stillwater intrusion, Montana, USA, 9, 125, 130
 stilpnomelane, 182, 226, 229
 Stokes law, 41
 stoping, 41
 strontianite, 139
 structural geology, 157, 166, 253
 sub-arc intrusion, 99
 subduction zone, 68, 89, 104, 121, 185, 201
 cold, 185, 198, 250, 251
 serpentinization, 204
 suprasubduction-zone ophiolite, 74
 Sudbury intrusion, Canada, 125, 129, 130
 sulfide mineral, 280
 sulfide ore body, 242, 243, 244,
See also volcanogenic massive sulfide deposit
 sulfur-bearing fluid, 125
 sulphur-bearing fluid, 171, 242, 244, 280
 Sunda-Banda island arc, 89, 98
 Super High Resolution Ion Microprobe (SHRIMP), 171
 supercritical fluid, 212
 Superior province, Canada, 256, 257
 supracrustal rocks, 257
 Suswa, Kenya, 117
 syenite, 50, 54, 56, 91, 140, 155
 monzo-, 43, 133
 nepheline, 127
 synchysite, 139
 syncline, 216
 system, thermodynamic, 19, 172
 tabular feldspar, 7, 133, 162, 186
 Taconic orogeny, 233
 talc*, 275
 Tambora, Indonesia, 90
 tantalum, 155
 Taos, New Mexico, USA, 164
 TAS diagram, classification, 5
 tectonic texture, 165
 tectonic thickening, 148, 149, 151
 tectosilicate, 184
 Tellnes Ti-deposit, Norway, 133
 tephrite, 115, 119
 terminal reaction, 174, 222, 223
 Tethys sea, 216, 252
 Teton Range, Wyoming, USA, 200
 thermal anomaly, 254
 thermobarometry, 158, 162, 171, 191, 193, 194–197, 199
 thermocouple, 39
 thermodynamic database, 162
 thermodynamics, 19, 39, 171, 205
 thermometry, 197, 198
 tholeiite, 40, 57, 58, 66, 83, 100, 121,
See also basalt
 melt viscosity, 40
 olivine, 8, 66, 112, 116
 quartz, 66
 thrust fault, 185
 Tibetan plateau, 151
 tie line flip reaction, 174, 222, 223, 228
 tiltmeter, 96
 tin ore, 147
 titanite. *See* sphene
 Toba, Indonesia, 90
 Tobago, West Indies, 89, 93–94, 99, 102
 tonalite, 93, 97, 99, 102, 145, 155, 200
 Tonga-Kermadec island arc, 89
 topaz, 154
 topology, 172, 173, 174
 Toutle River, Washington, USA, 95
 trachyte, 54, 100, 115
 transform fault, 75
 Trans-Hudson orogeny, 256
 transition metals, 56, 91, 254
 tremolite*, 272
 trench, 88, 91, 101, 218
 Tristan da Cunha, 83, 109
 troctolite, 4, 77, 78
 Troodos, Cyprus, 74, 84
 tschermakite, 274
 tuff, 11, 12, 114
 tungsten ore, 148
 Tuolumne pluton, California, USA. *See* Sierra Nevada batholith, California, USA
 turbidite, 163
 Turino, Italy, 253
 twinning, 264, 266, 279
 albite, 264, 265, 266
 Carlsbad, 264, 265
 pericline, 265
 polysynthetic, 265, 273
 tartan, 267
 ultrahigh pressure (UHP) metamorphism, 198, 200
 ultrahigh temperature (UHT) metamorphism, 198, 199
 ultramafic rock, 5, 93, 99, 102, 111, 119, 126, 174
 ulvöspinel*, 280
 undulatory extinction, 263
 Val Malenco. *See* Malenco serpentinite, European Alps
 variance, 19, 183, 209, 221, 240
 variation diagram, 58, 80, 99, 100, 103, 111, 118, 119, *See also* Harker diagram
 vein, 121, 141, 148, 244, 254
 vesicle, 10, 66, 164
 Voisey's Bay deposit, Canada, 133
 volatile, 7, 11, 37–39, 68, 99, 139, 154, 158, 239, 255
 devolatilization, 222, 238, 240
 Volcan Gelaras, Columbia, 148
 volcanic deposit, 10–12, 90, 93, 96–97
 air fall, 11, 13, 113
 lava flow, 8, 85, 92, 95, 108, 119
 pyroclastic flow, 11, 13, 14, 95, 96
 volcanic eruption type
 fissure, 85, 108, 110
 phreatomagmatic, 11
 plinian, 11, 13
 strombolian, 11, 13
 Volcanic Explosivity Index (VEI), 90, 96
 volcanic gas, 97, 148
 volcanic hazard prediction, 96, 97, 113
 volcanic hazards, occurrence
 convergent margin, 90, 96–97
 intracontinental, 113
 oceanic, 85
 volcanic neck, 13, 14
 volcanic winter, 90
 volcanogenic massive sulfide (VMS), 84
 wairakite, 184
 Wasatch Mountains, Utah, USA, 240
 wehrlite, 93
 welding, 12
 Wenatchee Mountains, Washington, USA, 217
 whiteschist, 229, 275
 whiteschist facies, 201, 230, 231
 Willow Creek pass, Colorado, USA, 9
 Wind River Range, Wyoming, USA, 114, 199
 Windimurra anorthosite complex, Australia, 131
 Wyoming province, 132
 xenocryst, 36, 44, 98, 120, 134
 xenolith, 15, 67, 83, 120, 256
 X-normal method, 265
 X-ray diffraction, 206, 224
 Yellowknife, Northwest Territories, Canada, 163
 Yellowstone hot spot, USA, 12, 109, 112, 113, 114, 147, 148, 159
 Yilgarn province, Australia, 258, 259
 Yosemite National Park, California, USA, 95
 Zarza, Baja, Mexico, 53, 54
 zeolite, 164
 zeolite facies, 184, 187, 198, 224, 250, 254
 correlation to Barrovian zone, 229
 Zermatt-Saas ophiolite, Switzerland, 201, 206, 252
 zircon, Zr, 58, 138, 140, 145, 281
 zoisite*, 279
 zonation, zoning
 in granite, 97, 148, 150
 normal, 264
 in plagioclase, 8, 9, 98, 266
 reverse, 44, 265
 in ultramafic rocks, 214

